Alexandr I. Korotkin

Fluid Mechanics and its Applications

Added Masses of Ship Structures

Springer

Added Masses of Ship Structures

FLUID MECHANICS AND ITS APPLICATIONS
Volume 88

Series Editor: R. MOREAU
MADYLAM
Ecole Nationale Supérieure d'Hydraulique de Grenoble
Boîte Postale 95
38402 Saint Martin d'Hères Cedex, France

Aims and Scope of the Series

The purpose of this series is to focus on subjects in which fluid mechanics plays a fundamental role.

As well as the more traditional applications of aeronautics, hydraulics, heat and mass transfer etc., books will be published dealing with topics which are currently in a state of rapid development, such as turbulence, suspensions and multiphase fluids, super and hypersonic flows and numerical modeling techniques.

It is a widely held view that it is the interdisciplinary subjects that will receive intense scientific attention, bringing them to the forefront of technological advancement. Fluids have the ability to transport matter and its properties as well as to transmit force, therefore fluid mechanics is a subject that is particularly open to cross fertilization with other sciences and disciplines of engineering. The subject of fluid mechanics will be highly relevant in domains such as chemical, metallurgical, biological and ecological engineering. This series is particularly open to such new multidisciplinary domains.

The median level of presentation is the first year graduate student. Some texts are monographs defining the current state of a field; others are accessible to final year undergraduates; but essentially the emphasis is on readability and clarity.

For other titles published in this series, go to
www.springer.com/series/5980

Alexandr I. Korotkin

Added Masses of Ship Structures

Springer

Alexandr I. Korotkin
Krylov Shipbuilding Research Institute
Moskovskoye Shosse, 44
St. Petersburg 196158
Russia

А.И. Короткин

**ПРИСОЕДИНЕННЫЕ
МАССЫ
СУДОСТРОИТЕЛЬНЫХ
КОНСТРУКЦИЙ**

Справочник

**Санкт-Петербург
Мор Вест
2007**

This is an updated and revised translation of the original Russian work entitled «Присоединенные массы судостроительных конструкций», by A. Korotkin, Morwest, St. Petersburg, Russia, 2007.

ISBN 978-1-4020-9431-6 e-ISBN 978-1-4020-9432-3

Library of Congress Control Number: 2008938548

Printed on acid-free paper

9 8 7 6 5 4 3 2 1

springer.com

Preface

Masses that are added to a ship's bulk will determine the inertial properties of that ship under motion. Computation of the effect of such added masses of various bodies has been the subject of many journal articles, as well as chapters in various textbooks and research monographs on theoretical and applied hydrodynamics. This book is part of that literature.

The present volume is a revised translation of the second edition of the author's book "Added masses of ship structures" published in 2007 in Russian by Morwest Publishers (St. Petersburg). The first Russian edition was published in 1986; in the second edition the author also reviewed results obtained in this field over the intervening 20 years.

In particular, we included a brief overview of existing numerical methods for determination of added masses (Chap. 9). The well-developed numerical methods allow us to go far beyond pure theoretical considerations which give explicit results only for simple models. However, in many cases, for practical engineering purposes one needs to know the dependence of various added masses on the main parameters of the system for various models. In particular, these model cases can be used to verify the accuracy of numerical results.

It is the purpose of this book to collect the main theoretical results on added masses and to describe some experimental methods of their determination; we hope that it can serve as a useful tool to engineers dealing with various structures moving in fluid. Besides marine engineering, this book can be used in machine engineering, aviation engineering and hydrotechnique studies.

The author would like to offer an apology to the reader for a certain notational inconsistency: the period is used in decimal numbers in the main text of the book. However, the comma is used for the same purpose in pictures which were inherited from the Russian edition of the book. To avoid a tedious process of re-drawing these figures we assume $0.5 = 0,5 = 1/2$ in this book; we hope this inconsistency will not confuse the reader significantly.

Some sections of this reference book were written by other authors. Sect. 9.6 is written by V.S. Boyanovskij and O.I. Babko; Sect. 4.1—by Yu.V. Gurjev; Sects. 7.1, 7.2—by E.I. Ivanjuta; Sect. 2.6—by A.I. Nemzer; Sect. 9.5—by S.N. Okunjov, Sect. 7.4—by A.S. Samsonov; Sect. 6.10—by V.N. Fedorov; Chap. 6 and Sect. 8.3—by E.N. Schukina, Sect. 5.14—by I.V. Sturova and E.V. Ermanjuk; Sect. 8.5—by A.M. Vishnevskij, A.J. Lapovok and S.A. Kirillov.

I.V. Sturova made several important comments on Chap. 5 of the Russian edition; these comments are taken into account in the English edition of the book.

The second Russian edition was published due to friendly recommendations of A.S. Ginevskij.

I express my deep gratitude to N.A. Sizova who prepared the second Russian edition for publication. Finally, I thank D. Korotkin who edited both the content and the language of the English version of the book.

St. Petersburg *Alexandr I. Korotkin*
July 2008

Contents

Chapter 1
General Discussion of Body Motion in an Ideal Infinite Fluid

The notion of added mass was first introduced by Dubua in 1776 (see [24]), who experimentally studied the small oscillations of a spherical pendulum. An exact mathematical expression for the added mass of a sphere was obtained by Green in 1833 and Stokes in 1843 (see [133]). Stokes also studied the motion of a sphere in a finite volume of fluid. Later, as a result of efforts of many researchers, the notion of added mass was generalized to an arbitrary body moving in different regimes. Under motion of a body in real incompressible fluid, the hydrodynamic forces and torques are determined by inertial and viscous properties of the fluid. In certain approximations one can distinguish the forces and torques of inertial nature, which can be computed assuming that the fluid is ideal (non-viscous), and the forces (torques) are related to viscosity. The forces and torques of the inertial nature can be expressed in terms of the added masses of the body. The hydrodynamic forces and torques can also be expressed in terms of added masses not only in the case of accelerated motion, but also in the case of motion with constant velocity. It is especially important to take the added masses (or added moments of inertia) into account if they are comparable with the mass (or moments of inertia) of the body itself.

The added masses are especially important in studies of the rolling of a vessel and in studies of vessel control, as well as in the problems of analysis of local and global vibration of a vessel and its parts (rudders, propellers).

1.1 Formulation of the Problem

Assume that the body with surface S is moving in an infinite homogeneous ideal fluid free from vortices. Consider two systems of coordinates: the stationary one (we denote it by XYZ) and the coordinate system moving together with the body (we denote it by $Oxyz$). Let us assume that at a given moment these two systems of coordinates coincide. The vortex-free condition implies the existence of a potential $\varphi(X, Y, Z, t)$ such that the components of the fluid velocity are given by:

$$v_X = \frac{\partial \varphi}{\partial X}; \qquad v_Y = \frac{\partial \varphi}{\partial Y}; \qquad v_Z = \frac{\partial \varphi}{\partial Z}. \tag{1.1}$$

The continuity and incompressibility of the fluid imply the Laplace equation

$$\frac{\partial^2 \varphi}{\partial X^2} + \frac{\partial^2 \varphi}{\partial Y^2} + \frac{\partial^2 \varphi}{\partial Z^2} = 0. \tag{1.2}$$

The boundary conditions for Eq. (1.2) look as follows:

1. The watertight condition, valid on the surface S:

$$\left.\frac{\partial\varphi}{\partial n}\right|_S = u_n, \tag{1.3}$$

   where $(\partial\varphi/\partial n)|_S$ is a projection of fluid velocity on the (external) normal direction n to surface S; u_n is the projection of velocity of a point of the body on the normal n.
2. Stationarity condition at infinity:

$$\lim_{r\to\infty}\frac{\partial\varphi}{\partial X} = \lim_{r\to\infty}\frac{\partial\varphi}{\partial Y} = \lim_{r\to\infty}\frac{\partial\varphi}{\partial Z} = 0, \tag{1.4}$$

   where $r^2 = X^2 + Y^2 + Z^2$ (r is the distance from the origin to a fluid point).

The function φ vanishes at infinity as r^{-2}, whereas its first-order coordinate derivatives vanish as r^{-3} [116, 221].

From the formulation of our problem (1.2)–(1.4) we see that function φ depends on time t via the right-hand side of boundary condition (1.3). Let us write down this condition in more detail. Choose the origin O to coincide with an arbitrary point of the body. Denote velocity of the point O by $\vec{u}_O$ (components u_{0x}, u_{0y}, u_{0z} are projections of the vector $\vec{u}_O$ on coordinate axes attached to the body). Denote by $\vec{\omega}$ the angular velocity of the body with respect to the point O (components of $\vec{\omega}$ in the same coordinate system are denoted by $\omega_x, \omega_y, \omega_z$). The velocity of an arbitrary point of the body, including any point of its surface S, is determined by the following relation

$$\vec{u} = \vec{u}_0 + \vec{\omega} \times \vec{r}, \tag{1.5}$$

where $\vec{r}$ is the vector determining the position of the point. In components Eq. (1.5) looks as follows:

$$\begin{aligned} u_x &= u_{0x} + \omega_y z - \omega_z y,\\ u_y &= u_{0y} + \omega_z x - \omega_x z,\\ u_z &= u_{0z} + \omega_x y - \omega_y x. \end{aligned} \tag{1.6}$$

On the surface S we have

$$u_n = u_x \cos(n,x) + u_y \cos(n,y) + u_z \cos(n,z). \tag{1.7}$$

Writing $\alpha \equiv \cos(n,x)$, $\beta \equiv \cos(n,y)$, $\gamma \equiv \cos(n,z)$ and substituting (1.6) into (1.7), we come to the following form of the boundary condition (1.3):

$$\begin{aligned} \left.\frac{\partial\varphi}{\partial n}\right|_S = u_n = u_{0x}\alpha + u_{0y}\beta + u_{0z}\gamma + \omega_x(y\gamma - z\beta)\\ + \omega_y(z\alpha - x\gamma) + \omega_z(x\beta - y\alpha). \end{aligned} \tag{1.8}$$

In the formula (1.8) the variables α, β, γ, $y\gamma - z\beta$, $z\alpha - x\gamma$, $x\beta - y\alpha$ are determined only by the shape of the surface body. The body motion and the dynamics of the flow are determined by the functions u_{0x}, u_{0y}, u_{0z}, ω_x, ω_y, ω_z.

Linearity of the problem allows us to represent the potential φ as the sum

$$\varphi = u_{0x}\varphi_1 + u_{0y}\varphi_2 + u_{0z}\varphi_3 + \omega_x\varphi_4 + \omega_y\varphi_5 + \omega_z\varphi_6. \tag{1.9}$$

The formula (1.9) shows that φ_i, $i = 1, 2, 3$ are the flow potentials corresponding to the body moving along the axes x, y, z at unit linear velocities, respectively. On the other hand, φ_i, $i = 4, 5, 6$ are potentials corresponding to rotation of the body around the same axes at unit angular velocities (respectively). We see that the problem of body motion in an ideal infinite fluid gives rise to solution of six problems.

The first problem can be formulated as follows: find the solution of the Laplace equation $\Delta\varphi_1 = 0$ with the following boundary conditions: the function

$$\frac{\partial\varphi_1}{\partial n} = \alpha$$

is given on the surface S and

$$\frac{\partial\varphi_1}{\partial X} = \frac{\partial\varphi_1}{\partial Y} = \frac{\partial\varphi_1}{\partial Z} \to 0 \quad \text{as } r \to \infty.$$

The last (sixth) problem, taking (1.8) into account, can be formulated as follows: find the solution of the Laplace equation $\Delta\varphi_6 = 0$ with the following boundary conditions: the function $\partial\varphi_6/\partial n = x\beta - y\alpha$ is given on the surface S, and

$$\frac{\partial\varphi_6}{\partial X} = \frac{\partial\varphi_6}{\partial Y} = \frac{\partial\varphi_6}{\partial Z} \to 0 \quad \text{as } r \to \infty.$$

We see that the functions φ_i $(i = 1, 2, \ldots, 6)$ do not depend on $\vec{u}_0$ and $\vec{\omega}$. These functions are determined only by the shape of the surface S of the body and the choice of coordinate system $Oxyz$ attached to the body.

1.2 Kinetic Energy of the Fluid

The kinetic energy of the fluid confined between the surface S of the moving body and the stationary sphere Σ of radius a containing the body together with surrounding fluid, is defined by the integral

$$T = \frac{1}{2}\rho\iiint_V v^2\,dV = \frac{1}{2}\rho\iiint_V\left[\left(\frac{\partial\varphi}{\partial x}\right)^2 + \left(\frac{\partial\varphi}{\partial y}\right)^2 + \left(\frac{\partial\varphi}{\partial z}\right)^2\right]dx\,dy\,dz,$$

where ρ is the density of the fluid.

Using Green's transformation for two functions (φ_1, φ_2),

$$\begin{aligned}&\iiint_V\left(\frac{\partial\varphi_1}{\partial x}\frac{\partial\varphi_2}{\partial x} + \frac{\partial\varphi_1}{\partial y}\frac{\partial\varphi_2}{\partial y} + \frac{\partial\varphi_1}{\partial z}\frac{\partial\varphi_2}{\partial z}\right)dx\,dy\,dz\\ &\quad= -\iint_{S+\Sigma}\varphi_1\frac{\partial\varphi_2}{\partial n}dS - \iiint_V\varphi_1\left(\frac{\partial^2\varphi_2}{\partial x^2} + \frac{\partial^2\varphi_2}{\partial y^2} + \frac{\partial^2\varphi_2}{\partial z^2}\right)dx\,dy\,dz\end{aligned}$$

and taking into account that in our case $\varphi_1 = \varphi_2 = \varphi$ and $\Delta\varphi = 0$, we get the expression

$$T = -\frac{\rho}{2}\iint_S \varphi \frac{\partial \varphi}{\partial n} dS - \frac{\rho}{2}\iint_\Sigma \varphi \frac{\partial \varphi}{\partial n} dS. \tag{1.10}$$

The second term in the right-hand side of Eq. (1.10) tends to zero as $a \to \infty$ by virtue of the asymptotical behavior of φ and its first derivatives as $r \to \infty$. Therefore, we obtain the following formula for the total kinetic energy of the fluid outside of the surface S:

$$T = -\frac{\rho}{2}\iint_S \varphi \frac{\partial \varphi}{\partial n} dS. \tag{1.11}$$

Substituting the expression (1.9) into (1.11) and writing

$$u_{0x} = u_1, \quad u_{0y} = u_2, \quad u_{0z} = u_3, \quad \omega_x = u_4, \quad \omega_y = u_5, \quad \omega_z = u_6,$$

we obtain

$$T = \frac{1}{2}\sum_{i=1}^{6}\sum_{k=1}^{6} \lambda_{ik} u_i u_k,$$

where the values

$$\boxed{\lambda_{ik} = -\rho \iint_S \frac{\partial \varphi_i}{\partial n}\varphi_k \, dS} \tag{1.12}$$

are called the *added masses* (in the sequel we shall sometimes use the abbreviation AM) of the body. Some authors prefer to call λ_{ik} the *virtual masses* of the body. The added masses do not depend on the kinematics of the motion, since velocities u_i do not enter (1.12). Applying Green's formula to functions φ_i and φ_k in the volume V between the surfaces Σ and S,

$$\iiint_V (\varphi_i \Delta\varphi_k - \varphi_k \Delta\varphi_i)\, dV = \iint_\Sigma \left(\varphi_i \frac{\partial \varphi_k}{\partial n} - \varphi_k \frac{\partial \varphi_i}{\partial n}\right) dS - \iint_S \left(\varphi_i \frac{\partial \varphi_k}{\partial n} - \varphi_k \frac{\partial \varphi_i}{\partial n}\right) dS,$$

we see that the left-hand side of the equation equals zero, since $\Delta\varphi_i = \Delta\varphi_k = 0$, and the first term of the right-hand side of the equation tends to zero at $a \to \infty$. Therefore, for the infinite fluid surrounding the body, the following condition holds:

$$\iint_S \varphi_i \frac{\partial \varphi_k}{\partial n} dS = \iint_S \varphi_k \frac{\partial \varphi_i}{\partial n} dS,$$

thus $\lambda_{ik} = \lambda_{ki}$. Therefore, out of 36 values λ_{ik} $(i, k = 1, 2, \ldots, 6)$ only 21 values are independent. The (multiplied by the factor of 2) kinetic energy of the fluid under an arbitrary body motion can be written as follows:

$$
\begin{aligned}
2T = {} & \lambda_{11}u_1^2 + \lambda_{22}u_2^2 + \lambda_{33}u_3^2 + 2\lambda_{12}u_1u_2 + 2\lambda_{13}u_1u_3 + 2\lambda_{23}u_2u_3 \\
& + 2u_1(\lambda_{14}u_4 + \lambda_{15}u_5 + \lambda_{16}u_6) + 2u_2(\lambda_{24}u_4 + \lambda_{25}u_5 + \lambda_{26}u_6) \\
& + 2u_3(\lambda_{34}u_4 + \lambda_{35}u_5 + \lambda_{36}u_6) + \lambda_{44}u_4^2 + \lambda_{55}u_5^2 + \lambda_{66}u_6^2 \\
& + 2\lambda_{45}u_4u_5 + 2\lambda_{46}u_4u_6 + 2\lambda_{56}u_5u_6. \qquad (1.13)
\end{aligned}
$$

The values for the AM λ_{ik} depend on the shape of the body, chosen coordinate system and fluid density ρ. The variables λ_{ik} $(i,k = 1,2,3)$ have dimension of mass, values for λ_{ik} $(i = 1,2,3;\ k = 4,5,6)$ have dimension of static moment, values for λ_{ik} $(i,k = 4,5,6)$ dimension of moment of inertia.

Similarly to the formula (1.13), the expression for kinetic energy of the body of mass m, with coordinates of the center of inertia x_c, y_c, z_c, with diagonal moments of inertia J_x, J_y, J_z and products of inertia J_{xy}, J_{xz}, J_{yz}, is represented in the following form:

$$
\begin{aligned}
2T_0 = {} & mu_1^2 + mu_2^2 + mu_3^2 + 2u_1(mz_cu_5 - my_cu_6) \\
& + 2u_2(mx_cu_6 - mz_cu_4) + 2u_3(my_cu_4 - mx_cu_5) \\
& + J_xu_4^2 + J_yu_5^2 + J_zu_6^2 - 2J_{yz}u_5u_6 - 2J_{xz}u_4u_6 - 2J_{xy}u_4u_5. \qquad (1.14)
\end{aligned}
$$

In spite of certain similarities between the formulas (1.13) and (1.14), there are also essential differences between them. Let for example the body have only two non-vanishing components of velocity: u_1 and u_2. Then the kinetic energy of the body is defined by the formula $T_0 = m(u_1^2 + u_2^2)/2$, while the kinetic energy of the fluid is given by $T = (\lambda_{11}u_1^2 + \lambda_{22}u_2^2 + 2\lambda_{12}u_1u_2)/2$. An additional term in the last formula can be interpreted as describing the interaction of two currents corresponding to the motion of the body with velocities u_1 and u_2.

Some data on kinetic energy of fluid enclosed within closed contours (ellipse, ideal triangle, segments of a circle) rotating with constant velocity around an axis orthogonal to the plane of these contours are given in [36, 114]. Kinetic energy of fluid can in these cases be expressed via variables which are analogous to added masses. We do not consider this type of motion in this work since it does not correspond to the problem formulated in Section 1.1.

1.3 Transformation of Added Masses under a Change of Coordinate System

Transformation laws for the added masses under a change of the coordinate system can be derived from invariance of quadratic form (1.13) under a change of coordinate systems.

Let λ_{ik} $(i,k = 1,2,\ldots,6)$ be the added masses of the body computed in the coordinate system xyz. Let us find the added masses λ'_{ik} $(i,k = 1,2,\ldots,6)$ of the same body in the new coordinate system $x_1y_1z_1$; we denote the coordinates of the origin of the new coordinate system in the coordinate system xyz by ξ_1, ξ_2, ξ_3. Let us consider the matrix of cosines of the angles between the axes of the coordinate systems xyz and $x_1y_1z_1$:

$$\begin{array}{cccc} & x & y & z \\ x_1 & \alpha_{11} & \alpha_{12} & \alpha_{13} \\ y_1 & \alpha_{21} & \alpha_{22} & \alpha_{23} \\ z_1 & \alpha_{31} & \alpha_{32} & \alpha_{33} \end{array}$$

The elements of this matrix satisfy the standard orthogonality relations

$$\sum_{i=1}^{3} \alpha_{pi}\alpha_{iq} = \delta_{pq},$$

where $p, q = 1, 2, 3$; δ_{pq} is the Kronecker symbol: $\delta_{pq} = 0$ if $p \neq q$ and $\delta_{pq} = 1$ if $p = q$.

The velocity of the origin O_1 of the new coordinate system we denote by $\vec{u}'$ (u'_1, u'_2, u'_3 are its projections onto the axes x_1, y_1 and z_1). The vector $\vec{u}$ is determined by the relation

$$\vec{u}' = \vec{u} + \vec{\omega} \times \vec{r}, \tag{1.15}$$

where $\vec{u}$ (u_1, u_2, u_3) is the velocity of the origin of coordinate system (x, y, z); the vector $\vec{r}$ with components (ξ_1, ξ_2, ξ_3) is the radius-vector of the point O_1 in coordinate system xyz; the projections of the vector $\vec{\omega}$ onto the axes $x_1y_1z_1$ are denoted by u'_4, u'_5, u'_6.

It follows from the formula (1.15) that $\vec{u} = \vec{u}' - \vec{\omega} \times \vec{r}$, or, in components,

$$u_1 = \sum_{m=1}^{3} u'_m \alpha_{m1} - (\omega_2\xi_3 - \omega_3\xi_2);$$
$$u_2 = \sum_{m=1}^{3} u'_m \alpha_{m2} - (\omega_3\xi_1 - \omega_1\xi_3);$$
$$u_3 = \sum_{m=1}^{3} u'_m \alpha_{m3} - (\omega_1\xi_2 - \omega_2\xi_1),$$

where

$$\omega_i = u_{3+i} = \sum_{m=1}^{3} u'_{3+m}\alpha_{mi}, \quad i = 1, 2, 3.$$

Substituting the expressions for u_i $(i = 1, 2, \ldots, 6)$ into the right-hand side of the expression (1.13) and collecting the terms in front of the factors $u'_i u'_k$ $(i, k = 1, 2, \ldots, 6)$, we obtain the formulas for the added masses in the coordinate system

$x_1y_1z_1$:

$$\lambda'_{kr} = \sum_{i=1}^{3}\sum_{j=1}^{3}\lambda_{ij}\alpha_{ki}\alpha_{rj}, \quad k,r = 1,2,3; \tag{1.16}$$

$$\lambda'_{kr} = \sum_{i=1}^{3}\sum_{j=4}^{6}\lambda_{ij}\alpha_{ki}\alpha_{rj} + \sum_{i=1}^{3}\sum_{j=1}^{3}\lambda_{ij}\alpha_{ki}(\alpha_{r,2+j}\xi_{j+1} - \alpha_{r,j+1}\xi_{j+2}), \tag{1.17}$$

for $k = 1,2,3$, $r = 4,5,6$,

$$\begin{aligned}\lambda'_{kr} = &\sum_{i=4}^{6}\sum_{j=4}^{6}\lambda_{ij}\alpha_{ki}\alpha_{rj} + \sum_{i=1}^{3}\sum_{j=4}^{6}\lambda_{ij}\alpha_{kj}(\alpha_{r,2+i}\xi_{1+i} - \alpha_{r,1+i}\xi_{2+i})\\ &+\sum_{i=1}^{3}\sum_{j=4}^{6}\lambda_{ij}\alpha_{rj}(\alpha_{k,2+i}\xi_{1+i} - \alpha_{k,1+i}\xi_{2+i})\\ &+\sum_{i=1}^{3}\sum_{j=1}^{3}\lambda_{ij}(\alpha_{k,i+2}\xi_{i+1} - \alpha_{k,i+1}\xi_{i+2})(\alpha_{r,j+2}\xi_{j+1} - \alpha_{r,j+1}\xi_{j+2}),\end{aligned} \tag{1.18}$$

for $k,r = 4,5,6$.

In the formulas (1.16)–(1.18) one should assume

$$\begin{aligned}&\alpha_{i4} = \alpha_{i1}, && \alpha_{i5} = \alpha_{i2}, && \alpha_{i6} = \alpha_{i3};\\ &\alpha_{4i} = \alpha_{1i}, && \alpha_{5i} = \alpha_{2i}, && \alpha_{6i} = \alpha_{3i};\\ &\xi_4 = \xi_1, && \xi_5 = \xi_2, && \xi_6 = \xi_3.\end{aligned}$$

Choosing in these general formulas

$$\begin{aligned}&\alpha_{11} = \cos\beta, \quad \alpha_{21} = -\sin\beta, \quad \alpha_{12} = \sin\beta,\\ &\alpha_{22} = \cos\beta, \quad \alpha_{33} = 1,\\ &\xi_1 = \xi, \quad \xi_2 = \eta,\\ &\alpha_{13} = \alpha_{31} = \alpha_{23} = \alpha_{32} = \xi_3 = 0,\end{aligned} \tag{1.19}$$

we obtain the transformation formulas for the added masses for the case of the planar motion [183, 206]:

$$\begin{aligned}&\lambda'_{11} = \lambda_{11}\cos^2\beta + \lambda_{22}\sin^2\beta + \lambda_{12}\sin 2\beta;\\ &\lambda'_{22} = \lambda_{11}\sin^2\beta + \lambda_{22}\cos^2\beta - \lambda_{12}\sin 2\beta;\\ &\lambda'_{12} = 0.5(\lambda_{22} - \lambda_{11})\sin 2\beta + \lambda_{12}\cos 2\beta;\\ &\lambda'_{16} = (\lambda_{16} + \lambda_{11}\eta - \lambda_{12}\xi)\cos\beta + (\lambda_{26} - \lambda_{22}\xi + \lambda_{12}\eta)\sin\beta;\\ &\lambda'_{26} = -(\lambda_{16} + \lambda_{11}\eta - \lambda_{12}\xi)\sin\beta + (\lambda_{26} - \lambda_{22}\xi + \lambda_{12}\eta)\cos\beta;\\ &\lambda'_{66} = \lambda_{66} + \lambda_{11}\eta^2 + \lambda_{22}\xi^2 - 2\lambda_{12}\xi\eta + 2(\lambda_{16}\eta - \lambda_{26}\xi).\end{aligned} \tag{1.20}$$

In the case of the planar motion of the three-dimensional body such that the coordinate system moves in the same plane, the expressions (1.20), according to the formulas (1.19), should be complemented by the transformation formulas for the other added masses, which follow from (1.16)–(1.18):

$$
\begin{aligned}
&\lambda'_{33} = \lambda_{33}; \qquad \lambda'_{13}\cos\beta + \lambda_{23}\sin\beta; \qquad \lambda'_{23} = -\lambda_{13}\sin\beta + \lambda_{23}\cos\beta;\\
&\lambda'_{14} = \left[\lambda_{13}(\xi\sin\beta - \eta\cos\beta) + \lambda_{14}\cos\beta + \lambda_{15}\sin\beta\right]\cos\beta\\
&\qquad + \left[\lambda_{23}(\xi\sin\beta - \eta\cos\beta) + \lambda_{24}\cos\beta + \lambda_{25}\sin\beta\right]\sin\beta;\\
&\lambda'_{15} = \left[\lambda_{13}(\xi\cos\beta + \eta\sin\beta) - \lambda_{14}\sin\beta + \lambda_{15}\cos\beta\right]\cos\beta\\
&\qquad + \left[\lambda_{23}(\xi\cos\beta + \eta\sin\beta) - \lambda_{24}\sin\beta + \lambda_{25}\cos\beta\right]\sin\beta;\\
&\lambda'_{24} = -\left[\lambda_{13}(\xi\sin\beta - \eta\cos\beta) + \lambda_{14}\cos\beta + \lambda_{15}\sin\beta\right]\sin\beta\\
&\qquad + \left[\lambda_{23}(\xi\sin\beta - \eta\cos\beta) + \lambda_{24}\cos\beta + \lambda_{25}\sin\beta\right]\cos\beta;\\
&\lambda'_{25} = -\left[\lambda_{13}(\xi\cos\beta + \eta\sin\beta) - \lambda_{14}\sin\beta + \lambda_{15}\cos\beta\right]\sin\beta\\
&\qquad + \left[\lambda_{23}(\xi\cos\beta + \eta\sin\beta) - \lambda_{24}\sin\beta + \lambda_{25}\cos\beta\right]\cos\beta;\\
&\lambda'_{34} = \lambda_{34}\cos\beta + \lambda_{35}\sin\beta + \lambda_{33}(\xi\sin\beta - \eta\cos\beta);\\
&\lambda'_{35} = -\lambda_{34}\sin\beta + \lambda_{35}\cos\beta + \lambda_{33}(\xi\cos\beta + \eta\sin\beta);\\
&\lambda'_{36} = \lambda_{13}\eta - \lambda_{23}\xi + \lambda_{36};\\
&\lambda'_{44} = \lambda_{33}(\xi\sin\beta - \eta\cos\beta)^2 + \lambda_{44}\cos^2\beta + \lambda_{55}\sin^2\beta\\
&\qquad + 2\lambda_{45}\sin\beta\cos\beta + 2\lambda_{34}\cos\beta(\xi\sin\beta - \eta\cos\beta)\\
&\qquad + 2\lambda_{35}(\xi\sin\beta - \eta\cos\beta)\sin\beta;\\
&\lambda'_{55} = \lambda_{33}(\xi\cos\beta + \eta\sin\beta)^2 + \lambda_{44}\sin^2\beta + \lambda_{55}\cos^2\beta - 2\lambda_{45}\cos\beta\sin\beta\\
&\quad - 2\lambda_{34}(\xi\cos\beta + \eta\sin\beta)\sin\beta + 2\lambda_{35}(\xi\cos\beta + \eta\sin\beta)\cos\beta;\\
&\lambda'_{66} = \lambda_{11}\eta^2 + \lambda_{22}\xi^2 - 2\lambda_{12}\xi\eta + \lambda_{66} + 2\lambda_{16}\eta - 2\lambda_{26}\xi;\\
&\lambda'_{45} = \lambda_{33}(\xi\sin\beta - \eta\cos\beta)(\xi\cos\beta + \eta\sin\beta) - \lambda_{44}\sin\beta\cos\beta + \lambda_{55}\sin\beta\cos\beta\\
&\qquad + \lambda_{45}\cos 2\beta + \lambda_{34}(\xi\cos 2\beta + \eta\sin 2\beta) + \lambda_{35}(\xi\sin 2\beta - \eta\cos 2\beta);\\
&\lambda'_{46} = (\lambda_{46} - \lambda_{13}\eta^2 + \lambda_{23}\xi\eta + \lambda_{14}\eta - \lambda_{24}\xi - \lambda_{36}\eta)\cos\beta\\
&\qquad + (\lambda_{56} + \lambda_{13}\xi\eta - \lambda_{23}\xi^2 + \lambda_{15}\eta - \lambda_{25}\xi + \lambda_{36}\xi)\sin\beta;\\
&\lambda'_{56} = -(\lambda_{46} - \lambda_{13}\eta^2 + \lambda_{23}\xi\eta + \lambda_{14}\eta - \lambda_{24}\xi - \lambda_{36}\eta)\sin\beta\\
&\qquad + (\lambda_{56} + \lambda_{13}\xi\eta - \lambda_{23}\xi^2 + \lambda_{15}\eta - \lambda_{25}\xi + \lambda_{36}\xi)\cos\beta.
\end{aligned}
$$

Let us derive the transformation formulas for the case when the axes of the new coordinate system $x_1y_1z_1$ are parallel to the axes of the old one. Let the origin of the new coordinate system $x_1y_1z_1$ in the system xyz have coordinates $\xi_1 = \xi$; $\xi_2 = \eta$; $\xi_3 = \zeta$. Then, taking into account the equations $\alpha_{11} = \alpha_{22} = \alpha_{33} = 1$, $\alpha_{ik} = 0$ $(i \neq k)$ we get from expressions (1.16)–(1.18):

$$\left.\begin{aligned}
&\lambda'_{11}=\lambda_{11}; \quad \lambda'_{22}=\lambda_{22}; \quad \lambda'_{33}=\lambda_{33};\\
&\lambda'_{12}=\lambda_{12}; \quad \lambda'_{13}=\lambda_{13};\\
&\lambda'_{23}=\lambda_{23}; \quad \lambda'_{36}=\lambda_{36}+\lambda_{13}\eta-\lambda_{23}\xi;\\
&\lambda'_{14}=\lambda_{12}\zeta-\lambda_{13}\eta+\lambda_{14}; \quad \lambda'_{15}=\lambda_{15}-\lambda_{11}\zeta+\lambda_{13}\xi;\\
&\lambda'_{16}=\lambda_{16}+\lambda_{11}\eta-\lambda_{12}\xi; \quad \lambda'_{24}=\lambda_{24}+\lambda_{22}\zeta-\lambda_{23}\eta;\\
&\lambda'_{25}=\lambda_{25}+\lambda_{23}\xi-\lambda_{12}\zeta; \quad \lambda'_{26}=\lambda_{26}-\lambda_{22}\xi+\lambda_{12}\eta;\\
&\lambda'_{44}=\lambda_{22}\zeta^2+\lambda_{33}\eta^2-2\lambda_{23}\eta\zeta+\lambda_{44}+2\lambda_{24}\zeta-2\lambda_{34}\eta;\\
&\lambda'_{55}=\lambda_{11}\zeta^2+\lambda_{33}\xi^2-2\lambda_{13}\xi\zeta+\lambda_{55}-2\lambda_{15}\zeta+2\lambda_{35}\xi;\\
&\lambda'_{66}=\lambda_{11}\eta^2+\lambda_{22}\xi^2-2\lambda_{12}\xi\eta+\lambda_{66}+2\lambda_{16}\eta-2\lambda_{26}\xi;\\
&\lambda'_{45}=-\lambda_{33}\xi\eta-\lambda_{12}\zeta^2+\lambda_{13}\eta\zeta+\lambda_{23}\xi\zeta+\lambda_{45}-\lambda_{14}\zeta\\
&\qquad+\lambda_{25}\zeta+\lambda_{34}\xi-\lambda_{35}\eta;\\
&\lambda'_{56}=-\lambda_{11}\eta\zeta+\lambda_{12}\xi\zeta+\lambda_{13}\xi\eta-\lambda_{23}\xi^2+\lambda_{56}+\lambda_{15}\eta\\
&\qquad-\lambda_{16}\zeta-\lambda_{25}\xi+\lambda_{36}\eta;\\
&\lambda'_{46}=-\lambda_{22}\xi\zeta+\lambda_{12}\eta\zeta-\lambda_{13}\eta^2+\lambda_{23}\xi\eta+\lambda_{46}+\lambda_{14}\eta\\
&\qquad-\lambda_{24}\xi+\lambda_{26}\zeta-\lambda_{36}\eta;\\
&\lambda'_{34}=-\lambda_{33}\eta+\lambda_{23}\zeta+\lambda_{34}; \quad \lambda'_{35}=\lambda_{33}\xi-\lambda_{13}\zeta+\lambda_{35}.
\end{aligned}\right\} \tag{1.21}$$

In the partial case ($\eta = 0$) the formulas (1.21) give the formulas derived by Lavrentijev [25].

If the coordinate system $x_1 y_1 z_1$ is obtained from the initial coordinate system by subsequent rotation of the initial coordinate system xyz by the angles β, ψ and θ around corresponding axes (see Fig. 1.1), and the origins of both coordinate systems coincide (i.e. $\xi_i = 0$, $i = 1, 2, 3$) then the expressions for α_{ik} ($i, k = 1, 2, 3$) have the following form:

$$\begin{aligned}
&\alpha_{11} = \cos\beta\cos\psi; \quad \alpha_{12} = \sin\beta\cos\psi; \quad \alpha_{22} = -\sin\psi;\\
&\alpha_{21} = \cos\beta\sin\psi\sin\theta - \sin\beta\cos\theta; \quad \alpha_{22} = \sin\beta\sin\psi\sin\theta + \cos\beta\cos\theta;\\
&\alpha_{23} = \cos\psi\sin\theta; \quad \alpha_{31} = \cos\beta\sin\psi\cos\theta + \sin\beta\sin\theta;\\
&\alpha_{32} = \sin\beta\sin\psi\cos\theta - \cos\beta\sin\theta; \quad \alpha_{33} = \cos\psi\cos\theta.
\end{aligned}$$

It is easy to derive these transformation laws from the formulas (1.16)–(1.18) taking into account that $\xi_i = 0$ ($i = 1, 2, 3$). Sometimes one can choose the coordi-

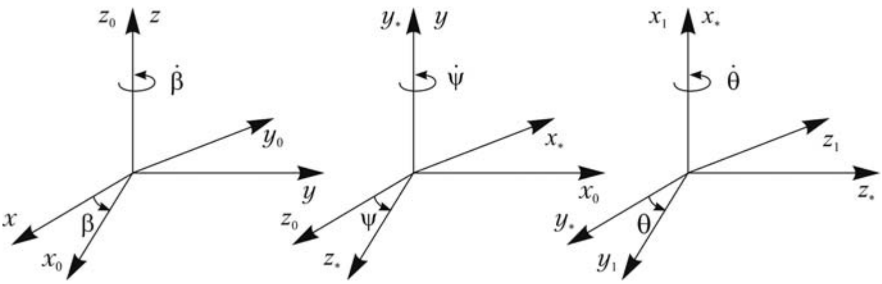

Fig. 1.1 Subsequent positions of the coordinate system under rotation around different axes

nates of the origin of the new coordinate system and angles of rotation of the new coordinate system with respect to the initial one such that some added masses in the new coordinate system vanish.

For example, from the third equality in (1.20), we see that for the case of planar flow we can choose the rotation angle β such that $\lambda'_{12} = 0$. Simultaneously, from the fourth and fifth equalities of (1.20) we see that choosing ξ and η to be solutions for the following system:

$$\begin{cases} \lambda_{12}\xi - \lambda_{11}\eta = \lambda_{16}, \\ \lambda_{22}\xi - \lambda_{12}\eta = \lambda_{26}, \end{cases}$$

it is possible to provide the vanishing of the added masses λ'_{16} and λ'_{26}.

For the three-dimensional case, using formulas (1.21) it is possible to choose ξ, η and ζ such that three values λ'_{ik} $(i = 1,2,3;\ k = 4,5,6)$ out of six vanish. For example, to get $\lambda'_{14} = \lambda'_{15} = \lambda'_{24} = 0$, one should solve the following system of equations with respect to ξ, η, ζ:

$$\begin{cases} \lambda_{13}\eta - \lambda_{12}\zeta = \lambda_{14}, \\ \lambda_{23}\eta - \lambda_{22}\zeta = \lambda_{24}, \\ \lambda_{11}\zeta - \lambda_{13}\xi = \lambda_{15}. \end{cases}$$

Notice that two out of three values λ'_{ik} must have the coinciding second index (k). Applying transformation formulas (1.21), we can calculate the coordinates of the central point of the body. The point ξ_0, η_0, ζ_0 is called central if, choosing this point as the origin of the new coordinate system, we have $\lambda'_{15} = \lambda'_{24}$; $\lambda'_{16} = \lambda'_{34}$; $\lambda'_{26} = \lambda'_{35}$. Writing down these equations in the initial coordinate system, we obtain the following system of equations on variables ξ_0, η_0, ζ_0:

$$\begin{cases} \lambda_{13}\xi_0 + \lambda_{23}\eta_0 - (\lambda_{22} + \lambda_{11})\zeta_0 = \lambda_{24} - \lambda_{15}; \\ \lambda_{12}\xi_0 - (\lambda_{11} + \lambda_{33})\eta_0 + \lambda_{23}\zeta_0 = \lambda_{16} - \lambda_{34}; \\ -(\lambda_{22} + \lambda_{33})\xi_0 + \lambda_{12}\eta_0 + \lambda_{13}\zeta_0 = \lambda_{35} - \lambda_{26}. \end{cases}$$

Generically the problem of finding of three main directions, i.e. such directions of axes that $\lambda'_{12} = \lambda'_{13} = \lambda'_{23} = 0$, is more difficult, due to complicated expressions for λ'_{12}, λ'_{13}, λ'_{23} in terms of the angles β, ψ, θ and added masses λ_{ik}, $i,k = 1,2,3$. The method of finding the main directions is considered in Section 1.5. If the body has at least one symmetry plane, the main directions can be easily determined: two of them lie in the symmetry plane, and the angle between the axes of the initial coordinate system and the new one can be computed using the formula derived in the case of planar motion (see the third formula in (1.20)). The third main direction is normal to the symmetry plane.

1.4 Force and Torque Influencing a Body Moving in an Ideal Incompressible Fluid

Consider a non-stationary motion of a body in an ideal infinite fluid. Then the hydrodynamic force and torque acting on the body are defined by the following expressions [116]:

$$\vec{R} = -\frac{\partial \vec{B}}{\partial t} - \vec{\omega} \times \vec{B};$$
$$\vec{L} = -\frac{\partial \vec{J}}{\partial t} - \vec{\omega} \times \vec{J} - \vec{u}_0 \times \vec{B},$$

where $\vec{R}$ is the vector of force, applied to the origin of the non-stationary coordinate system attached to the body; $\vec{B}$ is the main vector of the system of momenta of pressures acting on the surface of the body; $\vec{\omega}$ is the vector of angular velocity of body rotation around the axis passing through the origin of the non-stationary coordinate system; $\vec{L}$ is the hydrodynamic torque influencing the body (computed with respect to the origin of the non-stationary coordinate system); $\vec{J}$ is the main hydrodynamic moment influencing the surface of the body computed with respect to the origin of the non-stationary coordinate system; $\vec{u}_0$ is the vector of velocity of the origin of the non-stationary coordinate system.

Projecting $\vec{R}$ and $\vec{L}$ onto the axes of the non-stationary coordinate system, we obtain:

$$R_x = -\frac{\partial B_x}{\partial t} - \omega_y B_z + \omega_z B_y;$$
$$R_y = -\frac{\partial B_y}{\partial t} - \omega_z B_x + \omega_x B_z;$$
$$R_z = -\frac{\partial B_z}{\partial t} - \omega_x B_y + \omega_y B_x;$$
$$L_x = -\frac{\partial J_x}{\partial t} - \omega_y J_z + \omega_z J_y - u_{0y} B_z + u_{0z} B_y;$$
$$L_y = -\frac{\partial J_y}{\partial t} - \omega_z J_x + \omega_x J_z - u_{0z} B_x + u_{0x} B_z;$$
$$L_z = -\frac{\partial J_z}{\partial t} - \omega_x J_y + \omega_y J_x - u_{0x} B_y + u_{0y} B_x,$$

where the projections of the vectors $\vec{B}$ and $\vec{J}$ are determined by the following formulas [116]:

$$B_x = \frac{\partial T}{\partial u_{0x}} = \frac{\partial T}{\partial u_1}; \qquad B_y = \frac{\partial T}{\partial u_{0y}} = \frac{\partial T}{\partial u_2}; \qquad B_z = \frac{\partial T}{\partial u_{0z}} = \frac{\partial T}{\partial u_3};$$
$$J_x = \frac{\partial T}{\partial \omega_x} = \frac{\partial T}{\partial u_4}; \qquad J_y = \frac{\partial T}{\partial \omega_y} = \frac{\partial T}{\partial u_5}; \qquad J_z = \frac{\partial T}{\partial \omega_z} = \frac{\partial T}{\partial u_6}.$$

Taking into account the expression (1.13) for the kinetic energy T of the fluid, we get the following formulas for the force and torque of potential nature influencing the body:

$$\begin{aligned} R_x = -\Big[& \lambda_{11}\frac{\partial u_1}{\partial t} + \lambda_{12}\frac{\partial u_2}{\partial t} + \lambda_{13}\frac{\partial u_3}{\partial t} + \lambda_{14}\frac{\partial u_4}{\partial t} + \lambda_{15}\frac{\partial u_5}{\partial t} + \lambda_{16}\frac{\partial u_6}{\partial t} \\ & + \lambda_{33}u_3u_5 + \lambda_{13}u_1u_5 + \lambda_{23}u_2u_5 + \lambda_{34}u_4u_5 + \lambda_{35}u_5^2 \\ & + (\lambda_{36} - \lambda_{25})u_5u_6 - \lambda_{22}u_2u_6 - \lambda_{12}u_1u_6 - \lambda_{23}u_3u_6 \\ & - \lambda_{24}u_4u_6 - \lambda_{26}u_6^2 \Big]; \end{aligned} \tag{1.22}$$

$$\begin{aligned} R_y = -\Big[& \lambda_{12}\frac{\partial u_1}{\partial t} + \lambda_{22}\frac{\partial u_2}{\partial t} + \lambda_{23}\frac{\partial u_3}{\partial t} + \lambda_{24}\frac{\partial u_4}{\partial t} + \lambda_{25}\frac{\partial u_5}{\partial t} + \lambda_{26}\frac{\partial u_6}{\partial t} \\ & + \lambda_{11}u_1u_6 + \lambda_{12}u_2u_6 + \lambda_{13}u_3u_6 + (\lambda_{14} - \lambda_{36})u_4u_6 + \lambda_{15}u_5u_6 \\ & + \lambda_{16}u_6^2 - \lambda_{33}u_3u_4 - \lambda_{13}u_1u_4 - \lambda_{23}u_2u_4 - \lambda_{34}u_4^2 - \lambda_{35}u_4u_5 \Big]; \end{aligned} \tag{1.23}$$

$$\begin{aligned} R_z = -\Big[& \lambda_{13}\frac{\partial u_1}{\partial t} + \lambda_{23}\frac{\partial u_2}{\partial t} + \lambda_{33}\frac{\partial u_3}{\partial t} + \lambda_{34}\frac{\partial u_4}{\partial t} + \lambda_{35}\frac{\partial u_5}{\partial t} + \lambda_{36}\frac{\partial u_6}{\partial t} \\ & + \lambda_{12}u_1u_4 + \lambda_{22}u_2u_4 + \lambda_{23}u_3u_4 + \lambda_{24}u_4^2 + (\lambda_{25} - \lambda_{14})u_4u_5 \\ & + \lambda_{26}u_4u_6 - \lambda_{11}u_1u_5 - \lambda_{12}u_2u_5 - \lambda_{13}u_3u_5 - \lambda_{15}u_5^2 - \lambda_{16}u_5u_6 \Big]; \end{aligned} \tag{1.24}$$

$$\begin{aligned} L_x = -\Big[& \lambda_{14}\frac{\partial u_1}{\partial t} + \lambda_{24}\frac{\partial u_2}{\partial t} + \lambda_{34}\frac{\partial u_3}{\partial t} + \lambda_{44}\frac{\partial u_4}{\partial t} + \lambda_{45}\frac{\partial u_5}{\partial t} + \lambda_{46}\frac{\partial u_6}{\partial t} \\ & + (\lambda_{66} - \lambda_{55})u_5u_6 + \lambda_{16}u_1u_5 + (\lambda_{26} + \lambda_{35})u_2u_5 \\ & + (\lambda_{36} - \lambda_{25})u_3u_5 + \lambda_{46}u_4u_5 + \lambda_{56}u_5^2 - \lambda_{15}u_1u_6 \\ & + (\lambda_{36} - \lambda_{25})u_2u_6 - (\lambda_{26} + \lambda_{35})u_3u_6 - \lambda_{45}u_4u_6 - \lambda_{56}u_6^2 \\ & + (\lambda_{33} - \lambda_{22})u_2u_3 + \lambda_{13}u_1u_2 + \lambda_{23}u_2^2 + \lambda_{34}u_2u_4 \\ & - \lambda_{12}u_1u_3 - \lambda_{23}u_3^2 - \lambda_{24}u_3u_4 \Big]; \end{aligned} \tag{1.25}$$

$$\begin{aligned} L_y = -\Big[& \lambda_{15}\frac{\partial u_1}{\partial t} + \lambda_{25}\frac{\partial u_2}{\partial t} + \lambda_{35}\frac{\partial u_3}{\partial t} + \lambda_{45}\frac{\partial u_4}{\partial t} + \lambda_{55}\frac{\partial u_5}{\partial t} + \lambda_{56}\frac{\partial u_6}{\partial t} \\ & + (\lambda_{44} - \lambda_{66})u_4u_6 + (\lambda_{14} - \lambda_{36})u_1u_6 + \lambda_{24}u_2u_6 \\ & + (\lambda_{34} + \lambda_{16})u_3u_6 + \lambda_{45}u_5u_6 + \lambda_{46}u_6^2 - (\lambda_{16} + \lambda_{34})u_1u_4 \\ & - \lambda_{26}u_2u_4 + (\lambda_{14} - \lambda_{36})u_3u_4 - \lambda_{46}u_4^2 - \lambda_{56}u_4u_5 \\ & + (\lambda_{11} - \lambda_{33})u_1u_3 + \lambda_{12}u_2u_3 + \lambda_{13}u_3^2 + \lambda_{15}u_3u_5 \\ & - \lambda_{13}u_1^2 - \lambda_{23}u_1u_2 - \lambda_{35}u_1u_5 \Big]; \end{aligned} \tag{1.26}$$

$$\begin{aligned} L_z = -\Bigg[&\lambda_{16}\frac{\partial u_1}{\partial t} + \lambda_{26}\frac{\partial u_2}{\partial t} + \lambda_{36}\frac{\partial u_3}{\partial t} + \lambda_{46}\frac{\partial u_4}{\partial t} + \lambda_{56}\frac{\partial u_5}{\partial t} + \lambda_{66}\frac{\partial u_6}{\partial t} \\ &+ (\lambda_{55} - \lambda_{44})u_4u_5 + (\lambda_{15} + \lambda_{24})u_1u_4 + (\lambda_{25} - \lambda_{14})u_2u_4 \\ &+ \lambda_{35}u_3u_4 + \lambda_{45}u_4^2 + \lambda_{56}u_4u_6 - \lambda_{14}u_1u_5 - (\lambda_{24} + \lambda_{15})u_2u_5 \\ &- \lambda_{34}u_3u_5 - \lambda_{45}u_5^2 - \lambda_{46}u_5u_6 + \lambda_{12}u_1^2 + (\lambda_{22} - \lambda_{11})u_1u_2 \\ &+ \lambda_{23}u_1u_3 + \lambda_{25}u_1u_5 + \lambda_{26}u_1u_6 - \lambda_{12}u_2^2 - \lambda_{13}u_2u_3 - \lambda_{16}u_2u_6 \Bigg]. \end{aligned} \tag{1.27}$$

The expressions for forces and torques (1.22)–(1.27) make it possible to simplify the matrix of added masses λ_{ik} if the body has one, two or three planes of symmetry. Suppose that the body has the plane of symmetry xOy. Consider the forces and torques influencing the body when it starts moving from rest ($u_i = 0, i = 1, 2, \dots, 6$) along the axis Ox with acceleration $\partial u_1/\partial t$ (we assume that $\partial u_i/\partial t = 0$, $i = 2, 3, \dots, 6$). Then we obtain

$$\begin{aligned} &R_x = -\lambda_{11}\frac{\partial u_1}{\partial t}; \qquad R_y = -\lambda_{12}\frac{\partial u_1}{\partial t}; \qquad R_z = -\lambda_{13}\frac{\partial u_1}{\partial t}; \\ &L_x = -\lambda_{14}\frac{\partial u_1}{\partial t}; \qquad L_y = -\lambda_{15}\frac{\partial u_1}{\partial t}; \qquad L_z = -\lambda_{16}\frac{\partial u_1}{\partial t}. \end{aligned} \tag{1.28}$$

Due to the symmetry under the plane xOy we have $R_z = 0$, $L_x = 0$, $L_y = 0$ which, taking into account (1.28), implies $\lambda_{13} = \lambda_{14} = \lambda_{15} = 0$. Similarly, assuming the non-vanishing of acceleration $\partial u_2/\partial t$ while all other accelerations vanish, $\partial u_i/\partial t = 0$, $i = 1, 3, 4, 5, 6$, we get

$$\begin{aligned} &R_x = -\lambda_{12}\frac{\partial u_2}{\partial t}; \qquad R_y = -\lambda_{22}\frac{\partial u_2}{\partial t}; \qquad R_z = -\lambda_{23}\frac{\partial u_2}{\partial t}; \\ &L_x = -\lambda_{24}\frac{\partial u_2}{\partial t}; \qquad L_y = -\lambda_{25}\frac{\partial u_2}{\partial t}; \qquad L_z = -\lambda_{26}\frac{\partial u_2}{\partial t}. \end{aligned}$$

Taking into account the equations $R_z = L_x = L_y = 0$ which follow from the symmetry condition, we obtain $\lambda_{23} = \lambda_{24} = \lambda_{25} = 0$.

If we give to the body the angular acceleration around the axis z, assuming $\partial u_6/\partial t \neq 0$ while $u_i = 0$, $i = 1, 2, \dots, 6$ and $\partial u_i/\partial t = 0$, $i = 1, 2, \dots, 5$, then, using Eqs. (1.22)–(1.27) and $R_z = L_x = L_y = 0$, we get the relations $\lambda_{36} = \lambda_{46} = \lambda_{56} = 0$. Thus, if the body's plane of symmetry coincides with the coordinate plane xOy, the following added masses vanish:

$$\lambda_{13} = \lambda_{14} = \lambda_{15} = \lambda_{23} = \lambda_{24} = \lambda_{25} = \lambda_{36} = \lambda_{46} = \lambda_{56} = 0. \tag{1.29}$$

If the body's plane of symmetry coincides with the coordinate plane xOz, then

$$\lambda_{12} = \lambda_{14} = \lambda_{16} = \lambda_{23} = \lambda_{25} = \lambda_{34} = \lambda_{36} = \lambda_{45} = \lambda_{56} = 0.$$

If the plane of symmetry coincides with the plane yOz, then

$$\lambda_{12} = \lambda_{14} = \lambda_{13} = \lambda_{25} = \lambda_{26} = \lambda_{35} = \lambda_{36} = \lambda_{45} = \lambda_{46} = 0.$$

We can simplify the formulas (1.22)–(1.27) using (1.29). Let us write them down, using for clarity the original notation for the angular velocities:

$$R_x = -\left(\lambda_{11}\frac{\partial u_1}{\partial t} + \lambda_{12}\frac{\partial u_2}{\partial t} + \lambda_{16}\frac{\partial \omega_z}{\partial t} + \lambda_{33}u_3\omega_y + \lambda_{34}\omega_x\omega_y + \lambda_{35}\omega_y^2 \right.$$
$$\left. - \lambda_{12}u_1\omega_z - \lambda_{22}u_2\omega_z - \lambda_{26}\omega_z^2\right); \tag{1.30}$$

$$R_y = -\left(\lambda_{12}\frac{\partial u_1}{\partial t} + \lambda_{22}\frac{\partial u_2}{\partial t} + \lambda_{26}\frac{\partial \omega_z}{\partial t} + \lambda_{11}u_1\omega_z + \lambda_{12}u_2\omega_z + \lambda_{16}\omega_z^2 \right.$$
$$\left. - \lambda_{33}u_3\omega_x - \lambda_{34}\omega_x^2 - \lambda_{35}\omega_x\omega_y\right); \tag{1.31}$$

$$R_z = -\left(\lambda_{33}\frac{\partial u_3}{\partial t} + \lambda_{34}\frac{\partial \omega_x}{\partial t} + \lambda_{35}\frac{\partial \omega_y}{\partial t} + \lambda_{12}u_1\omega_x + \lambda_{22}u_2\omega_x \right.$$
$$\left. + \lambda_{26}\omega_x\omega_z - \lambda_{11}u_1\omega_y - \lambda_{12}u_2\omega_y - \lambda_{16}\omega_y\omega_z\right); \tag{1.32}$$

$$L_x = -\left[\lambda_{34}\frac{\partial u_3}{\partial t} + \lambda_{44}\frac{\partial \omega_x}{\partial t} + \lambda_{45}\frac{\partial \omega_y}{\partial t} + (\lambda_{26} + \lambda_{35})(u_2\omega_y - u_3\omega_z) \right.$$
$$+ \lambda_{16}u_1\omega_y + \lambda_{34}u_2\omega_x - \lambda_{12}u_1u_3 - \lambda_{45}\omega_x\omega_z + (\lambda_{33} - \lambda_{22})u_2u_3$$
$$\left. + (\lambda_{66} - \lambda_{55})\omega_y\omega_z\right]; \tag{1.33}$$

$$L_y = -\left[\lambda_{35}\frac{\partial u_3}{\partial t} + \lambda_{45}\frac{\partial \omega_x}{\partial t} + \lambda_{55}\frac{\partial \omega_y}{\partial t} + (\lambda_{16} + \lambda_{34})(u_3\omega_z - u_1\omega_x) \right.$$
$$+ \lambda_{12}u_2u_3 + \lambda_{45}\omega_y\omega_z - \lambda_{26}u_2\omega_x - \lambda_{35}u_1\omega_y + (\lambda_{11} - \lambda_{33})u_1u_3$$
$$\left. + (\lambda_{44} - \lambda_{66})\omega_x\omega_z\right]; \tag{1.34}$$

$$L_z = -\left[\lambda_{16}\frac{\partial u_1}{\partial t} + \lambda_{26}\frac{\partial u_2}{\partial t} + \lambda_{66}\frac{\partial \omega_z}{\partial t} + \lambda_{12}\left(u_1^2 - u_2^2\right) + \lambda_{45}\left(\omega_x^2 - \omega_y^2\right) \right.$$
$$+ \lambda_{35}u_3\omega_x + \lambda_{26}u_1\omega_z - \lambda_{34}u_3\omega_y - \lambda_{16}u_2\omega_z + (\lambda_{55} - \lambda_{44})\omega_x\omega_y$$
$$\left. + (\lambda_{22} - \lambda_{11})u_1u_2\right]. \tag{1.35}$$

Let us now consider the case when the body has two planes of symmetry, and these planes of symmetry coincide with the coordinate planes xOy and xOz of the coordinate system attached to the body. Then, in addition to the vanishing of the added masses (1.29), we have the vanishing of the following added masses:

$$\lambda_{12} = \lambda_{16} = \lambda_{34} = \lambda_{45} = 0. \tag{1.36}$$

Taking into account (1.36), the forces and torques of inertial nature (1.30)–(1.35) for the body with two planes of symmetry can be written down in the following form:

$$R_x = -\left(\lambda_{11}\frac{\partial u_1}{\partial t} + \lambda_{33}u_3\omega_y + \lambda_{35}\omega_y^2 - \lambda_{22}u_2\omega_z - \lambda_{26}\omega_z^2\right); \tag{1.37}$$

$$R_y = -\left(\lambda_{22}\frac{\partial u_2}{\partial t} + \lambda_{26}\frac{\partial \omega_z}{\partial t} + \lambda_{11}u_1\omega_z - \lambda_{33}u_3\omega_x - \lambda_{35}\omega_x\omega_y\right); \tag{1.38}$$

$$R_z = -\left(\lambda_{33}\frac{\partial u_3}{\partial t} + \lambda_{35}\frac{\partial \omega_y}{\partial t} + \lambda_{22}u_2\omega_x + \lambda_{26}\omega_x\omega_z - \lambda_{11}u_1\omega_y\right); \tag{1.39}$$

$$\begin{aligned} L_x = -\bigg[&\lambda_{44}\frac{\partial \omega_x}{\partial t} + (\lambda_{26} + \lambda_{35})(u_2\omega_y - u_3\omega_z) + (\lambda_{33} - \lambda_{22})u_2u_3 \\ &+ (\lambda_{66} - \lambda_{55})\omega_y\omega_z\bigg]; \end{aligned} \tag{1.40}$$

$$\begin{aligned} L_y = -\bigg[&\lambda_{35}\frac{\partial u_3}{\partial t} + \lambda_{55}\frac{\partial \omega_y}{\partial t} - \lambda_{26}u_2\omega_x - \lambda_{35}u_1\omega_y + (\lambda_{11} - \lambda_{33})u_1u_3 \\ &+ (\lambda_{44} - \lambda_{66})\omega_x\omega_z\bigg]; \end{aligned} \tag{1.41}$$

$$\begin{aligned} L_z = -\bigg[&\lambda_{26}\frac{\partial u_2}{\partial t} + \lambda_{66}\frac{\partial \omega_z}{\partial t} + \lambda_{35}u_3\omega_x + \lambda_{26}u_1\omega_z + (\lambda_{55} - \lambda_{44})\omega_x\omega_y \\ &+ (\lambda_{22} - \lambda_{11})u_1u_2\bigg]. \end{aligned} \tag{1.42}$$

If the body with two planes of symmetry (xOy and xOz) is the body of revolution whose axis coincides with the axis Ox, then its rotation in an ideal fluid around the Ox axis at an arbitrary velocity ω_x does not generate fluid motion.

Then the total potential (1.9) of the flow does not contain the term $\omega_x\varphi_4$; the kinetic energy of fluid and hydrodynamic forces influencing the body do not depend on ω_x. Besides, in an ideal fluid the hydrodynamic forces act orthogonally to the surface. Therefore, in the case of the body of revolution all hydrodynamic forces pass through the axis of rotation, which implies the equation $L_x = 0$. From the last equation, making use of the formula (1.40) and equations $\lambda_{22} = \lambda_{33}$, $\lambda_{55} = \lambda_{66}$, we deduce that for the body of rotation, $\lambda_{26} = -\lambda_{35}$. As a result we get from expressions (1.37)–(1.42):

$$R_x = -\lambda_{11}\frac{\partial u_1}{\partial t} - \lambda_{22}(u_3\omega_y - u_2\omega_z) + \lambda_{26}\left(\omega_y^2 + \omega_z^2\right); \tag{1.43}$$

$$R_y = -\lambda_{22}\frac{\partial u_2}{\partial t} - \lambda_{26}\frac{\partial \omega_z}{\partial t} - \lambda_{11}u_1\omega_z; \tag{1.44}$$

$$R_z = -\lambda_{22}\frac{\partial u_3}{\partial t} + \lambda_{26}\frac{\partial \omega_y}{\partial t} + \lambda_{11}u_1\omega_y; \tag{1.45}$$

$$L_x = 0; \tag{1.46}$$

$$L_y = \lambda_{26}\frac{\partial u_3}{\partial t} - \lambda_{55}\frac{\partial \omega_y}{\partial t} - \lambda_{26}u_1\omega_y + (\lambda_{33} - \lambda_{11})u_1u_3; \tag{1.47}$$

$$L_z = -\lambda_{26}\frac{\partial u_2}{\partial t} - \lambda_{55}\frac{\partial \omega_z}{\partial t} - \lambda_{26}u_1\omega_z - (\lambda_{22} - \lambda_{11})u_1u_2. \tag{1.48}$$

The formulas (1.43)–(1.48) admit further simplification if the origin is shifted along the Ox axis by $\xi = \lambda_{26}/\lambda_{22}$. Then applying the transformation formulas (1.21) to the case of the parallel shift of the coordinate system we get $\lambda'_{26} = 0$, $\lambda'_{55} = \lambda'_{66} = \lambda_{66} - \lambda^2_{26}/\lambda_{22}$. The forces and torques in the new coordinate system look as follows:

$$R^*_x = -\lambda_{11}\frac{\partial u^*_1}{\partial t} - \lambda_{22}\big(u^*_3\omega_y - u^*_2\omega_z\big); \qquad R^*_y = -\lambda_{22}\frac{\partial u^*_2}{\partial t} - \lambda_{11}u^*_1\omega_z;$$
$$R^*_z = -\lambda_{22}\frac{\partial u^*_3}{\partial t} + \lambda_{11}u^*_1\omega_y; \qquad L^*_x = 0;$$
$$L^*_y = -\lambda'_{55}\frac{\partial \omega_y}{\partial t} + (\lambda_{33} - \lambda_{11})u^*_1u^*_3; \qquad L^*_z = -\lambda'_{55}\frac{\partial \omega_z}{\partial t} - (\lambda_{22} - \lambda_{11})u^*_1u^*_2,$$

where u^*_1, u^*_2, u^*_3 are the components of the velocity of the origin of the new coordinate system (with respect to immovable coordinate system XYZ) in the new coordinate system.

Let us consider also the case when the body has three planes of symmetry: xOy, xOz and yOz. Then from the formulas (1.41), (1.42) we conclude that $\lambda_{26} = \lambda_{35} = 0$, since under accelerations of this symmetric body from rest—along the axis Oz (resp. Oy) the torque L_y (resp. L_z) is not generated.

Then the formulas (1.37)–(1.42) simplify further to give

$$R_x = -\lambda_{11}\frac{\partial u_1}{\partial t} - \lambda_{33}u_3\omega_y + \lambda_{22}u_2\omega_z;$$
$$R_y = -\lambda_{22}\frac{\partial u_2}{\partial t} - \lambda_{11}u_1\omega_z + \lambda_{33}u_3\omega_x;$$
$$R_z = -\lambda_{33}\frac{\partial u_3}{\partial t} - \lambda_{22}u_2\omega_x + \lambda_{11}u_1\omega_y;$$

$$L_x = -\lambda_{44}\frac{\partial \omega_x}{\partial t} + (\lambda_{55} - \lambda_{66})\omega_y\omega_z + (\lambda_{22} - \lambda_{33})u_2u_3;$$
$$L_y = -\lambda_{55}\frac{\partial \omega_y}{\partial t} + (\lambda_{66} - \lambda_{44})\omega_z\omega_x + (\lambda_{33} - \lambda_{11})u_3u_1;$$
$$L_z = -\lambda_{66}\frac{\partial \omega_z}{\partial t} + (\lambda_{44} - \lambda_{55})\omega_x\omega_y + (\lambda_{11} - \lambda_{22})u_1u_2.$$

1.5 Ellipsoids of Added Masses and Ellipsoids of Added Moments of Inertia

Let us describe a way of finding a coordinate system attached to the body where the matrix of added masses λ_{ik} has the simplest form.

In relation to the formula for kinetic energy of the fluid (1.13) consider the following two surfaces of second order:

$$\lambda_{11}x^2 + \lambda_{22}y^2 + \lambda_{33}z^2 + 2\lambda_{12}xy + 2\lambda_{13}xz + 2\lambda_{23}yz = 1; \tag{1.49}$$

and

$$\lambda_{44}x^2 + \lambda_{55}y^2 + \lambda_{66}z^2 + 2\lambda_{45}xy + 2\lambda_{46}xz + 2\lambda_{56}yz = 1. \tag{1.50}$$

Since in the left-hand side of Eq. (1.49) (respectively (1.50)) the coefficients $\lambda_{11}, \lambda_{22}, \lambda_{33}$ (respectively $\lambda_{44}, \lambda_{55}, \lambda_{66}$) have the same sign (they are positive, since they define the kinetic energy of the fluid as the body moves along or around the corresponding axis), then both surfaces are ellipsoids [65]. It follows from the formulas (1.49), (1.50) that if the point $M\ (x, y, z)$ belongs to the surface of one of these ellipsoids, then the point $M_1\ (-x, -y, -z)$ also belongs to that surface. Thus, the points of the surfaces form symmetric pairs with respect to the origin, and, therefore, these surfaces are central. Let us show how the surface (1.49) can be transformed to the simplest form by rotation of the coordinate system around the origin. The symmetric matrix of added masses

$$\Lambda := \begin{pmatrix} \lambda_{11} & \lambda_{12} & \lambda_{13} \\ \lambda_{12} & \lambda_{22} & \lambda_{23} \\ \lambda_{13} & \lambda_{23} & \lambda_{33} \end{pmatrix}$$

in the new coordinate system diagonalizes, i.e., values $\lambda'_{12}, \lambda'_{13}, \lambda'_{23}$ in the new coordinate system vanish; the corresponding axes Ox_1, Oy_1, Oz_1 will be called the *main* axes. Let us denote a vector pointing in one of the main directions (an eigenvector of matrix λ_{ij}) by $\vec{a}$; its projections onto the axes of the initial coordinate system we denote by (l, m, n). To determine l, m, n we first need to solve the characteristic (eigenvalue) equation

$$\det(\Lambda - kI) \equiv \begin{vmatrix} \lambda_{11} - k & \lambda_{12} & \lambda_{13} \\ \lambda_{12} & \lambda_{22} - k & \lambda_{23} \\ \lambda_{13} & \lambda_{23} & \lambda_{33} - k \end{vmatrix} = 0 \tag{1.51}$$

where I is the 3×3 unit matrix. This equation has three solutions (eigenvalues of the matrix λ_{ij}), denoted by k_1, k_2 and k_3, which correspond to three main directions. Taking one of them, say k_1, we get the homogeneous linear system for components of a corresponding eigenvector $\vec{a}_1 := (l_1, m_1, n_1)$:

$$\begin{cases} (\lambda_{11} - k_1)l_1 + \lambda_{12}m_1 + \lambda_{13}n_1 = 0, \\ \lambda_{12}l_1 + (\lambda_{22} - k_1)m_1 + \lambda_{23}n_1 = 0, \\ \lambda_{13}l_1 + \lambda_{23}m_1 + (\lambda_{33} - k_1)n_1 = 0, \end{cases}$$

which, due to (1.51), has a non-zero solution for l_1, m_1, n_1. Similarly, the other two eigenvalues k_2, k_3 correspond to eigenvectors $\vec{a}_2$ (l_2, m_2, n_2) and $\vec{a}_3$ (l_3, m_3, n_3). Since the matrix Λ is symmetric, the vectors $\vec{a}_1$, $\vec{a}_2$ and $\vec{a}_3$ are pairwise orthogonal.

Therefore, we can introduce the unit basic vectors (orths) $\vec{i}'$, $\vec{j}'$, $\vec{k}'$ pointing in the main directions $\vec{a}_1, \vec{a}_2, \vec{a}_3$; they are related to the orths of the initial coordinate system $\vec{i}$, $\vec{j}$, $\vec{k}$ by the formulas

$$\vec{i}' = \frac{\vec{a}_1}{|\vec{a}_1|} = \frac{l_1}{\sqrt{l_1^2 + m_1^2 + n_1^2}}\vec{i} + \frac{m_1}{\sqrt{l_1^2 + m_1^2 + n_1^2}}\vec{j} + \frac{n_1}{\sqrt{l_1^2 + m_1^2 + n_1^2}}\vec{k},$$
$$\vec{j}' = \frac{\vec{a}_2}{|\vec{a}_2|} = \frac{l_2}{\sqrt{l_2^2 + m_2^2 + n_2^2}}\vec{i} + \frac{m_2}{\sqrt{l_2^2 + m_2^2 + n_2^2}}\vec{j} + \frac{n_2}{\sqrt{l_2^2 + m_2^2 + n_2^2}}\vec{k},$$
$$\vec{k}' = \frac{\vec{a}_3}{|\vec{a}_3|} = \frac{l_3}{\sqrt{l_3^2 + m_3^2 + n_3^2}}\vec{i} + \frac{m_3}{\sqrt{l_3^2 + m_3^2 + n_3^2}}\vec{j} + \frac{n_3}{\sqrt{l_3^2 + m_3^2 + n_3^2}}\vec{k}.$$

Comparing these formulas with the usual transformation formulas for the orths of different coordinate systems:

$$\vec{i}' = \cos\alpha_1\vec{i} + \cos\beta_1\vec{j} + \cos\gamma_1\vec{k},$$
$$\vec{j}' = \cos\alpha_2\vec{i} + \cos\beta_2\vec{j} + \cos\gamma_2\vec{k},$$
$$\vec{k}' = \cos\alpha_3\vec{i} + \cos\beta_3\vec{j} + \cos\gamma_3\vec{k},$$

it is easy to find the cosines of the angles between the axes of the new and the initial coordinate system. Then we can write down the corresponding transformation of coordinates:

$$x = x'\cos\alpha_1 + y'\cos\alpha_2 + z'\cos\alpha_3,$$
$$y = x'\cos\beta_1 + y'\cos\beta_2 + z'\cos\beta_3,$$
$$z = x'\cos\gamma_1 + y'\cos\gamma_2 + z'\cos\gamma_3.$$

Similarly we can find the main axes of the ellipsoid of the added moments of inertia by diagonalizing the matrix

$$\tilde{\Lambda} := \begin{pmatrix} \lambda_{44} & \lambda_{45} & \lambda_{46} \\ \lambda_{45} & \lambda_{55} & \lambda_{56} \\ \lambda_{46} & \lambda_{56} & \lambda_{66} \end{pmatrix}.$$

In the new coordinate system the equation of the ellipsoid of added masses (1.49) looks as follows:

$$\lambda'_{11}x^2 + \lambda'_{22}y^2 + \lambda'_{33}z^2 = 1,$$

or, equivalently,

$$\frac{x^2}{(1/\sqrt{\lambda'_{11}})^2} + \frac{y^2}{(1/\sqrt{\lambda'_{22}})^2} + \frac{z^2}{(1/\sqrt{\lambda'_{33}})^2} = 1.$$

The main axes of the ellipsoid have the following property: if the body moves with constant velocity in an ideal fluid without rotation along the main axis, then the hydrodynamic forces and torques are equal to zero. Indeed, the added masses $\lambda'_{12}, \lambda'_{13}, \lambda'_{23}$ vanish in the coordinate system, whose axes coincide with the main axes. The vanishing of forces and torques follows from expressions (1.22)–(1.27) since in the new coordinate system $R_x = R_y = R_z = L_x = L_y = L_z = 0$. The motion with constant velocity along one of main axes is stable; along the two other main axes such motion is unstable.

Let the main axes be chosen such that $\lambda_{11} < \lambda_{22} < \lambda_{33}$. Suppose that a body moving with constant velocity along the axis Ox_1 receives a deviation—a rotation around the axis Oz_1 in the negative (clockwise) direction (Fig. 1.2) by an angle $\Delta\varphi$. Then the velocity gets the second component u_2 in the direction of the main axis Oy_1 attached to the body. Equation (1.27) shows that in this situation the body is acted upon by torque $L_z = -(\lambda_{22} - \lambda_{11})u_1\, u_2$ which is negative since $\lambda_{22} > \lambda_{11}$, $u_1 > 0$, $u_2 > 0$. This torque, acting in clockwise direction, increases the angle $\Delta\varphi$. Therefore, the motion with constant velocity along the axis Ox_1 is unstable. Analogously one can verify that the motion with constant velocity along the axis Oy_1 is also unstable with respect to a turn around the axis Ox_1. The only stable motion is the motion with constant velocity along the axis Oz_1. In that case a rotation around the axis Oy_1 generates the restoring torque which reduces the angle of deviation in the plane x_1Oz_1. Consider a small turn of the body in the positive direction in the y_1Oz_1, such that u_2 and u_3 are positive. Then, according to formula (1.25), the torque L_x is negative, i.e., we also get a restoring force.

Besides the main axes of the ellipsoid of added masses (1.49) we can consider the main axes of ellipsoid of the added moments of inertia (1.50). By the main axes of ellipsoid (1.50) we mean such axes that $\lambda_{45} = \lambda_{46} = \lambda_{56} = 0$. The procedure of determining the main axes of the ellipsoid of the added moments of inertia is completely analogous to the process of determining the main axes of the ellipsoid of added masses (1.49).

The formulas (1.22)–(1.27) show that if the body uniformly rotates in an ideal fluid around one of the main axes of ellipsoid (1.50), then the hydrodynamic forces

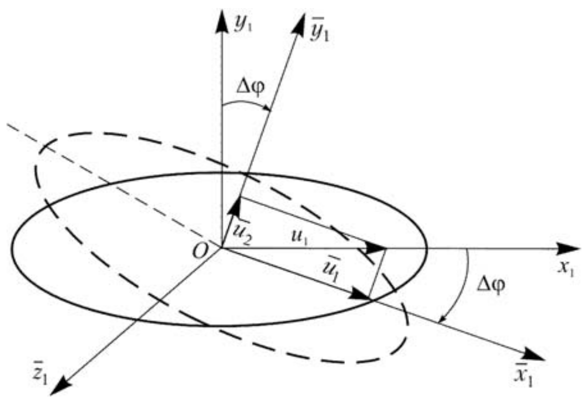

Fig. 1.2 Projections of velocity to the axes of the coordinate system attached to the body when the body turns

and torques do not influence it. Assume that the main axes are chosen such that $\lambda_{44} < \lambda_{55} < \lambda_{66}$. Let the body rotating with constant angular velocity around the axis Ox_1 receive a random turn in the plane x_1Oy_1 by the angle $\Delta\varphi$ (Fig. 1.2). Then the vector of angular velocity projects on the axes Ox_1 and Oy_1. The projections u_4 and u_5 of this vector are positive, since $\Delta\varphi$ is negative. The formula (1.27) shows that it generates the torque $L_z = -(\lambda_{55} - \lambda_{44})u_4u_5$ which tends to increase the angle $\Delta\varphi$, since $L_z < 0$. Therefore, the rotation with constant angular velocity around the axis Ox_1 is unstable. In the same way we can show that the rotation with constant angular velocity around the axis Oy_1 is unstable with respect to a small turn around the axis Ox_1. The only axis of stable rotation with constant angular velocity is the axis Oz_1, which corresponds to the maximal moment of inertia λ_{66}.

We stress that in general the main axes of the ellipsoid of added masses (1.49) and the ellipsoid of added moments of inertia (1.50) do not coincide.

In solution of various problems of dynamics of a real body in the fluid it makes sense to introduce the notion of so-called ellipsoids of modified masses and ellipsoids of modified moments of inertia. By modified masses and moments of inertia we mean the masses and moments of inertia of the system body-fluid [16]. The notions of modified masses and modified moments of inertia are very useful in investigation of equations of motion of a solid body in a fluid. In the monograph of Basin [16] the general equations of motion of this kind are presented, and various cases of the inertial motion of a solid body in a fluid are considered.

Chapter 2
The Added Masses of Planar Contours Moving in an Ideal Unlimited Fluid

For calculation of added masses of various elongated bodies the planar sections technique (see Chap. 3) is widely applied. Application of this method requires a knowledge of the added masses of corresponding cross sections in a planar flow. Theory of functions of a complex variable allows us to describe explicitly the planar flow around most planar contours that correspond to real ship structures. In this chapter we discuss added masses of various planar contours moving in an infinite two-dimensional fluid. We give the main formulas for computation of added masses using techniques due to Sedov [206].

2.1 Sedov's Technique

Using Sedov's technique one can efficiently determine the added masses of planar contours moving in an infinite fluid [206]. Consider the function of a complex variable

$$z = f(\zeta) = \frac{k}{\zeta} + k_0 + k_1\zeta + k_2\zeta^2 + \cdots, \tag{2.1}$$

which defines the conformal map of the unit disc in ζ-plane to exterior (filled with fluid) of a given contour C in z-plane (the "uniformization map"). Then the added masses of the contour C moving in the fluid are given by the formulas:

$$\lambda_x = -\rho\big[S - 2\pi k\bar{k} + \pi(kk_1 + \bar{k}\bar{k}_1)\big]; \tag{2.2}$$

$$\lambda_y = -\rho\big[S - 2\pi k\bar{k} - \pi(kk_1 + \bar{k}\bar{k}_1)\big]; \tag{2.3}$$

$$\lambda_{xy} = i\rho\pi(kk_1 - \bar{k}\bar{k}_1); \tag{2.4}$$

$$\lambda_{x\omega} = \rho\big[Sy_* - \pi(kc_1 + \bar{k}\bar{c}_1)\big]; \tag{2.5}$$

$$\lambda_{y\omega} = \rho\big[-Sx_* + \pi i(kc_1 - \bar{k}\bar{c}_1)\big]; \tag{2.6}$$

$$\lambda_\omega = \frac{i\rho}{2}\oint_l \bar{w}_3\left(\frac{1}{\zeta}\right)\frac{dw_3}{d\zeta}d\zeta. \tag{2.7}$$

A.I. Korotkin, *Added Masses of Ship Structures*,

In formulas (2.2)–(2.7) we use the following notations: contour of integration l is the unit circle $|\zeta|=1$ taken in positive (counterclockwise) direction; $f(\zeta)$ is the "uniformization" function (2.1). Let us introduce the function $\bar{f}$ defined by its Laurent series at $\zeta=\infty$:

$$\bar{f}\left(\frac{1}{\zeta}\right):=\bar{k}\zeta+\bar{k}_0+\frac{\bar{k}_1}{\zeta}+\frac{k_2}{\zeta^2}+\cdots,$$

where k, k_j $(j=0,1,2,\ldots)$ are the coefficients in the Laurent expansion (2.1). The function w_3 is defined as follows:

$$w_3(\zeta)=-\frac{1}{4\pi}\oint_l f(\eta)\bar{f}\left(\frac{1}{\eta}\right)\frac{\eta+\zeta}{\eta-\zeta}\frac{d\eta}{\eta};$$
$$\frac{dw_3}{d\zeta}=-\frac{1}{2\pi}\oint_l f(\eta)\bar{f}\left(\frac{1}{\eta}\right)\frac{d\eta}{(\eta-\zeta)^2};$$
$$\left(\frac{dw_3}{d\zeta}\right)_{\zeta=0}=c_1=-\frac{1}{2\pi}\oint_l f(\eta)\bar{f}\left(\frac{1}{\eta}\right)\frac{d\eta}{\eta^2}.$$

Similarly we define the analytic function $\bar{w}_3$: if the function w_3 has the Taylor series $w_3(\zeta)=c_1\zeta+c_2\zeta^2+\cdots$, then

$$\bar{w}_3\left(\frac{1}{\zeta}\right):=\frac{\bar{c}_1}{\zeta}+\frac{\bar{c}_2}{\zeta^2}+\cdots.$$

The integral

$$S=-\frac{i}{2}\oint_l\overline{f(\zeta)}\frac{df}{d\zeta}d\zeta$$

gives the area of the interior of the contour C (notice that, in contrast to the function $\bar{f}(\zeta^{-1})$ which is holomorphic, the function $\overline{f(\zeta)}$ is an *antiholomorphic* function);

$$z_*\equiv x_*+iy_*:=-\frac{i}{2S}\oint_l f(\zeta)\overline{f(\zeta)}\frac{df}{d\zeta}d\zeta$$

is the complex coordinate of the centroid of the figure bounded by the contour C. The overline here denotes ordinary complex conjugation.

These formulas show that the added masses of the contour C can be found if the conformal map (2.1) is known. Then the integrals over contour l can be computed by the residue theorem.

Below we use the formulas (2.2)–(2.7) for calculation of added masses of various contours. Due to the Cauchy theorem, the function $w_3(\zeta)$ can be found as follows [206]. Let us write $(i/2)f(\zeta)\bar{f}(1/\zeta)$ as $f_1(\zeta)+f_2(\zeta)$, where $f_1(\zeta)$ is regular for $|\zeta|<1$, and $f_2(\zeta)$ is regular for $|\zeta|>1$. Then $w_3(\zeta)=2f_1(\zeta)$.

Below we use this techniques to find added masses of various simple contours.

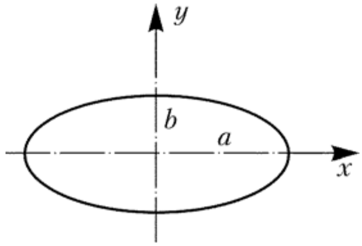

Fig. 2.1 Elliptic contour

2.2 The Added Masses of Simple Contours

2.2.1 Elliptic Contour, Circular Contour and Interval (Plate)

The map of the exterior of the ellipse with half-axes a and b (Fig. 2.1) to the interior of the unit circle in the ζ-plane is given by the function

$$z = f(\zeta) = -\frac{1}{2}\left[(a-b)\zeta + (a+b)\frac{1}{\zeta}\right].$$

Using the general formulas (2.2)–(2.7), we obtain

$$\begin{aligned} \lambda_{11} = \rho\pi b^2; \qquad \lambda_{22} = \rho\pi a^2;\\ \lambda_{66} = \frac{\rho\pi}{8}\left(a^2 - b^2\right)^2;\\ \lambda_{12} = \lambda_{16} = \lambda_{26} = 0. \end{aligned} \tag{2.8}$$

Circle. The added masses of the circular contour are given by the formulas (2.8) assuming $a = b = r$. Then $\lambda_{11} = \lambda_{22} = \rho\pi r^2$; $\lambda_{12} = \lambda_{16} = \lambda_{26} = \lambda_{66} = 0$.

Interval (plate). The added masses of the interval (plate) of length $2a$ are given by the formulas (2.8) assuming $b = 0$. Then $\lambda_{22} = \rho\pi a^2$; $\lambda_{66} = \rho\pi a^4/8$; $\lambda_{11} = \lambda_{12} = \lambda_{16} = \lambda_{26} = 0$.

2.2.2 Elliptic Contour with One Rib, T-shape Contour

The conformal map of the exterior of an ellipse with one rib (Fig. 2.2) in the z-plane to the unit disc in the ζ-plane is given by

$$\begin{aligned} z = f(\zeta) = \frac{ci}{2}\Bigg\{ &\frac{(a+b)(1+m)}{4c}\left(\zeta + \frac{1}{\zeta}\right) + \frac{m-1}{2}\frac{a+b}{c} \\ &+ \frac{a+b}{c}\left[\left(\frac{1+m}{4}\frac{1}{\zeta} + \frac{1+m}{4}\zeta + \frac{m-1}{2}\right)^2 - 1\right]^{1/2} \\ &+ \frac{c/(a+b)}{\frac{m-1}{2} + \frac{1+m}{4}(\zeta + \frac{1}{\zeta}) + [(\frac{1+m}{4}\zeta + \frac{1+m}{4}\frac{1}{\zeta} + \frac{m-1}{2})^2 - 1]^{1/2}}\Bigg\}, \end{aligned} \tag{2.9}$$

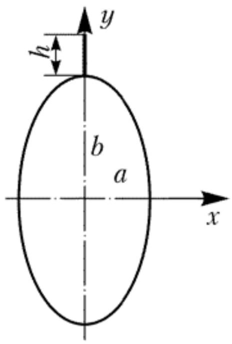

Fig. 2.2 Elliptic contour with one rib

where a, b are the half-axes of the ellipse; $c=\sqrt{b^2-a^2}$; h is the height of the rib; $m=(b+h)/(a+b)+a/(b+h+\sqrt{a^2+h^2+2bh})$; $i=\sqrt{-1}$. By expanding the right-hand side of (2.9) in powers of ζ, we obtain

$$k=i\frac{(a+b)(1+m)}{4};\qquad k_0=i\frac{(a+b)(m-1)}{2};$$
$$k_1=i\frac{(a+b)^2(m^2+2m-3)+4(b^2-a^2)}{4(a+b)(m+1)};\qquad k_2=i\frac{4a(m-1)}{(m+1)^2};$$
$$k_3=-i\frac{2a(3m^2-10m+7)}{(1+m)^3};\qquad c_1=-\frac{i}{4}\left(m^2-1\right)(a+b)^2.$$

Using the general Sedov formulas we obtain the following expressions for the added masses:

$$\lambda_{11}=\frac{\rho\pi b^2}{4}\left[(m+1)^2\left(1+\frac{a}{b}\right)^2-4\frac{a}{b}\left(2+\frac{a}{b}\right)\right];$$
$$\lambda_{22}=\pi\rho a^2;\qquad \lambda_{16}=-\frac{\pi\rho b^3}{8}\left(1+\frac{a}{b}\right)^3\left(m^2-1\right)(m+1);$$
$$\lambda_{66}=\rho\pi\frac{(a+b)^2}{2^7}\left[(a+b)^2\left(9m^4+4m^3-10m^2+4m-7\right)+16(b-a)^2\right];$$
$$\lambda_{12}=\lambda_{26}=0. \tag{2.10}$$

Dependence of coefficients

$$k_{11}=\frac{\lambda_{11}}{\pi\rho b^2};\qquad k_{16}=\frac{8\lambda_{16}}{\pi\rho b^3};$$
$$k_{66}=\frac{128\lambda_{66}}{\pi\rho b^4}$$

on parameters h/b and a/b is shown in Figs. 2.4–2.6.

Fig. 2.3 T-shape profile

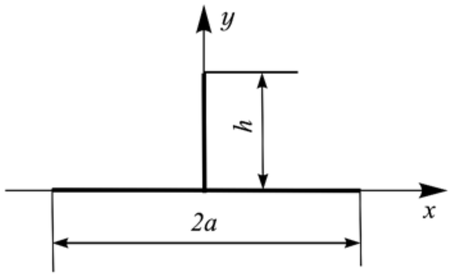

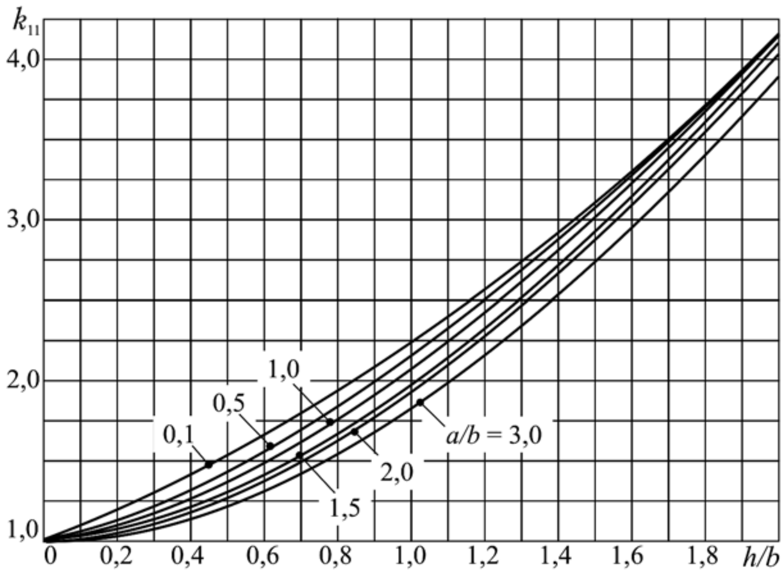

Fig. 2.4 Coefficient k_{11} of added masses of an ellipse with one rib

T-shape. The added masses of the T-shape (Fig. 2.3) can be obtained from formulas (2.10) assuming that $b = 0$:

$$m = \frac{h}{a} + \frac{a}{h + \sqrt{a^2 + h^2}};$$

$$\lambda_{11} = \frac{\pi}{4}\rho a^2\left[(m+1)^2 - 4\right]; \qquad \lambda_{22} = \pi\rho a^2;$$

$$\lambda_{16} = -\frac{\pi}{8}\rho a^3\left(m^2 - 1\right)(m+1);$$

$$\lambda_{66} = \frac{\pi}{2^7}\rho a^4\left(9m^4 + 4m^3 - 10m^2 + 4m + 9\right); \qquad \lambda_{12} = \lambda_{26} = 0.$$

The coefficients $k_{11} = \lambda_{11}/(\rho\pi a^2)$; $k_{16} = (8\lambda_{16})/(\rho\pi a^3)$; $k_{66} = (128\lambda_{66})/(\pi\rho a^4)$ are presented in Table 2.1 for $0.1 \le h/a \le 5$.

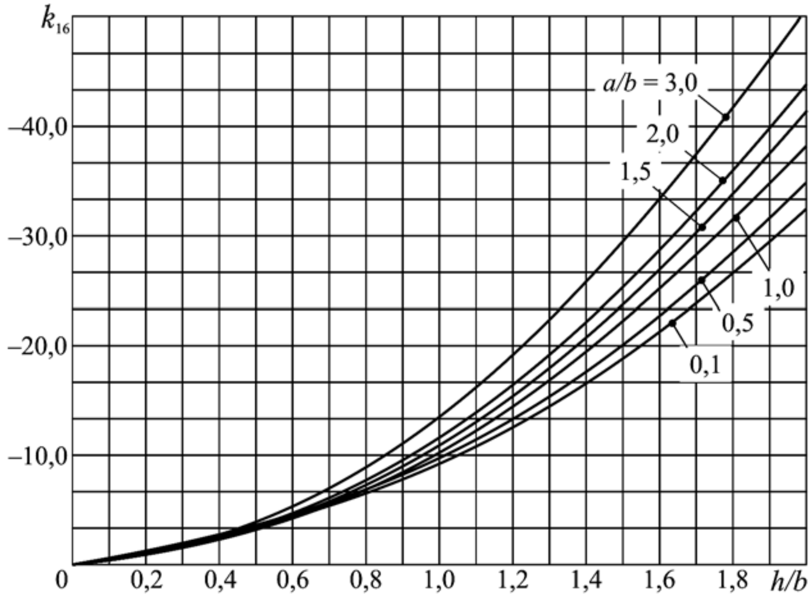

Fig. 2.5 Coefficient k_{16} of added masses of an ellipse with one rib

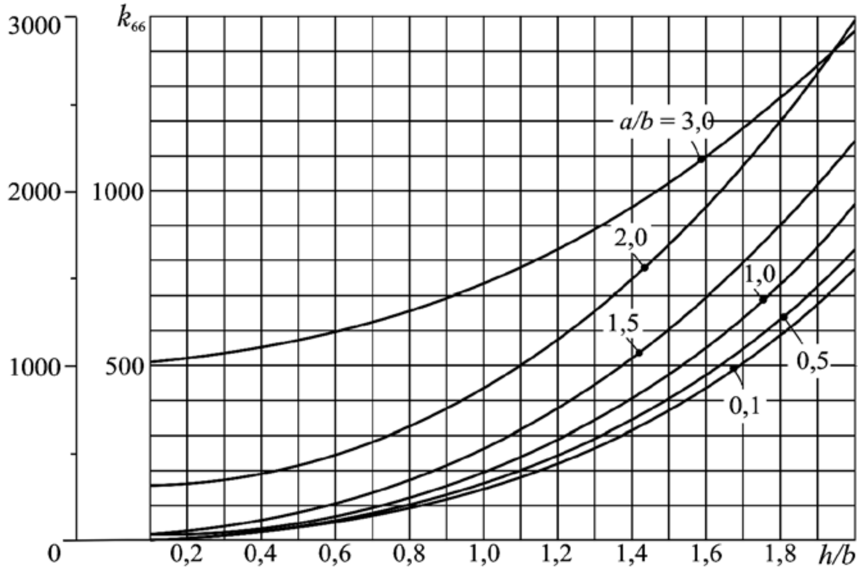

Fig. 2.6 Coefficients k_{66} of added masses of an ellipse with one rib. The *left vertical axis* corresponds to the curve $a/b = 3.0$; the *right vertical axis* corresponds to other values of a/b

Table 2.1 Coefficients of added masses of T-shape profile

h/a	k_{11}	k_{16}	k_{66}
0.1	0.005	−0.020	16.2
0.2	0.020	−0.082	16.7
0.3	0.044	−0.184	17.5
0.4	0.079	−0.332	18.8
0.5	0.122	−0.529	20.6
0.7	0.233	−1.090	24.0
1.0	0.457	−2.41	42.0
1.5	0.964	−6.31	102.0
2.0	1.62	−12.9	238
3.0	3.33	−37.4	853
4.0	5.56	−82.0	2690
5.0	8.30	−152	6380

2.2.3 *Elliptic Contour with Two Symmetric Ribs*

The exterior of the contour in the z-plane (Fig. 2.7) is mapped to the unit disc in the ζ-plane by function

$$z = f(\zeta) = \frac{c}{2}\left[\frac{m(a+b)}{2c}\left(\zeta + \frac{1}{\zeta}\right) + \frac{a+b}{c}\sqrt{\frac{m^2}{4}\left(\zeta + \frac{1}{\zeta}\right)^2 - 1}\right.$$
$$\left. + \frac{c}{a+b}\frac{1}{\frac{m}{2}(\zeta + \frac{1}{\zeta}) + \sqrt{\frac{m^2}{4}(\zeta + \frac{1}{\zeta})^2 - 1}}\right],$$

where

$$c = \sqrt{a^2 - b^2}; \qquad m = \frac{a+h}{a+b} + \frac{b}{a+h+\sqrt{b^2+h^2+2ah}};$$

h is the height of the ribs.

Expanding the function $f(\zeta)$ in powers of ζ, we obtain the coefficients

$$k = \frac{1}{2}(a+b)m; \qquad k_0 = 0; \qquad k_1 = \frac{1}{2m}\big[(a+b)\big(m^2-1\big) + a - b\big];$$
$$k_2 = 0; \qquad k_3 = \frac{(m^2-1)b}{m^3}.$$

Then it is easy to find the added masses

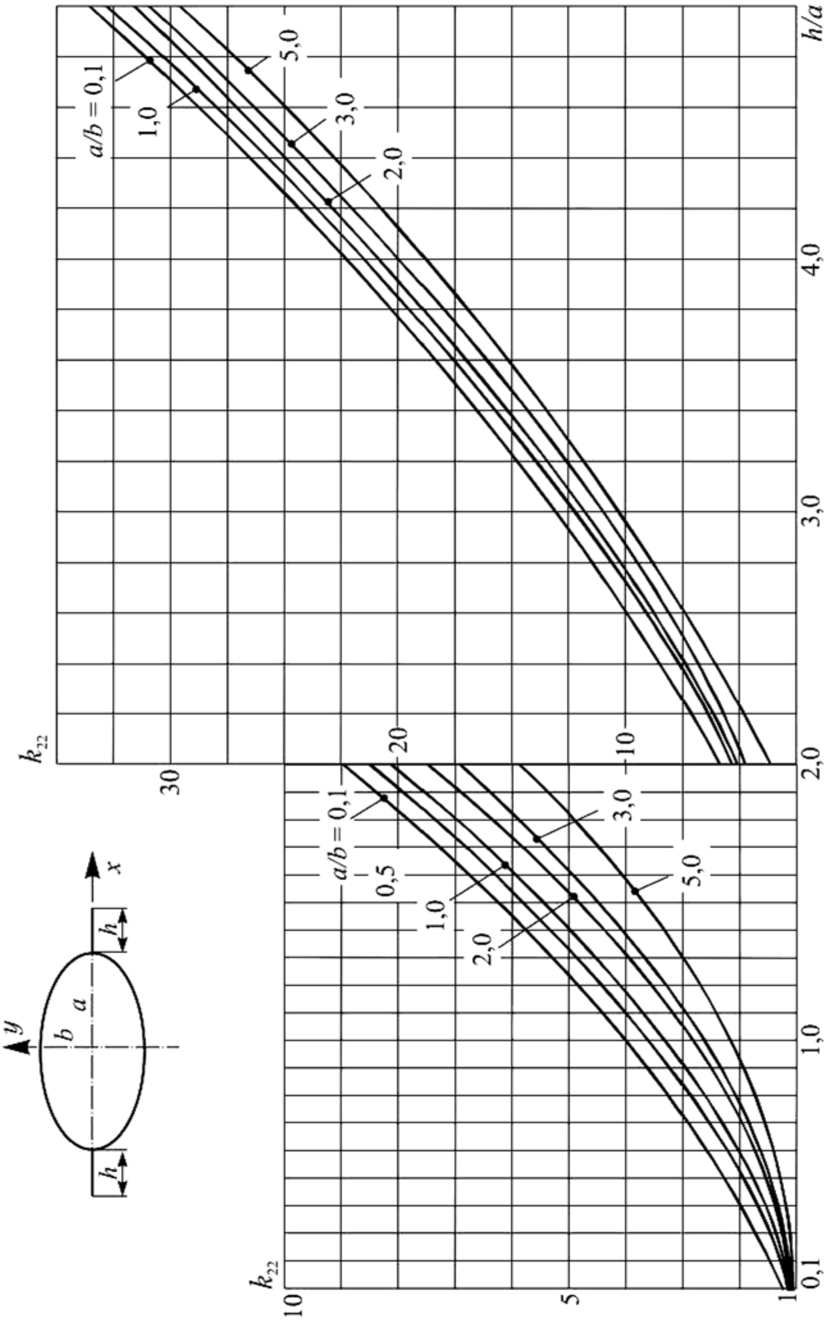

Fig. 2.7 Coefficient k_{22} for elliptic contour with two ribs

$$\lambda_{11} = \rho\pi b^2; \qquad \lambda_{22} = \rho\pi a^2\left[m^2\left(1+\frac{b}{a}\right)^2 - 2\frac{b}{a} - \frac{b^2}{a^2}\right];$$
$$\lambda_{66} = \frac{\pi}{8}\rho(a+b)^2\left[(a+b)^2\left(m^4-1\right)+(a-b)^2\right];$$
$$\lambda_{12} = \lambda_{16} = \lambda_{26} = 0. \tag{2.11}$$

The values of coefficients $k_{22} = \lambda_{22}/(\pi\rho a^2)$ and $k_{66} = (8\lambda_{66})/(\pi\rho a^4)$ are given in Figs. 2.7–2.9.

Choosing in (2.11) $b = a$, we obtain the expressions for the added masses of a circle with two ribs.

Alternative expressions for the added masses of the circle of radius a with two symmetric ribs of height h are given in the book [158]:

$$\lambda_{22} = \pi\rho s^2\left(1-\frac{a^2}{s^2}+\frac{a^4}{s^4}\right); \qquad s = a+h;$$
$$\lambda_{66} = \frac{\pi\rho s^4}{8}\left\{\left[\left(1+R^2\right)^2\arctan\frac{1}{R}\right]^2 + 2R\left(1-R^2\right)\left(R^4-6R^2+1\right)\arctan\frac{1}{R} - \pi^2R^4 + R^2\left(1-R^2\right)^2\right\}$$

where $R = a/(a+h)$.

2.2.4 Elliptic Contour with Horizontal and Vertical Ribs

The added masses of an elliptic contour with two horizontal ribs of the same height and with two vertical ribs of different height (Fig. 2.10) are defined by the formulas [158]

$$\lambda_{22} = \pi\rho\left(4c^2 - k^2 - 2ab - b^2\right),$$
$$\lambda_{33} = \pi\rho\frac{s^2(a^2+b^2)+2ab^2(a-b)-2abs(s^2-a^2+b^2)^{1/2}}{(a-b)^2}$$

where the parameters c and k can be found from the following equations:

$$k = \frac{as-b(s^2+a^2-b^2)^{1/2}}{a-b}; \qquad c = \frac{f_1+f_2}{4};$$
$$f_1^2 = k^2 + \left[\tau_1 + \frac{(a+b)^2}{4\tau_1}\right]^2; \qquad f_2^2 = k^2 + \left[\tau_2 + \frac{(a+b)^2}{4\tau_2}\right]^2;$$
$$\tau_1 = \frac{1}{2}\left[t_1 + \left(t_1 - a^2 + b^2\right)^{1/2}\right]; \qquad \tau_2 = \frac{1}{2}\left[t_2 + \left(t_2 - a^2 + b^2\right)^{1/2}\right].$$

The values a, b, s, t_1, t_2 are defined as shown in Fig. 2.10.

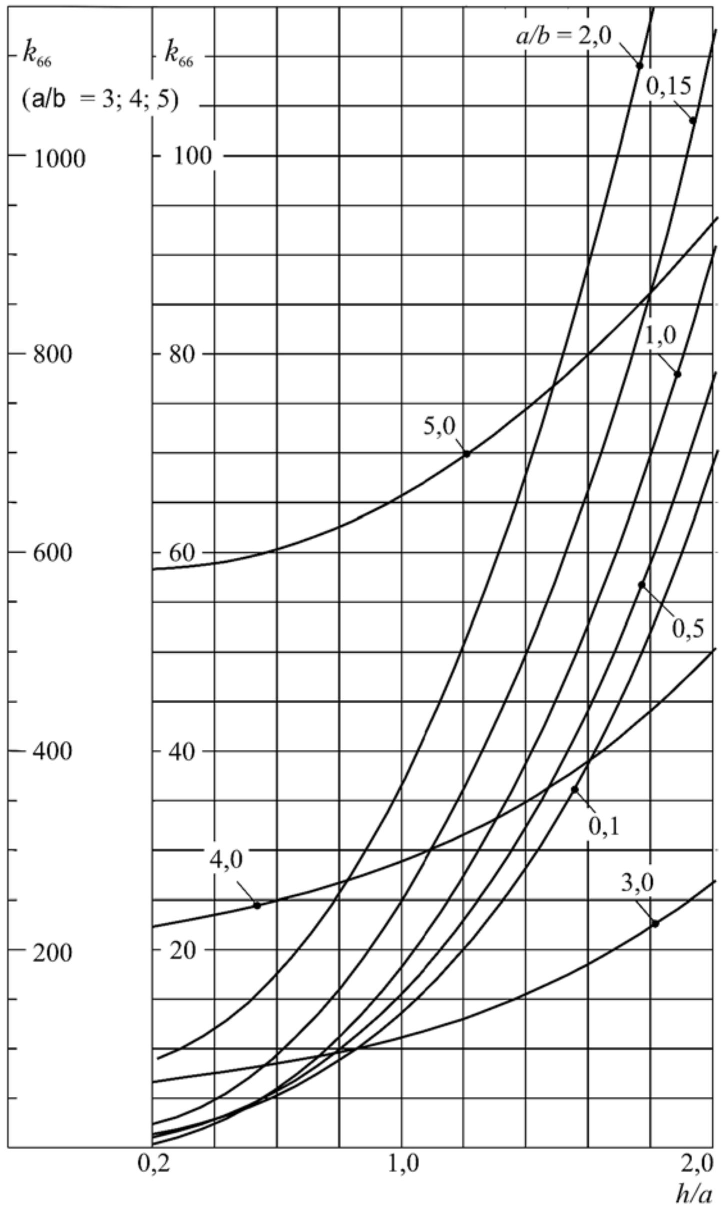

Fig. 2.8 Coefficient k_{66} for an elliptic contour with two ribs. The *left vertical axis* corresponds to values $a/b = 3, 4, 5$; the *right vertical axis* corresponds to all other values of a/b

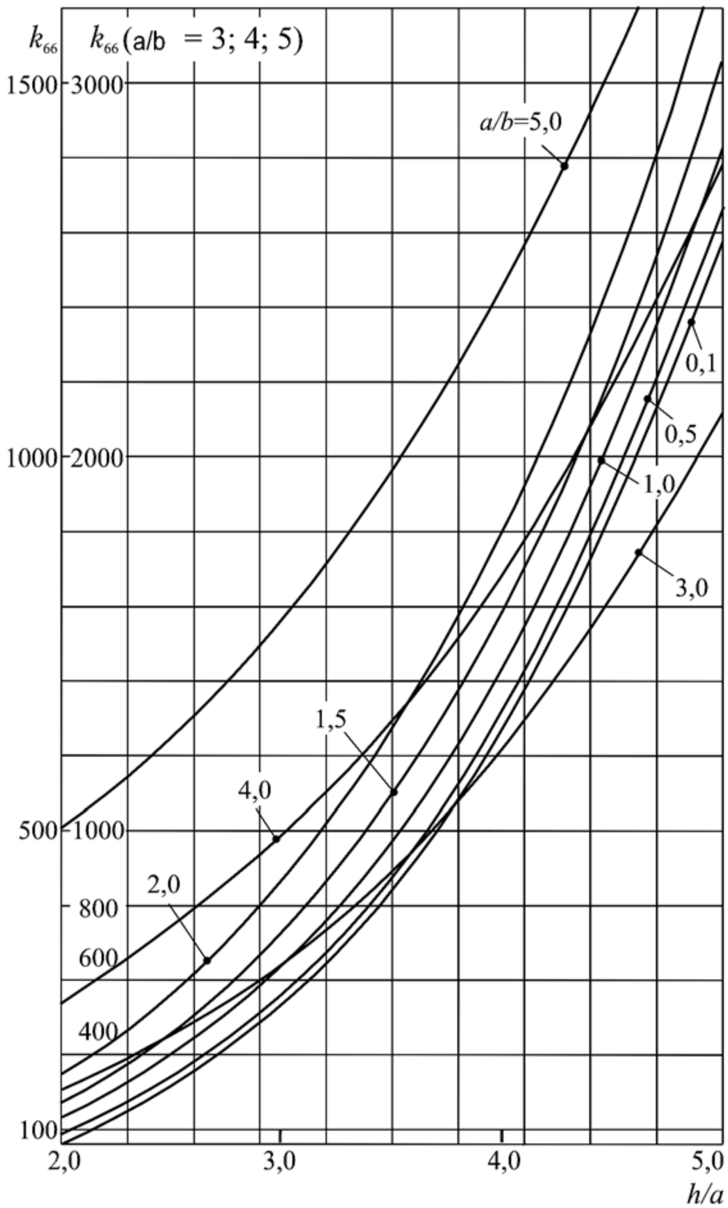

Fig. 2.9 Coefficient k_{66} for elliptic contour with two ribs. The *left vertical axis* corresponds to the values of a/b equal to 3, 4, 5; the *right vertical axis* corresponds to all other values of a/b

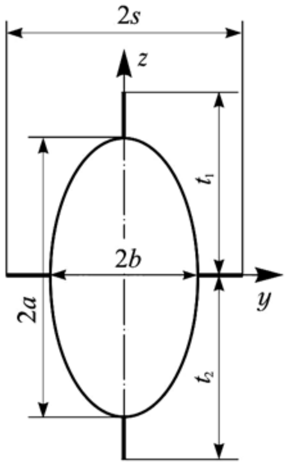

Fig. 2.10 Elliptic contour with four ribs

2.2.5 Symmetrical Profile Made up of Two Intersecting Intervals (Plates)

For this type of profile (Fig. 2.11) the added masses can be obtained as a partial case of formulas (2.11) assuming that $a = 0$:

$$m = \frac{h}{b} + \frac{b}{h + \sqrt{b^2 + h^2}};$$
$$\lambda_{11} = \pi\rho b^2; \qquad \lambda_{22} = \rho\pi h^2;$$
$$\lambda_{66} = \pi\rho b^4 \frac{m^4}{8}; \qquad \lambda_{12} = \lambda_{16} = \lambda_{26} = 0.$$

The values of the coefficient $k_{66} = (8\lambda_{66})/(\pi\rho b^4)$ are given in Table 2.2.

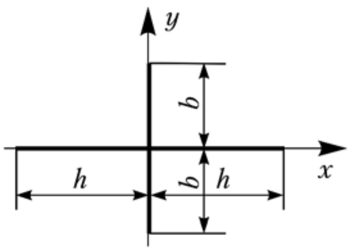

Fig. 2.11 Symmetric profile consisting of two plates intersecting at a right angle

Table 2.2 Coefficient k_{66} for some values of h/b

h/b	0.1	0.2	0.3	0.4	0.5	0.7	1.0	1.5	2.0	3.0	4.0	5.0
k_{66}	1.02	1.08	1.19	1.34	1.56	2.22	4.0	10.6	25.0	100.0	289.0	676.0

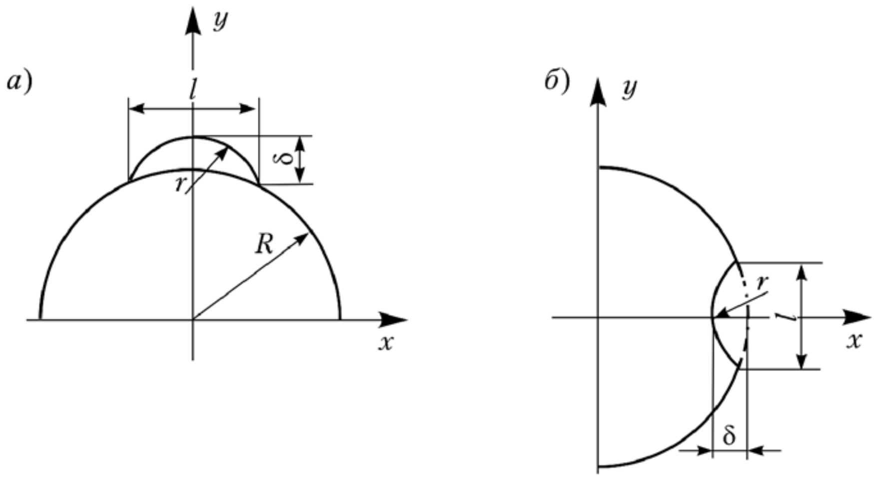

Fig. 2.12 Circle with two external **(a)** and two internal **(b)** hitches

2.2.6 Circle with Two Hitches

The added masses of the circular contour with two external hitches (Fig. 2.12a) are determined by the method of electro-hydrodynamic analogy (see Chap. 9) in [48]. The parameters of the hitch are: $\delta/r = 0.077$; $l/r = 0.76$; $s/(\pi R^2) = 0.027$ where δ is the height of the hitch, r is the radius of curvature of the hitch, l is the length of the hitch, s is the area of the hitch, R is the radius of the circle. The coefficients of added masses for the circle with external hitches are given by: $k_{11} = \lambda_{11}/\pi\rho R^2 = 1.09$; $k_{22} = \lambda_{22}/\pi\rho R^2 = 0.954$. If there are two internal hitches (Fig. 2.12b) with parameters $\delta/r = 0.115$; $l/r = 0.55$; $s/(\pi R^2) = 0.03$, then $k_{11} = 1.06$.

For other positions of hitches on the circle and other contours the added masses were also found in [48].

2.2.7 Circle with Two Side Ribs

The added masses of the circle with two plates located at the angle of 45 degrees to the diameter are found in [201]. The experimental results can be presented as the following graphs:

$$k_{22} = \frac{\lambda_{22}}{\rho\pi R^2} = f_1\left(\frac{h}{2R}\right); \qquad k_{33} = \frac{\lambda_{33}}{\rho\pi R^2} = f_2\left(\frac{h}{2R}\right),$$

where R is the radius of the main circle; h is the height of the ribs. These curves are shown in Fig. 2.13. In the same figure we show the dependence of dimensionless coordinate $l/2R$ of the point of application of inertial forces on $h/2R$. Knowing l one can compute the added mass $\lambda_{24} = l\lambda_{22}$.

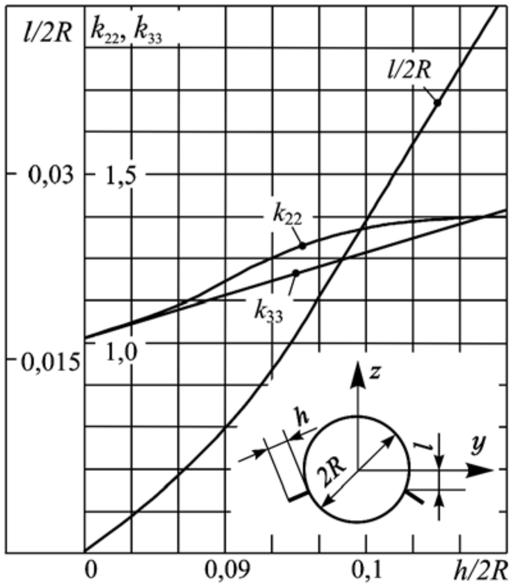

Fig. 2.13 Coefficient of added masses of circle with two side ribs

2.2.8 Circle with Cross-like Positioned Ribs

The formulas for the added masses of the circle with cross-like positioned ribs of the same height are as follows [158]:

$$\lambda_{22} = \lambda_{33} = \pi\rho s^2\left(1 - \frac{a^2}{s^2} + \frac{a^4}{s^4}\right),$$

where a is the radius of the circle; $s = a + h$; h is the height of the ribs (Fig. 2.14). The added mass $\lambda_{66} = 2\rho s^4 k_{66} a/(\pi s)$, where the coefficient k_{66} can be found from Fig. 2.14 (the curve I).

For comparison in the same Fig. 2.14 we draw the curve II which shows the dependence of the coefficient $k_{66} = (8\lambda_{66})/(\pi\rho s^4)$ on a/s for the circle with *two* symmetric ribs (the angle between the ribs is equal to π).

If the heights of vertical ribs on the circle differ from the heights of the horizontal ribs, then the added masses of the contour are as follows:

$$\lambda_{22} = \frac{\pi\rho s^2}{4}\left\{\frac{b^2}{s^2}\left(1 + \frac{a^4}{b^4}\right) + \frac{c^2}{s^2}\left(1 + \frac{a^4}{c^4}\right) - 2\left(1 + \frac{a^2}{s^2}\right)^2 \right.$$
$$\left. + 2\left[\left(1 + \frac{a^4}{s^2 b^2}\right)\left(1 + \frac{b^2}{s^2}\right)\left(1 + \frac{a^4}{s^2 c^2}\right)\left(1 + \frac{c^2}{s^2}\right)\right]^{1/2}\right\};$$
$$\lambda_{33} = \pi\rho s^2\left(1 - \frac{a^2}{s^2} + \frac{a^4}{s^4}\right).$$

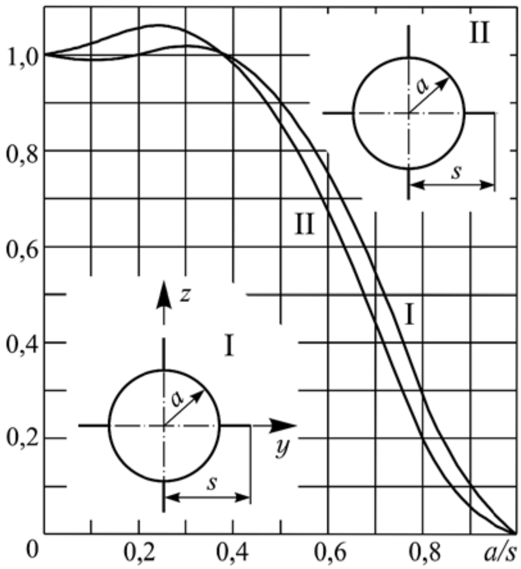

Fig. 2.14 Coefficient of added masses of a circle with four cross-like positioned ribs

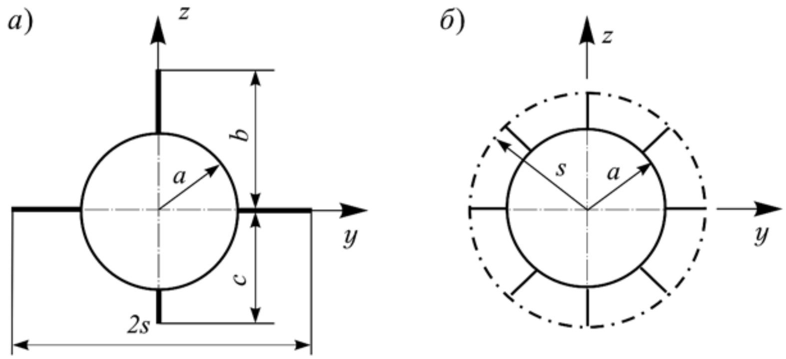

Fig. 2.15 Circle with asymmetric **(a)** and symmetric **(b)** lateral ribs

If on the circle there are three or more equidistant ribs (see Fig. 2.15b), then

$$\lambda_{22} = \lambda_{33} = 2\pi\rho s^2 \left\{ \left[\frac{1 + (a^2/s^2)^{n/2}}{2} \right]^{4/n} - \frac{1}{2}\left(\frac{a}{s}\right)^2 \right\};$$

$$\lambda_{66} = 0.533\rho s^4, \quad \text{if } n = 3,\ a = 0;$$
$$\lambda_{66} = \frac{2}{\pi}\rho s^4, \quad \text{if } n = 4,\ a = 0;$$
$$\lambda_{66} = \frac{\pi}{2}\rho s^4, \quad \text{if } n = \infty,\ a = 0.$$

2.2.9 Circle with Two Tangent Horizontal Ribs

If two horizontal ribs of span $2s$ are tangent to circle of radius a (Fig. 2.16) and also there are two vertical ribs of different heights, then the added masses are given by [158]:

$$\lambda_{22} = 2\pi\rho\left\{c^2 - \frac{a^2}{2} + \frac{4c^2 \sin\lambda \cos^2(\lambda/2)}{3(\lambda + \sin\lambda)}\left[\sin^2\frac{\lambda}{2} - \frac{3\lambda\cos^2(\lambda/2)}{\lambda + \sin\lambda}\right] + 2\left(r^2 - c^2\right)\right\},$$

$$\lambda_{33} = 2\pi\rho\left\{c^2 - \frac{a^2}{2} - \frac{4c^2 \sin\lambda \cos^2(\lambda/2)}{3(\lambda + \sin\lambda)}\left[\sin^2\frac{\lambda}{2} - \frac{3\lambda\cos^2(\lambda/2)}{\lambda + \sin\lambda}\right]\right\},$$

where the parameter λ is defined from the equation

$$\frac{a}{s} = \frac{1}{\pi}\left\{\operatorname{arcsh}\left(\frac{\lambda}{2}\tan\frac{\lambda}{2}\right)^{1/2} + \left[\frac{\lambda}{2}\tan\frac{\lambda}{2} + \left(\frac{\lambda}{2}\right)^2\tan^2\frac{\lambda}{2}\right]^{1/2}\right\}.$$

Then one finds the values $c = a\pi/(\lambda + \sin\lambda)$; variable h is determined by the equation

$$2 + \frac{b}{2} = \pi\left(\frac{\lambda}{h/c + 1} + \arctan\frac{\sin\lambda}{h/c - \cos\lambda}\right)^{-1};$$

the parameter f is determined by the equation

$$\frac{d}{a} = \pi\left(\frac{\lambda}{f/c - 1} + \arctan\frac{\sin\lambda}{f/c + \cos\lambda}\right)^{-1}.$$

Then we compute

$$r = \frac{1}{4}\left(h + \frac{c^2}{h} + f + \frac{c^2}{f}\right).$$

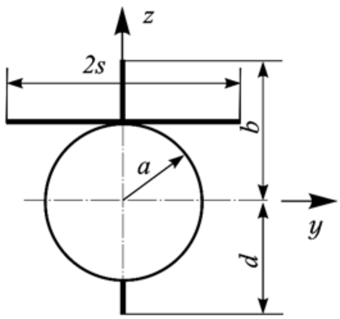

Fig. 2.16 Circle with horizontal ribs located in a tangent plane

2.2.10 Regular Inscribed Polygon

The values for the added masses of the regular polygon inscribed in the circle with the radius a depend on the number of its sides n and are defined by the following formulas [158]:

$$\begin{aligned}
\lambda_{22} = \lambda_{33} &= 0.654\pi\rho a^2, \quad \text{if } n = 3,\\
\lambda_{22} = \lambda_{33} &= 0.787\pi\rho a^2, \quad \text{if } n = 4,\\
\lambda_{22} = \lambda_{33} &= 0.823\pi\rho a^2, \quad \text{if } n = 5,\\
\lambda_{22} = \lambda_{33} &= 0.867\pi\rho a^2, \quad \text{if } n = 6.
\end{aligned}$$

2.2.11 Zhukowskiy's Foil Profile

The expressions for the added masses of the Zhukowskiy foil profile (Fig. 2.17) were derived by L. Sedov [206]:

$$\lambda_{11} = \frac{\pi\rho a^2}{4}\left(r^2 + R^2 - 2\cos 2\alpha\right); \qquad \lambda_{22} = \frac{\pi\rho a^2}{4}\left(r^2 + R^2 + 2\cos 2\alpha\right);$$

$$\lambda_{12} = \frac{\pi\rho a^2}{2}\sin 2\alpha; \qquad \lambda_{16} = \frac{\pi\rho a^3}{8}\left[r^2 + R^2 + 4(r+R)\cos\alpha\right]\sin\alpha;$$

$$\lambda_{26} = \frac{\rho\pi a^3}{8}\left[r^3 + R^3 + \left(r^2 + R^2\right)\cos\alpha + 2(r+R)\cos 2\alpha\right];$$

$$\lambda_{66} = \frac{\rho\pi a^4}{8}\left(8r^2R^2\cos^4\alpha - 2rR\sin^2 2\alpha + \cos 4\alpha\right)r^2R^2, \tag{2.12}$$

where the parameters a, α, R, r of the formulas can be approximately expressed via the geometrical characteristics of the given profile [110]: the value of the chord c,

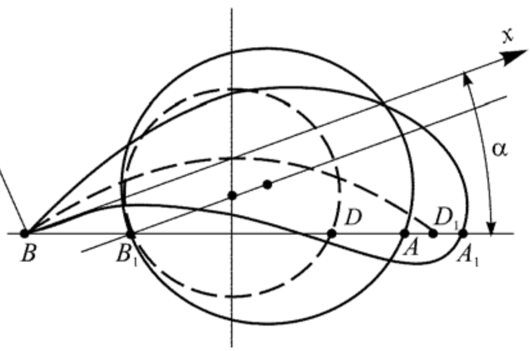

Fig. 2.17 Foil profile of Zhukowskiy

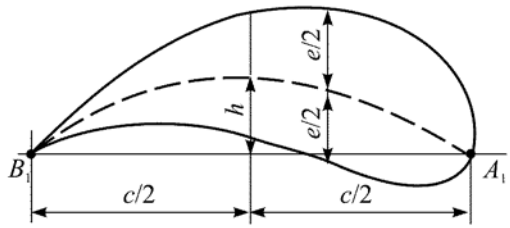

Fig. 2.18 Characteristic dimensions of foil profile of N.E. Zhukowskiy

the maximal thickness of the profile e_m and the height of the arch h (Fig. 2.18):

$$\mu = 0.77\frac{e_m}{c - 0.6e_m}; \qquad a = \frac{c}{2(1+\mu^2)};$$
$$R = \frac{1+\mu}{\cos\alpha}; \qquad r = \frac{1+\mu}{\cos\alpha(1+2\mu)}; \qquad \tan\alpha = \frac{2h}{c}\left(1+\mu^2\right).$$

The chord c of the profile is determined by the length of the interval A_1B_1 connecting the profile back edge with the frontal point A_1 posed at maximal distance from the back edge. The local thickness of the profile e, the skeleton line position (dotted line on the figure), and the arch height h are defined by the scheme shown in Fig. 2.18. For convenience we show in Figs. 2.19–2.23 the graphs obtained by using

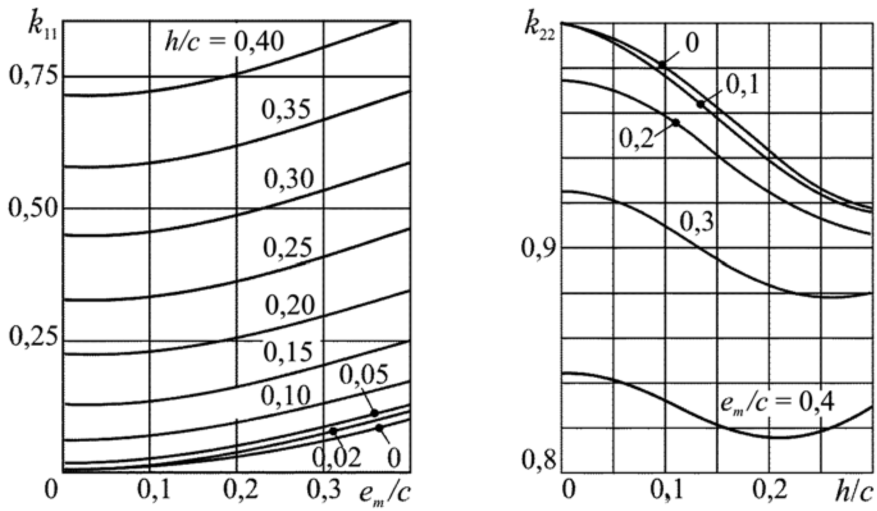

Fig. 2.19 Coefficients of added masses k_{11} and k_{22} of foil profile of Zhukowskiy

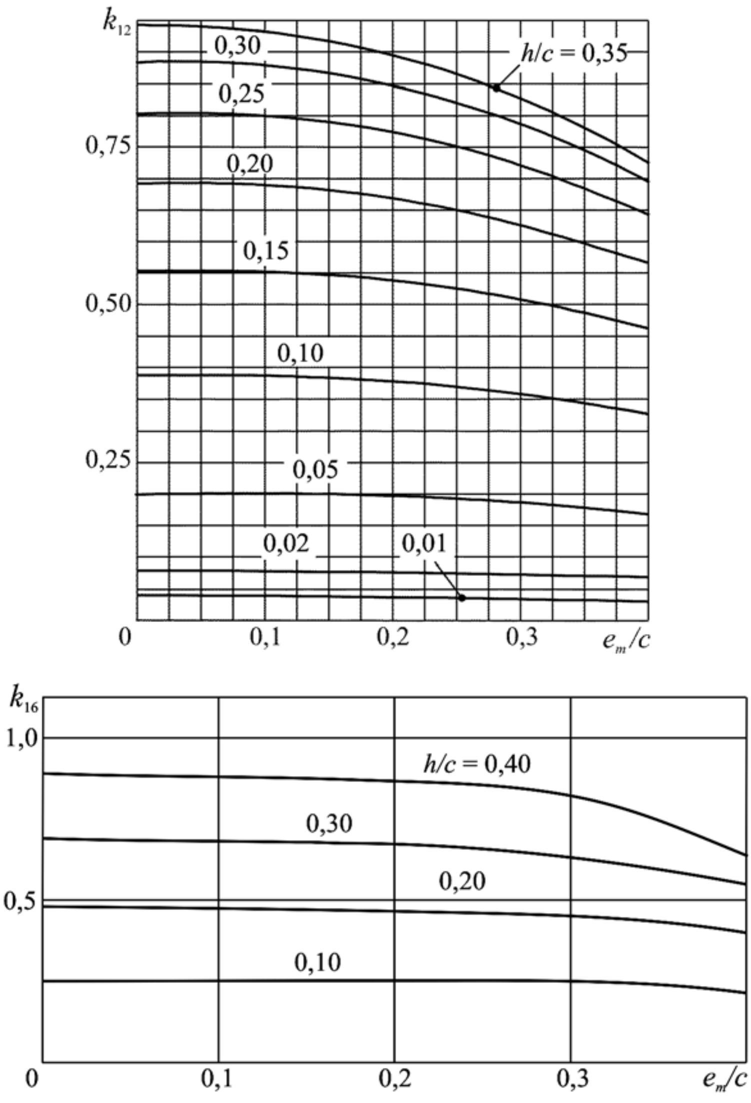

Fig. 2.20 Coefficients of added masses k_{12} (*above*) and k_{16} of Zhukowskiy's foil profile

the expressions (2.12).

$$k_{11}\left(\frac{h}{c}, \frac{e_m}{c}\right) := \frac{4\lambda_{11}}{\rho\pi c^2}; \qquad k_{22}\left(\frac{h}{c}, \frac{e_m}{c}\right) := \frac{4\lambda_{22}}{\rho\pi c^2}; \qquad k_{12}\left(\frac{h}{c}, \frac{e_m}{c}\right) := \frac{8\lambda_{12}}{\rho\pi c^2};$$

$$k_{16}\left(\frac{h}{c}, \frac{e_m}{c}\right) := \frac{8\lambda_{16}}{\rho\pi c^3}; \qquad k_{26}\left(\frac{h}{c}, \frac{e_m}{c}\right) := \frac{8\lambda_{26}}{\rho\pi c^3}; \qquad k_{66}\left(\frac{h}{c}, \frac{e_m}{c}\right) := \frac{16\lambda_{66}}{\rho\pi c^4};$$

$$\tan\alpha = \tan\alpha\big[(h/c, e_m/c)\big]; \qquad \mu = \mu\left(\frac{e_m}{c}\right).$$

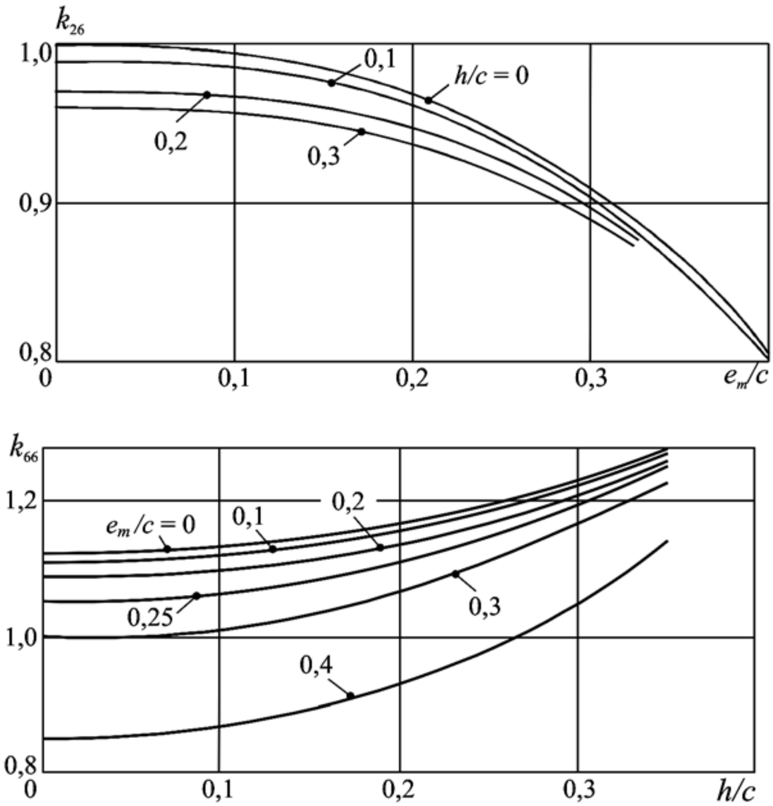

Fig. 2.21 Coefficients of added masses k_{26} (*above*) and k_{66} of Zhukowskiy's foil profile

We stress here that the coordinate system xy has its origin at the back edge of the profile, and the axis x has the angle α with the chord of the profile A_1B_1 (Fig. 2.17).

2.2.12 Arch of the Circle under Different Positions of Coordinate Axes

The added masses of the arch of a circle under various choices of coordinate system (Fig. 2.24) are given by the formulas [206]:

$$\lambda_{11} = \frac{\rho\pi a^2}{2}\tan^2\alpha; \qquad \lambda_{22} = \frac{\rho\pi a^2}{2}\left(1 + \frac{1}{\cos^2\alpha}\right); \qquad \lambda_{12} = \lambda_{26} = 0.$$

If the origin is located at the middle of the arch as shown in Fig. 2.24a, then

$$\lambda_{16} = \frac{\rho\pi a^3}{4}\frac{\sin\alpha}{\cos^3\alpha}, \qquad \lambda_{66} = \frac{\rho\pi a^4}{8}\frac{1}{\cos^4\alpha}.$$

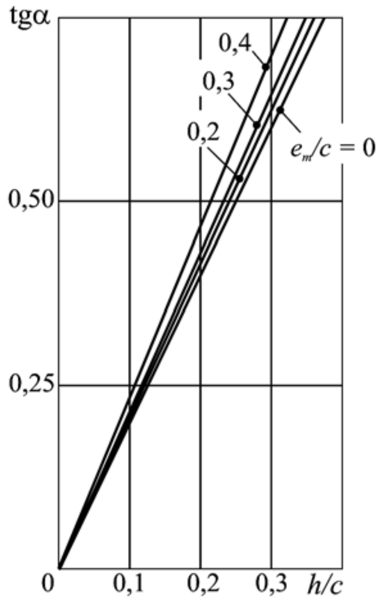

Fig. 2.22 Relation between the angle of (zero) lifting force with thickness and height of the arch of a Zhukowskiy profile

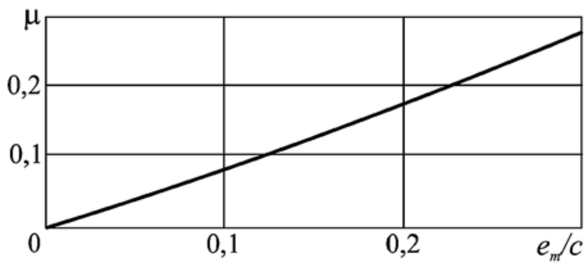

Fig. 2.23 Relation between the parameter μ and the relative width of Zhukowskiy's foil profile

If the origin coincides with the center of the circle as shown in Fig. 2.24b, then $\lambda_{16} = \lambda_{66} = 0$.

2.2.13 Lense Formed by Two Circular Arches

The added masses of the lens formed by two circular arches of radius R are given by [183]:

$$\lambda_{11} = \rho R^2 \left[\sin 2\beta - \frac{2\beta}{180}\pi + 2\pi \sin^2\beta \, \frac{\frac{\beta}{180}(2 - \frac{\beta}{180})}{3(1 - \frac{\beta}{180})^2} \right];$$

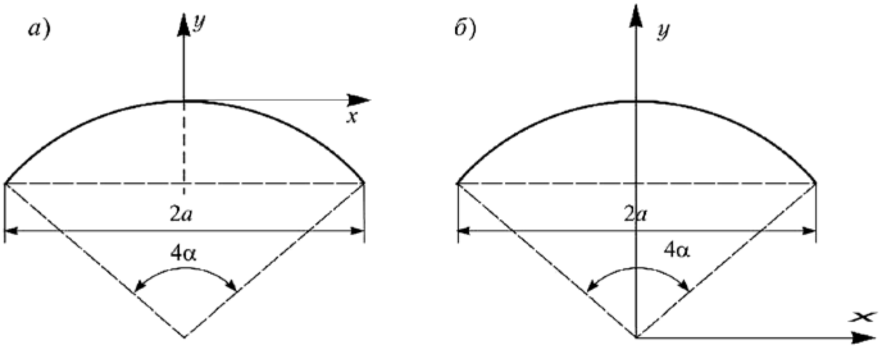

Fig. 2.24 Choice of coordinate axes for the arch of the circle

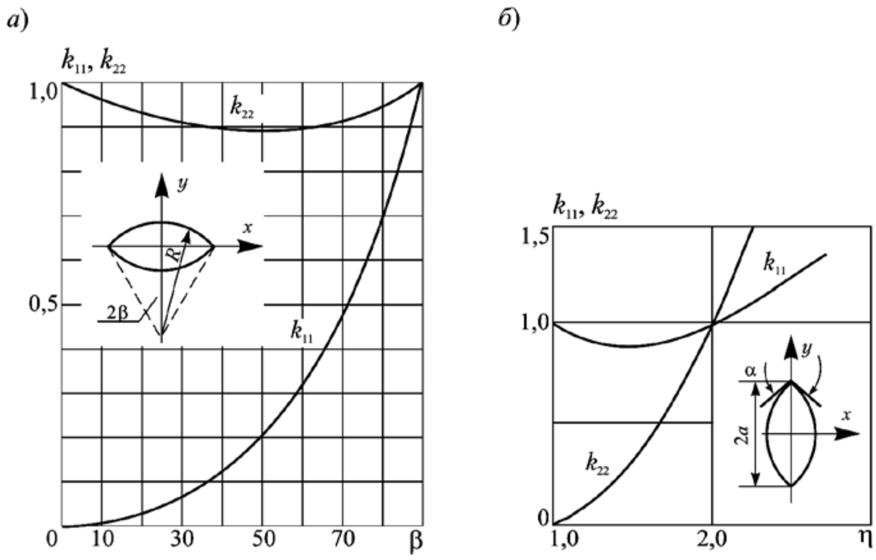

Fig. 2.25 Added masses of the lens formed by two circular arches

$$\lambda_{22} = \rho R^2 \left[\sin 2\beta - \frac{2\beta}{180}\pi + 2\pi \sin^2\beta \frac{3 - 4\frac{\beta}{180} + 2(\frac{\beta}{180})^2}{3(1 - \frac{\beta}{180})^2} \right],$$

where 2β is the central angle of the arches thus formed (in degrees). The coefficients $k_{11} = \lambda_{11}/(\rho\pi R^2 \sin^2\beta)$, $k_{22} = \lambda_{22}/(\rho\pi\ R^2 \sin^2\beta)$ can be found from Fig. 2.25a.

These results are generalized in the work [80]. The dependence of coefficients k_{11} and k_{22} on η is shown in Fig. 2.25b (where $k_{11} = \lambda_{11}/\pi\rho a^2$; $k_{22} = \lambda_{22}/\pi\rho a^2$; $\alpha = 2\pi/\eta$).

2.2.14 Hexagon, Rectangle, Rhomb, Octagon, Square with Four Ribs

The formulas for the added masses of hexagon (derived by Sokolov), rhomb and rectangle (Fig. 2.26) are presented in the works [183, 206].

The graphs for coefficient $k_{11} = \lambda_{11}/(\rho\pi b^2)$ as a function of d/b for the cases of a hexagon (for various angles β), a rectangular (curve I) and a rhomb (curve II) are shown in Fig. 2.26.

Let us consider the flow around two rhombs located next to each other in such a way that they touch each other at a corner and their orientation is the same. Then in the flow orthogonal to the line connecting centers of the rhombs, the values λ_{11} for the added mass of each rhomb in this system is 1.55 times higher in comparison with its added mass in an infinite fluid [177]. The added moments of inertia of a rectangle are computed in the work [246]. Dependence of coefficient $k_{66} = 8\lambda_{66}/\rho\pi b^4$ on the ratio a/b of the sides of the rectangle under rotation of the rectangle around the central point are shown in Fig. 2.27.

Under the rotation of a regular hexagon around the central point, its added moment of inertia is defined by approximate formula [246] $\lambda_{66} = 0.055\pi\rho a^4$, where $2a$ is the distance between the parallel opposite edges of the hexagon. The values for the added mass $\lambda_{11} = k_{11}\pi\rho a^2$ and the added moment of inertia $\lambda_{66} = k_{66}(\pi/8)\rho a^4$ of the square with the side $2a$ and four ribs of length d are presented in Fig. 2.28 as functions of the ratio d/a. The square is assumed to rotate around its central point.

2.2.15 Plate with Flap

The added masses of a plate with a flap are of particular practical interest, since such contour gives a good approximation to a flow around thin wing profiles with flaps of various relative length.

This scheme is also applied to determine the hydrodynamic characteristics of a system of two ships moving along a curved trajectory [177].

The added masses of the plate L_1 with flap of length L_2 located at an angle $\delta = \pi/2k$ to the main plate are calculated in [177] using Sedov's method. The exterior of the plate with a flap is mapped on the unit disc by a Christoffel–Schwarz integral. The values for the added masses are then calculated by formulas (2.2)–(2.7).

The coefficients of added masses $k_{11} = 4\lambda_{11}/(\pi\rho L_1^2)$; $k_{22} = 4\lambda_{22}/(\pi\rho L_1^2)$; $k_{12} = 4\lambda_{12}/(\pi\rho L_1^2)$; $k_{66} = 16\lambda_{66}/(\pi\rho L_1^4)$; $k_{16} = 8\lambda_{16}/(\pi\rho L_1^3)$; $k_{26} = 8\lambda_{26}/(\pi\rho L_1^3)$ as functions of the ratio L_1/L_2 are shown in Figs. 2.29–2.31. Parameter k shown in these figures is related to the angle between the plate and the flap by $\delta = \pi/2k$. The value $k = \infty$ corresponds to $\delta = 0$.

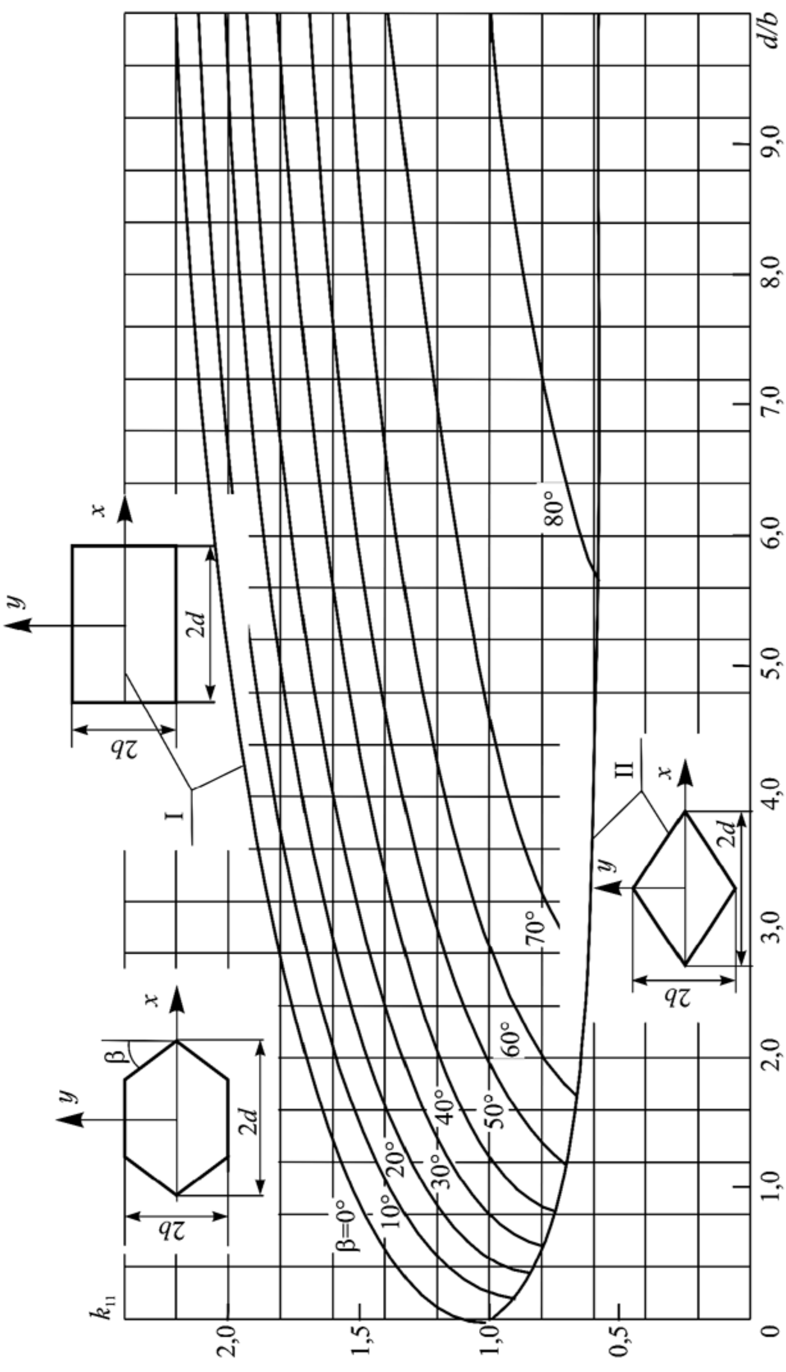

Fig. 2.26 Coefficients of added masses of *hexagon*, *rectangle* and *rhombus*

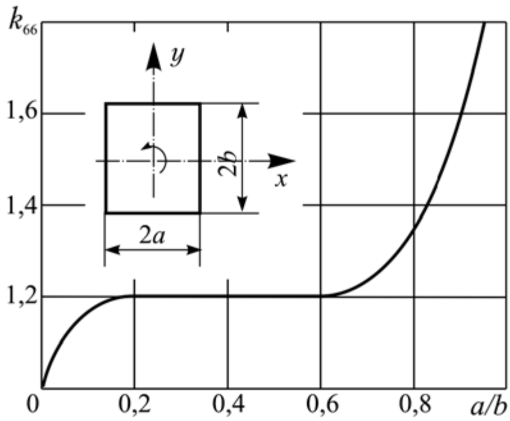

Fig. 2.27 Added moment of inertia of a *rectangle*

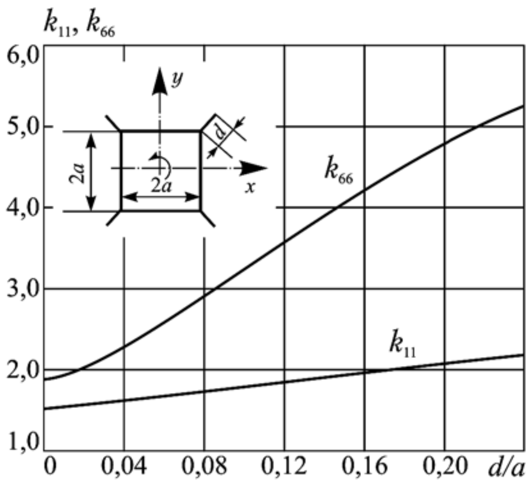

Fig. 2.28 Coefficients of added masses of *square* with ribs

2.3 Added Masses of Lattices

2.3.1 Two Plates Located on One Line

Formulas for the added masses of two intervals (plates) of lengths l_1 and l_2 located on the same line at distance d (Fig. 2.32) have the following form [183, 206]:

$$\lambda_{22} = \frac{\rho\pi}{4}\left(l_1^2 + l_2^2\right)\mu(p, q);$$

$$\lambda_{26} = \frac{\rho\pi}{16}(2p + q + 1)\left(q^2 - 1\right)l_1^3;$$

$$\lambda_{66} = \frac{\rho\pi}{64}\left[\frac{1}{2}\left(q^2 - 1\right)^2 + (2p + q + 1)^2\left(q^2 + 1\right)\right]l_1^4,$$

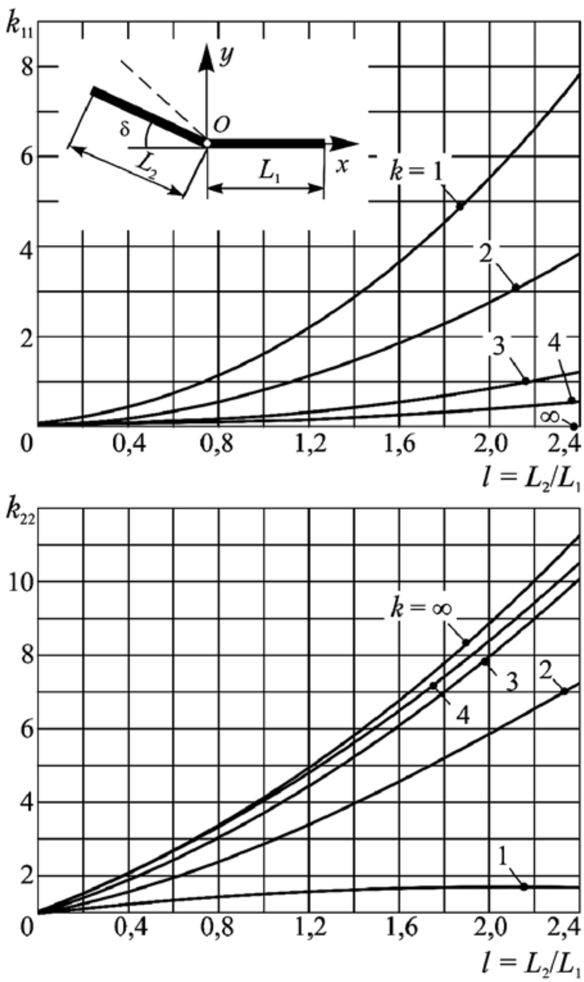

Fig. 2.29 Coefficients of added masses of a plate with flap

where $p = d/l_1$, $q = l_2/l_1$; the values for the coefficient $\mu(p,q) = \mu(p/q, 1/q)$ shown in Fig. 2.32 are defined via complete elliptic integrals of the first and second kind $F(k)$, $E(k)$:

$$\mu(p,q) = \frac{(1+2p+q)^2 - 4\frac{E(k)}{F(k)}(1+p)(p+q)}{1+q^2};$$

$$k^2 = \frac{q}{(1+p)(p+q)}.$$

In the computation of λ_{26}, λ_{66} we assumed that the origin is chosen to lie at an equal distance from the centers of the plates.

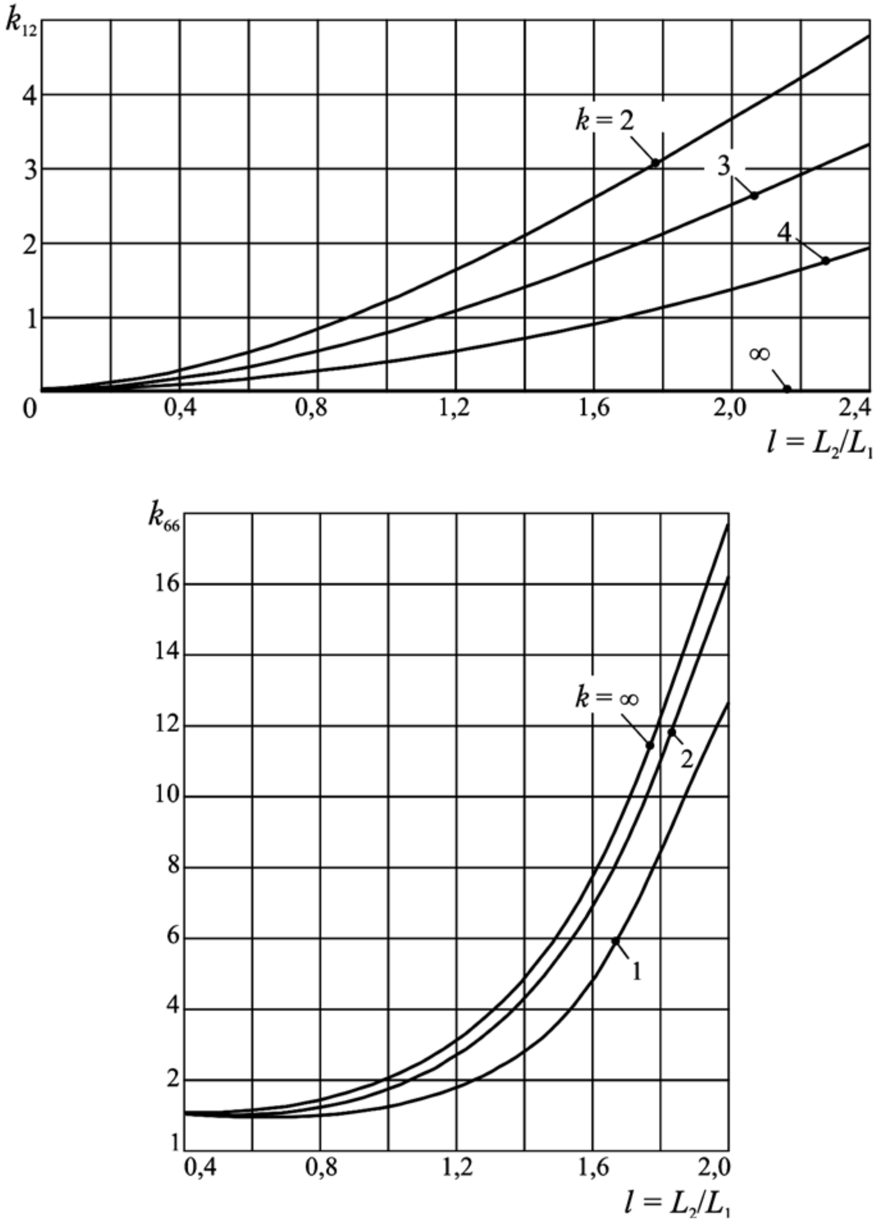

Fig. 2.30 Coefficients of added masses of a plate with flap

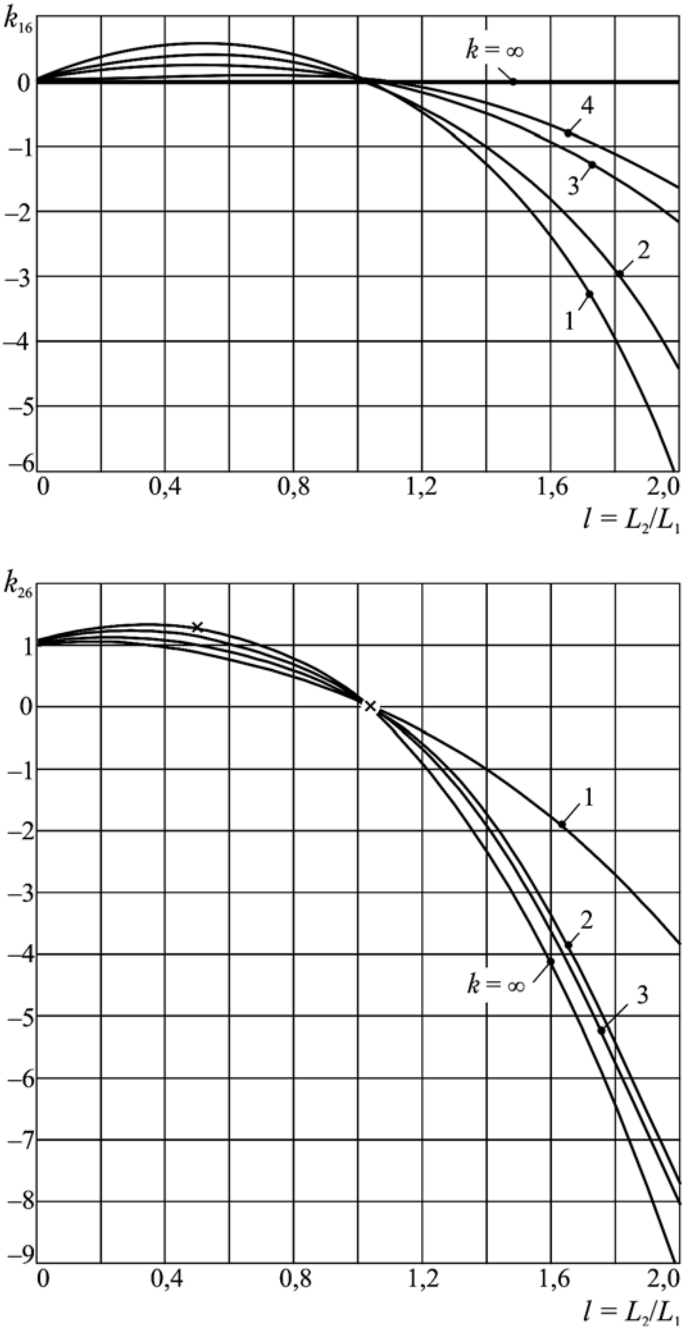

Fig. 2.31 Coefficients of added masses of a plate with flap

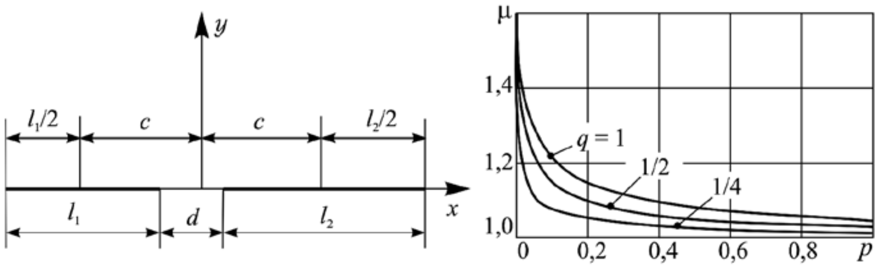

Fig. 2.32 Values of functions $\mu(p, q)$: $\mu(0, 1) = 2$; $\mu(0, 1/2) = 1.8$; $\mu(0, 1/4) = 1.46$

2.3.2 Three Plates Located on One Line

Formulas for the added masses of three plates symmetrically located on one line (Fig. 2.33) look as follows[1]:

$$\lambda_{22} = 2\pi\rho\left[\frac{1}{2}\left(c^2 + b^2 - a^2\right) - \left(c^2 - a^2\right)\frac{E(k)}{F(k)}\right];$$

$$\lambda_{66} = \frac{\pi\rho}{8}\left[\left(c^2 + b^2 - a^2\right)^2 - 4b^2\left(c^2 - a^2\right)\frac{E(k_1)}{F(k_1)}\right].$$

Here E, F are complete elliptic integrals of the first and second kind;

$$k^2 = \frac{c^2 - b^2}{c^2 - a^2}, \qquad k_1^2 = \frac{a^2(c^2 - b^2)}{b^2(c^2 - a^2)}.$$

The lengths of the plates are given by: $l_1 = 2a$, $l_2 = l_3 = c - b$. The gap between

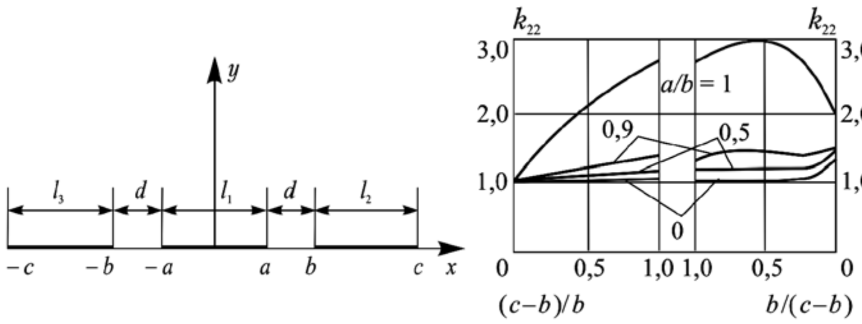

Fig. 2.33 Coefficients of added masses of three plates

[1]These formulas were derived by V.F. Shushpalov, see [183].

the plates equals $d = b - a$. The expressions for λ_{22} looks as follows:

$$\lambda_{22} = k_{22}\rho\pi\left[a^2 + \frac{(c-b)^2}{2}\right],$$

where dependence of k_{22} on a/b, $(c-b)/b$ for $(c-b)/b < 1$, or $b/(c-b)$ for $(c-b)/b > 1$ are shown in Fig. 2.33.

2.3.3 Lattice of Plates

Consider the lattice of parallel plates of width d (from a two-dimensional perspective these are intervals of length d). The axis of the lattice is assumed to have an inclination β to the plane of the plates. The interval between the plates calculated along the axis of the lattice is denoted by l (Fig. 2.34).

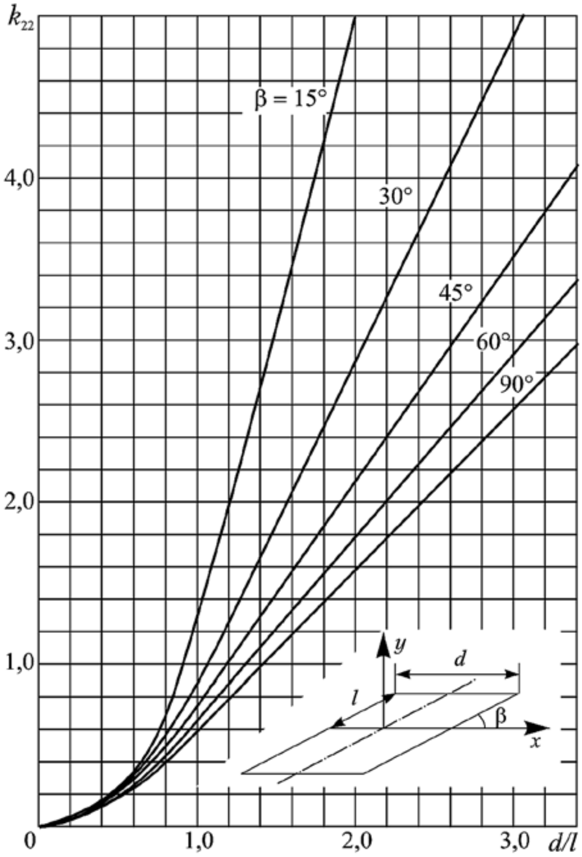

Fig. 2.34 Coefficients of added masses of a plate lattice

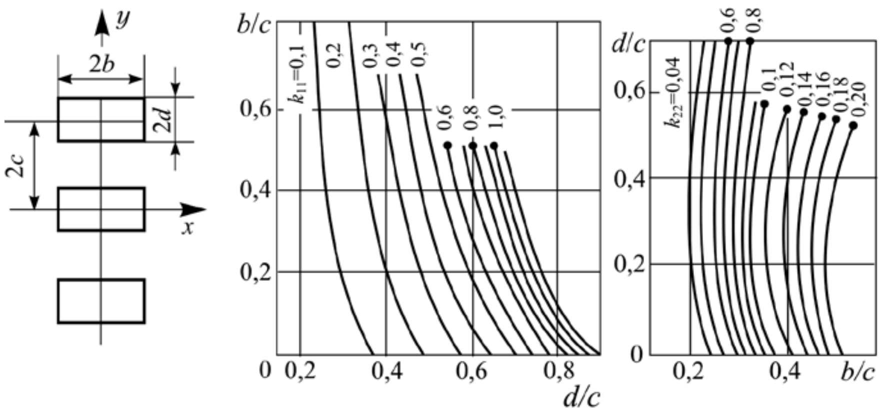

Fig. 2.35 Coefficients of added masses of a lattice of *rectangles*

Dependence of coefficient $k_{22} = \lambda_{22}/pl^2$ on parameters β and d/l is presented in Fig. 2.34. If the lattice consists of intervals lying on one line (lattice of horizontal plates), then $\beta = 0$ and

$$k_{22} = -\frac{2}{\pi} \ln \cos \frac{\pi d}{2l}.$$

If $\beta = \pi/2$ (vertical lattice of parallel plates) then

$$k_{22} = \frac{2}{\pi} \ln \cosh \frac{\pi d}{2l}.$$

2.3.4 Lattice of Rectangles

Consider the lattice with interval $2c$ of rectangles of width $2b$ and height $2d$ (Fig. 2.35). The added masses of each rectangle were computed in [91]. The values for coefficients $k_{11} = \lambda_{11}/(4\rho c^2)$, $k_{22} = \lambda_{22}/(4\rho c^2)$ as functions of b/c and d/c are shown in Fig. 2.35.

2.4 Added Masses of a Duplicated Shipframe Contour Moving in Unlimited Fluid

Let us briefly describe the method of computing of the added masses in this case. The description of motion of a two-dimensional contour in an ideal incompressible two-dimensional fluid reduces to computation of the complex potential of the planar flow $w(\tau) = \varphi(y,z) + i\psi(y,z)$ [116]. Knowing the potential $w(\tau)$ one can find the components of velocity v_y, v_z in the whole plane of $\tau = y + iz$. Then, using the

Cauchy–Lagrange formula one can determine the pressure at any point, including the points of the contour. To find the function $w(\tau)$ it is sufficient to find the current function $\psi(y, z)$; the function φ can be found from the Cauchy–Riemann equations $\partial\varphi/\partial y = \partial\psi/\partial z$; $\partial\varphi/\partial z = -\partial\psi/\partial y$.

The vortex-free condition leads to Laplace equation $\Delta\psi = 0$. The boundary conditions for this equation can be formulated as follows. If at infinity the fluid does not move, then $v_y = \partial\psi/\partial z = 0$ and $v_z = -\partial\psi/\partial y = 0$. On the contour we have the water-tightness condition

$$v_n = u_n, \tag{2.13}$$

where v_n is the normal component of velocity of fluid at the contour and u_n is the normal component of the velocity of the same point of the contour.

For v_n we have

$$\begin{aligned} v_n &= v_y \cos(n, y) + v_z \cos(n, z) = v_y \sin\alpha - v_z \cos\alpha \\ &= v_y \frac{dz}{ds} - v_z \frac{dy}{ds} = \frac{\partial\psi}{\partial z}\frac{dz}{ds} + \frac{\partial\psi}{\partial y}\frac{dy}{ds} = \frac{d\psi}{ds}, \end{aligned}$$

where α is the angle between the element ds of the current line and the axis $0y$ (Fig. 2.36). For u_n we get

$$u_n = u_y \sin\alpha - u_z \cos\alpha = (U_y - \omega z)\frac{dz}{ds} - (U_z + \omega y)\frac{dy}{ds},$$

where U_y, U_z are components of the velocity vector of the origin of the moving coordinate system yOz attached to the contour onto the axes Oy, Oz (we assume that for the moment of observation the stationary and non-stationary coordinate systems coincide); ω is the angular velocity of the contour rotation. Now condition (2.13) can be written down in a more detailed form:

$$\frac{d\psi}{ds} = (U_y - \omega z)\frac{dz}{ds} - (U_z + \omega y)\frac{dy}{ds}. \tag{2.14}$$

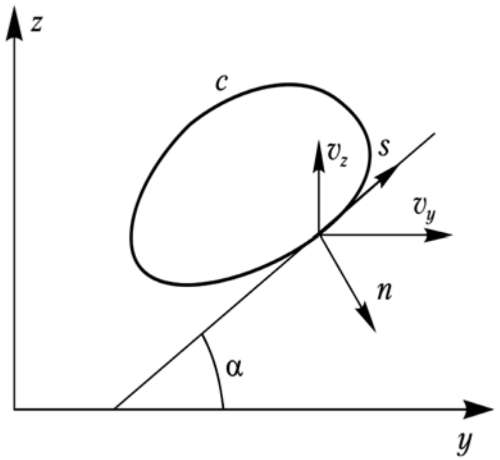

Fig. 2.36 System of coordinates

Using the formula (2.14) we get (up to an arbitrary additive constant) the condition

$$\psi = U_y z - U_z y - \frac{\omega}{2}\left(y^2 + z^2\right), \tag{2.15}$$

to be fulfilled on the contour. Taking into account (2.15) one represents the function $w(\tau)$ in the form

$$w(\tau) = U_y w_2(\tau) + U_z w_3(\tau) + \omega w_4(\tau),$$

where the functions $w_2(\tau)$, $w_3(\tau)$ and $w_4(\tau)$ are determined by geometric properties (i.e. the shape) of the contour only; these functions characterize the perturbed potential flow of the fluid under the motion of the contour with unit velocities along the axes Oy, Oz and under rotation, respectively. The functions $w_k(\tau) = \varphi_k(\tau) + i\psi_k(\tau)$ are regular outside of the contour and vanish at infinity. On the contour C their imaginary parts, according to (2.15), satisfy the conditions

$$\psi_2|_C = z; \qquad \psi_3|_C = -y; \qquad \psi_4|_C = -\frac{1}{2}\left(y^2 + z^2\right). \tag{2.16}$$

To find the potential of the fluid around contour C in the τ-plane it is sufficient to find the function

$$\tau = y + iz = f(\zeta), \tag{2.17}$$

which conformally maps the exterior of the contour to the exterior of the unit circle in the plane of $\zeta = \xi + i\eta$ [116, 127, 129, 130, 206], since the potential of the fluid flow around the circle is known.

The function $f(\zeta)$ can be in general represented as the following series:

$$f(\zeta) = k\zeta + k_0 + \frac{k_1}{\zeta} + \frac{k_2}{\zeta^2} + \cdots. \tag{2.18}$$

If the contour C (Fig. 2.37) is symmetric with respect to the z-axis, then the expansion (2.18) contains only terms of odd order.

Consider the following form of the function f [100]:

$$f(\zeta) \equiv y + iz := -\frac{iT}{1+p+q}\left(\zeta + p\zeta^{-1} + q\zeta^{-3}\right), \tag{2.19}$$

where the coefficients k, k_1, k_3 are replaced by the combinations of the value T (the waterdraft of the frame) and the parameters p, q. On the unit circle, $\zeta = e^{i\theta}$. By substituting this value into the formula (2.19) and separating the real and imaginary parts, we obtain the parametrical description of the contour C:

$$\begin{cases} y = T\dfrac{(1-p)\sin\theta - q\sin 3\theta}{1+p+q}; \\ z = -T\dfrac{(1+p)\cos\theta + q\cos 3\theta}{1+p+q}. \end{cases} \tag{2.20}$$

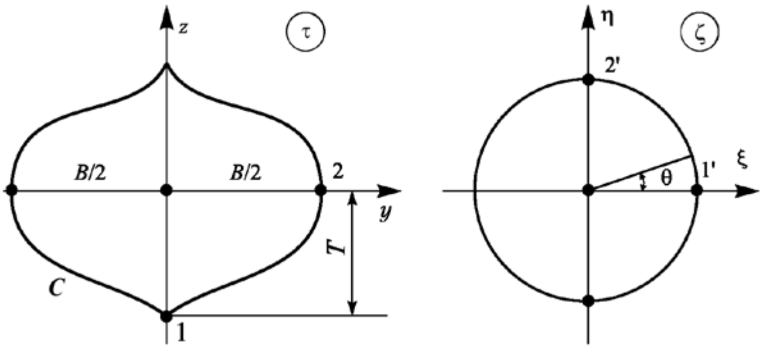

Fig. 2.37 Map of a duplicated shipframe to the unit circle

The chosen form of the function $f(\zeta)$ gives $z = -T$, $y = 0$ when $\theta = 0$. The second condition, $y = B/2$, $z = 0$ when $\theta = \pi/2$, gives one relation between the parameters p and q:

$$\frac{1+p+q}{1-p+q} = 2\frac{T}{B}.$$

By calculating the area bounded by the contour C: $S = 2\int_0^{B/2} z\,dy$, taking into account Eqs. (2.20) and using the usual notation $\beta = S/BT$ for the coefficient of the plumpness of the shipframe, we find the second relation between the parameters p and q:

$$\beta = \frac{\pi}{4}\frac{1-p^2-3q^2}{(1+p+q)^2}\frac{2T}{B}.$$

Therefore, for each pair of values β and $2T/B$ one can find corresponding values p and q, and draw a contour C in the τ-plane, using (2.20).

The tables for values p, q for $0.5 \le \beta \le 1$ and $0.2 \le 2T/B \le 10$ are given in the monograph by Huskind [100].

Let us turn to determining of the characteristic functions $w_k(\tau) = \varphi_k(\tau) + i\psi_k(\tau)$ ($k = 2, 3, 4$). Imaginary parts of these functions have to satisfy conditions (2.16) on the contour C; these conditions, taking into account (2.17), can be rewritten as

$$\Im w_2 = \Im\tau; \qquad \Im w_3 = -\Re\tau; \qquad \Im w_4 = -\frac{\tau\bar{\tau}}{2}. \tag{2.21}$$

On the basis of (2.19), (2.21) we can find the following relation for the function w_2:

$$\Im w_2 = \Im\left[-\frac{iT}{1+p+q}\left(\zeta + p\zeta^{-1} + q\zeta^{-3}\right)\right].$$

Taking into account that $\Im(i\zeta) = \Re\zeta$ and on the unit circle $\Re\zeta = \Re\zeta^{-1}$, we can rewrite the previous equation as

$$\Im w_2 = \Im\left\{-\frac{iT}{1+p+q}\big[(1+p)\zeta^{-1} + q\zeta^{-3}\big]\right\}.$$

Therefore, we have found the function ψ_2 which satisfies the water-tightness conditions on the contour and also the stationarity condition at infinity (when $\zeta \to \infty$). Now the function w_2 can be taken in the form

$$w_2 = -\frac{iT}{1+p+q}\big[(1+p)\zeta^{-1} + q\zeta^{-3}\big]. \tag{2.22}$$

Similar arguments lead (using the relation $\Im\zeta = -\Im\zeta^{-1}$ valid on the unit circle) to the formulas for w_3, w_4:

$$w_3 = -\frac{T}{1+p+q}\big[(p-1)\zeta^{-1} + q\zeta^{-3}\big], \tag{2.23}$$

$$w_4 = -\frac{iT^2}{(1+p+q)^2}\big[p(1+q)\zeta^{-2} + q\zeta^{-4}\big]. \tag{2.24}$$

In the right-hand side of (2.24) we omit an unessential constant. By separating in the expressions (2.22), (2.23), (2.24) the real and imaginary parts, we obtain φ_k, ψ_k ($k = 2, 3, 4$). By using the formulas for the added masses

$$\lambda_{ik} = -\rho\int_{C_1}\varphi_i\, d\psi_k,$$

where the integration is performed only over one half of the duplicated shipframe contour (in the plane of the fluid), which corresponds to integration from $-\pi/2$ to $\pi/2$ over θ in the ζ-plane, it is easy to find the dependence of the added masses on parameters determining the profile of the shipframe:

$$\lambda_{22} = \rho\frac{\pi T^2}{2}\frac{(1+p)^2 + 3q^2}{(1+p+q)^2} = \rho\frac{\pi T^2}{2}k_{22};$$

$$\lambda_{33} = \rho\frac{\pi B^2}{8}\frac{(1-p)^2 + 3q^2}{(1-p+q)^2} = \rho\frac{\pi B^2}{8}k_{33};$$

$$\lambda_{24} = \frac{\rho T^3}{2}\frac{1}{(1+p+q)^2}\left\{\frac{8}{3}p(1+p) + \frac{16}{35}q^2(20+7p)\right.$$
$$\left. + q\left[\frac{4}{3}(1+p)^2 - \frac{4}{5}(1-p)(7-5p)\right]\right\} = \frac{\rho T^3}{2}k_{24};$$

$$\lambda_{44} = \rho\frac{\pi B^4}{256}\frac{16[p^2(1+q)^2 + 2q^2]}{(1-p+q)^4} = \rho\frac{\pi B^4}{256}k_{44}.$$

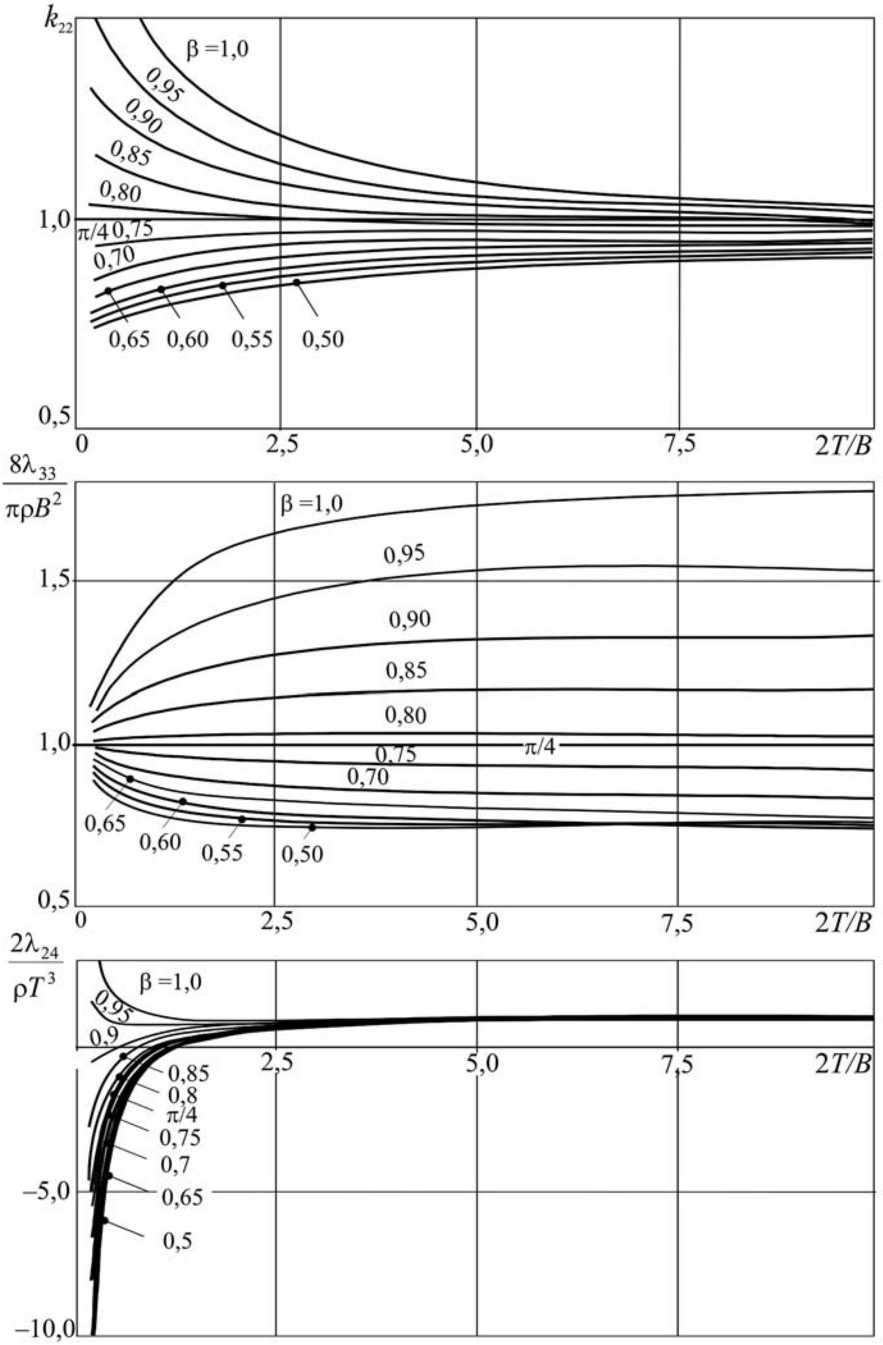

Fig. 2.38 Coefficients of added masses of shipframes determined via the method of a duplicated contour

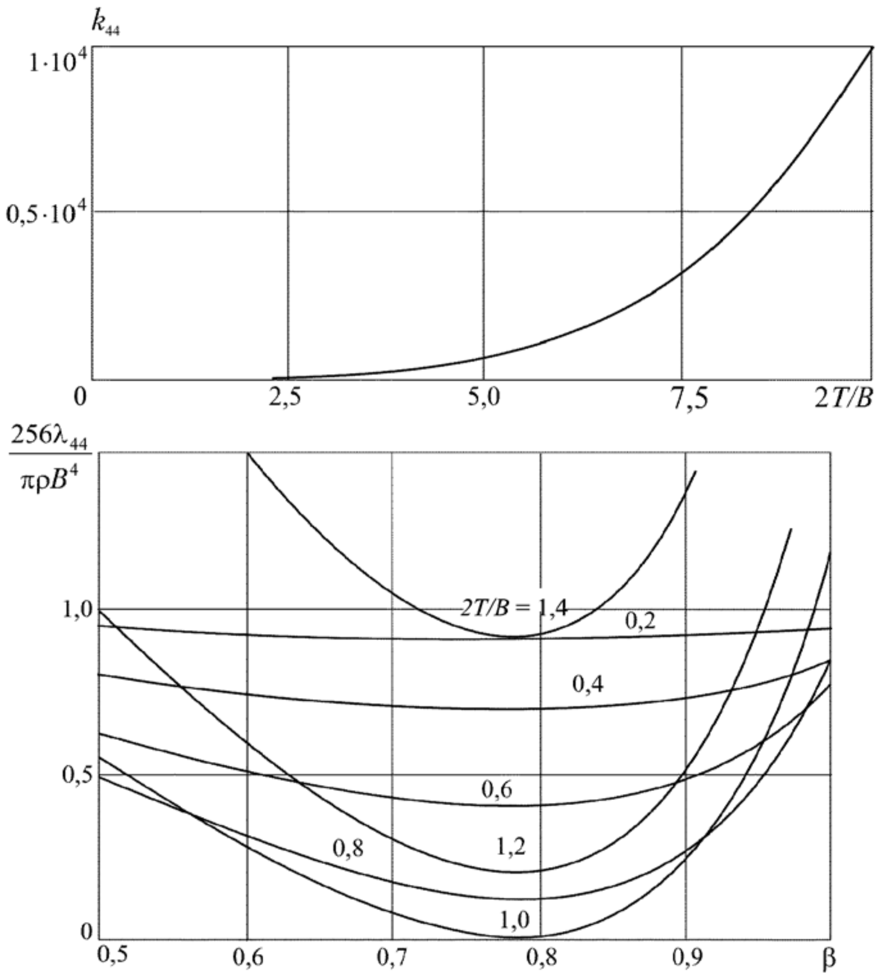

Fig. 2.39 Coefficients of added masses of shipframes determined via the method of a duplicated contour

The graphs of dependencies $k_{ij}(\beta, 2T/b)$ are presented in Figs. 2.38, 2.39.[2]

The profiles of shipframe corresponding to functions $f(\zeta)$ having three terms in their Laurent series are shown in Figs. 2.40–2.43 (these profiles were drawn by Dorofeuk [50]; for $B/2T = 0.2$; 0.4; 0.6; 0.8; 1; 1.2; 1.5; 2 these profiles were obtained by Lewis in [131]). Notice that dependence of Lewis shipframes on only two parameters $B/2T$ and β imposes certain restrictions on their applicability. In Fig. 2.44 we present a diagram showing the range of parameters where the Lewis form of the shipframe can be used in practice. In Table 2.3 for each profile we

[2]Similar graphs for the range $T/B \leq 1$ were found in the work [151].

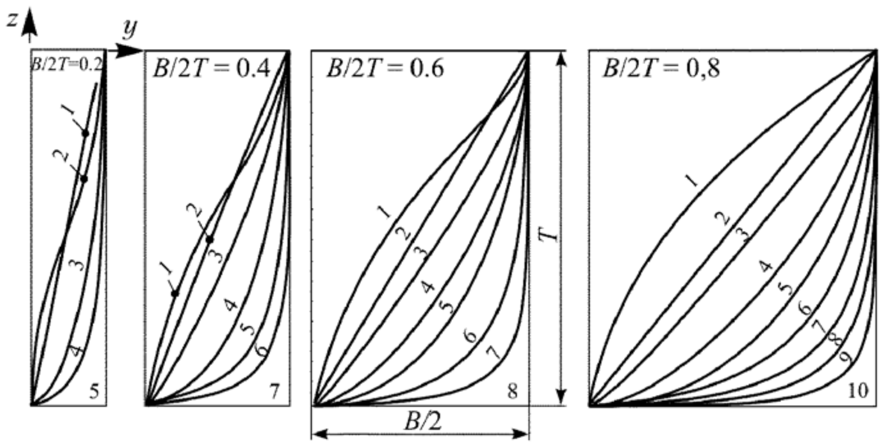

Fig. 2.40 Shape of a Lewis shipframe for different $B/2T$ and β

present corresponding values of β, $k_{22} = 2\lambda_{22}/(\pi\rho T^2)$ and $k_{33} = 8\lambda_{33}/(\pi\rho B^2)$. The last coefficient in the calculations of the ship oscillations is usually denoted by c_v. Indexes v and h correspond to the added masses in vertical and horizontal directions, respectively.

Dorofeuk calculated also several shipframe profiles and their inertial characteristics keeping six terms in the Laurent series of function $f(\zeta)$ (Fig. 2.45, Fig. 2.46, Table 2.4). In Tables 2.3 and 2.4 the values of k_{240} were computed taking into account the presence of free surface; in computation of other coefficients the presence of free surface is non-essential.

Besides the added masses of the "analytical" ships frames obtained on the basis of a function of the type (2.18), one is also interested in the added masses of the real shipframes. For two ships whose shipframes are shown in Fig. 2.47 and Fig. 2.48 the characteristics of these shipframes are given in Table 2.5 (they were found by Pavlov using the method of electro-hydrodynamic analogy (EHDA), see Chap. 9). The added masses of shipframes in the vertical direction can be found from the formula

$$\lambda_{33} = \frac{\pi\rho B^2}{8} k_{33}. \tag{2.25}$$

The added masses of shipframes in the horizontal direction (which are computed taking into account the presence of the free surface) can be found from the formula

$$\lambda_{220} = \frac{2\rho T^2}{\pi} k_{220}. \tag{2.26}$$

In the formulas (2.25), (2.26) B is the frame width on the water-line, T is the waterdraft of the frame. We notice the difference of the constant coefficients in the formulas (2.25) and (2.26).

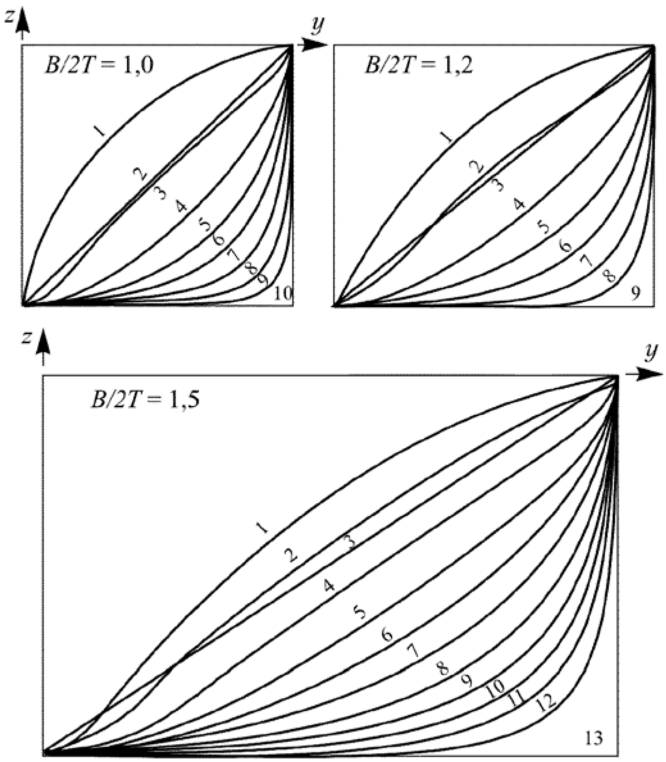

Fig. 2.41 Shape of a Lewis shipframe for different $B/2T$ and β

In practice it is convenient to use an approximate analytical representation of the coefficients

$$k_{33} = c_v = \frac{\lambda_{33}}{(\pi/2)\rho(B/2)^2} \quad \text{and} \quad k_{220} = c_h = \frac{\lambda_{220}}{(2/\pi)\rho T^2}$$

(see Fig. 2.49) in terms of characteristic dimensions of the frames. Possible inaccuracies arising from the use of this approximation can be corrected by use of computer simulation.

Now we present the formulas for k_{33} derived by Ivanuta and Boyanovsky [35]. Similar formulas for k_{220} are given in Chap. 5.

One can use the relation obtained in the work [128]

$$k_{33} = \frac{(1+k_1)^2 + \sum_{n=3}^{\infty} n k_n^2}{b_k^2},$$

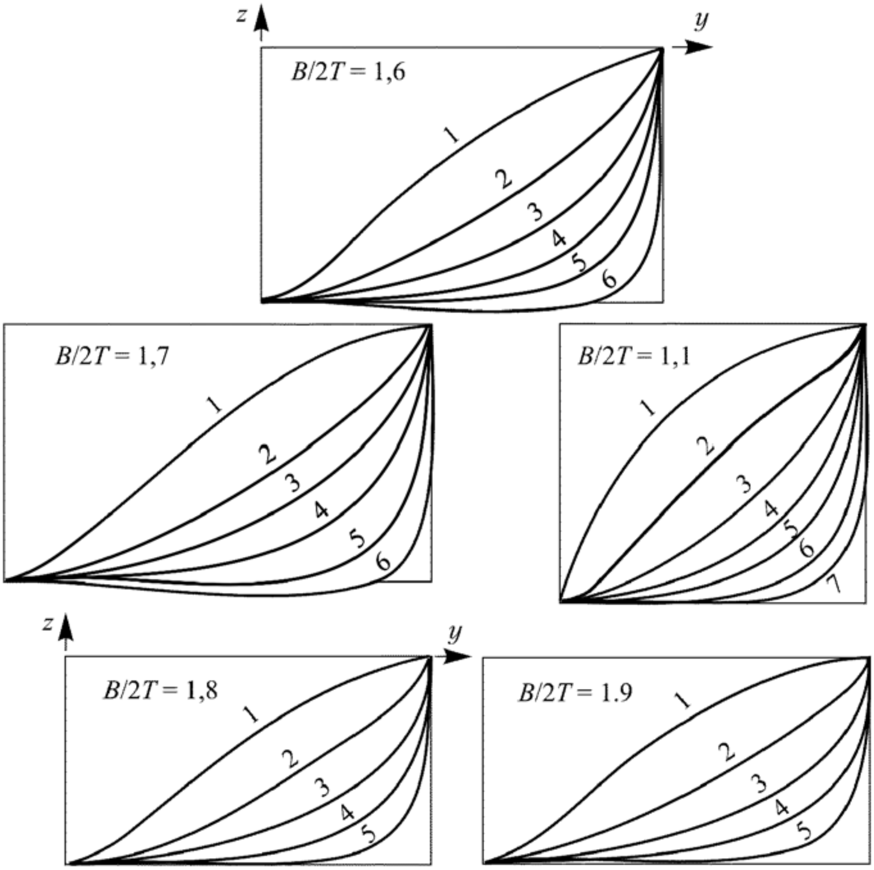

Fig. 2.42 Shape of a Lewis shipframe for different $B/2T$ and β

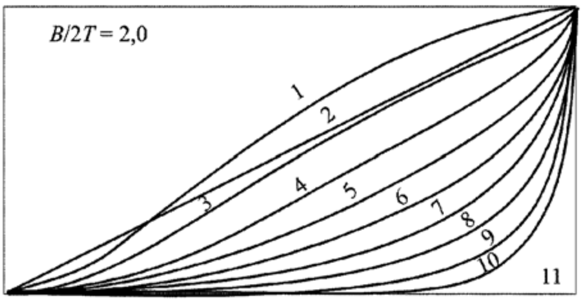

Fig. 2.43 Shape of a Lewis shipframe for different $B/2T$ and β

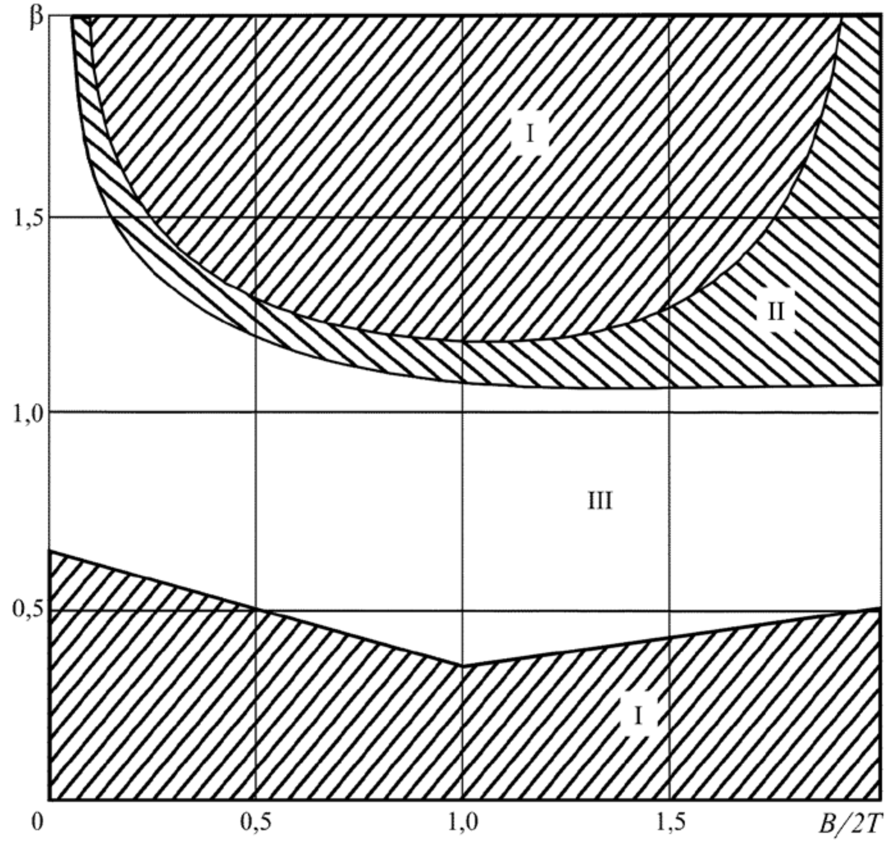

Fig. 2.44 Domains of applicability of a Lewis shipframe: *I*—Lewis shape of shipframe is not used; *II*—Lewis shape of shipframe is not recommended; *III*—Lewis shape of shipframe is recommended

Table 2.3 Coefficients of added masses of Lewis shipframes

$B/2T$	Cont. No.	β	k_{22}	$k_{220} = c_h$	$k_{33} = c_v$	$k_{44} = c_{\text{tor}}$	$k_{240} = c_{\text{incl}}$
0.2	1	0.500	–	–	0.611	–	–
	2	0.535	0.906	0.98	0.75	1.02	1.01
	3	0.785	1.00	1.00	1.00	1.00	1.00
	4	0.920	1.06	0.995	1.40	1.01	1.01
	5	1.000	–	–	1.98	–	–
0.3	1	0.505	0.87	1.03	0.75	1.08	1.02
	2	0.785	1.00	1.00	1.00	1.00	1.00
	3	0.925	1.10	1.11	1.40	1.04	1.04

(*continued on next page*)

Table 2.3 (continued)

$B/2T$	Cont. No.	β	k_{22}	$k_{220} = c_h$	$k_{33} = c_v$	$k_{44} = c_{\text{tor}}$	$k_{240} = c_{\text{incl}}$
0.4	1	0.470	0.84	1.05	0.75	1.16	1.06
	2	0.500	–	–	0.65	–	–
	3	0.630	0.91	1.01	0.80	1.05	1.00
	4	0.785	1.00	1.00	1.00	1.00	1.00
	5	–	–	–	1.20	–	–
	6	0.940	1.12	1.02	1.40	2.15	1.11
	7	1.00	–	–	1.76	–	–
0.5	1	0.440	0.80	1.08	0.75	1.35	1.09
	2	0.610	0.87	1.00	0.80	1.13	1.00
	3	0.785	1.00	1.00	1.00	1.00	1.00
	4	0.880	1.07	1.00	1.20	1.06	1.06
	5	0.945	1.10	1.04	1.40	1.23	1.15
0.6	1	0.410	0.79	1.12	0.75	1.69	1.15
	2	0.500	–	–	0.69	–	–
	3	0.615	0.87	1.03	0.80	1.24	1.0
	4	0.710	0.90	1.02	0.90	1.05	0.98
	5	0.785	1.00	1.00	1.00	1.00	1.00
	6	0.885	1.10	1.02	1.20	1.14	1.11
	7	0.955	1.2	1.05	1.40	1.53	1.27
	8	1.000	–	–	1.64	–	–
0.7	1	0.495	0.79	1.09	0.75	2.21	1.10
	2	0.595	0.84	1.04	0.80	1.63	1.02
	3	0.705	0.91	1.01	0.90	1.13	0.97
	4	0.785	1.00	1.00	1.00	1.00	1.00
	5	0.910	1.16	1.03	1.20	1.57	1.28
	6	0.960	1.25	1.06	1.40	2.24	1.50
0.8	1	0.350	0.76	1.22	0.75	5.85	1.47
	2	0.500	–	–	0.73	–	–
	3	0.565	0.82	1.07	0.80	2.95	1.02
	4	0.700	0.92	1.02	0.90	1.36	0.93
	5	0.785	1.00	1.00	1.00	1.00	1.00
	6	0.850	1.08	1.01	1.10	1.31	1.19
	7	0.895	1.14	1.02	1.20	1.98	1.37
	8	0.935	1.23	1.05	1.30	3.31	1.67
	9	0.970	1.25	1.07	1.40	4.80	1.94
	10	1.00	–	–	1.57	–	–

(*continued on next page*)

Table 2.3 (continued)

$B/2T$	Cont. No.	β	k_{22}	$k_{220} = c_h$	$k_{33} = c_v$	$k_{44} = c_{\text{tor}}$	$k_{240} = c_{\text{incl}}$
0.9	1	0.325	0.74	1.27	0.75	24.55	2.10
	2	0.550	0.79	1.08	0.80	10.24	1.04
	3	0.700	0.91	1.01	0.90	2.74	0.80
	4	0.785	1.00	1.00	1.00	1.00	1.00
	5	0.860	1.05	1.01	1.10	2.94	1.53
	6	0.900	1.15	1.03	1.20	6.28	1.96
	7	0.945	1.26	1.06	1.30	12.9	2.68
	8	0.980	1.36	1.10	1.40	21.0	3.45
1.0	1	0.295	0.74	1.33	0.75	0.035	−0.011
	2	0.500	–	–	0.76	–	–
	3	0.540	0.80	1.10	0.80	0.014	−0.0002
	4	0.690	0.90	1.02	0.90	0.003	0.002
	5	0.785	1.00	1.00	1.00	0	0
	6	0.850	1.08	1.01	1.10	0.002	−0.004
	7	0.910	1.20	1.04	1.20	0.005	−0.010
	8	0.950	1.29	1.08	1.30	−0.008	−0.017
	9	0.990	1.38	1.12	1.40	0.011	−0.026
	10	1.000	–	–	1.51	–	–
1.1	1	0.265	0.74	1.40	0.75	34.00	−0.475
	2	0.520	0.76	1.12	0.80	14.70	0.98
	3	0.680	0.84	1.02	0.90	3.79	1.30
	4	0.785	1.00	1.00	1.00	1.00	1.00
	5	0.850	1.06	1.01	1.10	3.12	0.40
	6	0.910	1.18	1.05	1.20	9.60	−0.49
	7	0.955	1.26	1.09	1.30	18.20	−1.41
1.2	1	–	–	–	0.76	–	–
	2	0.510	0.64	1.14	0.80	4.98	1.00
	3	0.500	–	–	0.78	–	–
	4	0.680	0.92	1.03	0.90	1.83	1.16
	5	0.785	1.00	1.00	1.00	1.00	1.00
	6	0.860	1.16	1.01	1.10	1.64	0.64
	7	0.920	1.31	1.05	1.20	3.50	0.13
	8	0.960	1.43	1.11	1.30	6.23	-0.45
	9	1.00	–	–	1.47	–	–
1.3	1	0.500	0.80	1.17	0.80	3.03	1.00
	2	0.675	0.88	1.03	0.90	1.43	1.14
	3	0.785	1.00	1.00	1.00	1.00	1.00

(*continued on next page*)

Table 2.3 (continued)

$B/2T$	Cont. No.	β	k_{22}	$k_{220} = c_h$	$k_{33} = c_v$	$k_{44} = c_{\text{tor}}$	$k_{240} = c_{\text{incl}}$
	4	0.860	1.12	1.02	1.10	1.35	0.72
	5	0.920	1.27	1.07	1.20	2.24	0.34
	6	0.970	1.42	1.13	1.30	3.80	-0.17
1.4	1	0.480	0.75	1.20	0.80	2.32	1.02
	2	0.675	0.87	1.03	0.90	1.27	1.12
	3	0.785	1.00	1.00	1.00	1.00	1.00
	4	0.870	1.14	1.02	1.10	1.23	0.77
	5	0.930	1.29	1.07	1.20	1.87	0.41
	6	0.975	1.43	1.15	1.30	2.88	-0.01
1.5	1	–	–	–	0.78	–	–
	2	0.470	0.78	1.24	0.80	1.96	1.02
	3	0.500	–	–	0.81	–	–
	4	–	–	–	0.85	–	–
	5	0.665	0.87	1.07	0.90	1.21	1.11
	6	–	–	–	0.95	–	–
	7	0.785	1.00	1.00	1.00	1.00	1.00
	8	–	–	–	1.05	–	–
	9	0.875	1.17	1.03	1.10	1.18	0.77
	10	–	–	–	1.15	–	–
	11	0.930	1.28	1.08	1.20	1.62	0.47
	12	0.985	1.49	1.19	1.25	2.40	0.07
	13	1.000	–	–	1.42	–	–
1.6	1	0.455	0.74	1.26	0.80	1.75	1.02
	2	0.660	0.84	1.04	0.90	1.16	1.11
	3	0.785	1.00	1.00	1.00	1.00	1.00
	4	0.870	1.14	1.03	1.10	1.12	0.89
	5	0.940	1.34	1.09	1.20	1.49	0.50
	6	0.990	1.50	1.18	1.30	2.04	0.03
1.7	1	0.440	0.73	1.30	0.80	1.62	1.02
	2	0.655	0.81	1.05	0.90	1.13	1.10
	3	0.785	1.00	1.00	1.00	1.00	1.00
	4	0.880	1.14	1.04	1.10	1.12	0.79
	5	0.940	1.32	1.10	1.20	1.39	0.53
	6	1.01	1.59	1.23	1.30	1.96	0.11

(*continued on next page*)

Table 2.3 (continued)

$B/2T$	Cont. No.	β	k_{22}	$k_{220} = c_h$	$k_{33} = c_v$	$k_{44} = c_{tor}$	$k_{240} = c_{incl}$
1.8	1	0.425	0.75	1.33	0.80	1.53	1.02
	2	0.650	0.86	1.05	0.90	1.11	1.10
	3	0.785	1.00	1.00	1.00	1.00	1.00
	4	0.875	1.20	1.03	1.10	1.08	0.80
	5	0.955	1.43	1.14	1.20	1.41	0.47
1.9	1	0.410	0.84	1.35	0.80	1.45	1.05
	2	0.645	0.93	1.06	0.90	1.10	1.11
	3	0.785	1.00	1.00	1.00	1.00	1.00
	4	0.885	1.35	1.04	1.10	1.08	0.80
	5	0.965	1.58	1.15	1.20	1.37	0.50
2.0	1	0.400	0.63	1.41	0.81	1.48	1.03
	2	0.500	–	–	0.84	–	–
	3	–	–	–	0.85	–	–
	4	0.640	0.85	1.06	0.90	1.09	1.11
	5	–	–	–	0.95	–	–
	6	0.785	1.00	1.00	1.00	1.00	1.00
	7	–	–	–	1.05	–	–
	8	0.885	1.24	1.04	1.10	1.07	0.81
	9	–	–	–	1.15	–	–
	10	0.960	1.45	1.15	1.20	1.27	0.54
	11	1.000	–	–	1.36	–	–

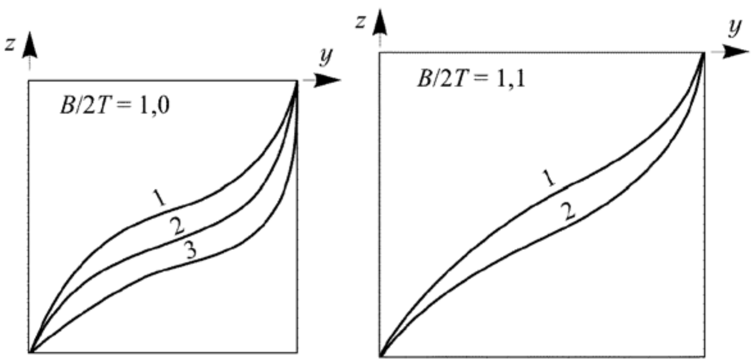

Fig. 2.45 Shape of a Lewis shipframe if six terms of function f are non-trivial

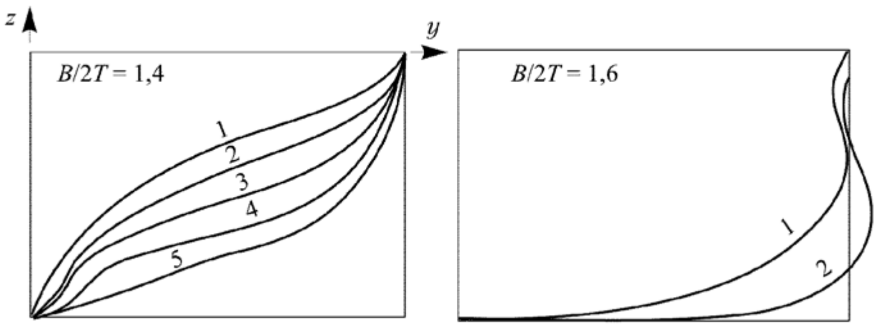

Fig. 2.46 Shape of a Lewis shipframe if six terms of function f are non-trivial

Table 2.4 Inertial characteristics of shipframe profiles

$B/2T$	Cont. No.	β	$k_{220} = c_h$	$k_{33} = c_v$	$k_{44} = c_{\text{tor}}$	$k_{240} = c_{\text{incl}}$
1	1	0.505	0.94	0.925	0.020	0.430
	2	0.610	0.83	1.02	0.012	0.474
	3	0.695	0.80	1.09	0.008	0.522
1.1	1	0.510	0.99	0.875	16.5	1.11
	2	0.605	0.90	0.915	8.97	1.43
1.4	1	0.400	1.07	0.88	3.35	0.87
	2	0.490	0.97	0.91	2.16	0.09
	3	0.575	0.86	0.95	2.15	0.10
	4	0.665	0.85	0.99	1.67	1.06
	5	0.755	0.89	1.01	1.34	1.04
1.6	1	–	1.06	1.14	1.41	0.76
	2	–	1.06	1.42	2.69	0.12

where $b_k^2 = (\pi/8\beta)(B/T)(1 - \sum_{n=1}^{\infty} nk_n^2)$; β is the coefficient of the plumpness of the shipframe, k_n are the coefficients in the expansion

$$z = f(\zeta) = \zeta + \frac{k_1}{\zeta} + \frac{k_3}{\zeta^3} + \frac{k_5}{\zeta^5} + \cdots .$$

If only values for k_1 and k_3 are assumed to be non-vanishing, we get the following formulas:

$$k_{33} = c_v = \left(\frac{2T}{B} - a\right)\left(\frac{2T}{B} - a + 1\right) + 1, \tag{2.27}$$

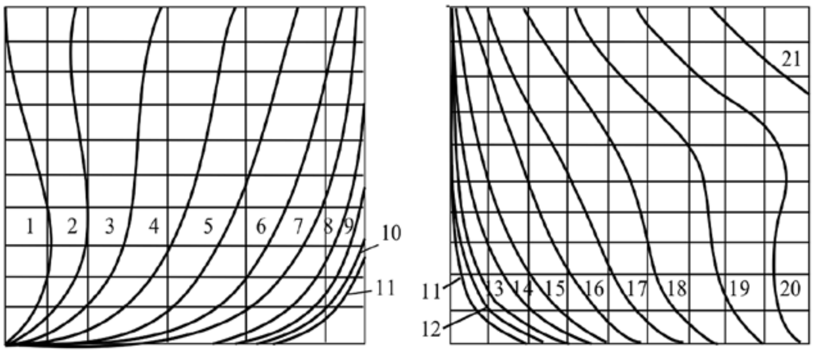

Fig. 2.47 Shipframe shapes for ship A

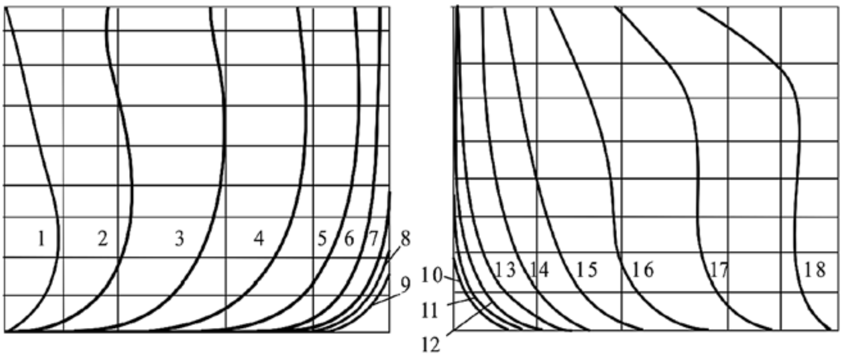

Fig. 2.48 Shipframe shapes for ship B

where

$$a = \frac{3}{2}\left(1 + \frac{2T}{B}\right) - \frac{1}{2}\sqrt{1 + \frac{20T}{B} + \frac{4T^2}{B^2} - \frac{64\beta T}{\pi B}}. \tag{2.28}$$

The expression under the square root is negative when $\beta > (\pi/32)(2T/B + B/2T + 10)$. This inequality distinguishes the shipframes of bulb-type shape. Therefore, for the shipframes of bulb-type shape the formula (2.27) is not applicable. For three main positions of the bulb-type shipframe with respect to the water surface (Fig. 2.50) Ivanuta and Boyanovsky derived the following approximate formulas:

- for position I: $\lambda_{33} = 0.5\rho\pi b_S^2$,
- for position II: $\lambda_{33} = \rho\pi b_S(1 - b_S^2/2H_S^2)$,
- for position III: $\lambda_{33} = \pi\rho b_{S1}^2(1 - b_{S1}^2/2H_{S1}^2)$,

where the characteristic lengths b_S, b_{S1}, H_S, H_{S1} are shown in Fig. 2.50. The values in the brackets take into account the influence of water surface in the first approx-

Table 2.5 Coefficients of added masses of shipframes

S.F. No.	Ship A				Ship B			
	$B/2T$	β	$k_{220}=c_h$	$k_{33}=c_v$	$B/2T$	β	$k_{220}=c_h$	$k_{33}=c_v$
1	–	–	0.515	–	–	–	0.585	–
2	0.240	1.035	0.950	2.20	0.320	1.13	0.960	2.81
3	0.520	0.788	0.965	1.04	0.675	0.99	1.18	1.56
4	0.773	0.736	0.978	0.872	0.970	0.94	1.22	1.225
5	0.985	0.775	1.07	0.880	1.15	0.91	1.255	1.15
6	1.170	0.762	1.13	0.850	1.23	0.926	1.370	1.19
7	1.19	0.886	1.21	1.065	1.26	0.985	1.49	1.32
8	1.19	0.930	1.27	1.160	1.27	0.99	1.51	1.37
9	1.19	0.945	1.285	1.205	1.27	0.99	1.51	1.44
10	1.19	0.960	1.304	1.235	1.27	0.99	1.51	1.42
11	1.19	0.993	1.350	1.280	1.27	0.98	1.49	1.38
12	1.19	0.990	1.348	1.275	1.27	0.975	1.44	1.26
13	1.19	0.960	1.304	1.235	1.195	0.945	1.39	1.18
14	1.19	0.930	1.348	1.160	1.195	0.930	1.34	1.15
15	1.17	0.865	1.160	1.030	1.10	0.875	1.155	1.04
16	1.15	0.790	1.10	0.920	0.960	0.785	1.05	0.917
17	1.07	0.733	1.145	0.823	0.745	0.635	1.05	0.740
18	0.933	0.666	1.110	0.729	0.497	0.308	0.70	0.397
19	0.773	0.505	0.946	0.650	–	–	–	–
20	0.586	0.303	0.794	0.790	–	–	–	–
21	0.320	0.927	1.570	0.742	–	–	–	–

imation. More precise formulas for taking into account the influence of the water surface on the added masses of a circular cylinder can be found in Chap. 5.

If $0.5 \leq \beta \leq 0.9$, then for approximate calculations one can use the formula

$$\lambda_{33} = \frac{1}{2}\rho\beta B^2.$$

2.5 Added Masses of an Inclined Shipframe

The above results can be generalized [121, 225] to computation of added masses λ_{22} and λ_{24} of inclined shipframes, whose contour can not be considered symmetric with respect to any vertical axis. The problem was solved under the assumption that on the water surface (which was assumed to be flat) the water-tightness condition is imposed.

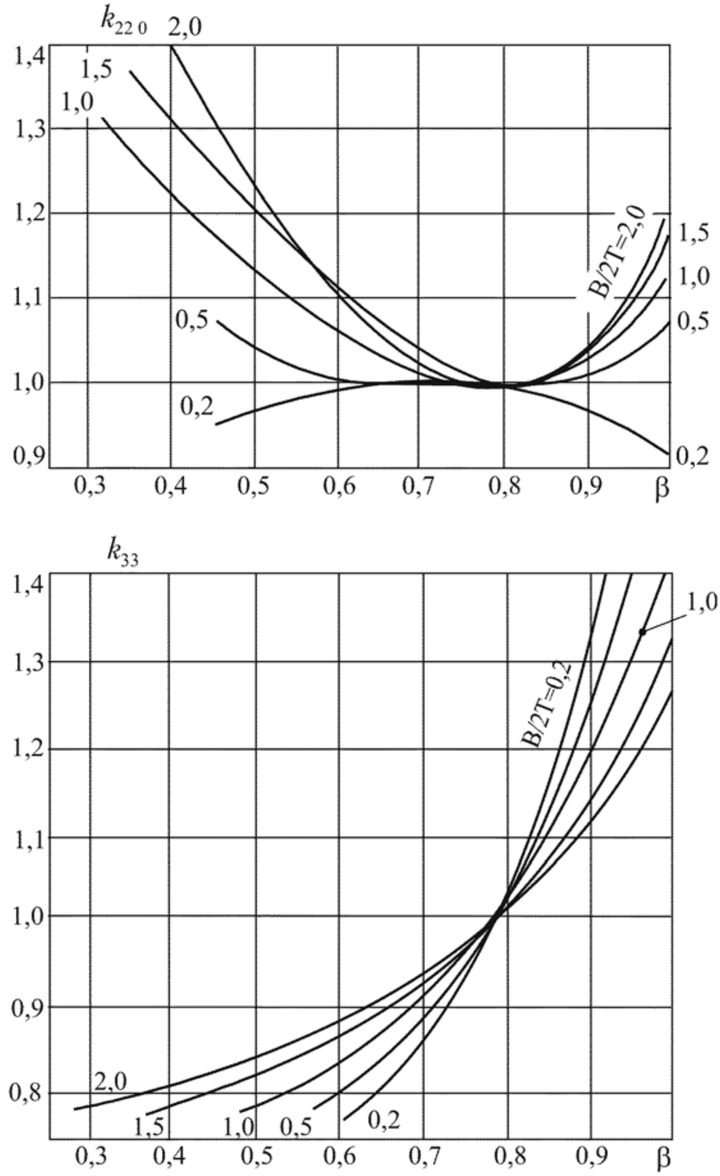

Fig. 2.49 Graphs of analytic representation of coefficients k_{220} and k_{33} in terms of characteristic dimensions of shipframes

Mapping the exterior of the contour of a duplicated shipframe in the τ-plane (Fig. 2.51) to the exterior of the unit circle in the ζ-plane by the function

$$\tau = y + iz = f(\zeta) = \frac{B}{2(1+p+q)}\left(\zeta + p\zeta^{-1} + a\zeta^{-2} + q\zeta^{-3} - a\right),$$

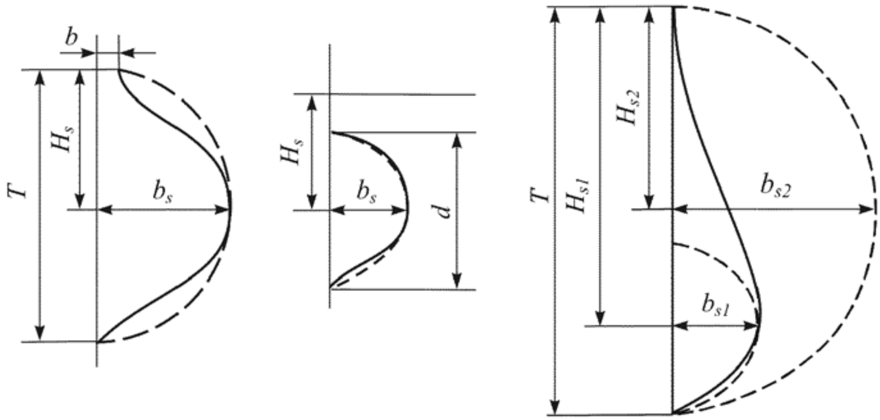

Fig. 2.50 Typical positions of bulb-type shipframes: from left to right: position I, position II and position III

where B is the shipframe width computed at the waterline, we can get the parametrical expression for the frame contour:

$$\begin{aligned} y &= \frac{B}{2(1+p+q)}\big[(1+p)\cos\theta + a\cos 2\theta + q\cos 3\theta - a\big]; \\ z &= \frac{B}{2(1+p+q)}\big[(1-p)\sin\theta - a\sin 2\theta - q\sin 3\theta\big]. \end{aligned} \tag{2.29}$$

The difference between formulas (2.29) and formulas (2.20) is in the presence of a non-zero parameter a and, also, in coefficients in front of the brackets in the formulas for $f(\zeta)$.

The graphs of coefficients $k_{22} = (\beta, \bar{y}_m, B/T) = 2\lambda_{22}/(\pi\rho T^2)$ and $k_{24} = \lambda_{24}/(\rho T^3)$ calculated by Usachev [225] are shown in Figs. 2.51–2.54. The value $\bar{y}_m := 2y_m/B$ (Fig. 2.51) determines the asymmetry of the contour.

2.6 Added Masses of Catamarans and Twin Rudders

The added masses of catamarans can be determined via the added masses of a single body [8][3]:

$$\lambda_{11c} = \kappa_1\lambda_{11}, \qquad \lambda_{22c} = \kappa_2\lambda_{22},$$
$$\lambda_{66c} = \kappa_2\left(\lambda_{66} + \frac{B_1^2}{4}\lambda_{22}\right) + \kappa_1\frac{B_1^2}{4}\lambda_{11}$$

[3]This section was written by A.I. Nemzer.

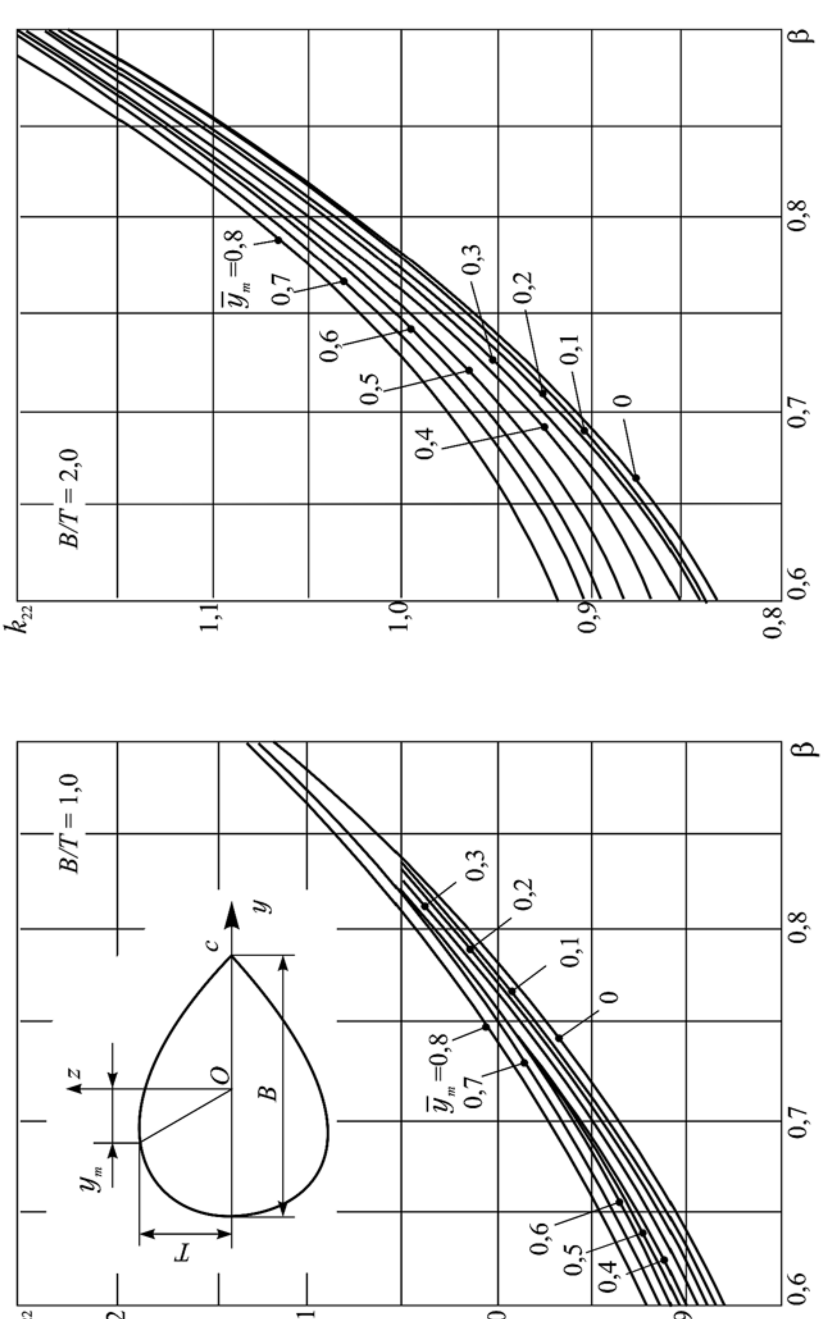

Fig. 2.51 Coefficients of added masses of an inclined shipframe

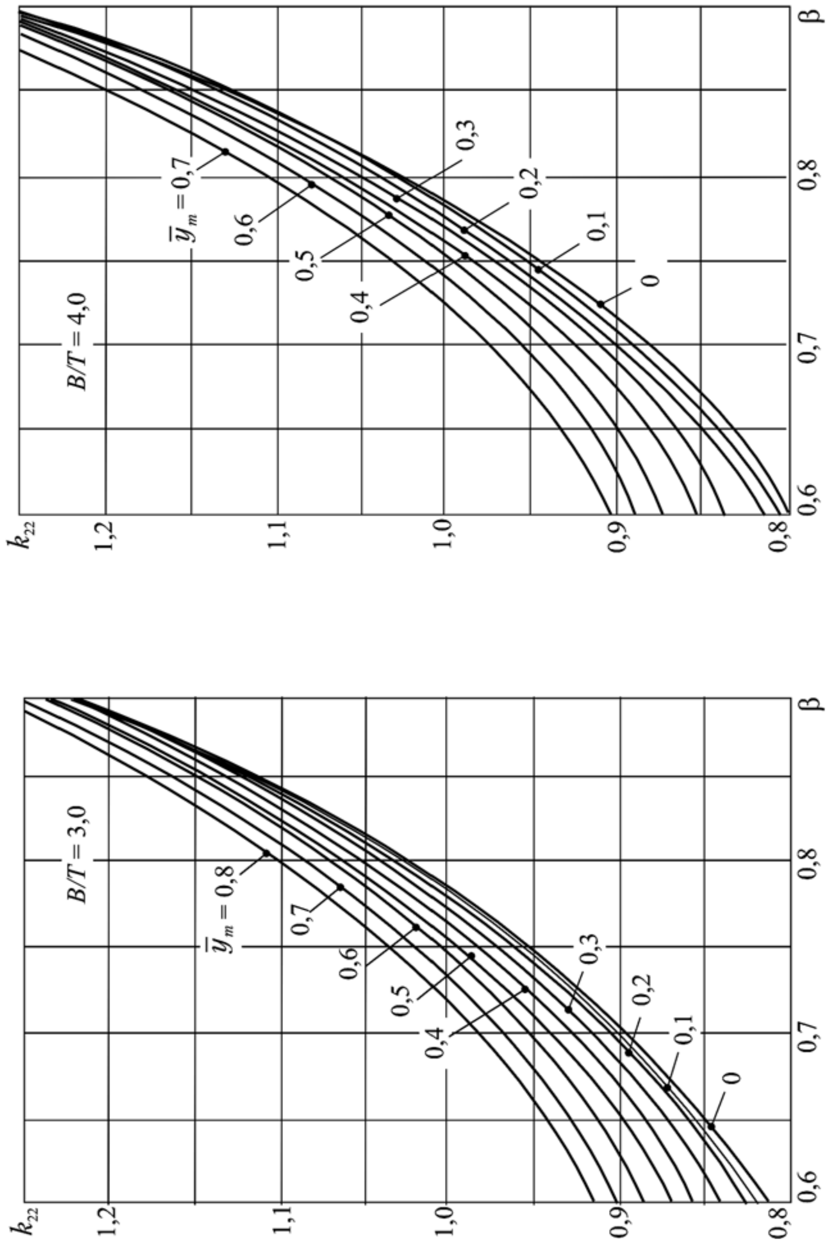

Fig. 2.52 Coefficients of added masses of an inclined shipframe

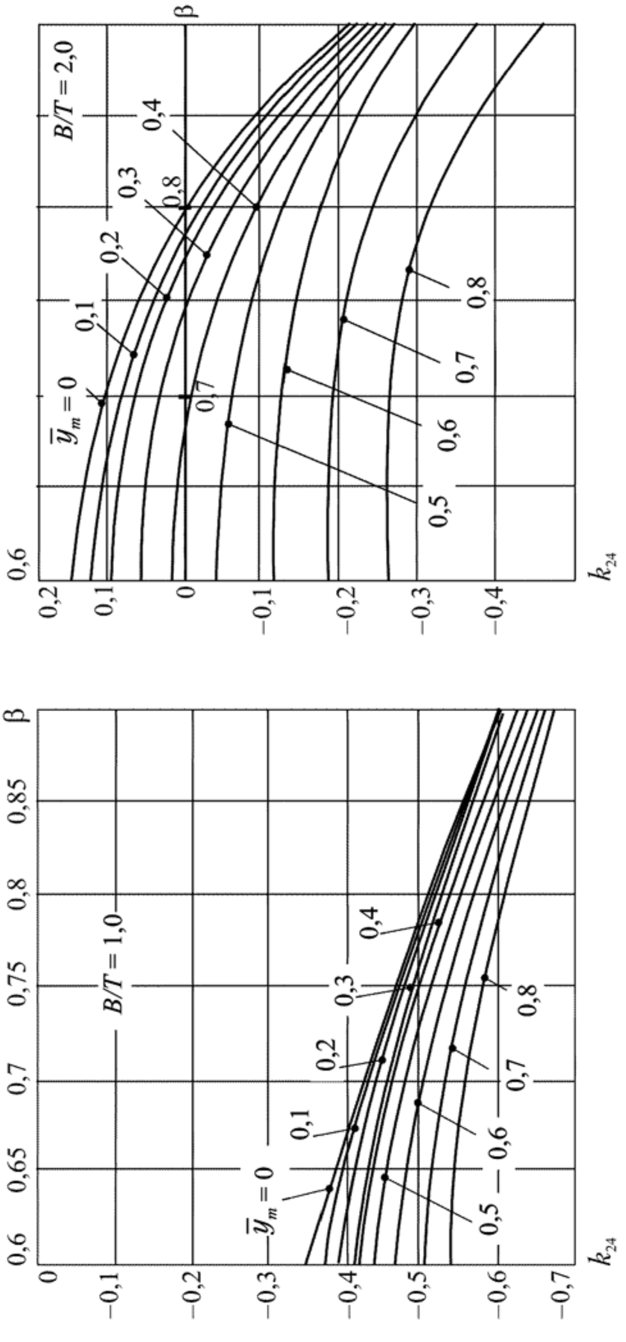

Fig. 2.53 Coefficients of added masses of an inclined shipframe

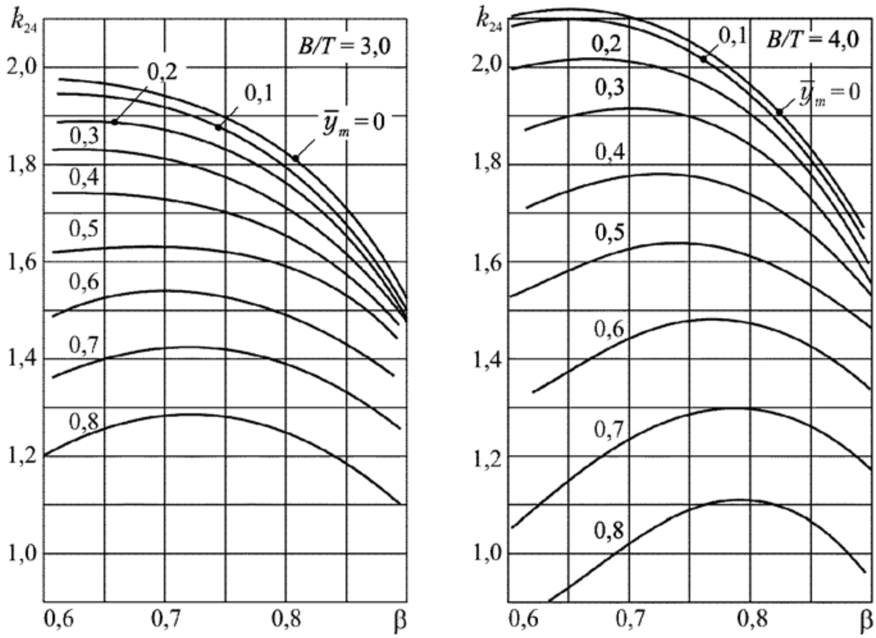

Fig. 2.54 Coefficients of added masses of an inclined shipframe

where $\lambda_{11}, \lambda_{22}$ and λ_{66} are added masses and added moment of inertia of the single body; B_1 is the distance between the symmetry planes (diameter planes) of the bodies; κ_1 and κ_2 are coefficients taking into account the mutual position of the bodies. These coefficients are determined by the formulas:

$$\kappa_1 = 2 + e^{-\bar{c}}, \qquad \kappa_2 = 2 - 0.8e^{-2\bar{c}}, \qquad \bar{c} = \frac{C}{B},$$

where C is the distance between the internal surfaces of the bodies, measured along the waterline, B is the width of one body of the catamaran.

Other interesting results for added masses of a shipframe considered as a part of a catamaran obtained in [48]:

$$\lambda_{22csf} = k_{22}\lambda_{22sf}, \qquad \lambda_{33csf} = k_{33}\lambda_{33sf},$$

where $\lambda_{22sf}, \lambda_{33sf}$ are added masses of the shipframe of each of the bodies forming the catamaran; k_{22} and k_{33} are coefficients taking into account the mutual position of the bodies.

The coefficients k_{22} and k_{33} for the different shapes of the shipframes are shown in Fig. 2.55.

On catamarans, as well as on single-body vessels, one could use twin rudders (Fig. 2.56). The added mass of the rudders in the direction of the y axis is determined as follows [2, 230]:

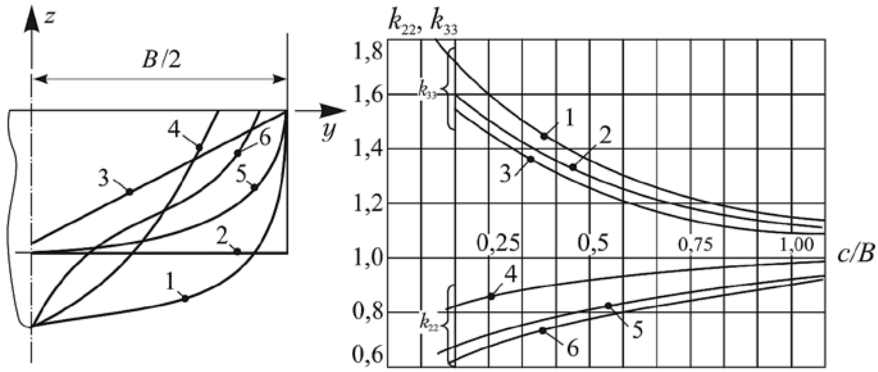

Fig. 2.55 Coefficients of added masses of a single hull considered as part of a catamaran

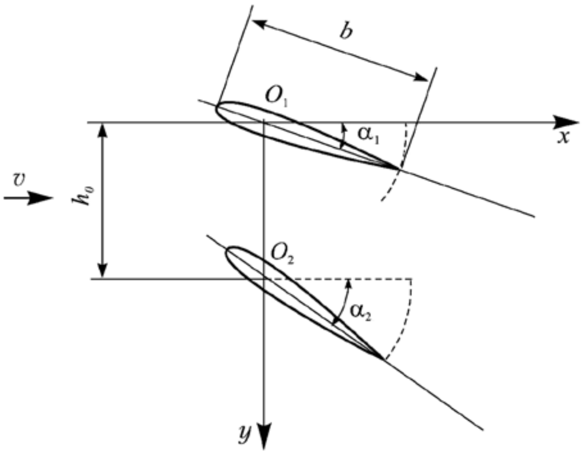

Fig. 2.56 Positions of twin rudders

$$\lambda_y = K_y \rho b^2 l,$$

where b is the chord of the rudder, l is the span of the rudder, K_y is the coefficient determined from the graphs shown in Figs. 2.57–2.60 as functions of parameters

$$\alpha_1, \alpha_2, \bar{\alpha}, \bar{h}_0/b, \lambda,$$

where α_1 and α_2 are the attack angles of the twin rudders, $\bar{\alpha} := \alpha_2/\alpha_1$, h_0 is the distance between the axes of the stocks, and λ is the elongation (ratio of the chord to the span) of the rudder.

Graphs shown in Figs. 2.57–2.60 are obtained under assumption that $\alpha_2 \geq \alpha_1$ and therefore $\bar{\alpha} \geq 1$. Therefore if $\alpha_1 \neq \alpha_2$ we choose the larger angle α_2 in determining the coefficient K_y. If $\alpha_1 > \alpha_2$, then the indices of the angle should be interchanged, i.e., α_1 should be chosen as an argument on the graphs in Figs. 2.57–2.60, and parameter $\bar{\alpha}$ is determined as $\bar{\alpha} = \alpha_1/\alpha_2$.

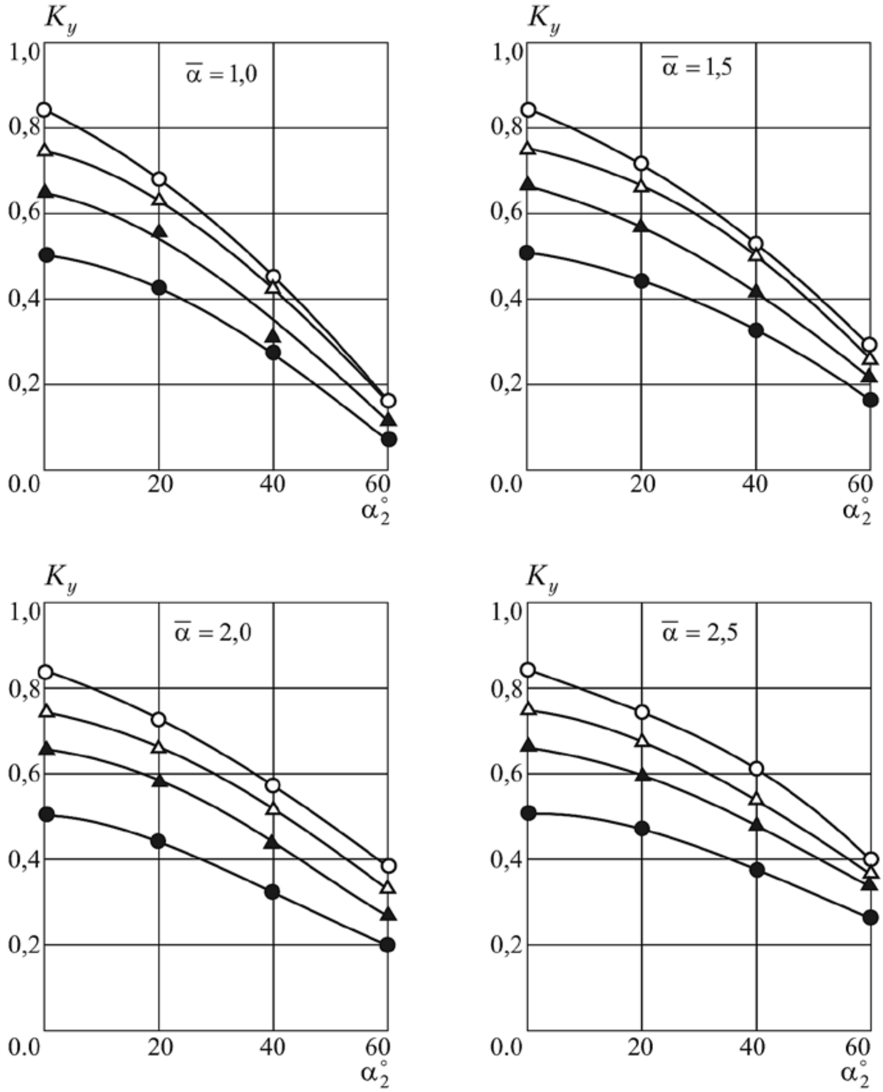

Fig. 2.57 Values of coefficient K_y for $h_0/b = 0.8$. *Black circles* correspond to $\lambda = 0.5$, *black triangles* to $\lambda = 0.75$, *white triangles* to $\lambda = 1.0$, *white circles* to $\lambda = 1.25$

The total added masses of the system vessel-rudder are determined by the formulas

$$\lambda_{22}^{\text{total}} = \lambda_{22} + \lambda_y, \qquad \lambda_{26}^{\text{total}} = \lambda_{26} - l_b\lambda_y, \qquad \lambda_{66}^{\text{total}} = \lambda_{66} - l_b^2\lambda_y,$$

where l_b is the distance from the rudder stock to the center of mass of the vessel.

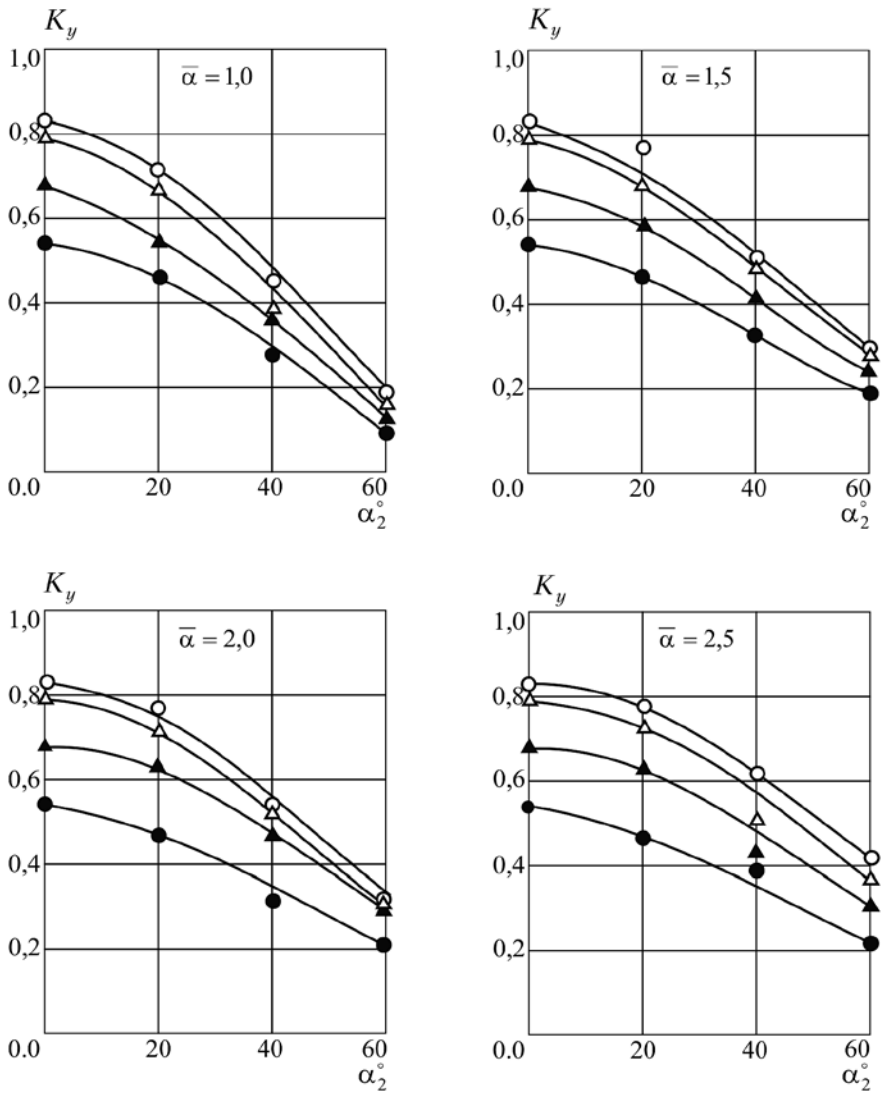

Fig. 2.58 Values of coefficient K_y for $h_0/b = 1.0$. *Black circles* correspond to $\lambda = 0.5$, *black triangles* to $\lambda = 0.75$, *white triangles* to $\lambda = 1.0$, *white circles* to $\lambda = 1.25$

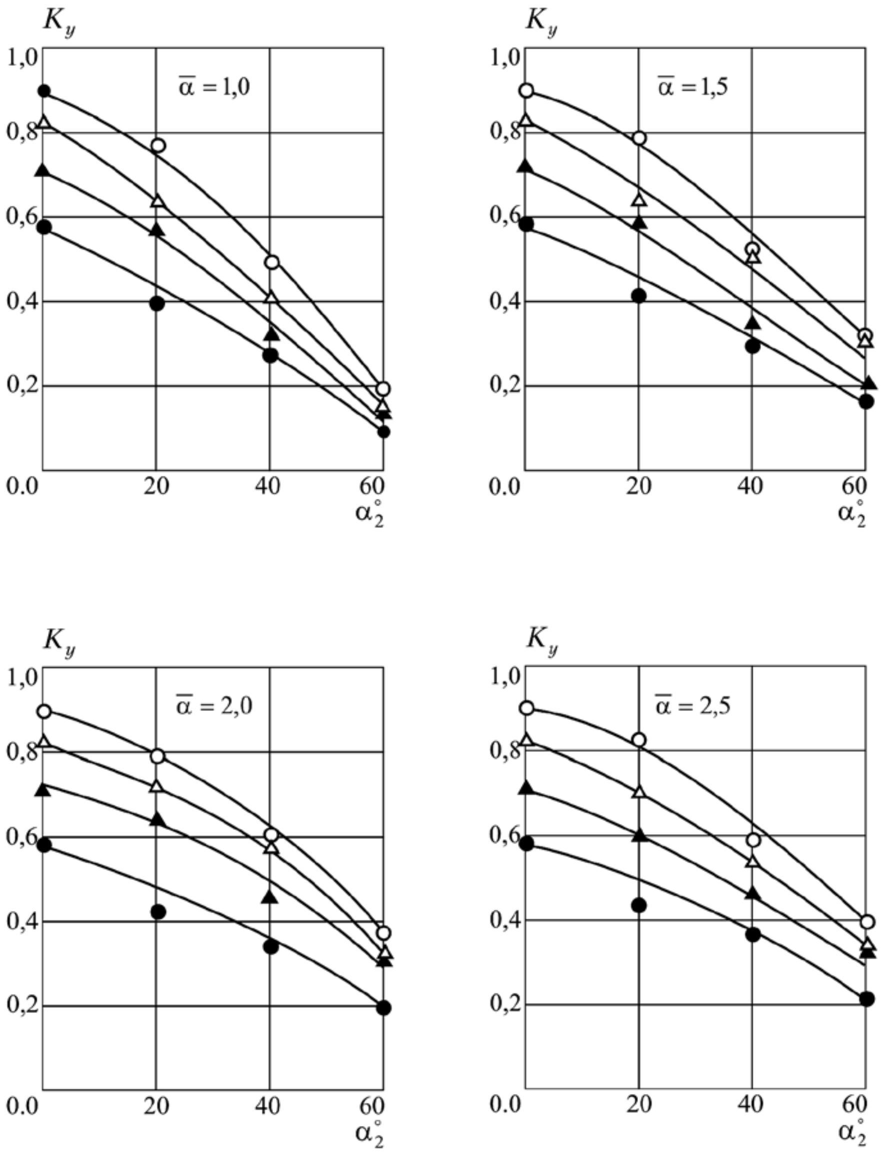

Fig. 2.59 Values of coefficient K_y for $h_0/b = 1.2$. *Black circles* correspond to $\lambda = 0.5$, *black triangles* to $\lambda = 0.75$, *white triangles* to $\lambda = 1.0$, *white circles* to $\lambda = 1.25$

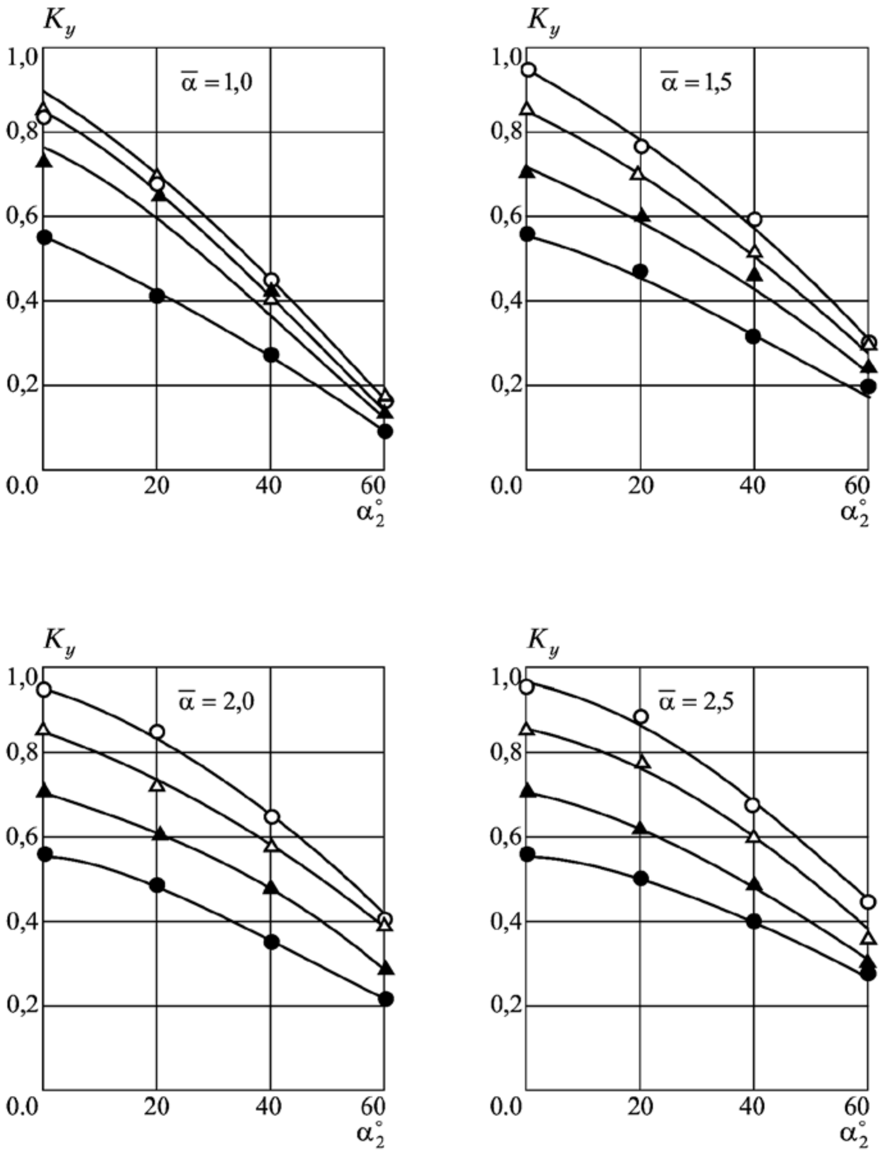

Fig. 2.60 Values of coefficient K_y for $h_0/b = 1.4$. *Black circles* correspond to $\lambda = 0.5$, *black triangles* to $\lambda = 0.75$, *white triangles* to $\lambda = 1.0$, *white circles* to $\lambda = 1.25$

Chapter 3
Added Masses of Three-Dimensional Bodies in Infinite Fluid

From the general expressions for added masses of a solid body moving in fluid (1.12) one sees that the added masses and moments can be computed if one knows the potentials of velocity fields arising in the fluid under the motion of the body along and around coordinate axes. Therefore, the problem of computation of added masses involves solving the Laplace equation with given boundary conditions on the surface of the body and at infinity. The methods of solutions of the Laplace equation which are most commonly applied in hydrodynamics are the method of separation of variables and the singularity method [4, 133, 139]. According to the method of separation of variables, the general solution of a Laplace equation is represented as a sum of particular solutions with constant coefficients, which are defined from the boundary conditions. In this method it is convenient to use an orthogonal curvilinear coordinate system chosen such that one of the coordinate "planes" coincides with the surface of the body. For example, the problem can be solved in a relatively simple way for ellipsoids if one uses an elliptic coordinate system. For an arbitrary body of revolution the solution is rather complicated [139]; the solution can be simplified assuming that the length of the body is large compared to its width.

The method of singularities is also based on linearity of the Laplace equation; the potential in question is obtained by summing up potentials of elementary hydrodynamic singularities: sources, dipoles and vortices. Posing the singularities inside of the body and on its surface, one can find their distribution using the water-tightness condition on the surface of the body. The method of singularities is widely used in numerical analysis of this type of problems [21, 22].

In this chapter we discuss added masses of some simple bodies obtained from exact solutions of a Laplace equation. Then we discuss approximate methods of computation of added masses of three-dimensional bodies.

3.1 Added Masses of an Ellipsoid Moving in an Infinite Fluid

Motion of an ellipsoid in infinite ideal fluid is one of very few cases which can be analyzed explicitly. Formulation of the problem and its solution is treated in detail in standard courses of hydrodynamics [116, 133]. In these textbooks one can also find the following formulas for added masses of three-axial ellipsoid with half-axes $a > b > c$:

$$\lambda_{11} = \frac{4}{3}\pi\rho abc\frac{A_0}{2-A_0}; \qquad \lambda_{22} = \frac{4}{3}\pi\rho abc\frac{B_0}{2-B_0};$$

A.I. Korotkin, *Added Masses of Ship Structures*,

$$\lambda_{33} = \frac{4}{3}\pi\rho abc\frac{C_0}{2-C_0};$$

$$\lambda_{44} = \frac{4}{15}\pi\rho\frac{abc(b^2-c^2)^2(C_0-B_0)}{2(b^2-c^2)+(B_0-C_0)(b^2+c^2)};$$

$$\lambda_{55} = \frac{4}{15}\pi\rho\frac{abc(a^2-c^2)^2(A_0-C_0)}{2(c^2-a^2)+(C_0-A_0)(c^2+a^2)};$$

$$\lambda_{66} = \frac{4}{15}\pi\rho\frac{abc(a^2-b^2)^2(B_0-A_0)}{2(a^2-b^2)+(A_0-B_0)(a^2+b^2)}.$$

In these formulas

$$A_0 = abc\int_0^\infty \frac{du}{(a^2+u)\sqrt{(a^2+u)(b^2+u)(c^2+u)}},$$

$$B_0 = abc\int_0^\infty \frac{du}{(b^2+u)\sqrt{(a^2+u)(b^2+u)(c^2+u)}},$$

$$C_0 = abc\int_0^\infty \frac{du}{(c^2+u)\sqrt{(a^2+u)(b^2+u)(c^2+u)}},$$

we notice that $A_0 + B_0 + C_0 = 2$.

Computations of added masses on the basis of these formulas were performed by Gurevich and Riman.

Taking into account that the mass of fluid inside of the ellipsoid is $m = (4/3)\pi\rho abc$, and moments of inertia with respect to the axes Ox, Oy, Oz are

$$J_{xx} = \frac{4}{15}\pi\rho abc\left(b^2+c^2\right);$$

$$J_{yy} = \frac{4\pi\rho}{15}abc\left(a^2+c^2\right);$$

$$J_{zz} = \frac{4\pi\rho}{15}abc\left(a^2+b^2\right),$$

it makes sense to consider dependence of coefficients of added masses

$$k_{11} = \frac{\lambda_{11}}{m}, \qquad k_{22} = \frac{\lambda_{22}}{m}, \qquad k_{33} = \frac{\lambda_{33}}{m},$$

$$k_{44} = \frac{\lambda_{44}}{J_{xx}}, \qquad k_{55} = \frac{\lambda_{55}}{J_{yy}}, \quad k_{66} = \frac{\lambda_{66}}{J_{zz}}$$

on parameters $p = a/b$, $q = c/b$. These functions are shown in Figs. 3.1–3.3.

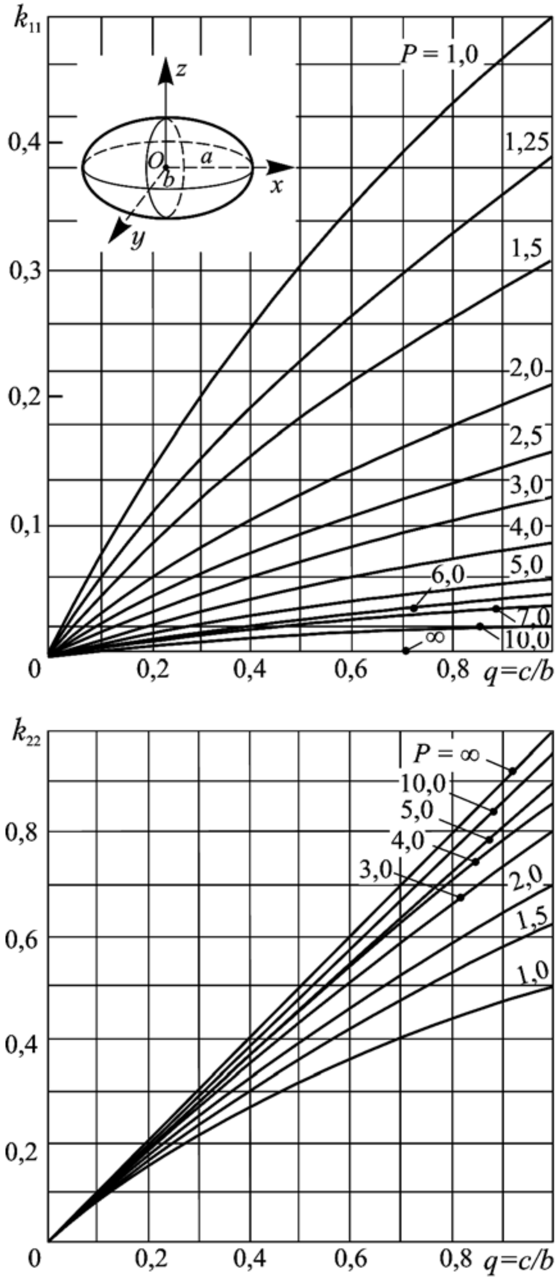

Fig. 3.1 Coefficients of added masses of *three-axial ellipsoids*

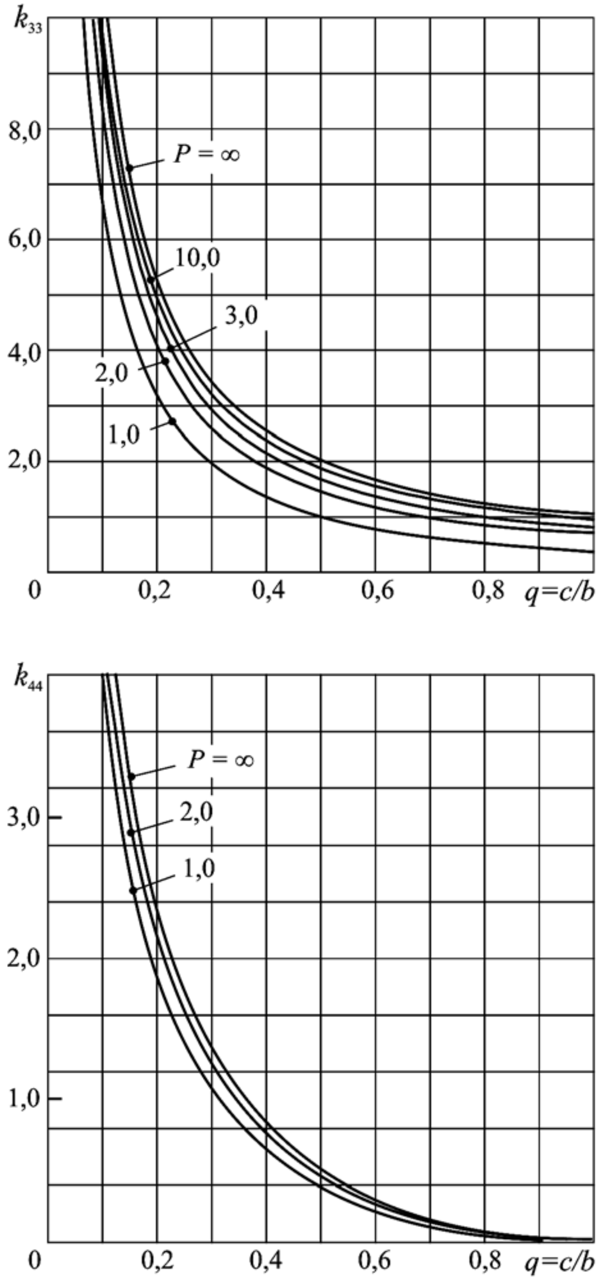

Fig. 3.2 Coefficients of added masses of *three-axial ellipsoids*

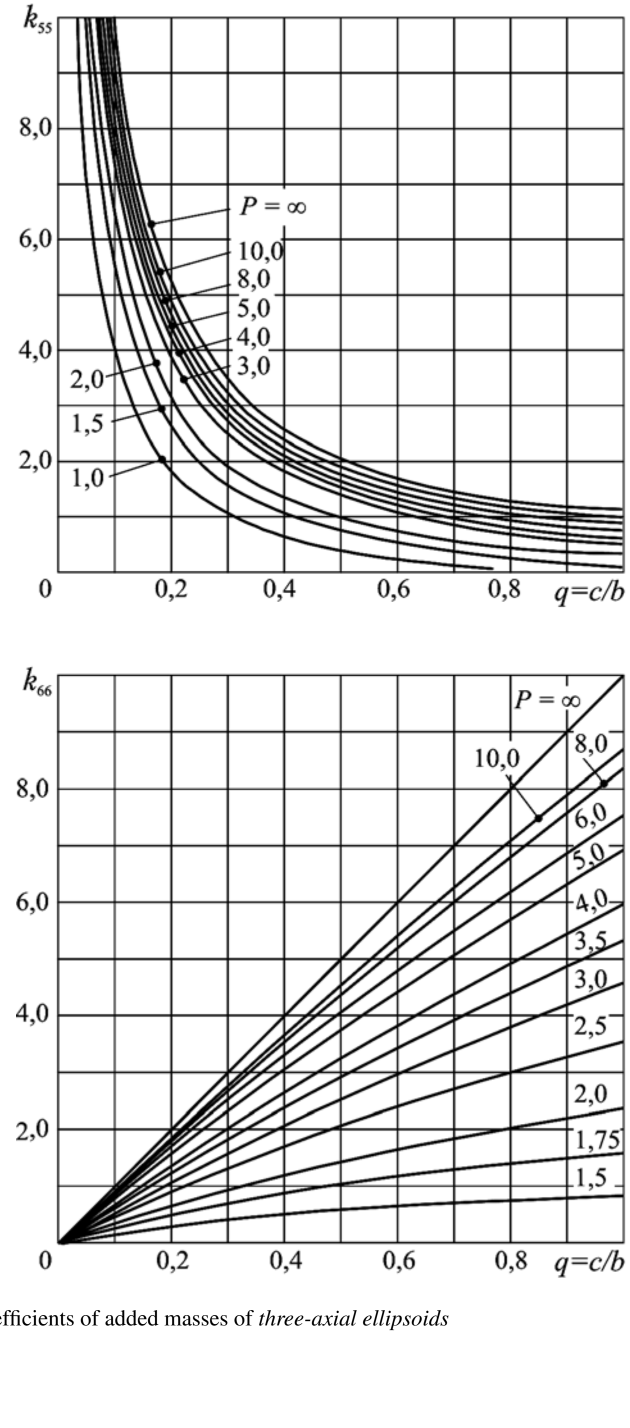

Fig. 3.3 Coefficients of added masses of *three-axial ellipsoids*

3.2 Oblate Spheroid, Elongated Ellipsoid of Revolution, Sphere, Disc and Elliptic Plates

For an oblate spheroid (oblate ellipsoid of revolution) $p = a/b = 1$, and the following equalities hold [183]:

$$A_0 = B_0 = \frac{q}{(1-q^2)^{3/2}}\left[\arcsin\sqrt{1-q^2} - q\sqrt{1-q^2}\right];$$

$$C_0 = \frac{2q}{(1-q^2)^{3/2}}\left[\frac{1}{q}\sqrt{1-q^2} - \arcsin\sqrt{1-q^2}\right];$$

$$q = c/b.$$

Coefficients of added masses can be found from general expressions [183]:

$$k_{11} = \frac{A_0}{B_0 + C_0}; \qquad k_{22} = \frac{B_0}{A_0 + C_0}; \qquad k_{33} = \frac{C_0}{A_0 + B_0};$$

$$k_{44} = \frac{(1-q^2)^2}{1+q^2}\,\frac{C_0 - B_0}{2(1-q^2) + (B_0 - C_0)(1+q^2)};$$

$$k_{55} = \frac{(q^2-p^2)^2}{p^2+q^2}\,\frac{A_0 - C_0}{2(q^2-p^2) + (C_0 - A_0)(q^2+p^2)};$$

$$k_{66} = \frac{(p^2-1)^2}{p^2+1}\,\frac{B_0 - A_0}{2(p^2-1) + (A_0 - B_0)(p^2+1)}.$$

For $p = 1$, $q = 0$ the spheroid degenerates to the disc of radius a, whose added masses look as follows:

$$\lambda_{33} = \frac{8}{3}\rho a^3; \qquad \lambda_{44} = \lambda_{66} = \frac{16}{45}\rho a^5; \qquad \lambda_{11} = \lambda_{22} = \lambda_{55} = 0.$$

For $p = 1$, $q = 1$ the spheroid turns into the sphere whose added masses are given by

$$\lambda_{11} = \lambda_{22} = \lambda_{33} = \frac{2}{3}\pi\rho a^3; \qquad \lambda_{44} = \lambda_{55} = \lambda_{66} = 0.$$

It is convenient to normalize the added masses of a spheroid which is oblate in the direction of the z-axis. For that purpose we divide these added masses by the corresponding added masses of the disc of radius a introducing the coefficients

$$k_{11} = \frac{3\lambda_{11}}{8\rho a^3} = k_{22}; \qquad k_{33} = \frac{3\lambda_{33}}{8\rho a^3}; \qquad k_{44} = k_{55} = \frac{45\lambda_{44}}{16\rho a^5}.$$

Graphs of the coefficients $k_{11}(c/a)$, $k_{33}(c/a)$ and $k_{44}(c/a)$ are shown in Fig. 3.4.

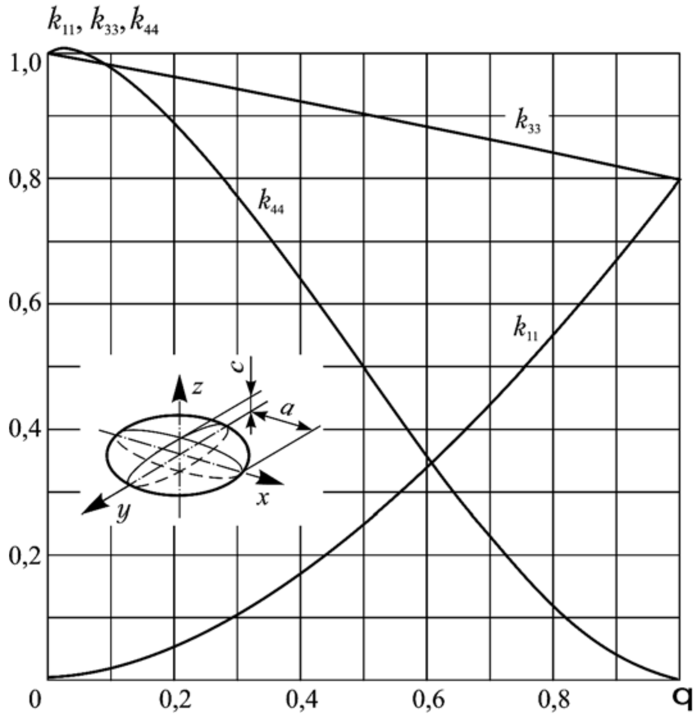

Fig. 3.4 Coefficients of added masses of an *oblate spheroid* as functions of $q = c/a$

For the elongated ellipsoid of revolution ($q = c/b = 1$) we have

$$A_0 = \frac{2v}{(v^2-1)^{3/2}}\left[\ln\left(\sqrt{v^2-1}+v\right) - \frac{\sqrt{v^2-1}}{v}\right];$$

$$B_0 = C_0 = \frac{v^2}{v^2-1}\left[1 - \frac{v^2}{\sqrt{v^2-1}}\ln\left(\sqrt{v^2-1}+v\right)\right],$$

where $v = a/b$.

In terms of the eccentricity

$$e = \sqrt{1-\frac{b^2}{a^2}} = \frac{\sqrt{v^2-1}}{v}$$

of the meridian section of the ellipsoid, the previous formulas can be rewritten as follows:

$$A_0 = \frac{2(1-e^2)}{e^3}\left[\frac{1}{2}\ln\frac{1+e}{1-e} - e\right];$$

$$B_0 = C_0 = \frac{1}{e^2} - \frac{1-e^2}{2e^3} \ln \frac{1+e}{1-e}.$$

It is convenient to introduce the coefficients

$$k_{11} = \frac{3\lambda_{11}}{4\pi\rho ab^2}; \qquad k_{22} = k_{33} = \frac{3\lambda_{22}}{4\pi\rho ab^2};$$

$$k_{55} = k_{66} = \frac{15\lambda_{55}}{4[\pi\rho ab^2(a^2+b^2)]}; \qquad k_{44} = 0.$$

The graphs of functions $k_{11}(b/a)$, $k_{22}(b/a)$ and $k_{55}(b/a)$ are shown in Fig. 3.5.

The added masses of elliptic plates with half-axes a and b can be obtained from general formulas for the added masses of three-axes ellipsoids in the limit $q \to 0$ [183]. The graphs of coefficients equal to ratios of the added masses of the elliptic plates to the added masses and added moments of inertia of the disc of radius a,

$$k_{11} = k_{22} = 0; \qquad k_{33} = \frac{\lambda_{33}}{8\rho a^3/3};$$

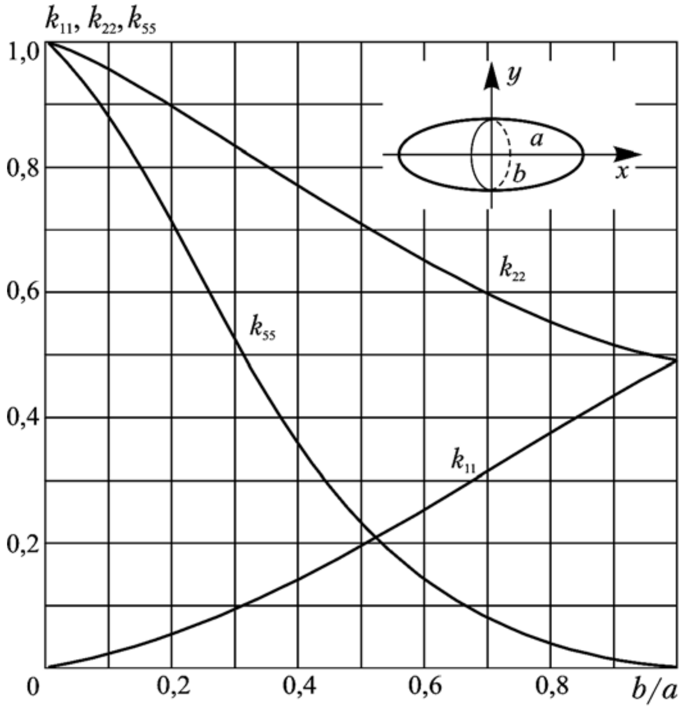

Fig. 3.5 Coefficients of added masses of an *elongated ellipsoid* of revolution

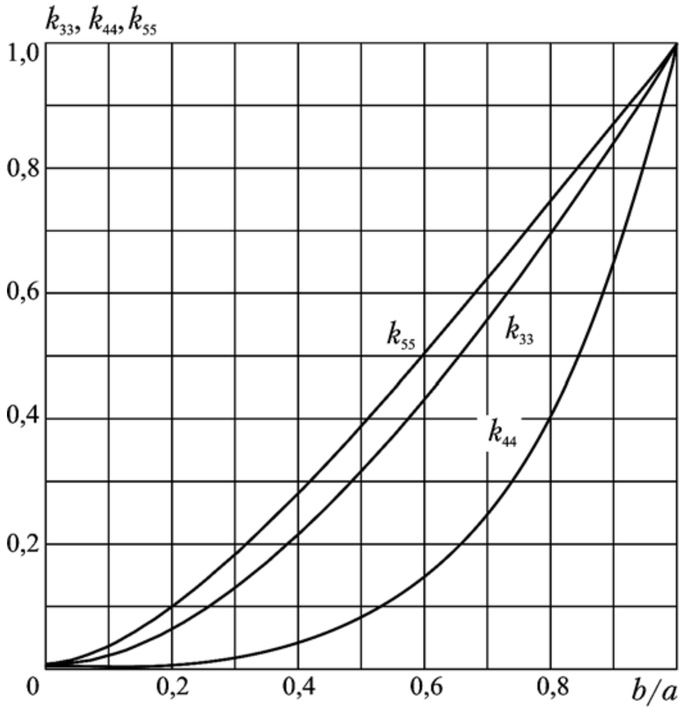

Fig. 3.6 Coefficients of added masses of *elliptic plates*

$$k_{44} = \frac{\lambda_{44}}{16\rho a^5/45}; \qquad k_{55} = \frac{\lambda_{55}}{16\rho a^5/45}; \qquad k_{66} = 0,$$

are shown in Fig. 3.6.

3.3 Added Masses of Thin Finite-Span Airfoils

Added masses of finite-span foils are computed in [21, 22] by the method of the vortex surface. The plane shape of the airfoils is characterized by the following parameters (see Fig. 3.7): b—the root chord; l—the wing span; l_k—the tip chord; S—the area of the airfoil; φ_0 is the front edge wing sweep angle; $\lambda = l^2/S$—the coefficient of relative elongation of the airfoil; $\eta = b/b_k$—the wing taper ratio.

The origin of the coordinate system xyz is chosen in the middle of the central chord; the plane xOz coincides with the plane of the airfoil. Taking into account that the airfoil is assumed to be thin, one computes only the added masses λ_{22}, λ_{26}, λ_{44} and λ_{66}. In Figs. 3.8–3.10 we demonstrate dependence of the coefficients $k_{22} = \lambda_{22}/(\rho Sb)$, $k_{26} = \lambda_{26}/(\rho Sb^2)$, $k_{44} = \lambda_{44}/(\rho Sb^3)$, $k_{66} = \lambda_{66}/(\rho Sb^3)$ on λ, η and φ_0.

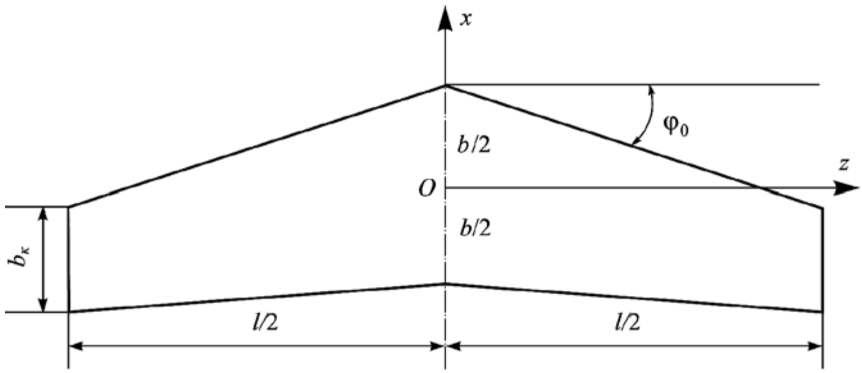

Fig. 3.7 Scheme of a monoplane airfoil ($\eta = b/b_k, \lambda = l^2/S$)

To get an idea about the accuracy of these theoretical results one can consider Fig. 3.11 where one compares theoretical and experimental results for the coefficients k_{22} and k_{66} in the case of rectangular airfoils of various elongation.

For the coefficients of added masses k_{22} of rectangular wings of elongation λ and $1/\lambda$ one can get the relation [21] $k_{22}(\lambda) = \lambda k_{22}(1/\lambda)$ which follows from some obvious equalities that are valid for a rectangular wing of span l and chord b: $\lambda_{22}(\lambda) = \lambda_{22}(1/\lambda) := \lambda_{22}$; $k_{22}(\lambda) = \lambda_{22}/(\rho S b)$; $k_{22}(1/\lambda) = \lambda_{22}/(\rho S l)$.

Sometimes it is convenient to use the following relations valid for the airfoils shown in Fig. 3.7:

$$S = \frac{l(b_k + b)}{2} = \frac{bl(1 + \eta^{-1})}{2};$$

$$\frac{l}{b} = \frac{\lambda(1 + \eta^{-1})}{2}.$$

The added mass λ_{22} of a thin symmetric triangular airfoil with base l and angle φ_0 between each side and the base is given by the formula [36]:

$$\lambda_{22} = \frac{\rho l^3}{\pi}(\tan\varphi_0)^{3/2}.$$

3.4 Added Masses of Thin Circular Cylindrical Airfoils

A thin circular cylindrical airfoil of diameter D and chord of profile b represents a thin cylindrical shell of diameter D and length b. Its added masses were obtained by Kapustina and presented in [21]. The origin of the coordinate system is situated in the center of the axis of the airfoil; the x-axis is chosen to coincide with the axis of the airfoil (Fig. 3.12). Coefficients $k_{22} := \lambda_{22}/(\rho D b^2)$ and $k_{66} := \lambda_{22}/(\rho D b^4)$ as functions of elongation $\lambda = D/b$ of the annular airfoil are shown in Fig. 3.13.

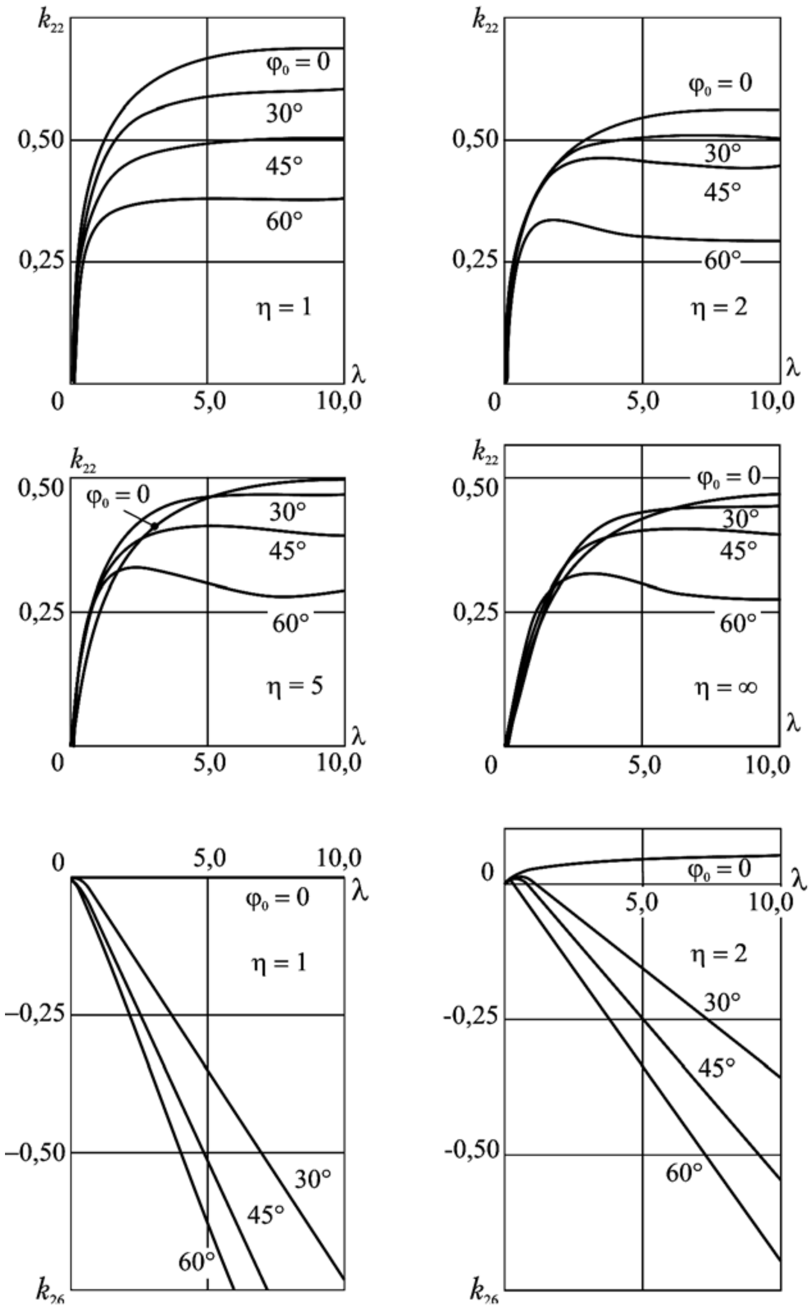

Fig. 3.8 Coefficients of added masses of *finite-span airfoils*

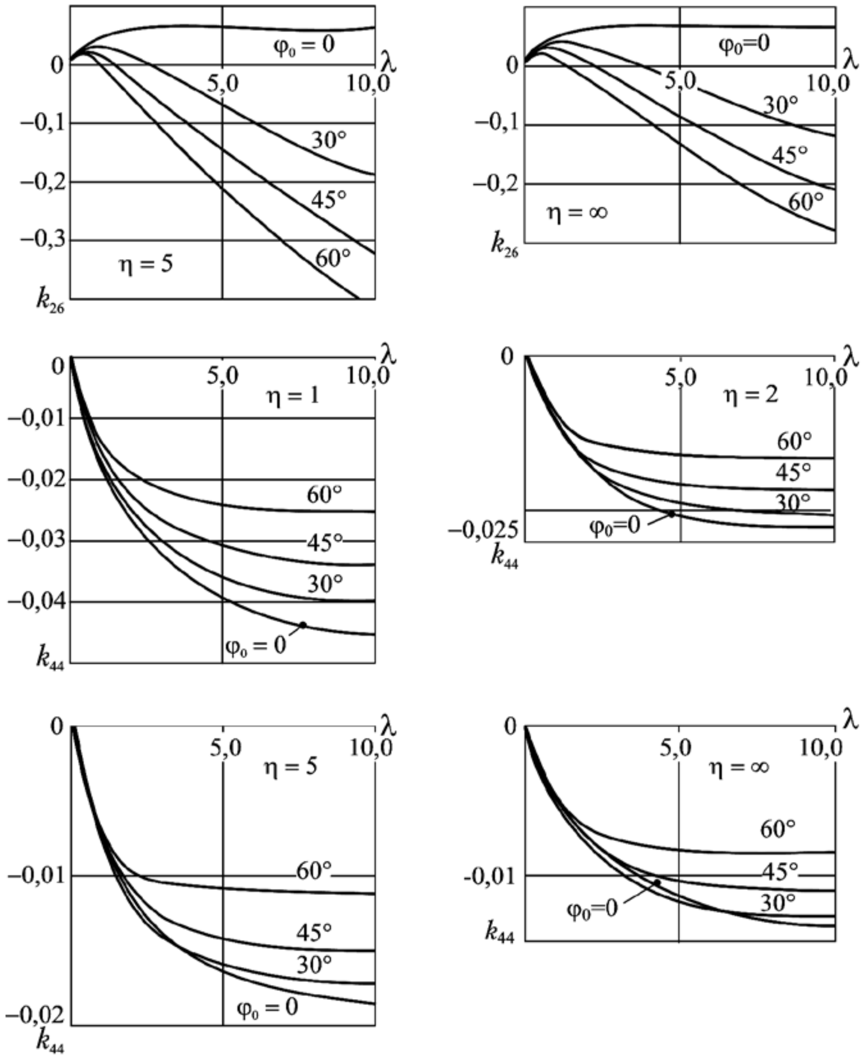

Fig. 3.9 Coefficients of added masses of *finite-span airfoils*

3.5 Approximate Methods to Determine Added Masses of 3D Bodies

For most real ship structures it is impossible to compute added masses explicitly and one needs to make use of various approximate methods.

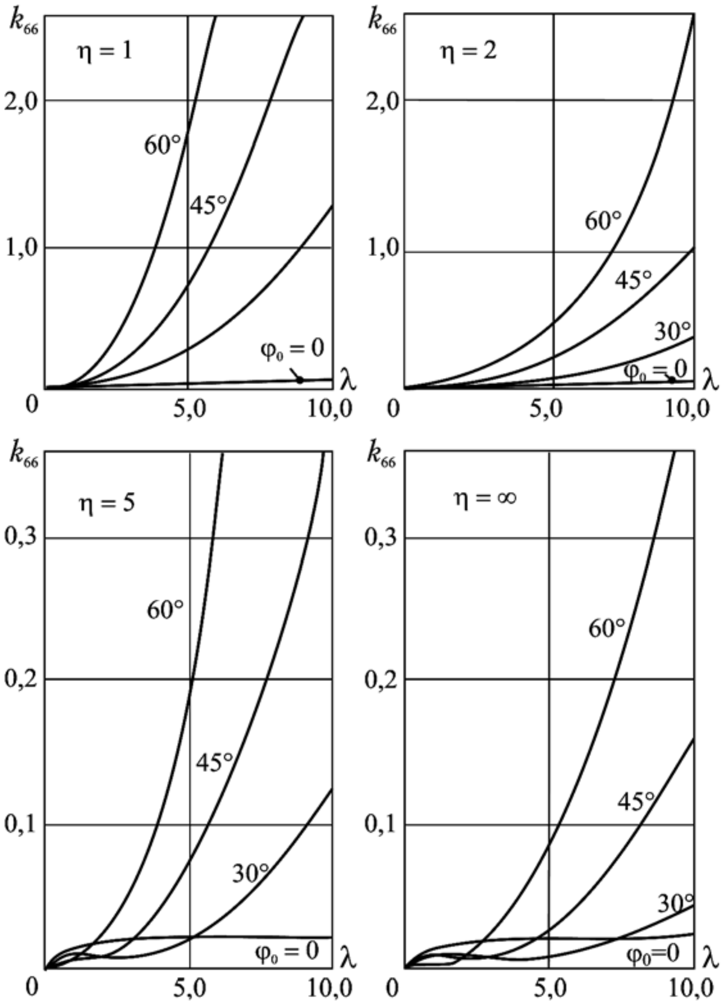

Fig. 3.10 Coefficients of added masses of *finite-span airfoils*

3.5.1 Method of Plane Sections

If a body is elongated along one of its axes (typically this axis is assumed to coincide with the x-axis) the added masses in orthogonal directions (i.e., along y and z-axes) can be computed by the method of plane sections. The idea of this method is that one computes the added masses of all plane sections orthogonal to the x-axis and then integrates them along x. One assumes that the motion of fluid in the x-direction is negligible if the body moves in any direction orthogonal to the x axis. This assumption is well-satisfied for prolate bodies, when the ratio of the length of the body (L) to its diameter (B or $2T$) is large enough ($\lambda := L/B \geq 9$). When λ

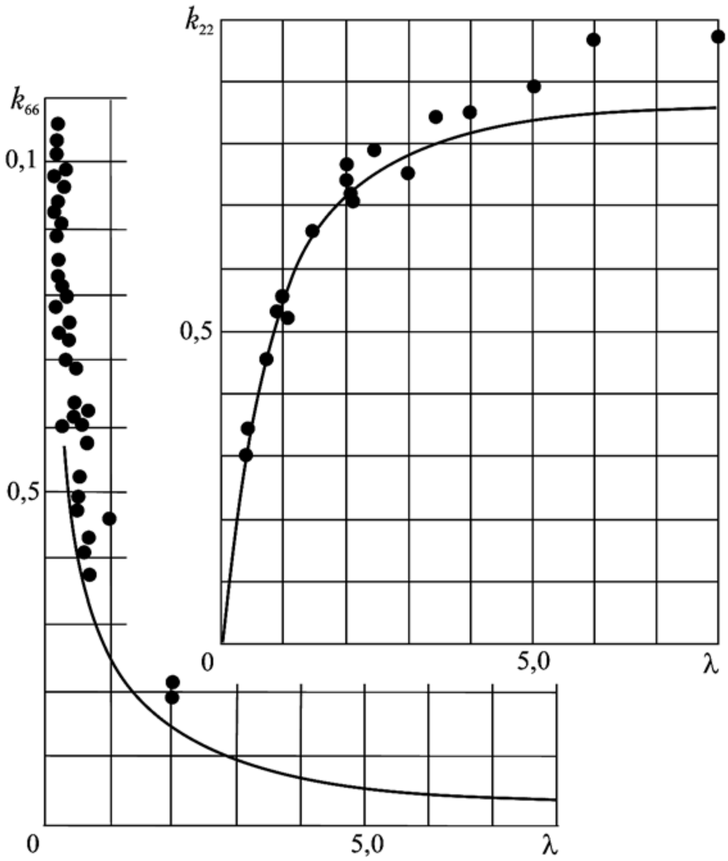

Fig. 3.11 Comparison of theoretical and experimental results for added masses of *rectangular airfoils* ($k_{22} = 4\lambda_{22}/(\rho\pi Sb)$, $k_{66} = 48\lambda_{66}/(\rho\pi l^2 b^3)$). The *solid curves* are theoretical; *dots* correspond to experimental data

gets smaller the motion of fluid along the x-axis becomes essential, and the added masses computed by the method of plane sections have to be corrected.

The formulas for added masses computed via the method of plane sections can be written as follows:

$$\lambda_{22} = \mu\left(\lambda = \frac{L}{2T}\right)\int_{L_1}^{L_2} \lambda_{220}(x)\,dx; \tag{3.1}$$

$$\lambda_{33} = \mu\left(\lambda = \frac{L}{B}\right)\int_{L_1}^{L_2} \lambda_{330}(x)\,dx; \tag{3.2}$$

$$\lambda_{24} = \mu\left(\lambda = \frac{L}{2T}\right)\int_{L_1}^{L_2} \lambda_{240}(x)\,dx; \tag{3.3}$$

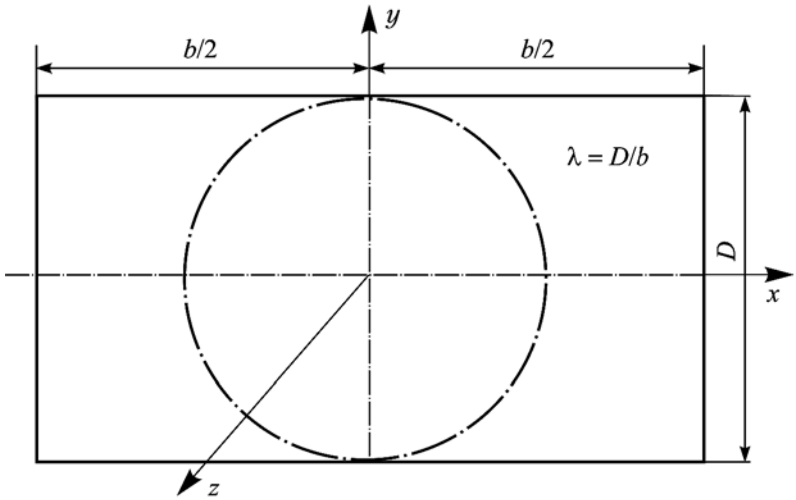

Fig. 3.12 Scheme of a *circular cylindrical airfoil*

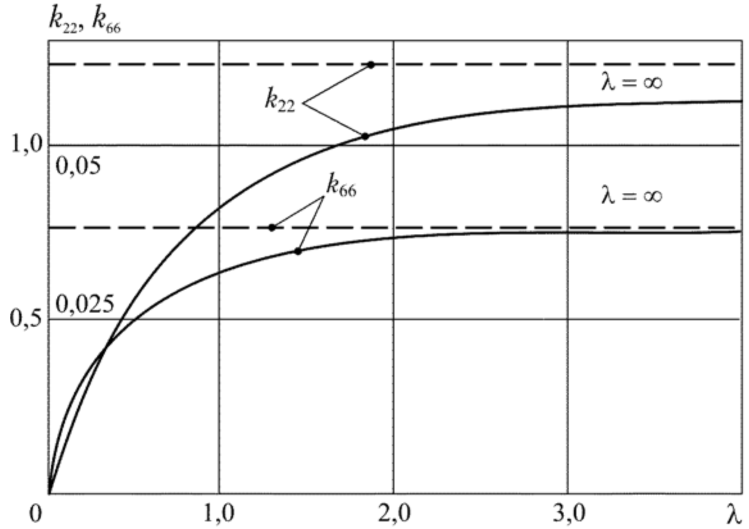

Fig. 3.13 Added masses of a *circular cylindrical airfoil*

$$\lambda_{34} = \mu\left(\lambda = \frac{L}{B}\right)\int_{L_1}^{L_2} \lambda_{340}(x)\,dx; \tag{3.4}$$

$$\lambda_{44} = \mu\left(\lambda = \frac{L}{2T}\right)\int_{L_1}^{L_2} \lambda_{440}(x)\,dx; \tag{3.5}$$

$$\lambda_{26} = \mu_1\left(\lambda = \frac{L}{2T}\right)\int_{L_1}^{L_2} \lambda_{220}(x)x\,dx; \tag{3.6}$$

$$\lambda_{35} = -\mu_1\left(\lambda = \frac{L}{B}\right)\int_{L_1}^{L_2} \lambda_{330}(x)x\,dx; \tag{3.7}$$

$$\lambda_{55} = \mu_1\left(\lambda = \frac{L}{B}\right)\int_{L_1}^{L_2} \lambda_{330}(x)x^2\,dx; \tag{3.8}$$

$$\lambda_{66} = \mu_1\left(\lambda = \frac{L}{2T}\right)\int_{L_1}^{L_2} \lambda_{220}(x)x^2\,dx. \tag{3.9}$$

In the formulas (3.1)–(3.9) the integration is performed between the endpoints of the body whose x-coordinates equal L_1 and L_2; $\mu(\lambda)$ and $\mu_1(\lambda)$ are corrections related to fluid motion along the x-axis; these corrections are different since the motion of fluid along the x-axis is different for cases of linear motion of the body and its rotation. Notice the different sign in the formulas (3.6) and (3.7). There is a subtlety related to the choice of correct sign while computing the added masses having the dimension of static moment by the method of plane sections. Consider for example the added mass λ_{35} of the body M which is symmetric under the x_1Oy_1 plane in the coordinate system $x_1y_1z_1$ (Fig. 3.14). For the body M (as well as for any other body) one can find such a coordinate system xyz that $\lambda_{35} = 0$. Indeed, in the interval $[L_1, L_2]$, where $\lambda_{330}(x) \geq 0$, we have from the mean value theorem:

$$\int_{L_1}^{L_2} \lambda_{330}(x)x\,dx = x_c\int_{L_1}^{L_2} \lambda_{330}(x)\,dx$$

for some x_c. Shifting the origin of the coordinate system along the x-axis to the point $x = x_c$, we get $\lambda_{35} = 0$. Let coordinate system $x_1y_1z_1$ be shifted in the negative direction of the axis Ox with respect to the coordinate system xyz by Δx. Then the integral $\int_{L_1-\Delta x}^{L_2-\Delta x} \lambda_{330}(x)x\,dx$ defining the added mass $\lambda_{35}^{(1)}$ in the coordinate system

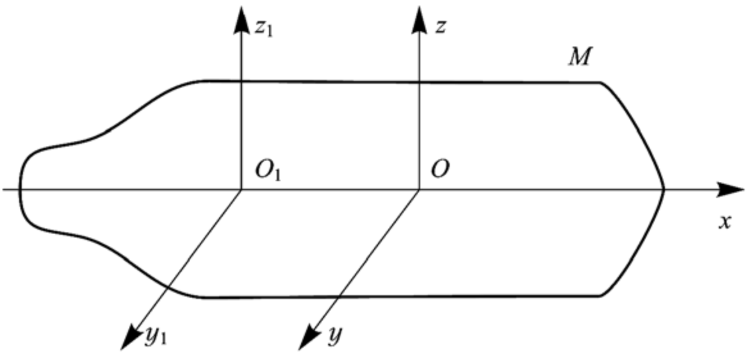

Fig. 3.14 Coordinate systems for an elongated body

$x_1y_1z_1$ is positive (in this qualitative discussion we assume that the correction coefficient μ in (3.7) equals 1). However, the added mass $\lambda_{35}^{(1)}$ itself is in fact negative in this case, which follows from the following reasoning.

Suppose the body M starts moving from rest in the ideal fluid in the direction of the axis Oz_1 with acceleration

$$\frac{du_3}{dt} > 0. \tag{3.10}$$

Then in the coordinate system (x_1, y_1, z_1) the body is influenced by torque

$$M_{y_1} > 0 \tag{3.11}$$

since the body starts rotating in the clockwise direction (from the point of view of an observer situated at the "end" of the y_1-axis). This direction of rotation is positive in the left coordinate system $x_1y_1z_1$. From the formula (1.26) it follows that the torque M_{y_1} is related to acceleration du_3/dt by the formula

$$M_{y_1} = -\lambda_{35}\frac{du_3}{dt}. \tag{3.12}$$

Comparing expressions (3.10), (3.11) and (3.12) we conclude that in the coordinate system $x_1y_1z_1$ the added mass $\lambda_{35} < 0$.

In general the signs of added masses can be found using laws of transformation of the added masses under a change of coordinate system (1.17). Suppose that in the coordinate system xyz we have $\lambda_{35} = 0$. Consider now the coordinate system $x_2y_2z_2$ obtained from xyz by shifting the axis Ox in the positive direction by Δx. Then according to (1.21), $\lambda_{35}^{(2)} = \Delta x \lambda_{33}$. Therefore, computing $\lambda_{35}^{(2)}$ by the method of plane sections one should use the formula

$$\lambda_{35}^{(2)} = -\int_{L_1}^{L_2} \lambda_{330}(x) x\, dx,$$

since the integral itself is negative for this direction of shift.

Analogously, for $\lambda_{26}^{(2)}$ we get $\lambda_{26}^{(2)} = -\Delta x \lambda_{22}$; thus $\lambda_{26}^{(2)}$ should be computed using the formula $\lambda_{26}^{(2)} = \int_{L_1}^{L_2} \lambda_{220}(x) x\, dx$. Similarly one can choose the correct signs in front of all other integrals for computation of all added static moments by the method of plane sections.[1]

The smaller the elongation of the body, the less precise is the method of plane sections. To decrease the arising error one introduces the correction coefficients μ and μ_1 related to flow of fluid along the body. These correction terms can be found both experimentally and theoretically, using the known exact solutions. The most well-known experimental correction is the Pabst correction derived empirically from

[1] The problem with the choice of correct signs for the added static moments was indicated in [16, 183].

experiments with rectangular plates:

$$\mu(\lambda) = \frac{\lambda}{\sqrt{1+\lambda^2}}\left(1 - 0.425\frac{\lambda}{1+\lambda^2}\right), \tag{3.13}$$

where $\lambda = L/B$ is the elongation of the plate.

In computations of added masses of hulls, the use of Pabst correction might be insufficient due to the specific shape of the ship frames. Another issue is the influence of viscosity of the real fluid on these corrections. Therefore it is reasonable to determine the corrections related to finiteness of the length of the hull by using exact solutions (see Sect. 3.1) for three-axial ellipsoids; this allows also us to take into account the relative thickness of the hull.

For a three-axial ellipsoid the added mass in the direction of the z-axis is determined by the formula

$$\lambda_{33} = k_{33}\frac{4}{3}\rho\pi abc,$$

where the coefficient $k_{33} = k_{33}(\lambda = a/b, q = c/b)$ can be found from Fig. 3.2.

Computing the added mass by the method of plane sections, we find

$$\lambda_{33pl} = 2\pi\rho b^2 \int_0^a \left(1 - \frac{x^2}{a^2}\right) dx = \frac{4}{3}\pi\rho ab^2.$$

Therefore, the correction related to the 3D character of the flow can be found from relation $\mu(\lambda, q) = \lambda_{33}/\lambda_{33pl} = k_{33}q$. Graphs of the function $\mu(\lambda, q)$ are shown in Fig. 3.15. The dashed line shows the dependence of Pabst correction on parameter λ.

We notice that the Pabst corrections found in experiments with plates significantly differ from corrections $\mu(\lambda, 0)$ obtained theoretically for elliptic plates; the experimental correction is actually closer to $\mu(\lambda, 1)$. This fact is probably due to the difference between real and theoretical structure of the fluid flow.

Analogously one can get a correction related to the 3D character of the flow for the added moment of inertia. The exact value of the added mass is

$$\lambda_{66} = k_{66}(\lambda, q)\frac{4}{15}\rho\pi abc\left(a^2 + b^2\right),$$

where the coefficient $k_{66}(\lambda, q)$ is shown on the graphs in Sect. 3.1.

The added mass λ_{66}, computed by the method of plane sections, is expressed by the formula

$$\lambda_{66}^{\text{planar}} = 2\rho\pi b^2 \int_0^a \left(1 - \frac{x^2}{a^2}\right) x^2\, dx = \frac{4}{15}\rho\pi b^2 a^3.$$

Therefore, the correction for the added moment of inertia is written in the form

$$\mu_1(\lambda, q) = \frac{\lambda_{66}}{\lambda_{66}^{\text{planar}}} = k_{66}(\lambda, q) q\left(1 + \frac{1}{\lambda^2}\right).$$

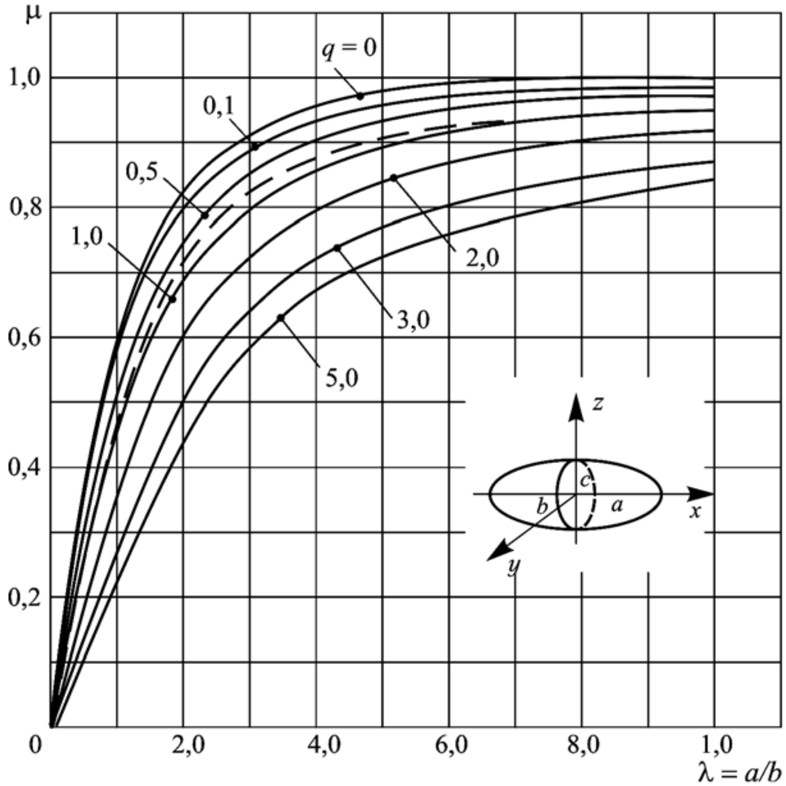

Fig. 3.15 Corrections related to the 3D character of flow to added masses computed by the method of plane sections

Graphs of the function $\mu_1(\lambda, q)$ are shown in Fig. 3.16.

The corrections $\mu(\lambda, q)$ and $\mu_1(\lambda, q)$ can be used to determine the added masses by the method of plane sections for bodies with relatively smooth boundaries.

Experimental data for correction μ_1 for rectangular plates with different ratios of the length L to the width B are shown in Fig. 3.16. The correction μ_1 is found as the ratio of an experimentally measured variable λ_{55} to the added moment of inertia of the rectangular plate $\pi\rho B^2 L^3/48$ computed via the method of plane sections. The solid curve in Fig. 3.16 approximates the experimental data and corresponds to the formula

$$\mu_1(\lambda) = 1 - e^{-0.4\lambda}. \tag{3.14}$$

If the plate has the shape of a double trapezeum (see Fig. 3.17) then the added moment of inertia is equal to the added moment of inertia of a rectangular plate of the same length and the same area, multiplied with coefficient ξ (Fig. 3.17) depending on the ratio B_1/B_2, where B_1 and B_2 are characteristic sizes shown in Fig. 3.17.

Let us comment on the use of formulas (3.13) and (3.14). The experimental formula (3.13) derived for plates can be also applied to bodies of finite thickness, since

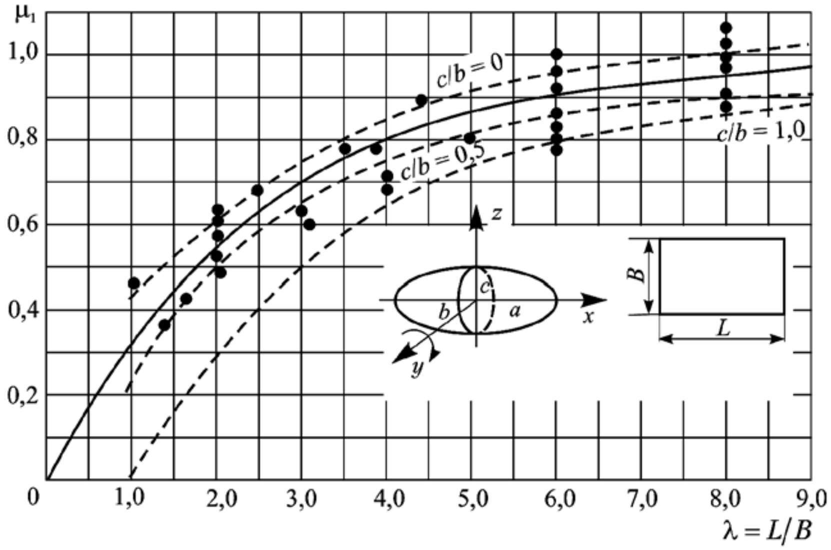

Fig. 3.16 Correction μ_1 taking into account 3D effects in computation of the added moment of inertia: *solid line*—approximation of experimental data; *dots*—experimental data; *dashed line*—computation for ellipsoids

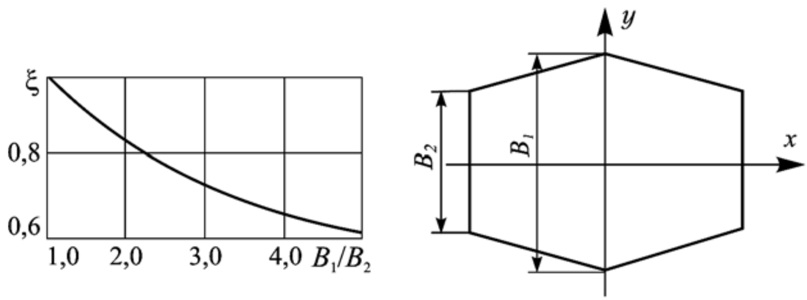

Fig. 3.17 Ratio of added moment of inertia of double trapezeum to added moment of inertia of a *rectangular plate* of the same length and area

the ratio of thickness to width of the body does not significantly influence the correction coefficient $\mu(\lambda)$. On the other hand, the correction coefficient $\mu_1(\lambda)$ essentially depends on the ratio $B/2T$. Indeed, for a body of revolution we have $B/2T = 1$, and if $\lambda = L/B$ tends to 1 the correction μ_1 tends to 0, since for the sphere the added moment of inertia is absent. On the other hand, for a plate with $\lambda = 1$ the correction μ_1 is different; it can be computed by formula (3.14). Therefore, in practical computations it makes sense to find correction μ_1 using the data for ellipsoids.

Correction coefficients which take into account 3D effects in computation of added masses by the method of plane sections are given in Sect. 7.3 of this book.

3.5.2 Method of an Equivalent Ellipsoid

The problem of finding the added masses of an elongated body of volume V with sizes L along the x-axis, B along the y-axis, $2T$ along the z-axis can be approximately reduced to the problem of finding the added masses of an equivalent ellipsoid. The sizes of the ellipsoid are chosen as follows: assume the length of the longest axis to coincide with the length of the body ($2a = L$); the volume of the ellipsoid equals the volume of the body ($V = (4/3)\pi abc$). For computation of λ_{33} and λ_{55} one assumes that $2b = B$ (the third axis $2c$ of the ellipsoid is then determined from condition $V = (4/3)\pi abc$). For computation of λ_{22} and λ_{66} one should assume $2c = 2T$ (then the axis $2b$ is found from the same condition $V = (4/3)\pi abc$).

In computation of the added masses λ_{11} and λ_{44} one fixes the volume of the ellipsoid ($V = (4/3)\pi abc$) and two axes $2b = B$ and $2c = 2T$.

3.5.3 Approximate Formulas for Added Masses of the Hull

For the hull with symmetric waterline defined by equation

$$y(x) = \frac{B}{2}\left[1 - \left(\frac{2x}{B}\right)^n\right], \tag{3.15}$$

and diametral section defined by equation

$$z(x) = -T\left[1 - \left(\frac{2x}{B}\right)^m\right], \tag{3.16}$$

the following added masses were obtained by Huskind [100] using the method of plane sections:

$$\lambda_{33} = \lambda_{33}^M \frac{2\alpha^2 L}{1+\alpha}\mu\left(\lambda = \frac{L}{B}\right); \tag{3.17}$$

$$\lambda_{22} = \lambda_{22}^M \frac{2\beta_0^2 L}{1+\beta_0}\mu\left(\lambda = \frac{L}{2T}\right); \tag{3.18}$$

$$\lambda_{55} = \lambda_{33}^M \frac{\alpha^2 L^3}{6(3-2\alpha)(3-\alpha)}\mu_1\left(\lambda = \frac{L}{B}\right); \tag{3.19}$$

$$\lambda_{66} = \lambda_{22}^M \frac{\beta_0^2 L^3}{6(3-2\beta_0)(3-\beta_0)}\mu_1\left(\lambda = \frac{L}{2T}\right); \tag{3.20}$$

$$\lambda_{24} = \lambda_{24}^M \frac{L}{1-S_1^2}\left(\frac{2\alpha^2}{1+\alpha} - S_1^2\right)\mu\left(\lambda = \frac{L}{2T}\right); \tag{3.21}$$

$$\lambda_{44} = \lambda_{44}^M \frac{L}{(S_1^2 - 1)^2} \left[S_1^4 - \frac{4S_1^2\alpha^2}{1+\alpha} + \frac{12\alpha^4}{(1+\alpha)(2+\alpha)(1+3\alpha)} \right] \mu\left(\lambda = \frac{L}{2T}\right). \tag{3.22}$$

In the formulas (3.17)–(3.22) the area coefficient of the waterplane α and of the diametral section β_0 are related to degrees m and n in (3.15), (3.16) by relations $\alpha = n/(n+1)$, $\beta_0 = m/(m+1)$; variables λ_{ik}^M are added masses of the midship frame; $S_1 = 2T/B$.

In practice, for a rough evaluation one can use the following simplified formulas:

1. For the added mass λ_{33} of the hull:

$$\lambda_{33} = \rho V \left(1.2 + \frac{B}{3T}\right);$$

2. For the added mass λ_{22} of the hull:

$$\lambda_{22} = \rho V \left(0.3 + 0.3\frac{T}{B}\right).$$

In these formulas V is the cubic displacement of the hull, B is the maximal width, T is the average draft, L is the length of the hull. The formulas (3.17)–(3.22) can be used in approximate computations under various types of ship motion which are taken into account for computation of coefficients λ_{ik}^M.

Chapter 4
Added Masses of Interacting Bodies

If a body is moving in a fluid close to other bodies (moving or not), then its added masses differ from the added masses corresponding to motion in an infinite fluid. This difference arises due to different boundary conditions: for an isolated body in an infinite fluid one has only a boundary condition (water-tightness) on the body surface and a boundary condition at infinity. In the presence of other bodies one should also impose boundary conditions on their surfaces. A partial case of such a situation is the motion of a body near a wall, which in the case of an ideal fluid can be substituted by the mirror image of the body. In this chapter we consider added masses of interacting bodies and added masses of bodies moving near hard walls.

4.1 Added Masses of Interacting Bodies Moving in a Fluid

4.1.1 Formulation of the Problem

We can distinguish three essentially different cases of interaction of bodies moving in a fluid[1]:

1. Motion of a body which consists of several parts which are rigidly connected among themselves.
2. Motion of a body in the presence of one or more stationary bodies.
3. Motion of two or more bodies, such that each body is moving independently, possessing (in the general case) six degrees of freedom.

A typical example of the first case is given by two-hull vessels (catamarans), where two hulls are rigidly connected to each other and preserve their relative position under arbitrary motion (for example, under roll). Other examples of interaction of this type are given by interaction of the hull with rudder, keel and other external objects. The characteristic feature of this type of motion is that all elements of the structure move as a single body which possesses not more than six degrees of freedom.

For these problems one can apply an ordinary approach of finding added masses of a single body in an infinite fluid. However, in practice this problem is essentially more difficult in comparison with the case of single bodies whose surface can be described by some analytical function (say, an ellipsoid). A few examples when one can find added masses for compound bodies theoretically are given in Chap. 2 of this book.

[1]This section is written by Yu.V. Gurjev.

In the general case one has to compute the added masses of each element of construction separately, and then find the added masses of the whole construction by summation. Of course, then we encounter the problem of evaluation of mutual influence of various elements of the construction. For example, the transversal added masses of the keel (which in the first approximation can be considered as a flat plate of small elongation) increase with presence of the hull. To approximately model the influence of the hull in this case one can substitute the hull near the keel by a flat wall; the influence of the wall can be taken into account by the method of mirror image, by doubling the length of the plate. After computing the added masses of this new plate we have to divide them by two to find the added masses of the keel near the hull. In the general case, to take into account the interaction of various elements of construction is much more difficult; such problems can be solved either semiempirically or numerically.

The second and third cases of interaction mentioned above are typically classified as cases of non-stationary interaction of bodies in a fluid. The word "non-stationary" is used here in the sense that the mutual positions of bodies change; in this sense that motion can be non-stationary even if the velocities of the bodies remain constant. Examples of non-stationary motion are given by motion of two ships under overtaking or divergence, docking of a ship to a wall etc. In this case the system consists of N bodies, each of which has six degrees of freedom. Therefore, the system as a whole can have $6N$ degrees of freedom.

Under non-stationary motion the mutual positions of bodies in fluid continuously change, as well as the degree of their mutual influence and their hydrodynamic characteristics. Even when they move with constant velocities, all hydrodynamic characteristics of the fluid flow (velocities, potentials, pressure) change. Therefore, kinetic energy of the fluid motion also changes, which leads to similar changes for the added masses.

Therefore, under non-stationary interaction of the bodies the added masses become variables depending on coordinates of positions of the interacting bodies. This is the principal difference between the problem of non-stationary motion and the motion of a single body in fluid. Recall that for a single body the added masses forming the 6×6 matrix are constants, determined only by the shape of the body and choice of the coordinate system. Taking into account constancy of this matrix we have obtained formulas for (1.22)–(1.27) for inertial hydrodynamic forces and torques. Use of these formulas for the case of non-stationary interaction of bodies in fluid is not correct any more [94].

The common feature of the situation when a body moves near immovable objects and the situation when there are several moving bodies is that in both cases the added masses become time-dependent variables. Simultaneously, there is a significant difference between these types of situations. For example, when a body moves near a rigid wall, there are only added masses of the body itself, and their number is the same as the number of added masses of a body moving in an infinite fluid. In the case of simultaneous motion of several bodies the number of added masses is larger. The increase in the number of added masses is not only due to the fact that each of the bodies has 36 added masses, but also due to appearance of new added

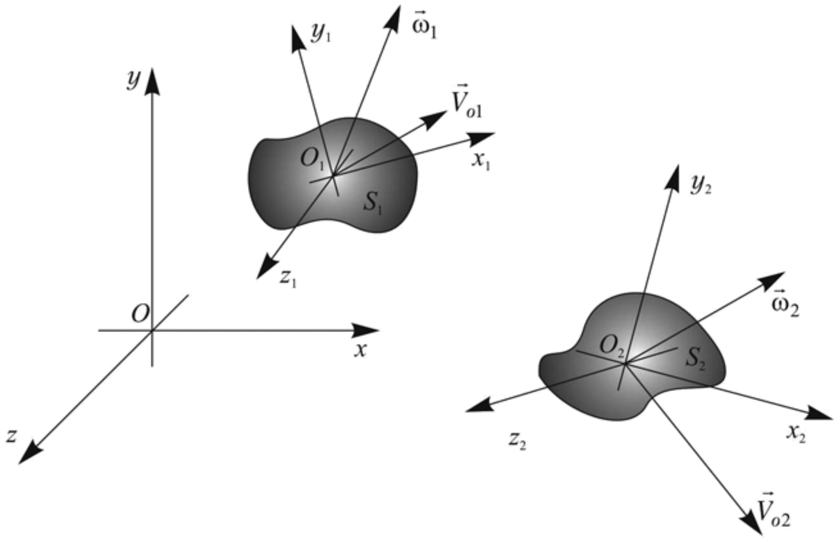

Fig. 4.1 Coordinate systems of interacting bodies

masses, called the added masses of interaction. For example, for two bodies moving in an infinite fluid the total number of added masses equals 144.

For simplicity consider the interaction of two bodies moving in a fluid; for a higher number of bodies the analysis remains essentially the same. Let two bodies (see Fig. 4.1) of an arbitrary shape move independently in an inviscous ideal fluid. Consider three coordinate systems: an absolute (immovable) system x, y, z and two movable ones: x_1, y_1, z_1 which is rigidly attached to the 1st body and x_2, y_2, z_2 which is rigidly attached to the 2nd body. The origin of the nth coordinate system $(n = 1, 2)$ we denote by O_n; this point is considered as the pole (center of rotation) of the nth body. Then velocity of a point P belonging to the nth body is given by the formula

$$\vec{V}_n(P) = \vec{V}_{O_n} + \vec{\omega}_n \times \vec{r}_n, \tag{4.1}$$

where $\vec{r}_n = O_n P$ is the radius-vector of the point P with respect to the pole O_n.

We assume the flow to be vortex-free, with single-valued potential Φ. The problem of finding the potential gives rise to a solution of the Laplace equation

$$\frac{\partial^2 \Phi}{\partial x^2} + \frac{\partial^2 \Phi}{\partial y^2} + \frac{\partial^2 \Phi}{\partial z^2} = 0 \tag{4.2}$$

with the following boundary conditions:

- Water-tightness condition on the surface of each body:

$$\left.\frac{\partial \Phi}{\partial n}\right|_{S_1} = \vec{V}_1 \cdot \vec{n}, \qquad \left.\frac{\partial \Phi}{\partial n}\right|_{S_2} = \vec{V}_2 \cdot \vec{n}, \tag{4.3}$$

where $\vec{n}$ is the unit vector of the external normal to the surface of the body.

- Asymptotic condition:

$$\operatorname{grad}\Phi \to 0, \quad \text{as } R = \sqrt{x^2 + y^2 + z^2} \to \infty. \tag{4.4}$$

Linearity of this problem allows us to use the superposition principle and represent the potential as a sum of 12 potentials (according to the total number of degrees of freedom). As well as in the case of the motion of a single body in an unlimited fluid one can introduce so-called elementary potentials φ_{in} in terms of which the solution can be written in the form

$$\Phi = \sum_{i=1}^{6} v_{i1} \cdot \varphi_{i1} + \sum_{i=1}^{6} v_{i2} \cdot \varphi_{i2}. \tag{4.5}$$

In this formula one has the generalized velocities v_{i1} and v_{i2} of the first and the second bodies. These velocities are given by projections of linear and angular velocities of the nth body to the axes of the coordinate system associated to this body:

$$\begin{aligned} &v_{11} = V_{O1x}, \quad v_{21} = V_{O1y}, \quad v_{31} = V_{O1z}, \quad v_{41} = \omega_{1x},\\ &v_{51} = \omega_{1y}, \quad v_{61} = \omega_{1z}, \quad v_{12} = V_{O2x}, \quad v_{22} = V_{O2y},\\ &v_{32} = V_{O2z}, \quad v_{42} = \omega_{2x}, \quad v_{52} = \omega_{2y}, \quad v_{62} = \omega_{2z}. \end{aligned} \tag{4.6}$$

The elementary potentials φ_{i1} correspond to the motion of the first body with unit ith velocity such that all other velocities of this body, as well as all velocities of the second body, equal zero. Potentials φ_{i1} are defined analogously. In analogy to analysis of Chap. 1 of the motion of an isolated body, substituting (4.5) and (4.1) in the boundary conditions (4.3) we obtain a set of conditions for the 12 potentials on the boundaries of both bodies:

1. On the surface S_1

$$\begin{aligned} &\frac{\partial\varphi_{11}}{\partial n_1} = \cos(n_1, x_1); \qquad \frac{\partial\varphi_{21}}{\partial n_1} = \cos(n_1, y_1) = l_2;\\ &\frac{\partial\varphi_{31}}{\partial n_1} = \cos(n_1, z_1) = l_3; \qquad \frac{\partial\varphi_{41}}{\partial n_1} = y_1 l_3 - z_1 l_2 = l_4;\\ &\frac{\partial\varphi_{51}}{\partial n_1} = z_1 l_1 - x_1 l_3 = l_5; \qquad \frac{\partial\varphi_{61}}{\partial n_1} = x_1 l_2 - y_1 l_1 = l_6; \qquad \frac{\partial\varphi_{i2}}{\partial n_1} = 0. \end{aligned} \tag{4.7}$$

2. On the surface S_2:

$$\begin{aligned} &\frac{\partial\varphi_{12}}{\partial n_2} = \cos(n_2, x_2) = m_1; \qquad \frac{\partial\varphi_{22}}{\partial n_2} = \cos(n_2, y_2) = m_2;\\ &\frac{\partial\varphi_{32}}{\partial n_2} = \cos(n_2, z_2) = m_3; \qquad \frac{\partial\varphi_{42}}{\partial n_2} = y_2 m_3 - z_2 m_2 = m_4;\\ &\frac{\partial\varphi_{52}}{\partial n_{21}} = z_2 m_1 - x_2 m_3 = m_5; \qquad \frac{\partial\varphi_{62}}{\partial n_2} = x_2 m_2 - y_2 m_1 = m_6; \qquad \frac{\partial\varphi_{i1}}{\partial n_2} = 0. \end{aligned} \tag{4.8}$$

From these boundary conditions we observe that each of the elementary potentials φ_{in} corresponds to the motion of the nth body with ith unit velocity under assumption that the second body remains at rest.

As well as in the case of an isolated body in an infinite fluid the total kinetic energy of the fluid enclosed between the surfaces of the bodies and the sphere of large radius equals (in the limit when the radius of the sphere tends to infinity)

$$T = -\frac{\rho}{2}\int_{S_1} \Phi \frac{\partial \Phi}{\partial n_1}\, dS - \frac{\rho}{2}\int_{S_2} \Phi \frac{\partial \Phi}{\partial n_2}\, dS. \tag{4.9}$$

Substituting the linear decomposition of the potential (4.5) in this expression and taking into account the boundary conditions (4.8) and (4.9) for the unit potentials, one can obtain an expression for the kinetic energy of the fluid, which contains 144 terms.

Using the formulas for the added masses in terms of the elementary potentials, the expression (4.9) can be written in the form [94, 95]

$$\begin{aligned} 2T = {} & \sum_{i=1}^{6}\sum_{j=1}^{6} v_{i1}v_{j1}A_{ij} + \sum_{i=1}^{6}\sum_{j=1}^{6} v_{i2}v_{j2}D_{ij} + \sum_{i=1}^{6}\sum_{j=1}^{6} v_{i1}v_{j2}B_{ij} \\ & + \sum_{i=1}^{6}\sum_{j=1}^{6} v_{i1}v_{j2}C_{ij}. \end{aligned} \tag{4.10}$$

The added masses entering (4.10) are contained in four 6×6 matrices A_{ij}, B_{ij}, C_{ij} and D_{ij} given by

$$\begin{aligned} A_{ij} &= -\rho \iint_{S_1} \varphi_{i1}\frac{\partial \varphi_{j1}}{\partial n}\, dS, & D_{ij} &= -\rho \iint_{S_2} \varphi_{i2}\frac{\partial \varphi_{j2}}{\partial n}\, dS, \\ B_{ij} &= -\rho \iint_{S_1} \varphi_{i2}\frac{\partial \varphi_{j1}}{\partial n}\, dS, & C_{ij} &= -\rho \iint_{S_2} \varphi_{i1}\frac{\partial \varphi_{j2}}{\partial n}\, dS. \end{aligned} \tag{4.11}$$

The matrices A_{ij} and D_{ij} are the matrices of added masses of the first and second bodies, respectively. However, these matrices are obtained taking into account the mutual hydrodynamic influence of the bodies; therefore, they are different from the added masses of the corresponding single body in an infinite fluid. The matrices B_{ij} and C_{ij} contain new added masses, which can be called the added masses of interaction. Since B_{ij} are expressed via integrals over the surface of the first body, they are called the added masses of interaction of the first body; C_{ij} are called the added masses of interaction of the second body.

We stress again, that all these added masses essentially depend on mutual positions of the bodies, and, therefore, change in the process of motion.

The total number of added masses which determine the kinetic energy of the fluid under independent motion of two bodies equals 144 (four matrices, each of which contains 36 entries). However, the number of independent added masses is much smaller. One can show, for example, that $B_{ij} = C_{ij}$ [94–96]. Taking into account this property the formula (4.10) for kinetic energy can be rewritten as follows:

$$2T = \sum_{i=1}^{6}\sum_{j=1}^{6} v_{i1}v_{j1}A_{ij} + \sum_{i=1}^{6}\sum_{j=1}^{6} v_{i2}v_{j2}D_{ij} + 2\sum_{i=1}^{6}\sum_{j=1}^{6} v_{i1}v_{j2}B_{ij}.$$

Therefore, each body has 21 added masses (similarly to the case of motion of an isolated body in an infinite fluid); in addition there are 36 added masses of interaction. The total number of independent added masses is therefore equal to 78.

Consider now the case of interaction of two bodies one of which is moving and another is staying at rest. According to our terminology, such interaction is considered as non-stationary. There are the following modifications in formulation of the problem of fluid motion in that case in comparison with the motion of two bodies:

First, the boundary conditions (4.3) on the boundary of the second (immovable) body transform as follows (while the boundary conditions on the surface of the first body remain the same):

$$\left.\frac{\partial \Phi}{\partial n}\right|_{S_1} = \vec{V}_1 \cdot \vec{n}, \qquad \left.\frac{\partial \Phi}{\partial n}\right|_{S_2} = 0.$$

Second, now the system of two bodies possesses only six degrees of freedom (instead of 12 in the case when both bodies move). The potential of fluid flow can be represented as the sum of only six terms: $\varphi = \sum_{i=1}^{6} v_{i1} \cdot \varphi_{i1}$. Boundary conditions for the elementary potentials φ_{i1} on the surfaces of moving body (S_1) and immovable body (S_2) differ from (4.7) and (4.8). Namely, in these formulas the boundary conditions for the elementary potentials of the second body (φ_{i2}) are absent, since these potentials equal zero. On the surface of the immovable body one has to impose boundary conditions for the elementary potentials of the first (moving) body: $\partial\varphi_{i1}/\partial n|_{S_2} = 0$. It follows from (4.11) that under these conditions the added masses of the second body D_{ij}, as well as all added masses of interaction (B_{ij} and C_{ij}) of both bodies, vanish. Therefore, we conclude that under interaction of a moving body with an immovable one there exist only added masses of the moving body, which are variable functions of coordinates determining its position with respect to the immovable body.

The absence of the added masses of the second body, as well as of the added masses of interaction is explained by the fact that the body can create some kinetic energy of the fluid flow only if it is moving. If it is immovable, its boundaries can only influence the flow created by the motion of the other body (and, therefore, on its added masses). Mathematically this influence is expressed in the form of an additional water-tightness condition on the surface of the immovable body, which leads to the change of added masses of the moving body.

4.1.2 Motion of Two Spheres in an Infinite Fluid

The main features of the flow caused by the motion of two bodies in a fluid can be observed in the case of motion of two spheres [117, 133, 181]. Let two spheres

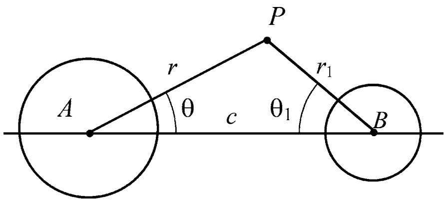

Fig. 4.2 Scheme of motion of two spheres along the line connecting their centers

with radii a and b move along the line connecting their centers with velocities u and u_1. The distance between the centers of the spheres is denoted by c. For an arbitrary point P of the fluid we have (Fig. 4.2): $AP = r$, $BP = r_1$, $\angle PAB = \theta$, $\angle PBA = \theta_1$. The potential of velocities can be represented in the form $u\varphi + u_1\varphi_1$ where the functions φ and φ_1 satisfy the following conditions:

1. $\Delta\varphi = 0$; $\Delta\varphi_1 = 0$.
2. At infinity all coordinate derivatives of functions φ and φ_1 vanish.
3. On the surface of the sphere A we have $\partial\varphi/\partial r = -\cos\theta$, $\partial\varphi_1/\partial r = 0$; on the surface of the sphere B we have $\partial\varphi/\partial r_1 = 0$, $\partial\varphi_1/\partial r_1 = -\cos\theta_1$.

We see that the function φ is the potential of the velocity in the case when the sphere A moves with unit velocity towards the sphere B which stays at rest. The function φ_1 has a similar meaning: this is the potential of fluid corresponding to the situation when the sphere A stays at rest while the sphere B moves towards the sphere A with unit velocity. Complexity of this problem is due to necessity to satisfy the water-tightness condition simultaneously on the surfaces of both spheres. The method of successive approximation allows us to find the functions φ, φ_1 and get an expression for kinetic energy of the fluid:

$$2T = Lu^2 + 2Muu_1 + Nu_1^2, \tag{4.12}$$

where

$$L = \frac{2}{3}\rho\pi a^3\left[1 + 3\frac{a^3b^3}{c^3f_1^3} + 3\frac{a^6b^6}{c^3f_1^3(c-f_2)^3f_2^3} + \cdots\right];$$

$$M = 2\pi\rho\frac{a^3b^3}{c^3}\left[1 + \frac{a^3b^3}{f_{10}^3(c-f_{20})^3} + \frac{a^6b^6}{f_{10}^3f_{30}^3(c-f_{20})^3(c-f_{40})^3} + \cdots\right];$$

$$N = \frac{2}{3}\pi\rho b^3\left[1 + 3\frac{a^3b^3}{c^3f_{10}^3} + 3\frac{a^6b^6}{c^3f_{10}^3(c-f_{20})^3f_{20}^3} + \cdots\right];$$

$$f_1 = c - \frac{b^2}{c}; \qquad f_2 = \frac{a^2c}{c^2-b^2}; \qquad f_{10} = c - \frac{a^2}{c}; \qquad f_{20} = \frac{b^2c}{c^2-a^2};$$

$$f_{30} = c - \frac{a^2}{c-f_{20}}; \qquad f_{40} = \frac{b^2}{f_{30}}.$$

The formula (4.12) is analogous to the formula for kinetic energy of a body with two degrees of freedom moving in a fluid; for example, this body can move only along axes Ox and Oy in the coordinate system attached to the body.

If the sphere B stays at rest ($u_1 = 0$), then the added mass of the sphere A equals $\lambda_{11} = L$, which follows from expression (4.12). If the ratios a/c and b/c are small, then one can derive approximate expressions for L, M and N:

$$L = \frac{2}{3}\pi\rho a^3\left(1 + \frac{3a^3b^3}{c^6}\right); \qquad M = 2\pi\rho\frac{a^3b^3}{c^3}; \qquad N = \frac{2}{3}\pi\rho b^3\left(1 + \frac{a^3b^3}{c^6}\right).$$

If the spheres move orthogonally to the line connecting their centers with velocities v and v_1, then in the formula for kinetic energy of the fluid

$$2T = Pv^2 + 2Qvv_1 + Rv_1^2$$

coefficients can be found approximately under assumption that the ratios a/c and b/c are small [133]:

$$P = \frac{2}{3}\pi\rho a^3\left(1 + \frac{3}{4}\frac{a^3b^3}{c^6}\right); \qquad Q = \pi\rho\frac{a^3b^3}{c^3};$$

$$R = \frac{2}{3}\pi\rho b^3\left(1 + \frac{3}{4}\frac{a^3b^3}{c^6}\right).$$

Added masses of two interacting bodies were also studied in [36].

4.2 Added Masses of Bodies Moving Close to a Solid Boundary

4.2.1 Sphere Moving Close to a Flat Wall

By substituting into the formulas derived in the previous section $a = b$, $c = 2h$, where h is the distance to a flat solid wall, we find in the case when the sphere moves orthogonally to the wall:

$$\lambda_{22} = \frac{2}{3}\pi\rho a^3\left(1 + \frac{3}{8}\frac{a^3}{h^3} + \cdots\right). \tag{4.13}$$

When the motion is parallel to the wall:

$$\lambda_{11} = \frac{2}{3}\pi\rho a^3\left(1 + \frac{3}{16}\frac{a^3}{h^3} + \cdots\right). \tag{4.14}$$

We assume that the x axis is parallel to the wall, and the y axis is orthogonal to the wall. If in the computations one keeps the terms up to the order $(a/h)^{12}$, one gets the following more precise version of the formulas (4.13), (4.14) [193]:

$$\lambda_{22} = \frac{2}{3}\pi\rho a^3\left(1 + \frac{3}{8}\delta^3 + \frac{3}{2^6}\delta^6 + \frac{9}{2^8}\delta^8 + \frac{3}{2^9}\delta^9 + \frac{9}{2^9}\delta^{10} + \frac{9}{2^{10}}\delta^{11} + \frac{33}{2^{12}}\delta^{12} + \cdots\right);$$

$$\lambda_{11} = \frac{2}{3}\pi\rho a^3\left(1 + \frac{3}{16}\delta^3 + \frac{3}{2^8}\delta^6 + \frac{3}{2^8}\delta^8 + \frac{3}{2^{12}}\delta^9 + \frac{27}{2^{12}}\delta^{10} + \frac{3}{2^{11}}\delta^{11} + \frac{195}{2^{16}}\delta^{12} + \cdots\right),$$

where $\delta = a/h$.

4.2.2 Circular Cylinder Moving Near a Flat Wall

When an infinite cylinder of radius a moves hear a flat solid wall situated at a distance h from its axis, its added masses are determined by the following formula [193]:

$$\lambda_{11} = \lambda_{22} = \pi\rho a^2\left(1 + \frac{1}{2}\delta^2 + \frac{1}{2^3}\delta^4 + \frac{3}{2^5}\delta^6 + \frac{1}{2^4}\delta^8 + \frac{23}{2^9}\delta^{10} + \frac{71}{2^{11}}\delta^{12} + \cdots\right).$$

The x-axis is parallel to the wall; the y-axis is orthogonal to the wall, the z-axis coincides with the axis of the cylinder, $\delta = a/h$.

If a circular cylinder touches the wall ($\delta = 1$), then its added mass λ_{11} looks as follows [77]:

$$\lambda_{11} = \pi\rho a^2\left(\frac{\pi^2}{3} - 1\right) = 2.29\pi\rho a^2.$$

Consider an infinite circular cylinder of radius a situated in the central plane of a channel of infinite depth bounded by two vertical walls; the distance between the walls of the channel is denoted by h. The added mass of the cylinder along axis x (which is chosen to be parallel to the walls) is given by the formula [36]:

$$\lambda_{11} = \pi\rho a^2\left[1 + \frac{2}{3}\left(\frac{\pi a}{h}\right)^2 + \cdots\right].$$

The added mass of a plate of width b under the same conditions of motion (the plane of the plate is orthogonal to the boundaries of the channel) is given by [36]:

$$\lambda_{11} = \frac{\pi\rho b^2}{4}\left(1 + \frac{\pi^2 b^2}{24h^2} + \cdots\right).$$

If an infinite circular cylinder of radius a is situated in the center of an infinite cylinder of square section with side s, then its added mass in the direction orthogonal to the axis of the cylinder and one of the walls is given by the formula [36]:

$$\lambda_{11} = \pi\rho a^2\left(1 + 6.88\frac{a^2}{s^2} + \cdots\right)$$

under condition $a/s \ll 1$.

4.2.3 Elliptic Cylinder Moving Near a Flat Wall

Consider an elliptic cylinder moving near a flat solid wall such that the larger axis of its cross-section is parallel to the wall and coincides with the x-axis. The smaller axis (coinciding with the y-axis) is orthogonal to the wall. Then the added masses (per unit of length of the cylinder) are given by the formulas [194]:

$$\lambda_{11} = \rho\pi ab\frac{2 - (1-e^2)^{1/2} - (1-\eta^{-2})^{1/2}}{(1-e^2)^{-1/2} - 2 + (1-\eta^{-2})^{1/2}} := k_{11}\rho\pi ab;$$

$$\lambda_{22} = \rho\pi ab\frac{(1-e^2)^{-1/2} - (1-\eta^{-2})^{1/2}}{(1-\eta^{-2})^{1/2} - (1-e^2)^{1/2}} := k_{22}\rho\pi ab;$$

$$\begin{aligned}\lambda_{66} &= \frac{\pi\rho ab(a^2+b^2)e^2}{8(2-e^2)}\frac{(1-e^2)^{-1/2}[1-(1-e^2)^{1/2}]^2 + 2[1-(1-\eta^{-2})^{1/2}]^2}{e^{-2}[1-(1-e^2)^{1/2}]^2 - [1-(1-\eta^{-2})^{1/2}]^2}\\ &:= k_{66}\frac{1}{4}\rho\pi ab\big(a^2+b^2\big),\end{aligned} \tag{4.15}$$

where $e^2 = 1 - (b/a)^2$; $\eta = [1 + 4h^2/(a^2 - b^2)]^{1/2}$; a is the large semi-axis of the ellipse, b—small semi-axis; h is the distance between the large semi-axis of the ellipse and the wall. We consider ratios of these added masses to added masses of elliptic cylinder in infinite volume to get coefficients k_{11}, k_{22} and k_{66} per unit of length.

In Figs. 4.3, 4.4 we show the graphs of functions $k_{11}(a/b, b/h)$; $k_{22}(a/b, b/h)$ and $k_{66}(a/b, b/h)$.

4.2.4 Elliptic Cylinder Moving Between Two Flat Walls in the Direction Parallel to the Walls

The problem of such motion was considered in the paper [70, 234]. An approximate solution was used obtained under an assumption that the motion of the cylinder can be substituted by the motion of three cylinders (the original cylinder and two of

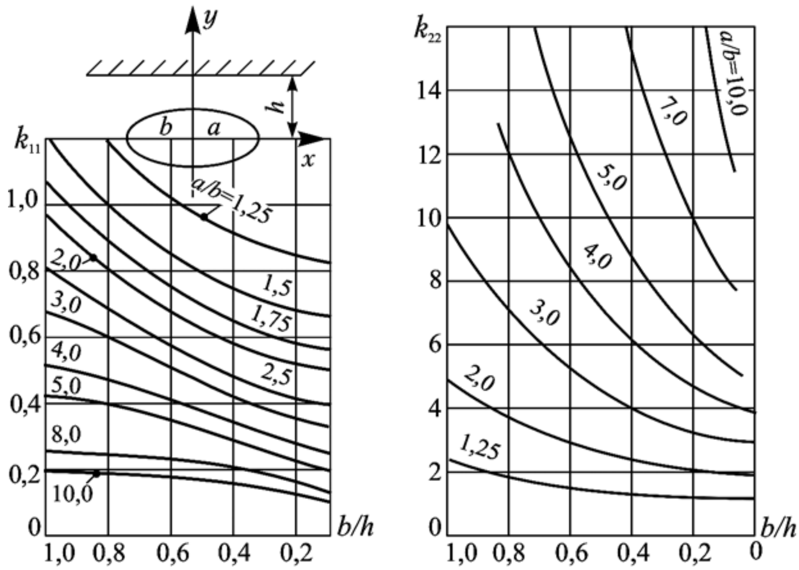

Fig. 4.3 Coefficients of added masses of an *elliptic cylinder* moving near a *flat solid wall* ($k_{11} := \lambda_{11}/\pi\rho ab$, $k_{22} := \lambda_{22}/\pi\rho ab$)

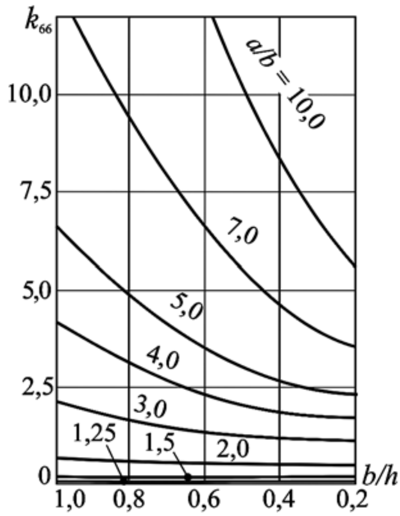

Fig. 4.4 Coefficients of added masses of *elliptic cylinder* moving near a *flat solid wall* ($k_{66} = \lambda_{66}/\{\pi\rho ab(a^2 + b^2)\}$)

its mirror images) in infinite fluid (the exact solution would require analyzing an infinite lattice of such cylinders). Results of computation of the added mass

$$k_{11} = \frac{\lambda_{11}}{\pi\rho ab} = f\left(\frac{b}{a}, \frac{b}{h}\right),$$

where h is a half of the distance between walls, are shown in Fig. 4.5.

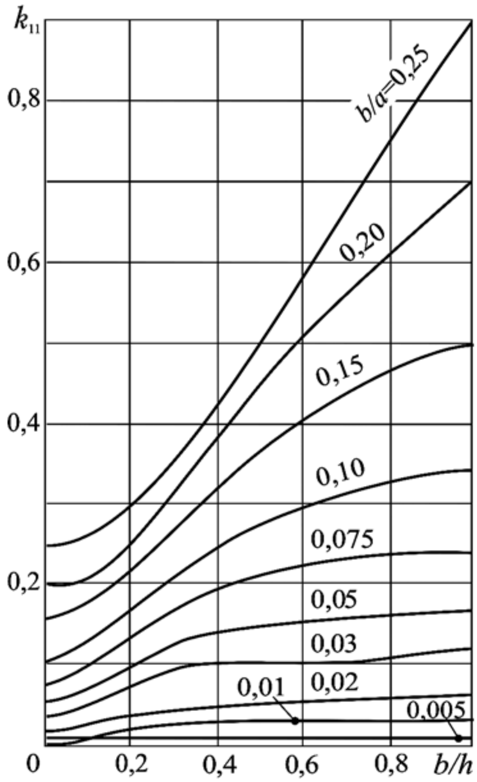

Fig. 4.5 Coefficient of added mass of an elliptic cylinder moving between two parallel walls in the direction parallel to the walls

4.2.5 Motion of Parallelepipeds in Infinite Fluid and Between Flat Walls

The added mass λ_{11} of parallelepipeds was determined experimentally [233] by the method of small oscillations (see Chap. 9). It was considered only the motion along the x-axis which is parallel to the flat walls. The y-axis was also parallel to the walls, so the added mass λ_{22} can be obtained by a simple substitution. The sizes of the parallelepiped along x, y and z axes are denoted by B, L and $2T$. In Fig. 4.6 we show the graph of the function

$$k_{11} = \frac{\lambda_{11}}{2\rho(BT)^{3/2}} = f_1\left(\frac{B}{L}, \frac{L}{T}\right)$$

for the case of motion in infinite fluid. The influence of hard walls situated at the distance $z = \pm H$ from the xOy-plane is shown in Fig. 4.7 in the form of ratio

$$\frac{k_{11\infty}}{k_{11H}} = f_2\left(\frac{B}{L}, \frac{T}{H}\right).$$

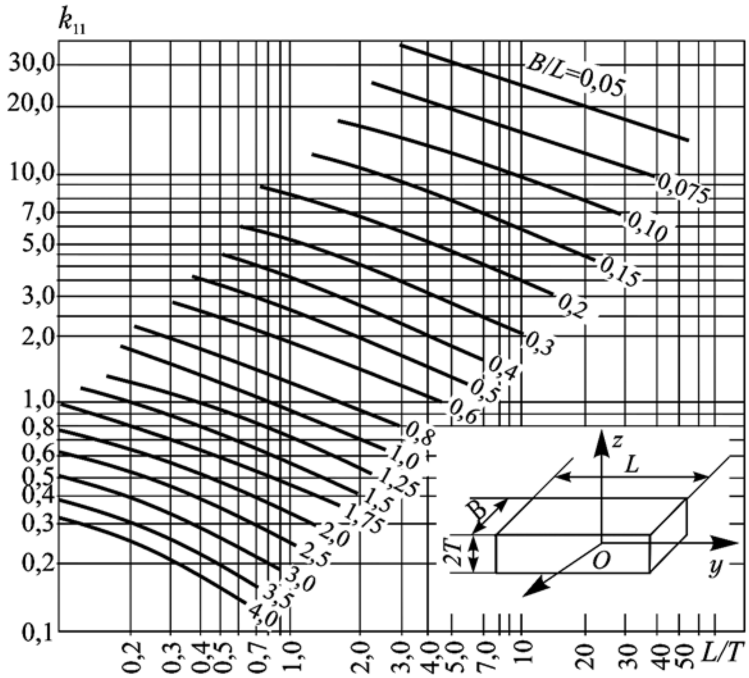

Fig. 4.6 Coefficient of added mass of a parallelepiped moving in an infinite fluid

4.2.6 Ellipsoid of Revolution Moving Near a Flat Wall

Consider an ellipsoid of revolution moving near a solid flat wall such that its symmetry axis (coinciding with the x-axis) remains parallel to the wall; the y-axis is chosen to be orthogonal to the wall. Then the added masses are expressed by the formulas [193]:

$$\lambda_{11} = k_{11}\frac{4\pi}{3}\rho ab^2; \qquad \lambda_{22} = k_{22}\frac{4\pi}{3}\rho ab^2;$$

$$\lambda_{33} = k_{33}\frac{4\pi}{3}\rho ab^2; \qquad \lambda_{55} = k_{55}\frac{4\pi}{15}\rho\left(a^2+b^2\right)ab^2.$$

In these formulas a is the semi-axis of the ellipsoid corresponding to its symmetry axis, b is another semi-axis; coefficients k_{11}, k_{22}, k_{33}, k_{55} are shown in Fig. 4.8, Fig. 4.9 as functions of a/b and b/h, where h is the distance from the center of the ellipsoid to the wall. The dashed lines in Fig. 4.8, Fig. 4.9 correspond to exact formulas in the cases of a sphere and an infinite cylinder.

Added masses of the ellipsoid of revolution moving near a hard boundary were also given by Farell [68] for $3 < a/b < 15$.

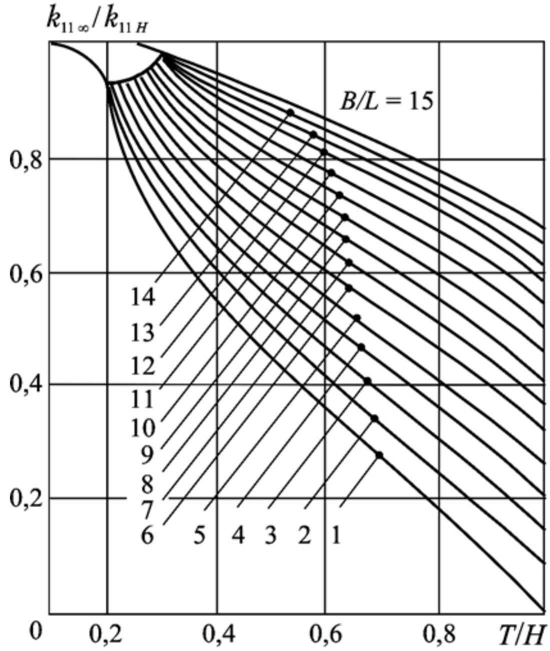

Fig. 4.7 Coefficient of added mass of a parallelepiped moving between two walls

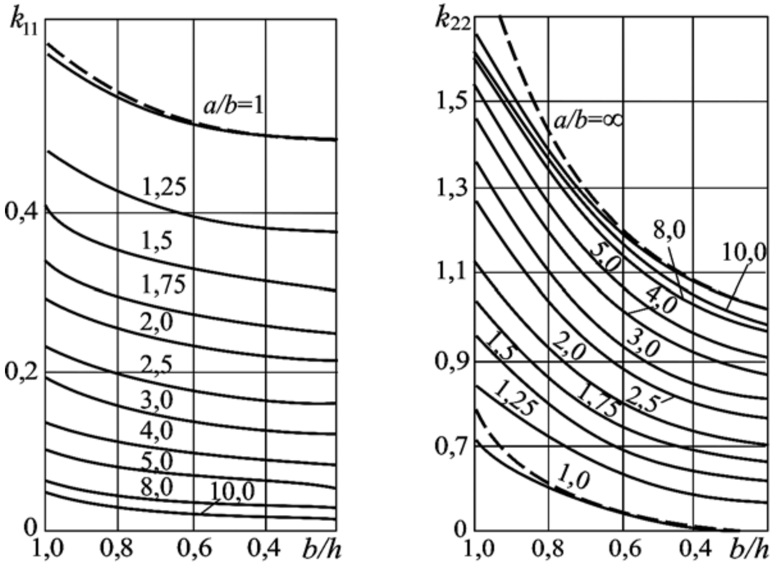

Fig. 4.8 Coefficients of added masses of a cylinder of revolution moving near a flat solid wall

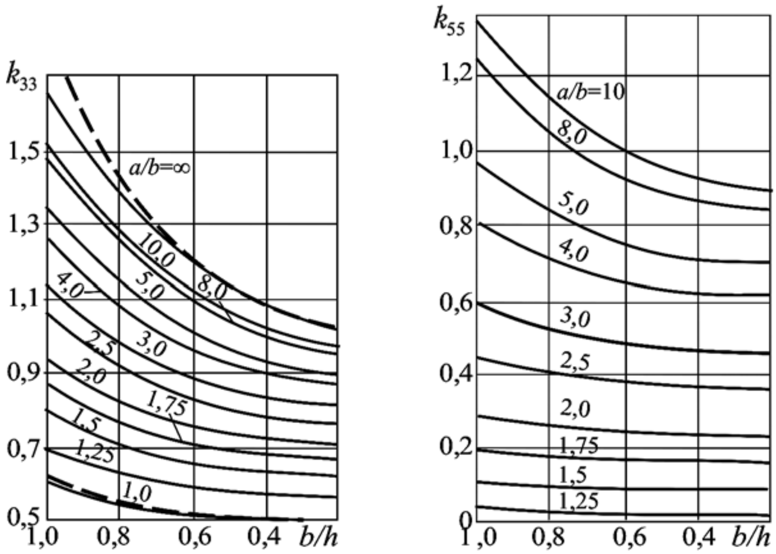

Fig. 4.9 Coefficients of added masses of a cylinder of revolution moving near a flat solid wall

4.2.7 Three-Axial Ellipsoid Moving Near a Flat Wall

In first approximation the added masses of a three-axial ellipsoid moving near a flat hard wall can be computed via a method proposed by Bloch and Ginevsky [30]. Let us briefly outline this method for the case of motion of two bodies in an ideal fluid which does not move at infinity. The potential of velocities Φ of the fluid motion can be represented in the form

$$\Phi = \Phi_1 + \Phi_2,$$

where Φ_1 is the potential of velocities corresponding to the motion of the first body in the presence of the second body, which stays at rest; Φ_2 is the potential of velocities corresponding to the motion of the second body in the presence of the first body, assuming that the first body stays at rest.

Obviously, the potential Φ_1 differs from the potential Φ_1^0 which corresponds to the motion of the first body in an infinite fluid, when the second body is absent; this difference is due to the water-tightness boundary condition on the surface of the second body when it is present. If the distance between two bodies is large enough in comparison with their sizes, then in the formula

$$\Phi_1^0 = \Phi_1 + \delta\Phi_1 \tag{4.16}$$

the first-order correction $\delta\Phi_1$ can be found as follows. First compute the velocity δu_1 caused by the motion of the first body at the position of the second one. Assume that the second body moves with this velocity. Then the second term in the right-hand side of (4.4) will be written in the form $\varphi_2 \delta u_1$, where φ_2 is the potential arising in the fluid under the motion of the second body with unit speed in the direction of velocity δu_1 in the presence of the first body. Then we come to the equation

$$\Phi_1^0 = \Phi_1 + \varphi_2 \delta u_1. \tag{4.17}$$

Analogously for the second body we find

$$\Phi_2^0 = \Phi_2 + \varphi_1 \delta u_2. \tag{4.18}$$

The unknowns in Eqs. (4.17), (4.18) are φ_1, φ_2, Φ_1, Φ_2; the potentials φ_1 and Φ_1 are also related to each other (as well as φ_2 and Φ_2), since they are entirely determined by the motion of the first (respectively second) body. From the system (4.17), (4.18) we can express either $\Phi_{1,2}$ or $\varphi_{1,2}$.

If, for example, the body moves with linear velocity u_0 along a hard flat wall then, considering the mirror image of the body, we get that $\delta u_1 = \delta u_2 = \delta u$ is the velocity induced by the body at the location of its mirror image,

$$\Phi_1 = u_0 \varphi_1, \qquad \Phi_1^0 = u_0 \varphi_1^0, \qquad \Phi_2 = u_0 \varphi_2, \qquad \Phi_2^0 = u_0 \varphi_2^0.$$

The system of Eqs. (4.17), (4.18) then takes the form

$$\varphi_1^0 = \varphi_1 + \varphi_2 \delta \bar{u},$$
$$\varphi_2^0 = \varphi_2 + \varphi_1 \delta \bar{u},$$

where $\delta \bar{u} \equiv \delta u / u_0$.

Solutions of this system can be written in the form

$$\varphi_1 = \frac{\varphi_1^0 - \varphi_2^0 \delta \bar{u}}{1 - (\delta \bar{u})^2}, \qquad \varphi_2 = \frac{\varphi_2^0 - \varphi_1^0 \delta \bar{u}}{1 - (\delta \bar{u})^2}$$

and allows us to find the required potential

$$\varphi \equiv \frac{\Phi}{u_0} = \varphi_1 + \varphi_2 = \frac{\varphi_1^0 + \varphi_2^0}{1 + \delta \bar{u}}.$$

The formula for the elementary potential has the same form for the case when the body moves orthogonally to the wall. Potentials φ_1^0 and φ_2^0 correspond to the motion of isolated bodies in an unlimited fluid. If the body moves near a free surface of the fluid then (imposing on the free surface the boundary condition $\varphi = 0$) the formula for the total potential takes the form $\varphi = (\varphi_1^0 - \varphi_2^0)/(1 - \delta \bar{u})$.[2] In Fig. 4.10 we show dependence of the coefficient of the added mass $k_{11} = \lambda_{11}/[(4/3)\pi \rho a b]$ of the three-axial ellipsoid with half-axes $a > b > c$, on c/b [30]. The positions of the axes are chosen as follows: the largest axis, coinciding with coordinate axis Ox, is parallel to the wall, while the smallest axis is either orthogonal to the wall (left half of the figure), or parallel to the wall (right half of the figure). The ratio of half-axes a/b in this example equals 5.

[2]More detailed description of this approximate method is contained in the work [30] and in the monograph [117].

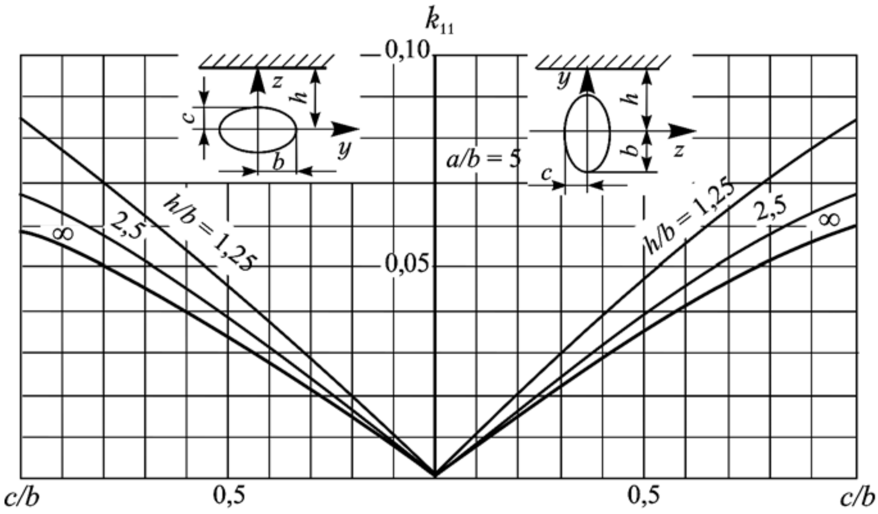

Fig. 4.10 Coefficient k_{11} of added mass of a three-axis ellipsoid moving near a flat solid wall

The problem of motion of a three-axial ellipsoid near the wall was considered in [52, 75, 188, 236]. The influence of the wall was substituted by the influence of the mirror image of the ellipsoid. The axes Ox and Oy were assumed to be parallel to the wall, the Oz axis—orthogonal to the wall. The half-axes were assumed to satisfy the condition $a > b > c$. The distance from the xOy plane of the ellipsoid to the wall was denoted by h. Motion along the Ox and Oy axes was considered. The results of computation of the added masses

$$k_{11} = \frac{\lambda_{11}}{(4/3)\pi\rho abc} = f_1\left(\frac{c}{a}, \frac{c}{h}\right);$$

$$k_{22} = \frac{\lambda_{22}}{(4/3)\pi\rho abc} = f_2\left(\frac{c}{a}, \frac{c}{h}\right)$$

are shown in Figs. 4.11–4.15 for fixed values of he ratio b/a.

4.2.8 System of Oblate Ellipsoids of Revolution

For computations of added masses of chains and lattices of prolate ellipsoids of revolution one can use the method of Bloch and Ginevsky [82]. The small semi-axis of the ellipsoid is denoted by c, the large is denoted by a; the dimensionless parameter is $\bar{a} = a/c$. In the case of the infinite chain of the ellipsoids posed at a distance of $2H$ from one another along the z-axis (Fig. 4.16), the coefficient $k_{11} = \lambda_{11}/[(4/3)\pi\rho a^2 c]$ of each of the ellipsoids (with small axis directed along the x-axis) depends on parameters $\bar{a}$ and $\bar{H} = H/a$. Graphs of this dependence are shown in Fig. 4.16a; the curve $\bar{a} = 1$ corresponds to the chain of spheres.

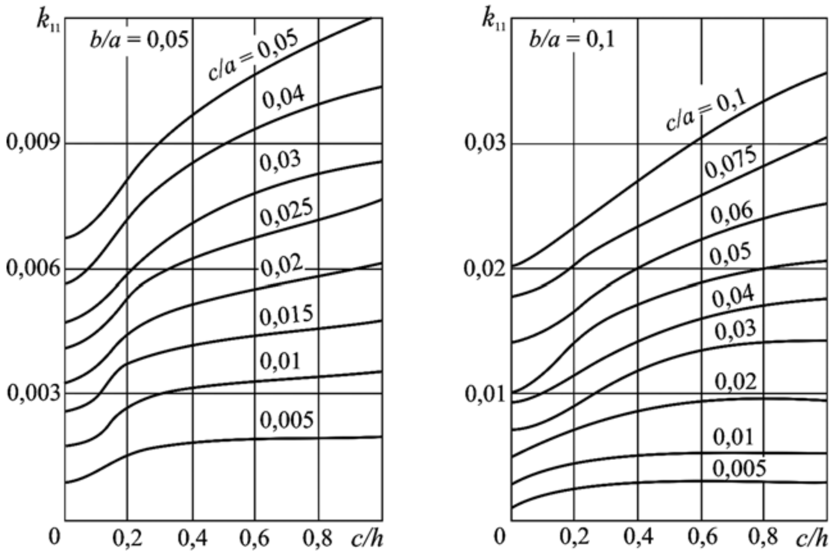

Fig. 4.11 Coefficients of added masses of a three-axial ellipsoid moving near a solid flat wall

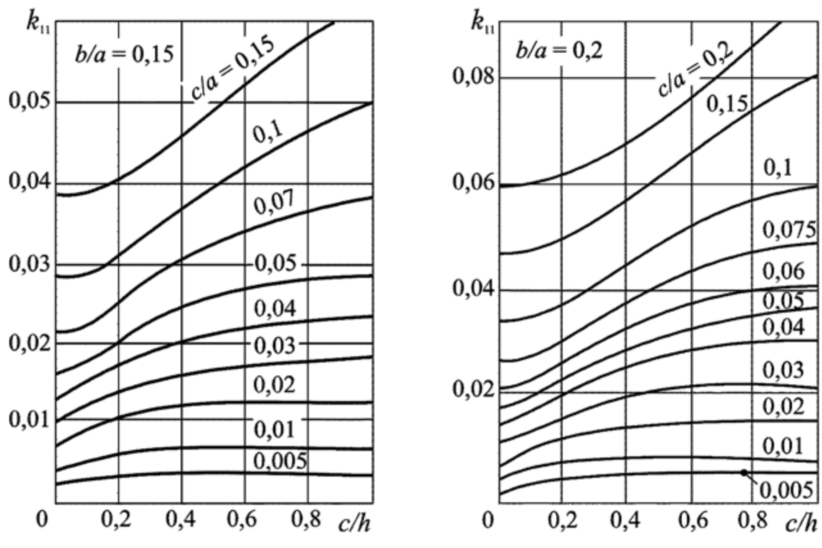

Fig. 4.12 Coefficients of added masses of a three-axial ellipsoid moving near a solid flat wall

For the square lattice of the ellipsoids, when their centers are posed in the vortices of square lattice with side $2H$ in the yOz-plane, and small axes are parallel to the x-axis, the functions $k_{11}(\bar{a}, \bar{H})$ computed using the formula presented above, are shown in Fig. 4.16b. Dots in Fig. 4.16b correspond to experimental data obtained by the authors of [82].

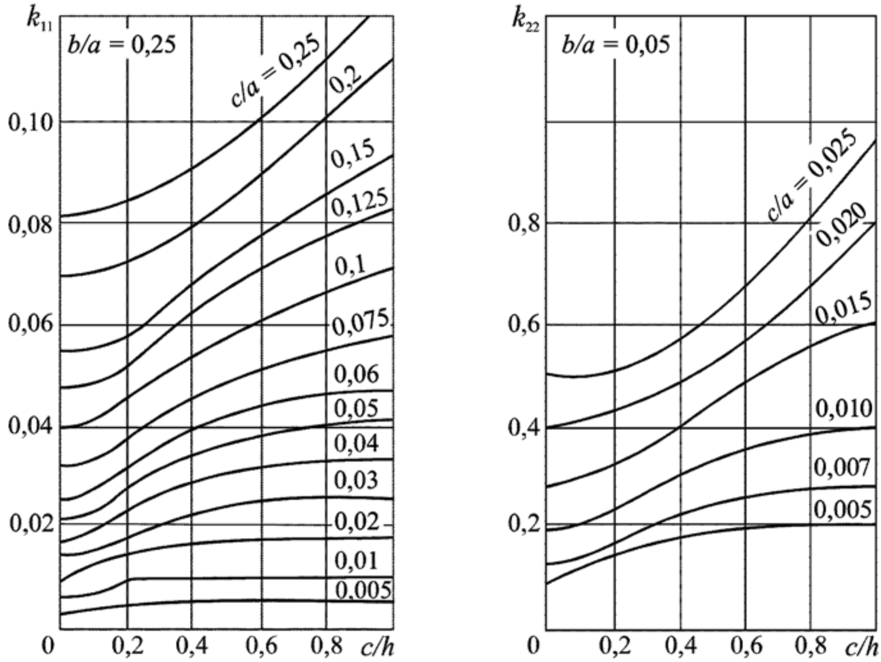

Fig. 4.13 Coefficients of added masses of three-axial ellipsoid moving near a solid flat wall

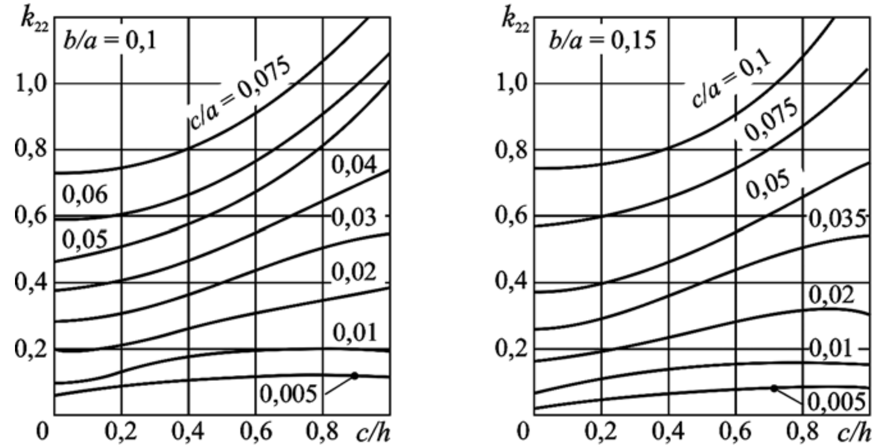

Fig. 4.14 Coefficients of added masses of three-axial ellipsoid moving near a solid flat wall

4.2.9 Infinite Chain of Three-Axial Ellipsoids

In the problem of motion of a three-axial ellipsoid in a flat channel between two walls, the influence of the walls is modeled by an infinite chain of the ellipsoids

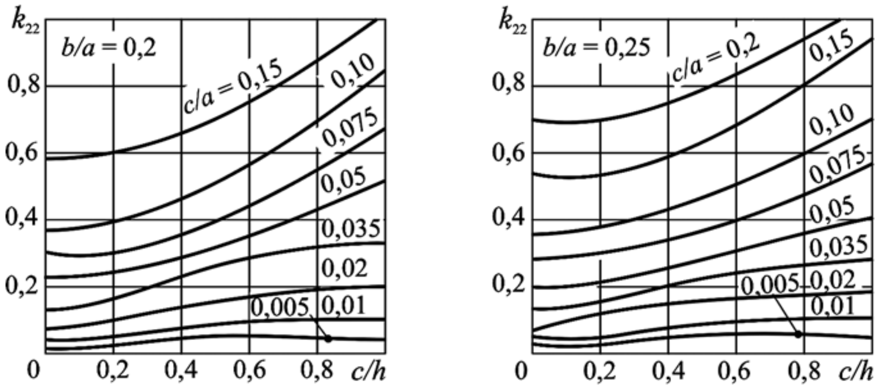

Fig. 4.15 Coefficients of added masses of a three-axial ellipsoid moving near a flat solid wall

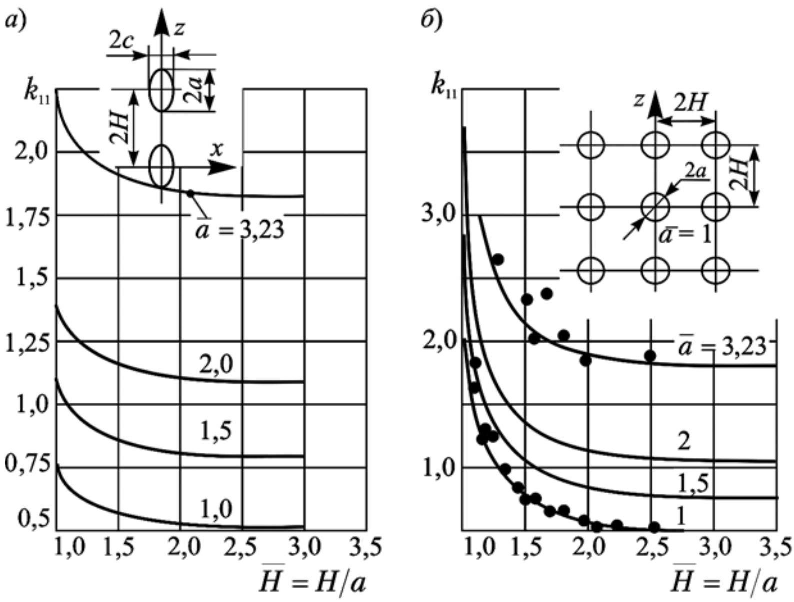

Fig. 4.16 Coefficient of added mass of an oblate ellipsoid of revolution, considered an element of an infinite chain **(a)** and an infinite lattice **(b)**

posed such that the distance between their centers equals the distance between the walls of the channel. The plane xOy of the ellipsoids is parallel to the walls of the channel; the z-axis is orthogonal to the walls. The half-axes of the ellipsoid are $a > b > c$. Coefficients of added masses of each ellipsoid in such a chain

$$k_{11} = \frac{\lambda_{11}}{(4/3)\pi\rho abc} = f_1\left(\frac{c}{h}, \frac{c}{a}\right),$$

$$k_{22} = \frac{\lambda_{22}}{(4/3)\pi\rho abc} = f_1\left(\frac{c}{h}, \frac{c}{a}\right),$$

computed by the method of Bloch and Ginevsky [236], are shown in Figs. 4.17 and 4.18 for different values of b/a. Here $2h$ is the distance between centers of two neighbor ellipsoids.

4.2.10 *Sphere in Various Systems (Chains, Lattices)*

In [48] by the method of electro-hydrodynamic analogy (EHDA, see Chap. 9) the added masses of spheres posed in an infinite chain along the x-axis (curve 1 in Fig. 4.19), in a chain along the y-axis (curve 2), in a flat square 2D lattice in the yz-plane (curve 3) and in a 3D cubic lattice (curve 4) were obtained. The radius of the sphere is denoted by R; the distance between centers of close neighbors is h. The considered coefficient of added mass is $k_{11} = \lambda_{11}/[(4/3)\pi\rho R^3]$. Notice smaller values of the coefficient k_{11} in the case of a horizontal chain in comparison with the same coefficient for an isolated sphere ($k_{110} = 0.5$).

The added masses of spheres posed in various chains and lattices are computed in [213].

4.2.11 *Ellipsoid of Revolution Moving in the Bisecting Plane of a Dihedral Angle*

To find the potential of the flow one uses the method of Bloch–Ginevsky by substituting the influence of the walls by a system of mirror ellipsoids [85]. The coordinate system is shown in Fig. 4.20. Added masses were computed for the ellipsoid of revolution with ratio of the axes $b/a = 0.208$. Results of the computations for the functions

$$k_{11} = \frac{\lambda_{11}}{(4/3)\pi\rho ab^2} = f_1\left(\frac{b}{H}, \theta\right);$$

$$k_{22} = \frac{\lambda_{22}}{(4/3)\pi\rho ab^2} = f_2\left(\frac{b}{H}, \theta\right)$$

are shown in Fig. 4.20. The distance H from the center of the ellipsoid to the wall is computed along the normal to bisecting plane; 2θ is the dihedral angle. Apart from theoretical results for k_{11} and k_{22}, there were also obtained experimental results via the method of small oscillations. Experimental results for the same coefficients $k_{11e} = f_3(b/H, \theta)$ and $k_{22e} = f_4(b/H, \theta)$ are shown in Fig. 4.21.

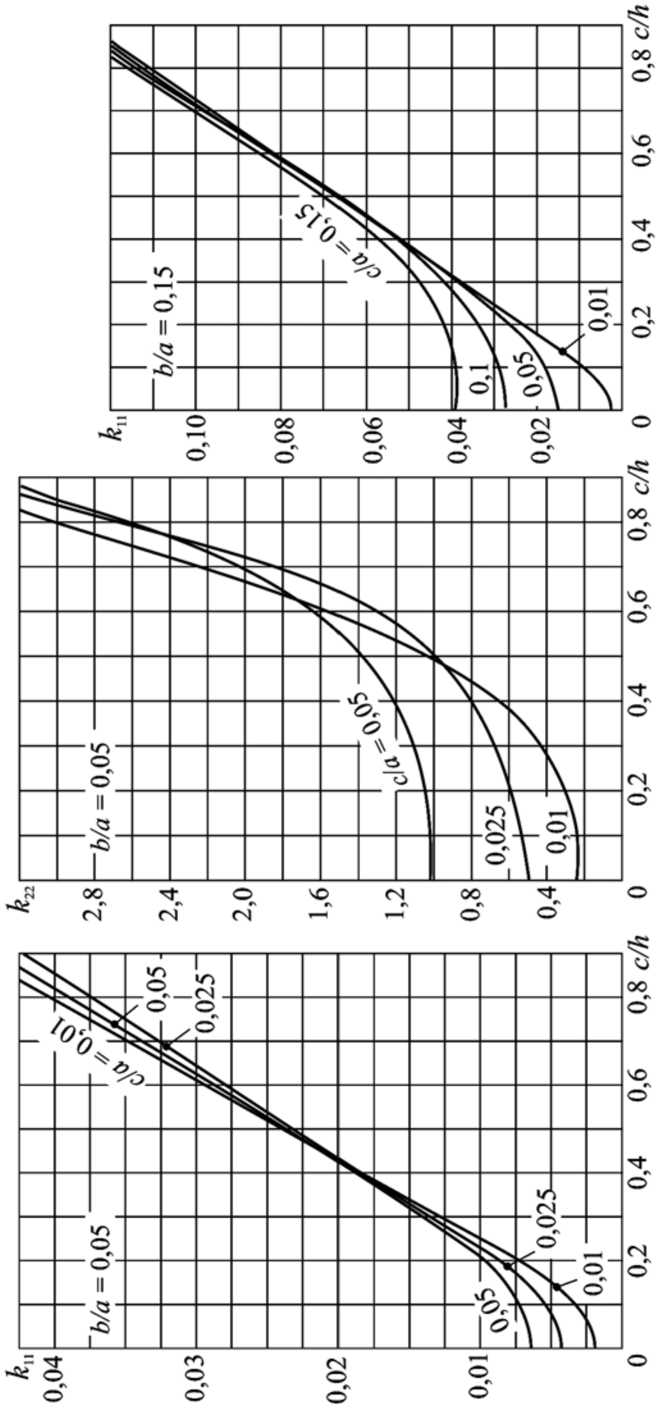

Fig. 4.17 Added masses of a three-axial ellipsoid considered as an element of an infinite chain

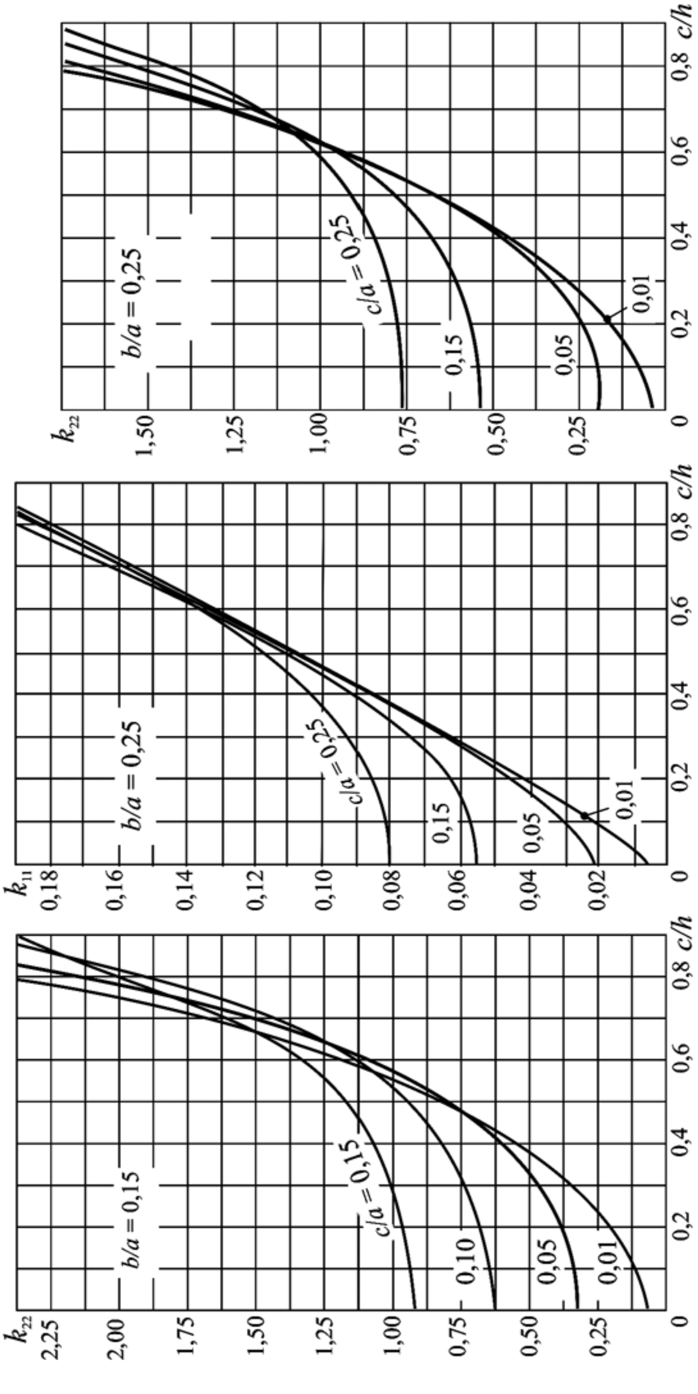

Fig. 4.18 Added masses of a three-axial ellipsoid considered as an element of an infinite chain

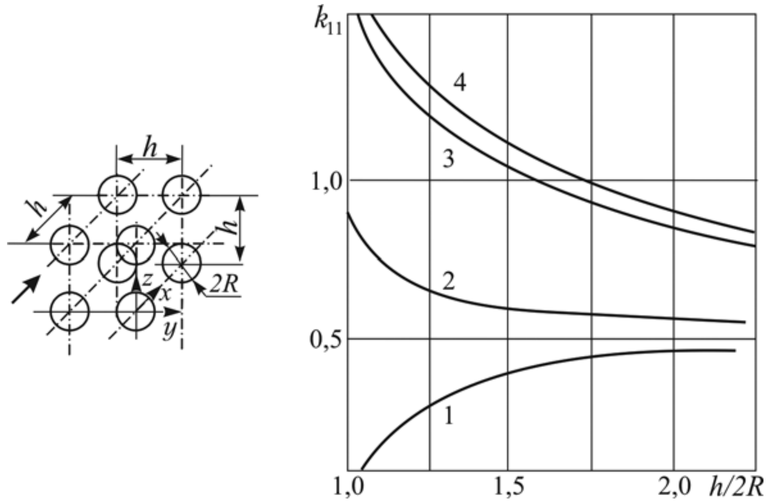

Fig. 4.19 Coefficients of added masses of a single sphere in various configurations

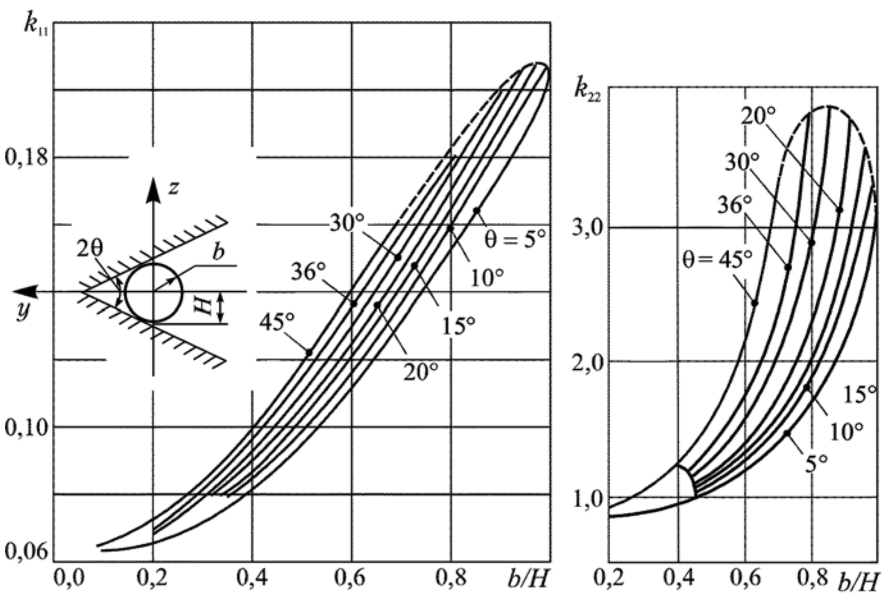

Fig. 4.20 Theoretical results for added masses of an ellipsoid of revolution moving in the bisecting plane of a dihedral angle

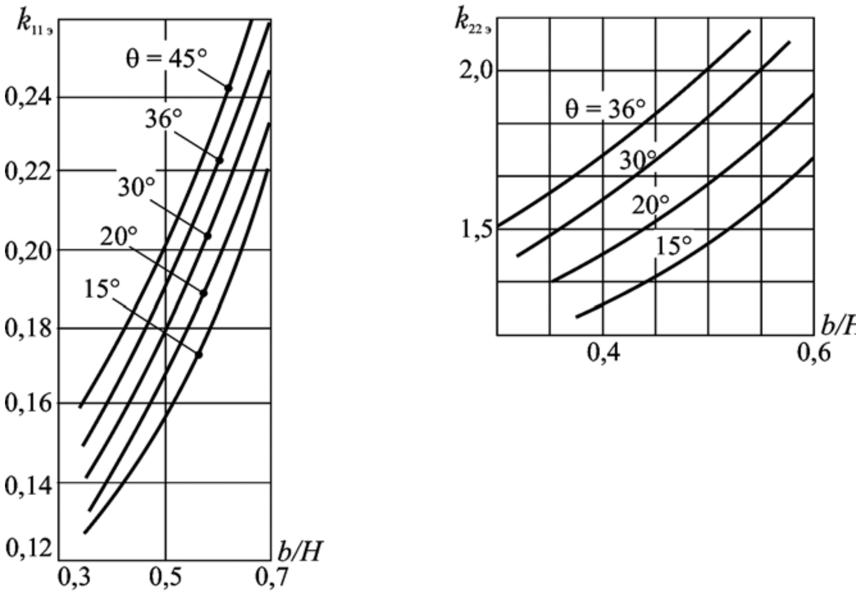

Fig. 4.21 Experimental results for added masses of an ellipsoid of revolution moving in the bisecting plane of a dihedral angle

4.2.12 Influence of the Boundary and the Free Surface on Added Masses of Foils

If a foil is moving near a hard boundary or near the free surface, then the added masses depend on the distance of the body to the boundary or the free surface. In the case of a hard wall the added masses increase when the foil approaches the wall. In the case of an under-water foil moving near a free surface with relatively high velocity (this allows us to assume that on the surface the velocity potential vanishes, $\varphi = 0$), then its added mass decreases when the foil approaches the surface.

The coefficients $k_{22}^{*}(h/B) = \lambda_{22}^{*}/\lambda_{22\infty}$ and $k_{22}^{**}(h/B) = \lambda_{22}^{**}/\lambda_{22\infty}$ shown in Fig. 4.22 [18] determine the change of the added mass of the foil near the hard wall (k_{22}^{*}) and near the free surface (k_{22}^{**}). Here $\lambda_{22\infty}$ is the added mass of the foil in an infinite fluid; b is the chord of the foil; h is the distance of the foil trailing edge from the wall or free surface. For small attack angles the added masses of the foil near a hard wall or a free surface can be found using the data for elliptic cylinders (see Sect. 4.2.3), depending on the relative width of the profile and the distance to the boundary.

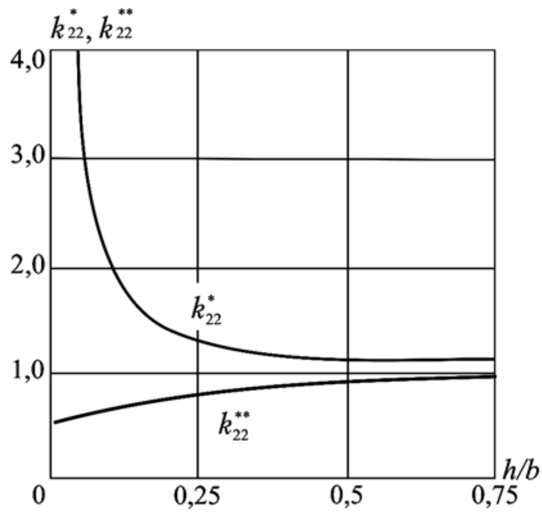

Fig. 4.22 Coefficients of added masses of a foil moving near hard wall (k^*_{22}) and free surface (k^{**}_{22})

4.3 Added Masses of Bodies Moving in an Enclosed Space Filled with a Fluid

4.3.1 Motion of a Sphere in the Fluid Contained Within a Spherical Concentric Shell

Motion of the fluid is determined by the Laplace equation $\Delta\varphi = 0$ and the following boundary conditions [133]:

- On the surface of the sphere of radius a: $\partial\varphi/\partial r = -U\cos\theta$ for $r = a$, where U is the velocity of the sphere.
- On the surface of a spherical immovable shell of radius b ($b > a$): $\partial\varphi/\partial r = 0$ for $r = b$.

Considering the solution of the Laplace equation in the form

$$\varphi = \left(Ar + \frac{B}{r^2}\right)\cos\theta,$$

we get from the boundary conditions:

$$A = \frac{a^3}{b^3 - a^3}U; \qquad B = \frac{1}{2}\frac{a^3b^3}{b^3 - a^3}U.$$

The result for an added mass is as follows:

$$\lambda_{11} = \frac{2}{3}\pi\rho\frac{b^3 + 2a^3}{b^3 - a^3}a^3.$$

We see that when b decreases from ∞ to a the added mass of the sphere increases from its value in an unlimited fluid to ∞.

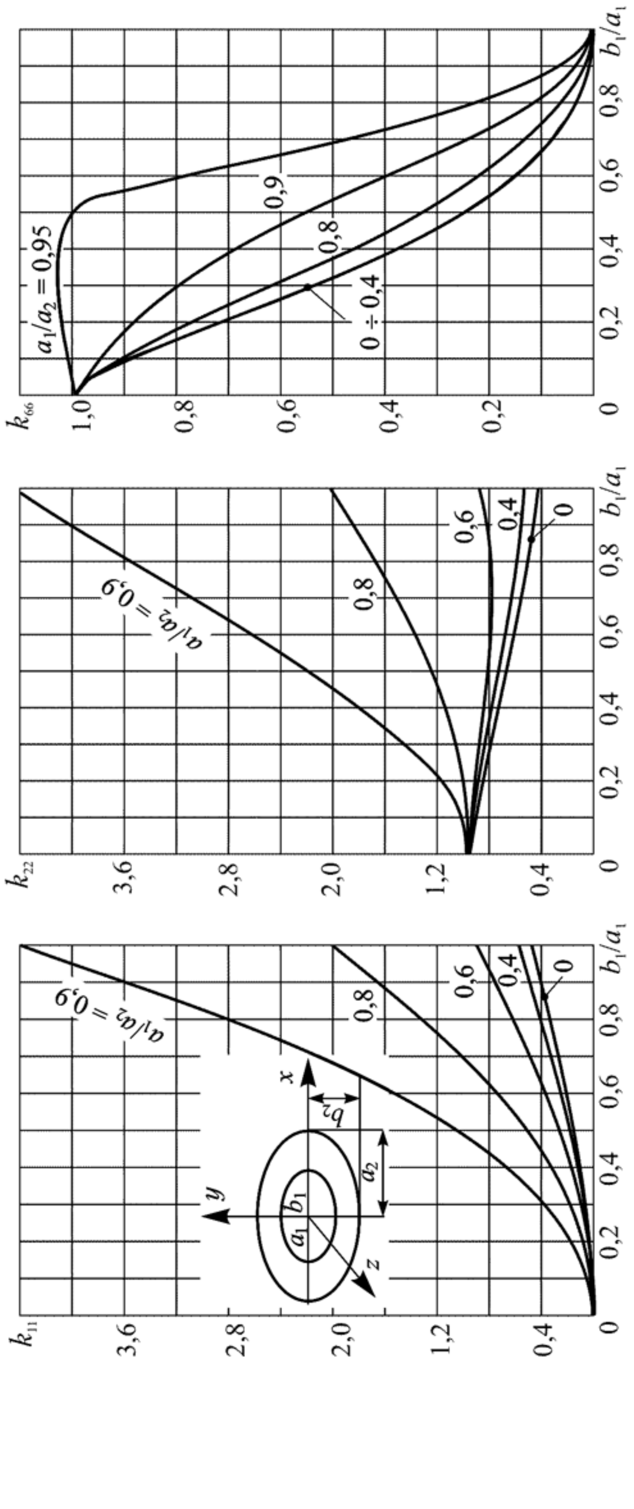

Fig. 4.23 Coefficient of added mass of an ellipsoid of revolution moving in a fluid within a confocal elliptic cavity

4.3.2 Ellipsoid of Revolution Moving in a Fluid Within a Confocal Elliptic Cavity

This problem [148] is a generalization of the problem considered before. Let the space between two confocal spheroids with half-axes a_1, b_1, b_1 and a_2, b_2, b_2 be filled with a fluid of density ρ. Then the added masses of an internal spheroid are determined by the formulas

$$\lambda_{11} = k_{11}\frac{4\pi}{3}\rho a_1 b_1^2; \qquad \lambda_{22} = k_{22}\frac{4\pi}{3}\pi\rho a_1 b_1^2;$$

$$\lambda_{66} = k_{66}\frac{4\pi}{15}\rho a_1 b_1^2\left(a_1^2 + b_1^2\right).$$

The dependence of the coefficients k_{11}, k_{22}, k_{66} on b_1/a_1 and a_1/a_2 is shown in Fig. 4.23; recall that for confocal spheroids we have $a_1^2 - b_1^2 = a_2^2 - b_2^2$.

Chapter 5
Added Masses of Bodies Moving Close to a Free Surface

5.1 Boundary Conditions on a Free Surface

Description of motion of a body near a free surface of a fluid is significantly different from description of body motion in an infinite fluid. The difference is due to the presence of a boundary condition (constancy of pressure) on the free surface. Below we consider typical ways of dealing with this boundary condition for various cases.

5.1.1 Boundary Conditions on a Free Surface at Impact of a Floating Body

Consider a body floating in an immovable fluid. When the body suffers an impact the fluid particles situated in a small neighborhood of the body surface gain finite velocities v_x, v_y, v_z during an infinitely small interval of time τ. Consider the Navier–Stokes equations of motion of incompressible fluid

$$\frac{\partial \vec{v}}{\partial t} + (\vec{v}\nabla)\vec{v} = -\frac{1}{\rho}\nabla p + \vec{g} + \frac{\mu}{\rho}\Delta\vec{v} \tag{5.1}$$

where $\vec{g}$ is the vector of free fall acceleration with components g_x g_y and g_z; μ is the dynamical viscosity; Δ is the Laplacian. Let us integrate these equations between 0 and τ (for brevity we consider only the first equation):

$$\begin{aligned} v_x &+ \int_0^\tau \left(v_x \frac{\partial v_x}{\partial x} + v_y \frac{\partial v_x}{\partial y} + v_z \frac{\partial v_z}{\partial z} \right) dt \\ &= \int_0^\tau g_x\, dt - \frac{1}{\rho}\frac{\partial}{\partial x}\int_0^\tau p\, dt + \nu \int_0^\tau \Delta v_x\, dt, \end{aligned} \tag{5.2}$$

where we took into account that $v_x = v_y = v_z = 0$ at $t = 0$.

Taking into account that velocities, their derivatives and forces g_x, g_y, g_z remain finite in the limit, we get from (5.2) in the limit $\tau \to 0$:

$$v_x = -\frac{\partial}{\partial x}\left(\frac{p_t}{\rho}\right) \tag{5.3}$$

and, analogously, from the remaining two equations of motion we get

$$v_y = -\frac{\partial}{\partial y}\left(\frac{p_t}{\rho}\right); \tag{5.4}$$

$$v_z = -\frac{\partial}{\partial z}\left(\frac{p_t}{\rho}\right), \tag{5.5}$$

where the variable $p_t = \int_0^\tau p\,dt$, called the pressure momentum, has finite value as $\tau \to 0$. The formulas (5.3)–(5.5) imply the existence of potential φ such that $v_x = \partial\varphi/\partial x$, $v_y = \partial\varphi/\partial y$, $v_z = \partial\varphi/\partial z$.

Due to (5.3)–(5.5) we get

$$\varphi = -\frac{p_t}{\rho}. \tag{5.6}$$

Applying Eq. (5.6) to the free surface we get the boundary condition

$$\varphi = 0. \tag{5.7}$$

Since on a free surface the pressure is always constant and to equal p_0, and $\tau \to 0$, we see that $p_t = 0$.

5.1.2 Boundary Conditions on a Free Surface under Periodic Oscillations of a Floating Body

Periodic oscillations of a body floating close to the free surface of a fluid cause periodic wave motion. Denote the amplitude of the waves by r, the wavelength by λ (the wave number is $k_0 = 2\pi/\lambda$) and the circular frequency by σ. Consider the Navier–Stokes equations (5.1). Introducing the following dimensionless variables [100]:

$$t_0 = \sigma t, \qquad x_0 = k_0 x, \qquad y_0 = k_0 y, \qquad z_0 = k_0 z,$$

$$\vec{u} = \frac{\vec{v}}{r\sigma}, \qquad q = \frac{p}{\rho g r},$$

we can rewrite the Navier–Stokes equation in the dimensionless form:

$$\frac{\partial \vec{u}}{\partial t_0} + rk_0(\vec{u}\nabla)\vec{u} = -\frac{gk_0}{\sigma^2}\nabla q + \frac{\vec{g}}{r\sigma^2} + \frac{\nu k_0^2}{\sigma}\Delta\vec{u}, \tag{5.8}$$

where $g := |\vec{g}|$, $\nu := \mu/\rho$.

Under the usual assumption $r \ll \lambda$, or $rk_0 \ll 1$, the second term in the left-hand side of Eq. (5.8) can be neglected, which leads to the linearized equation

$$\frac{\partial \vec{v}}{\partial t} = -\frac{1}{\rho}\nabla p + \vec{g} + \nu\Delta\vec{v}. \tag{5.9}$$

The next essential assumption is related to neglecting the viscosity while considering the wave motion. As one can see from the right-hand side of (5.8), the viscosity can be neglected if the coefficient in front of the last term is small: $\nu k_0^2/\sigma \ll 1$.

According to Huskind's estimate, for water $\nu k_0^2/\sigma \sim 8.9 \cdot 10^{-6}\lambda^{-3/2}$, where the wavelength λ is measured in meters. It is clear that viscosity can be essential only for small wavelengths. Neglecting viscosity, we get from (5.9):

$$\frac{\partial \vec{v}}{\partial t} = -\frac{1}{\rho}\nabla p + \vec{g}, \tag{5.10}$$

where the vector $\vec{v}$ has components v_x, v_y and v_z. From (5.10) follows the existence of potential $\varphi(x, y, z)$ such that $\vec{v} = \nabla\varphi$.

Due to continuity the potential φ satisfies the Laplace equation $\Delta\varphi = 0$ and condition (5.10). Then in the coordinate system chosen such that the xOy plane coincides with the undisturbed water surface and the z axis is directed upwards, we get the integral

$$p - p_0 = -\rho\frac{\partial\varphi}{\partial t} - \rho g z, \tag{5.11}$$

where p_0 is the pressure over a free water surface.

On the free surface at $z = \zeta$ (where function $\zeta(x, y)$ determines the shape of the free surface) we have $p = p_0$ and Eq. (5.11) can be written as follows:

$$\frac{\partial\varphi}{\partial t} + g\zeta = 0. \tag{5.12}$$

Differentiating expression (5.12) in time, taking into account the approximate equality $\partial\zeta/\partial t \sim v_z = \partial\varphi/\partial z$, we get

$$\frac{\partial^2\varphi}{\partial t^2} + g\frac{\partial\varphi}{\partial z} = 0. \tag{5.13}$$

Under the assumption of small amplitude of the waves, the condition (5.13) can be imposed on the unperturbed surface at $z = 0$.

Oscillations of floating and immersed bodies, and also scattering of surface waves on immovable bodies we considered in detail in the monograph [135].

Taking into account the surface tension force, one can get the following relation by projecting the equilibrium condition of a surface element (Fig. 5.1) on the vertical axis:

$$\alpha(\sin\theta_2 - \sin\theta_1) + (p - p_0)\,dx = 0,$$

where α is the force of surface tension.

Assuming the angles θ_1 and θ_2 to be small, we can write:

$$\sin\theta_1 \sim \tan\theta_1 = \left.\frac{\partial\zeta}{\partial x}\right|_{x=x_1}, \qquad \sin\theta_2 \sim \tan\theta_2 = \left.\frac{\partial\zeta}{\partial x}\right|_{x=x_2},$$

Fig. 5.1 Forces acting on an element of the free surface

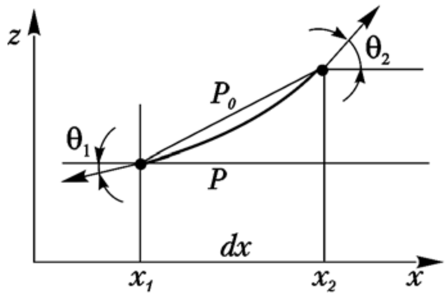

which allows us to rewrite the previous equality as

$$\alpha \frac{\partial^2 \zeta}{\partial x^2} + p - p_0 = 0. \tag{5.14}$$

Substituting in expression (5.14) the value $p - p_0$ from (5.11) and following the derivation of (5.13) from (5.11), we arrive at the following boundary condition on the free surface, taking into account the surface tension force:

$$\frac{\partial^2 \varphi}{\partial t^2} + g \frac{\partial \varphi}{\partial z} - \frac{\alpha}{\rho} \frac{\partial^3 \varphi}{\partial z \partial x^2} = 0. \tag{5.15}$$

It is possible to show (see [116]) that if the wavelength is significantly greater than $\lambda_0 = 1.78$ cm, then the surface tension can be neglected.

The function φ corresponding to waves on a free surface can be represented in the form

$$\varphi = \varphi_1(y, z) \sin(\sigma t - k_0 x).$$

Then condition (5.13) on the free surface implies for the function φ_1:

$$\frac{\partial \varphi_1}{\partial z} - \frac{\sigma^2}{g} \varphi_1 = 0. \tag{5.16}$$

For flat waves condition (5.15) can be written as

$$\frac{\partial \varphi_1}{\partial z} - \frac{\sigma^2}{g + \alpha k_0^2/\rho} \varphi_1 = 0. \tag{5.17}$$

Parameters σ and k_0 are related to each other in each concrete problem. Their relationship is determined by conditions (5.13), (5.15) and the Laplace equation with appropriate boundary conditions. For the case of sinusoidal waves on deep water, when

$$\varphi = C e^{k_0 z} \sin(\sigma t - k_0 x),$$

condition (5.17) gives $\sigma^2 = k_0(g + \alpha k_0^2/\rho)$ or, neglecting the surface tension, $\sigma^2 = k_0 g$. Using these equations we can rewrite the boundary conditions (5.16), (5.17) in the form

$$\frac{\partial \varphi_1}{\partial z} - k_0 \varphi_1 = 0. \tag{5.18}$$

If k_0 is small then boundary condition (5.18) takes the form

$$\left. \frac{\partial \varphi_1}{\partial z} \right|_{z=0} = 0. \tag{5.19}$$

This condition is equivalent to assumption of water-tightness of the separation surface.

If k_0 is very large (short waves) the condition (5.18) takes the form (5.7). This happens under vibration of a body submerged close to a free surface. Obviously, when determining whether the waves should be considered short or long one should compare the wavelength with a characteristic size of the body.

The limiting cases (5.7) or (5.19) of the boundary condition (5.13) or (5.16) can be interpreted as the cases of ultra-light or ultra-heavy fluid, respectively [100]. In the case of ultra-light fluid the acceleration of the fluid particles is essentially greater than the acceleration of the free fall. In the case of ultra-heavy fluid the acceleration of the fluid particles is essentially lower than the acceleration of the free fall.

Behavior of the added masses in the limits of low and high frequencies is discussed in the works [6, 7, 146, 209] and others.

5.1.3 *Boundary Conditions on a Free Surface when the Method of a Duplicated Model is Applied*

In the limiting cases ($k_0 \to 0$, $k_0 \to \infty$) one often uses the method of a duplicated model. If on the free surface one has the condition (5.7): $\varphi(z = 0) = 0$ (as $k_0 \to \infty$) then the function $\varphi(x, y, z)$ can be continued to the upper half-space assuming it to be an odd function of coordinate z by insertion in the upper half-space of the mirror image S_1 of the surface S; then $\varphi(x, y, z, t) = -\varphi(x, y, -z, t)$. Then we get the following symmetry relations for velocities:

$$\begin{aligned} v_x(x, y, z, t) &= -v_x(x, y, -z, t); \\ v_y(x, y, z, t) &= -v_y(x, y, -z, t); \\ v_z(x, y, z, t) &= v_z(x, y, -z, t). \end{aligned} \tag{5.20}$$

Expressions (5.20) show that if we consider the motion of the duplicated hull in an infinite fluid only along the z-axis, then the flow around its lower part is the same as the flow around the immersed part of the original single hull under boundary condition $\varphi|_{z=0} = 0$. If one considers the motion along axes x or y, the upper part of the duplicated contour should move in the opposite direction to the lower part.

Therefore, to calculate the added masses λ_{33}, λ_{35}, λ_{55} one can calculate first the added masses of the duplicated hull and then divide them by 2.

If on a free surface we have the boundary condition

$$\left.\frac{\partial\varphi}{\partial z}\right|_{z=0} = 0$$

(see (5.19)) in the limit $k_0 \to 0$, one can continue function $\varphi(x, y, z, t)$ to the upper half-space as an even function:

$$\varphi(x, y, z, t) = \varphi(x, y, -z, t),$$

which implies for velocities:

$$\begin{aligned} v_x(x, y, z, t) &= v_x(x, y, -z, t); \\ v_y(x, y, z, t) &= v_y(x, y, -z, t); \\ v_z(x, y, z, t) &= -v_z(x, y, -z, t). \end{aligned} \tag{5.21}$$

Formulas (5.21) show that the flow around the duplicated hull under the motion along the x and y axes is the same as the flow around the single hull along the same axis. However, the motion of the duplicated hull along the z-axis gives the same picture as the motion of the single hull if two halfs of the duplicated hull move in opposite directions. Therefore, the added masses λ_{11}, λ_{22}, λ_{26}, λ_{66} of the hull can be computed under the boundary condition (5.19) as halfs of corresponding added masses of the duplicated hull moving in an infinite fluid.

Therefore, in computation of added masses of the hull one should consider the following problems:

1. Computation of added masses of the duplicated hull moving in an infinite fluid (in this way one can compute added masses). If the case of boundary condition $\varphi|_{z=0} = 0$ (this boundary condition is considered in studies of hull vibration) in this way we compute the added masses λ_{33}, λ_{35}, λ_{55}. In the case of boundary condition $\partial\varphi/\partial z|_{z=0} = 0$ (this boundary condition corresponds to the motion of a ship in ice) we get in this way the added masses λ_{11}, λ_{22}, λ_{26}, λ_{66}.
2. Computation of remaining added masses λ_{11}, λ_{22}, λ_{26}, λ_{66} under the boundary condition $\varphi|_{z=0} = 0$.
3. Computation of remaining added masses λ_{33}, λ_{35}, λ_{55} of the hull under the boundary condition $\partial\varphi/\partial z|_{z=0} = 0$.
4. Computation of added masses of the hull under general boundary condition (5.16), which corresponds to the roll of the ship on a perturbed water surface.

There exist two simplified models of the hull: the model of thin hull and the model of long hull. Denote the length of the hull by L, the width by B and the draft by T. The model of thin hull is applicable when $B/L \ll T/B$ and T/B is of the order of 1. The model of elongated hull is applicable if B/L and T/L are both small and have the same order of magnitude.

Below we use both of these models for computation of added masses of hull.

In computation of added masses of a hull the method of planar sections is commonly used (see Sect. 3.5). Therefore we present below results of computation of added masses of shipframes obtained under various boundary conditions. We also present some data on added masses of simple bodies moving under the free surface or crossing the free surface.

5.2 Added Masses of Vertical Cylindrical Obstacles

A systematic description of the interaction of an ideal incompressible fluid with cylindrical obstacles in case of presence of the free surface is contained in the monograph by M.D. Huskind [100].

Consider surface waves with a linear wavefront in the presence of an immovable vertical cylinder crossing the free surface (Fig. 5.2). The shape of the wave is given by expression

$$A \sin(\sigma t + k_0 x), \tag{5.22}$$

where A is the amplitude of waves, σ is the time frequency, t is time; $k_0 = 2\pi/\lambda$ is the space frequency related to the wavelength λ; x is the coordinate chosen in the direction of wave propagation.

If the radius of the cylinder a is small in comparison with the wavelength (i.e., $a/\lambda \ll 1$) then one can consider a flat flow around each cross-section of the cylinder with velocity which is given by the formula $u(z,t) = u_*(z)\sin\sigma t$. The amplitude $u_*(z)$ depends on the immersion depth of the section (Fig. 5.2). The hydrodynamic forces arising due to non-stationary character of the flow are determined in each section by the ordinary added mass $\lambda_{11} = \rho\pi a^2$ and the corresponding local acceleration of the flow.

Consider now the case $\lambda \sim a$. In that case we can not consider the incoming flow to be homogeneous in space (along the x-coordinate). The influence of the non-homogeneity of the flow is characterized by the parameter $k_0 a = 2\pi a/\lambda$. Dependence of the added mass of the circular cylinder on this parameter is shown in Fig. 5.3, where the vertical axis corresponds to the variable $[\lambda_{11}(k_0 a)]/[\lambda_{11}(k_0 a = 0)]$, where $\lambda_{11}(k_0 a = 0) = \pi\rho a^2$ (curve 1). In the same figure we show the curve corresponding to the vertical flat plate of width $2a$ posed orthogonally to the direction of incoming waves (curve 2).

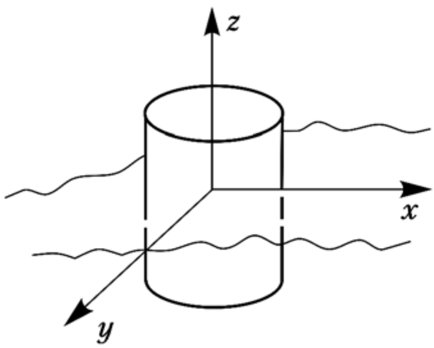

Fig. 5.2 Vertical cylinder crossing the free surface of fluid

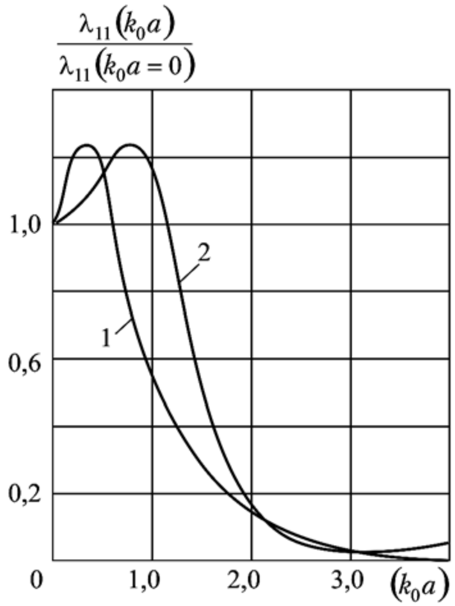

Fig. 5.3 Coefficients of added masses of the circular cylinder (*curve 1*) and vertical plate (*curve 2*) crossing the free surface of a fluid

5.3 Added Masses of Shipframes when a Ship is Oscillating on a Free Surface

Hydrodynamic forces acting on a ship rolling on a free surface under the influence of incoming waves can be determined under the following simplifying assumptions [100]. Relative wave amplitudes are assumed to be small, which allows us to use the linear wave theory. Oscillations of the hull are also assumed small. The fluid is assumed to be ideal. The velocity potential is represented in the form

$$\varphi(x,y,z,t) = \varphi_1(x,y,z) + \varphi_2(x,y,z,t) + \varphi_3(x,y,z,t) + \varphi_4(x,y,z,t),$$

where φ_1 is the potential corresponding to stationary movement of the ship with constant linear and angular velocities on a still free surface; φ_2 is the potential of the incoming system of waves; φ_3 is the diffraction potential characterizing the wave motion arising as a result of interaction of the incoming system of waves with the ship, considered as an immovable obstacle; φ_4 is the potential corresponding to forced oscillation of the ship on a still surface.

The problem of a body moving linearly with constant velocity in the presence of periodic wave motion was discussed in [156] in the linear approximation. In contrast to rolling in absence of linear velocity, here the matrix of added masses is not symmetric; it depends not only on characteristics of the body and wave frequency, but also on velocity. This problem is usually considered in the coordinate system attached to the body. The most well-studied case is the circular cylinder completely immersed under free surface of an infinitely deep fluid [89, 111, 123, 208, 248, 252]. In [248] the values of λ_{11}, λ_{33} and λ_{13} are given as functions of the frequency of oscillations of the cylinder for $h = 2a$, $U/\sqrt{ga} = 0.4$, where a is the radius of the cylinder, h is the distance of the cylinder's axis to the free surface, U is the velocity of incoming flow. Added masses for a circular cylinder immersed in a fluid of finite depth are determined in [247]; for an elliptic cylinder whose large semi-axis is parallel to the unperturbed water surface and $a/b = 4$ the added masses were found in [112].

The added masses for a completely immersed sphere in the presence of homogeneous flow were determined in [253] (for the case of infinite depth) and in [249] (for the case of finite depth). The added masses of an ellipsoid of revolution with $a/b = 5$ completely submerged under the surface of an infinitely deep fluid are given in [106].

The influence of small linear velocities on added masses of a (completely or partially submerged) circular cylinder for an infinitely deep fluid was studied in [255]; for the case of a floating rectangular pontoon—in [164].

In computation of added masses of a rolling ship, the influence of its stationary linear motion is typically neglected; only the apparent frequency of incoming waves is taken into account.

On the surface of the ship one imposes water-tightness boundary conditions; on the free surface of the fluid one imposes a condition of constancy of pressure. If the fluid has infinite depth, one assumes that the velocity vector vanishes as $z \to -\infty$. If the fluid has finite depth, one imposes the water-tightness condition at the bottom. Besides, for potentials φ_3 and φ_4 one imposes the so-called radiation condition at infinity [100]. The physical meaning of the radiation condition for example, for the case of the diffraction potential φ_3, is that the system of incoming waves gets partially reflected by the hull, and partially goes through.

In the general case, assuming that all these conditions are fulfilled, the hydrodynamic forces X_1, X_2, X_3 and moments X_4, X_5, X_6 acting on a rolling ship (on regular periodic waves) can be written in the form [100]:

$$X_m = -\sum_{s=1}^{6}\left(\lambda_{ms}\frac{dv_s}{dt} + \nu_{ms}v_s\right), \quad m = 1, 2, \ldots, 6, \tag{5.23}$$

where λ_{ms} are generalized added masses of the ship, which depend not only on the shape of the hull, but also on frequency of waves; ν_{ms} are coefficients of damping forces; appearance of these coefficients is related to the fact that under the roll of a ship part of the energy is spent to wave generation.

Notice that in the right-hand side of (5.23) the terms containing pairwise products of velocities with coefficients given by added masses λ_{ms}, $m, s = 1, 2, \ldots, 6$, are absent. This is related to linearity of the formulation of this problem. If one needs to take the non-linear terms into account one can use general formulas (1.22)–(1.27), where λ_{ms} have to be defined taking into account the presence of free surface.

For real ships, computation of added masses is carried out by the method of plane sections (see Sect. 3.3); to use this method one should know the added masses of each shipframe. Added masses of shipframes on waved water surface are computed in [196, 197]. The shape of shipframe was chosen to coincide with a Lewis shipframe keeping three terms in the corresponding Taylor expansion (see Chap. 2).

In Figs. 5.4–5.17 and in Table 5.1 we show dependence of dimensionless added masses λ_{22}, λ_{33}, λ_{24}, λ_{44} of different shipframes on dimensionless wave number $Bk_0/2 = B\pi/\lambda$, where B is the width of the shipframe, λ is the wavelength. Results were given for different values of shipframe coefficient β and half of the ratio of the shipframe width to the draft: $B/2T$. We notice that the value $B\pi/\lambda$ shown along the horizontal axis can be represented in the form $B\pi/\lambda = B\sigma^2/2g$, where σ is the time frequency; to get this formula one should take into account that for small waves described by Eq. (5.22) we have $\sigma^2 = k_0 g$, $k_0 = 2\pi/\lambda$.

Similar computations of coefficients of added masses of shipframes under roll were carried out in works by Tasai (some results of these computations are given in [26, 200]).

Detailed tables of added masses $\lambda_{22}, \lambda_{33}, \lambda_{24}, \lambda_{44}$ of a Lewis shipframe are presented in [182]. These results essentially coincide with results of [196, 197]. To take into account not only the influence of shipframe coefficient, but more subtle characteristics of shipframe shape on the added mass λ_{33}, one can use results of Porter [32].

If a planar contour floating (vertically) on a one-dimensional free surface of a two-dimensional fluid oscillates in vertical direction under finite depth of fluid H, then following Havelock [97] one can write

$$\lambda_{33\,H} = \lambda_{33H=\infty} k\left(\frac{H}{T}\right)$$

where T is the draft of the contour; $\lambda_{33\,H=\infty}$ is the added mass of the contour at infinite depth.

Graphs of function $k(H/T)$ are shown in Fig. 5.18. The curve 1 was obtained in [97]; the curve 2 was obtained in [9]; two points correspond to the circular cylinder [90]. The analytic form of these curves looks as follows:

$$k\left(\frac{H}{T}\right) = 1 + \frac{1}{2}\left(\frac{H}{T}\right)^2, \quad \text{(curve 1)},$$

$$k\left(\frac{H}{T}\right) = \frac{1 + 8(H/T)^2 + 8(H/T)^4}{8(H/T)^4 - 1}, \quad \text{(curve 2)}.$$

Under a rolling motion in shallow water the added moment of inertia can be written as

$$\lambda_{44H} = \lambda_{44H=\infty} k_1\left(\frac{H}{T}\right).$$

The coefficient $k_1(H/T)$ was determined in [31] experimentally to have the form

$$k_1\left(\frac{H}{T}\right) = 1 + 0.2\left(\frac{T}{H}\right)^2 + 0.1\left(\frac{T}{H}\right)^3.$$

Experiments show that the influence of the bottom is negligible for $H \geq 4T$. The influence of the bottom on added masses of shipframes (the Lewis class, discussed

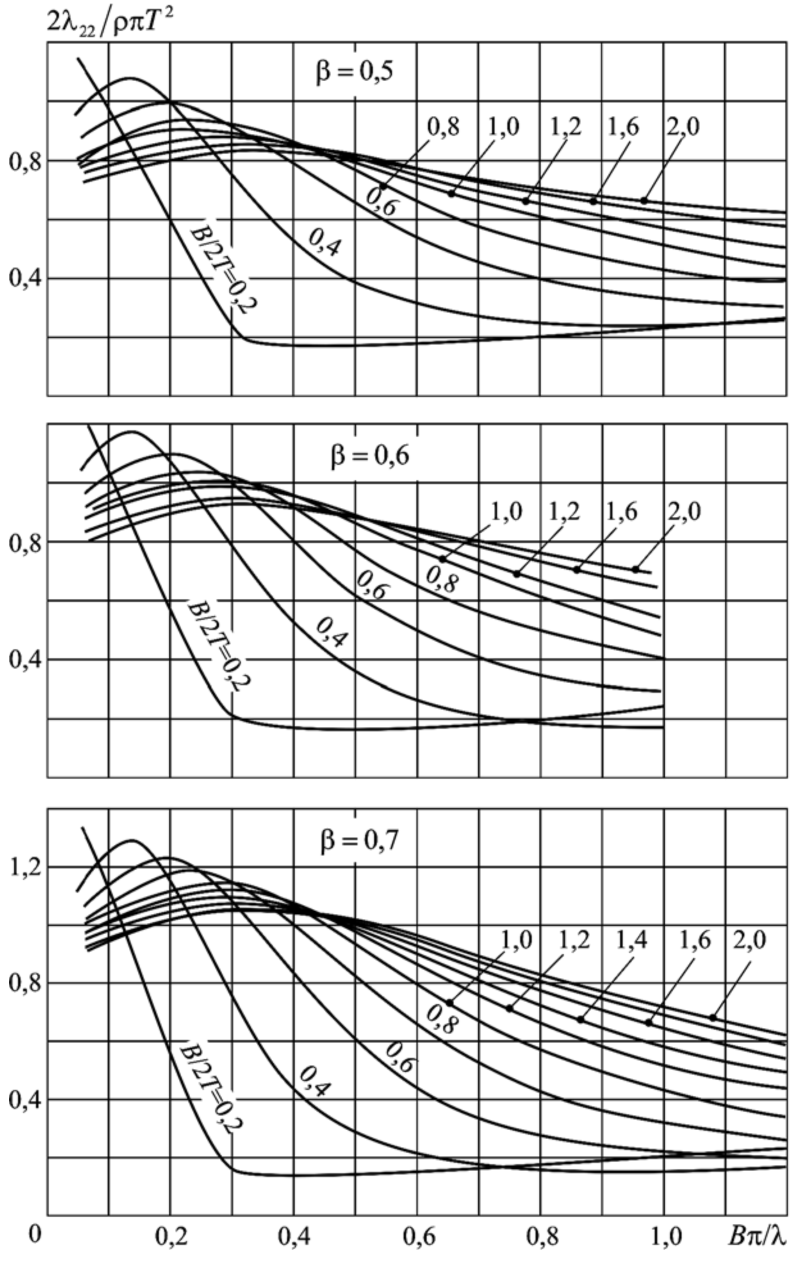

Fig. 5.4 Coefficients of added masses of shipframes depending on dimensionless frequency of oscillations $\sigma^2 B/2g = B\pi/\lambda$

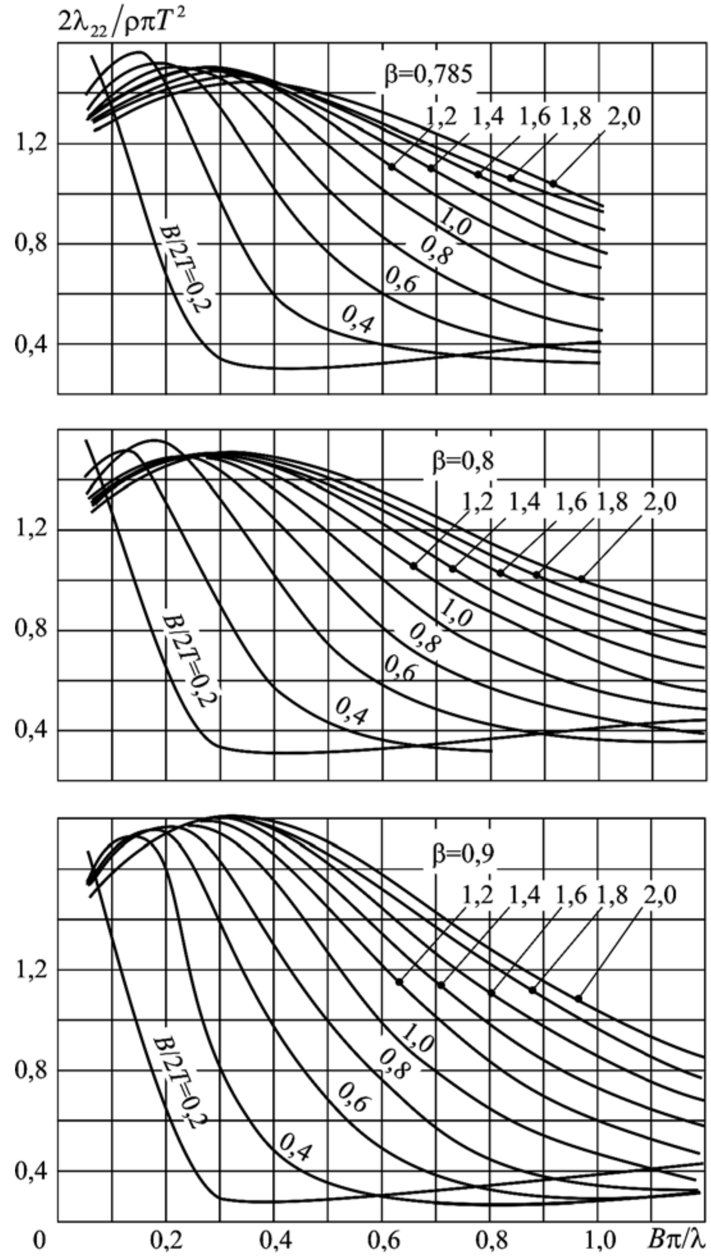

Fig. 5.5 Coefficients of added masses of shipframes depending on dimensionless frequency of oscillations $\sigma^2 B/2g = B\pi/\lambda$

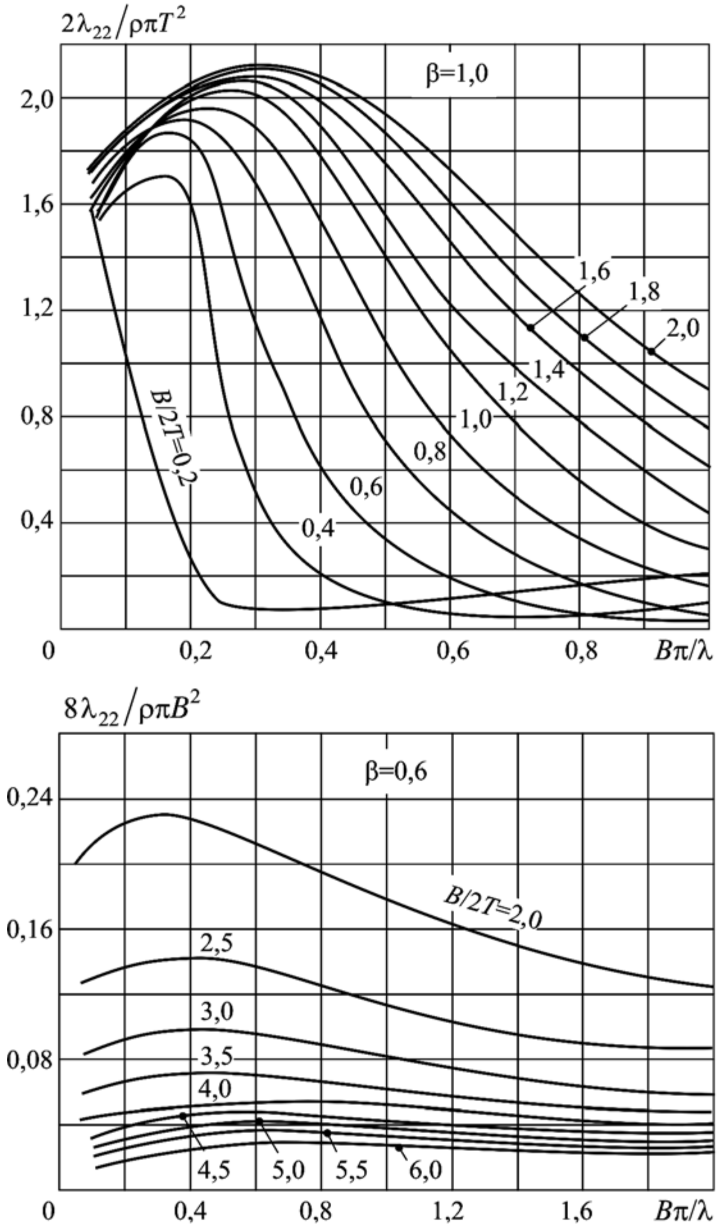

Fig. 5.6 Coefficients of added masses of shipframes depending on dimensionless frequency of oscillations $\sigma^2 B/2g = B\pi/\lambda$

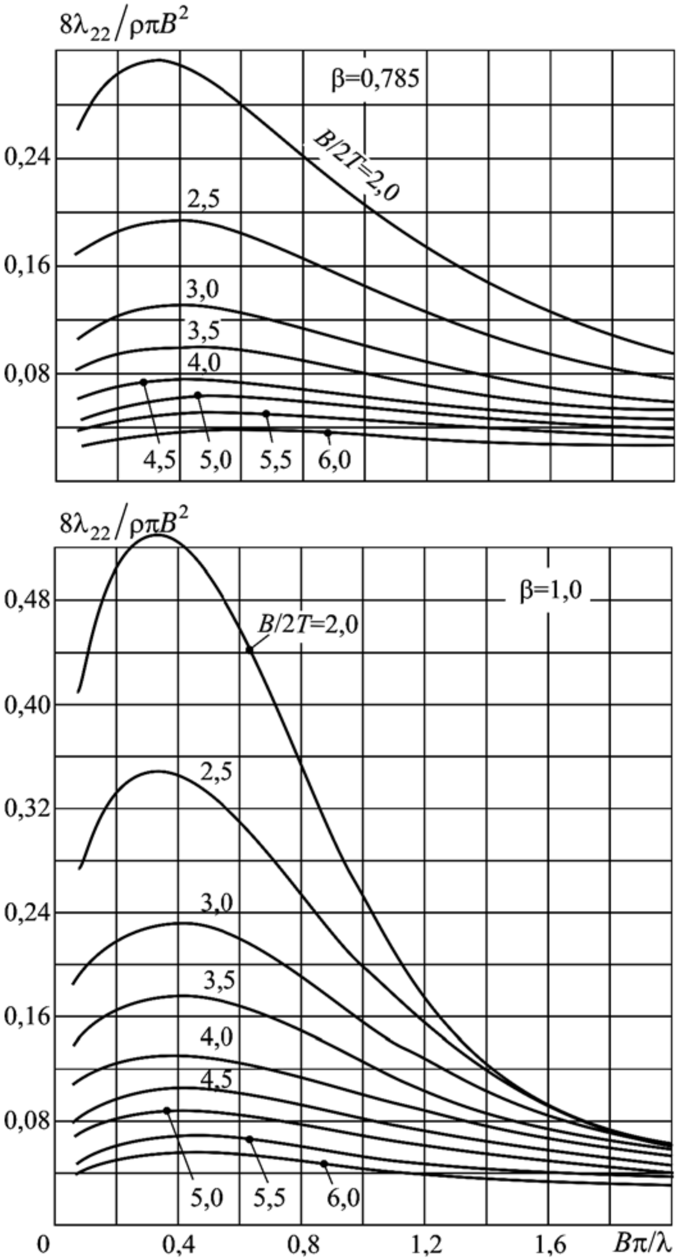

Fig. 5.7 Coefficients of added masses of shipframes depending on dimensionless frequency of oscillations $\sigma^2 B/2g = B\pi/\lambda$

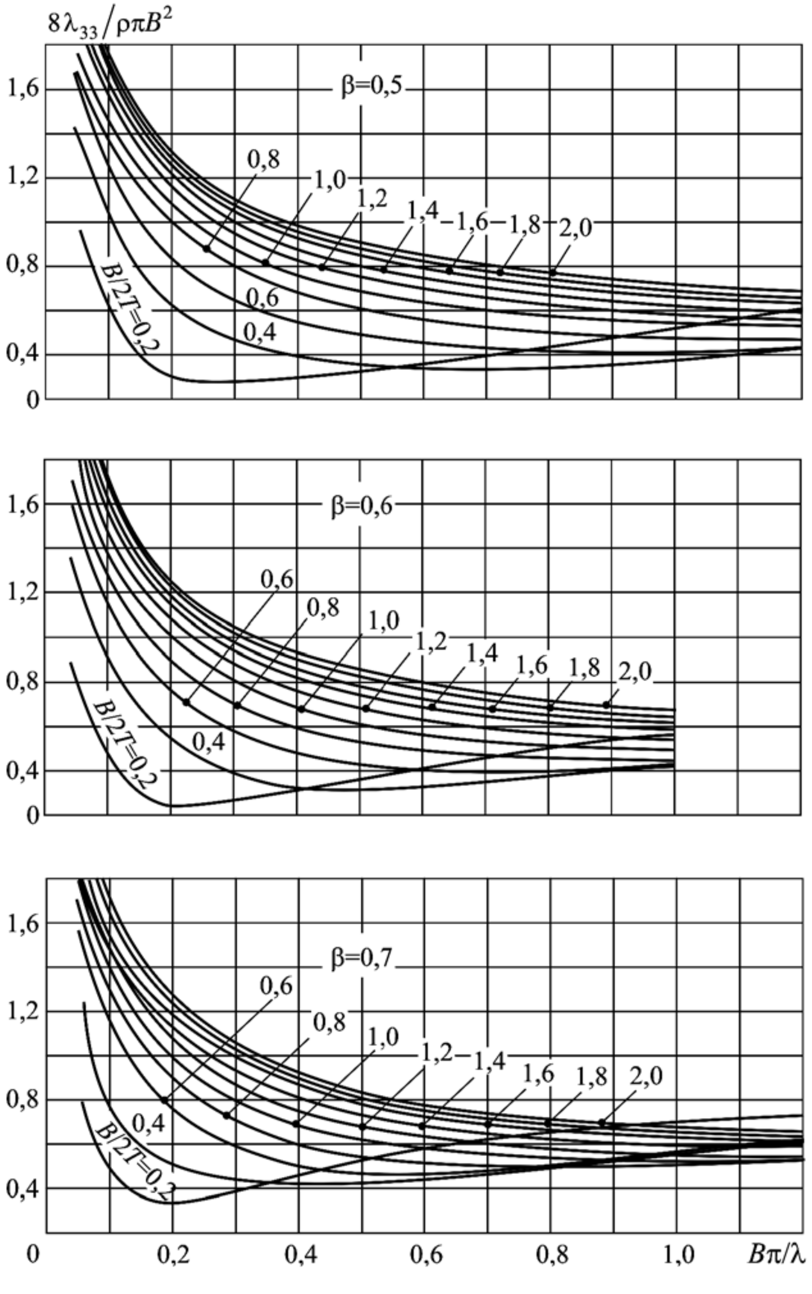

Fig. 5.8 Coefficients of added masses of shipframes depending on dimensionless frequency of oscillations $\sigma^2 B/2g = B\pi/\lambda$

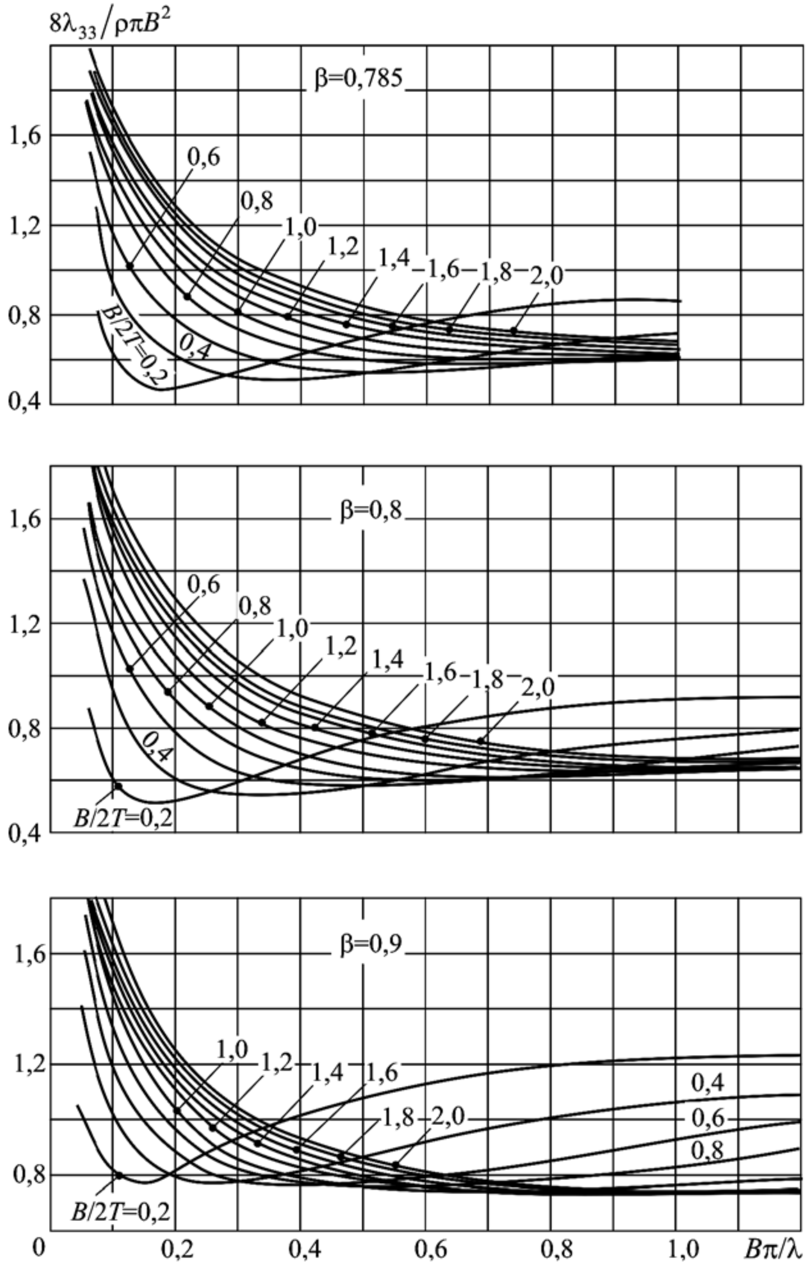

Fig. 5.9 Coefficients of added masses of shipframes depending on dimensionless frequency of oscillations $\sigma^2 B/2g = B\pi/\lambda$

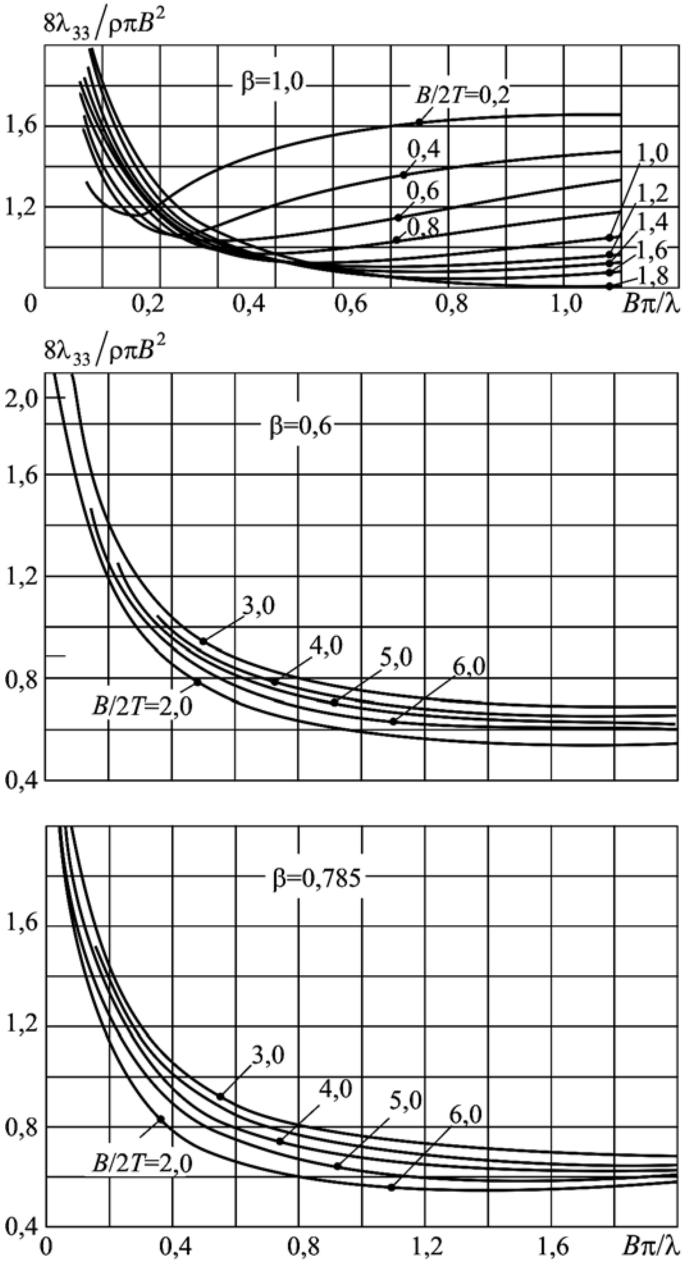

Fig. 5.10 Coefficients of added masses of shipframes depending on dimensionless frequency of oscillations $\sigma^2 B/2g = B\pi/\lambda$

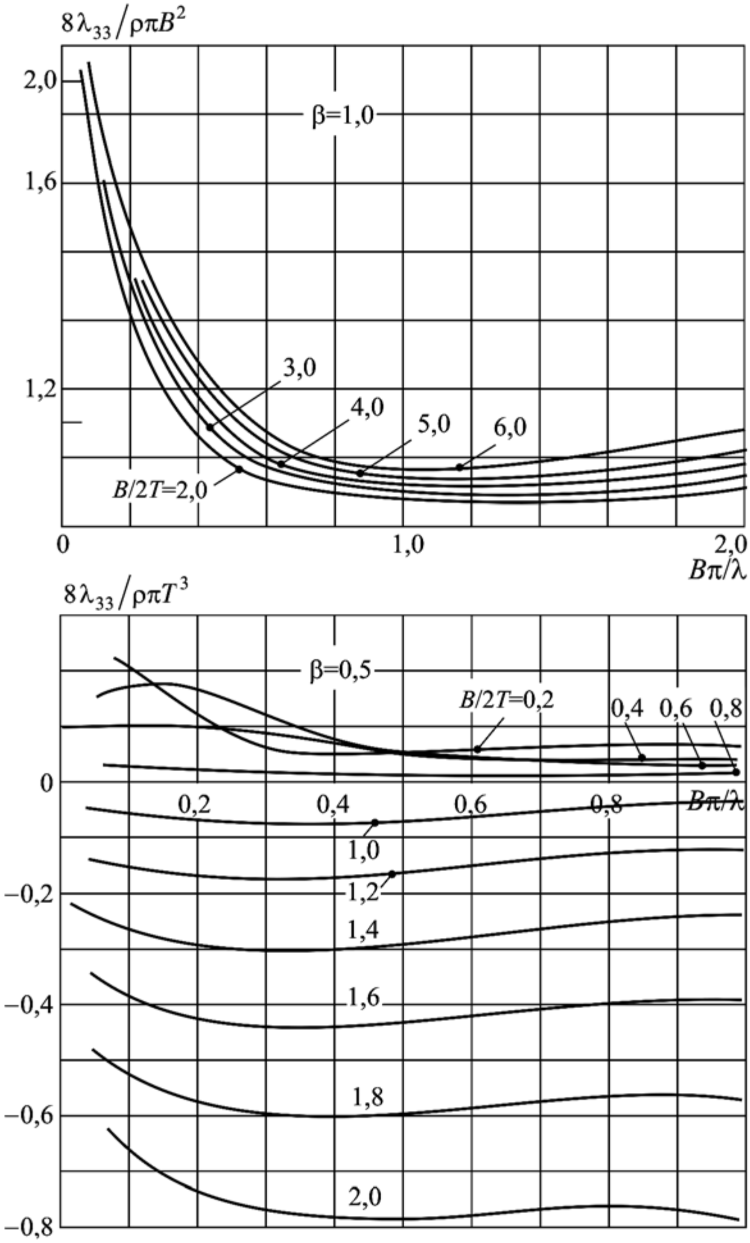

Fig. 5.11 Coefficients of added masses of shipframes depending on dimensionless frequency of oscillations $\sigma^2 B/2g = B\pi/\lambda$

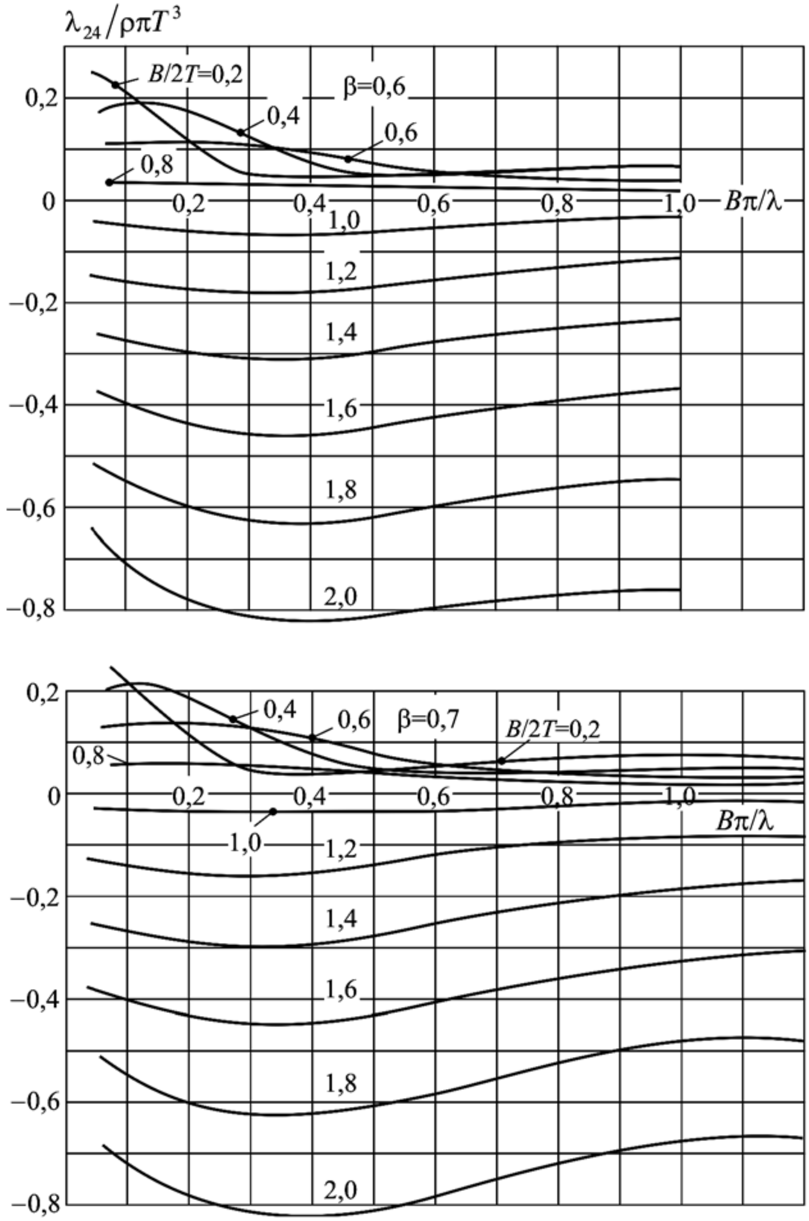

Fig. 5.12 Coefficients of added masses of shipframes depending on dimensionless frequency of oscillations $\sigma^2 B/2g = B\pi/\lambda$

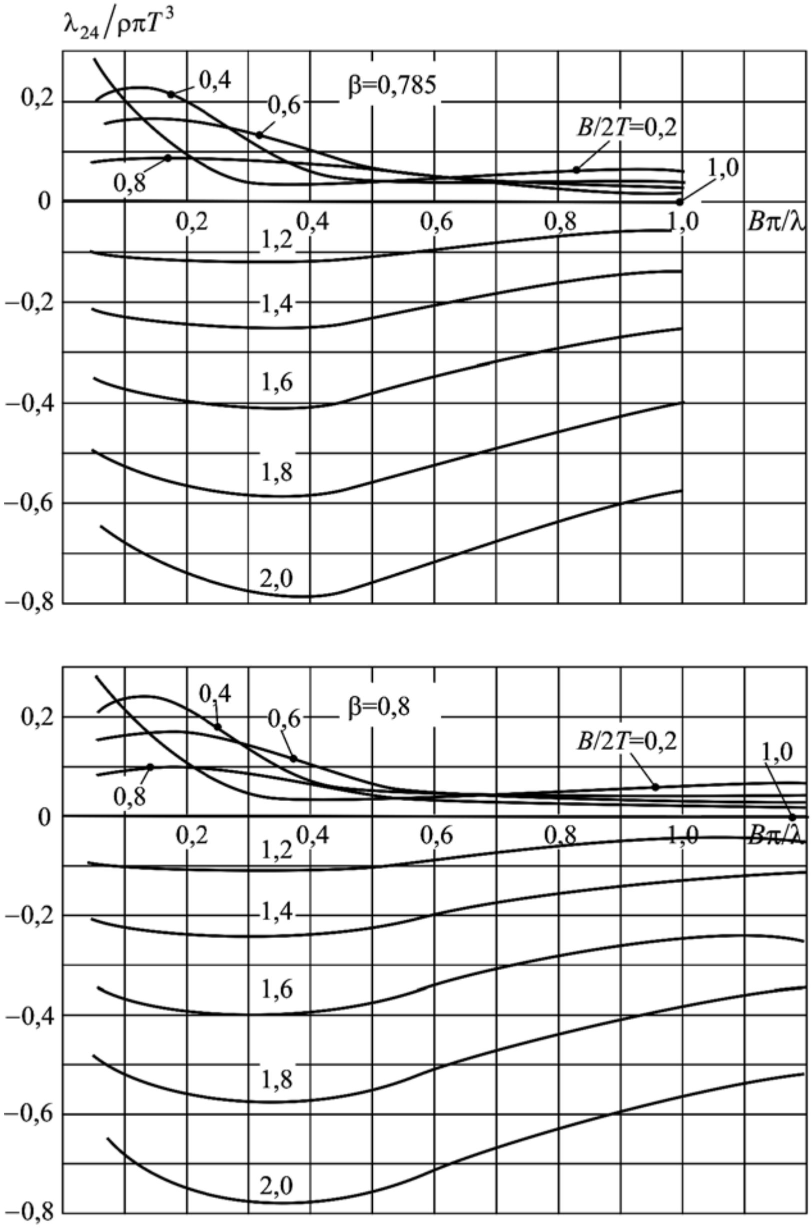

Fig. 5.13 Coefficients of added masses of shipframes depending on dimensionless frequency of oscillations $\sigma^2 B/2g = B\pi/\lambda$

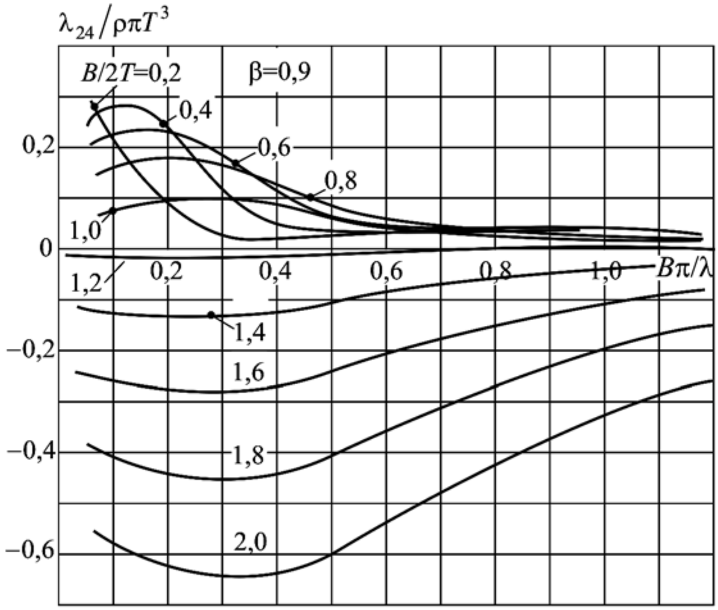

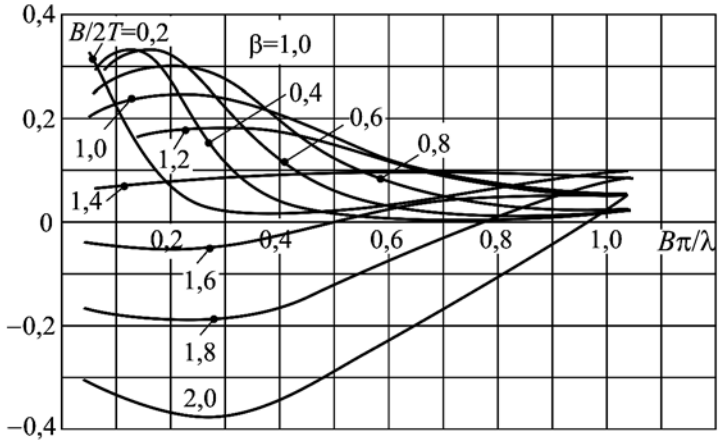

Fig. 5.14 Coefficients of added masses of shipframes depending on dimensionless frequency of oscillations $\sigma^2 B/2g = B\pi/\lambda$

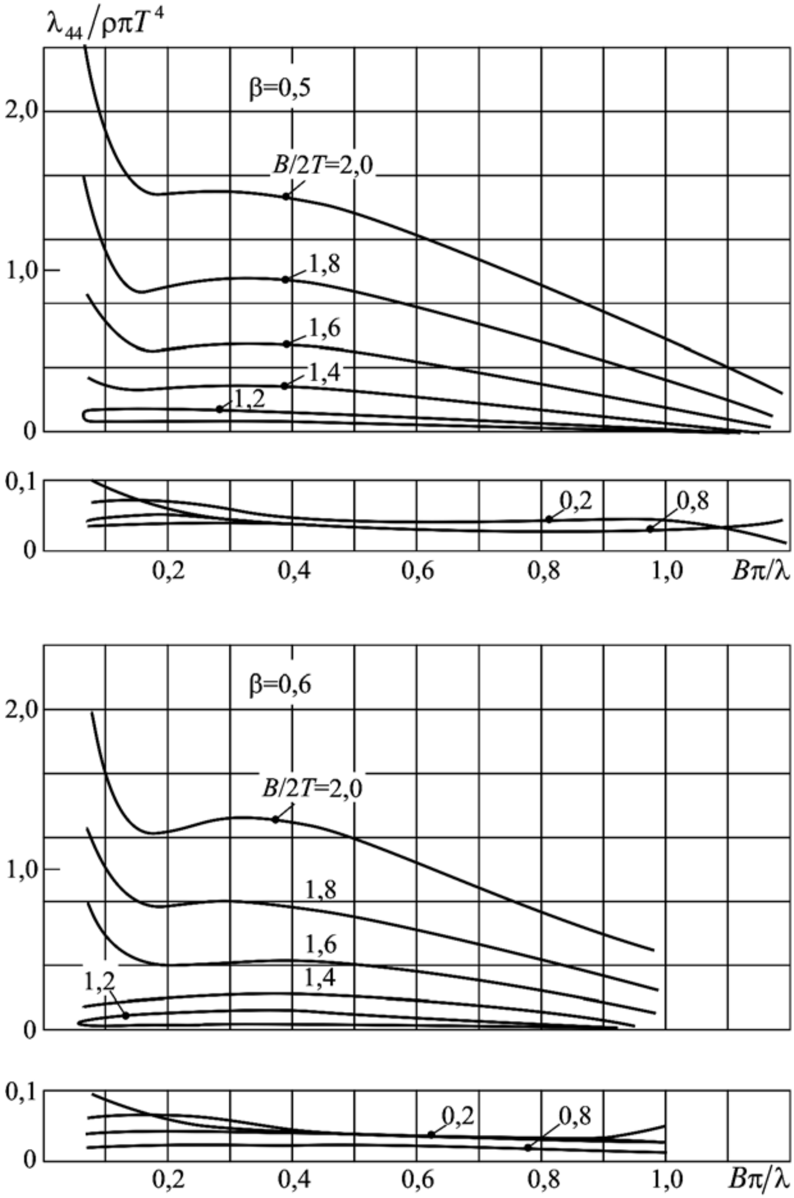

Fig. 5.15 Coefficients of added masses of shipframes depending on dimensionless frequency of oscillations $\sigma^2 B/2g = B\pi/\lambda$

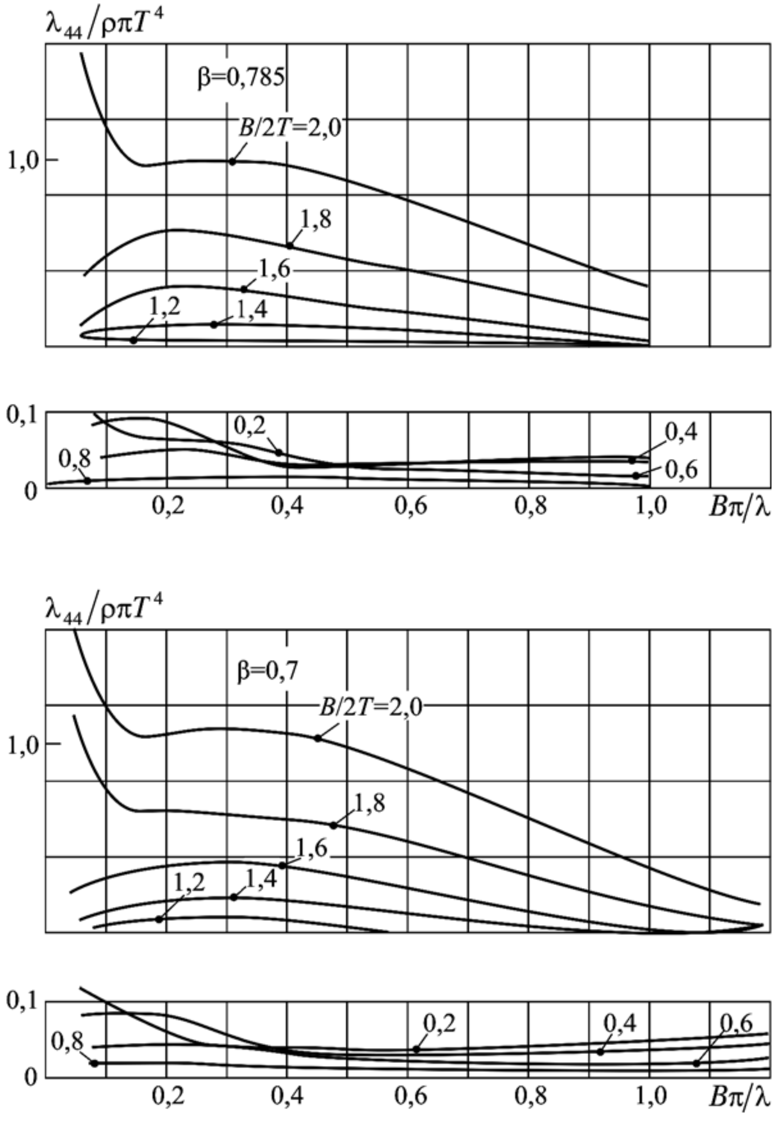

Fig. 5.16 Coefficients of added masses of shipframes depending on dimensionless frequency of oscillations $\sigma^2 B/2g = B\pi/\lambda$

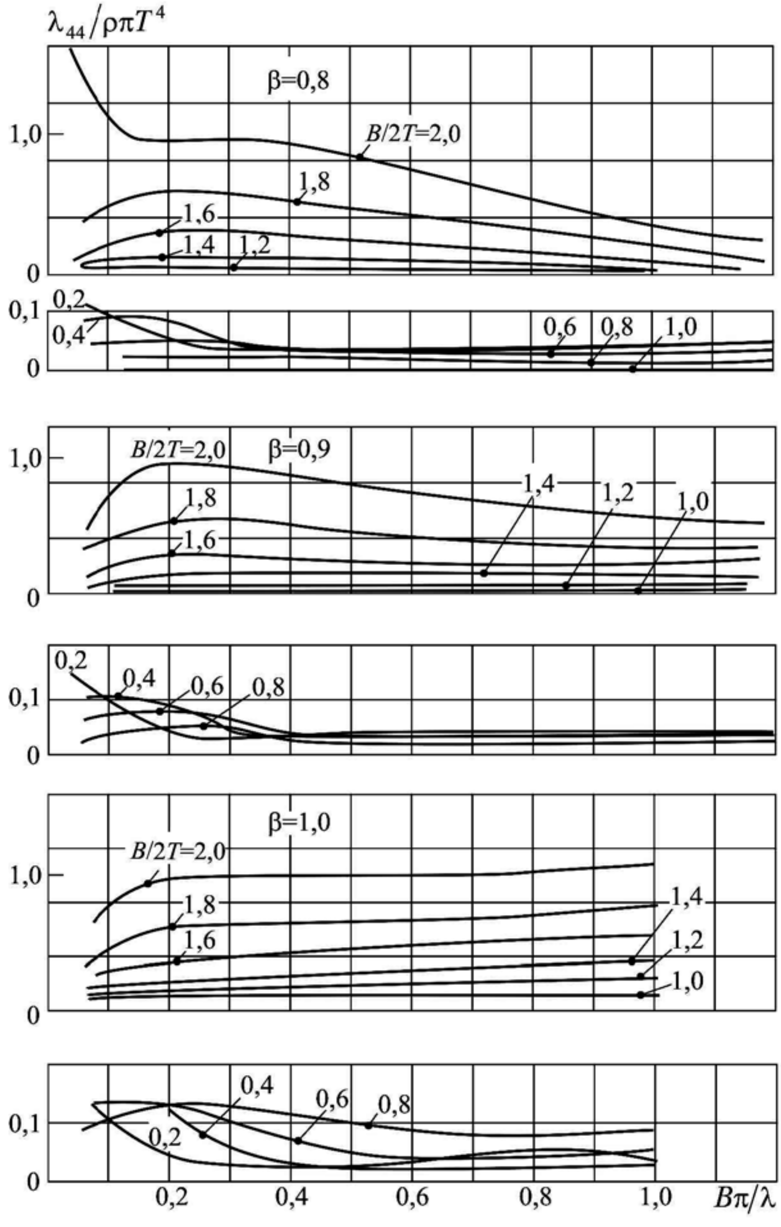

Fig. 5.17 Coefficients of added masses of shipframes depending on dimensionless frequency of oscillations $\sigma^2 B/2g = B\pi/\lambda$

Table 5.1 Values of coefficients of added masses λ_{44} and λ_{24}

	β	$\frac{B}{2T}$	$\frac{B\pi}{\lambda}=\frac{\sigma^2 B}{2g}$								
			0.06	0.15	0.30	0.45	0.60	0.60	1.20	1.60	2.00
$\frac{16\lambda_{44}}{\rho\pi B^4}$	0.6	2.0	0.138	0.078	0.065	0.078	0.067	0.048	0.011	−0.020	−0.045
		3.0	0.167	0.095	0.102	0.096	0.086	0.070	0.046	0.010	0
		4.0	0.185	0.108	0.106	0.102	0.093	0.078	0.048	0.025	0.012
		6.0	0.194	0.114	0.109	0.104	0.097	0.085	0.059	0.040	0.031
	0.785	2.0	0.103	0.061	0.062	0.056	0.047	0.033	0.011	0	0.003
		3.0	0.145	0.081	0.087	0.082	0.073	0.033	0.018	0.018	0.014
		4.0	0.152	0.090	0.096	0.091	0.083	0.070	0.045	0.030	0.025
		6.0	0.177	0.133	0.102	0.098	0.091	0.079	0.056	0.042	0.038
	1.0	2.0	0.038	0.059	0.062	0.063	0.063	0.065	0.074	0.085	0.093
		3.0	0.116	0.075	0.077	0.074	0.070	0.063	0.055	0.057	0.065
		4.0	0.131	0.081	0.086	0.083	0.077	0.068	0.054	0.050	0.055
		6.0	0.147	0.089	0.095	0.092	0.086	0.075	0.058	0.049	0.049
$\frac{8\lambda_{24}}{\rho\pi B^3}$	0.6	2.0	−0.084	−0.095	−0.101	−0.102	−0.099	−0.095	−0.095	−0.105	−0.119
		3.0	−0.060	−0.069	−0.074	−0.077	−0.079	−0.081	−0.090	−0.103	−0.115
		4.0	−0.045	−0.052	−0.057	−0.061	−0.064	−0.068	−0.081	−0.094	−0.105
		6.0	−0.028	−0.034	−0.039	−0.043	−0.047	−0.053	−0.067	−0.081	−0.089
	0.785	2.0	−0.082	−0.091	−0.098	−0.097	−0.090	−0.080	−0.067	−0.062	−0.059
		3.0	−0.062	−0.071	−0.076	−0.078	−0.077	−0.074	−0.071	−0.070	−0.068
		4.0	−0.048	−0.056	−0.060	−0.063	−0.064	−0.065	−0.067	−0.069	−0.068
		6.0	−0.031	−0.038	−0.042	−0.045	−0.047	−0.051	−0.058	−0.064	−0.064
	1.0	2.0	−0.040	−0.044	−0.046	−0.039	−0.026	0.009	0.015	0.030	0.039
		3.0	−0.047	−0.055	−0.060	−0.059	−0.052	−0.040	−0.019	−0.004	0.010
		4.0	−0.042	−0.050	−0.054	−0.054	−0.052	−0.046	−0.033	−0.021	−0.009
		6.0	−0.031	−0.038	−0.041	−0.043	−0.043	−0.043	−0.040	−0.036	−0.027

in Chap. 2) for the case of shallow water was studied by Vorobjov [238–240]. He computed the added mass λ_{33} for high frequency vertical oscillations of contours where the ratio $B/2T$ was between 0.4 and 1.4, and shipframe coefficient β (equal to the ratio of the area of shipframe to the product of its maximal width to maximal height) was between $\beta = 0.5$ and $\beta = 1.0$. In Fig. 5.19, we present the dependence of dimensionless coefficients $k_{33} = \lambda_{33}/(\rho\beta BT)$ on the relative depth H/T. In Fig. 5.19 circles correspond to a Lewis shipframe ($B/2t = 1.0$, $\beta = 1.0$), crosses correspond to a circle ($\beta = \pi/4 = 0.785$).

Following [238–240], in Fig. 5.20 we show dimensionless added masses of three ships which oscillate with a high frequency in shallow water. Ship I had the average form coefficient of immersed part (i.e. the ratio of the volume of its immersed part to the product of its maximal width to maximal length and maximal immersion depth) $\delta = 0.6$, the waterplane area coefficient (i.e., ratio of the area of the waterplane to the

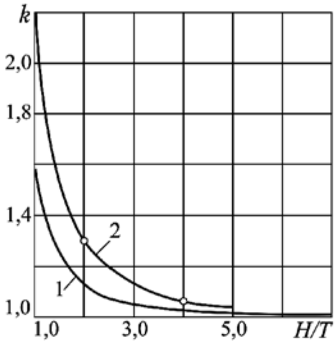

Fig. 5.18 Dependence of ratio $k = \lambda_{33\,H}/\lambda_{33\,\infty}$ on the depth of fluid

product of maximal length to maximal width) $\alpha = 0.706$; other parameters were given by $L/B = 7.5$, $B/T = 2.5$. Ship II had the following parameters: $\delta = 0.7$, $\alpha = 0.785$, $L/B = 7.0$, $B/T = 2.5$; ship III had the following parameters: $\delta = \alpha = 0.785$, $L/B = 7.0$, $B/T = 2.5$. The values of added masses are divided by the ship displacement $V = \delta LBT$. For these three ships Vorobjov computed the added masses λ_{33} and λ_{55} as functions of the dimensionless frequency of vertical oscillations $\delta\sqrt{L/g}$ (Fig. 5.21).

5.4 Added Masses of Inclined Ship Frames Rolling on a Free Surface

Added masses of inclined ship frames rolling on a free surface according to harmonic law with frequency σ were computed by Ya.M. Elis [56, 57]. Denote by S the area of the immersed part of a non-inclined ship frame; the width of shipframe is denoted by B.

Coefficients of added masses $k_{22} = \lambda_{22}/\rho S$, $k_{23} = \lambda_{23}/\rho S$, $k_{33} = \lambda_{33}/\rho S$, $k_{24} = 2\lambda_{24}/\rho SB$, $k_{22} = 2\lambda_{34}/\rho SB$, $k_{44} = 4\lambda_{44}/\rho SB^2$ as functions of dimensionless frequency parameter $\zeta = \sigma^2 T/g$ for different values of B/T (T is the draft of non-inclined shipframe), β (area coefficient of the immersed part of a non-inclined shipframe), α (angle of roll) and parameter $\alpha_n = \arctan[2(H-T)/B]$ (the roll angle when the deck touches the water surface) are shown in Table 5.2.

The parameter ζ was changing between 0.1 and 1.35. The variable H is the height of the non-inclined shipframe. Values k_{ij} were determined in coordinate system xyz (Fig. 5.22), where the z-axis is normal to free undisturbed water surface downward; the y axis lies in the plane of the shipframe and directed along the water surface; positive direction of rotation is assumed to be clockwise. General formulas for added masses of inclined shipframes oscillating with small amplitude (either in vertical, or in horizontal direction, as well as rotational oscillations) on a free surface of a fluid having finite depth, are given in [55].

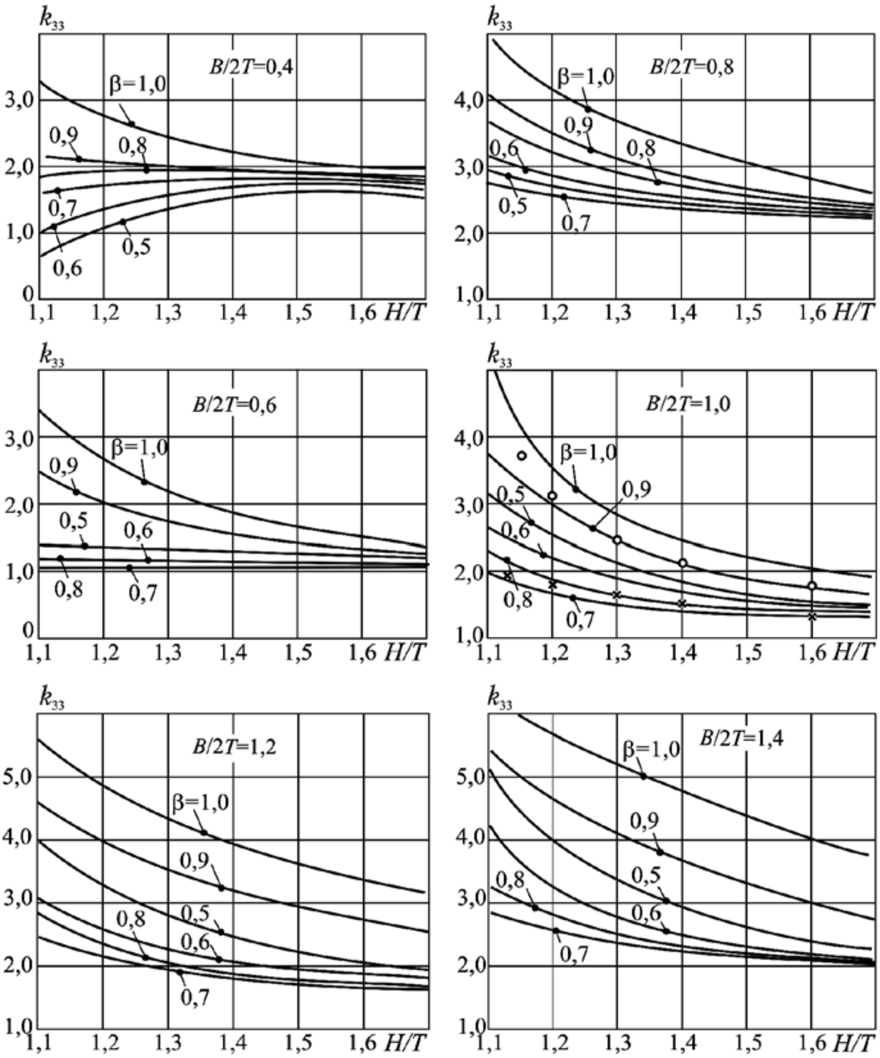

Fig. 5.19 Dependence of coefficient k_{33} of added mass on relative depth of water.

5.5 Added Masses of a Shipframe in Case of Hull Vibration on an Undisturbed Free Surface

Under vertical vibration of a shipframe its added mass λ_{33} is equal to $1/2$ of the added mass of the duplicated shipframe (see Sect. 5.1); it is defined by formulas given in Chap. 2.

The added mass $\lambda_{22\,0}$ under a horizontal vibration should be determined via the formula (5.7). Results of computations carried out by Dorofeuk in 1953–1954 for shipframes presented in Fig. 2.40–2.43, are collected in Table 2.3.

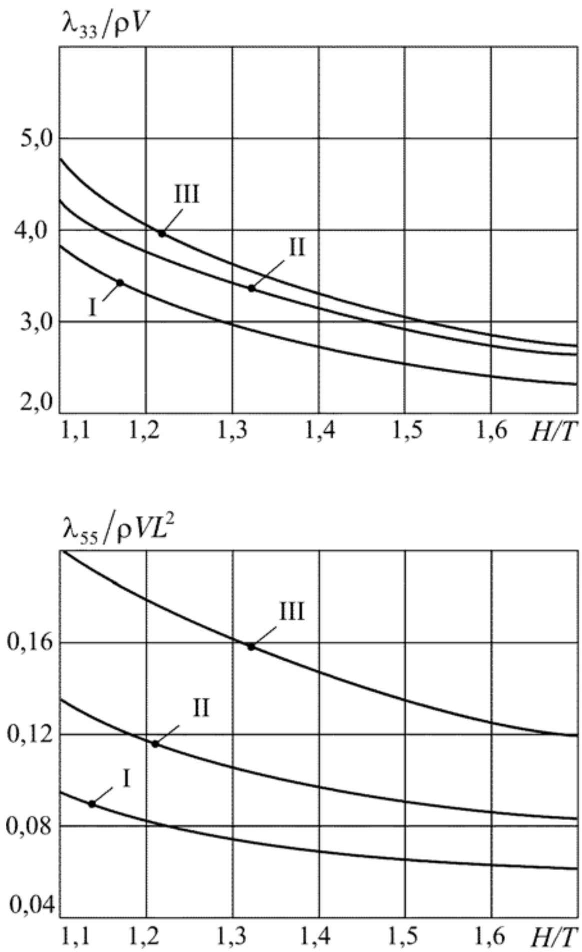

Fig. 5.20 Dimensionless added masses λ_{33}, λ_{55} of three ships under high frequency vertical oscillations on shallow water

Coefficient $k_{22\,0}$ (also often denoted by c_h, from "horizontal" in studies of vibration), is equal to the ratio

$$k_{22\,0} = c_h = \frac{\lambda_{22\,0}}{(2/\pi)\rho T^2}; \tag{5.24}$$

the denominator equals the added mass of the half-immersed ellipse with the vertical semi-axis T, under a horizontal impact [206].

It is sometimes convenient to use the following approximate formula for $k_{22\,0}$ proposed by Ivanjuta and Boyanovsky on the basis of work [128] (analogously to formulas for k_{33}, see Sect. 2.4):

$$k_{22\,0} = c_h = 1 + \frac{B^2}{3T^2}\left(\frac{2T}{B} - a + 1\right)^2,$$

where a is determined by expression (2.28).

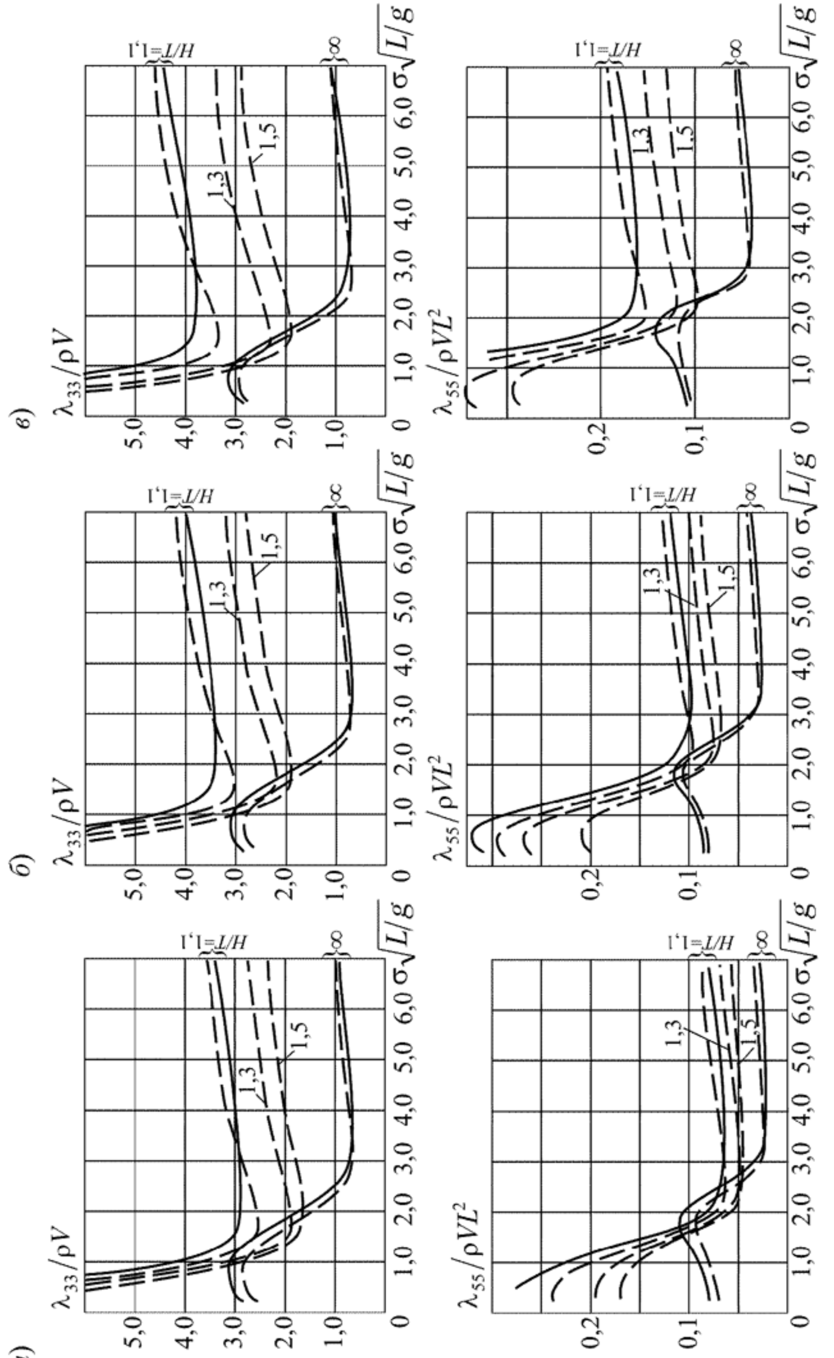

Fig. 5.21 Dependence of generalized added masses of three ships on dimensionless frequency of vertical oscillations. *Left*—for ship I; *center*—for ship II; *right*—for ship III. *Solid line* corresponds to thin ship; *dashed line* corresponds to elongated ship

Table 5.2 Coefficients of added masses of inclined ship frames

ξ	$\alpha_n = 40°$					30°	20°		10°		
	$\alpha = 0°$	10°	20°	30°	40°	40°	30°	20°	20°	30°	40°
	Contour $B/T = 0.8$; $\beta = 0.6$										
	Coefficient k_{22}										
0.10	3.207	3.111	2.711	2.068	1.317	2.179	3.352	3.739	5.310	7.449	8.428
0.35	3.835	3.732	3.272	2.516	1.611	2.704	4.090	4.612	5.899	6.798	7.139
0.60	3.273	3.187	2.820	2.180	1.412	2.193	2.987	2.989	3.047	2.211	1.737
0.85	2.158	2.084	1.833	1.396	0.905	1.244	1.600	1.359	1.485	0.927	0.510
1.10	1.428	1.362	1.175	0.869	0.555	0.690	0.916	0.665	0.954	0.647	0.301
1.35	1.051	0.992	0.837	0.599	0.373	0.432	0.622	0.395	0.782	0.634	0.337
	Coefficient k_{23}										
0.10	0.0	0.379	0.666	0.778	0.668	0.947	1.053	1.376	0.904	1.739	2.367
0.35		0.471	0.830	0.981	0.848	1.221	1.345	1.792	1.084	1.857	2.501
0.60		0.463	0.830	0.997	0.887	1.201	1.202	1.497	0.753	1.045	1.283
0.85		0.370	0.666	0.803	0.735	0.912	0.884	1.009	0.533	0.788	0.967
1.10		0.293	0.525	0.632	0.584	0.693	0.662	0.756	0.457	0.748	0.933
1.35		0.247	0.441	0.526	0.488	0.569	0.562	0.642	0.435	0.767	0.970

continued on next page

Table 5.2 (continued)

ξ	$\alpha_n = 40°$					30°	20°		10°		
	$\alpha = 0°$	10°	20°	30°	40°	40°	30°	20°	20°	30°	40°
	Coefficient k_{24}										
0.10	−2.698	−2.624	−2.238	−1.603	−0.868	−1.943	−3.383	−4.420	−6.155	−10.82	−13.51
0.35	−3.115	−3.040	−2.610	−1.885	−1.024	−2.342	−3.999	−5.326	−6.609	−9.749	−12.08
0.60	−2.632	−2.571	−2.231	−1.625	−0.900	−1.935	−2.965	−3.618	−3.603	−3.807	−3.978
0.85	−1.806	−1.750	−1.511	−1.089	−0.609	−1.197	−1.744	−1.925	−2.096	−2.327	−2.299
1.10	−1.303	−1.250	−1.061	−0.747	−0.414	−0.773	−1.173	−1.225	−1.658	−2.131	−2.144
1.35	−1.068	−1.016	−0.847	−0.582	−0.315	−0.582	−0.951	−0.973	−1.573	−2.248	−2.339
	Coefficient k_{33}										
0.10	0.855	0.913	1.054	1.187	1.217	1.589	1.468	2.137	1.263	2.020	3.186
0.35	0.391	0.457	0.627	0.809	0.878	1.156	1.001	1.598	0.726	1.439	2.535
0.60	0.259	0.330	0.515	0.727	0.826	1.076	0.876	1.453	0.595	1.298	2.398
0.85	0.207	0.272	0.443	0.644	0.756	0.968	0.772	1.323	0.571	1.344	2.498
1.10	0.188	0.247	0.400	0.580	0.689	0.892	0.725	1.282	0.594	1.431	2.627
1.35	0.185	0.240	0.379	0.543	0.645	0.857	0.715	1.292	0.651	1.508	2.731

continued on next page

Table 5.2 (continued)

ξ	$\alpha_n = 40°$					30°	20°		10°		
	$\alpha = 0°$	10°	20°	30°	40°	40°	30°	20°	20°	30°	40°
	Coefficient k_{34}										
0.10	0.0	−0.362	−0.631	−0.702	−0.523	−1.231	−1.455	−2.639	−1.525	−3.895	−6.883
0.35		−0.433	−0.756	−0.851	−0.646	−1.407	−1.667	−2.932	−1.623	−3.887	−6.863
0.60		−0.429	−0.760	−0.874	−0.687	−1.413	−1.549	−2.662	−1.291	−2.926	−5.483
0.85		−0.366	−0.652	−0.758	−0.618	−1.217	−1.277	−2.212	−1.104	−2.710	−4.993
1.10		−0.318	−0.565	−0.660	−0.550	−1.074	−1.129	−2.004	−1.059	−2.731	−5.032
1.35		−0.292	−0.519	−0.606	−0.509	−1.000	−1.068	−1.928	−1.062	−2.803	−5.170
	Coefficient k_{44}										
0.10	2.776	2.724	2.350	1.701	0.934	2.521	4.385	7.201	8.585	19.21	29.77
0.35	3.054	3.004	2.600	1.883	1.021	2.840	4.912	8.172	8.914	17.73	28.11
0.60	2.653	2.614	2.292	1.687	0.942	2.521	3.953	6.388	5.764	10.02	15.88
0.85	2.047	2.007	1.768	1.318	0.771	1.942	2.877	4.627	4.324	8.354	13.63
1.10	1.706	1.665	1.461	1.093	0.656	1.613	2.401	3.921	3.985	8.308	13.64
1.35	1.565	1.522	1.327	0.990	0.598	1.467	2.235	3.686	3.983	8.611	14.11

continued on next page

Table 5.2 (continued)

ξ	$\alpha_n = 40°$					30°	20°		10°		
	$\alpha = 0°$	10°	20°	30°	40°	40°	30°	20°	20°	30°	40°
	Contour $B/T = 0.8$; $\beta = 0.8$										
	Coefficient k_{22}										
0.10	2.770	2.850	2.398	1.810	1.147	2.133	3.612	3.351	4.671	6.291	7.347
0.35	3.399	3.482	2.917	2.185	1.369	2.542	3.995	3.610	4.605	4.215	3.796
0.60	2.560	3.457	2.104	1.558	1.010	1.523	1.753	1.585	1.641	0.977	0.720
0.85	1.379	1.257	1.118	0.837	0.579	0.701	0.691	0.638	0.644	0.389	0.288
1.10	0.769	0.692	0.635	0.487	0.355	0.372	0.371	0.340	0.396	0.335	0.306
1.35	0.505	0.459	0.430	0.337	0.252	0.249	0.284	0.252	0.358	0.404	0.418
	Coefficient k_{23}										
0.10	0.0	0.306	0.500	0.570	0.465	0.770	0.936	0.933	0.652	1.174	1.542
0.35		0.402	0.654	0.747	0.606	1.021	1.196	1.177	0.763	1.092	1.269
0.60		0.353	0.592	0.684	0.580	0.841	0.778	0.796	0.431	0.542	0.659
0.85		0.241	0.423	0.500	0.455	0.576	0.489	0.523	0.281	0.408	0.547
1.10		0.175	0.312	0.380	0.364	0.433	0.370	0.422	0.231	0.377	0.548
1.35		0.138	0.251	0.313	0.308	0.361	0.320	0.376	0.217	0.386	0.577

continued on next page

Table 5.2 (continued)

ξ	$\alpha_n = 40°$					30°	20°		10°		
	$\alpha = 0°$	10°	20°	30°	40°	40°	30°	20°	20°	30°	40°
	Coefficient k_{24}										
0.10	−2.448	−2.557	−2.003	−1.353	−0.666	−1.913	−4.005	−3.660	−5.460	−8.717	−10.86
0.35	−2.916	−3.041	−2.378	−1.600	−0.782	−2.259	−4.357	−3.914	−5.242	−5.867	−6.164
0.60	−2.160	−2.117	−1.704	−1.150	−0.597	−1.421	−1.979	−1.901	−1.975	−1.717	−1.831
0.85	−1.194	−1.121	−0.941	−0.652	−0.372	−0.739	−0.928	−0.961	−0.975	−1.081	−1.331
1.10	−0.730	−0.685	−0.590	−0.420	−0.254	−0.469	−0.639	−0.679	−0.788	−1.121	−1.467
1.35	−0.551	−0.527	−0.455	−0.327	−0.202	−0.374	−0.588	−0.612	−0.816	−1.300	−1.722
	Coefficient k_{33}										
0.10	0.625	0.691	0.803	0.893	0.911	1.204	1.151	1.520	0.954	1.422	2.120
0.35	0.292	0.353	0.468	0.581	0.602	0.851	0.801	1.033	0.587	0.992	1.585
0.60	0.217	0.280	0.391	0.510	0.541	0.762	0.688	0.919	0.517	0.970	1.636
0.85	0.203	0.259	0.348	0.452	0.490	0.684	0.641	0.893	0.540	1.045	1.784
1.10	0.209	0.262	0.331	0.419	0.458	0.652	0.645	0.916	0.582	1.120	1.892
1.35	0.224	0.274	0.330	0.406	0.442	0.646	0.663	0.952	0.620	1.175	1.967

continued on next page

Table 5.2 (continued)

ξ	$\alpha_n = 40°$					30°	20°		10°		
	$\alpha = 0°$	10°	20°	30°	40°	40°	30°	20°	20°	30°	40°
	Coefficient k_{34}										
0.10	0.0	−0.340	−0.531	−0.565	−0.401	−1.104	−1.523	−1.940	−1.183	−2.734	−4.685
0.35		−0.413	−0.637	−0.672	−0.457	−1.244	−1.723	−1.993	−1.221	−2.483	−4.066
0.60		−0.373	−0.592	−0.639	−0.458	−1.120	−1.315	−1.656	−0.878	−1.875	−3.464
0.85		−0.285	−0.470	−0.527	−0.408	−0.932	−1.058	−1.453	−0.752	−1.797	−3.464
1.10		−0.237	−0.398	−0.459	−0.374	−0.840	−0.968	−1.394	−0.729	−1.816	−3.562
1.35		−0.214	−0.363	−0.427	−0.355	−0.799	−0.942	−1.384	−0.734	−1.863	−3.657
	Coefficient k_{44}										
0.10	2.404	2.585	1.972	1.308	0.623	2.365	5.340	5.333	7.227	14.180	21.230
0.35	2.762	2.959	2.248	1.478	0.689	2.670	5.682	5.614	6.846	10.380	14.910
0.60	2.091	2.131	1.892	1.155	0.595	1.982	3.193	3.632	3.241	5.071	8.889
0.85	1.305	1.304	1.101	0.810	0.477	1.416	2.113	2.720	2.250	4.433	8.430
1.10	0.955	0.970	0.846	0.654	0.413	1.192	1.853	2.467	2.138	4.628	8.810
1.35	0.838	0.868	0.758	0.595	0.384	1.116	1.838	2.428	2.235	4.961	9.302

continued on next page

Table 5.2 (continued)

ξ	$\alpha_n = 40°$					30°	20°		10°		
	$\alpha = 0°$	10°	20°	30°	40°	40°	30°	20°	20°	30°	40°
	Contour $B/T = 0.8$; $\beta = 1.0$										
	Coefficient k_{22}										
0.10	2.798	2.870	2.445	1.722	1.147	1.973	3.533	3.681	4.458	6.070	7.175
0.35	3.476	3.486	2.918	2.019	1.283	2.054	3.266	2.814	3.712	1.410	2.184
0.60	2.022	1.838	1.581	1.150	0.790	0.992	0.971	0.891	0.873	0.197	0.520
0.85	0.778	0.689	0.652	0.531	0.436	0.484	0.349	0.420	0.255	0.354	0.429
1.10	0.320	0.301	0.328	0.304	0.288	0.315	0.227	0.331	0.163	0.603	0.548
1.35	0.167	0.179	0.223	0.227	0.229	0.263	0.229	0.343	0.193	0.827	0.692
	Coefficient k_{23}										
0.10	0.0	0.274	0.441	0.470	0.344	0.462	0.761	0.672	0.568	1.433	0.977
0.35		0.382	0.610	0.644	0.457	0.608	0.934	0.738	0.641	0.506	0.613
0.60		0.273	0.456	0.515	0.395	0.445	0.459	0.404	0.255	0.122	0.294
0.85		0.143	0.266	0.331	0.297	0.304	0.235	0.260	0.113	0.087	0.236
1.10		0.080	0.166	0.229	0.234	0.230	0.149	0.202	0.063	0.115	0.238
1.35		0.050	0.115	0.174	0.197	0.189	0.113	0.180	0.047	0.156	0.256

continued on next page

Table 5.2 (continued)

ξ	$\alpha_n = 40°$					30°	20°		10°		
	$\alpha = 0°$	10°	20°	30°	40°	40°	30°	20°	20°	30°	40°
	Coefficient k_{24}										
0.10	−2.835	−2.900	−2.289	−1.356	−0.656	−1.566	−4.121	−4.115	−5.614	−8.214	−10.51
0.35	−3.442	−3.445	−2.689	−1.576	−0.730	−1.652	−3.805	−3.230	−4.581	−2.826	−3.660
0.60	−1.957	−1.782	−1.447	−0.908	−0.482	−0.883	−1.195	−1.237	−1.125	−0.891	−1.389
0.85	−0.766	−0.688	−0.619	−0.437	−0.299	−0.505	−0.509	−0.752	−0.444	−1.388	−1.354
1.10	−0.361	−0.350	−0.348	−0.270	−0.220	−0.378	−0.398	−0.673	−0.398	−2.001	−1.604
1.35	−0.250	−0.266	−0.274	−0.218	−0.189	−0.341	−0.429	−0.704	−0.490	−2.525	−1.873
	Coefficient k_{33}										
0.10	0.594	0.648	0.726	0.736	0.750	0.963	0.999	1.258	0.899	1.563	1.605
0.35	0.356	0.405	0.477	0.506	0.461	0.591	0.747	0.809	0.652	1.409	1.216
0.60	0.332	0.375	0.430	0.455	0.403	0.521	0.669	0.775	0.641	1.521	1.367
0.85	0.350	0.379	0.406	0.411	0.372	0.504	0.655	0.818	0.677	1.601	1.512
1.10	0.374	0.396	0.405	0.392	0.360	0.511	0.666	0.871	0.711	1.649	1.600
1.35	0.397	0.414	0.412	0.384	0.358	0.526	0.683	0.918	0.738	1.681	1.657

continued on next page

Table 5.2 (continued)

ξ	$\alpha_n = 40°$					30°	20°		10°		
	$\alpha = 0°$	10°	20°	30°	40°	40°	30°	20°	20°	30°	40°
	Coefficient k_{34}										
0.10	0.0	−0.366	−0.571	−0.512	−0.357	−0.811	−1.415	−1.732	−1.163	−4.485	−3.427
0.35		−0.465	−0.706	−0.630	−0.367	−0.784	−1.555	−1.561	−1.199	−2.984	−2.692
0.60		−0.360	−0.575	−0.546	−0.345	−0.678	−1.067	−1.280	−0.765	−2.486	−2.532
0.85		−0.243	−0.417	−0.426	−0.308	−0.602	−0.844	−1.212	−0.628	−2.531	−2.623
1.10		−0.190	−0.348	−0.357	−0.288	−0.573	−0.777	−1.220	−0.594	−2.635	−2.723
1.35		−0.168	−0.303	−0.323	−0.278	−0.565	−0.760	−1.233	−0.593	−2.737	−2.802
	Coefficient k_{44}										
0.10	3.090	3.212	2.456	1.343	0.569	1.761	5.752	6.013	7.897	18.631	19.11
0.35	3.637	3.704	2.809	1.518	0.613	1.813	5.409	5.087	6.506	10.580	10.070
0.60	2.122	2.014	1.645	0.998	0.492	1.265	2.410	3.069	2.266	7.594	7.197
0.85	0.981	0.965	0.899	0.635	0.399	0.996	1.650	2.621	1.522	8.857	7.419
1.10	0.627	0.671	0.671	0.508	0.358	0.909	1.552	2.586	1.544	10.280	7.941
1.35	0.555	0.873	0.621	0.471	0.342	0.887	1.615	2.654	1.717	11.290	8.427

continued on next page

Table 5.2 (continued)

ξ	$\alpha_n = 40°$					30°	20°		10°		
	$\alpha = 0°$	10°	20°	30°	40°	40°	30°	20°	20°	30°	40°
	Contour $B/T = 1.6$; $\beta = 0.6$										
	Coefficient k_{22}										
0.10	1.527	1.466	1.353	1.041	0.727	1.251	1.831	2.305	2.257	3.224	3.965
0.35	1.698	1.652	1.564	1.221	0.860	1.509	2.196	2.814	2.526	3.654	4.811
0.60	1.355	1.338	1.294	1.026	0.752	1.221	1.734	1.963	1.674	1.984	2.725
0.85	0.981	0.960	0.905	0.708	0.534	0.756	1.056	0.976	0.982	0.890	1.049
1.10	0.752	0.721	0.645	0.488	0.366	0.453	0.639	0.471	0.648	0.468	0.390
1.35	0.624	0.585	0.496	0.361	0.264	0.289	0.421	0.243	0.495	0.314	0.150
	Coefficient k_{23}										
0.10	0.0	0.117	0.230	0.289	0.271	0.274	0.243	0.183	0.107	0.071	−0.052
0.35		0.139	0.279	0.360	0.340	0.347	0.290	0.211	0.106	−0.004	−0.170
0.60		0.135	0.280	0.376	0.369	0.353	0.272	0.173	0.072	−0.022	−0.168
0.85		0.120	0.249	0.338	0.344	0.300	0.225	0.138	0.067	0.042	−0.046
1.10		0.109	0.222	0.298	0.305	0.251	0.196	0.132	0.080	0.114	0.060
1.35		0.103	0.203	0.268	0.273	0.218	0.185	0.141	0.100	0.173	0.133

continued on next page

Table 5.2 (continued)

ξ	$\alpha_n = 40°$					30°	20°		10°		
	$\alpha = 0°$	10°	20°	30°	40°	40°	30°	20°	20°	30°	40°
	Coefficient k_{24}										
0.10	−0.156	−0.171	−0.188	−0.102	−0.011	−0.213	−0.487	−0.843	−0.608	−1.420	−2.220
0.35	−0.150	−0.172	−0.199	−0.108	−0.006	−0.252	−0.570	−1.026	−0.659	−1.594	−2.676
0.60	−0.129	−0.145	−0.167	−0.087	0.001	−0.210	−0.463	−0.752	−0.460	−0.910	−1.574
0.85	−0.118	−0.125	−0.131	−0.064	0.006	−0.140	−0.306	−0.413	−0.308	−0.458	−0.667
1.10	−0.118	−0.118	−0.111	−0.049	0.009	−0.092	−0.209	−0.230	−0.239	−0.283	−0.303
1.35	−0.122	−0.117	−0.102	−0.042	0.010	−0.065	−0.158	−0.144	−0.210	−0.221	−0.169
	Coefficient k_{33}										
0.10	1.580	1.530	1.492	1.396	1.314	1.626	1.808	2.220	1.775	2.317	3.104
0.35	0.799	0.785	0.799	0.793	0.779	0.949	1.020	1.347	0.944	1.411	2.039
0.60	0.596	0.592	0.624	0.649	0.658	0.806	0.848	1.215	0.784	1.334	1.982
0.85	0.520	0.519	0.560	0.596	0.614	0.771	0.814	1.242	0.768	1.410	2.099
1.10	0.492	0.495	0.540	0.578	0.596	0.777	0.832	1.314	0.800	1.508	2.233
1.35	0.488	0.492	0.542	0.577	0.591	0.801	0.870	1.393	0.847	1.594	2.345

continued on next page

Table 5.2 (continued)

ξ	$\alpha_n = 40°$					30°	20°		10°		
	$\alpha = 0°$	10°	20°	30°	40°	40°	30°	20°	20°	30°	40°
	Coefficient k_{34}										
0.10	0.0	0.013	0.032	0.081	0.144	−0.019	−0.095	−0.244	−0.132	−0.233	−0.446
0.35		−0.016	−0.030	−0.010	0.041	−0.091	−0.122	−0.198	−0.091	−0.070	−0.113
0.60		−0.026	−0.051	−0.042	0.004	−0.118	−0.129	−0.181	−0.075	−0.032	−0.066
0.85		−0.031	−0.060	−0.057	−0.015	−0.125	−0.124	−0.172	−0.072	−0.054	−0.135
1.10		−0.034	−0.065	−0.065	−0.026	−0.125	−0.121	−0.175	−0.074	−0.088	−0.212
1.35		−0.036	−0.068	−0.069	−0.033	−0.124	−0.120	−0.181	−0.077	−0.118	−0.274
	Coefficient k_{44}										
0.10	0.109	0.104	0.106	0.093	0.090	0.126	0.240	0.539	0.299	0.982	1.968
0.35	0.109	0.102	0.102	0.082	0.072	0.128	0.259	0.604	0.307	1.043	2.175
0.60	0.108	0.100	0.096	0.074	0.064	0.119	0.234	0.515	0.261	0.754	1.557
0.85	0.108	0.099	0.091	0.068	0.057	0.105	0.197	0.397	0.227	0.560	1.055
1.10	0.109	0.099	0.089	0.064	0.053	0.095	0.174	0.330	0.213	0.484	0.847
1.35	0.109	0.099	0.087	0.061	0.049	0.089	0.162	0.297	0.207	0.456	0.770

continued on next page

Table 5.2 (continued)

ξ	$\alpha_n = 40°$					30°	20°		10°		
	$\alpha = 0°$	10°	20°	30°	40°	40°	30°	20°	20°	30°	40°
	Contour $B/T = 1.6$; $\beta = 0.8$										
	Coefficient k_{22}										
0.10	1.361	1.402	1.271	1.010	0.708	1.211	1.711	2.207	2.531	3.898	4.418
0.35	1.541	1.578	1.433	1.134	0.792	1.358	1.878	2.404	2.283	2.571	3.618
0.60	1.048	1.054	0.981	0.805	0.597	0.914	1.116	1.315	0.919	0.707	1.112
0.85	0.614	0.615	0.584	0.503	0.400	0.536	0.589	0.631	0.413	0.289	0.407
1.10	0.394	0.397	0.380	0.340	0.285	0.342	0.354	0.350	0.256	0.220	0.248
1.35	0.288	0.292	0.281	0.257	0.223	0.246	0.252	0.237	0.215	0.243	0.239
	Coefficient k_{23}										
0.10	0.0	0.056	0.109	0.145	0.150	0.099	0.045	−0.079	−0.119	−0.418	−0.581
0.35		0.073	0.143	0.190	0.194	0.125	0.052	−0.127	−0.167	−0.484	−0.757
0.60		0.068	0.137	0.187	0.199	0.117	0.042	−0.114	−0.113	−0.242	−0.420
0.85		0.056	0.113	0.160	0.179	0.097	0.035	−0.074	−0.065	−0.115	−0.207
1.10		0.046	0.094	0.137	0.159	0.083	0.032	−0.041	−0.035	−0.055	−0.100
1.35		0.040	0.081	0.120	0.144	0.075	0.033	−0.016	−0.016	−0.026	−0.045

continued on next page

Table 5.2 (continued)

ξ	$\alpha_n = 40°$					30°	20°		10°		
	$\alpha = 0°$	10°	20°	30°	40°	40°	30°	20°	20°	30°	40°
	Coefficient k_{24}										
0.10	−0.239	−0.257	−0.190	−0.075	0.025	−0.122	−0.369	−0.599	−0.868	−1.780	−2.116
0.35	−0.264	−0.281	−0.208	−0.080	0.031	−0.137	−0.403	−0.643	−0.764	−1.094	−1.619
0.60	−0.178	−0.187	−0.142	−0.057	0.025	−0.096	−0.241	−0.344	−0.299	−0.244	−0.381
0.85	−0.107	−0.113	−0.088	−0.037	0.016	−0.059	−0.130	−0.157	−0.134	−0.077	−0.071
1.10	−0.074	−0.079	−0.062	−0.028	0.012	−0.040	−0.082	−0.081	−0.089	−0.068	−0.027
1.35	−0.059	−0.065	−0.050	−0.023	0.008	−0.031	−0.062	−0.052	−0.082	−0.096	−0.051
	Coefficient k_{33}										
0.10	1.155	1.163	1.166	1.121	1.048	1.304	1.402	1.773	1.449	1.917	2.514
0.35	0.591	0.595	0.605	0.593	0.571	0.691	0.741	0.982	0.821	1.279	1.676
0.60	0.476	0.481	0.490	0.482	0.464	0.570	0.634	0.882	0.795	1.353	1.714
0.85	0.457	0.463	0.468	0.454	0.431	0.552	0.639	0.915	0.862	1.483	1.843
1.10	0.470	0.477	0.478	0.456	0.425	0.570	0.678	0.980	0.937	1.585	1.958
1.35	0.495	0.503	0.500	0.470	0.430	0.599	0.724	1.046	1.000	1.657	2.043

continued on next page

Table 5.2 (continued)

ξ	$\alpha_n = 40°$					30°	20°		10°		
	$\alpha = 0°$	10°	20°	30°	40°	40°	30°	20°	20°	30°	40°
	Coefficient k_{34}										
0.10	0.0	−0.030	−0.041	−0.013	0.048	−0.108	−0.175	−0.338	−0.175	−0.267	−0.492
0.35		−0.032	−0.050	−0.035	0.011	−0.081	−0.105	−0.128	−0.030	0.073	−0.126
0.60		−0.034	−0.056	−0.047	−0.006	−0.081	−0.093	−0.095	−0.030	−0.028	−0.000
0.85		−0.034	−0.058	−0.054	−0.017	−0.082	−0.093	−0.103	−0.050	−0.120	−0.147
1.10		−0.035	−0.060	−0.058	−0.025	−0.085	−0.098	−0.121	−0.070	−0.184	−0.254
1.35		−0.035	−0.061	−0.061	−0.030	−0.088	−0.103	−0.140	−0.086	−0.226	−0.328
	Coefficient k_{44}										
0.10	0.046	0.055	0.040	0.025	0.028	0.031	0.108	0.286	0.365	1.128	1.733
0.35	0.049	0.058	0.043	0.025	0.026	0.031	0.107	0.250	0.299	0.649	1.133
0.60	0.034	0.041	0.033	0.023	0.024	0.027	0.071	0.155	0.132	0.220	0.431
0.85	0.023	0.029	0.025	0.021	0.022	0.024	0.049	0.100	0.076	0.150	0.270
1.10	0.018	0.023	0.022	0.019	0.021	0.022	0.039	0.079	0.063	0.161	0.270
1.35	0.016	0.021	0.020	0.019	0.019	0.022	0.036	0.072	0.064	0.190	0.309

continued on next page

Table 5.2 (continued)

ξ	$\alpha_n = 40°$					30°	20°		10°		
	$\alpha = 0°$	10°	20°	30°	40°	40°	30°	20°	20°	30°	40°
	Contour $B/T = 1.6$; $\beta = 1.0$										
	Coefficient k_{22}										
0.10	1.625	1.633	1.424	1.146	0.817	1.395	1.916	2.496	2.636	3.625	5.078
0.35	1.772	1.734	1.477	1.139	0.807	1.308	1.681	2.012	1.836	1.751	2.025
0.60	0.815	0.796	0.765	0.667	0.537	0.757	0.766	0.937	0.520	0.525	0.795
0.85	0.313	0.327	0.387	0.410	0.377	0.490	0.415	0.568	0.201	0.314	0.643
1.10	0.136	0.163	0.242	0.302	0.302	0.380	0.299	0.454	0.139	0.309	0.681
1.35	0.075	0.107	0.188	0.256	0.266	0.334	0.264	0.426	0.146	0.354	0.754
	Coefficient k_{23}										
0.10	0.0	0.026	0.031	0.021	0.046	−0.084	−0.144	−0.383	−0.218	−0.601	−1.231
0.35		0.057	0.070	0.045	0.065	−0.102	−0.151	−0.458	−0.201	−0.526	−1.018
0.60		0.042	0.058	0.045	0.064	−0.087	−0.116	−0.341	−0.145	−0.336	−0.612
0.85		0.011	0.026	0.029	0.056	−0.075	−0.106	−0.263	−0.142	−0.281	−0.457
1.10		−0.011	−0.002	0.013	0.048	−0.068	−0.108	−0.219	−0.150	−0.266	−0.397
1.35		−0.027	−0.023	−0.001	0.041	−0.063	−0.112	−0.192	−0.158	−0.266	−0.377

continued on next page

Table 5.2 (continued)

ξ	$\alpha_n = 40°$					30°	20°		10°		
	$\alpha = 0°$	10°	20°	30°	40°	40°	30°	20°	20°	30°	40°
	Coefficient k_{24}										
0.10	−0.662	−0.633	−0.403	−0.155	0.011	−0.134	−0.527	−0.594	−1.274	−1.675	−2.047
0.35	−0.724	−0.671	−0.418	−0.152	0.015	−0.113	−0.454	−0.416	−0.876	−0.744	−0.523
0.60	−0.344	−0.320	−0.230	−0.105	−0.005	−0.086	−0.228	−0.197	−0.265	−0.228	−0.185
0.85	−0.143	−0.143	−0.129	−0.082	−0.020	−0.081	−0.146	−0.149	−0.118	−0.162	−0.254
1.10	−0.073	−0.081	−0.089	−0.072	−0.028	−0.083	−0.120	−0.149	−0.091	−0.179	−0.354
1.35	−0.050	−0.061	−0.074	−0.069	−0.033	−0.086	−0.114	−0.161	−0.097	−0.212	−0.437
	Coefficient k_{33}										
0.10	1.027	1.053	1.033	0.995	0.935	1.202	1.236	1.616	1.296	1.597	2.245
0.35	0.633	0.639	0.583	0.523	0.486	0.615	0.675	0.895	0.858	1.081	1.579
0.60	0.613	0.615	0.534	0.446	0.395	0.517	0.630	0.825	0.917	1.167	1.624
0.85	0.656	0.656	0.557	0.446	0.373	0.513	0.674	0.865	1.018	1.296	1.738
1.10	0.705	0.703	0.594	0.468	0.376	0.538	0.732	0.926	1.098	1.395	1.833
1.35	0.746	0.744	0.629	0.494	0.388	0.570	0.785	0.984	1.153	1.463	1.907

continued on next page

Table 5.2 (continued)

ξ	$\alpha_n = 40°$					30°	20°		10°		
	$\alpha = 0°$	10°	20°	30°	40°	40°	30°	20°	20°	30°	40°
	Coefficient k_{34}										
0.10	0.0	−0.068	−0.096	−0.093	−0.056	−0.259	−0.238	−0.540	−0.158	−0.266	−0.654
0.35		−0.071	−0.082	−0.056	−0.030	−0.114	−0.089	−0.147	−0.048	0.017	−0.022
0.60		−0.071	−0.084	−0.054	−0.028	−0.086	−0.080	−0.107	−0.081	−0.079	−0.167
0.85		−0.065	−0.084	−0.058	−0.032	−0.081	−0.091	−0.121	−0.106	−0.157	−0.298
1.10		−0.060	−0.083	−0.062	−0.036	−0.085	−0.105	−0.146	−0.122	−0.211	−0.394
1.35		−0.057	−0.083	−0.066	−0.040	−0.091	−0.118	−0.173	−0.132	−0.247	−0.460
	Coefficient k_{44}										
0.10	0.341	0.325	0.190	0.084	0.052	0.150	0.297	0.628	0.808	1.272	2.585
0.35	0.363	0.341	0.194	0.081	0.052	0.113	0.236	0.379	0.594	0.617	0.989
0.60	0.211	0.208	0.145	0.077	0.051	0.103	0.174	0.285	0.307	0.376	0.776
0.85	0.130	0.141	0.118	0.075	0.50	0.101	0.156	0.266	0.242	0.376	0.856
1.10	0.102	0.117	0.107	0.075	0.049	0.102	0.154	0.269	0.235	0.413	0.968
1.35	0.094	0.109	0.103	0.076	0.049	0.103	0.157	0.280	0.243	0.453	1.065

continued on next page

Table 5.2 (continued)

ξ	$\alpha_n = 40°$					30°	20°		10°		
	$\alpha = 0°$	10°	20°	30°	40°	40°	30°	20°	20°	30°	40°
	Contour $B/T = 2.4$; $\beta = 0.6$										
	Coefficient k_{22}										
0.10	0.991	0.974	0.957	0.779	0.626	1.091	1.445	2.069	1.969	2.382	2.812
0.35	1.026	1.042	1.066	0.904	0.713	1.259	1.675	2.346	2.021	2.769	3.091
0.60	0.792	0.806	0.831	0.716	0.586	0.912	1.197	1.320	1.128	1.702	1.462
0.85	0.607	0.595	0.582	0.498	0.418	0.550	0.699	0.594	0.616	0.820	0.561
1.10	0.501	0.469	0.426	0.357	0.302	0.340	0.421	0.284	0.405	0.426	0.237
1.35	0.411	0.396	0.336	0.274	0.232	0.227	0.279	0.157	0.321	0.262	0.125
	Coefficient k_{23}										
0.10	0.0	0.028	0.068	0.111	0.129	0.013	−0.069	−0.330	−0.263	−0.426	−0.596
0.35		0.028	0.077	0.138	0.165	0.012	−0.112	−0.470	−0.395	−0.640	−0.847
0.60		0.022	0.072	0.144	0.180	0.008	−0.129	−0.419	−0.360	−0.595	−0.661
0.85		0.919	0.065	0.134	0.172	0.006	−0.107	−0.295	−0.257	−0.418	−0.418
1.10		0.018	0.061	0.123	0.158	0.007	−0.077	−0.203	−0.170	−0.274	−0.272
1.35		0.020	0.061	0.114	0.145	0.009	−0.050	−0.143	−0.105	−0.175	−0.187

continued on next page

Table 5.2 (continued)

ξ	$\alpha_n = 40°$					30°	20°		10°		
	$\alpha = 0°$	10°	20°	30°	40°	40°	30°	20°	20°	30°	40°
	Coefficient k_{24}										
0.10	0.288	0.214	0.133	0.113	0.115	0.013	−0.070	−0.143	−0.119	−0.505	−0.837
0.35	0.306	0.234	0.149	0.130	0.135	0.008	−0.094	−0.497	−0.146	−0.617	−0.955
0.60	0.226	0.174	0.112	0.105	0.117	−0.002	−0.085	−0.310	−0.094	−0.405	−0.476
0.85	0.159	0.119	0.074	0.075	0.091	−0.004	−0.058	−0.147	−0.043	−0.189	−0.175
1.10	0.118	0.085	0.050	0.056	0.073	−0.002	−0.035	−0.064	−0.012	−0.075	−0.054
1.35	0.093	0.064	0.037	0.044	0.061	0.002	−0.019	−0.023	0.005	−0.020	−0.005
	Coefficient k_{33}										
0.10	2.219	2.049	1.885	1.669	1.503	1.804	2.145	2.433	2.458	2.871	2.880
0.35	1.206	1.110	1.029	0.925	0.848	1.013	1.221	1.511	1.462	1.801	1.923
0.60	0.966	0.887	0.829	0.753	0.695	0.856	1.048	1.417	1.354	1.686	1.870
0.85	0.881	0.812	0.768	0.700	0.645	0.833	1.034	1.460	1.390	1.715	1.929
1.10	0.854	0.793	0.759	0.691	0.634	0.856	1.070	1.533	1.454	1.776	2.009
1.35	0.852	0.797	0.773	0.701	0.639	0.896	1.121	1.605	1.516	1.838	2.082

continued on next page

Table 5.2 (continued)

ξ	$\alpha_n = 40°$					30°	20°		10°		
	$\alpha = 0°$	10°	20°	30°	40°	40°	30°	20°	20°	30°	40°
	Coefficient k_{34}										
0.10	0.0	0.114	0.216	0.283	0.332	0.265	0.238	0.327	0.132	0.346	0.447
0.35		0.061	0.116	0.149	0.180	0.147	0.173	0.359	0.210	0.471	0.630
0.60		0.047	0.090	0.113	0.138	0.124	0.173	0.386	0.259	0.531	0.647
0.85		0.043	0.081	0.096	0.117	0.121	0.182	0.388	0.284	0.532	0.606
1.10		0.042	0.079	0.088	0.106	0.125	0.192	0.385	0.294	0.519	0.572
1.35		0.044	0.081	0.086	0.100	0.132	0.201	0.380	0.296	0.503	0.544
	Coefficient k_{44}										
0.10	0.133	0.087	0.068	0.080	0.110	0.068	0.099	0.296	0.217	0.467	0.654
0.35	0.142	0.090	0.058	0.058	0.076	0.051	0.097	0.323	0.222	0.503	0.704
0.60	0.115	0.074	0.049	0.047	0.062	0.047	0.099	0.292	0.217	0.458	0.553
0.85	0.090	0.060	0.042	0.039	0.051	0.047	0.099	0.254	0.207	0.397	0.438
1.10	0.074	0.050	0.038	0.034	0.044	0.048	0.099	0.229	0.197	0.354	0.380
1.35	0.054	0.045	0.037	0.032	0.040	0.049	0.098	0.214	0.188	0.327	0.394

continued on next page

Table 5.2 (continued)

ξ	$\alpha_n = 40°$					30°	20°		10°		
	$\alpha = 0°$	10°	20°	30°	40°	40°	30°	20°	20°	30°	40°
	Contour $B/T = 2.4$; $\beta = 0.8$										
	Coefficient k_{22}										
0.10	0.954	0.952	0.899	0.785	0.625	1.096	1.366	2.010	1.845	2.952	3.284
0.35	0.981	0.983	0.932	0.815	0.657	1.140	1.406	2.005	1.510	2.033	2.902
0.60	0.620	0.628	0.616	0.564	0.482	0.721	0.827	0.977	0.640	0.671	1.100
0.85	0.382	0.389	0.398	0.382	0.344	0.442	0.473	0.490	0.325	0.330	0.493
1.10	0.263	0.270	0.286	0.288	0.267	0.307	0.312	0.312	0.223	0.259	0.326
1.35	0.206	0.210	0.228	0.237	0.224	0.242	0.240	0.249	0.195	0.262	0.293
	Coefficient k_{23}										
0.10	0.0	−0.041	−0.046	−0.012	0.042	−0.116	−0.237	−0.512	−0.447	−0.983	−1.089
0.35		−0.052	−0.057	−0.012	0.055	−0.154	−0.316	−0.688	−0.564	−1.140	−1.404
0.60		−0.049	−0.054	−0.010	0.057	−0.148	−0.289	−0.556	−0.427	−0.722	−0.946
0.85		−0.043	−0.048	−0.009	0.054	−0.127	−0.239	−0.413	−0.319	−0.500	−0.643
1.10		−0.039	−0.044	−0.009	0.050	−0.109	−0.200	−0.321	−0.254	−0.392	−0.486
1.35		−0.036	−0.042	−0.010	0.046	−0.095	−0.173	−0.264	−0.214	−0.338	−0.403

continued on next page

Table 5.2 (continued)

ξ	$\alpha_n = 40°$					30°	20°		10°		
	$\alpha = 0°$	10°	20°	30°	40°	40°	30°	20°	20°	30°	40°
	Coefficient k_{24}										
0.10	0.141	0.135	0.133	0.130	0.126	0.052	0.013	−0.277	−0.084	−0.616	−0.924
0.35	0.140	0.135	0.136	0.136	0.136	0.051	0.009	−0.271	−0.064	−0.355	−0.741
0.60	0.089	0.086	0.088	0.093	0.100	0.029	0.006	−0.111	−0.003	−0.010	−0.167
0.85	0.058	0.055	0.057	0.061	0.071	0.016	0.010	−0.028	0.035	0.072	0.018
1.10	0.044	0.042	0.041	0.044	0.054	0.011	0.013	0.004	0.047	0.079	0.059
1.35	0.038	0.036	0.034	0.034	0.043	0.010	0.017	0.015	0.050	0.066	0.054
	Coefficient k_{33}										
0.10	1.613	1.594	1.514	1.365	1.210	1.496	1.769	2.065	1.985	2.524	2.786
0.35	0.883	0.870	0.819	0.731	0.651	0.806	0.988	1.259	1.242	1.816	1.949
0.60	0.752	0.739	0.684	0.599	0.526	0.680	0.865	1.168	1.198	1.767	1.847
0.85	0.740	0.724	0.661	0.568	0.489	0.666	0.863	1.185	1.251	1.806	1.844
1.10	0.766	0.747	0.674	0.571	0.482	0.686	0.896	1.228	1.316	1.859	1.878
1.35	0.803	0.782	0.701	0.588	0.489	0.718	0.939	1.275	1.375	1.908	1.919

continued on next page

Table 5.2 (continued)

ξ	$\alpha_n = 40°$					30°	20°		10°		
	$\alpha = 0°$	10°	20°	30°	40°	40°	30°	20°	20°	30°	40°
	Coefficient k_{34}										
0.10	0.0	0.016	0.053	0.112	0.179	0.083	0.003	0.048	−0.066	0.097	0.177
0.35		0.014	0.032	0.061	0.098	0.063	0.055	0.220	0.113	0.478	0.643
0.60		0.017	0.320	0.051	0.077	0.068	0.084	0.262	0.160	0.464	0.614
0.85		0.020	0.034	0.049	0.068	0.078	0.101	0.269	0.170	0.424	0.555
1.10		0.022	0.037	0.049	0.064	0.085	0.111	0.265	0.166	0.389	0.510
1.35		0.024	0.039	0.049	0.062	0.091	0.116	0.258	0.158	0.362	0.477
	Coefficient k_{44}										
0.10	0.025	0.024	0.025	0.035	0.056	0.020	0.044	0.211	0.158	0.652	0.871
0.35	0.025	0.024	0.025	0.032	0.047	0.020	0.043	0.194	0.128	0.461	0.684
0.60	0.017	0.017	0.018	0.024	0.036	0.020	0.040	0.153	0.103	0.298	0.421
0.85	0.013	0.013	0.014	0.018	0.028	0.019	0.038	0.125	0.085	0.231	0.308
1.10	0.012	0.012	0.012	0.015	0.023	0.019	0.035	0.107	0.074	0.205	0.262
1.35	0.011	0.011	0.011	0.013	0.020	0.019	0.033	0.097	0.067	0.198	0.246

continued on next page

Table 5.2 (continued)

ξ	$\alpha_n = 40°$					30°	20°		10°		
	$\alpha = 0°$	10°	20°	30°	40°	40°	30°	20°	20°	30°	40°
	Contour $B/T = 2.4$; $\beta = 1.0$										
	Coefficient k_{22}										
0.10	1.158	1.165	1.072	0.952	0.749	1.305	1.605	3.979	2.043	3.082	4.850
0.35	1.105	1.086	0.972	0.848	0.688	1.128	1.272	3.004	1.207	1.350	2.128
0.60	0.473	0.494	0.524	0.528	0.477	0.672	0.646	1.463	0.416	0.541	0.917
0.85	0.192	0.230	0.315	0.376	0.369	0.475	0.417	0.982	0.221	0.408	0.768
1.10	0.088	0.131	0.230	0.310	0.319	0.397	0.338	0.847	0.179	0.410	0.800
1.35	0.051	0.094	0.190	0.280	0.294	0.366	0.312	0.824	0.183	0.445	0.866
	Coefficient k_{23}										
0.10	0.0	−0.093	−0.155	−0.148	−0.052	−0.275	−0.459	−1.306	−0.608	−1.274	−2.105
0.35		−0.097	−0.171	−0.170	−0.061	−0.339	−0.538	−1.531	−0.617	−1.144	−1.848
0.60		−0.076	−0.142	−0.151	−0.057	−0.299	−0.437	−1.171	−0.433	−0.781	−1.183
0.85		−0.074	−0.130	−0.139	−0.054	−0.261	−0.371	−0.939	−0.359	−0.644	−0.939
1.10		−0.078	−0.129	−0.133	−0.052	−0.234	−0.334	−0.806	−0.332	−0.588	−0.839
1.35		−0.084	−0.128	−0.130	−0.050	−0.216	−0.312	−0.726	−0.322	−0.567	−0.800

continued on next page

Table 5.2 (continued)

ξ	$\alpha_n = 40°$					30°	20°		10°		
	$\alpha = 0°$	10°	20°	30°	40°	40°	30°	20°	20°	30°	40°
	Coefficient k_{24}										
0.10	−0.160	−0.118	0.002	0.090	0.113	0.032	−0.058	−0.514	−0.369	−0.625	−1.487
0.35	−0.174	−0.128	−0.006	0.080	0.106	0.034	−0.032	−0.283	−0.217	−0.145	−0.269
0.60	−0.097	−0.080	−0.023	0.029	0.056	−0.001	−0.028	−0.114	−0.083	−0.010	0.011
0.85	−0.050	−0.049	−0.028	0.003	0.027	−0.021	−0.032	−0.091	−0.048	−0.021	−0.054
1.10	−0.026	−0.031	−0.028	−0.010	0.012	−0.032	−0.037	−0.106	−0.040	−0.053	−0.151
1.35	−0.014	−0.022	−0.025	−0.017	0.003	−0.039	−0.041	−0.131	−0.042	−0.084	−0.237
	Coefficient k_{33}										
0.10	1.387	1.402	1.357	1.269	1.101	1.424	1.644	3.357	1.771	2.286	3.150
0.35	0.875	0.863	0.783	0.697	0.590	0.788	0.983	2.128	1.228	1.692	2.426
0.60	0.865	0.838	0.715	0.600	0.486	0.684	0.901	1.958	1.250	1.646	2.236
0.85	0.930	0.896	0.739	0.590	0.458	0.674	0.919	1.955	1.343	1.700	2.214
1.10	1.000	0.962	0.785	0.608	0.457	0.693	0.961	2.000	1.429	1.762	2.235
1.35	1.056	1.019	0.810	0.633	0.465	0.718	1.005	2.050	1.496	1.817	2.268

continued on next page

Table 5.2 (continued)

ξ	$\alpha_n = 40°$					30°	20°		10°		
	$\alpha = 0°$	10°	20°	30°	40°	40°	30°	20°	20°	30°	40°
	Coefficient k_{34}										
0.10	0.0	−0.021	−0.043	−0.042	0.034	−0.134	−0.191	−0.527	−0.075	−0.164	−0.215
0.35		−0.001	−0.004	−0.010	0.019	−0.045	−0.015	0.020	0.129	0.232	0.397
0.60		−0.001	0.007	0.006	0.019	−0.008	0.036	0.126	0.131	0.233	0.327
0.85		−0.004	0.009	0.014	0.022	0.012	0.053	0.156	0.109	0.205	0.285
1.10		−0.006	0.006	0.018	0.024	0.023	0.056	0.160	0.085	0.175	0.258
1.35		−0.008	0.004	0.018	0.025	0.029	0.053	0.154	0.065	0.150	0.242
	Coefficient k_{44}										
0.10	0.116	0.107	0.080	0.077	0.069	0.125	0.205	0.905	0.363	0.934	2.568
0.35	0.120	0.109	0.077	0.074	0.069	0.115	0.163	0.669	0.272	0.537	1.368
0.60	0.111	0.105	0.075	0.065	0.058	0.105	0.142	0.556	0.227	0.407	1.050
0.85	0.103	0.102	0.075	0.060	0.050	0.098	0.130	0.499	0.207	0.375	0.990
1.10	0.099	0.099	0.075	0.057	0.045	0.093	0.124	0.468	0.205	0.375	0.999
1.35	0.096	0.098	0.074	0.055	0.042	0.089	0.121	0.452	0.209	0.387	1.028

continued on next page

Table 5.2 (continued)

ξ	$\alpha_n = 40°$					30°	20°		10°		
	$\alpha = 0°$	10°	20°	30°	40°	40°	30°	20°	20°	30°	40°
	Contour $B/T = 3.2$; $\beta = 0.6$										
	Coefficient k_{22}										
0.10	0.723	0.741	0.776	0.731	0.651	1.144	1.357	2.195	1.403	2.220	3.125
0.35	0.701	0.749	0.821	0.785	0.701	1.235	1.466	2.250	1.437	2.294	2.960
0.60	0.523	0.551	0.600	0.583	0.534	0.804	0.920	1.057	0.848	1.125	1.147
0.85	0.408	0.407	0.417	0.407	0.383	0.476	0.520	0.464	0.482	0.518	0.461
1.10	0.345	0.324	0.310	0.303	0.292	0.308	0.324	0.249	0.317	0.296	0.255
1.35	0.309	0.277	0.249	0.243	0.239	0.224	0.230	0.172	0.244	0.216	0.199
	Coefficient k_{23}										
0.10	0.0	−0.046	−0.059	−0.016	0.036	−0.192	−0.324	−0.769	−0.390	−0.800	−1.211
0.35		−0.064	−0.082	−0.020	0.049	−0.255	−0.445	−1.036	−0.554	−1.119	−1.584
0.60		−0.072	−0.090	−0.020	0.055	−0.249	−0.433	−0.824	−0.532	−0.925	−1.114
0.85		−0.071	−0.086	−0.019	0.053	−0.216	−0.363	−0.601	−0.437	−0.670	−0.767
1.10		−0.067	−0.079	−0.017	0.049	−0.187	−0.300	−0.465	−0.351	−0.506	−0.589
1.35		−0.062	−0.071	−0.016	0.044	−0.165	−0.253	−0.385	−0.287	−0.406	−0.494

continued on next page

Table 5.2 (continued)

ξ	$\alpha_n = 40°$					30°	20°		10°		
	$\alpha = 0°$	10°	20°	30°	40°	40°	30°	20°	20°	30°	40°
	Coefficient k_{24}										
0.10	0.432	0.336	0.232	0.177	0.158	0.041	0.023	−0.463	0.133	−0.344	−0.945
0.35	0.418	0.336	0.238	0.188	0.172	0.027	−0.003	−0.531	0.098	−0.413	−0.955
0.60	0.306	0.241	0.166	0.136	0.134	−0.005	−0.032	−0.304	0.037	−0.233	−0.406
0.85	0.232	0.174	0.112	0.094	0.098	−0.016	−0.030	−0.151	0.029	−0.094	−0.161
1.10	0.191	0.138	0.083	0.069	0.076	−0.016	−0.018	−0.081	0.041	−0.024	−0.076
1.35	0.167	0.117	0.068	0.055	0.063	−0.013	−0.006	−0.048	0.053	0.009	−0.049
	Coefficient k_{33}										
0.10	2.791	2.535	2.250	1.923	1.671	2.014	2.471	2.763	2.889	3.228	3.315
0.35	1.605	1.443	1.271	1.073	0.927	1.143	1.465	1.854	1.776	2.189	2.405
0.60	1.353	1.212	1.065	0.888	0.759	0.989	1.311	1.763	1.644	2.101	2.292
0.85	1.277	1.148	1.014	0.837	0.708	0.974	1.307	1.770	1.662	2.103	2.274
1.10	1.263	1.143	1.016	0.834	0.699	1.004	1.346	1.810	1.712	2.133	2.304
1.35	1.273	1.162	1.039	0.849	0.707	1.047	1.394	1.855	1.764	2.169	2.346

continued on next page

Table 5.2 (continued)

ξ	$\alpha_n = 40°$					30°	20°		10°		
	$\alpha = 0°$	10°	20°	30°	40°	40°	30°	20°	20°	30°	40°
	Coefficient k_{34}										
0.10	0.0	0.164	0.314	0.397	0.439	0.422	0.399	0.676	0.273	0.590	0.891
0.35		0.090	0.180	0.222	0.245	0.266	0.309	0.717	0.278	0.714	1.117
0.60		0.079	0.157	0.185	0.199	0.254	0.329	0.746	0.342	0.781	1.084
0.85		0.083	0.159	0.176	0.181	0.265	0.358	0.743	0.394	0.791	1.028
1.10		0.091	0.168	0.176	0.175	0.281	0.381	0.738	0.426	0.786	0.994
1.35		0.100	0.179	0.180	0.174	0.296	0.398	0.733	0.476	0.777	0.971
	Coefficient k_{44}										
0.10	0.282	0.190	0.138	0.136	0.157	0.128	0.173	0.480	0.272	0.561	0.903
0.35	0.274	0.184	0.123	0.102	0.109	0.100	0.168	0.516	0.275	0.595	0.940
0.60	0.203	0.139	0.098	0.082	0.087	0.099	0.173	0.480	0.274	0.567	0.761
0.85	0.156	0.109	0.083	0.069	0.073	0.102	0.180	0.441	0.273	0.525	0.652
1.10	0.129	0.093	0.077	0.064	0.066	0.107	0.182	0.413	0.269	0.490	0.597
1.35	0.113	0.085	0.075	0.061	0.062	0.110	0.182	0.396	0.263	0.465	0.569

continued on next page

Table 5.2 (continued)

ξ	$\alpha_n = 40°$					30°	20°		10°		
	$\alpha = 0°$	10°	20°	30°	40°	40°	30°	20°	20°	30°	40°
	Contour $B/T = 3.2$; $\beta = 0.8$										
	Coefficient k_{22}										
0.10	0.718	0.750	0.804	0.765	0.681	1.184	1.381	2.276	1.516	2.730	3.265
0.35	0.675	0.701	0.762	0.738	0.674	1.136	1.285	1.949	1.135	1.747	2.489
0.60	0.408	0.423	0.483	0.500	0.482	0.680	0.706	0.860	0.496	0.630	0.916
0.85	0.254	0.267	0.323	0.359	0.359	0.435	0.425	0.469	0.277	0.368	0.490
1.10	0.177	0.190	0.245	0.288	0.294	0.326	0.308	0.350	0.206	0.319	0.394
1.35	0.138	0.151	0.205	0.251	0.260	0.278	0.260	0.320	0.188	0.326	0.389
	Coefficient k_{23}										
0.10	0.0	−0.127	−0.194	−0.129	−0.032	−0.279	−0.493	−0.886	−0.654	−1.404	−1.466
0.35		−0.163	−0.245	−0.159	−0.038	−0.360	−0.637	−1.110	−0.813	−1.573	−1.736
0.60		−0.157	−0.236	−0.153	−0.036	−0.331	−0.564	−0.840	−0.648	−1.072	−1.161
0.85		−0.142	−0.216	−0.143	−0.034	−0.287	−0.477	−0.641	−0.524	−0.827	−0.853
1.10		−0.130	−0.200	−0.135	−0.033	−0.253	−0.417	−0.529	−0.449	−0.710	−0.705
1.35		−0.120	−0.188	−0.130	−0.032	−0.229	−0.376	−0.464	−0.404	−0.652	−0.629

continued on next page

Table 5.2 (continued)

ξ	$\alpha_n = 40°$					30°	20°		10°		
	$\alpha = 0°$	10°	20°	30°	40°	40°	30°	20°	20°	30°	40°
	Coefficient k_{24}										
0.10	0.273	0.265	0.216	0.172	0.142	0.045	0.050	−0.401	0.110	−0.493	−0.958
0.35	0.245	0.236	0.196	0.162	0.142	0.030	0.031	−0.363	0.071	−0.279	−0.710
0.60	0.147	0.140	0.115	0.098	0.095	−0.002	0.003	−0.165	0.051	−0.029	−0.214
0.85	0.098	0.093	0.072	0.061	0.063	−0.014	−0.001	−0.079	0.059	0.034	−0.074
1.10	0.078	0.073	0.053	0.042	0.045	−0.017	0.002	−0.049	0.066	0.040	−0.048
1.35	0.070	0.066	0.045	0.032	0.035	−0.016	0.005	−0.042	0.069	0.029	−0.057
	Coefficient k_{33}										
0.10	2.055	2.057	1.903	1.607	1.350	1.673	2.148	2.355	2.490	3.104	2.981
0.35	1.202	1.209	1.100	0.896	0.732	0.942	1.311	1.588	1.697	2.398	2.241
0.60	1.075	1.082	0.965	0.757	0.599	0.821	1.193	1.480	1.643	2.249	2.061
0.85	1.080	1.085	0.949	0.726	0.560	0.808	1.187	1.464	1.676	2.214	2.000
1.10	1.124	1.125	0.970	0.730	0.554	0.828	1.213	1.481	1.724	2.222	1.956
1.35	1.177	1.174	1.003	0.747	0.562	0.858	1.247	1.506	1.769	2.244	2.011

continued on next page

Table 5.2 (continued)

ξ	$\alpha_n = 40°$					30°	20°		10°		
	$\alpha = 0°$	10°	20°	30°	40°	40°	30°	20°	20°	30°	40°
	Coefficient k_{34}										
0.10	0.0	−0.001	0.072	0.179	0.264	0.202	0.091	0.313	−0.046	0.263	0.557
0.35		0.006	0.047	0.099	0.144	0.143	0.137	0.464	0.143	0.640	0.903
0.60		0.026	0.064	0.094	0.120	0.156	0.190	0.493	0.235	0.658	0.842
0.85		0.042	0.084	0.101	0.114	0.174	0.225	0.497	0.273	0.648	0.795
1.10		0.053	0.098	0.108	0.114	0.190	0.246	0.496	0.285	0.634	0.769
1.35		0.059	0.108	0.115	0.116	0.202	0.258	0.493	0.286	0.625	0.754
	Coefficient k_{44}										
0.10	0.137	0.139	0.111	0.090	0.098	0.078	0.155	0.391	0.323	0.890	0.987
0.35	0.123	0.126	0.104	0.080	0.076	0.074	0.156	0.389	0.293	0.755	0.867
0.60	0.088	0.093	0.082	0.063	0.060	0.075	0.152	0.341	0.265	0.616	0.656
0.85	0.072	0.078	0.070	0.054	0.050	0.077	0.147	0.307	0.242	0.542	0.562
1.10	0.067	0.073	0.066	0.050	0.046	0.078	0.142	0.285	0.226	0.504	0.521
1.35	0.066	0.071	0.064	0.048	0.043	0.078	0.138	0.272	0.214	0.487	0.504

continued on next page

Table 5.2 (continued)

ξ	$\alpha_n = 40°$					30°	20°		10°		
	$\alpha = 0°$	10°	20°	30°	40°	40°	30°	20°	20°	30°	40°
	Contour $B/T = 3.2$; $\beta = 1.0$										
	Coefficient k_{22}										
0.10	0.894	0.916	1.125	0.876	0.753	1.327	1.523	2.433	1.785	2.991	4.136
0.35	0.760	0.771	0.823	0.730	0.669	1.095	1.122	1.716	0.929	1.204	2.300
0.60	0.328	0.366	0.425	0.477	0.467	0.643	0.597	0.808	0.364	0.553	0.940
0.85	0.145	0.192	0.282	0.367	0.370	0.463	0.420	0.558	0.233	0.469	0.706
1.10	0.073	0.122	0.232	0.320	0.326	0.395	0.361	0.500	0.207	0.486	0.698
1.35	0.045	0.094	0.215	0.300	0.305	0.371	0.345	0.500	0.214	0.525	0.741
	Coefficient k_{23}										
0.10	0.0	−0.156	−0.486	−0.229	−0.082	−0.354	−0.636	−0.967	−0.843	−1.694	−1.975
0.35		−0.177	−0.581	−0.269	−0.098	−0.434	−0.744	−1.102	−0.859	−1.483	−1.976
0.60		−0.148	−0.492	−0.249	−0.093	−0.377	−0.620	−0.817	−0.637	−1.059	−1.284
0.85		−0.133	−0.428	−0.232	−0.088	−0.329	−0.538	−0.654	−0.536	−0.903	−1.007
1.10		−0.129	−0.387	−0.222	−0.084	−0.295	−0.490	−0.565	−0.490	−0.840	−0.887
1.35		−0.128	−0.362	−0.215	−0.082	−0.271	−0.459	−0.515	−0.470	−0.815	−0.833

continued on next page

Table 5.2 (continued)

ξ	$\alpha_n = 40°$					30°	20°		10°		
	$\alpha = 0°$	10°	20°	30°	40°	40°	30°	20°	20°	30°	40°
	Coefficient k_{24}										
0.10	0.053	0.079	0.185	0.152	0.120	0.004	0.030	−0.438	−0.093	−0.511	−1.422
0.35	0.014	0.039	0.132	0.117	0.103	−0.008	0.018	−0.296	−0.056	−0.098	−0.635
0.60	−0.018	−0.006	0.070	0.050	0.052	−0.036	−0.012	−0.149	−0.025	−0.001	−0.190
0.85	−0.017	−0.014	0.052	0.018	0.025	−0.048	−0.022	−0.113	−0.016	−0.016	−0.151
1.10	−0.008	−0.011	0.047	0.004	0.010	−0.053	−0.027	−0.111	−0.016	−0.048	−0.190
1.35	0.000	−0.008	0.045	−0.004	0.002	−0.055	−0.031	−0.119	−0.019	−0.081	−0.242
	Coefficient k_{33}										
0.10	1.706	1.705	1.954	1.473	1.181	1.501	1.979	2.135	2.237	2.906	3.134
0.35	1.100	1.077	1.284	0.854	0.645	0.867	1.281	1.460	1.660	2.304	2.452
0.60	1.096	1.047	1.220	0.751	0.540	0.707	1.190	1.347	1.649	2.169	2.191
0.85	1.178	1.112	1.239	0.737	0.513	0.764	1.193	1.329	1.715	2.163	2.110
1.10	1.263	1.188	1.275	0.749	0.512	0.782	1.221	1.340	1.785	2.188	2.094
1.35	1.332	1.254	1.311	0.770	0.520	0.806	1.252	1.359	1.845	2.221	2.103

continued on next page

Table 5.2 (continued)

ξ	$\alpha_n = 40°$					30°	20°		10°		
	$\alpha = 0°$	10°	20°	30°	40°	40°	30°	20°	20°	30°	40°
	Coefficient k_{34}										
0.10	0.0	−0.011	−0.170	0.006	0.136	0.035	−0.150	0.040	−0.103	−0.076	0.326
0.35		0.013	0.024	0.008	0.072	0.053	0.008	0.257	0.155	0.328	0.763
0.60		0.026	0.053	0.030	0.065	0.083	0.081	0.292	0.210	0.362	0.661
0.85		0.030	0.090	0.046	0.067	0.104	0.116	0.302	0.211	0.364	0.622
1.10		0.028	0.106	0.056	0.070	0.119	0.132	0.306	0.199	0.359	0.607
1.35		0.026	0.113	0.063	0.074	0.129	0.140	0.306	0.183	0.354	0.603
	Coefficient k_{44}										
0.10	0.128	0.128	0.264	0.118	0.085	0.113	0.274	0.500	0.456	1.192	1.791
0.35	0.123	0.121	0.228	0.110	0.076	0.115	0.247	0.437	0.375	0.846	1.246
0.60	0.122	0.116	0.196	0.092	0.063	0.112	0.223	0.380	0.326	0.698	0.962
0.85	0.123	0.116	0.179	0.082	0.056	0.110	0.206	0.349	0.301	0.640	0.879
1.10	0.124	0.117	0.168	0.077	0.051	0.108	0.195	0.331	0.291	0.620	0.858
1.35	0.124	0.11	0.161	0.074	0.049	0.105	0.187	0.322	0.289	0.618	0.862

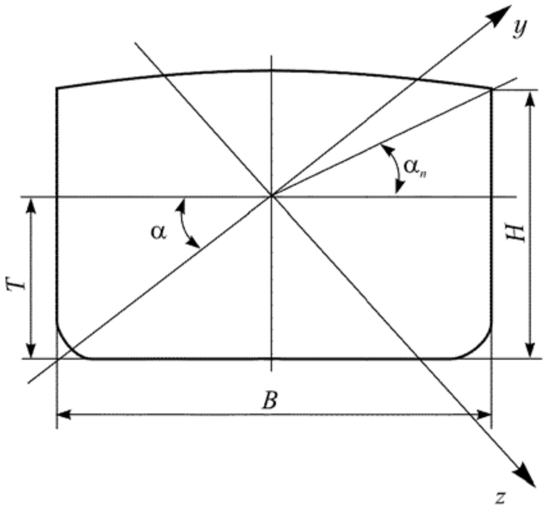

Fig. 5.22 Coordinate axes and notations for inclined ship frame

For three types of bulb-shaped shipframes considered in Sect. 2.4 (see Fig. 2.50) they proposed the following formulas:

$$\text{Type I:} \qquad \lambda_{22\,0} = \frac{\pi}{2}\rho b_s^2;$$

$$\text{Type II:} \qquad \lambda_{22\,0} = \pi\rho b_s^2\left(1 - \frac{b_s^2}{2H_s^2}\right);$$

$$\text{Type III:} \qquad \lambda_{22\,0} = \frac{\pi}{2}\rho b_{s\,2}^2.$$

Under torsional oscillations of a hull vibrating on a free surface, the added moment of inertia of shipframe with respect to the x-axis (which is directed along the axis of the ship and lies in the plane of waterline) can be found from formula $\lambda_{44} = 0.5\lambda_{44}^*$, where λ_{44}^* is the added moment of inertia of a duplicated contour under rotation around the same axis in an infinite fluid. If coefficients in the Laurent series of the function mapping the exterior of the contour to the interior of the unit disc are known, then λ_{44}^* can be found using Sedov's formulas [206], given in Chap. 2.

For shipframes shown in Fig. 2.45 and Fig. 2.46 the following formulas are due to Dorofeuk. For the coefficient k_{44} we have:

$$k_{44} = c_{\text{tor}} = \frac{\lambda_{44}}{(\pi/16)\rho T^4(B^2/4T^2 - 1)^2} \tag{5.25}$$

where the variable in the denominator is equal to the added moment of inertia of the half-ellipse with half-axes $B/2$ and T. Variables k_{44} are given in Table 2.3. In computation of λ_{44} one can also use the formula given in Sect. 2.4, and Fig. 2.39. Suppose one needs to compute the added moment of inertia $\lambda_{44\,1}$ with respect to the axis x_1, which is also contained in the centerline plane of the hull but shifted by z_0 (which could be either positive or negative) with respect to the waterline. Then one has to use the transformation formulas (see Chap. 1), which imply

$$\lambda_{44\,1} = \lambda_{44} + z_0^2\lambda_{22\,0} + 2z_0\lambda_{24\,0},$$

where $\lambda_{22\,0}$ is defined by the formula (5.24), and

$$\lambda_{24\,0} = \frac{1}{3}\rho T^3\left(\frac{B^2}{4T^2} - 1\right)k_{24\,0}. \tag{5.26}$$

The coefficients $k_{24\,0}$, which are also typically denoted in computations of vibrations by c_{incl} (from “inclination”), are presented in Tables 2.3 and 2.4.

For $B/2T = 1$ instead of formulas (5.25), (5.26) one has to use the relations

$$\lambda_{44} = k_{44}2\pi\rho T^4, \qquad \lambda_{24\,0} = k_{24\,0}\frac{8\rho T^3}{105},$$

where k_{44} and $k_{24\,0}$ are shown in Table 2.3.

On the basis of results discussed above one can find the functions $c_v = k_{33}(\beta, B/2T)$ and $c_h = k_{22\,0}(\beta, B/2T)$, shown in Fig. 2.49.

Approximate analytical formulas for coefficients $k_{44} = c_{\text{tor}}$ and $k_{24\,0} = c_{\text{incl}}$, obtained by Ivanjuta and Boyanovsky, have the following form:

$$k_{44} \equiv c_{\text{tor}} = \frac{(1 + a_3)^2 + 2(a_3/a_1)^2}{(1 + a_3)^2};$$

$$k_{24\,0} \equiv c_{\text{incl}} = \frac{1}{35}\,\frac{7(5 - 5a_1 + 9a_3)\,a_1(1 + a_3) + 2a_3(7 - 7a_1 - 45a_3)}{a_1(1 + a_3)(1 - a_1 + a_3)}.$$

Here

$$a_1 = \frac{1 - 2T/B}{1 + 2T/B}(1 + a_3);$$

$$a_3 = \frac{1 - 2k_{33} - 2T/B + (1 + 2T/B)\sqrt{4k_{33} - 3}}{2(k_{33} - 1 - 2T/B - 4T^2/B^2)},$$

where k_{33} is defined by formulas (2.27), (2.28).

To evaluate the influence of the depth of water on added mass λ_{33} for various shapes of shipframe, one can use the experimental data by Prohasky [200] obtained by the method of small oscillations. In Fig. 5.23 we show graphs of coefficient $k_{33} = 8\lambda_{33}/\pi\rho B^2$, where B is the width of shipframe measured at the level of waterline, on parameters h/T (h is the depth of water, T is the draught of the shipframe), β is the area coefficient of the shipframe. The curves presented in Fig. 5.23 are enumerated according to the numbers of shipframes shown in the same figure.

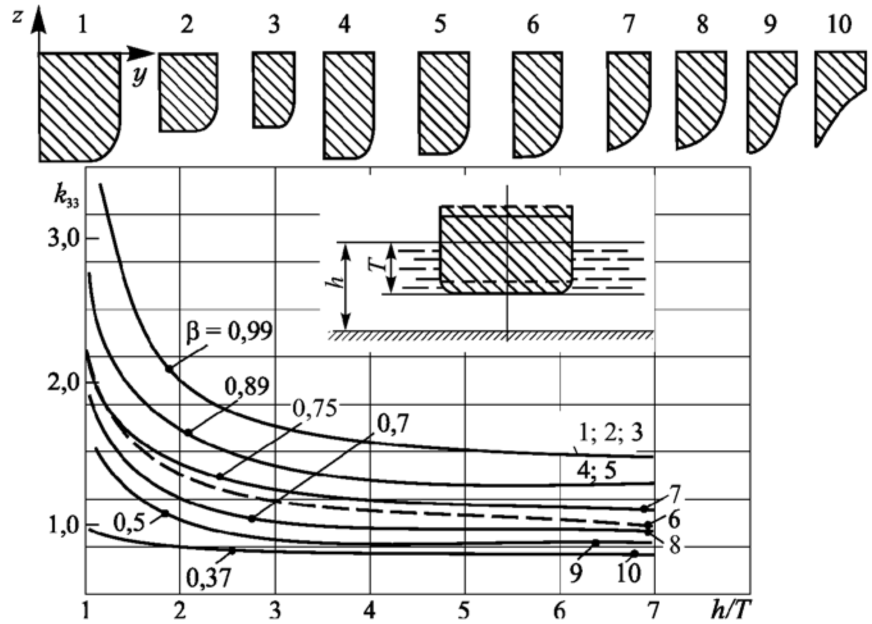

Fig. 5.23 Dependence of coefficient k_{33} of various shipframes on the depth of water

5.6 Influence of a Free Surface on Added Masses of Submerged Cylinders and Ellipsoids

A body moving under the free surface of a fluid generates surface waves. However, in some cases like motion with high velocity or acceleration, high frequency oscillation of the body, motion starting from rest under the impact etc., the surface waves can be neglected. Physically this corresponds to assuming that gravity forces can be neglected in comparison with inertial forces.

In this section added masses of a body moving under the free surface are determined under the following conditions:

- Velocity potential satisfies Laplace equation

$$\Delta\varphi = 0. \tag{5.27}$$

- On a free surface the following boundary condition is satisfied:

$$\varphi = 0. \tag{5.28}$$

- At infinity the fluid remains at rest:

$$\operatorname{grad}\varphi|_{\infty} = 0. \tag{5.29}$$

- On the surface of the body

$$\frac{\partial \varphi}{\partial n} = u_n, \tag{5.30}$$

where u_n is the normal component of velocity of a point of the surface of the body.

Conditions (5.27)–(5.30) completely determine the function $\varphi(x, y, z)$.

5.6.1 Completely Submerged Sphere

Added mass of a sphere under horizontal motion along the x-axis under a free surface is expressed by the formula [191]:

$$\lambda_{11} = \frac{4}{3}\pi r^3 \rho k_{11},$$

where

$$k_{11} = \frac{1}{2}\frac{1 - \delta^3/8}{1 + \delta^3/16},$$

$\delta = r/h$; r is the radius of the sphere; h is the distance from the center of the sphere to the free surface.

Under vertical motion (i.e. motion along z-axis) of a sphere under free surface the added mass is given by approximate formula

$$\lambda_{33} = \frac{4}{3}\pi r^3 \rho k_{33},$$

where

$$k_{33} = \frac{1}{2}\frac{1 - \delta^3/4}{1 + \delta^3/8}.$$

A more precise formula has the form [192]:

$$k_{33} = \frac{1}{2}\left(1 - \frac{3}{2^3}\delta^3 + \frac{3}{2^6}\delta^6 + \frac{9}{2^8}\delta^8 - \frac{3}{2^9}\delta^9 + \frac{9}{2^9}\delta^{10} - \frac{9}{2^{10}}\delta^{11} + \cdots\right).$$

Experimental data on added masses of sphere and disc which oscillate in the vertical direction under a free water surface are shown in Fig. 5.24, see [183].

For a sphere oscillating under the free surface of a fluid of infinite depth the dependence of the added masses λ_{11} and λ_{33} on oscillation frequencies is studied in [211, 244] for various immersion depths.

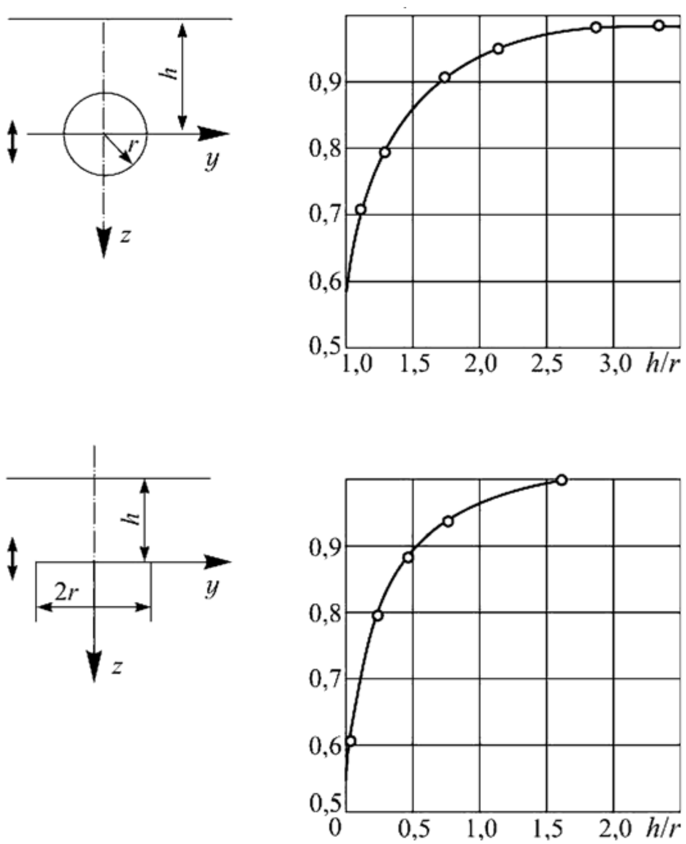

Fig. 5.24 Coefficient $\lambda_{33}/\lambda_{33\,\infty}$ of added masses of a sphere (*above*) and a disc (*below*) oscillating in the vertical direction near the free surface

5.6.2 Circular Cylinder

Added mass per unit of length of the circular cylinder whose axis (y) is parallel to the free surface, is given by the formula [183]:

$$\lambda_{11} = \lambda_{33} = \pi r^2 \rho k_{11} = \pi r^2 \rho k_{33},$$

where

$$k_{11} = k_{33} = \frac{1 - \delta^2/4}{1 + \delta^2/4};$$

$\delta = r/h$; r is the radius of the cylinder; h is the distance from the axis of the cylinder to the free surface.

A more precise formula has the form

$$k_{11} = k_{33} = 1 - \delta^2/2 + \frac{\delta^4}{2^3} + \frac{\delta^6}{2^5} - 3\frac{\delta^{10}}{2^9} - 9\frac{\delta^{12}}{2^{11}} + \cdots .$$

Dependence of added masses of an oscillating cylinder on the immersion depth h are given in [87] in the limiting cases of high-frequency and low-frequency oscillations. Dependence of added masses of a completely immersed cylinder on the frequency of oscillations is given in [53, 87]. A distinctive feature of a circular cylinder completely immersed under the free surface of an infinitely deep fluid is the equality $\lambda_{11} = \lambda_{33}$ and vanishing of all other entries of the matrix of added masses. For $h/r < 1.125$ the added masses λ_{11} and λ_{33} of an oscillating cylinder are negative in certain intervals of frequencies; explanations of this phenomenon are given in [147].

Dependence of the added masses λ_{11} and λ_{33} on the frequency of oscillations of an immersed cylinder of square section are given in [53].

Dependence of λ_{11} and λ_{33} of a system of two identical circular cylinders completely immersed under the surface of an infinitely deep fluid was studied in [42]. The author considered two cases: when the centers of the cylinders are situated on a horizontal line, and when the cases are situated on a vertical line.

5.6.3 Ellipsoid of Revolution

Let an ellipsoid of revolution be fully submerged in water such that its long axis is parallel to the free surface. The x-axis is chosen to coincide with the long axis of the ellipsoid; the z-axis is orthogonal to free surface and directed downwards; the y axis is parallel to free surface. Half-axes of the ellipsoid are denoted by a and b; the distance of the axis of the ellipsoid to the free surface is denoted by h.

Added masses of the ellipsoid are given by the formulas [192]:

$$\lambda_{11} = \frac{4}{3}\pi ab^2\rho k_{11}\left(\frac{a}{b}, \frac{h}{b}\right), \qquad \lambda_{22} = \frac{4}{3}\pi ab^2\rho k_{22}\left(\frac{a}{b}, \frac{h}{b}\right),$$

$$\lambda_{33} = \frac{4}{3}\pi ab^2\rho k_{33}\left(\frac{a}{b}, \frac{h}{b}\right), \qquad \lambda_{66} = \frac{4}{15}\pi a(a^2 + b^2)ab^2\rho k_{66}\left(\frac{a}{b}, \frac{h}{b}\right).$$

Coefficients $k_{ii}(a/b, h/b)$ are shown in Fig. 5.25. Dashed curves correspond to exact values of coefficients of added masses for the sphere ($a/b = 1$) and the infinite circular cylinder ($a/b = \infty$).

For an oscillating completely immersed ellipsoid of revolution the dependence of all coefficients of added masses on the oscillation frequency was studied in [254] for different ratios of axes of the ellipsoid and different distances to the free surface (the fluid was assumed infinitely deep).

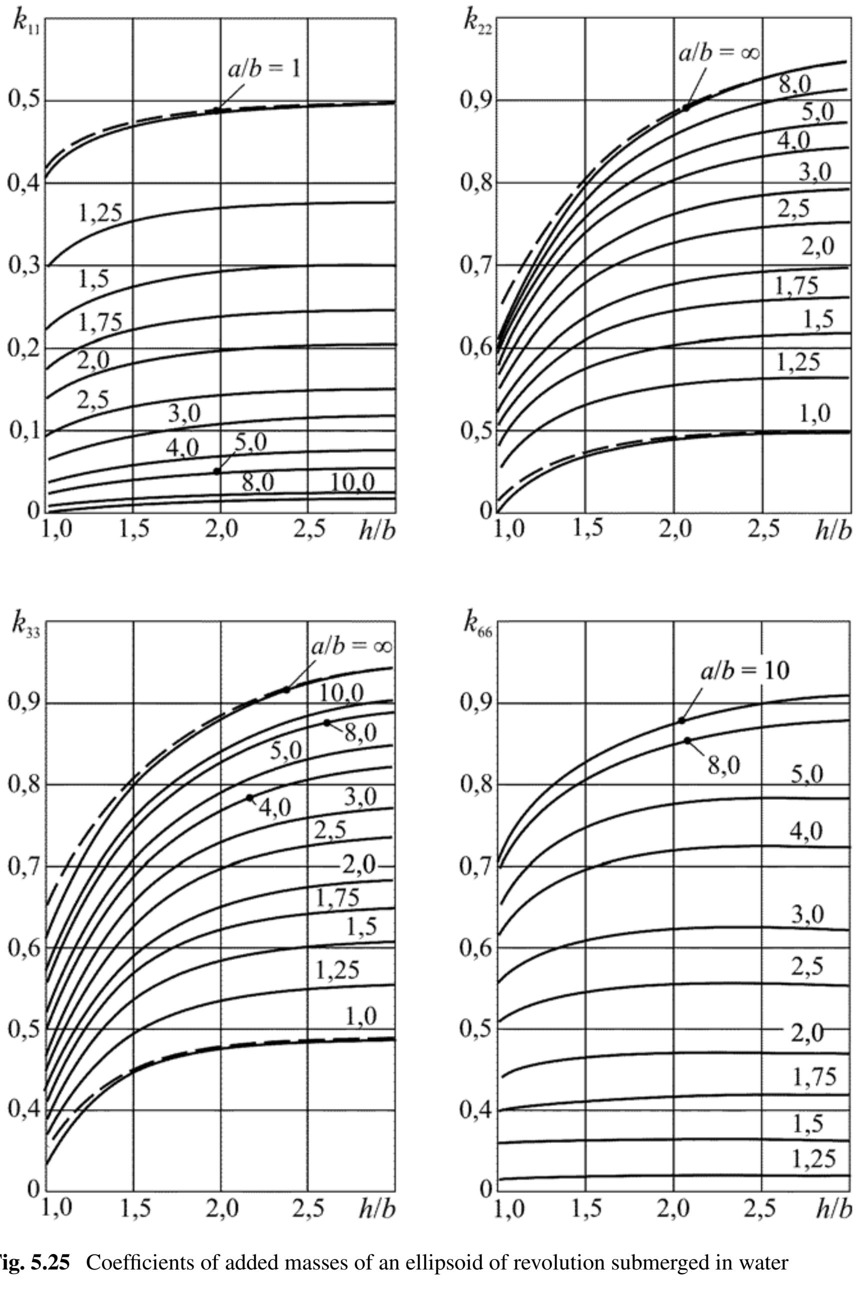

Fig. 5.25 Coefficients of added masses of an ellipsoid of revolution submerged in water

5.6.4 Elliptic Cylinder

Let an elliptic cylinder be submerged in water such that the large axis of its cross-section is parallel to the free surface and coincides with the x-axis. The smaller axis (coinciding with the y-axis) is orthogonal to the free surface; it is directed downwards.

Assuming that the Froude numbers are large [194], the added masses of elliptic cylinder are given by the formulas:

$$\begin{aligned}
\lambda_{11} &= \rho\pi ab\frac{(1-\eta^{-2})^{1/2}-(1-e^2)^{1/2}}{(1-e^2)^{-1/2}-(1-\eta^{-2})^{1/2}} := k_{11}\rho\pi ab;\\
\lambda_{22} &= \rho\pi ab\frac{(1-e^2)^{-1/2}+(1-\eta^2)^{1/2}-2}{2-(1-e^2)^{1/2}-(1-\eta^{-2})^{1/2}} := k_{22}\rho\pi ab;\\
\lambda_{66} &= \frac{1}{4}\rho\pi ab\big(a^2+b^2\big)\\
&\quad\times\frac{e^2}{2-e^2}\,\frac{(1-e^2)^{-1/2}[1-(1-e^2)^{1/2}]^2-2[1-(1-\eta^{-2})^{1/2}]^2}{2e^{-2}[1-(1-e^2)^{1/2}]^2+2[1-(1-\eta^{-2})^{1/2}]^2}\\
&:= \frac{1}{4}\rho\pi ab\big(a^2+b^2\big)k_{66}.
\end{aligned}$$

Here $e^2 = 1-(b/a)^2$, $\eta = [1+4h^2/(a^2-b^2)]^{1/2}$; a is the long semi-axis of the cross-section of the cylinder; b is the short semi-axis; h is the distance of the large semi-axis from the free surface. In Fig. 5.26 we show graphs of coefficients $k_{11}=k_{11}(a/b, b/h)$, $k_{22}=k_{22}(a/b, b/h)$, $k_{66}=k_{66}(a/b, b/h)$.

5.6.5 Three-Axial Ellipsoid Moving under a Free Surface

The added mass $\lambda_{11}=k_{11}(4/3)\rho\pi abc$ of the three-axial ellipsoid with half-axes $a>b>c$ in the case of a motion close to the water surface for large Froude numbers can be determined by the method due to Bloch and Ginevsky [30].

In Fig. 5.27 we show the graph of function $k_{11}(h/b, c/b)$ for an ellipsoid with the ratio $a/b=5$. The position of the ellipsoid is such that the semi-axis a (coinciding with the x-axis) is parallel to the free surface; the semi-axis c is either orthogonal to the free surface (the left half of the graph) or parallel to the surface (the right half of the graph).

5.7 Added Masses of Simplest Bodies Floating on a Water Surface

Consider a body floating on a water surface. The xOy coordinate plane is assumed to coincide with the water surface; the Oz axis is directed downwards. The motion

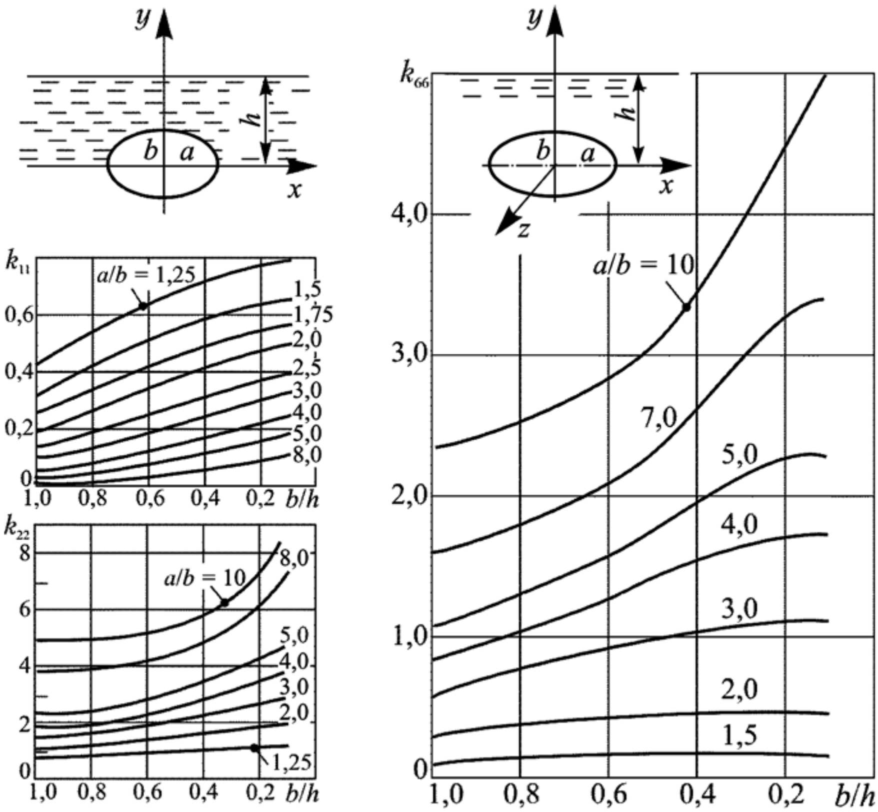

Fig. 5.26 Coefficients of added masses of a submerged elliptic cylinder

of an ideal non-compressible fluid is assumed to be potential. The potential of velocities φ satisfies the Laplace equation and the following boundary conditions (see Sect. 5.1): on a free surface $\varphi = 0$; on the part of the surface of the body which is immersed in water $\partial\varphi/\partial n = v_n$, where v_n is the projection of velocity of a point of the body surface to the normal (to the body surface); $\partial\varphi/\partial n$ equals the projection of velocity of fluid particles to the same normal. Notice that the same problem corresponds to vibration of a body on a free surface. If the fluid is bounded by hard walls, then on these walls the water-tightness condition $\partial\varphi/\partial n = 0$ should be fulfilled.

The first boundary condition leads to formulas (5.20), which are applicable if the duplicated body either moves after impact along the Oz axis or rotates around some horizontal axis. Therefore, under a vertical impact, the motion of the duplicated body in an infinite fluid generates in the half-space $z > 0$ the same velocities as the original body floating on a free surface of fluid of infinite depth. Therefore, in this case the added masses of a floating body are equal to $1/2$ of the corresponding added masses of the duplicated body floating in an infinite fluid. In the presence of hard walls, the problem of computation of added masses becomes more complicated.

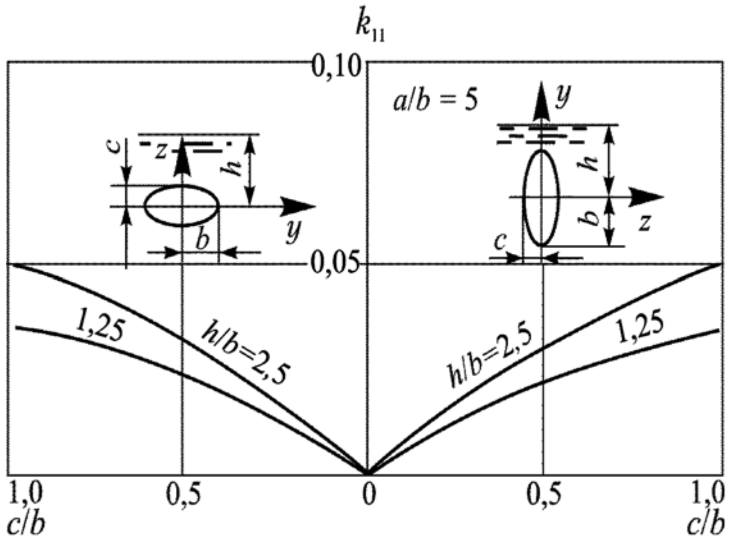

Fig. 5.27 The coefficient of the added mass $k_{11} = 3\lambda_{11}/(4\pi\rho abc)$ of a three-axial ellipsoid submerged close to the free surface

The same formulas (5.20) show that the motion of a floating body under horizontal impact can not be described via the motion of a duplicated model moving as a whole in an infinite fluid. In that case one has to consider a model where the mirror image of a body moves along a free surface in the direction which is opposite to the direction of motion of the body itself.

Physically it can be explained by the fact that under motion in the horizontal plane close to a free surface the pressure (additional to normal air pressure) vanishes during the whole motion. Thus, the pressure at waterline arising due to the body motion is absent, while at motion of the duplicated body in an infinite fluid the pressure at the body surface in the waterplane is maximal. On the other hand, under a vertical impact the difference in stress at waterline upon a floating body and its duplicated model does not take place.

5.7.1 Elliptic Cylinder, Circular Cylinder, Wedge and Plate Floating on the Surface of an Unlimited Fluid

Under vertical impact added masses of elliptic contour half-immersed in fluid are given by [206]:

$$\lambda_{33} = \frac{1}{2}\rho\pi a^2, \qquad \lambda_{44} = \frac{\rho\pi}{16}\left(a^2 - b^2\right)^2, \tag{5.31}$$

where a is the horizontal semi-axis, b is the vertical semi-axis. The origin is placed at the geometric center of the ellipse.

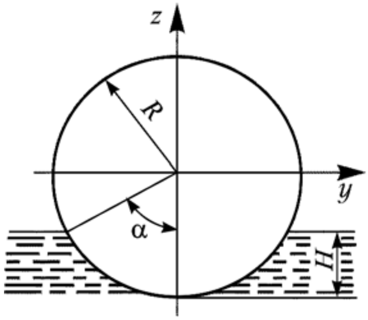

Fig. 5.28 Coordinate axes and notations for a floating cylinder

For a circular cylinder of radius a we get from formulas (5.31): $\lambda_{33} = \rho\pi a^2/2$, $\lambda_{44} = 0$. For a flat plate of width $2a$ placed at the water surface we get from the same formulas:

$$\lambda_{33} = \frac{1}{2}\rho\pi a^2, \qquad \lambda_{44} = \frac{1}{16}\rho\pi a^4.$$

If a circular cylinder of radius R is floating on a surface of an infinite fluid, being immersed to depth H (Fig. 5.28), then its added mass per unit of length is expressed by the following formula [67]:

$$\lambda_{33} = \rho R^2\left[\frac{\pi \sin^2\alpha}{6k^2}\left(1+2k^2\right) - \alpha + \frac{1}{2}\sin 2\alpha\right],$$

where α is 1/2 of the angle of the immersed arc of the circle; $k = 1 - \alpha/\pi$; $h = R(1-\cos\alpha)$.

If the cylinder is completely immersed ($\alpha = \pi$, $H = 2R$, $k = 0$) then

$$\lambda_{33} = \pi\rho R^2\left(\frac{\pi^2}{6} - 1\right).$$

Half-immersed cylinder ($\alpha = \pi/2$, $k = 0.5$) has added mass $\lambda_{33} = 0.5\pi R^2\rho$.

Dependence of the added masses λ_{11} and λ_{33} on the oscillation frequency of a floating cylinder for different values of α are given in [53, 87]. Typically in the range of low frequencies the added mass λ_{33} logarithmically grows with frequency. The added mass λ_{11} is negative in certain ranges of frequencies for $\alpha > 2\pi/3$ (in contrast to a completely submerged cylinder, the added masses λ_{11} and λ_{33} do not coincide for a floating cylinder).

Added mass of a wedge (Fig. 5.29) under vertical impact is equal to 1/2 of added mass of the rhombus corresponding to the immersed part of the wedge; it is defined by the formula

$$\lambda_{33} = \frac{\rho l^2}{2}\left[\frac{\Gamma(3/2-\beta/\pi)\Gamma(\beta/\pi)}{\Gamma(\beta/\pi+1/2)\Gamma(1-\beta/\pi)} - 1\right]\sin 2\beta,$$

where l is the length of the immersed side of the wedge; $\Gamma(x)$ is the gamma-function; β is the angle between planes of the wedge and free surface.

Fig. 5.29 Coordinate axes and notations in the problem of vertical impact of a wedge

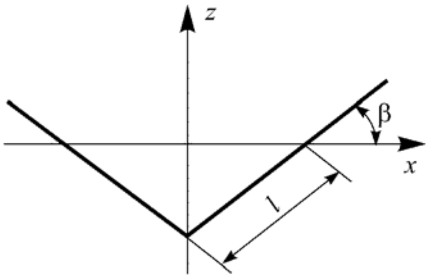

The coefficient of added mass $k_{33} = \lambda_{33}/(0.5\rho\pi l^2 \cos^2\beta)$ as a function of $\tan\beta$ is represented in Fig. 2.26 by curve II (for rhombus $d/b = \tan\beta$).

For angles β between 0 and 45° the formula for added mass of a wedge can be written in simplified form [224]:

$$\lambda_{33} = \frac{\rho h \pi^3}{8}\left(1 - \frac{\beta}{\pi}\right)\cot\beta,$$

where h is the depth of immersion of the tip of the wedge. This formula takes into account the increase of the level of a free surface near the faces of the wedge under a vertical motion.

Dependence of λ_{11} and λ_{33} on frequency for an oscillating floating wedge with $\beta = \pi/3$ is obtained in [155]. The theoretical results agree well with experiment [243].

Under a vertical impact of two plates floating horizontally on a free surface (Fig. 5.30) their added mass is determined via formula [88]

$$\lambda_{33} = \rho\pi\left(\frac{b^2 + a^2}{2} - c^2\right),$$

where c^2 is the ratio of two elliptic integrals:

$$c^2 = \left[\int_a^b \frac{x^2\,dx}{(x^2 - a^2)(b^2 - x^2)}\right]\left[\int_a^b \frac{dx}{(x^2 - a^2)(b^2 - x^2)}\right]^{-1}.$$

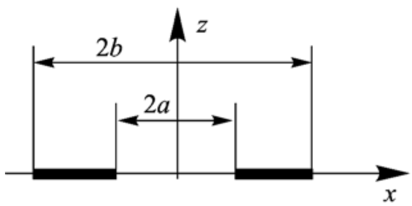

Fig. 5.30 Coordinate axes and notations in the problem of vertical impact of two plates

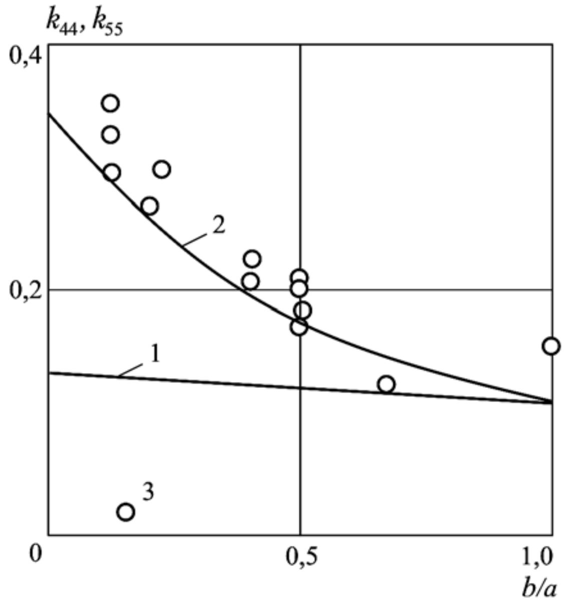

Fig. 5.31 Dependence of coefficients k_{55} and k_{44} on elongation of the plate b/a: *1*—coefficient k_{44}; *2*—coefficient k_{55}; *circles (3)* correspond to experimental data for k_{55}

Added mass of a floating rectangular plate with sides a and b under vertical impact can be computed via the Pabst formula:

$$\lambda_{33} = \frac{\pi}{8}\rho\frac{a^2b^2}{\sqrt{a^2+b^2}}\left(1 - 0{,}425\frac{ab}{a^2+b^2}\right).$$

Some corrections to this formula were found in [226]. In the same paper the added moments of inertia of a plate under rotation at the moment of impact around the "short" symmetry axis y were found:

$$\lambda_{55} = \frac{\pi\rho}{16}a^2b^2k_{55},$$

as well as around the "long" symmetry axis x:

$$\lambda_{44} = \frac{\pi\rho}{16}ab^3k_{44}.$$

In these formulas the sides of the plate are equal to $2a$ and $2b$ along the axes x and y, respectively. In Fig. 5.31 we show the dependence of coefficients k_{55} (curve 1) and k_{44} (curve 2) on the elongation of the plate b/a. Points 3 correspond to experimental data for coefficient k_{55}.

5.7.2 Sphere and Ellipsoid of Revolution Floating on the Surface of a Fluid of Unlimited Depth

The problem of finding added masses of a half-immersed ellipsoid of revolution (in particular, a sphere) was solved by Bloch [28, 29].

We introduce a coefficient equal to the ratio of an added mass of a half-immersed sphere to a mass of water contained in a submerged part of the sphere. Under boundary condition $\varphi = 0$ on a free surface (inertial forces under impact significantly exceed the gravity forces, thus the fluid can be assumed to be massless) we have:

$$\lambda_{11} = k_{11}\frac{2}{3}\pi a^3\rho; \qquad k_{11} = 0.273224; \qquad \lambda_{22} = \lambda_{11};$$

$$\lambda_{33} = k_{33}\frac{2}{3}\pi a^3\rho; \qquad k_{33} = 0.5$$

where a is the radius of the sphere (Fig. 5.32). We observe that the coefficient of added mass of a floating hemisphere in the horizontal direction is essentially lower than the same coefficient (equal to 0.5) in the case of an infinite fluid.

If we impose the boundary condition $\partial\varphi/\partial z$ on the free surface (the inertial forces in this case are assumed to be negligible in comparison with gravity forces, which corresponds to ultra-heavy fluid) we have:

$$\lambda_{11} = k_{11}\frac{2\pi}{3}a^3\rho; \qquad k_{11} = 0.5; \qquad \lambda_{22} = \lambda_{11};$$

$$\lambda_{33} = k_{33}\frac{2\pi}{3}a^3\rho; \qquad k_{33} = 0.8308.$$

In this case the coefficient k_{33} is higher than the corresponding coefficient of added mass of a hemisphere in an infinite fluid.

In [27–29] there were considered two positions of an ellipsoid of revolution on the free surface: in the first case its axis of rotation is orthogonal to free surface; in the second case the axis of rotation lies in the plane of free surface (Fig. 5.33).

Added masses of the vertical ellipsoid of revolution are given by

$$\lambda_{11} = \lambda_{22} = k_{11}\frac{2\pi}{3}ab^2\rho, \qquad \lambda_{33} = k_{33}\frac{2\pi}{3}ab^2\rho;$$

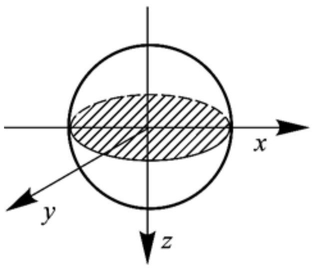

Fig. 5.32 Coordinate system for a floating sphere

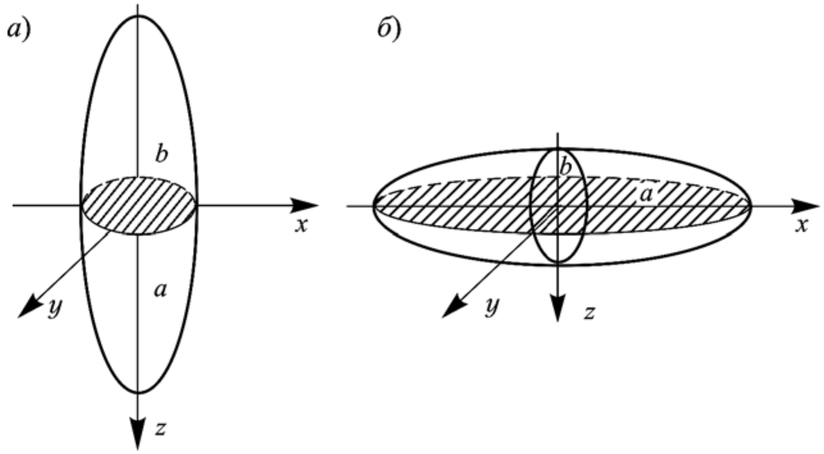

Fig. 5.33 Coordinate system for ellipsoid of revolution floating vertically **(a)** and horizontally **(b)**

Fig. 5.34 Coefficients of added masses of vertically floating ellipsoid of revolution as functions of parameter $n = 1/(1 + a/b)$

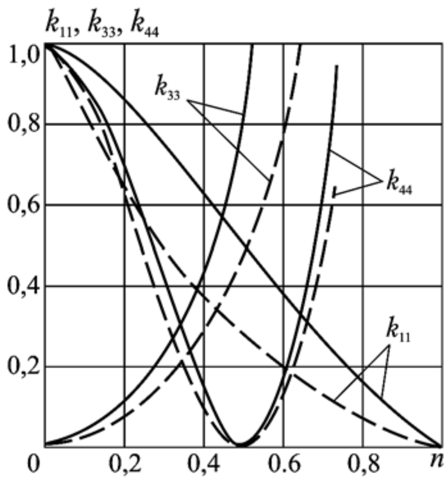

$$\lambda_{44} = \lambda_{55} = k_{44}\frac{2\pi}{15}ab^2\left(a^2 + b^2\right)\rho, \qquad \lambda_{66} = 0,$$

where coefficients k_{ii} were computed by Bloch (Fig. 5.34). Continuous curves correspond to solution of the problem with boundary condition $\partial\varphi/\partial z|_{z=0} = 0$; dashed curves correspond to the boundary condition $\varphi|_{z=0} = 0$.

Analogous coefficients of added masses of a horizontal ellipsoid for two boundary conditions are also shown in Fig. 5.35. Notice that added masses of completely immersed bodies (see Sect. 5.6) computed under condition $\varphi|_{z=0} = 0$ on a free surface can be considered as added masses of corresponding bodies under impact.

Added masses under a vertical impact of the axially symmetric body obtained by rotation of a circle arc around a line connecting the endpoints of the arc, were

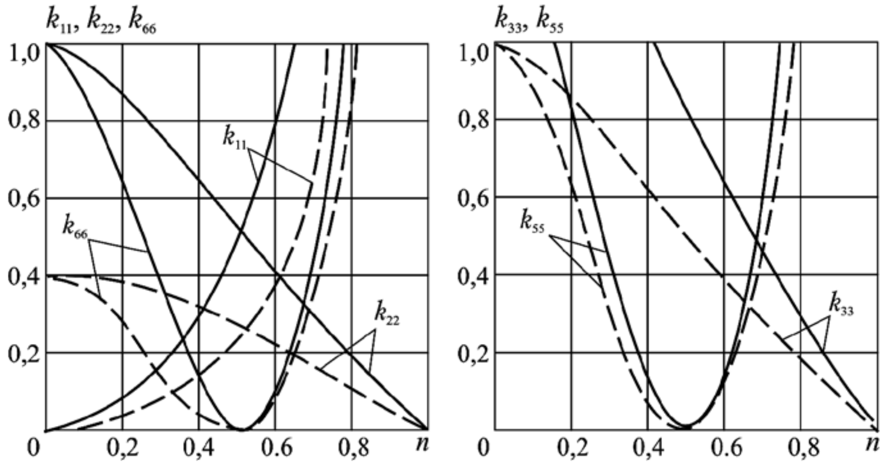

Fig. 5.35 Coefficients of added masses of a horizontally floating ellipsoid of revolution as functions of parameter $n = b/(a + b)$

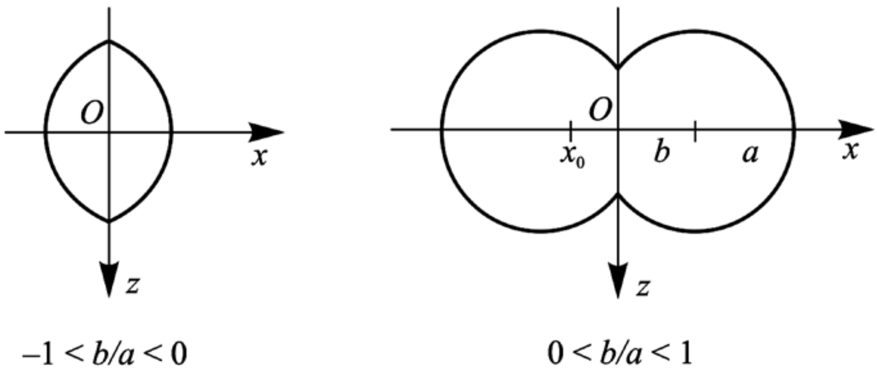

Fig. 5.36 Coordinate system for a body of revolution floating on a free surface

computed by Norkin [160–162]. The body is half-immersed in a fluid of infinite depth (Fig. 5.36). The radius of the circle is denoted by a; the distance from the center of the arc to the axis of the rotation is denoted by b. The direction of vertical impact can in general be shifted from the axis of rotation by x_0. Therefore, besides the vertical shift along the z-axis there can also be present a rotation around the y-axis orthogonal to the xOz plane. In [160] there were obtained added masses $\lambda_{33} = k_{33}(b/a)\rho a^3$ and $\lambda_{55} = k_{55}(b/a)\rho a^5$. Coefficients $k_{33}(b/a)$ and $k_{55}(b/a)$ are shown in Table 5.3.

The linear velocity v after impact is related to the angular velocity ω by relation $\lambda_{33} v x_0 = \lambda_{55}\omega$.

Added masses of an ellipsoid of revolution floating on a free surface such that its axis of rotation is orthogonal to the free surface, and its geometric center is situated

Table 5.3 Coefficients k_{33} and k_{55}

b/a	k_{33}	k_{55}	b/a	k_{33}	k_{55}
−0.7	0.022	0.003	0.3	2.456	0.067
−0.5	0.112	0.009	0.5	3.919	0.288
−0.3	0.331	0.009	0.7	5.914	0.827
−0.1	0.745	0.002	0.8	7.145	1.282
0.0	$\pi/3$	0	0.9	8.553	1.903
0.1	1.426	0.004	1.0	10.158	2.728

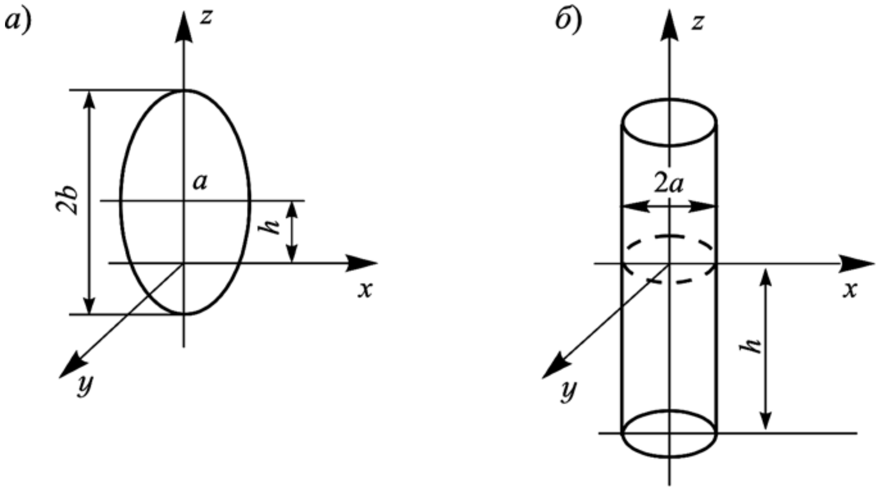

Fig. 5.37 Coordinate system for vertical floating ellipsoid of revolution **(a)** and vertical circular cylinder **(b)**

at distance h from the free surface (Fig. 5.37a), are computed in [14]. Boundary conditions on the free surface are assumed to be $\partial\varphi/\partial z = 0$. The z-axis is directed along the rotation axis; the x-axis is parallel to the water surface. The length of the ellipsoid along the z-axis is denoted by $2b$; the radius of maximal section is a. Coefficients of added masses

$$k_{33} = \frac{\lambda_{33}}{\rho V}; \qquad k_{55} = \frac{\lambda_{55}}{\rho V a^2}; \qquad k_{15} = \frac{\lambda_{15}}{\rho V a},$$

where V is the volume of the submerged part of the ellipsoid, are given in Table 5.4.

Coefficients k_{33}, k_{55}, k_{15} were also computed in the same paper [14] for the case of a circular cylinder of radius a vertically submerged in fluid to depth h (Fig. 5.37b). Values of these coefficients divided by the volume of the submerged part and radius of the cylinder are shown in Table 5.5.

Table 5.4 Added masses of floating ellipsoid of revolution for different distances from its geometric center to free surface

h/b	$b/a = 0.5$			$b/a = 1.0$			$b/a = 2.0$		
	k_{33}	k_{55}	k_{51}	k_{33}	k_{55}	k_{51}	k_{33}	k_{55}	k_{51}
−0.5	0.915	0.064	0.059	0.392	0.153	0.309	0.157	1.180	0.900
−0.4	1.037	0.045	0.001	0.439	0.094	0.238	0.173	0.932	0.789
−0.3	1.212	0.043	−0.055	0.508	0.051	0.171	0.198	0.720	0.683
−0.2	1.433	0.057	−0.102	0.600	0.021	0.108	0.231	0.541	0.581
−0.1	1.697	0.082	−0.143	0.701	0.005	0.051	0.273	0.393	0.483
0	2.005	0.117	−0.177	0.836	0.000	0.000	0.323	0.272	0.391
0.1	2.364	0.157	−0.204	0.991	0.005	−0.049	0.385	0.177	0.303
0.2	2.781	0.201	−0.224	1.176	0.018	−0.090	0.459	0.106	0.221
0.3	3.274	0.244	−0.238	1.398	0.038	−0.124	0.551	0.056	0.145
0.4	3.867	0.284	−0.245	1.671	0.061	−0.152	0.667	0.024	0.075
0.5	4.605	0.318	−0.244	2.018	0.086	−0.171	0.816	0.010	0.013

Table 5.5 Coefficients of added masses of a floating vertical cylinder

h/a	k_{33}	k_{55}	k_{51}	h/a	k_{33}	k_{55}	k_{51}
0.1	8.725	0.762	−0.150	1.5	0.464	0.332	0.416
0.7	3.894	0.353	−0.107	2.0	0.340	0.663	0.629
0.4	1.885	0.153	−0.031	4.0	0.162	3.449	1.526
0.6	1.277	0.104	0.045	6.0	0.102	8.585	2.469
0.8	0.904	0.105	0.124	8.0	0.075	16.215	3.372
1.0	0.714	0.139	0.205	10.0	0.057	26.160	4.292

5.7.3 Elliptic Cylinder and Plate Floating on a Water Surface near Hard Walls

Consider an elliptic cylinder floating on the free surface of a fluid filling a cylindrical channel whose section also has an elliptic shape (Fig. 5.38), and, moreover, the focuses of both ellipses coincide. In this case the added masses are determined in [43, 73, 76, 81, 149, 168, 174, 176, 190].

We introduce the added mass $\lambda_{33\infty} = 0.5\rho\pi a^2$ corresponding to the same cylinder on the free surface of a fluid filling the whole lower half-space. Dependence of $\lambda_{33}/\lambda_{33\infty}$ on the ratio a/b of axes of the ellipse and the ratio a/A, where A is the maximal depth of the channel, is shown in Fig. 5.38.

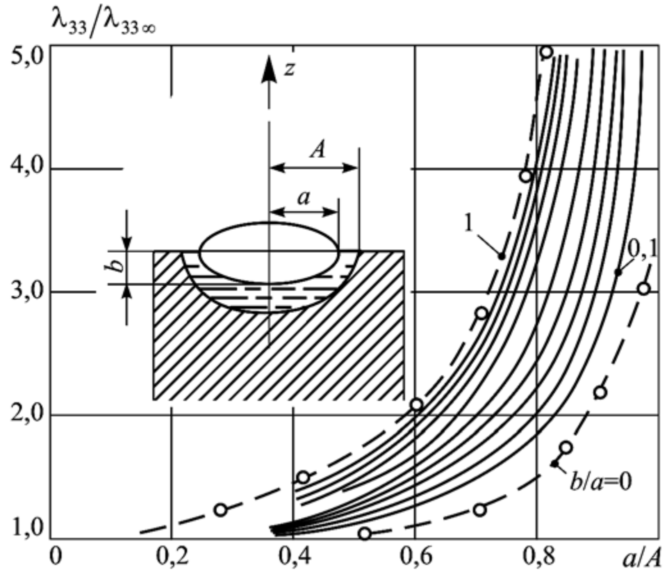

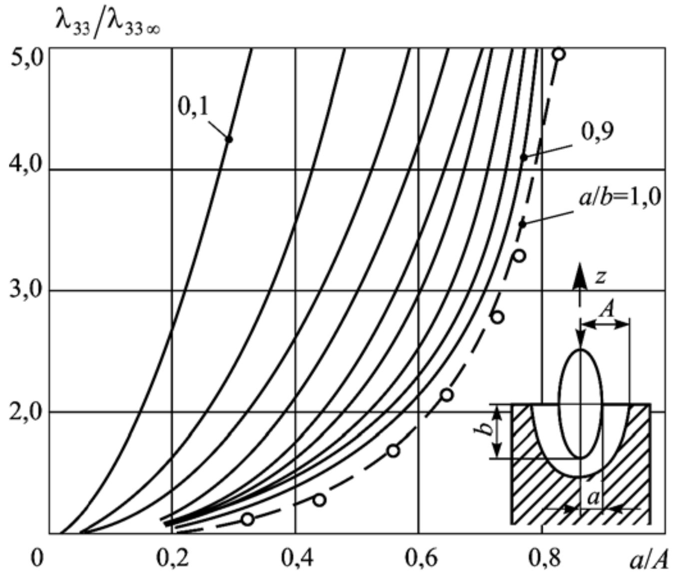

Fig. 5.38 Coefficients of added masses of an elliptic cylinder floating in a cylindrical channel

Under boundary condition $\varphi = 0$ on the free surface, the formula for added mass λ_{33} has the form

$$\lambda_{33} = \frac{\pi\rho a^2}{2} \frac{1 - \frac{b}{a}\sqrt{1 - (1 - \frac{b^2}{a^2})\frac{a^2}{A^2}}}{\sqrt{1 - (1 - \frac{b^2}{a^2})\frac{a^2}{A^2}} - \frac{b}{a}}. \tag{5.32}$$

The added mass λ_{44} of an ellipse in a confocal channel under an impact (boundary condition $\varphi = 0$ on the free surface) is defined by the formula

$$\lambda_{44} = \frac{\pi\rho}{16}\left(a^2 - b^2\right)^2 \coth\left[2(\alpha_2 - \alpha_1)\right], \tag{5.33}$$

where α_1 and α_2 depend on the sizes of the channel and ellipse:

$$\cosh\alpha_1 = \frac{a}{\sqrt{a^2 - b^2}}, \qquad \cosh\alpha_2 = \frac{A}{\sqrt{a^2 - b^2}}.$$

In [190] there were also defined the following added masses under the same boundary condition $\varphi = 0$:

$$\lambda_{22} = \frac{16}{\pi}\rho b^2 \sum_{n=1}^{s} \frac{n}{(4n^2 - 1)^2} \coth\left[2n(\alpha_2 - \alpha_1)\right]; \tag{5.34}$$

$$\lambda_{24} = \frac{1}{3}\rho b\left(a^2 - b^2\right)\coth\left[2(\alpha_2 - \alpha_1)\right]. \tag{5.35}$$

Taking in these formulas the limit $\alpha_2 \to \infty$, one can get the formulas for added masses of an elliptic cylinder floating on a free surface of fluid filling the lower half-space:

$$\lambda_{22\infty} = \frac{2}{\pi}\rho b^2; \qquad \lambda_{33\infty} = 0.5\rho\pi a^2;$$
$$\lambda_{24\infty} = \frac{1}{3}\rho b\left(a^2 - b^2\right); \qquad \lambda_{44\infty} = \frac{1}{16}\pi\rho\left(a^2 - b^2\right)^2. \tag{5.36}$$

Graphs of functions $\lambda_{22}/\lambda_{22\infty} = f(a/A, b/a)$, $\lambda_{44}/\lambda_{44\infty} = f_1(a/A, b/a)$ are shown in Fig. 5.39. Choosing in (5.32)–(5.35) $b = 0$ we get expressions for added masses of the plate of width $2a$ floating in elliptic channel:

$$\lambda_{22} = \lambda_{24} = 0, \qquad \lambda_{33} = 0.5\frac{\pi\rho a^2}{\sqrt{1 - a^2/A^2}};$$
$$\lambda_{44} = \frac{\pi}{16}\rho a^4 \coth 2\alpha_2. \tag{5.37}$$

If the fluid fills the whole half-space, one gets from the formulas (5.37) in the limit $A \to \infty$, $\alpha_2 \to \infty$:

$$\lambda_{33\infty} = 0.5\pi\rho a^2; \qquad \lambda_{44\infty} = \frac{\pi}{16}\rho a^4.$$

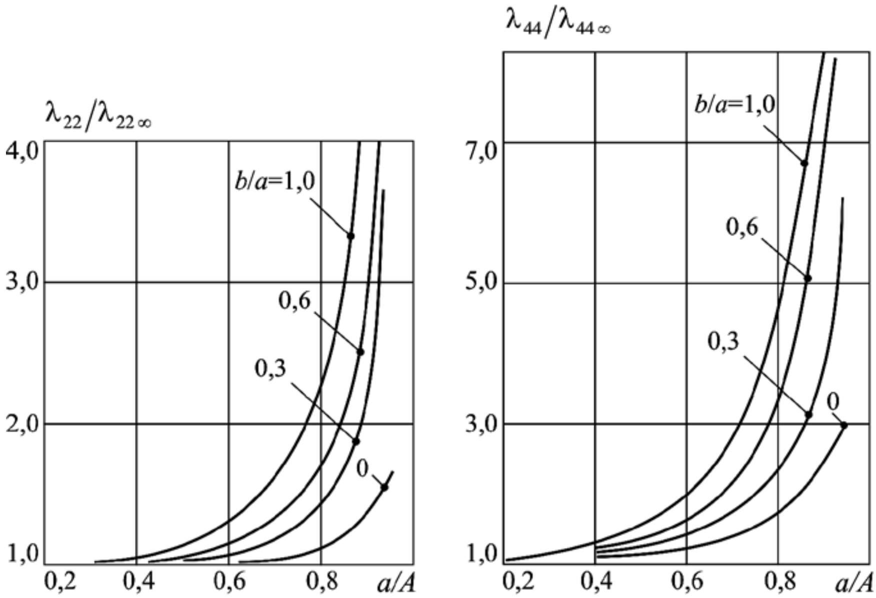

Fig. 5.39 Coefficients of added masses of an elliptic cylinder floating in a cylindrical channel

Choosing in the formulas (5.32)–(5.35) $a = 0$, we get added masses of a vertical plate immersed to depth b in the channel of an elliptic section:

$$\lambda_{22} = \frac{16}{\pi}\rho b^2 \sum_{n=1}^{\infty} \frac{n}{(4n^2-1)^2}\coth(2n\alpha_2);$$

$$\lambda_{33} = 0;$$

$$\lambda_{24} = -\frac{1}{3}\rho b^3 \coth 2\alpha_2; \qquad \lambda_{44} = \frac{\pi}{16}\rho b^4 \coth 2\alpha_2. \tag{5.38}$$

When the fluid fills the whole half-space ($\alpha_2 \to \infty$), formulas (5.38) take the form

$$\lambda_{22\infty} = \frac{2}{\pi}\rho b^2; \qquad \lambda_{33\infty} = 0; \qquad \lambda_{24\infty} = \frac{1}{3}\rho b^3; \qquad \lambda_{44\infty} = \frac{1}{16}\rho\pi b^4.$$

Formulas (5.32)–(5.35) allow us to get added masses of the circular cylinder of radius a floating in the concentric channel of radius R:

$$\lambda_{24} = \lambda_{44} = 0; \qquad \lambda_{22} = \frac{16}{\pi}\rho a^2 \sum_{n=1}^{\infty} \frac{n}{(4n^2-1)^2}\frac{R^{4n}+a^{4n}}{R^{4n}-a^{4n}}.$$

The value of the added mass λ_{33} for the circular cylinder is given in Sect. 5.7.4.

It is interesting to compare the added mass of a half-submerged ellipse floating on the surface of a fluid of infinite depth under horizontal impact, and an analogous added mass of the same ellipse moving in an infinite fluid. Denote a half of the added mass of an ellipse immersed in an infinite fluid by $\lambda_{22\infty} = \pi\rho b^2/2$ and compute the coefficient $k = \lambda_{22}/\lambda_{22\infty} = 4/\pi^2$. This coefficient is approximately equal to 0.40528; it shows how much the added mass of a contour moving in a horizontal direction decreases when the contour moves near a free surface in comparison with the motion in an infinite fluid.

For the circular cylinder of radius a we get from formulas (5.36):

$$\lambda_{22} = \frac{2}{\pi}\rho a^2; \qquad \lambda_{24} = 0.$$

The added masses of an elliptic cylinder floating in a confocal elliptic channel half-filled by ultra-heavy fluid (very small Froude numbers) were considered in [190]. The boundary condition on a free surface was taken to be $\partial\varphi/\partial z = 0$.

Formulas for added masses are written as follows:

$$\begin{aligned}
\lambda_{22} &= 0.5\pi\rho b^2 \coth(\alpha_2 - \alpha_1);\\
\lambda_{24} &= \frac{2}{3}\rho b\left(a^2 - b^2\right)\coth(\alpha_2 - \alpha_1);\\
\lambda_{44} &= \frac{8}{\pi}\rho\left(a^2 - b^2\right)^2 \sum_{n=0}^{\infty} \frac{\coth[(2n+1)(\alpha_2 - \alpha_1)]}{(2n+1)(2n-1)^2(2n+3)^2}.
\end{aligned} \tag{5.39}$$

Taking in formulas (5.39) the limit $\alpha_2 \to \infty$, we get added masses of an elliptic cylinder half-submerged in an ultra-heavy fluid:

$$\begin{aligned}
\lambda_{22\infty} &= 0.5\rho\pi b^2; \qquad \lambda_{24\infty} = \frac{2}{3}\rho b\left(a^2 - b^2\right);\\
\lambda_{44\infty} &= \frac{\rho}{\pi}\left(a^2 - b^2\right)^2.
\end{aligned}$$

In Fig. 5.40 we present the dependencies

$$\frac{\lambda_{44}}{\lambda_{44\infty}} = 8\sum_{n=0}^{\infty} \frac{\coth\left[(2n+1)(\alpha_2 - \alpha_1)\right]}{(2n+1)(2n-1)^2(2n+3)^2} = f\left(\frac{a}{A}, \frac{b}{a}\right).$$

Notice that the added mass λ_{33} is absent in formulas (5.39). This is due to the fact that in incompressible fluid potential φ_3, corresponding to vertical motion of an ellipse in an elliptic channel, does not exist under boundary condition $\partial\varphi/\partial z$ on free surface (i.e., the corresponding boundary value problem for the Laplace equation is unsolvable).

Choosing in formulas (5.39) $b = 0$, we find added masses of a plate of width $2a$ floating on the surface of an ultra-heavy fluid in an elliptic channel:

$$\lambda_{22} = \lambda_{24} = 0; \qquad \lambda_{44} = \frac{8}{\pi}\rho a^4 \sum_{n=0}^{\infty} \frac{\coth\left[(2n+1)\alpha_2\right]}{(2n+1)(2n-1)^2(2n+3)^2}.$$

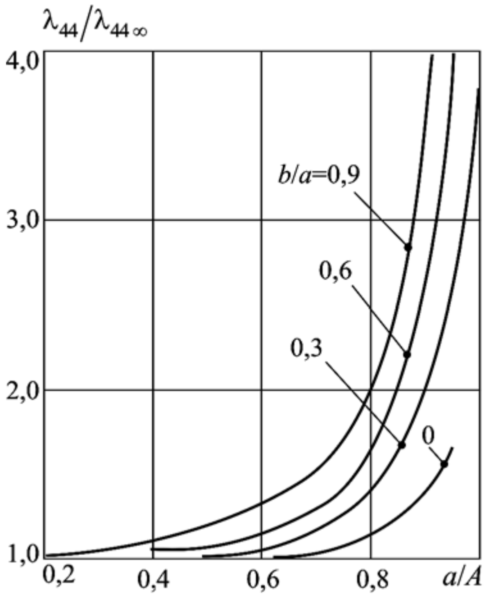

Fig. 5.40 Added mass λ_{44} of an elliptic cylinder floating in an elliptic channel on the surface of an ultra-heavy fluid (boundary condition $\partial\varphi/\partial z = 0$)

If the ultra-heavy fluid fills the whole lower half-space, we get from the previous formula

$$\lambda_{44\infty} = \frac{\rho}{\pi} a^4.$$

Formulas (5.39) allow us also to get added masses of the vertical plate immersed to depth b in an ultra-heavy fluid filling an elliptic channel. For that purpose one should assume in (5.39) $\alpha_1 = a = 0$:

$$\lambda_{22} = 0.5\pi\rho b^2 \coth\alpha_2; \qquad \lambda_{24} = -\frac{2}{3}\rho b^3 \coth\alpha_2;$$

$$\lambda_{44} = \frac{8}{\pi}\rho b^4 \sum_{n=0}^{\infty} \frac{\coth[(2n+1)\,\alpha_2]}{(2n+1)(2n-1)^2(2n+3)^2}.$$

If the plate is immersed vertically to the ultra-heavy fluid filling the whole lower half-space, then

$$\lambda_{22} = 0.5\pi\rho b^2; \qquad \lambda_{24} = -\frac{2}{3}\rho b^3; \qquad \lambda_{44} = \frac{\rho}{\pi} b^4.$$

On the basis of formulas (5.37) one can draw the graphs

$$\frac{2\lambda_{33}}{\pi\rho a^2} = k_{33}\left(\frac{a}{A}\right); \qquad \frac{16\lambda_{44}}{\pi\rho a^4} = k_{44}\left(\frac{a}{A}\right)$$

shown in Fig. 5.41a.

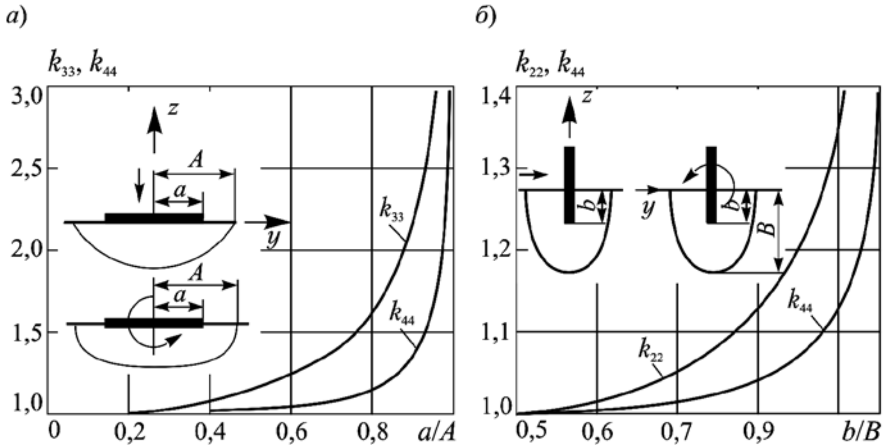

Fig. 5.41 Coefficients of added masses of horizontal **(a)** and vertical **(b)** plates in an elliptic channel

In Fig. 5.41b we show graphs of functions

$$k_{22}(b/B) = \frac{\pi\lambda_{22}}{2\rho b^2}; \qquad k_{44}(b/B) = \frac{16\lambda_{22}}{\pi\rho b^4}$$

found using formulas (5.38) for the case of a vertical plate immersed to depth b in a channel having an elliptic section.

The added mass λ_{33} of a plate of width a floating horizontally on the surface of a fluid filling a rectangular channel of width b and depth H under vertical impact is shown by the graph of function $f(a/b, H/b) = 8\lambda_{33}/\pi\rho a^2$ in Fig. 5.41a [176].

For a plate of width $2a$ floating on a free surface of fluid of depth H the added mass under vertical impact is defined by the graph $k_{33}(a/H) = 2\lambda_{33}/\pi\rho a^2$ shown in Fig. 5.42b. The problem of determining $k_{33}(a/H)$ was first considered by Keldysh [113]. Work [176, 241] contains more precise numerical computations.

If a plate of width $2a$ is floating horizontally on free surface of fluid filling a channel having section of half-circle of radius r, its added mass λ_{33} under vertical impact is given by the following formula [93]:

$$k_{33} = \frac{2\lambda_{33}}{\pi\rho a^2} = 1 + \frac{1}{2}x + \frac{1}{4}x^2 + \frac{7}{32}x^3 + \frac{5}{32}x^4 + \frac{9}{64}x^5 + \frac{29}{256}x^6 + \frac{851}{8192}x^7 + \frac{727}{8192}x^8 + \frac{1351}{16384}x^9 + \frac{2389}{32768}x^{10} + \cdots,$$

where $x = (a/r)^2$.

The graph of function $k_{33}(a/r)$ found by a simpler method in the paper [176] is shown in Fig. 5.43.

Consider the more general problem of computation of added mass of a plate of width a floating non-symmetrically on the surface of a half-cylindrical channel of

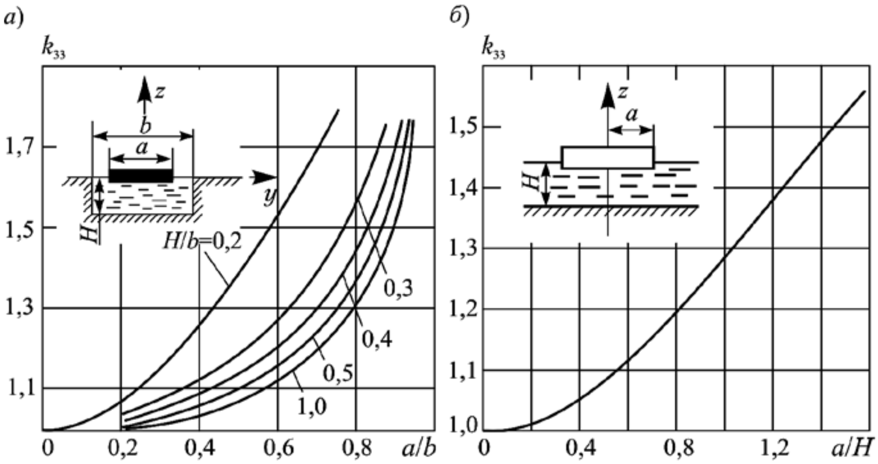

Fig. 5.42 Coefficient of added mass of a horizontal plate in a rectangular channel (*left*) and under vertical impact in the case of finite depth of fluid (*right*)

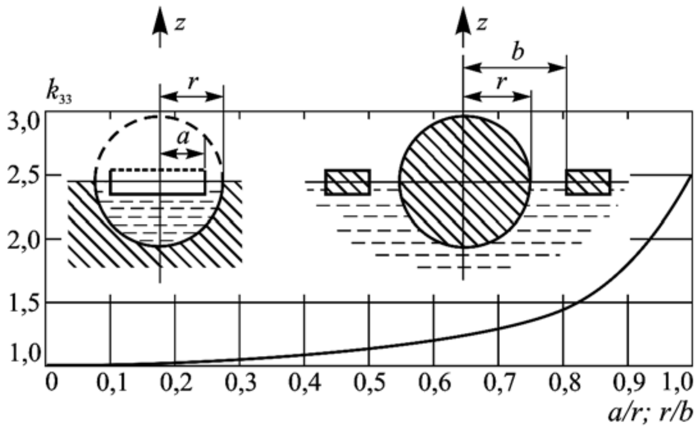

Fig. 5.43 Coefficient of added mass of a plate in a cylindrical channel and coefficient of added mass of a cylinder in a flat gap

radius r (Fig. 5.44). Values of the coefficient of added mass $k_{33}(a/r) = 8\lambda_{33}/\pi\rho a^2$ are shown in Fig. 5.44. The same curve expresses dependence of coefficient of added mass of width $2a$ floating symmetrically in a gap of width $2b$ (see Fig. 5.44). In this case the coefficient k_{33} is defined as follows: $k_{33}(a/b) = 2\lambda_{33}/\pi\rho a^2$.

Results of computation of the added mass of a plate floating in a channel of rectangular section are given in the work [228].

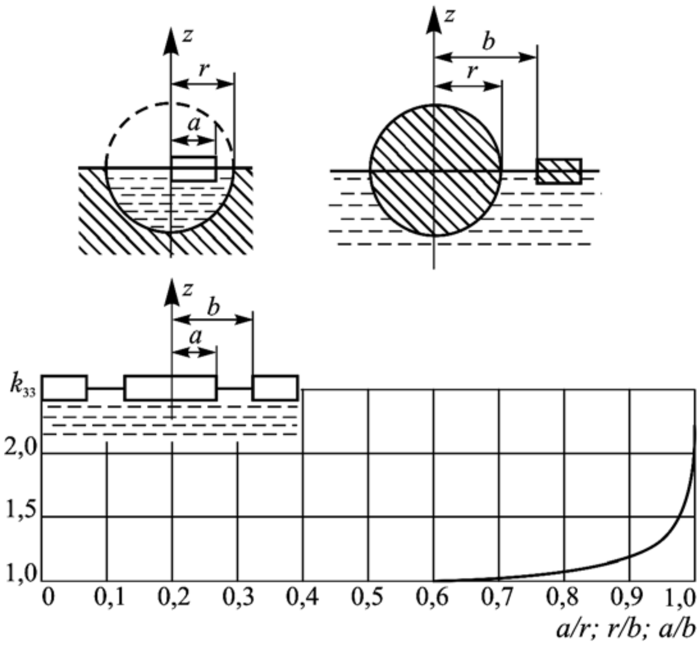

Fig. 5.44 Coefficient of added mass of a plate non-symmetrically floating in a cylindrical channel, and also in a gap; the same coefficient for a cylinder floating near a plate

5.7.4 Circular Cylinder Floating on a Free Surface Close to Solid Boundaries at Vertical Impact

The added mass λ_{33} of a circular cylinder of radius a which is symmetrically semi-submerged in a channel which has the shape of a semi-circle of radius A, was computed (under vertical impact) in [34, 261]. The graph of corresponding coefficients is shown in Fig. 5.38 by a curve corresponding to the ratio of axes of the ellipse $a/b = 1$. Here $\lambda_{33\,\infty} = \rho\pi a^2/2$. The added mass of a circular cylinder of radius r which is floating symmetrically in a gap of width $2b$, is determined by a curve shown in Fig. 5.43, where along the vertical axis we show the ratio $2\lambda_{33}/\pi\rho r^2$.

For a cylinder of radius r floating near an edge of a plate situated on a water surface, the added mass is determined by the curve shown in Fig. 5.44, where the vertical axis corresponds to the ratio $2\lambda_{33}/\pi\rho r^2$ (the distance from the axis of the cylinder to the edge of the plate is denoted by b). The added mass of a half-submerged circular cylinder of radius r_1 floating in a channel of half-cylindrical shape of radius r_2 is represented in Fig. 5.45a by function $f(r_1/r_2, l/r_2) := \lambda_{33}/\lambda_{33\,\infty}$; the distance from the axis of the floating cylinder to the axis of the channel is denoted by l; $\lambda_{33\,\infty} := \rho\pi r_1^2/2$.

For a half-submerged cylinder of radius r floating near a vertical wall such that the distance from the center of the cylinder to the wall equals l, the added mass

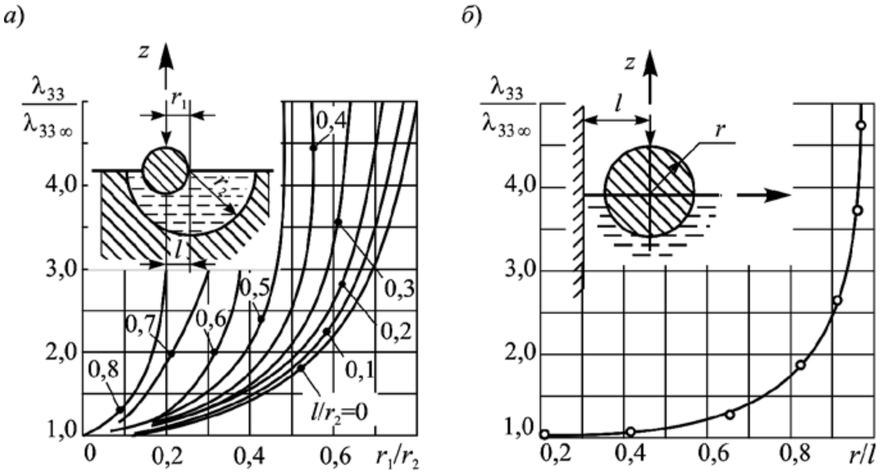

Fig. 5.45 Coefficient of added mass of a circular cylinder floating eccentrically in a channel of half-cylindrical shape under vertical impact (*left*). The coefficient of the added mass of a circular cylinder floating close to a vertical wall under a vertical impact (*right*)

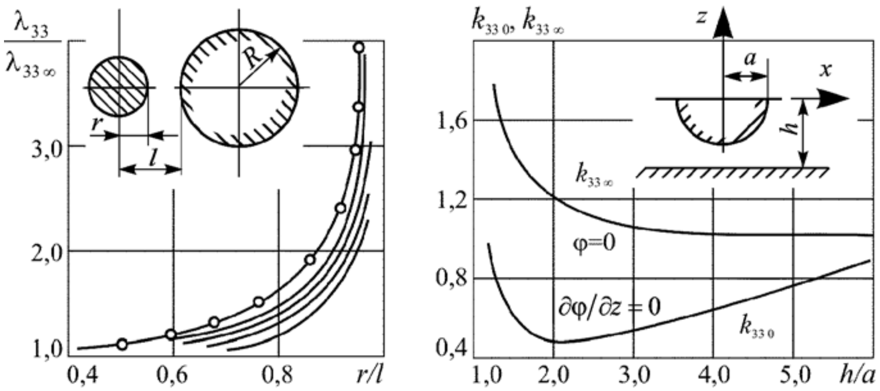

Fig. 5.46 The added mass of a circular cylinder floating near another cylinder, under a vertical impact **(a)**. Coefficients of the added mass of a circular cylinder floating in fluid of a finite depth under two different boundary conditions on free surface **(b)**

λ_{33} can be found from function $f(r/l) := \lambda_{33}/\lambda_{33\,\infty}$ shown in Fig. 5.45b, where $\lambda_{33\,\infty} = 0.5\rho\pi r^2$.

The added mass λ_{33} of a half-submerged cylinder of radius r floating on the free surface near a half-submerged cylinder of radius R is given by the function $f(r/l, r/R) := \lambda_{33}/\lambda_{33\,\infty}$ where $\lambda_{33\,\infty} = 0.5\rho\pi r^2$; l is the distance between the center of the first cylinder and the nearest point of the second cylinder.

Added masses of an oscillating half-submerged cylinder of radius a on the surface of fluid of depth h were computed in [13] (Fig. 5.46b). The vertical oscillations are assumed to be harmonic: $z = z_0 \sin \delta t$. In limiting cases $\delta \to 0$ (on a free sur-

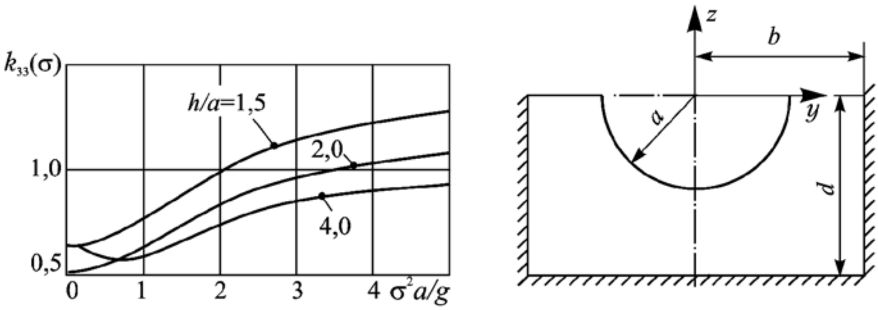

Fig. 5.47 Dependence of the coefficient of the added mass of a circular cylinder floating in the fluid of finite depth, on the frequency of vertical oscillations (*left*). Circular cylinder floating in a channel of rectangular section (*right*)

face one can assume the condition $\partial\varphi/\partial z = 0$) and $\delta \to \infty$ (on free surface one can assume the condition $\varphi = 0$) the functions $f_0(h/a) \equiv k_{33\,0} := 2\lambda_{33\,0}/\rho\pi a^2$ and $f_1(h/a) \equiv k_{33\,\infty} := 2\lambda_{33\,\infty}/\rho\pi a^2$ where $\lambda_{33\,0}$ and $\lambda_{33\,\infty}$ are corresponding limits of the added mass λ_{33}, are shown in Fig. 5.46b. Moreover, for some values of h/a there was computed the dependence of coefficient $k_{33} := 2\lambda_{33}/\rho\pi a^a$ on dimensionless frequency of oscillations (Fig. 5.47).

Dependence of λ_{33} on frequency for $h/a = 2$ and $h/a = 10$ was studied in [199] and [54]. The added mass λ_{33} of a half-submerged elliptic cylinder whose waterline coincides with the long axis was studied in [199] for $a = h = 2b$.

In a fluid of finite depth (in contrast to an infinitely deep fluid) the added mass λ_{33} remains finite as $\delta \to 0$.

Added masses of a half-submerged circular cylinder of radius a in a rectangular channel of depth d and width $2b$ under horizontal oscillations were found in [12] (see Fig. 5.47). Results of computation of coefficients $k_{22\,0} = \lambda_{22\,0}/2\rho a^2$ and $k_{22\,\infty} = \lambda_{22\,\infty}/2\rho a^2$ when the frequency of oscillations tends to 0 ($\lambda_{22\,0}$) and ∞ ($\lambda_{22\,\infty}$) [these limits correspond to boundary conditions $\partial\varphi/\partial z = 0$ and $\varphi = 0$, respectively], are shown in Table 5.6.

5.7.5 Ellipsoid of Revolution Floating in an Ellipsoid-Shape Vessel under Vertical Impact

This problem was solved by Polunin [176]. For an oblate ellipsoid of revolution (the rotation axis coincides with the Oz coordinate axis) floating in a vessel of ellipsoidal shape the added mass under vertical impact is equal to $\lambda_{33} = (2/3)\pi\rho a^2 b k_{33}$; the graphs of the coefficient $k_{33}(a/A, b/a)$ is shown in Fig. 5.48. The variable a is equal to the radius of the maximal cross-section of the ellipsoid; b is the smaller axis of the ellipsoid; A is the radius of the free surface of the vessel.

In a partial case, when $b = 0$, the added mass of a disc of radius a floating in the center of the surface of elliptical vessel with radius A of free surface, is given by

Table 5.6 Coefficients of added masses of a floating circular cylinder

d/a	b/a	$k_{22\,0}$	$k_{22\,\infty}$	d/a	b/a	$k_{22\,0}$	$k_{22\,\infty}$
1.2	1.05	3.4826	1.2917	2.0	1.05	1.9819	0.8119
1.2	1.10	3.3060	1.0009	2.0	1.10	1.7711	0.6428
1.2	1.20	3.1412	0.7547	2.0	1.20	1.5487	0.5039
1.2	1.30	3.0658	0.6390	2.0	1.30	1.4279	0.4432
1.2	1.50	3.0047	0.5278	2.0	1.50	1.3036	0.3884
1.2	2.00	2.9751	0.4202	5.0	1.05	1.8999	0.7809
1.2	3.00	2.9750	0.4149	5.0	1.10	1.6788	0.6142
1.2	4.00	2.9749	0.4131	5.0	1.20	1.4356	0.4787
1.2	5.00	2.9749	0.4130	5.0	1.30	1.2943	0.4188
1.2	10.00	2.9744	0.4126	5.0	1.50	1.1314	0.3652

$$\lambda_{33} = \frac{2}{3}\pi\rho a^3 \frac{1}{\arcsin\sqrt{1-(\frac{a}{A})^2} + \frac{a}{A}\sqrt{1-(\frac{a}{A})^2}}.$$

If $a/A \to 0$, we get $\lambda_{33\,\infty} = (4/3)\rho a^3$. In Fig. 5.49 we show the graph of function $f(a/A) := \lambda_{33}/\lambda_{33\,\infty}$.

In the case of an ellipsoid of revolution elongated along the Oz axis floating in confocal ellipsoidal vessel the function $f(a/b, b/B) := \lambda_{33}/\lambda_{33\,\infty}$ is shown in

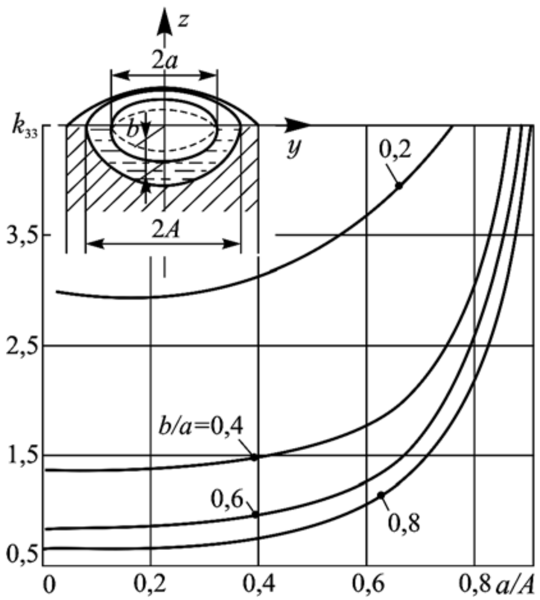

Fig. 5.48 Coefficient of the added mass of a half-submerged ellipsoid of revolution floating in an ellipsoidal vessel

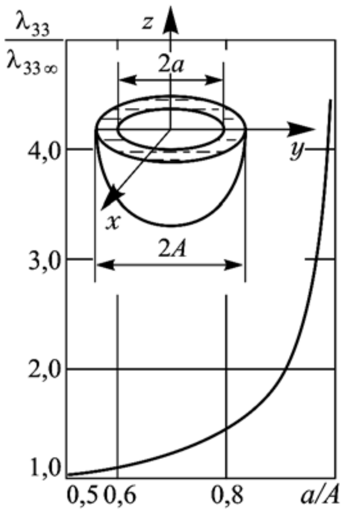

Fig. 5.49 Coefficient of the added mass of an elliptic plate floating in an ellipsoidal vessel

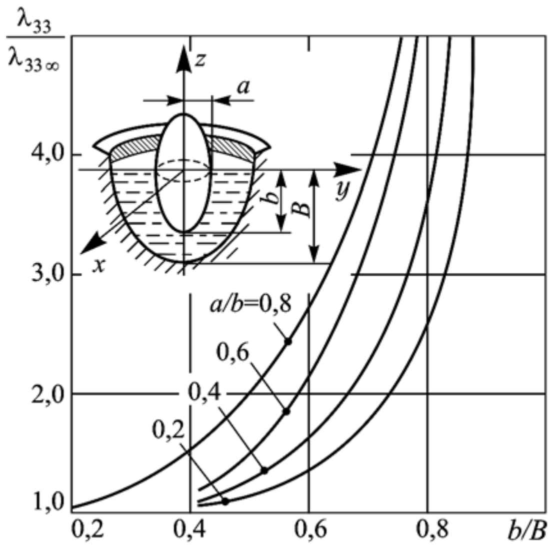

Fig. 5.50 Coefficient of added mass of elongated ellipsoid of revolution floating in an ellipsoidal vessel

Fig. 5.50. The value $\lambda_{33\infty}$ can be computed using results of [28, 29]; B is the depth of the ellipsoidal vessel.

5.7.6 Sphere Floating on a Fluid Surface Close to Solid Boundaries under Vertical Impact

The formula for the added mass of a sphere of radius a half-submerged in a spherical vessel of radius R, was obtained for the case of a vertical impact by Zhukowskiy

[263] and has the form

$$\lambda_{33} = \frac{\pi\rho a^3}{3}\frac{R^3 + 2a^3}{R^3 - a^3}.$$

If a sphere of radius a is half-submerged in a fluid of finite depth h, then the problem of computation of the velocity potential under a vertical impact is formulated as follows. One has to find a solution of the Laplace equation $\Delta\varphi = 0$ satisfying boundary conditions $\partial\varphi/\partial r = v\cos\theta$ for $r = a$ and $|\theta| < \pi/2$; $\varphi = 0$ for $r > a, \theta = \pm\pi/2$; $\partial\varphi/\partial z = 0$ for $z = h$; $\operatorname{grad}\varphi \to 0$ as $\sqrt{x^2 + y^2} \to \infty$, where the z-axis is directed downwards; x and y axes lie in the plane of free surface; (r, θ) are two out of three spherical coordinates; the angle θ is the angle between a radius-vector and z-axis.

Solution of this problem [233] gives the following approximate result for the added mass of the sphere:

$$\lambda_{33} = \lambda_{33\,\infty}(1 + 6\alpha),$$

where $\lambda_{33\,\infty} = \pi\rho a^3/3$ is the added mass of the half-submerged sphere for $h \to \infty$; value $1 + 6\alpha$ for different values of a/h is shown in the table:

a/h	0	1/5	2/7	1/3	2/5	1/2	10/11
$1 + 6\alpha$	1	1.0054	1.0158	1.0252	1.0439	1.0870	1.8510

In [162] there was obtained the following formula for the added mass of a half-submerged sphere floating on the surface of a fluid of finite depth, under a vertical impact:

$$\lambda_{33} = \lambda_{33\,\infty}\left[1 + \frac{9\cdot\zeta(3)}{16}\left(\frac{a}{h}\right)^3 + \frac{27\cdot\zeta^2(3)}{256}\left(\frac{a}{h}\right)^6 + \frac{81\cdot\zeta^3(3)}{4096}\left(\frac{a}{h}\right)^9 \right.$$
$$\left. + \frac{2025\cdot\zeta^2(5)}{32768}\left(\frac{a}{h}\right)^{10} + \frac{243\cdot\zeta^2(3)}{65536}\left(\frac{a}{h}\right)^{12} + \cdots\right],$$

where, as before, a is the radius of the sphere, h is the depth of the fluid; $\zeta(x) = \sum_{k=1}^{\infty} k^{-x}$ is the Riemann zeta-function; $\zeta(3) \approx 1.202$; $\zeta(5) \approx 1.037$; $\lambda_{33\,\infty}$ is the limit of λ_{33} as $a/h \to 0$.

The frequency dependence of added masses λ_{11} and λ_{33} of a sphere oscillating under the free surface of a fluid of a finite depth was studied in [134].

The influence of parallel vertical walls of a channel on diagonal coefficients of added masses λ_{11}, λ_{22}, λ_{33} of a sphere completely immersed under the free surface of an infinitely deep fluid was studied in [251]. It was shown that the frequency dependence of the added masses sharply changes near eigenfrequencies of the channel. The influence of the vertical walls becomes insignificant if their distance to the center of the wall is larger than $10a$.

Diagonal coefficients of added masses for a system of identical spheres whose centers are situated in a horizontal plane are determined in [250].

5.7.7 Disc Floating on a Free Surface Close to Solid Boundaries under Vertical Impact

Consider a disc of radius a floating on the surface of a fluid of depth h. Consider cylindrical coordinates where the z axis is directed downwards; r is the distance from the z-axis to a point; the origin O coincides with the center of the disc. The problem of description of vertical impact of the disc gives rise to solution of the following boundary value problem for the Laplace equation [242]: $\partial\varphi/\partial z = v$ for $z = 0$, $r \leq a$, where v is the velocity of the disc after the impact; $\varphi = 0$ for $z = 0$, $r > a$; $\partial\varphi/\partial z = 0$ for $z = h$; grad$\varphi \to 0$ as $r \to \infty$.

Approximate values of the added mass obtained after solution of this problem are contained in the following table; the added mass $\lambda_{33\,\infty} = (4/3)\rho a^3$ corresponds to $h = \infty$.

h/a	3	2	1.8	1.6	1.4	1.2	1.1
$\lambda_{33}/\lambda_{33\,\infty}$	1	1.01	1.01	1.02	1.03	1.04	1.05

If a disc is floating on the free surface of a fluid filling a cylindrical vertical vessel of radius R, then the problem of finding the potential φ is formulated as follows [33]. One has to find the solution of Laplace equation $\Delta\varphi = 0$, satisfying the following boundary conditions:

$$\begin{aligned}
&\frac{\partial\varphi}{\partial z} = v \quad \text{for } r \leq a,\ z = 0;\\
&\varphi = 0 \quad \text{for } a < r < R,\ z = 0;\\
&\frac{\partial\varphi}{\partial r} = 0 \quad \text{for } r = R,\ z \geq 0;\\
&\operatorname{grad}\varphi \to 0 \quad \text{as } r \to \infty.
\end{aligned}$$

In [33] the problem was solved in the interval $0 \leq a/R \leq 0.815$. For the added mass of the disc there was found the following approximate formula:

$$\begin{aligned}
\lambda_{33} = \frac{4}{3}\rho a^3\big[&1 + 0.33818x^3 + 0.10190x^5 + 0.11437x^6\\
&+ 0.05426x^7 + 0.06892x^8 + 0.07325x^9 + \cdots\big],
\end{aligned}$$

where $x = a/R$. Below we give the values of the correction term, which we denote by α, for different values of a/R:

a/R	0	0.1	0.2	0.3	0.4	0.5	0.6	0.7
α	1	1.0003	1.0028	1.0095	1.0233	1.0481	1.0897	1.1580

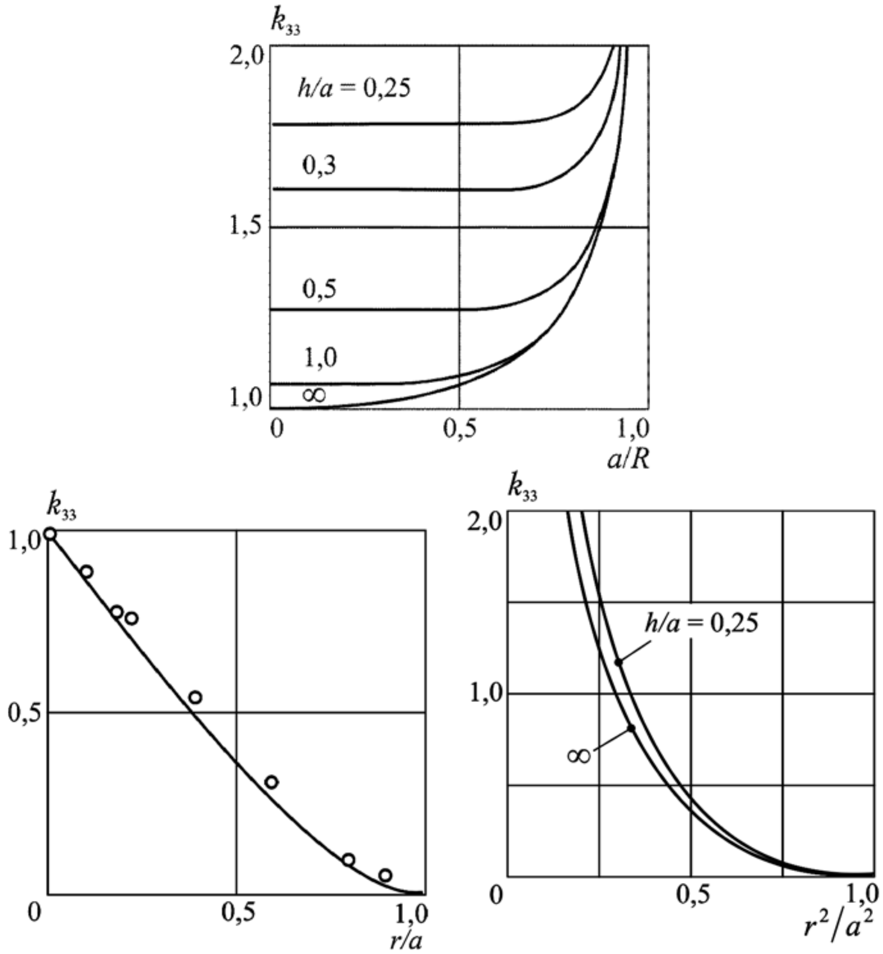

Fig. 5.51 Coefficients of added masses: *above*—of the disc; *below*—of the ring plate

Data on added masses of a disc floating on the free surface of an ellipsoidal vessel are given in Sect. 5.7.5.

The added mass of a disc of radius a floating in the center of a cylindrical vessel of radius R and depth R, under a vertical impact, depends on two parameters: a/R and h/a. Coefficients $k_{33}(a/R, h/a) = \lambda_{33}/((4/3)\rho a^3)$ obtained in [227], are shown in Fig. 5.51a.

For $a/R \to 0$ the following approximate equality holds:

$$k_{33} = -\frac{3}{4}\ln\left(1 - \frac{a}{R}\right).$$

For $a/R \to 0$ and small h/a another approximate formula holds:

$$k_{33} = \frac{3\pi a}{32h}.$$

For a disc plate of external radius a and internal radius r floating on a free surface, the coefficient of added mass $k_{33} = \lambda_{33}/((4/3)\rho a^3)$ as a function of ratio r/a was obtained in [227] (Fig. 5.51b). Small circles in Fig. 5.51b correspond to experimental results. For $r/a < 0.6$ one has the approximate formula $k_{33} = 1 - 1.25r/a$; if $r/a > 0.6$, one has another approximate formula:

$$k_{33} = \frac{3\pi^2}{32}\left(1+\frac{r}{a}\right)\left(1-\frac{r}{a}\right)^2.$$

In [227] there was also studied the added mass of a plate ring floating on the free surface of a fluid filling a cylindrical vessel whose diameter coincides with the external diameter of the plate ring. Under a vertical impact the plate ring slides along the surface of the vessel. The dependence $k_{33}(r^2/a^2)$ for two depths of the fluid ($h/a = 0.25$, $h/a = \infty$) is given in Fig. 5.51c. For $r^2/a^2 < 0.1$ one can use the formula $k_{33} = 3\pi^2/(16r/a)$.

5.7.8 Rectangular Pontoon Floating on a Fluid Surface

Added masses of an infinitely long rectangular pontoon of width $2a$ floating on the surface with the draught $T = a$ are discussed in [246].

Under a vertical motion $\lambda_{33} = 0.75\pi\rho a^2$; under a horizontal motion $\lambda_{22} = 0.25\pi\rho a^2$; under a rotation around the axis lying at the intersection of the waterline plane and the longitudinal vertical plane $\lambda_{44} = 0.117\pi\rho a^4$. The depth of the fluid is assumed to be infinite. The boundary condition for the velocity potential on the free surface is assumed to be in the form $\varphi = 0$.

The dependence of added masses λ_{11} and λ_{33} of an oscillating rectangular pontoon floating on the free surface of a fluid of an infinite depth on the oscillation frequency is given in [155]. The draught of the pontoon was equal to 1/2 of its width. For λ_{11} the theoretical predictions agree well with experimental data from [243] for all frequencies. Analogous results for a pontoon with the ratio of the sides $a/T = 1$ which is situated in the middle of the channel of the depth $6a$ were obtained in [54].

5.7.9 Rectangular Pontoon Floating Close to Flat Walls

The added mass λ_{33} of a rectangular pontoon of width $2a$ with draught $T = a$ moving close to a flat bottom such that the distance from the lower boundary of the pontoon to the bottom equals h, is given by $\lambda_{33} = k_{33}\pi\rho a^2$, where the values of the

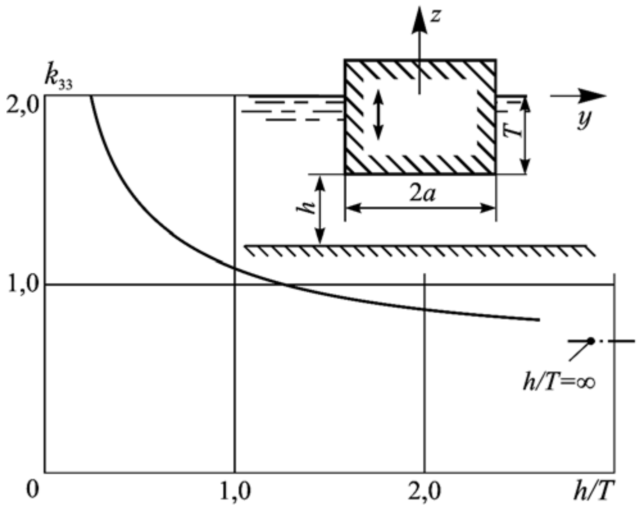

Fig. 5.52 The coefficient of the added mass of a rectangular pontoon floating on the free surface of a fluid of a finite depth

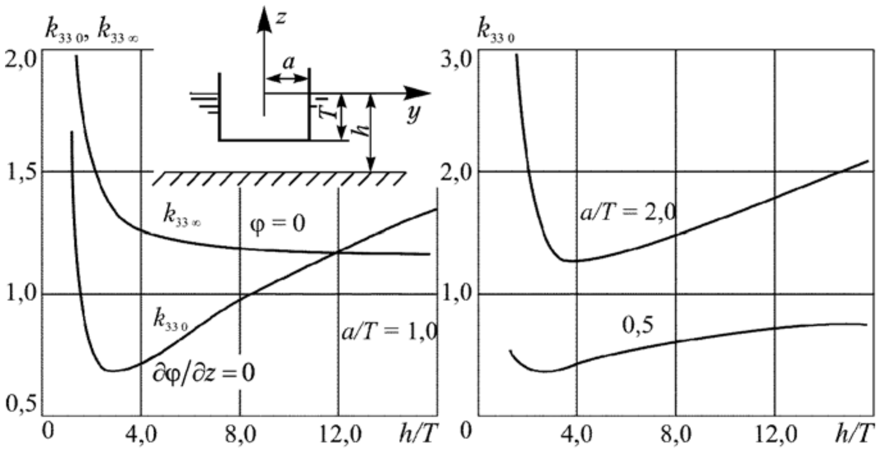

Fig. 5.53 The coefficient of the added mass of a rectangular pontoon floating on the free surface of a fluid of a finite depth, under different boundary conditions

coefficient $k_{33}(h/T)$ are given in Fig. 5.52 [246]. On the free surface the boundary condition $\varphi = 0$ is assumed.

In [13, 98] the added mass λ_{33} of the rectangular pontoon oscillating vertically according to the law $z = z_0 \sin \delta t$ were studied (see Fig. 5.53). In Fig. 5.53 we show the dependence of limit values of the coefficient k_{33} on the relative depth of the water. In Fig. 5.54 we show the dependence of the coefficient k_{33} on the dimensionless frequency of oscillations $\delta^2 a/g$ for some values of h/T.

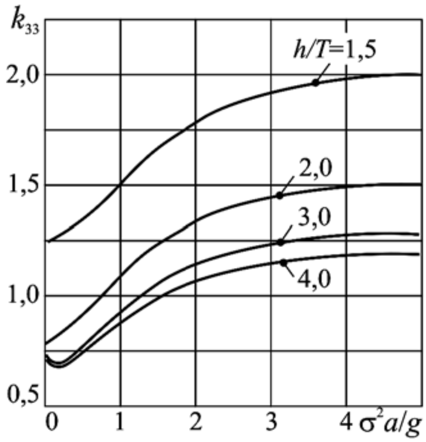

Fig. 5.54 Dependence of coefficient of added masses of rectangular pontoon on frequency of vertical oscillations

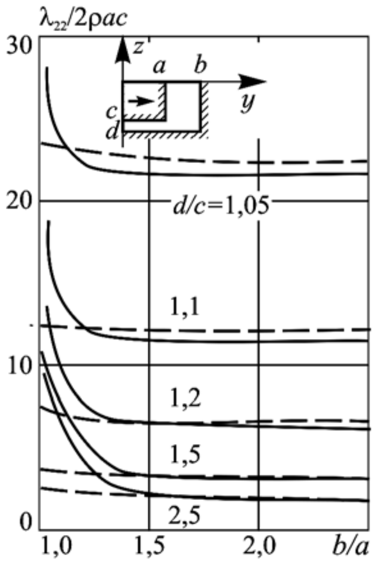

Fig. 5.55 The coefficient of the added mass of a rectangular pontoon under horizontal oscillations in a rectangular channel

In [54] the dependence of the added masses λ_{11} and λ_{33} on the frequency were studied for floating rectangular pontoons of two types: $a/T = 1$ and $h = T$, and, also $a/T = 1.5$ and $h/T = 5$.

The added mass of a rectangular pontoon of width $B = 2a$ symmetrically immersed in a rectangular channel of width $2b$ with draught c (the level of water in the channel equals d), is computed in [13, 37]. The velocity potential is found numerically assuming water-tightness boundary conditions on the hard walls and the free surface.

Results of solution of this problem are shown in Fig. 5.55 for various ratios b/a and d/c for a rectangular pontoon with $B/T = 2a/c$, where B is the width of the pontoon, T is the draught. The added mass is divided by the volume of fluid in

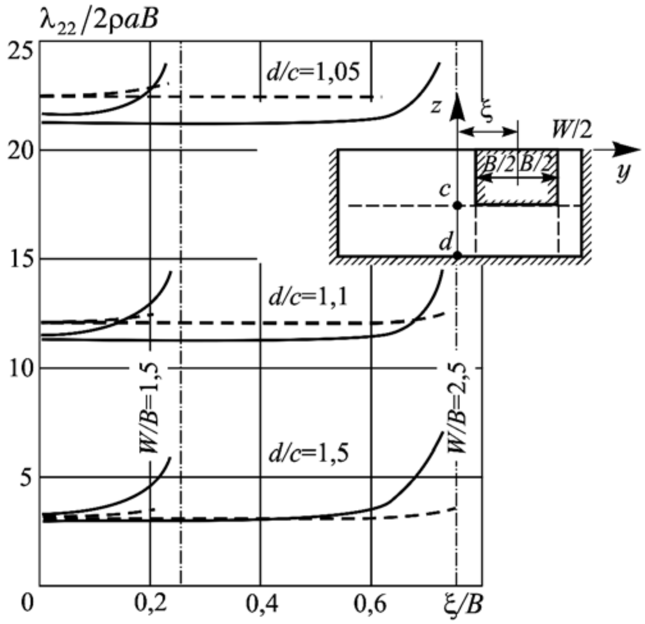

Fig. 5.56 Dimensionless added mass of rectangular pontoon eccentrically floating in rectangular channel

the submerged part of the pontoon. Dashed lines correspond to the data taken from [159].

In computation of the added mass λ_{22} of a rectangular pontoon in a rectangular channel under water-tightness boundary conditions on a free surface (see Fig. 5.55) one can use the formula

$$\lambda_{22} = \frac{2}{3}\rho c\left[\frac{cd}{b-a} + \frac{c\,(2a+b)}{d-c} + b - a\right],$$

obtained in [11] which gives acceptable results in the range $0 < (d-c)/a \leq 0.3$; $0 < (b-a)/c \leq 0.3$.

If the rectangular pontoon is shifted with respect to the axis of a rectangular channel by the distance ξ (Fig. 5.56) then its added mass changes depending on d/c, W/B, ξ/B, where W is the width of the channel. Corresponding curves are shown for $W/B = 1.5$ and $W/B = 2.5$ in Fig. 5.56 [72]. Dashed curves correspond to the data from [23, 159].

Besides added masses corresponding to a linear motion, the added masses of an oscillating rectangular pontoon near hard walls are also given in [72]. Formulation of this problem is different from the one considered above since on the free surface, when the oscillation frequency is high, one has to use the boundary condition $\varphi = 0$ instead of $\partial\varphi/\partial n = 0$, as follows from the general discussion of Sect. 5.1.

Results of computation of the added mass λ_{22} under horizontal oscillations close to a vertical wall on a shallow water are shown in Fig. 5.57b (solid curves). Dashed

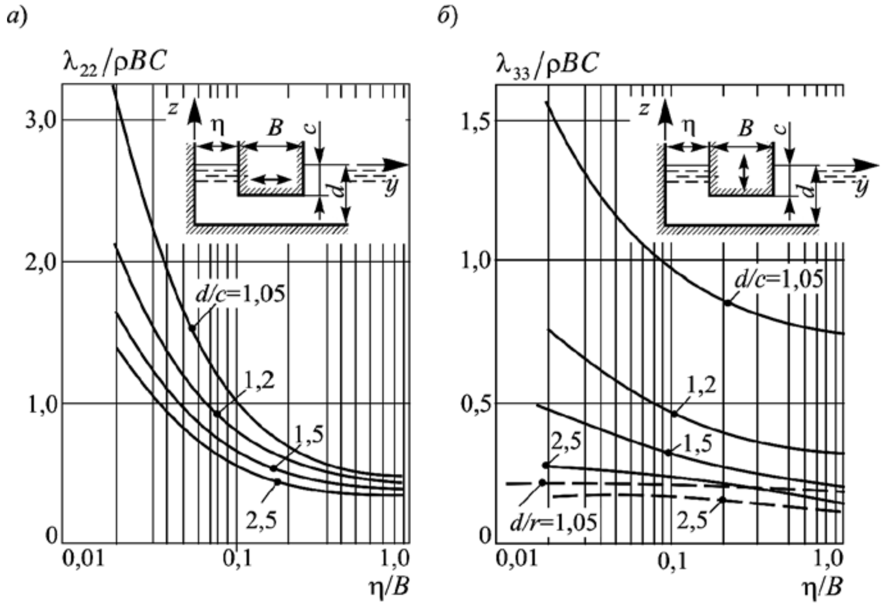

Fig. 5.57 Dimensionless added masses of a rectangular pontoon near a vertical wall in shallow water

curves correspond to the values of the coefficient $2\lambda_{33}/(\rho\pi r^2)$ of a half-submerged circular cylinder of radius r which oscillates vertically near a flat solid wall.

An interesting numerical investigation of the added mass λ_{22} of a rectangular pontoon floating in a rectangular channel (Fig. 5.58) is contained in [109]. Parameters of the problem had the following values: $l/T = 14.8$, $B/T = 4$, $h/T = 0.2$, where l is the width of the channel, T is the draught of the pontoon, B is the width of the pontoon, h is the distance from the bottom of the pontoon to the bottom of the channel. The distance from the pontoon to the wall of the channel (expressed via parameter $(l - l_1)/T$) was changing.

Importance of this research was determined by two factors:

- The boundary condition on the free surface was considered in the form

$$\frac{\partial\varphi}{\partial z} + b\varphi = 0,$$

  where the parameter b was changing between 0 and ∞.
- Both types of the flow: a separating flow and a non-separating flow were considered.

Results of this research are shown in Fig. 5.58a for a non-separating flow, and in Fig. 5.58b for a separating flow, when on the rear surface of the pontoon the boundary condition $\varphi = 0$ is fulfilled. In vertical axes we show the ratio of λ_{22} to $\lambda_{22\infty}$, where $\lambda_{22\infty}$ is the added mass computed for the case when the walls are

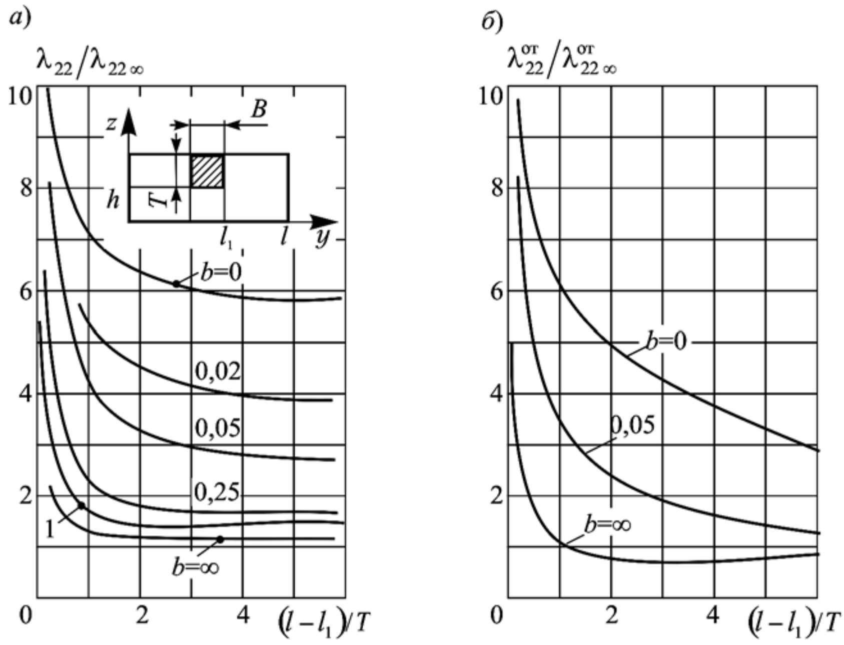

Fig. 5.58 Dimensionless added masses of a rectangular pontoon in a rectangular channel for a flow without separation and for a flow with separation

Fig. 5.59 Dimensionless added mass of a rectangular pontoon under vertical impact

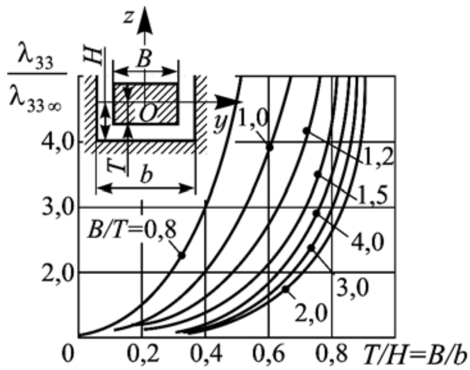

absent. It is shown that for all b the value of $\lambda_{22\,\infty}$ for the case of non-separating flow is about 1.7 times higher than $\lambda_{22\,\infty}$ for the case of separating flow.

Added masses of a rectangular pontoon of width B and draught T floating in a geometrically similar rectangular channel of depth H and width b, under a vertical impact, were computed in [175]. Graphs of functions $f(B/T, T/H) := \lambda_{33}/\lambda_{33\,\infty}$ are shown in Fig. 5.59. We have $\lambda_{33\,\infty} = \lambda_{33\,0}/2$, where $\lambda_{33\,0}$ is the added mass of the rectangle with sides B and $2T$ under its motion in an infinite fluid.

Fig. 5.60 Dimensionless added mass of polygonal contours under vertical impact

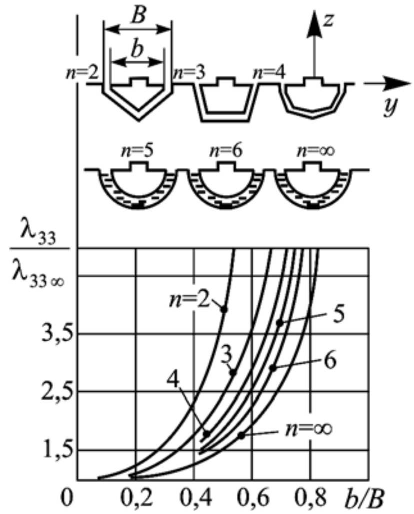

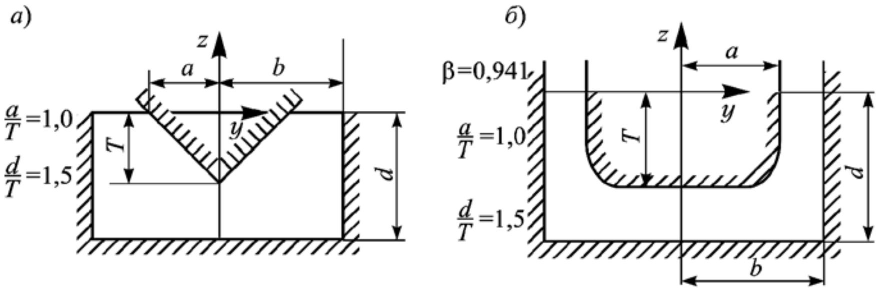

Fig. 5.61 Triangular cylinder (*left*) and shipframe (*right*) floating in a rectangular channel

Analogous dependencies for polygonal contours of various shape floating in geometrically similar channels are shown in Fig. 5.60.

The added masses $\lambda_{22\,0}$ (on the free surface one assumes the boundary condition $\partial\varphi/\partial z = 0$) and $\lambda_{22\,\infty}$ (on the free surface one assumes $\varphi = 0$) of a triangular cylinder (Fig. 5.61a; $a/T = 1.0$, $d/T = 1.5$) and the cylinder whose cross-section has the shape of a Lewis shipframe with the area coefficient 0.941 (Fig. 5.61b; $\beta = 0.941$, $a/T = 1.0$, $d/T = 1.5$), floating in a rectangular channel, were computed in [12]. We present these data in Tables 5.7 and 5.8.

5.8 Influence of the Separation of the Flow on a Body Surface on Added Masses

Usually added masses are computed under the assumption that the flow around a body does not separate on the body surface. However, there exist such regimes of

Table 5.7 Added masses of a triangular cylinder in a rectangular channel

b/a	$\lambda_{220}/(\rho a T)$	$\lambda_{220}/(\rho a T)$
1.05	2.2142	1.1412
1.10	2.1650	1.0299
1.20	2.0997	0.9212
1.30	2.0601	0.8646
1.50	2.0194	0.8048
2.00	1.9934	0.7480
2.50	1.9902	0.7292

Table 5.8 Added masses of a cylinder having cross-section in the shape of a Lewis shipframe in a channel of rectangular section

b/a	$\lambda_{220}/(\rho a T)$	$\lambda_{220}/(\rho a T)$
1.5	2.5769	0.4987
2.0	2.4483	0.4113
2.5	2.4338	0.3871
3.0	2.4320	0.3790
4.0	2.4315	0.3750
5.0	2.4307	0.3742

motion that this assumption is not applicable and the curves (surfaces) of the discontinuity of the velocity are formed (curves BD and CD in Fig. 5.62). In this case one should consider the flow around a body under the following boundary conditions on the body surface:

1. On the part AB and AC of the body where the flow does not separate one imposes the water-tightness condition $\partial\varphi/\partial n = 0$.
2. On the part BC of the body where the flow has separated from the body surface and the fluid is stagnant one assumes the constancy of the pressure, i.e., $\varphi = 0$.

In computation of added masses corresponding surface integrals (1.12) are computed only over the part BAC since on the part BC the integrand vanishes.

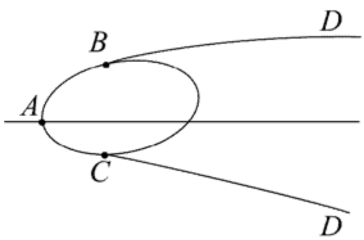

Fig. 5.62 Separation of the flow around a body

As an example we describe some data on added masses of bodies floating on a free surface under horizontal impact [120, 231]. It is assumed that there is separation of flow at the rear side (i.e., the side of the impact) of the body.

The z axis is chosen to be directed downwards; the z-coordinate of the point of the separation is assumed to be equal to $0.92b$ where b is the maximal immersion depth of the contour.

For a half-submerged horizontal elliptic cylinder,

$$\lambda_{22} = 0.56\frac{2\rho b^2}{\pi}; \qquad \lambda_{23} = 0.598\frac{2\rho ab}{\pi}; \qquad \lambda_{24} = -0.195\rho b\left(b^2 - a^2\right).$$

For the same cylinder in the case when the separation of the flow does not take place:

$$\lambda_{22} = \frac{2\rho b^2}{\pi}; \qquad \lambda_{23} = 0; \qquad \lambda_{24} = -\frac{1}{3}\rho b\left(b^2 - a^2\right).$$

For a half-submerged circular cylinder of radius a in the presence of the separation:

$$\lambda_{22} = 0.56\frac{2\rho a^2}{\pi}; \qquad \lambda_{23} = 0.598\frac{2\rho a^2}{\pi}; \qquad \lambda_{24} = 0.$$

For a vertical plate submerged to a depth b:

$$\lambda_{22} = 0.56\frac{2\rho b^2}{\pi}; \qquad \lambda_{23} = 0; \qquad \lambda_{24} = -0.195\rho b^3.$$

The horizontal plate of width l under a vertical impact leading to the separation of the flow, has the added mass $\lambda_{33} = 0.4224\rho l^2$ (see [92]).

Experimental data [192] show that the added mass of a cavitating disc of radius a equals $\lambda_{33} = 2.52\,\rho a^3$ and does not depend on the angle of inclination of the disc to the free surface [260]. The theoretical value of the added mass of a disc floating on the free surface under a vertical impact (see Sect. 5.7.7) is given by $\lambda_{33} = (4/3)\rho a^3$.

We stress the difference between the cavitating separation of flow, when the cavern near the surface of the body is filled by a gas (air or steam), and the viscous separation of the flow, when behind the point of separation one has the stagnant zone of a fluid of the same density as the density of the incoming fluid. Obviously, under an acceleration one has to take into account the influence of the fluid in the stagnant zone on the body surface.

5.9 Effect of Fluid Compressibility on Added Masses of a Floating Plate at an Impact

The problem of a vertical impact of a plate floating on the free surface of a compressible fluid is considered in [58, 59]. It is assumed that the vertical force acting on the plate starts at $t = 0$ and increases according to the law $F(t) = F_0(1 - e^{-\beta t})$, where the finiteness of the coefficient β reflects the compressibility of the fluid; for an incompressible fluid $\beta = 0$. The boundary conditions are formulated in the usual way: on the surface of the fluid $\varphi = 0$; on the surface of the plate the normal component of the velocity of the fluid is equal to the velocity of the plate; the perturbations arising due to the impact decay at infinity (the radiation condition).

The added mass of the plate is determined by the formula

$$\lambda_{33} = \frac{\rho\pi a^2}{2}\left(\frac{1 - e^{-\beta t}}{1 + (\rho\pi a^2/2m)e^{-\beta t}}\right),$$

where m is the mass of the plate. This formula shows that the added mass under an impact, taking into account the compressibility of the fluid, grows from the value $\lambda_{33} = 0$ at $t = 0$ to $\lambda_{33} = (1/2)\rho\pi a^2$ (as $t \to \infty$) which coincides with the value of λ_{33} in the case of an incompressible fluid. As $\beta \to \infty$ the added mass also tends to the added mass in an incompressible fluid: $\lambda_{33} \to (1/2)\rho\pi a^2$.

5.10 Added Masses of Elliptic Contour under its Lift from a Water Surface

Problems of this kind are rather common in shipbuilding.

Below we describe the solution of the problem of finding the added mass of a half-submerged elliptic contour under its lift from the water surface [39].

At $t = 0$ the elliptic contour with half-axes a and b is half-submerged such that the Ox axis coincides with the free surface (Fig. 5.63). In the process of motion the contour is lifted from the water along the axis Oy (y_c denotes the vertical coordinate of the center of the ellipse in the process of the lift).

The motion of fluid is assumed to be potential. On the free surface one imposes the following boundary conditions:

1. The normal component of velocity is absent:

$$\left.\frac{\partial\varphi}{\partial y}\right|_{y=0} = 0.$$

2. The component of velocity tangential to the free surface is given at points M_1 and M_2 where the contour intersects the free surface.

To solve this problem one should first take the mirror image of the flow with respect to the free surface. Then one maps the exterior of the resulting contour (for $t = 0$ this is an ellipse itself; for $t > 0$ it looks like an "elliptic lens") to the interior of the unit circle in the plane of the auxiliary complex variable. Applying Sedov's formulas, the author of [39] gets the following formula for the added mass of an elliptic contour under its lift from the water surface:

$$\lambda_{22} = \frac{2}{3\pi}\rho\left[10\frac{a(b - y_c)}{b}\sqrt{b^2 - y_c^2} + \pi ab - 2\frac{a}{b}\left(y_c\sqrt{b^2 - y_c^2} + b^2 \arcsin\frac{y_c}{b}\right)\right].$$

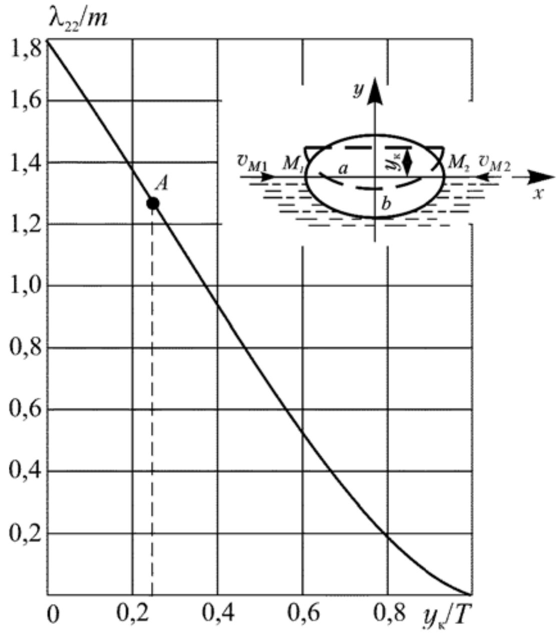

Fig. 5.63 Dimensionless added mass of an ellipse under its lift from water surface

This formula can be used for estimation of λ_{22} for various contours, if one denotes the width of the contour at waterline by $B = 2a$ and draught by $T = b$.

The formula for $\lambda_{22}(y_c/T)$ was verified in [39] experimentally. Results of these experiments (point A in Fig. 5.63) agree with theoretical predictions.

5.11 Added Masses of Inland Ships

In [115] added masses $\lambda_{22} = k_{22}\pi\rho T^2/2$ for typical shapes of inland vessel's shipframes were determined by the method of electro-hydrodynamic analogy (see Chap. 9).

Coefficient k_{22} as a function of B/T (B is width and T is the draught) and β (the area coefficient of the shipframe) is shown in Fig. 5.64.

In the same work under assumption that the Froude numbers are small (on the free surface one assumes the fulfillment of the water-tightness condition) the coefficients $k_{11} = \lambda_{11\,H}/\lambda_{11\,H=\infty}$, $k_{22} = \lambda_{22\,H}/\lambda_{22\,H=\infty}$ and $k_{66} = \lambda_{66\,H}/\lambda_{66\,H=\infty}$ were found as functions of the ratio T/H (H is the depth of fluid). Graphs of these functions are shown in Fig. 5.65, where curves I correspond to an ellipsoid, curves II correspond to the hull of an inland vessel.

If the added masses of an inland vessel are determined by the method of planar sections, then corrections μ and μ_1 related to spacial effects in the formulas (3.1), (3.9)

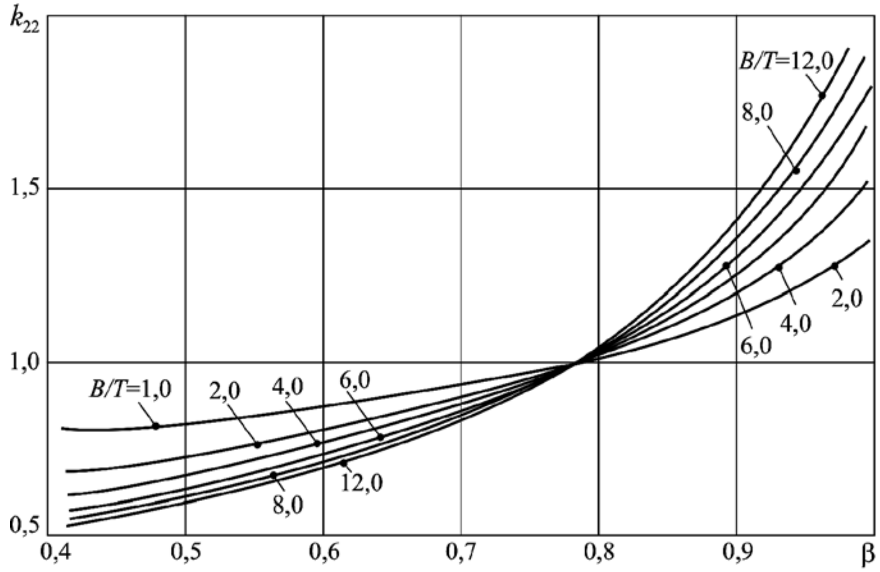

Fig. 5.64 Coefficients of added masses of inland vessels in the horizontal direction

$$\lambda_{22} = \mu \int_0^L \lambda_{22\,0}(x)\,dx; \qquad \lambda_{66} = \mu_1 \int_0^L \lambda_{22\,0}(x) x^2\,dx$$

can be taken in the following empirical form [78]:

$$\mu = 0.9 + 0.012\frac{B}{T}; \qquad \mu_1 = 0.44\left(\frac{B^2}{T^2} + 1\right)\left(\frac{L}{B}\right)^{1/3}$$

where L is the length of the boat.

Notice that correction μ is independent of L/T.

A systematic study of added masses of inland ships was carried out at the Novosibirsk institute of water transport in 1966–1971.

Systematic computations of added masses of three-axial ellipsoids moving in a channel of a rectangular section were carried out in the paper [235] using the method of [30]. On the basis of these computations there was proposed a method of determination of added masses of inland ships. On the basis of these results in [170] there were obtained the following approximate formulas for added masses of inland ships valid under the assumptions

$$T/H \leq 0.8; \qquad B/L \leq 0.25; \qquad 0.1 \leq T/B \leq 0.5; \qquad 0.5 \leq \delta \leq 0.92,$$

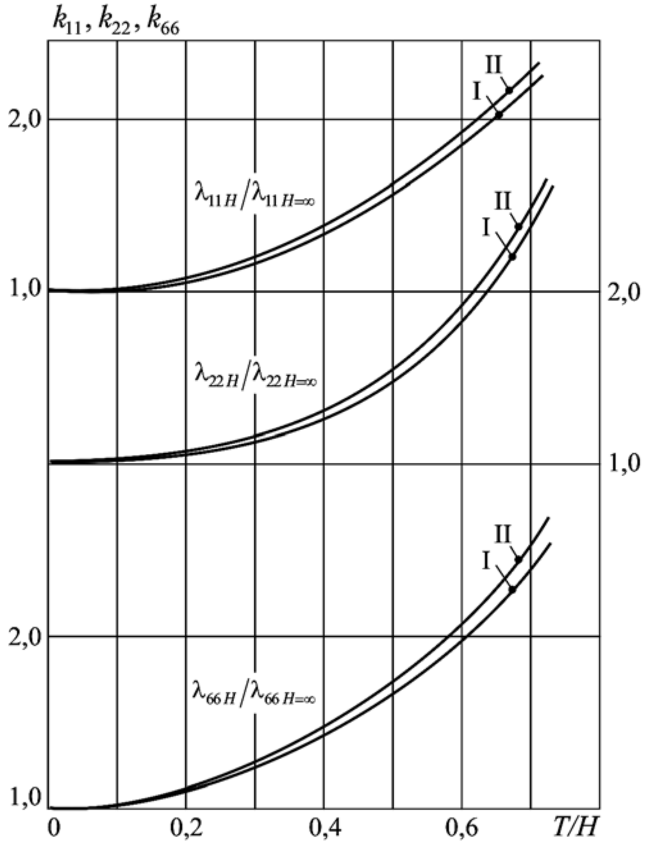

Fig. 5.65 Influence of the depth of the water on added masses of inland vessels

where δ is the volume coefficient of the submerged part of the boat (which is equal to the ratio of the volume of the submerged part of the hull to the product LBT);

$$\lambda_{11} = k_{11}\frac{D}{g}; \qquad \lambda_{22} = k_{22}\frac{D}{g}; \qquad \lambda_{66} = k_{66}J_z,$$

where D is the displacement of the ship; g is the gravity acceleration;

$$\begin{aligned} J_z &= \left(1+\delta^{4.5}\right)\frac{D}{24g}\left(L^2+B^2\right); \\ k_{11} &= (0.624+0.72\delta) \\ &\quad \times \frac{B}{L}\left\{\frac{2T}{B}\left[0.18+2.88\left(\frac{B}{L}\right)^2\right]\left[1-1.4\left(\frac{T}{H}\right)^{1.5}\right]+1.06\left(\frac{T}{H}\right)^{1.5}\right\}; \end{aligned} \tag{5.40}$$

$$k_{22} = 3.76\frac{T}{B}\frac{\sigma(1-\alpha\sigma)}{\alpha(1+\sigma)(2-\alpha-\sigma)} + \frac{0.27\sigma}{1+2.35(T/B)}\frac{T/H}{1-3.11(T/H)+3.77(T/H)^2-1.66(T/H)^3}; \tag{5.41}$$

$$k_{66} = \frac{1.68(T/B)}{1+(B/L)^2}\frac{2\sigma(9-6\alpha-6\sigma+4\alpha\sigma)(3-2\alpha-2\sigma+\alpha\sigma)}{a(6-5\alpha-5\sigma+4\alpha\sigma)(9-9\sigma+2\sigma^2)} + \frac{0.223\sigma^2}{1+3.68(T/B)-2.27(T/B)^2} \times \frac{T/H}{1-2.9(T/H)+3.37(T/H)^2-1.47(T/H)^3}, \tag{5.42}$$

where σ is the area coefficient of the diameter buttock; α is the area coefficient of the waterplane.

The formulas (5.40)–(5.42) are valid for small Froude numbers. If the Froude numbers are greater than 0.2, one should introduce experimental corrections to k_{11} [140, 145, 153, 232] which take into account an influence of the free surface at acceleration and deceleration. In some cases, in particular in studies of rolling on shallow water, one has to determine the added mass λ_{33}. To find λ_{33} of a given shipframe on shallow water one can use the formula $\lambda_{33\,H} = \varepsilon_H \lambda_{33\,\infty}$ [18] where the coefficient ε_H is shown in Fig. 5.66 as a function of the ratio H/T and dimensionless frequency of oscillations $\sigma^2 B/2g$ (H is the depth of the water).

These dependencies are obtained theoretically for a circular cylinder oscillating on shallow water. The value $\lambda_{33\,\infty}$ is the added mass of shipframe on deep water.

We notice also experimental results by Palagushkin for added masses of inland ships at acceleration and deceleration [165–167]. A family of models whose geometric characteristics are given in Table 5.9 was tested. The hull of the model No. 2 (chosen as the base model) is shown in Fig. 5.67. The models were tugged preserving the freedom of vertical motion and the trim angle motion. The tugging velocities corresponded to dimensionless Froude numbers $Fr = v/\sqrt{gL}$ (where L is the length of the model) varying between 0 and 0.25.

The velocity of a model varied in the range 0.05 m/sec $\le v \le$ 2.5 m/sec and measured with the precision 0.1%; an acceleration (deceleration) a of the model varied in the limits 0.015 m/sec^2 $\le |a| \le$ 0.2 m/sec^2. In the process of tugging, the longitudinal force acting on the model was measured.

Under a non-stationary motion the following equations of motion hold:

$$ma = X - R, \tag{5.43}$$

where m is the mass of the model; a is an acceleration; X is the force measured by a dynamometer; R is the hydrodynamic force acting on the model. The force R can be represented in the form:

$$R = R_1(a) + R_2(a, v) + R_3(v), \tag{5.44}$$

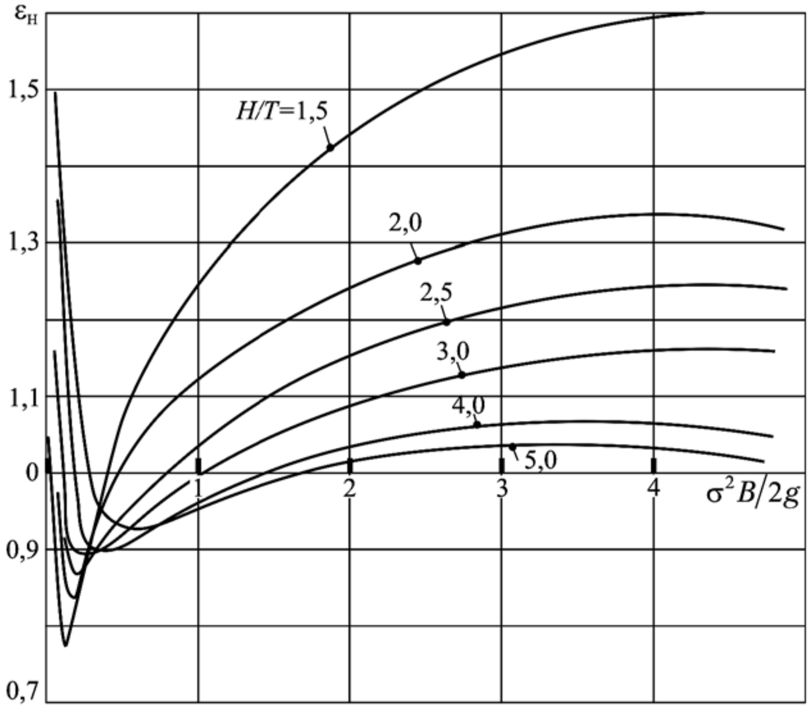

Fig. 5.66 Influence of the frequency of vertical oscillations on added masses of circular cylinder oscillating on shallow water

Table 5.9 Geometric characteristics of a family of models of inland cargo vessels

Model No.	1	2	3	4	5	6	7	8	9
Length L, m	4.25	3.4	2	3.4	3.4	3.4	3.4	3.4	3.4
Width B, m	0.5	0.5	0.5	0.5	0.5	0.5	0.5	0.5	0.5
Draught T, m	0.083	0.083	0.083	0.083	0.083	0.083	0.1346	0.0555	0.0357
Gen. area coeff. δ	0.85	0.85	0.85	0.809	0.907	0.931	0.85	0.85	0.85
L/B	8.5	6.8	4.0	6.8	6.8	6.8	6.8	6.8	6.8
B/T	6.0	6.0	6.0	6.0	6.0	6.0	3.71	9.0	14.0

where R_1 depends only on the acceleration a, R_2 depends on a and v; R_3 is determined by the velocity v only.

The term $R_3(v)$ is found by tugging of the model with a constant velocity.

It was assumed in [166] that the term R_3, which is independent of an acceleration, does not contribute to the added mass, i.e., the added mass is defined by relation

$$R_1 + R_2 = a\lambda_{11} \tag{5.45}$$

where λ_{11} is the added mass of the model in the longitudinal direction.

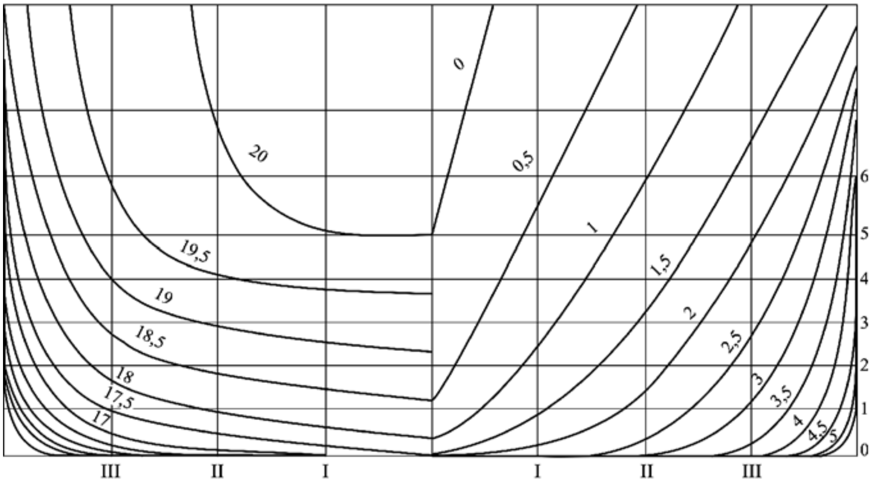

Fig. 5.67 Hull of base model of an inland cargo vessel

Substituting the formulas (5.44) and (5.45) in (5.43), we find:

$$k_{11} := \frac{\lambda_{11}}{m} = \frac{X - R_3}{ma} - 1. \tag{5.46}$$

Examples of experimental dependencies $k_{11} = k_{11}(Fr)$, obtained for the model number 2 under three relative depths of water ($T/H = 0$; 0.333; 0.667) where T is the draught of the model, H is the depth of water, are shown in Fig. 5.68. Curves 1, 3, 5 are obtained under an acceleration of the model; curves 2, 4, 6—under deceleration. Curve 7 in Fig. 5.68 corresponds to the coefficient k_{11} computed via the equivalent ellipsoid.

Approximation of these experimental data allowed the author to propose the following approximate formulas for determination of k_{11} under the forward motion; k_{11*} under the reverse motion and k_{22} under the log motion:

$$k_{11} = k_{11\infty}\bar{k}_{11} + c_{11}\Delta k_{11} f_1 f_2 f_3; \tag{5.47}$$

$$k_{11*} = k_{11}\left[1.09 - 0.042\left(\frac{T}{H}\right) + 0.018\left(\frac{T}{H}\right)^2\right]; \tag{5.48}$$

$$k_{22} = k_{22\infty}\bar{k}_{22} + D\Delta k_{22} f_1' f_2' f_3'. \tag{5.49}$$

In the formulas (5.47)–(5.49) the following notations are used:

$$k_{11\infty} := \frac{\pi}{10}\left(\frac{B}{L}\right)^{1.31}\left[\tanh\left(7.88\frac{T}{B}\right)\right]^{1.6};$$

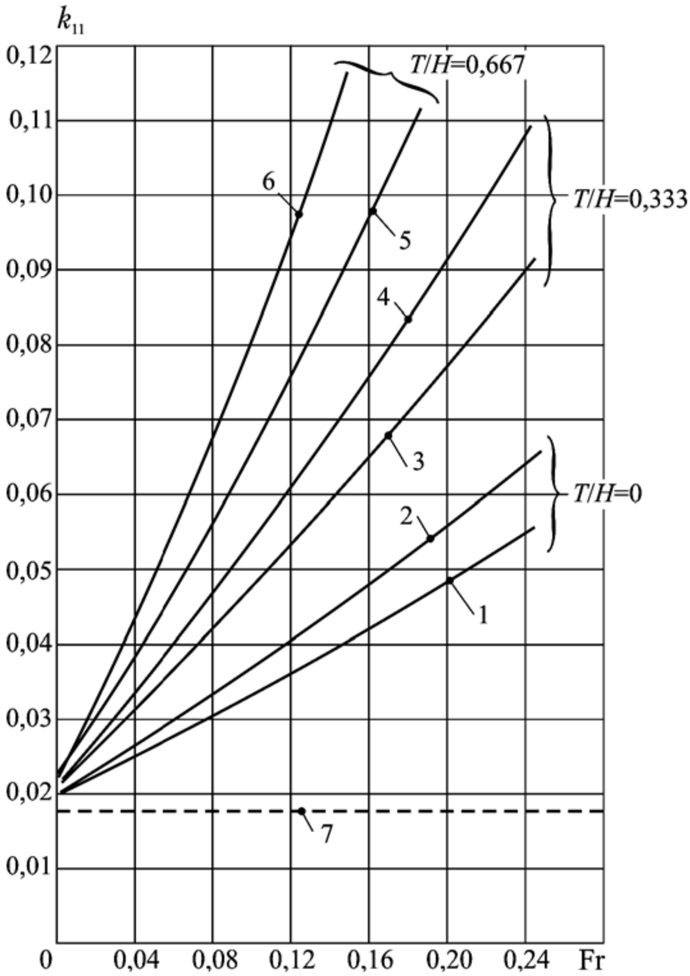

Fig. 5.68 Examples of experimental curves

$$\bar{k}_{11} := 1 + 0.1\left(\frac{T}{H}\right)^{1.24};$$

$$\Delta k_{11} := \left[0.156 + 0.674\left(\frac{T}{H}\right)^{1.28}\right] Fr^{1.03};$$

$$c_{11} := 1 - \left[0.13 - 0.138\frac{T}{H} + 0.198\left(\frac{T}{H}\right)^{2}\right] \mathrm{sign}(a);$$

$$f_1 := 1 + 2.56\left(\frac{B}{L} - 0.147\right)\frac{T}{H};$$

$$f_2 := 1 + 1.122(\delta - 0.85);$$

$$f_3 := 1 + 0.693\left(\frac{T}{B} - 0.167\right);$$

$$k_{22\infty} := 1.53\left(\frac{2T}{B}\right) - 0.685\left(\frac{2T}{B}\right)^2;$$

$$\bar{k}_{22} := 1 + 0.068\left(\frac{T}{H}\right)^{1.7};$$

$$\Delta k_{22} := \left[1.46 + 17.1\left(\frac{T}{H}\right)^{2.26}\right]\left(\frac{v}{\sqrt{gB}}\right)^{1.16+0.135(T/H)^2};$$

$$D := 1 - \left[0.121 - 0.115\frac{T}{H} + 0.112\left(\frac{T}{H}\right)^2\right]\operatorname{sign}(a).$$

Under an acceleration $\operatorname{sign}(a) = 1$; under a deceleration $\operatorname{sign}(a) = -1$.

$$f_1' := 1 - \left[2.41 - 4.54\frac{T}{H} + 5.58\left(\frac{T}{H}\right)^2\right]\left(\frac{B}{L} - 0.147\right);$$

$$f_2' := 1 + 1.48(\delta - 0.85);$$

$$f_3' := 1 - 1.62\left[1 - 2.27\frac{T}{H} - 2.81\left(\frac{T}{H}\right)^2\right]\left(\frac{T}{B} - 0.167\right)\left[1 - 3.18\left(\frac{T}{B} - 0.167\right)\right],$$

where L, is the length, B is the width, T is the draught, δ is the general area coefficient; H is the depth of water.

The domain of applicability of the formulas (5.47)–(5.49) looks as follows:

$$0.11 \le \frac{B}{L} \le 0.25; \qquad 0.07 \le \frac{T}{B} \le 0.28; \qquad 0.8 \le \delta \le 0.94; \qquad \frac{T}{H} \le 0.67;$$

$$Fr = \frac{v}{\sqrt{gL}} \le 0.24; \qquad \frac{v}{\sqrt{gB}} \le 0.28.$$

The fact that the coefficients k_{11} and k_{22} essentially depend on the Froude number is explained by wave formation. In experiments with an ellipsoid which was deeply submerged under the surface, the influence of velocity on added masses was negligible. These added masses exceeded theoretical values by 11%, which can be explained by the viscosity of water.

5.12 Added Masses of Barges Consists

Added masses of consists of barges were studied in [83, 84]. The added masses of consist are determined via added masses of separate vessels, and via inertial coefficients j_{km} which take into account an interaction of vessels. Both computations and experiments show that j_{km} significantly differ from 1 when the barges form a single line whose direction coincides with the direction of motion, as well as in the case when the consist is made of sections (a section consists of two barges which are lashed together by sideboards).

The added mass of consist can be computed by the following formula:

$$\lambda_{11} = j_{11} \sum_{i=1}^{n} \lambda_{11\,i},$$

where $\lambda_{11\,i}$ is the added mass of a single barge; values of coefficients j_{11} are given below:

- For a single line consist:

$T+1$	$j_{11} = 0.90$
$T+1+1$	$j_{11} = 0.74$
$T+1+1+1$	$j_{11} = 0.61$

- For a two-line consist:

$T+2$	$j_{11} = 1.49$
$T+2+2$	$j_{11} = 1.25$
$T+2+2+2$	$j_{11} = 1.14$

where T denotes the pusher tug; the numbers are the numbers of barges and their position in the consist.

In computation of added masses λ_{22}, λ_{26}, λ_{66} one has to introduce the inertial coefficients of a single section, which consists of several barges lashed by sideboards. Added masses of each section are determined by expressions

$$\lambda_{22}^{(s)} = j_{22}^{(s)} \sum_{i=1}^{m} \lambda_{22\,i}; \qquad \lambda_{66}^{(s)} = j_{66}^{(s)} \sum_{i=1}^{m} \lambda_{66\,i}.$$

One can always choose the origin in such a way that $\lambda_{26} = 0$; due to the specific shape of barges this point is typically close to the center of mass of the barge.

If a section consists of one barge then $j_{22} = j_{66} = 1$. If a section consists of two lashed barges then $j_{22} = 0.8$ and $j_{66} = 0.87$; for the section which consists of three lashed barges $j_{22} = 0.71$, $j_{66} = 0.75$.

In computation of added masses λ_{22}, λ_{26}, λ_{66} one usually neglects an interaction between separate sections. Taking also into account that $\lambda_{11\,i}$ is small in comparison with $\lambda_{22\,i}$ for each single barge, one gets the following formulas for the consist:

$$\lambda_{22} = \sum_{s=1}^{n} \lambda_{22}^{(s)} = \sum_{s=1}^{n} j_{22}^{(s)} \left(\sum_{i=1}^{m} \lambda_{22i} \right)_s ;$$

$$\lambda_{26} = \sum_{s=1}^{n} \lambda_{22}^{(s)} x_s = \sum_{s=1}^{n} j_{22}^{(s)} \left(\sum_{i=1}^{m} \lambda_{22i} \right)_s x_s;$$

$$\lambda_{66} = \sum_{s=1}^{n} \lambda_{66}^{(s)} + \sum_{s=1}^{n} \lambda_{22}^{(s)} x_s^2 = \sum_{s=1}^{n} j_{66}^{(s)} \left(\sum_{i=1}^{m} \lambda_{66i} \right)_s + \sum_{s=1}^{n} j_{22}^{(s)} \left(\sum_{i=1}^{m} \lambda_{22i} \right)_s x_s^2.$$

In these formulas x_s is the x-coordinate (the x-axis is chosen along the central line of the consist) of the center of mass of each section with respect to the origin which is chosen in the center of mass of the consist.

These formulas were verified by systematic model experiments.

5.13 Added Masses of Rafts

Added masses of a raft taking into account the bending effect were considered in [195]. Inertial characteristics of the raft were determined as functions of its length L, width B, and radius of curvature of its central line under bending R (or curvature $\kappa = 1/R$). The longitudinal axis Ox and the transversal axis Oy are chosen in the plane of the raft. Combining theoretical and experimental data one gets the following approximate formulas, which take into account the penetrability of the (unbent) raft:

$$k_{11} = \frac{\lambda_{11}}{m} = 1.3\left(0.041 - 0.0027\frac{L}{B}\right);$$

$$k_{22} = \frac{\lambda_{22}}{m} = 1.3\left(0.043 + 0.0085\frac{L}{B}\right),$$

where m is the mass of the raft. In [195] the following approximate formulas for added masses of a raft under bending were also proposed:

$$\lambda_{11}^{\kappa} = \lambda_{11} + \kappa^2 \lambda_{22} \frac{L^2}{12}; \qquad \lambda_{16}^{\kappa} = \kappa \lambda_{22} \frac{L^2}{12},$$

where λ_{11}^{κ} and λ_{16}^{κ} are added masses of the bent raft; κ is the curvature of the central line.

5.14 Influence of Density Stratification of Fluid on Added Masses

Sometimes underwater vehicles move in a fluid whose density increases with depth. Near the boundary separating layers with different density there may exist internal waves whose generation is related to additional energy losses.[1] Therefore it is necessary to study the influence of the gradient of fluid density to added masses of a body.

The most interesting case is the case of an infinite fluid with homogeneous stratification when the parameter $N(z) := [(-g/\rho)\, d\rho/dz]^{1/2}$ is independent of depth z: $N(z) = N_0$ (here $\rho(z)$ is the density of the fluid). For a weakly stratified fluid one usually uses the Boussinesque approximation. The homogeneous stratification is then approximated by the linear stratification. A general solution for hydrodynamic forces acting on a body immersed in such a fluid is derived in [62]; in this work there were deduced relationships between oscillations of bodies in homogeneous and linearly stratified fluids.

If the oscillation frequency $\sigma > N_0$, one considers an elliptic problem with watertightness conditions on the surface of the body and vanishing of the amplitude at infinity (problem 1). Let us rename the coordinates: $x_1 := x$, $x_2 := y$, $x_3 := z$. By an affine transformation of the form $\xi_i = a_i x_i$ (where $a_1 = a_2 = 1$; $a_3 = \alpha := (\Omega^2 - 1)^{1/2}/\Omega$ and $\Omega = \sigma/N_0$) the equation of motion of a linearly stratified fluid turns into a Laplace equation. The boundary conditions on the body also transform. In this way one gets an equivalent problem (problem 2) in the non-stratified fluid. The coefficients of added masses in the two problems, $k_{ij}^{(1)} := \lambda_{ij}^{(1)}/(\rho_0 W^{(1)})$ and $k_{ij}^{(2)} := \lambda_{ij}^{(2)}/(\rho_0 W^{(2)})$ (where $W^{(1)}$ and $W^{(2)}$ are volumes in the two problems in the 3D case and areas in the 2D case and ρ_0 is the density of fluid at the depth of the body motion), are related by $k_{ij}^{(1)} = k_{ij}^{(2)} a_i a_j$.

In problem 2 one introduces the characteristic linear sizes of the body b_1, b_2 and b_3 in three directions ξ_1, ξ_2 and ξ_3. One can then consider the coefficients $k_{ij}^{(2)}$ as functions of the ratios $e := b_2/b_1$ and $f := b_3/b_1$:

$$f_{ij}(e, f) := k_{ij}^{(2)}. \tag{5.50}$$

Therefore, a solution of the original problem 1 for the tensor of coefficients of added masses can be obtained from (5.50) by the substitution $q = q_0\alpha \equiv q_0(\Omega^2 - 1)^{1/2}/\Omega$:

$$k_{ij}^{(1)}(\Omega) = f_{ij}(e_0, q_0\alpha)\, a_i a_j. \tag{5.51}$$

For high frequency oscillations $\sigma \to \infty$ these solutions, obtained in the Boussinesque approximation, coincide with corresponding values of added masses in a homogeneous unlimited fluid.

For $\Omega < 1$ the original equation of problem 1 is the equation of hyperbolic type. Its solution can be obtained by the method of analytical continuation. One can introduce in this case the real parameter $\eta = (1 - \Omega^2)^{1/2}/\Omega$. The analytical continuation of α is given by $-i\eta$; coefficients a_i in (5.51) should be substituted by γ_i: $\gamma_1 = \gamma_2 = 1$, $\gamma_3 = -i\eta$. Solution (5.51) for $\Omega < 1$ takes the form

$$k_{ij}^{(1)}(\Omega) = f_{ij}(e_0, -iq_0\eta)\, \gamma_i \gamma_j. \tag{5.52}$$

[1]This section was written by I.V. Sturova and E.V. Ermanyuk.

From (5.51) and (5.52) we see that the values of $k_{ij}^{(1)}$ for families of affine equivalent bodies, which differ only by the value of q_0, can be represented by a universal curve.

In general case expressions for hydrodynamic pressures have complex form, where the real part is determined by the added mass:

$$\lambda_{ij} = \rho_0 W^{(1)} \Re\big(k_{ij}^{(1)}\big). \tag{5.53}$$

All solutions for bodies of simplest geometry known before ([126]—vertical oscillations of ellipsoids of revolution, [99]—oscillations of a vertical cylinder in an arbitrary direction) can be obtained as partial cases of the above construction. For example, for an elliptic cylinder $f_{11}(q) = q,\ f_{33}(q) = 1/q$. Substitution of these functions in (5.51), (5.52), (5.53) gives a solution obtained in [99]:

$$k_{11}^{(1)} = k_{33}^{(1)} \equiv 0 \quad \text{for } \Omega \le 1, \qquad k_{11}^{(1)} = k_{33}^{(1)} = \frac{(\Omega^2 - 1)^{1/2}}{\Omega} \quad \text{for } \Omega > 1. \tag{5.54}$$

A distinctive feature of solution (5.54) is the identical vanishing of the coefficients λ_{11} and λ_{33} for flat contours for $\sigma \le N_0$.

In Fig. 5.69 we show experimental and theoretical data for the coefficient $k_{11} = \lambda_{11}/(\pi\rho_0 a^2)$ for a circular cylinder which horizontally oscillates in an unlimited homogeneously stratified fluid. The solid line corresponds to a theoretical curve obtained by Hurley [99]; symbols correspond to experimental data of Ermanyuk [60]. Data obtained in a fluid of homogeneous density are shown by the dotted line and +'s. Experimental estimates of dependence of the added mass λ_{11} on the frequency are obtained by response function of the system corresponding to a single impuls using Fourier transform.

In Fig. 5.70 we present the theoretical and experimental data for the coefficient

$$k_{11} = \frac{\lambda_{11}}{(4/3)\pi\rho_0 a^2 b}$$

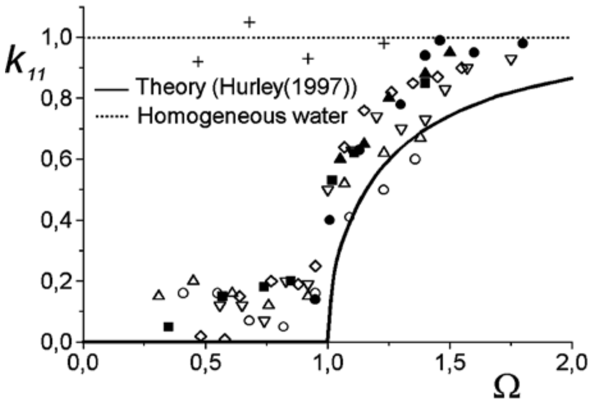

Fig. 5.69 Coefficient k_{11} for a circular cylinder oscillating in a homogeneously stratified fluid: *solid curve*—theory [99], *dotted curve* and +'s—data for a homogeneous fluid; *triangles*, *squares* and *circles* correspond to experimental data [60]

Fig. 5.70 Coefficient k_{11} for ellipsoids with vertical rotation axis, which horizontally oscillate in homogeneously stratified fluid [62]: *curves* correspond to theoretical predictions, *triangles* and *circles* represent corresponding experimental data (*1*—oblate ellipsoid with ratio of axes $a/b = 2$, *2*—sphere, *3*—prolate ellipsoid with ratio of axes $a/b = 1/2$)

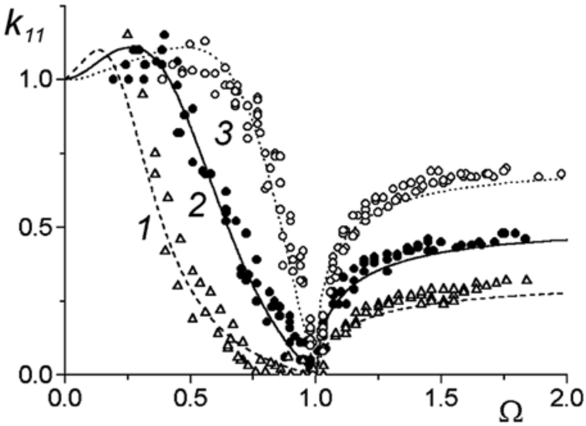

Fig. 5.71 Universal curves for $\Re k_{11}^{(1)}$ of ellipsoids with vertical axis of rotation of an arbitrary elongation in a homogeneously stratified fluid [62]: the *curve* corresponds to theoretical predictions; *triangles* and *circles* correspond to experimental data shown in Fig. 5.70 and recalculated via affine transformation

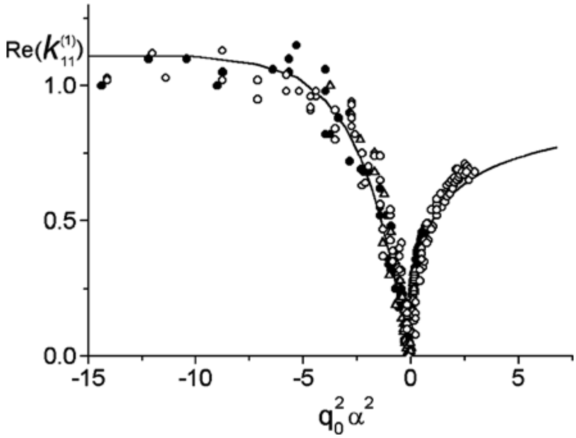

of ellipsoids with vertical axis of rotation in unlimited homogeneously stratified fluid. Curves correspond to theoretical results; symbols correspond to experimental data of Ermanyuk [62, 63]. Using the affine transformation the data shown in Fig. 5.70 can be shown in a universal form shown in Fig. 5.71.

From well-known formulas for fluids of homogeneous density (see for example Chaps. 2, 3) one can also get formulas of added masses of ellipsoids under oscillations in an arbitrary direction, contours with corners etc. In particular, added masses λ_{11} and λ_{33} for cylinders of rectangular section were derived in [61].

A typical stable configuration of sea medium looks as follows: two homogeneous layers of different density are separated by a layer with high gradient of density, called the pycnocline. When the gradient of density in pycnocline is high it can be modeled by a two-layer fluid. When the gradient of density at pycnocline is low, one can model the physical problem by a three-layer fluid; the pycnocline (the central layer) is assumed to be linearly stratified.

The three-layer fluid includes as partial cases both the linearly stratified fluid and the two-layer fluid. The first limiting case corresponds to an increase of the thickness of the central layer while keeping the value of the density gradient constant. The second case arises when the thickness of pycnocline tends to zero.

The motion of a body in a two-layer fluid is most well-studied. The upper layer is assumed to have density ρ_1 and thickness H_1. The lower level is assumed to have density $\rho_2 = \rho_1(1+\varepsilon)$ $(\varepsilon > 0)$ and thickness H_2.

Dependence of added masses on the frequency for a circular and elliptic cylinder completely submerged in an infinitely deep layer under the separation boundary of two layers was found by Sturova [217]. For the circular cylinder in this case $\lambda_{11} = \lambda_{33}$, as well as for a homogeneous fluid of infinite depth. Under low frequency oscillations $(\sigma \to 0)$ the separation surface behaves like a solid boundary, independently of the magnitude of the density jump and the thickness of the upper layer. An approximate dependence of added masses on frequency is obtained on assumption that the body is submerged deeply enough under the surface of separation. For an elliptic cylinder with the axes ratio $a/b = 2$ for $H_1 = h = b$ and $\varepsilon = 0.03$ the dependencies of added masses on frequencies were found numerically, by the method of hybrid finite elements (h is the distance between the center of the cylinder and the separation surface). The results are compared with analogous values of added masses for two-layer fluid bounded by a solid boundary ("cover") from the top, and with the values of added masses in a homogeneous fluid with free surface. For small values of σ mostly internal waves are generated; their characteristics almost coincide with the case of a two-layer fluid under the "cover". As the frequency grows the generation of internal waves decreases and the surface waves become dominant; the characteristics of the surface waves are essentially not influenced by a small jump of density.

The added masses λ_{11} for a circular cylinder and λ_{55} for a horizontal plate submerged under the separation surface in a two-layer unlimited fluid, are given in the book by Filippov [71].

The model of a two-layer fluid allows us also to study the influence of a slimy bottom on the motion of floating of a submerged body. Dependence of coefficient λ_{33} on the frequency for the Lewis shipframe floating on a free surface and not intersecting the separation boundary is given in [264]. It is assumed that the lower layer of fluid is viscous and its depth is essentially smaller than the depth of the upper layer. It is shown that the coefficient λ_{33} essentially depends on the frequency, the ratio of densities and thicknesses of the layers; however, it is essentially independent of viscosity of the oozy layer.

The added masses λ_{11}, λ_{33} and λ_{55} as functions of the oscillation frequency of a parallelepiped with square horizontal section floating on a free surface in the upper layer of a two-layer fluid were studied in [256].

Behavior of added masses λ_{11} and λ_{33} as functions of frequency for a circular cylinder crossing the separation surface of an unlimited two-layer fluid was studied in [152]. It was shown that under oscillations of a cylinder crossing the separation surface the values of added masses are typically higher than the values of added masses in a homogeneous fluid with free surface. This is explained by the fact that in the latter case the area of the surface of the body contacting with the fluid is smaller; thus a smaller amount of the fluid gets involved in oscillating motion.

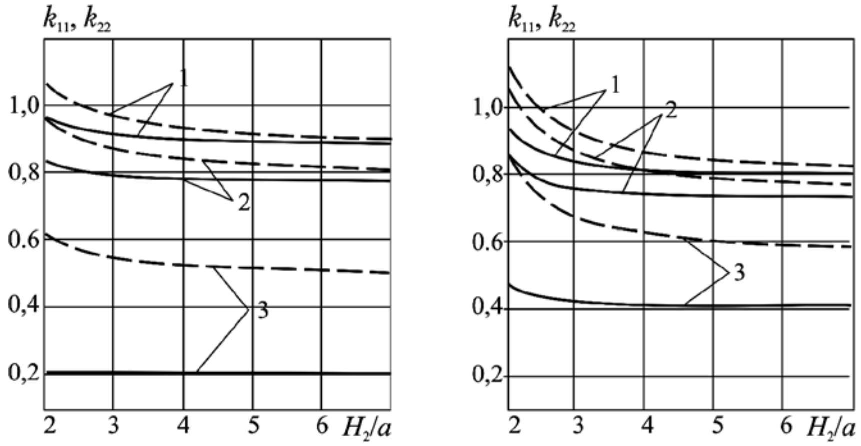

Fig. 5.72 Dependence of coefficients of added masses k_{11} (*solid curves*) and k_{22} (*dashed curves*) on the depth of the lower layer for a circular cylinder. *Left*: $h = 0$, $H_1/a = 2$; *right*: $h/a = 0.5$, $H_1/a = 1$. *Curves 1* correspond to $\varepsilon = 0$; *curves 2* correspond to $\varepsilon = 0.3$; *curves 3* correspond to $\varepsilon = \infty$

The influence of the depth of the lower layer on added masses of a circular and elliptic cylinder floating on the separation boundary of a two-layer weightless fluid which is bounded from above by free surface, is studied in [216]. As an example we present below the results of computation of added masses of a circular cylinder floating on the separation boundary.

The radius of the cylinder is denoted by a. On the free surface ($y = H_1$) one imposes the boundary condition $\varphi = 0$. On the hard bottom ($y = -H_2$) one assumes the water-tightness condition $\partial\varphi/\partial y = 0$. The distance from the center of the cylinder to the boundary between the layers ($y = 0$) is denoted by h. In Fig. 5.72 we show coefficients $k_{11} = \lambda_{11}/(\pi\rho_2 a^2)$ and $k_{22} = \lambda_{22}/(\pi\rho_2 a^2)$ as functions of H_2/a for several values of h/a (equal to 0 and 0.5), H_1/a (equal to 1 and 2) and ε (equal to 0, 0.3 and ∞). The case $\varepsilon = 0$ corresponds to a non-stratified fluid. The case $\varepsilon = \infty$ corresponds to the cylinder floating on a free surface.

Dependence of added masses λ_{11}, λ_{33}, λ_{55} and λ_{15} on the oscillation frequency for an elliptic cylinder (flat problem) floating on the separation surface of a two-layer fluid of finite density and finite depth bounded by a free surface was studied in [220].

The influence of the separation surface on λ_{33} for a Lewis shipframe floating on the free surface of a two-layer fluid was studied in [222] and [220]. In [222] there were compared the experimental results for a contour with the following characteristics: width $B = 20$ cm, draught $T = 12$ cm, area coefficient $\beta := S/(BT) = 0.9$. In the laboratory experiment there were used two non-mixing fluids (isoparaffine oil and water) with the difference of densities $\varepsilon = 0.3076$. The full fluid depth in all experiments was $H = 40$ cm. There were considered two cases, when the contour either crosses the separation boundary ($H_1 = 6$ cm, $H_2 = 34$ cm) or is completely floating in the upper layer ($H_1 = 15$ cm, $H_2 = 25$ cm). For comparison we

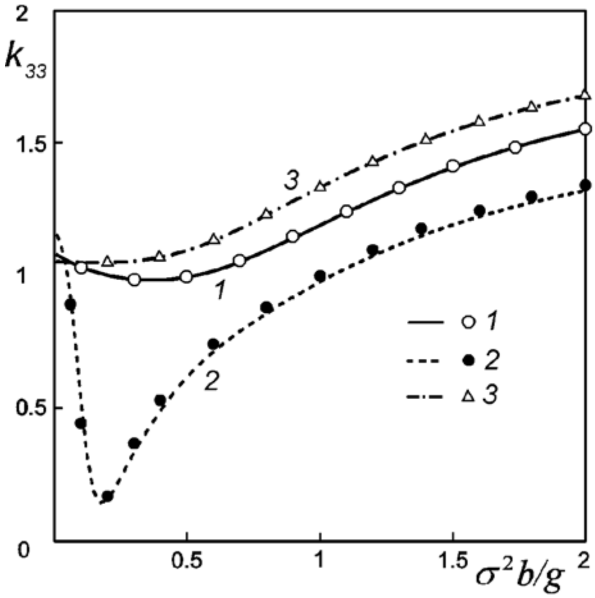

Fig. 5.73 Dependence of coefficient k_{33} on the frequency under vertical oscillations of the Lewis contour: *1*—$H_1 = 6$ cm, $H_2 = 34$ cm; *2*—$H_1 = 15$ cm, $H_2 = 25$ cm; *3*—homogeneous layer of depth $H = 40$ cm. Curves represent results of [222]; symbols correspond to results of [220]

present also the third case, when the contour is oscillating in the layer of homogeneous fluid of density ρ_2 for the same value of the depth H. In [222] it was revealed a good agreement between numerical and experimental data. In Fig. 5.73 we compare the numerical results of [222] and [220] for dependence of the coefficient $k_{33} = \lambda_{33}/(\rho_2 b^2)$ on the frequency, where $b = B/2$. Curves 1–3 show the results of [222] obtained by the method of boundary elements; symbols 1–3 show the results of [220] obtained by the method of hybrid finite elements. The numerical results of both methods agree well with each other. One observes that the stratification and position of the body significantly influence the coefficient of added mass k_{33}.

Hydrodynamic forces acting on an immersed body under its horizontal motion with constant velocity in the lower layer of a two-layer fluid were studied in [218] for a 2D problem. It is assumed that the lower layer is bounded by the solid "cover", while the lower layer has infinite depth. The full matrix of added masses for elliptic contour with $a/b = 2$ is computed.

The influence of pycnocline on added masses of a body immersed in a three-layer fluid were studied in the 2D case in [214, 215, 219]. Comparison of dependence of added masses λ_{11} and λ_{33} on the frequency of oscillations of a circular cylinder immersed in the lower layer (having finite depth) of two-layer and three-layer fluids was made in [214]. It was assumed that the upper level is bounded by a solid "cover". The influence of the pycnocline thickness and the depth of the lower layer was studied. It was shown that the behavior of added masses for the two-layer fluid and the three-layer fluid with thin pycnocline (with the same change of density) essentially coincide. When the thickness of the pycnocline increases, the maximal values of added masses increase, too.

The frequency dependence of added masses of a circular cylinder completely immersed in the linearly stratified layer is studied in [215]. It was shown that under increase of the thickness of the stratified layer, the values of added masses approach the corresponding values given by (5.54); this is especially manifest in the case of λ_{33}. The presence of thick homogeneous layers significantly influences the values of λ_{11} and λ_{33}.

An arbitrary position of a circular cylinder in a three-layer fluid under assumption of infinite thickness of the lower and upper layers was considered in [219]. The values of λ_{11} and λ_{33} were compared for different stratifications, from an unlimited two-layer fluid to a relatively deeply situated linearly stratified layer.

Experimental studies of λ_{11} for a circular cylinder and for a sphere oscillating in a waveguide (linearly stratified fluid of finite depth and two-layer system of miscible fluids with pycnocline of finite thickness) were carried out in [61, 64].

Chapter 6
Added Masses under Elastic Oscillations of Structures and Their Components

Here we discuss oscillations of the surface of a body immersed in a fluid and computation of added masses of the body under such oscillations.[1] Oscillations of this type typically occur as local oscillations of the hull surface. We give examples of computation of added masses in typical model oscillations.

6.1 General Discussion

When a system immersed in a fluid oscillates elastically, the added mass depends on whether the system is isolated or represents a part of a larger system because, in the latter case, added masses depend on the behavior of system parts that are neighbor to the system experiencing oscillations: if these parts are stable, then they serve as a solid screen; if they oscillate, this results in additional fluid flow.

Publications on the problem of added masses caused by elastic motions of various constructions and their separate parts are sparse. This is because of diversity of hydroelasticity problems, each of which is difficult and customarily needs a separate approach. At the same time, elastic motions of constructions are important in actual engineering.

The problem of finding added masses of an elastic rectangular plate attached to a solid screen was solved by Babaev [10] and the one for the circular plate was solved by Lamb [133]. In the first case, the problem was solved in application to a separate plate, whereas the rest of the ship's skin was assumed to be absolutely rigid. In reality, a single oscillating plate involves into motion neighbor parts of the skin, which can be thought of as a stiffened multispan elastic plate. Added masses of a multispan plate at various oscillation types were found by Schukina [202, 204] by taking into account the fluid flow into the neighbor spans. She also proposed a way to find added masses of fluid for oscillations of complex constructions taking into account interactions between separate elements of these constructions.

The added masses of rectangular, cantilever plates (solid and perforated) and the ones of the circular plates was found in paper [202]. The influence of the added mass on characteristics of oscillations of a flexible plate in the fluid flow was considered in [125, 203]. In [205], the dependence of the added mass of a plate on the presence of a solid boundary was found.

[1] This chapter was written by E.N. Schukina.

The influence of the free fluid surface and of the flow of fluid across the ship hull on the added mass of the ship bottom plating was estimated by Rostovtzev [187]. The problem of added masses of shells experiencing oscillations, which are axial- or skew-symmetric w.r.t. the generating line, was addressed in [3, 15, 40, 69, 79, 104, 141, 150, 173, 180, 207, 223, 259, 262].

The determination of added masses of ship propellers due to shaft oscillations [51] is important for dynamical calculations of shafting and propeller-shaft struts.

Calculations of added masses for various elastic constructions are performed below taking into account different factors such as the presence of a solid boundary and of the free fluid surface, oscillations of parts neighbor to the construction under study, dynamical interaction between elements entering the construction and volumes of fluid involved in motion by these elements.

6.2 Methods of Finding Added Masses under Structure Oscillations

Problems of determination of added masses under oscillations of bodies and constructions in fluid are being customarily solved under the assumption of the ideal fluid whose flow is potential. This is because the inertial properties of fluid depend weakly on thermodynamical effects and on fluid viscosity. Investigating the potential motion of an incompressible homogeneous fluid reduces to finding the velocity potential φ satisfying the Laplace equation and the corresponding boundary and initial conditions (see Chap. 1). The velocity potential φ can be also found using the method of sources and sinks [139]. The influence of an oscillating body is equivalent to the action of simple sources of capacity $q = \partial Z/\partial t$ continuously distributed over the body surface S (here $Z(A,t)$ is the normal (with respect to the surface) displacement of the body at the corresponding point). A source of capacity $q\,dS$ corresponds to the area element dS located at a point A of the surface S, and the velocity potential for this elementary source at a point M of the space filled with liquid is

$$d\varphi(M) = -q(A)\frac{dS(A)}{2\pi r(AM)},$$

where $r(AM)$ is the length of the radius-vector $\vec{AM} = r$ joining the elementary source at the point A with the space point M. Using the method of current superposition, we determine the velocity potential at the point M created by sources continuously distributed over the surface s as the integral

$$\varphi(M) = -\frac{1}{2\pi}\iint_S \frac{\partial Z(A)}{\partial t}\frac{dS(A)}{r(AM)}. \tag{6.1}$$

The integration ranges over the whole surface S.

If the domain of fluid motion is unbounded, the function φ tends to zero as the point M tends to infinity.

The kinetic energy T of the potential motion of an incompressible homogeneous fluid is given by the volume integral

$$T = \frac{1}{2}\rho \iiint_V \mathbf{v}^2 \, dV,$$

where the integration ranges over the whole fluid volume V and $\mathbf{v} = \operatorname{grad} \varphi$.

Using the Green's transformation, or the Ostrogradskii–Gauss formula, we can express the kinetic energy T of the fluid through the value of the velocity potential φ on the surface of the oscillating body S:

$$T = -\frac{\rho}{2} \iint_S \varphi \frac{\partial \varphi}{\partial n} \, dS. \tag{6.2}$$

Using relations (6.1) and

$$-\frac{\partial \varphi}{\partial n} = \frac{\partial Z}{\partial t},$$

we express dependence (6.2) in the form

$$T = \frac{\rho}{4\pi} \iint_S \frac{\partial Z(M)}{\partial t} \, dS(M) \iint_S \frac{\partial Z(A)}{\partial t} \frac{dS(A)}{r(AM)}. \tag{6.3}$$

Let us assume that the displacement $Z(A, t)$ can be represented in the form

$$Z(A, t) = F(A)\tau(t), \tag{6.4}$$

where $F(A)$ is the function characterizing changes in displacements at different points of the body surface (for instance, the oscillation amplitude) and $\tau(t)$ describes the time dependence of displacements. The assumption (6.4) means that the time dependence of displacement of all points of the body surface is the same for all points of the surface.

Then

$$T = \frac{\rho}{4\pi} \iint_S F(M) \frac{\partial \tau}{\partial t} \, dS(M) \iint_S F(A) \frac{\partial \tau}{\partial t} \frac{dS(A)}{r(AM)}.$$

Then one can introduce the time-independent quantities

$$M_{\mathrm{ad}} = \frac{\rho}{2\pi} \iint_S F(M) \, dS(M) \iint_S F(A) \frac{dS(A)}{r(AM)} \tag{6.5}$$

which can be naturally called the added masses. These quantities have the dimension of mass; they correspond to the diagonal entries λ_{11}, λ_{22} and λ_{33} of the matrix of added masses considered in Chap. 1. By using the decomposition of the potential φ into a linear combination of the elementary potentials φ_i, $i = 1, \ldots, 6$, similarly to (1.9) one can define all other added masses, which have dimensions of mass, static moment, and inertia moment.

We stress that the definition of natural time-independent variable M_{ad} corresponding to a given type of vibration is possible due to assumption (6.4), which is natural in considering the vibrating bodies. This notion of added mass is therefore different from the notion of added masses of interacting bodies considered in Sect. 4.1.1, since the latter are essentially time-dependent variables depending on mutual position of the interacting bodies.

In the sequel we shall for brevity omit some arguments in (6.5) and write (6.5) in the following schematic way:

$$M_{\mathrm{ad}} = \frac{\rho}{2\pi} \iint_S F(s')\, dS' \iint_S F(s) \frac{dS}{r}$$

where s and s' stand for integration points of the surface S.

6.3 Added Masses of Multi-span Plates

Plates are the most common elements of various engineering constructions in which they usually participate as multi-span (continuous) elements reinforced by beams (of the ship skin, of deck plating, of platforms, etc.).

Under oscillations in a fluid, velocity fields caused by a motion of a single plate span and the ones caused by a motion of the whole continuous construction are different in general because of flow of fluid from one span to another. The character of the fluid flow then depends on the nature of oscillations of a multi-span plate. To determine added masses of a continuous plate, let us consider oscillations of a rectangular panel (Fig. 6.1) reinforced by parallel stiffeners[2] attached to a screen and contacting with fluid from one side. We assume stiffeners to be rigid and non-deforming[3] and the plate to be flexible only in spans between the stiffeners.

Expressing plate oscillations in the form

$$Z(x, y, t) = w(t)\psi(x, y),$$

where x and y are the Cartesian coordinates, t is time, $w(t)$ is the generalized coordinate, and $\psi(x, y)$ is the function of elastic oscillations of a continuous plate, we replace the influence of an oscillating plate by the action of simple sources of capacity $q = \partial Z/\partial t$ continuously distributed over the surface s of the plate. Then, by virtue of (6.3), the expression for the kinetic energy of surrounding fluid is

$$T = \frac{\rho}{4\pi} \iint_S \frac{\partial Z}{\partial t}\, dS' \iint_S \frac{\partial Z}{\partial t} \frac{dS}{r}$$

or

$$T = \frac{\rho}{4\pi} \dot{w}^2 \iint_S \psi\, dS' \iint_S \psi \frac{dS}{r}. \tag{6.6}$$

[2] Panels reinforced by parallel stiffeners are often called fields.

[3] For the solution of the problem for a plate with flexible stiffeners, see Sect. 6.9.

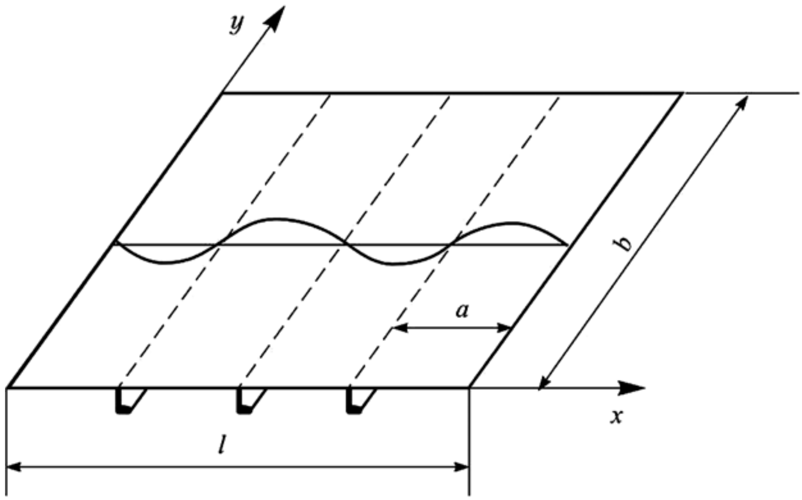

Fig. 6.1 The panel reinforced by parallel stiffeners

Here ρ is the fluid density, r is the distance between the points s and s', and $\dot{w}$ is the generalized velocity.[4]

The coefficient of the generalized coordinate in expression (6.6) is the added mass of the plate whose oscillations are described by the function $\psi(x, y)$. In actual calculations, dimensionless coefficients of added masses are more convenient [202],

$$\mu\left(\frac{l}{nb}\right) = \frac{n}{2\pi l} \frac{\iint_S \psi \, dS' \iint_S \psi \frac{dS}{r}}{\iint_S \psi^2 \, dS}, \tag{6.7}$$

where l and b are the lengths of the panel (continuous plate) sides (see Fig. 6.1), $l/n = a$ is the length of a single span of the continuous plate, and n is the number of spans into which the panel side l is separated by the stiffeners (the number of spans of the continuous plate participating in motion).

The added mass per the plate unit area is then

$$m = \rho \frac{l}{n} \mu\left(\frac{l}{nb}\right). \tag{6.8}$$

The coefficient $\mu(l/nb)$ depends therefore on the shape of oscillations of a continuous plate, on the number of spans involved in the oscillations, and on the ratio of sides of the supporting contour.

[4]The dot over the symbol indicates differentiation in time.

The numerical integration provided the coefficients [202] $\mu(l/nb)$ for the following forms of the plate oscillations (the axis y is directed along the stiffeners):

$$\left.\begin{aligned}
&\psi(x,y)=\sin\frac{n\pi x}{l}\sin\frac{\pi y}{b}; \qquad \psi(x,y)=\sin^2\frac{n\pi x}{l}\sin^2\frac{\pi y}{b};\\
&\psi(x,y)=\sin^2\frac{n\pi x}{l}\sin\frac{\pi y}{b}; \qquad \psi(x,y)=\sin\frac{n\pi x}{l};\\
&\psi(x,y)=\sin^2\frac{n\pi x}{l}.
\end{aligned}\right\} \tag{6.9}$$

The main difficulty in finding the coefficient μ is the evaluation of the integral

$$K=\iint_S \psi\, dS' \iint \psi \frac{dS}{r}. \tag{6.10}$$

For the circular plate, this integral was calculated exactly [133]. Calculating this integral for the rectangular one-span plate is difficult and was therefore performed by Babaev [10] only approximately.

Let us denote

$$F(x',y')=\iint \frac{\psi(x,y)}{r}\, dS. \tag{6.11}$$

Then

$$K=\iint_S F(x',y')\psi(x',y')\, dS'.$$

We split the surface of the whole (continuous) plate into a sufficiently large number of equal rectangles and assume the values of the functions F and ψ to be known at the geometrical centers of each of these rectangles. We can then write

$$K\approx \Delta x\Delta y\sum_i\sum_k F_{ik}\psi_{ik}. \tag{6.12}$$

To simplify calculations, we split each side of the plate into an even number of equal intervals, that is, we split the side l into $2nv$ intervals and the side b into $2p$ intervals. Expression (6.12) then becomes

$$K=4\Delta x\Delta y\sum_{i=1}^{nv}\sum_{k=1}^{p} F_{ik}\psi_{ik},$$

where $\Delta x=l/(2nv)$ and $\Delta y=b/(2p)$. Hence,

$$K=\frac{lb}{nvp}\sum_{i=1}^{nv}\sum_{k=1}^{p} F_{ik}\psi_{ik}. \tag{6.13}$$

The functions ψ_{ik} entering (6.13) are calculated for the oscillation forms under study (see (6.9)) as follows:

$$\left.\begin{aligned}
\psi_{ik} &= \sin\frac{(2i-1)\pi}{4v}\sin\frac{(2k-1)\pi}{4p};\\
\psi_{ik} &= \sin^2\frac{(2i-1)\pi}{4v}\sin^2\frac{(2k-1)\pi}{4p};\\
\psi_{ik} &= \sin^2\frac{(2i-1)\pi}{4v}\sin\frac{(2k-1)\pi}{4p};\\
\psi_{ik} &= \sin\frac{(2i-1)\pi}{4v}1; \qquad \psi_{ik} = \sin^2\frac{(2i-1)\pi}{4v}1.
\end{aligned}\right\} \tag{6.14}$$

To calculate F_{ik} we present expression (6.11) in the form

$$F_{ik} = \iint_{S_1}\frac{\psi(x,y)}{r}\,dS + \iint_{S_2}\frac{\psi(x,y)}{r}\,dS. \tag{6.15}$$

The integration in the first term is here performed over the surface S_1 of the element at whose geometrical center we calculate the function F_{ik}, whereas the integration in the second term is performed over the whole remaining surface S_2 of the plate except this element.

The first integral reduces to

$$\begin{aligned}
\iint_{S_1}\frac{\psi(x,y)}{r}\,dS &\approx \psi_{ik}\iint_{S_1}\frac{dx\,dy}{r}\\
&= 2\psi_{ik}\big[\Delta x\ln\tan(\beta/2+\pi/4) + \Delta y\ln\tan(\alpha/2+\pi/4)\big],
\end{aligned}$$

where $\alpha = \arctan(\Delta x/\Delta y)$ and $\beta = \arctan(\Delta y/\Delta x)$.

The second term in (6.15) can be calculated using the approximation

$$\iint_{S_2}\frac{\psi(x,y)}{r}\,dx\,dy \approx \Delta x\Delta y\sum_{j=1}^{2nv}\sum_{t=1}^{2p}\frac{\psi_{jt}}{r(x_i;y_k;x_j;y_t)}$$

where the indices j and t take all values except those when simultaneously $j=i$ and $t=k$.

The coefficients $\mu(l/(nb))$ were calculated for the following values of the ratio $l/(nb)$: 0.1; 0.3; 0.5; 0.7; 0.85; 1.0. In expressions (6.14), the number of spans n was taken to be 1, 2, 3, 4, and also $n=6$ for the oscillations of form $\sin\frac{n\pi x}{l}\sin^2\frac{\pi y}{b}$. All the calculations were performed with accuracy within 1%. The graphs of the dependence of the coefficient μ on the ratio of the sides of the supporting contour of the plate $l/(nb)$ for different forms of its oscillations (different kinds of fixation of its edges) are presented in Figs. 6.2–6.6, see [202].

Forms of oscillations under consideration (6.9) correspond to oscillations of the neighbor spans of the plate either in phase or in antiphase, i.e., they represent either the so-called symmetric or antisymmetric forms of deformations of continuous plates.

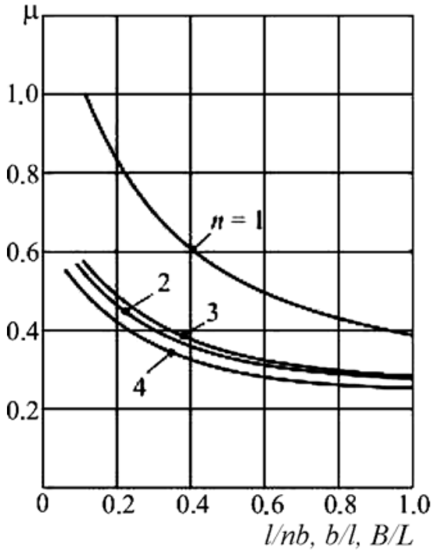

Fig. 6.2 The graph of dependence of the added mass coefficient μ on the ratio of sides of the plate freely supported along all the edges, $\psi(x, y) = \sin(n\pi x/l)\sin(\pi y/b)$

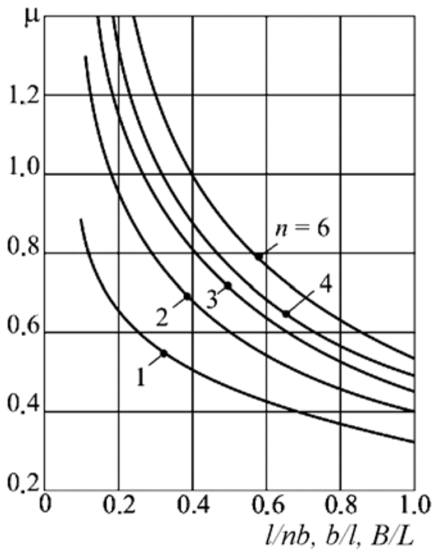

Fig. 6.3 The graph of dependence of the added mass coefficient μ on the ratio of sides of the plate rigidly clamped along all the edges, $\psi(x, y) = \sin^2(n\pi x/l)\sin^2(\pi y/b)$

The last two cases in expressions (6.9) correspond to the cylindrical deformations of the plate that is either freely supported (antisymmetric form of oscillations) or rigidly clamped (symmetric form of oscillations) along the long edges; this type of oscillations is possible for plates with the ratio of sides $a/b \geq 2.5$.

If a construction is surrounded by fluid from both sides (for instance, by outside water or by fluid in a cistern), one must add the added masses (it is doubled if the

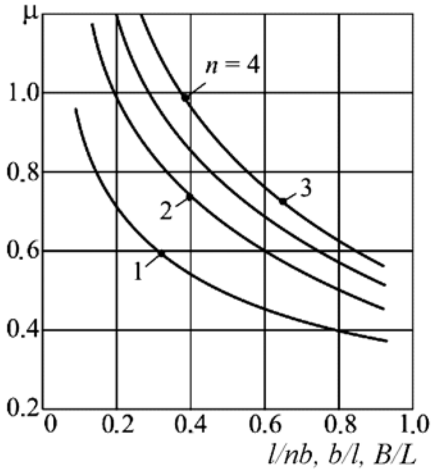

Fig. 6.4 The graph of dependence of the added mass coefficient μ on the ratio of sides of the plate rigidly clamped along one pair of parallel edges and freely supported along the other pair of parallel edges $\psi(x, y) = \sin^2(n\pi x/l) \times \sin(\pi y/b)$

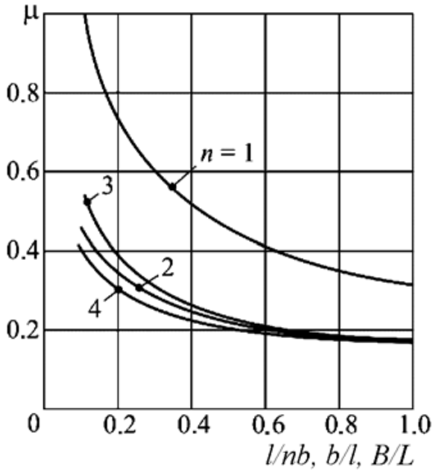

Fig. 6.5 The graph of dependence of the added mass coefficient μ on the ratio of sides of the plate freely supported along the pair of parallel long edges and experiencing cylindrical oscillations $\psi(x, y) = \sin(n\pi x/l)$

fluid density is equal from both sides of the construction):

$$m = \mu\left(\frac{l}{nb}\right)\frac{l}{n}(\rho + \rho_1), \tag{6.16}$$

where ρ and ρ_1 are the densities of fluid from the different sides of the construction.

It is worth mentioning that the curves in Figs. 6.2 and 6.3 for $n = 1$ exactly coincide with the curves obtained by Babaev [10] for the separate plate, which is attached to a rigid screen and is either freely supported or rigidly clamped along its edges.

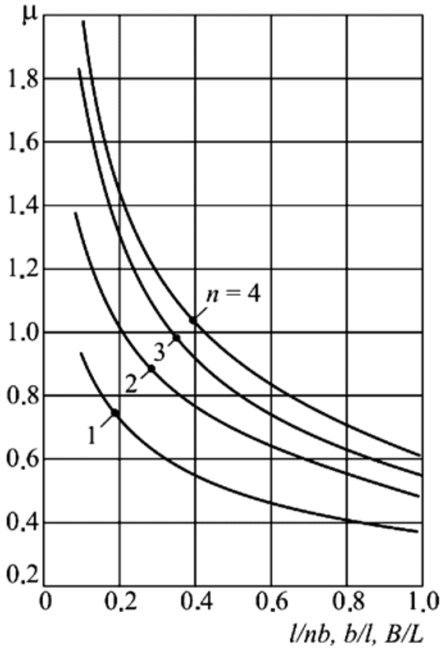

Fig. 6.6 The graph of dependence of the added mass coefficient μ on the ratio of sides of the plate rigidly clamped along the pair of parallel long edges and experiencing cylindrical oscillations $\psi(x, y) = \sin^2(n\pi x/l)$

The generalized added mass of a single span of the plate (with dimensions $a \times b$) whose oscillations have amplitude $\psi(x, y)$ by virtue of formulas (6.7) and (6.8) is

$$M = m \int_0^a \int_0^b \psi^2(x, y)\, dx\, dy. \tag{6.17}$$

Example. Let us find the added mass of the plate of a ship's external plating, which is reinforced by stiffeners and oscillates in the antisymmetric mode. The number of plate spans between longitudinal beams of the prime set (stringers) is $n = 4$. The plate dimensions are: the short side (the distance between stringers) $a = 0.40$ m, the long side $b = 1.60$ m. The construction is surrounded by fluid on both sides: by outer water on one side and by water in a cistern on the other side.

The added mass m per the unit area of the plate surface is given by formula (6.16). The coefficient μ can be found from Fig. 6.2 for the antisymmetric oscillation mode.

When the ratio of the plate sides

$$\frac{a}{b} = \frac{l}{nb} = \frac{0.40}{1.60} = 0.25; \qquad \mu\left(\frac{a}{b}\right) = 0.39,$$

we have

$$m = 2\rho a \mu\left(\frac{a}{b}\right) = 2 \cdot 1.0 \cdot 10^3 \cdot 0.40 \cdot 0.39 = 0.312 \cdot 10^3 \text{ kg/m}^2.$$

Here $\rho = 1.0 \cdot 10^3 \mathrm{kg/m^3}$ is the water density.

By virtue of formula (6.17), the generalized added mass of the plate is

$$M = m \int_0^a \int_0^b \psi^2(x, y)\, dx\, dy = m \int_0^a \int_0^b \sin^2 \frac{\pi x}{a} \sin^2 \frac{\pi y}{b}\, dx\, dy$$
$$= 0.312 \cdot 10^3 \frac{0.40 \cdot 1.60}{4} = 0.5 \cdot 10^2 \text{ kg}.$$

At plate thickness $\delta = 1.2 \cdot 10^{-2}$ m and for the steel ship's hull ($\rho_{\mathrm{m}} = 7.85 \cdot 10^3$ kg/m^3), the added mass corresponding to the antisymmetric mode of the plating oscillations (with water on both sides) is $m/m_{\mathrm{M}} = \frac{0.312 \cdot 10^3}{7.85 \cdot 10^3 1.2 \cdot 10^{-2}} = 3.3$ times bigger than the mass of the plate itself.

6.4 Plate Immersed in a Compressible Fluid in the Presence of a Solid Boundary

We consider the influence of a solid boundary on the added masses on the example of an infinite plane plate oscillating in an ideal compressible fluid in antisymmetric modes in two mutually perpendicular directions. Plate oscillations are assumed to be stable and harmonic in time. Taking into account linearity of the problem, we consider one Fourier harmonic of oscillation displacement described by the function

$$w(x, y, t) = f e^{i\omega t} \sin \frac{\pi x}{a} \sin \frac{\pi y}{b},$$

where f and ω are the respective amplitude and frequency of oscillations, a and b are the lengths of half-waves in the directions of axes x and y (Fig. 6.7), and t is time. The function w is complex-valued, and reality of displacement is restored in physically realistic situations when one considers a linear combination of various harmonics.

The motion of ideal compressible fluid is described by the wave equation

$$\frac{\partial^2 \varphi}{\partial x^2} + \frac{\partial^2 \varphi}{\partial y^2} + \frac{\partial^2 \varphi}{\partial z^2} = \frac{1}{c_0^2} \frac{\partial^2 \varphi}{\partial t^2}, \tag{6.18}$$

where φ is the potential of fluid velocities and c_0 is the sound velocity in the fluid.

Wave equation (6.18) must be supplemented by the following boundary conditions:

(1) the normal components of the fluid and plate velocities are equal on the plate surface, i.e.,

$$\text{for } z = 0, \quad \frac{\partial \varphi}{\partial z} = \frac{\partial w}{\partial t}; \tag{6.19}$$

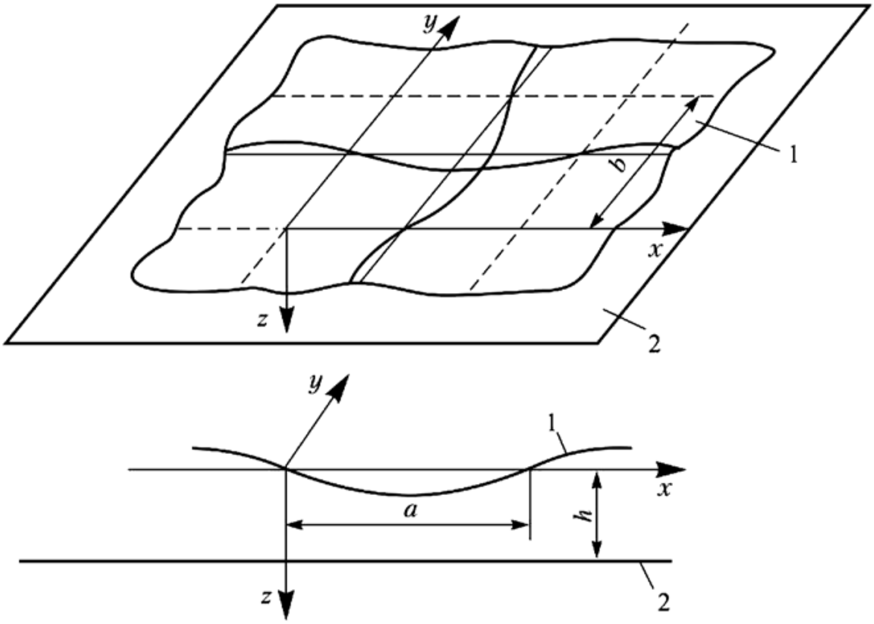

Fig. 6.7 An infinite plate oscillating near the solid boundary *1*—the plate; *2*—the solid boundary

(2) the condition of impenetrability of the solid boundary

$$\text{for } z = h, \quad \frac{\partial \varphi}{\partial z} = 0, \tag{6.20}$$

where h is the distance between the plate and the solid boundary (the boundary is parallel to the plate).

Because the fluid motion is stable, we consider only one harmonic and seek the solution of wave equation (6.18) in the form (this solution is complex, but a final linear combination of such solutions having a physical meaning should be real)

$$\varphi(x, y, z, t) = \psi(x, y, z)e^{i\omega t}. \tag{6.21}$$

Substituting (6.21) in Eq. (6.18), we obtain the equation on the function $\dot{\psi}(x, y, z)$:

$$\frac{\partial^2 \psi}{\partial x^2} + \frac{\partial^2 \psi}{\partial y^2} + \frac{\partial^2 \psi}{\partial z^2} + \left(\frac{\omega}{c_0}\right)^2 \psi = 0. \tag{6.22}$$

The boundary conditions for $\psi(x, y, z)$ by virtue of (6.19) and (6.20) are

$$\begin{aligned} &\text{for } z = 0, \quad \frac{\partial \psi}{\partial z} = i f \omega \sin\frac{\pi x}{a} \sin\frac{\pi y}{b}; \\ &\text{for } z = h, \quad \frac{\partial \psi}{\partial z} = 0. \end{aligned} \tag{6.23}$$

Looking for the solution of Eq. (6.22) in the form

$$\psi(x, y, z) = Z(z) \sin \frac{\pi x}{a} \sin \frac{\pi y}{b}, \tag{6.24}$$

where $Z(z)$ is a function of a single argument z (we assume that the axis z is directed perpendicular to the plate), and substituting ansatz (6.24) in Eq. (6.22), we obtain

$$\frac{d^2 Z}{dz^2} - a^2 Z = 0, \tag{6.25}$$

where

$$\alpha = \sqrt{\left(\frac{\pi}{a}\right)^2 + \left(\frac{\pi}{b}\right)^2 - \left(\frac{\omega}{c_0}\right)^2}. \tag{6.26}$$

The boundary conditions for Eq. (6.25) by virtue of (6.23) are:

$$\begin{aligned} &\text{for } z = 0, \quad \frac{dZ}{dz} = if\omega; \\ &\text{for } z = h, \quad \frac{dZ}{dz} = 0. \end{aligned} \tag{6.27}$$

The solution of Eq. (6.25) can be presented in the form

$$Z(z) = C_1 e^{az} + C_2 e^{-az}, \tag{6.28}$$

with C_1 and C_2 arbitrary constants.

For solution (6.28) to satisfy boundary conditions (6.27), we must set

$$\begin{aligned} C_1 &= -\frac{if\omega}{a} \frac{e^{-ah}}{e^{ah} - e^{-ah}}; \\ C_2 &= -\frac{if\omega}{a} \frac{e^{ah}}{e^{ah} - e^{-ah}}. \end{aligned} \tag{6.29}$$

By virtue of expressions (6.21), (6.24), (6.28), and (6.29), the desired potential of fluid velocities is

$$\varphi(x, y, z, t) = -\frac{if\omega}{a} e^{i\omega t} \frac{e^{a(h-z)} + e^{-a(h-z)}}{e^{ah} - e^{-ah}} \sin \frac{\pi x}{a} \sin \frac{\pi y}{b}.$$

The pressure on the plate surface (at $z = 0$) caused by its oscillations and calculated by a linearized Cauchy integral is

$$\begin{aligned} p = -\rho \frac{\partial \varphi}{\partial t}\bigg|_{z=0} &= \rho \frac{f\omega^2}{\alpha} e^{i\omega t} \frac{e^{\alpha h} + e^{-\alpha h}}{e^{\alpha h} - e^{-\alpha h}} \sin \frac{\pi x}{a} \sin \frac{\pi y}{b} \\ &= \rho \frac{f\omega^2}{\alpha} e^{i\omega t} \frac{1}{\operatorname{th} ah} \sin \frac{\pi x}{a} \sin \frac{\pi y}{b}. \end{aligned}$$

To calculate the added mass, we first find the generalized force caused by the fluid pressure on the plate part of dimensions $a \times b$:

$$P = \int_0^a \int_0^b p \sin\frac{\pi x}{a} \sin\frac{\pi y}{b}\, dx\, dy = \rho \frac{ab}{4}\frac{f\omega^2}{\alpha} e^{i\omega t}\frac{1}{\tanh \alpha h}.$$

Because $f\omega^2 e^{i\omega t}$ is the acceleration of the middle of the plate part under consideration, its proper added mass is[5]

$$M_{\text{ad}} = \rho \frac{ab}{4\alpha}\frac{1}{\tanh \alpha h}. \tag{6.30}$$

The added mass per unit area of the multi-span plate, calculated with accounting for the number of oscillating spans and in the presence of the solid boundary, is given by the formula

$$m = \rho \frac{l}{n} \mu\left(\frac{l}{nb}\right) \beta(\alpha, h),$$

where $l/n = a$ is the distance between the nodal lines or the stiffeners, n is the number of oscillating spans of the multi-span plate, $\mu(l/nb)$ is the added mass coefficient determined by Figs. 6.2–6.6, and $\beta(\alpha, h)$ is the coefficient taking into account the influence of the solid boundary and depending on the distance h between the plate and the boundary and on the conditions of fixing the plate on the supporting contour (on the oscillation type) characterized by the parameter α.

At the antisymmetric type of oscillations, the coefficient $\beta(\alpha, h) = \tanh(\alpha h)$ in the case where the fluid is constrained between the plate and the solid boundary and $\beta(\alpha, h) = 1 + 1/\tanh(\alpha h)$ in the case where the fluid is unlimited on the one side of the plate and is constrained by the solid boundary on the other side of the plate.

The obtained results indicate that the influence of the fluid compressibility is characterized by the ratio ω/c_0 (see formula (6.26)). If the square of this ratio is small as compared with the first two terms, then we may neglect the influence of the compressibility. Let a be the smallest half-wave length (or the interval between the stiffeners); then the condition

$$\left(\frac{\omega}{c_0}\right)^2 \le \left(\frac{\pi}{a}\right)^2$$

is satisfied if

$$\tau > 2T, \tag{6.31}$$

where $\tau = 2\pi/\omega$ is the period of plate oscillations and $T = 2a/c_0$ is the time during which the sound wave in fluid travels the distance equal to the doubled length of the shortest half-wave.

[5]The solution was obtained by V.A. Rodosskii.

Calculations of frequencies of oscillations of a ship's hull plates and other engineering constructions demonstrate that condition (6.31) is usually satisfied, and one can therefore neglect the fluid compressibility when considering antisymmetric types of oscillations of plates (and circular cylindrical shells). The expression for α is then

$$\alpha = \pi\sqrt{\frac{1}{a^2} + \frac{1}{b^2}}.$$

Besides, formula (6.30) yields that the added mass increases as the distance h between the solid boundary and the plate decreases.

We now find the minimal distance to the solid boundary at which we can neglect its influence on the fluid added mass, say, at which this influence will not exceed 10%. This is equivalent to the condition

$$\frac{1}{\tanh(\alpha h)} = \frac{e^{\alpha h} + e^{-\alpha h}}{e^{\alpha h} - e^{-\alpha h}} < 1.1, \quad \text{or} \quad e^{2\alpha h} > 21,$$

whence

$$2\alpha h > \ln 21 \text{ or } h > \frac{3.04}{2\pi\sqrt{a^{-2} + b^{-2}}}. \tag{6.32}$$

Inequality (6.32) yields

– for the plate oscillating in a cylinder-like mode ($b \to \infty$), $h > 0.484a$;
– for the square plate ($a = b$), $h > 0.342a$.

Therefore, if the distance between the plate and the solid boundary is greater than the half-length of the short half-wave of the plate ($h > a/2$), experiencing antisymmetric oscillations, then we can neglect the influence of the solid boundary on the added masses.

If the infinite plate reinforced by parallel stiffeners and oscillating in the symmetric mode (all spans oscillate in the same phase) is located near the solid boundary, then, due to the fluid incompressibility and the absence of its flow between the spans, the added mass becomes infinite.

6.5 Added Masses of Ship Hull Grillages and Fields

Grillages of ship hulls and other structures are systems of cross stiffeners (Fig. 6.8) sheathed with plating. Fields are parts of plating confined between prime and cross boarding joists and reinforced by parallel stiffeners. The nature of deformations of such plating, or of the field, is the same as the one of the plate restricted by its bounding contour. When determining the added masses of fields we can therefore apply the principles and formulas obtained for plates.

The added masses caused by grillage oscillations and taken per unit area of the grillage are determined by the respective formulas [204]

$$m_{\text{rel}} = \rho B\mu(B/L); \qquad m_{\text{ad}} = \rho b\mu(b/l), \tag{6.33}$$

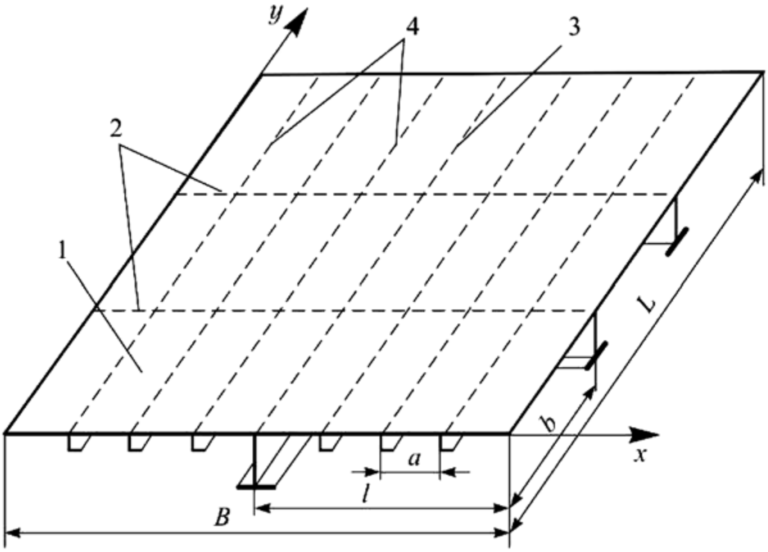

Fig. 6.8 The scheme of the ship hull grillage. *1*—plating; *2*—prime boarding joists; *3*—cross boarding joist; *4*—cross stiffeners

where B and L are the dimensions of the grillage and b and l are the dimensions of the field.

The coefficients $\mu(B/L)$ and $\mu(b/l)$ can be determined from Figs. 6.2–6.6 depending on the ratio of sizes of the supporting contour of the construction (the grillage or the field), on the type of its oscillations and on whether the neighbor constructions participate in motion (the number n).

For the bottom platings whose sizes are close to the transversal dimensions of the ship hull, the added masses must be determined taking into account the free water surface, i.e., taking into account the three-dimensional hydrodynamic flow. Rostovtzev [187] solved this problem and plotted the graphs of values of the added mass coefficients k (Fig. 6.9) taking into account the influence of the above factors. In accordance with this solution, for the principal mode of oscillations of the bottom plating of the ship hull, the added mass per unit area is $m_{\mathrm{rel}} = \rho Bk$.

Calculations demonstrate [187] that clamping the grillage on the edges does not substantially affect the value of the added mass per unit area. On the other hand, passing from the oscillations that are symmetric w.r.t. the transverse bulkheads to the oscillations that are antisymmetric reduces the coefficient by a factor of more than two.

Examples of calculations of the added masses of fields and grillages are presented in Sects. 6.9.1 and 6.9.2.

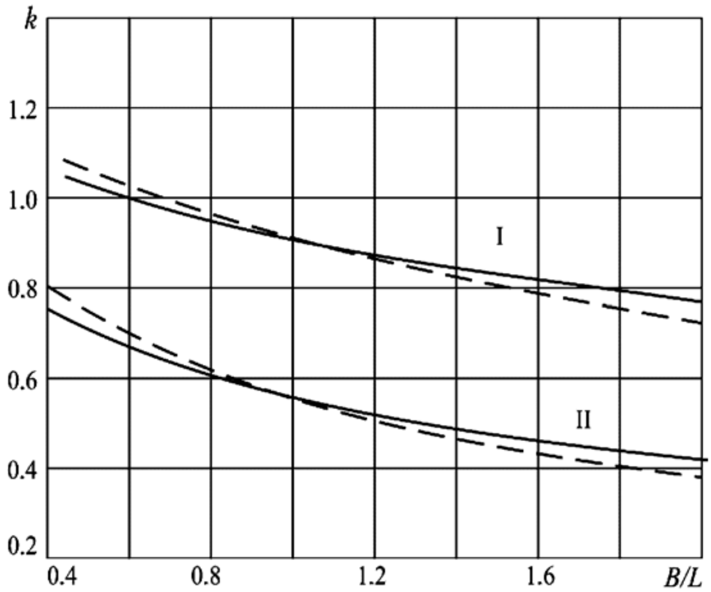

Fig. 6.9 Values of the added mass coefficient for the ship's bottom grillages; *I*—symmetric oscillations; *II*—antisymmetric oscillations; *dashed line*—the grillage is freely supported on the edges; *solid line*—the grillage is rigidly clamped on the edges

6.6 Added Masses of Cantilever Plates

For the first three modes of elastic oscillations of cantilever plates immersed in an unlimited fluid, the added mass per unit length is determined by the formula [132]

$$m = \frac{\pi \rho b^2}{4} \frac{1}{1 + k_i(\delta/b)b/2l}, \tag{6.34}$$

where l is the plate length (measured between the rigidly clamped and the freely supported edges), b and δ are the respective width and depth of the plate, and $k_i(\delta/b)$ is the coefficient determined by Fig. 6.10.

The adjoint inertia moment per unit length of the longitudinal axis of symmetry of the cantilever plate caused by its torsional oscillations is determined by the formula (at $b \gg \delta$)

$$J = \frac{1}{128} \pi \rho b^4. \tag{6.35}$$

The influence of the proximity of the free fluid surface on the added masses and on the inertia moment of the cantilever plate (when the plate surface is parallel to the free water surface) can be taken into account by multiplying the added mass value and the inertia moments calculated by formulas (6.34) and (6.35) by the coefficient k_{surf} determined from Fig. 6.11.

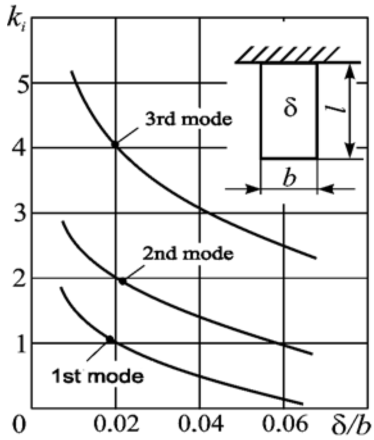

Fig. 6.10 Values of the coefficient determining the influence of elastic displacements of the cantilever plate on the added mass

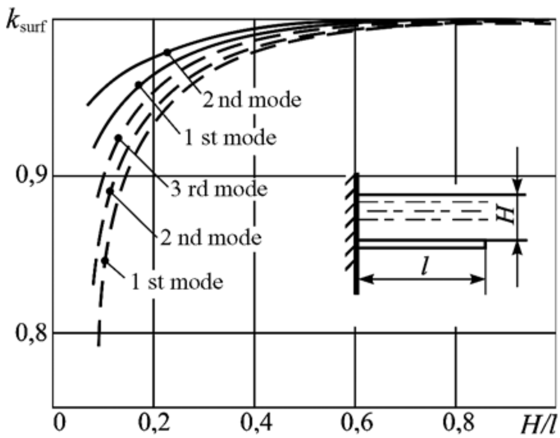

Fig. 6.11 Values of the coefficient determining the influence of the free fluid surface on the added mass of the cantilever plate *solid line*—torsional oscillations; *dashed line*—flexural oscillations

Example. Find the added mass of cantilever plates oscillating in an unlimited fluid for the first three modes of their oscillations. Plate dimensions and the calculation are presented in Table 6.1.

6.7 Added Masses of Shells

To find added masses of fluid involved in the motion of an oscillating shell, we must introduce into the equations describing the shell oscillations the pressure of the perturbed fluid and take into account the continuity of the normal component of the fluid velocity, which must be equal to the velocity of the shell deformation on the surface of the shell.

Table 6.1 Calculation results for added masses of cantilever plates

Plate parameters	Osc. mode	$k_i(\delta/b)$	$(1+k_i(\delta/b)/2l)^{-1}$	m given by (6.34)
$l=0.60$	1	0.95	0.865	$0.865\,\pi\rho b^2/4$
$b=0.20$	2	1.9	0.76	$0.76\,\pi\rho b^2/4$
$\delta=0.5\cdot 10^{-2}$	3	3.75	0.618	$0.618\,\pi\rho b^2/4$
$\delta/b=0.025$				
$l=0.60$	1	~ 0	~ 1	$\pi\rho b^2/4$
$b=0.20$	2	0.9	0.87	$0.87\,\pi\rho b^2/4$
$\delta=0.5\cdot 10^{-2}$	3	2.42	0.712	$0.712\,\pi\rho b^2/4$
$\delta/b=0.075$				

The law of pressure distribution and the one of the velocity of the perturbed fluid can be determined by solving the equations of motion and by taking into account the continuity of an ideal incompressible fluid.

Because it is necessary to find the added masses for types of the shell oscillations both dependent on and independent of the coordinate along the generatrix of the shell (that is, for shells of finite or infinite lengths), we solve this problem in the cases of both flat and spatial fluid flows.

6.7.1 Cylindrical Shell of Infinite Length

In the case of an infinitely long cylindrical shell (for which all the transversal sections oscillate in the same phase, and we can therefore consider it the circle of unit length segregated from the shell by two sections perpendicular to the symmetry axis) the equations of motion and continuity in the polar coordinates r and θ and under the assumption of the smallness of oscillations of the shell and of the ideal fluid are [116]

$$\frac{\partial v_r}{\partial t}=-\frac{1}{\rho}\frac{\partial p}{\partial r};\qquad \frac{\partial v_\theta}{\partial t}=-\frac{1}{\rho r}\frac{\partial p}{\partial \theta};\qquad \frac{\rho}{r}\frac{\partial(r v_r)}{\partial r}+\frac{\rho}{r}\frac{\partial v_\theta}{\partial_\theta}=0, \tag{6.36}$$

where v_r and v_θ are the respective radial and tangential components of the fluid velocity, $p(r,\theta,t)$ is the fluid pressure, ρ is the fluid density, and t is time.

Substituting the components of the fluid velocity from the first two equations of system (6.36) into the third equation, we obtain the following partial differential equation w.r.t. the unknown function p:

$$\frac{\partial}{\partial r}\left(r\frac{\partial^2 p}{\partial r\partial t}\right)+\frac{1}{r}\frac{\partial^3 p}{\partial \theta^2\partial t}=0.$$

Solving this equation, taking into account that the pressure is zero at large distance from the shell, we obtain the formula for the pressure in the outer domain,

$$p(r,\theta,t) = \frac{C}{r^n}\cos n\theta \cos \lambda t, \tag{6.37}$$

where C is the integration constant determined from the boundary condition on the shell surface, n is the number of wave lengths along the shell boundary, and λ is the oscillation frequency.

Substituting expression (6.37) in the first two equations of system (6.36) and integrating the latter, we obtain the formulas determining the velocity components of fluid surrounding the shell:

$$v_r = \frac{C_n}{\rho\lambda r^{n+1}}\cos(n\theta)\sin(\lambda t); \qquad v_\theta = \frac{C_n}{\rho\lambda r^{n+1}}\sin(n\theta)\sin(\lambda t). \tag{6.38}$$

The shell added mass can be determined by the energy method.

The coefficient ν, taking into account the influence of the added mass on the eigenfrequency of the cylindrical shell, is

$$\nu = \frac{\omega_n}{\lambda} = \sqrt{1+\frac{m}{m_{\text{sh}}}} = \sqrt{1+\frac{T}{T_{\text{sh}}}} \tag{6.39}$$

where ω_n and λ are the respective shell eigenfrequencies in air and in the fluid, m is the mass of fluid added per unit area of the shell surface, m_{sh} is the mass of the unit area of the shell surface, T is the kinetic energy of fluid involved in the motion by the oscillating shell, and T_{sh} is the shell kinetic energy.

The kinetic energy of the fluid involved into a motion by an oscillating ring is determined by the formula

$$T = 0.5\rho\int_0^{2\pi}\int_{r_{\text{sh}}}^{\infty}\left(v_r^2+v_\theta^2\right) r\,d\theta\,dr, \tag{6.40}$$

where r_{sh} is the shell radius.

Substituting the values of the velocity components (6.38) into formula (6.40), we obtain

$$T = \frac{\pi\rho n C^2}{2\lambda^2 r^{2n}}\sin^2(\lambda t).$$

The kinetic energy of the oscillating ring of unit length can be expressed analogously,

$$T_{\text{sh}} = \frac{\rho_{\text{sh}}\delta r_o}{2}\int_0^{2\pi}\left(\dot{w}^2+\dot{v}^2\right)d\theta,$$

where ρ_{sh} is the density of the shell material, δ is the shell thickness, and $\dot{w}$ and $\dot{v}$ are the respective normal and tangential components of the ring velocity determined by expressions (6.38) upon the substitution $r = r_{\text{sh}}$.

Substituting the values of $\dot{w}$ and $\dot{v}$ in the formula for the ring kinetic energy, we obtain

$$T_{\rm sh} = \frac{\pi \rho_{\rm sh} \delta r_{\rm sh}}{2} \frac{C^2(n^2+1)}{\rho^2 \lambda^2 r_{\rm sh}^{2n+2}} \sin^2(\lambda t).$$

The squared coefficient ν (6.39) for the cylindrical shell whose form of oscillations does not depend on x (the x-axis is directed along the shell axis of symmetry) is therefore

$$\nu^2 = 1 + \frac{n r_{\rm sh} \rho}{\rho_{\rm sh} \delta (n^2+1)}. \tag{6.41}$$

Comparing equalities (6.39) and (6.41) we find the added mass per unit area of the infinite cylindrical shell oscillating in the antisymmetric mode,

$$m = \frac{n r_{\rm sh} \rho}{n^2+1}. \tag{6.42}$$

It is worth mentioning that the least eigenfrequency of the shell oscillations corresponds to antisymmetric modes of oscillations at which the shell loses stability, which is accompanied by the appearance of a large number of waves along the circular boundary ($n \approx 15$–20 and more).

If we neglect the unity as compared with n^2, then expression (6.42) becomes merely

$$m = \frac{r_{\rm sh} \rho}{n}. \tag{6.43}$$

At the axial-symmetric oscillations of the infinite cylindrical shell (Fig. 6.12b) the notion of added mass becomes nonsense (tends to infinity), that is, the hypothesis of fluid incompressibility becomes invalid. Therefore, one must take into account

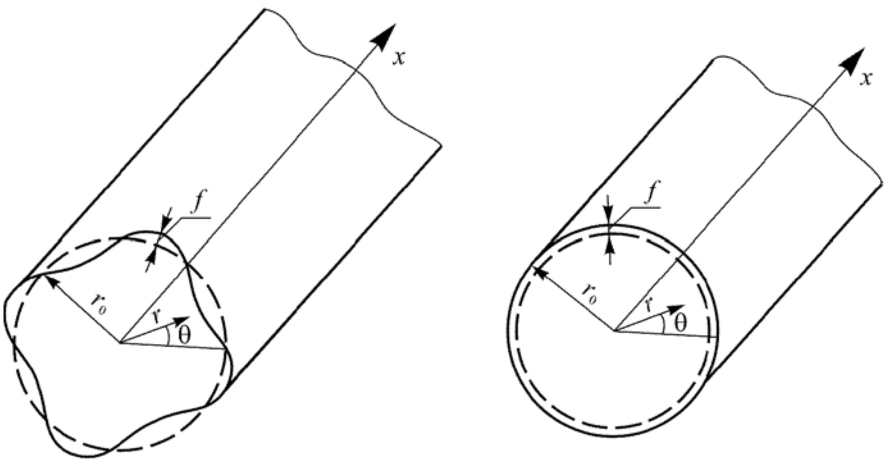

Fig. 6.12 The oscillation modes for the cylindrical shell of infinite length: *left*—antisymmetric; *right*—axial-symmetric; f is the shell oscillation amplitude

fluid compressibility when considering oscillations of the mode $n = 0$ for an infinite shell.

6.7.2 Cylindrical Shell of Finite Length

Equations of motion and continuity at the spatial flow of an ideal incompressible fluid (for a vortex-free motion) can be reduced to a single partial differential equation with the unknown φ, which is the Laplace equation taking the following form in cylindrical coordinates:

$$\frac{\partial^2\varphi}{\partial r^2} + \frac{1}{r}\frac{\partial\varphi}{\partial r} + \frac{1}{r^2}\frac{\partial^2\varphi}{\partial\theta^2} + \frac{1}{r_{\text{sh}}^2}\frac{\partial^2\varphi}{\partial\xi^2} = 0,$$

where $\xi = x/r_0$ and x is the coordinate along the generatrix with the origin at one of the ends of the shell.

Solving the Laplace equation, taking into account the boundary conditions, enables us to determine the components of the fluid velocity: the radial component v_r, the tangential component v_{sh}, and the component along the cylinder generatrix v_Z.

To find the added mass in the case of oscillations of the cylindrical shell of finite length (with n waves along the circle component and k half-waves along the axial component), we use the reasonings analogous to the ones in Sect. 6.7.1.[6]

We substitute the components of the fluid velocity into the formula for the kinetic energy of fluid involved into motion by an oscillating shell,

$$T = 0.5\rho r_{\text{sh}} \int_0^{2\pi} \int_{r_{\text{sh}}}^{\infty} \int_0^{l/r_{\text{sh}}} \left(v_r^2 + v_{\text{sh}}^2 + v_Z^2\right) r\, d\theta\, dr\, d\xi$$

(l is the shell length), simultaneously substituting the components of the shell oscillation velocity $\dot{w}$, $\dot{u}$, and $\dot{v}$ into the formula for the shell kinetic energy

$$T_{\text{sh}} = \frac{\rho\delta r_{\text{sh}}}{2} \int_0^{2\pi} \int_0^{l/r_{\text{sh}}} \left(\dot{w}^2 + \dot{u}^2 + \dot{v}^2\right) d\theta\, d\xi.$$

Omitting rather cumbersome calculations, we eventually obtain the coefficient v squared (see (6.39)), which takes into account the influence of the added mass on the shell eigenfrequencies, in the form

$$\nu^2 = \frac{\omega_n^2}{\lambda^2} = \frac{r_{\text{sh}}(\rho_{\text{sh}}\delta + \mu r_{\text{sh}}\rho)}{\rho_{\text{sh}}\delta r_{\text{sh}}} = 1 + \mu\frac{r_{\text{sh}}\rho}{\rho_{\text{sh}}\delta}, \tag{6.44}$$

where

$$\mu = \frac{1}{\sqrt{n^2 + \gamma_k^2}(1 + \frac{\gamma_k^2}{2(n^2+\gamma_k^2)^{3/2}})}. \tag{6.45}$$

[6]The solution was obtained by Novozhilov and Lefonova.

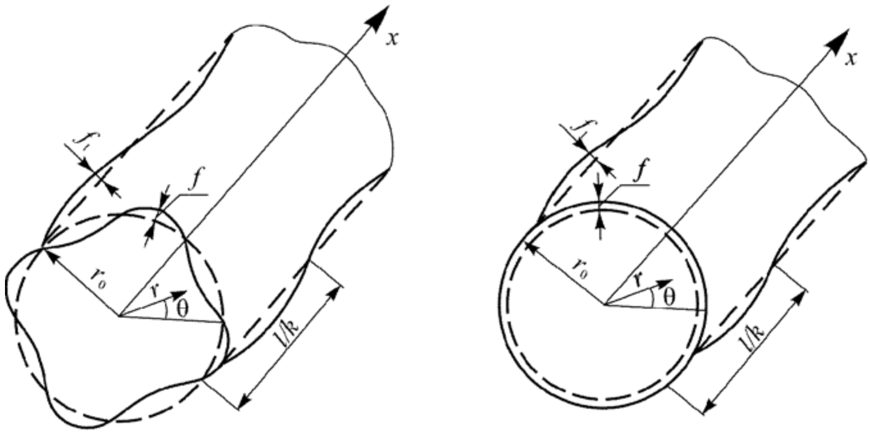

Fig. 6.13 The oscillation modes for the cylindrical shell of a finite length: *left*—antisymmetric; *right*—axial-symmetric; f and f_1 are the shell oscillation amplitudes

The added mass per unit area of the surface is therefore

$$m_{kn} = \mu r_{\text{sh}} \rho. \tag{6.46}$$

We use the following notation in expressions (6.44)–(6.46): μ is the dimensionless coefficient of the shell added mass, $\gamma_k = k\pi r_{\text{sh}}/l$, r_{sh} and l are the respective radius and the length (the size along the generatrix) of the shell, and k is the number of half-waves of the oscillation mode along the shell generatrix (Fig. 6.13a).

The number of waves n in the circular dimension that correspond to lacking stability and to the least eigenfrequency of the shell can be determined from Fig. 6.14.

For thin shells, formula (6.46) becomes

$$m_{kn} \approx \frac{r_{\text{sh}} \rho}{\sqrt{n^2 + \gamma_k^2}}, \tag{6.47}$$

because in this case the quantity $\gamma_k^2 (n^2 + \gamma_k^2)^{3/2}$ in expression (6.45) is small as compared to unity.

From dependence (6.47) we can easily obtain the formula determining the added mass of the infinite shell that does not experience deformations in the longitudinal dimension and undergoes n-waves deformation along the circular coordinate, that is, we do not allow fluid flows along the shell axis. Setting $\gamma_k = 0$ (i.e. $l \to \infty$) in (6.47), we obtain formula (6.43).

Comparing formulas (6.43) and (6.47) we obtain that with the increase of the number of waves in the circular direction, which is specific for a thin-wall shell of large radius, the influence of the fluid flow along the shell surface on the added masses decreases. We can neglect this influence if the wavelengths in the circular and longitudinal directions satisfy the inequality $n^2 \gg \gamma_k^2$.

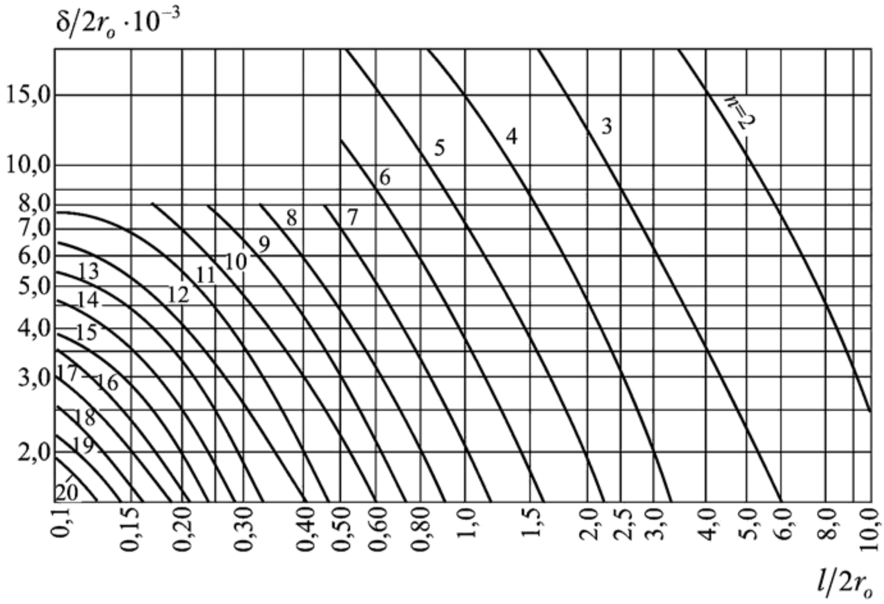

Fig. 6.14 The dependence of the number of waves in the circular dimension at which the cylindrical shell loses stability on the parameters of the shell

The above formulas were obtained under the assumption that the shell contacts fluid only from one side. If the fluid is on both sides of the shell, the added mass must be doubled.

For the added mass of the shell reinforced by the longitudinal stiffeners participating in oscillations, formulas (6.45) and (6.46) remain valid, but the values of quantities in these formulas must be changed.

We take the shell thickness to be the reduced thickness equal to

$$\delta_{\text{red}} = \delta + \frac{sF}{L},$$

where δ is the depth of the plating, s is the number of stiffeners along the shell length, F is the cross-section of the transversal stiffener, L is the shell length, $\gamma_k = k\pi r_{\text{sh}}/L$, and n is the number of waves along the circular direction created when a stiffener loses stability.

At the axial-symmetric oscillations of a shell of a finite length (Fig. 6.13b), the added mass per the unit area of the shell surface can be calculated using formulas (6.45) and (6.46) setting $n = 0$, i.e., $m_{kn} = 2r_{\text{sh}}\rho/(2\gamma_k + 1)$, or approximately $m_{kn} \approx r_{\text{sh}}\rho/\gamma_k$.

In Table 6.2 we present the added mass per unit area of the cylindrical shell caused by the shell oscillations in the antisymmetric mode with the least eigenfrequency (with the number of waves along the circular direction that corresponds to losing stability) and with one half-wave along the generatrix. We consider two cases: the non-reinforced shell and the reinforced shell.

Table 6.2 The added masses of the cylindrical shell

Shell	r_0	th.	l	n	k	γ_k	μ	m
Non-reinforced	100	0.6	15	18	1	21	$\frac{1}{27.7}$	37.0
With one stiffener	100	0.662	30	8	1	10.5	$\frac{1}{13.2}$	77.5

In Table 6.2 r_0 is the radius (cm); th. is the shell thickness (for non-reinforced case) or modified thickness (for reinforced case); l is the shell length; n is the number of waves when the shell loses its stability; k is the number of half-waves along the shell generating line; $\gamma_k = k\pi r_0/l$; μ is the coefficient of the added mass; m is the added mass per unit of the shell area, (kg/m^2).

6.8 Effect of a Solid Boundary on Added Masses of Shells

We estimate the influence of the solid boundary on the shell added mass on the example of oscillations of the thin (elastic) shell near the absolutely rigid cylindrical boundary situated co-centrically w.r.t. the shell (Fig. 6.15). For this we use the basic dependencies of the theory of incompressible fluid. We consider the plane fluid motion whose equation reads

$$\frac{\partial^2\varphi}{\partial r^2} + \frac{1}{r}\frac{\partial\varphi}{\partial r} + \frac{1}{r^2}\frac{\partial^2\varphi}{\partial\theta^2} = 0 \tag{6.48}$$

in the polar coordinates.

The boundary conditions are

$$\text{for } r = R, \quad \frac{\partial\varphi}{\partial r} = 0;$$
$$\text{for } r = r_{\text{sh}}, \quad \frac{\partial\varphi}{\partial r} = a\lambda\cos(n\theta)\cos(\lambda t),$$

where φ is the velocity potential for the fluid perturbed by the shell oscillations, r_{sh} and R are the respective radiuses of the thin and absolutely rigid (solid boundary) shells, a and λ are the respective amplitude and frequency of the shell oscillations, and n is the number of waves along the shell perimeter.

We seek the solution of Laplace equation (6.48) for the case of stable small oscillations of fluid under consideration in the form

$$\varphi(r,\theta,t) = \psi(r)\cos(n\theta)\cos(\lambda t). \tag{6.49}$$

Substituting (6.49) in (6.48), we come to the equation

$$\frac{\partial^2\psi}{\partial r^2} + \frac{1}{r}\frac{\partial\psi}{\partial r} - \frac{n^2}{r^2}\psi = 0 \tag{6.50}$$

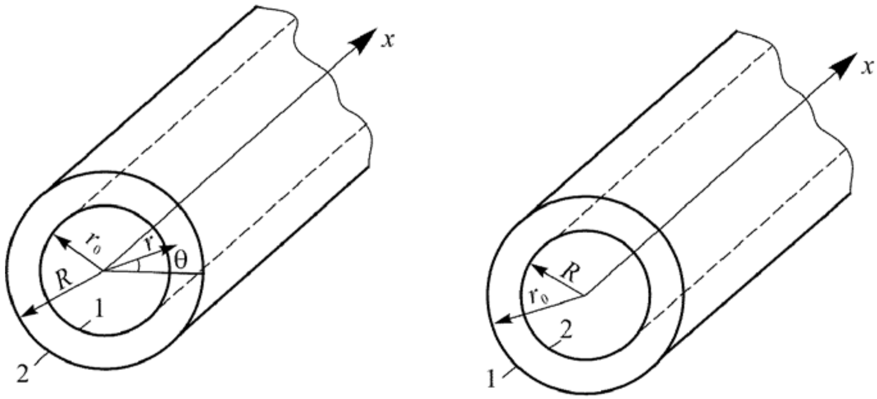

Fig. 6.15 Two co-centric cylindrical shells: *1*—the elastic shell, *2*—the absolutely rigid shell

with the boundary conditions

$$\text{for } r = R, \quad \frac{d\psi}{dr} = 0;$$
$$\text{for } r = r_{\text{sh}}, \quad \frac{d\psi}{dr} = a\lambda. \tag{6.51}$$

Looking for the solution of Eq. (6.50) in the form

$$\psi(r) = Cr^s, \tag{6.52}$$

where C is a constant, and substituting (6.52) in (6.50), we obtain $s = \pm n$.
Therefore,

$$\psi(r) = C_1 r^{-n} + C_2 r^n. \tag{6.53}$$

Imposing boundary conditions (6.51) on solution (6.53), we find

$$C_1 = \frac{a\lambda}{n} \frac{R^{2n}}{r_{\text{sh}}^{n-1} - R^{2n} r_{\text{sh}}^{-(n+1)}}; \qquad C_2 = \frac{a\lambda}{n} \frac{1}{r_{\text{sh}}^{n-1} - R^{2n} r_{\text{sh}}^{-(n+1)}},$$

and the expression for the potential then reads

$$\varphi(r,\theta,t) = \frac{a\lambda}{n} \frac{R^{2n} r^{-n} + r^n}{r_{\text{sh}}^{n-1} - R^{2n} r_{\text{sh}}^{-(n+1)}} \cos(n\theta)\cos(\lambda t).$$

The pressure on the surface of the elastic shell is then

$$p|_{r=r_{\text{sh}}} = -\rho \left.\frac{\partial\varphi}{\partial t}\right|_{r=r_{\text{sh}}}$$
$$= \rho \frac{a\lambda^2 r_{\text{sh}}}{n} \cos(n\theta)\sin(\lambda t)\,\text{sign}(\Delta r) \frac{(r_{\text{sh}}/R)^{2n} + 1}{(r_{\text{sh}}/R)^{2n} - 1}, \tag{6.54}$$

where $\Delta r = r_{sh} - R$ (see Fig. 6.15).

It follows from (6.54) that the influence of the proximity of a solid boundary on the shell added masses is characterized by the last factor taking into account the mutual locations of the elastic and rigid shells (sign Δr), i.e., taking into account whether the rigid shell is located inside or outside the elastic shell.

The added mass per unit area of the shell surface experiencing oscillations with n waves on the circle and with k half-waves along the generatrix can be therefore determined, by virtue of formulas (6.45), (6.47), and (6.54), using the expression[7]

$$m_{kn} = \frac{r_{sh}\rho}{\sqrt{\gamma_k^2 + n^2}} \operatorname{sign}(\Delta r) \frac{(r_{sh}/R)^{2\sqrt{\gamma_k^2+n^2}} + 1}{(r_{sh}/R)^{2\sqrt{\gamma_k^2+n^2}} - 1} \tag{6.55}$$

if the fluid is confined between the shell and the rigid boundary, and using the expression

$$\begin{aligned} m_{kn} &= \frac{r_{sh}\rho}{\sqrt{\gamma_k^2 + n^2}} \operatorname{sign}(\Delta r)\left(1 + \frac{(r_{sh}/R)^{2\sqrt{\gamma_k^2+n^2}} + 1}{(r_{sh}/R)^{2\sqrt{\gamma_k^2+n^2}} - 1}\right) \\ &= \frac{2r_{sh}\rho}{\sqrt{\gamma_k^2 + n^2}} \frac{\operatorname{sign}\Delta r}{1 - (R/r_{sh})^{2\sqrt{\gamma_k^2+n^2}}} \end{aligned} \tag{6.56}$$

if we have a solid boundary on one side of the shell and the unlimited fluid on the other side.

At the plane fluid flow (for an infinite shell) we must set $\gamma_k = 0$ in formulas (6.55) and (6.56).

We can use formulas (6.55) and (6.56) for both closed and non-closed shells (bend plates). In the latter case, the number n is the number of half-waves along the bend edge of a non-closed shell.

We now analyze the influence of the solid boundary on the added masses on the example of an infinite shell. This influence will not exceed 10% if the last multiplier in formula (6.54) does not exceed 1.1, or if

$$(r_{sh}/R)^{2n} > 20. \tag{6.57}$$

The influence of the solid boundary on the value of added masses is therefore diminished with the increase of the number of waves n along the circular boundary of the shell and with the increase in the distance between the shell and the solid boundary r_{sh}/R.

At $n = 20$, inequality (6.57) holds at $r_{sh}/R > 1.1$. The influence of the solid boundary on the added masses of a light shell, which customarily experiences oscillations with a large number of waves along the circular coordinate, is therefore negligible in practically all actual applications.

[7]These formulas were obtained by Schukina in collaboration with Rodosskii.

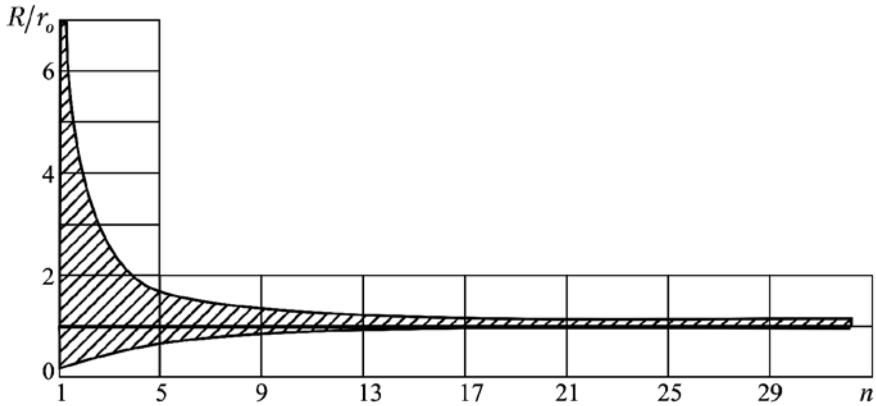

Fig. 6.16 The domain (*hatched*) of combinations R/r_0 and n, in which the shell experiences the influence of the proximity of the solid boundary

The formulas that take into account the influence of the solid boundary on the added mass of fluid confined between two co-centric shells one of which is rigid were also derived in [150]. The results of the above calculations coincide with the ones presented in [150].

In [150], the domain of values of the combinations R/r_{sh} and $n \neq 0$ within which the shell immersed in an incompressible fluid is affected by the presence of the solid boundary was found (the hatched domain in Fig. 6.16). The graph is depicted under the assumption that solid boundaries do not affect added masses if the extra increase of the added mass due to restrictions imposed by bounding the annulus-like layer of fluid in comparison with the added mass in an unlimited fluid does not exceed 1.05 (5%).

6.9 Added Masses at Complex Structure Motion

Above we have considered added masses caused by definite types of motions of either a solid or an elastic body. But in practice many bodies and constructions participate in a complex motion unifying many types or components of oscillation processes. Say, bending oscillations of beam structures (of the ship hull, of overhanging elements like cantilever wings, stabilizers, etc.) in fluid are customarily accompanied by torsional oscillations even in the case where center of masses of transversal sections coincide with the rigidity centers, which ensures the independence of these two types of oscillations for a system in vacuum. Or, for example, beams or other elements of a construction participate simultaneously in the motion together with the bearing structure and in the motion w.r.t. this structure. The grillage plating, first, oscillates with the prime boarding joists and, second, fluctuates w.r.t. these joists. When we have stiffeners reinforcing the plating (see Fig. 6.8), we add one more motion component—the stiffener bending due to the plating.

Each of the motion components of the construction involves into motion a definite amount of fluid—the added mass caused by this type of the construction oscillation. Interaction of the construction with the surrounding fluid is therefore complex, which results in many difficulties when applying the added mass principle: when combining different types of motion, the expression for the kinetic energy of fluid contains scalar products of velocities of components of motion (both radial and angular in the general case), that is, added masses and added inertia moments of fluid caused by different deformation types appear together with added static moments of fluid, which appear due to various combinations of these deformations.

6.9.1 Interaction of Plates with Reinforcing Stiffeners

We consider oscillations of the continuous plate reinforced by elastic stiffeners (Fig. 6.17). Oscillations of a specific mode of such construction can be regarded as oscillations of a system with two degrees of freedom whose motion can be described by a pair of generalized coordinates. The plate displacement can be then presented in the form

$$Z(x, y, t) = w_1(t)\eta(y) + w(t)\psi(x, y),$$

where $w_1(t)$ and $w(t)$ are the generalized coordinates characterizing the respective displacements of stiffeners, and displacements of the plate w.r.t. the stiffeners and

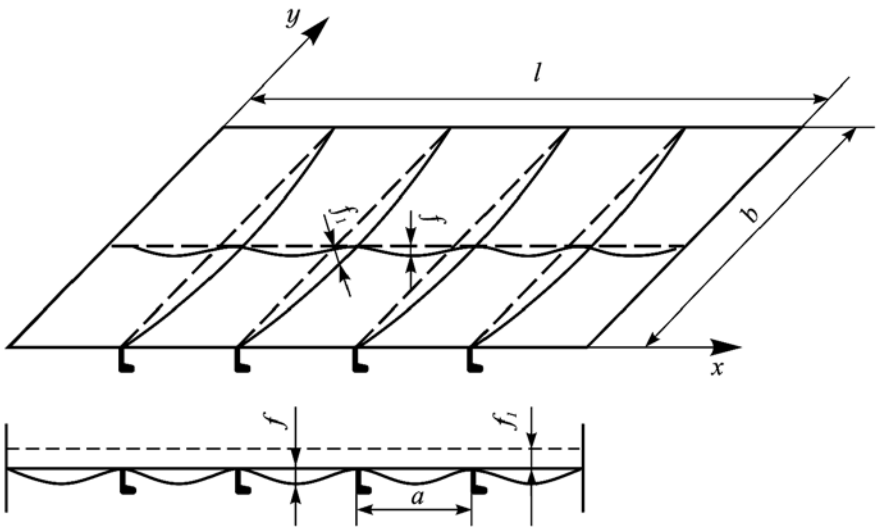

Fig. 6.17 The continuous plate reinforced by elastic stiffeners. The plate is rigidly attached to the stiffeners whereas the stiffeners and the short edges of the plate are freely supported, $\eta(y) = \sin(\pi y/b)$; $\psi(x, y) = \sin^2(n\pi x/l)\sin(\pi y/b)$

$\eta(y)$ and $\psi(x, y)$ are the functions describing the respective shapes of oscillations of stiffeners and the ones of the continuous plate.

The kinetic energy of fluid involved in motion by the oscillating system is, in accordance with expression (6.3),

$$\begin{aligned} T &= \frac{\rho}{4\pi} \iint_S \frac{\partial Z}{\partial t}\, dS' \iint \frac{\partial Z}{\partial t} \frac{dS}{r} \\ &= \frac{\rho}{4\pi} \iint_S (\dot{w}_1 \eta + \dot{w}\psi)\, dS' \iint (\dot{w}_1 \eta + \dot{w}\psi) \frac{dS}{r} \\ &= \frac{\rho}{4\pi} \left[\dot{w}_1^2 \iint_S \eta\, dS' \iint \eta \frac{dS}{r} \right. \\ &\quad + \dot{w}_1 \dot{w} \left(\iint_S \eta\, dS' \iint \psi \frac{dS}{r} + \iint_S \psi\, dS' \iint \eta \frac{dS}{r} \right) \\ &\quad \left. + \dot{w}^2 \iint_S \psi\, dS' \iint \psi \frac{dS}{r} \right]. \end{aligned} \tag{6.58}$$

The first term in expression (6.58) is the added mass of the field, i.e., the one of the continuous plate vibrating together with the stiffeners, whereas the last term is the added mass of the plate oscillating w.r.t. the stiffeners. The added masses of the field M_1 and the one of the plate M can be determined using the added mass coefficient μ, defined in Sect. 6.3,

$$M_1 = \frac{1}{2}\frac{\rho}{\pi} \iint_S \eta(y)\, dS' \iint \eta(y) \frac{dS}{r} = \rho b \mu\left(\frac{b}{l}\right) \int_0^l \int_0^b \eta^2(y)\, dx\, dy,$$

$$\begin{aligned} M &= \frac{1}{2}\frac{\rho}{\pi} \iint_S \psi(x, y)\, dS' \iint \psi(x, y) \frac{dS}{r} \\ &= \rho \frac{l}{n} \mu\left(\frac{l}{nb}\right) \int_0^l \int_0^b \psi^2(x, y)\, dx\, dy \end{aligned}$$

where l and b are the field dimensions and $\mu(b/l)$ and $\mu(l/nb)$ are the coefficients of the added masses caused by the respective oscillations of the field (the stiffeners) and the ones of the plate w.r.t. the stiffeners. They are determined by Figs. 6.2–6.6 depending on the oscillation type, on the ratio of sides of the supporting contour, and on the numbers of spans of the field[8] and the plate.

The sum of two integrals inside the parenthesis in expression (6.58) can be calculated as follows [205].

It was noted in Sect. 6.2 that the action of an oscillating plate on the surrounding fluid is equivalent to the action of simple density sources $(1/2\pi)\dot{Z}$ distributed over

[8]For an isolated field, $n = 1$. If the field enters a more complex structure (say, the grillage), then we take n to be the number of neighbor oscillating fields.

the plate surface. If we assume that we can replace the spatially variable distributions of density sources over the plate surface

$$-(1/2\pi)\dot{w}\psi(x,y) \quad \text{and} \quad -(1/2\pi)\dot{w}_1\eta(y)$$

by the constant sources

$$-(1/2\pi)\dot{w}\tilde{\psi} \quad \text{and} \quad -(1/2\pi)\dot{w}_1\tilde{\eta},$$

where

$$\tilde{\psi} = \sqrt{\frac{\iint_S \psi\, dS' \iint \psi \frac{dS}{r}}{\iint_S dS' \iint \frac{dS}{r}}} \quad \text{and} \quad \tilde{\eta} = \sqrt{\frac{\iint_S \eta\, dS' \iint \eta \frac{dS}{r}}{\iint_S dS' \iint \frac{dS}{r}}},$$

then using the mean value theorem, we obtain

$$\begin{aligned} M_{01} &= \frac{1}{2}\frac{\rho}{\pi}\left(\iint_S \eta\, dS' \iint \psi \frac{dS}{r} + \iint_S \psi\, dS' \iint \eta \frac{dS}{r}\right) \\ &\approx \frac{\rho}{\pi}\sqrt{\left\{\iint_S \eta\, dS' \iint \eta \frac{dS}{r}\right\}\left\{\iint_S \psi\, dS' \iint \psi \frac{dS}{r}\right\}} = 2\sqrt{M_1 M}. \end{aligned}$$

The fluid kinetic energy is therefore

$$T = \frac{1}{2}\left(M_1\dot{w}_1^2 + M_{01}\dot{w}_1\dot{w} + M\dot{w}^2\right).$$

The obtained value of the kinetic energy can be used in various dynamical problems of this construction immersed in a fluid, for instance, in the problem of free and forced oscillations. We stress that the added masses affect frequencies of collective free oscillations of plates and stiffeners (taking into account their interaction) more strongly than partial frequencies of the system, i.e., the frequencies calculated without taking into account interactions between elements of the construction, which seems unnatural at first glance. Let us present the example.

To find equations of motion of the plate reinforced by elastic stiffeners from energy considerations, we begin with expressions for the kinetic and potential energies of the system construction-fluid.

The kinetic energy T_Σ of such a system comprising the kinetic energies of the plate, the stiffeners, and fluid surrounding the system can be presented in the form

$$T_\Sigma = \frac{1}{2}\left[\dot{w}_1^2\left(M_1^k + M_1\right) + \dot{w}\dot{w}_1\left(2M_{01}^k + M_{01}\right) + \dot{w}^2\left(M^k + M\right)\right],$$

where

$$M_1^k = m_{\mathrm{pl}}\int_0^l\int_0^b \eta^2\, dx\, dy + (n-1)m_{\mathrm{st}}\int_0^b \eta^2\, dy;$$

$$M_{01}^k = m_{\mathrm{pl}}\int_0^l\int_0^b \eta\psi\, dx\, dy; \qquad M^k = m_{\mathrm{pl}}\int_0^l\int_0^b \psi^2\, dx\, dy. \tag{6.59}$$

The potential energy of the system comprising the potential energies of deformations of the plate and of the stiffeners is

$$\Pi = \frac{1}{2}\left(Cw^2 + C_1 w_1^2\right),$$

where

$$C = \frac{E\delta^3}{12(1-\nu^2)} \int_0^l \int_0^b \left[\left(\frac{\partial^2 \psi}{\partial x^2}\right)^2 + \left(\frac{\partial^2 \psi}{\partial y^2}\right)^2 + 2\nu \frac{\partial^2 \psi}{\partial x^2}\frac{\partial^2 \psi}{\partial y^2} + 2(1-\nu)\left(\frac{\partial^2 \psi}{\partial x \partial y}\right)^2 \right] dx\,dy,$$

$$C_1 = (n-1)Ei \int_0^b \left(\frac{\partial^2 \eta}{\partial y^2}\right)^2 dy. \tag{6.60}$$

We have introduced the following notation in expressions (6.59) and (6.60): δ is the plate thickness, m_{pl} is the mass per unit area of the plate, m_{st} is the mass per unit length of the stiffener (without the joining band), i is the inertia moment of the stiffener cross-section (with the joining band), $n-1$ is the number of stiffeners reinforcing the plate, and E and ν are the respective coefficient of normal elasticity and the Poisson coefficient of the construction material.

Using the Lagrange equations

$$\frac{d}{dt}\left(\frac{\partial T_\Sigma}{\partial \dot{w}_i}\right) + \frac{\partial \Pi}{\partial w_i} = 0,$$

we obtain the system of differential equations describing the construction oscillations:

$$\ddot{w} + A_0 \ddot{w}_1 + A_1 w = 0, \qquad \ddot{w}_1 + A_2 \ddot{w} + A_3 w_1 = 0, \tag{6.61}$$

where A_0, A_1, A_2, and A_3 are the quantities depending on the construction parameters, on conditions of its fixation on the contour (on the oscillation type), and on the conditions of its interaction with fluid:

$$A_0 = \frac{M_{01}^k + 0.5M_{01}}{M^k + M}; \qquad A_1 = \frac{C}{M^k + M};$$

$$A_2 = \frac{M_{01}^k + 0.5M_{01}}{M_1^k + M_1}; \qquad A_3 = \frac{C_1}{M_1^k + M_1}.$$

Here A_1 and A_3 are the squares of the proper partial (calculated under the assumption of isolated work) frequencies of plates and of the stiffeners.

Considering harmonic construction oscillations and equating to zero the determinant of system of Eqs. (6.61), we obtain the formula for determining eigenfrequencies of plate and stiffeners, taking into account their interactions and the influence

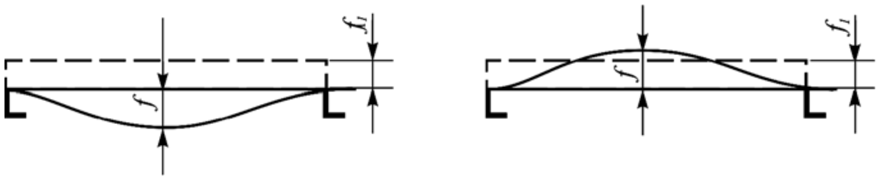

Fig. 6.18 The cross-section of modes of the joint oscillations of the plate and the reinforcing stiffeners; f_1 is the stiffener bending, f is the plate bending w.r.t. stiffeners, the *dashed line* indicates the equilibrium position, and the *solid line* indicates the position during the deformation process

of the environment [204]:

$$\lambda_{1.2}^2 = \frac{A_1 + A_3 \pm \sqrt{(A_1 + A_3)^2 - 4A_1 A_3(1 - A_0 A_2)}}{2(1 - A_0 A_2)}. \tag{6.62}$$

The limits of values of joint frequencies of plate and stiffeners become wider as compared with their partial frequencies, that is, the least among the partial frequencies decreases whereas the highest increases. Calculations of actual ship plates reinforced by stiffeners have demonstrated that the highest frequency may become several times higher approaching the corresponding frequency of oscillation of the construction in air. This is understandable: at the first frequency of the joint oscillations, stiffeners (the field) and the plate oscillate in the same phase (Fig. 6.18a), that is, the influence of added masses increases. At the second frequency when the field and separate plates oscillate in antiphase (Fig. 6.18b), a partial compensation of action of the added masses on the construction takes place. For special relations between amplitudes of the motion components, the second eigenfrequency of the construction may approach the one for the construction in air.

Note that the mechanical compliance of the set (w.r.t. transversal shifts) is important for those forms of oscillations of a continuous structure in which its spans oscillate in phase.[9] In this case, calculations of free and forced oscillations of plates and stiffeners must be performed with accounting for their interaction, which becomes stronger in the presence of the surrounding fluid.

We now present expressions for the quantities entering formula (6.62) for the main, most interesting practically, conditions of fixation of plates and reinforcing stiffeners on the supporting contour [204].

[9]For the symmetric forms of oscillations of a multi-span plate, its supporting frame behaves as an elastic one (elastic joists), whereas the same supporting frame behaves as a rigid frame for the antisymmetric forms of oscillations. This is due to the direction of forces acting on the joists of a continuous structure from the neighbor spans. These forces act in the same direction in the first case and they act in opposite directions in the second case.

(1) The plate is rigidly attached to stiffeners whereas the stiffeners and the short edges of the plate are freely supported (see Fig. 6.17):

$$\left.\begin{aligned}
A_0 &= \frac{4}{3m^*}\left(m_{\text{pl}} + \sqrt{\frac{3}{2}m_{\text{ad}}m}\right);\\
A_1 &= \frac{16D\pi^4}{3a^4m^*}\left[1 + 0.5\left(\frac{a}{b}\right)^2 + \frac{3}{16}\left(\frac{a}{b}\right)^4\right];\\
A_2 &= \frac{1}{2\cdot m^*_{\text{p+s}}}\left(m_{\text{pl}} + \sqrt{\frac{3}{2}m_{\text{ad}}m}\right);\\
A_3 &= \left(\frac{\pi}{b}\right)^4\frac{Ei}{m^*_{\text{p+s}}a}.
\end{aligned}\right\} \tag{6.63}$$

(2) The plate is rigidly clamped along the contour and the stiffeners are rigidly clamped at their ends (Fig. 6.19):

$$\left.\begin{aligned}
A_1 &= \frac{16D\pi^4}{3a^4m^*}\left[1 + \frac{2}{3}(a/b)^2 + (a/b)^4\right];\\
A_3 &= 16/3(\pi/b)^4\frac{Ei}{m^*_{\text{p+s}}a};
\end{aligned}\right\} \tag{6.64}$$

whereas A_0 and A_2 are determined by the corresponding expressions from Eq. (6.63).

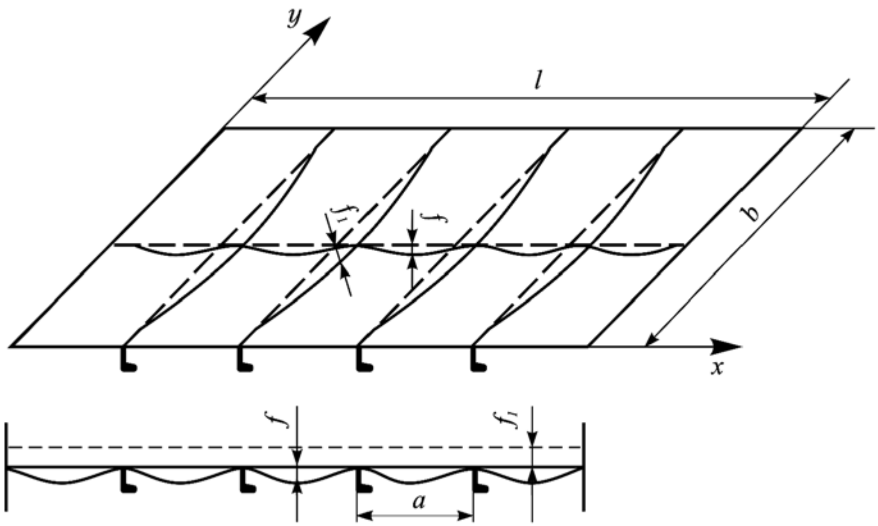

Fig. 6.19 The continuous plate reinforced by elastic stiffeners. The plate and the stiffeners are rigidly clamped along the supporting contour, $\eta(y) = \sin^2(\frac{\pi y}{b})$, $\psi(x, y) = \sin^2(\frac{n\pi x}{l})\sin^2(\frac{\pi y}{b})$

We have introduced the following notation in expressions (6.63) and (6.64): m_{pl} and $m^*_{\mathrm{p+s}}$ are the respective masses per unit area of the plate and of the plate together with the averaged masses of stiffeners, m_{ad} and m are the respective added masses per unit area of the plate and caused by the respective oscillations of the stiffeners and the ones of the plate w.r.t. the stiffeners (see formulas (6.33) and (6.8)), $m^* = m + m_{\mathrm{pl}}$, $m^*_{\mathrm{p+s}} = m_{\mathrm{ad}} + m^{\mathrm{st}}_{\mathrm{p+s}}$, $D = E\delta^3/(12(1-\nu^2))$ is the cylindrical stiffness of the plate, and Ei is the torsional stiffness of the stiffener with the attached belt.

(3) For the plate with the ratio of sides more than 2.5 (the cylindrical bending of plate), the expressions for A_1 and A_3 are

$$A_1 = \frac{16D\pi^4}{3a^4m^*}, \qquad A_3 = \frac{2V}{am^*_{\mathrm{p+s}}}, \tag{6.65}$$

and A_1 and A_2 are calculated by expressions (6.63).

The quantity V entering A_3 is the stiffness of the elastic support of the band-shaped beam that is the cross-section of the plate carved out across its long edges,

$$V = \frac{\alpha^4}{2b^4}Ei, \tag{6.66}$$

where α is the dimensionless parameter depending on fixing the ends of the stiffeners in the following way:

κ	0	0.25	0.50	0.75	1.0
α	3.14	3.46	3.81	4.22	4.73,

where κ is the coefficient of the supporting pair.

Example. Let us find eigenfrequencies of the plate of the grillage field and reinforcing stiffeners taking into account their interaction. The construction material is steel ($E = 19.6 \cdot 10^{10}$ kg/m^2, $\nu = 0.3$). The construction contacts with water on one side and has the following dimensions:

- the dimensions of the grillage field $l = 1.75$ m; $b = 1.00$ m; the plating thickness $\delta = 1 \cdot 10^{-2}$ m;
- the number of spans of the continuous plate $n = 5$; the distance between the stiffeners (the length of the short side of a separate plate) $a = l/n = 0.35$ m; the profile of the stiffeners is the flat-bulb No. 8[10], the mass of the unit plate area $m_{\mathrm{pl}} = 78.4$ kg/m^2;
- the mass of the unit plate area taking into account the averaged mass of stiffeners $m^{\mathrm{st}}_{\mathrm{p+s}} = 88.8$ kg/m^2; the inertia moment of the stiffener $i = 1.7 \cdot 10^{-6}$ m^4; the cylindrical stiffness of the plate $D = 1.79 \cdot 10^4$ N $\cdot$ m.

We consider the case where the edges and the plate are rigidly clamped along the supporting contour (see Fig. 6.19). We find quantities m and m_{ad} by formulas

[10] According to Russian GOST (State Standard) classification.

(6.8) and (6.33). The coefficients μ entering these formulas and taking into account the influence of the added masses are: $\mu(b/l) = 0.44$ is the coefficient determining the added masses due to the field oscillations; we can find it from Fig. 6.3 at $n = 1$; $\mu(l/nb) = 0.98$ is the coefficient determining the added masses due to plate oscillations w.r.t. the stiffeners; we can find it from Fig. 6.3 at $n = 5$. Then $m = 1 \cdot 10^3 \cdot 0.35 \cdot 0.98 = 343\ \mathrm{kg/m^2}$; $m_{\mathrm{ad}} = 1 \cdot 10^3 \cdot 1 \cdot 0.44 = 440\ \mathrm{kg/m^2}$.

In accordance with formulas (6.64) and (6.63),

$$A_1 = \frac{16 \cdot 1.79 \cdot 10^4 \cdot 3.14^4}{3 \cdot 0.35^4 \cdot 421.4}\left[1 + \frac{2}{3}\left(\frac{0.35}{1.0}\right)^2 + \left(\frac{0.35}{1.0}\right)^4\right] = 161.0 \cdot 10^4\ \mathrm{sec}^{-2};$$

$$A_3 = \frac{16}{3}\left(\frac{3.14}{1.0}\right)^4 \frac{19.6 \cdot 10^{10} \cdot 1.7 \cdot 10^{-6}}{528.85 \cdot 0.35} = 93.33 \cdot 10^4\ \mathrm{sec}^{-2};$$

$$A_0 = \frac{4}{3 \cdot 421.4}\left[78.4 + \sqrt{\frac{3}{2} \cdot 440 \cdot 343}\,\right] = 1.7534;$$

$$A_2 = \frac{1}{2 \cdot 528.85}\left[78.4 + \sqrt{\frac{3}{2} \cdot 440 \cdot 343}\,\right] = 0.5255.$$

Using formula (6.62), we find the eigenfrequencies of the plate and stiffeners taking into account their interaction: $\lambda_1 = 777\ \mathrm{sec}^{-1}$ and $\lambda_2 = 5645\ \mathrm{sec}^{-1}$.

The partial frequencies of the stiffeners and the plate are $\lambda_{\mathrm{st}} = \sqrt{A_3} = 970\ \mathrm{sec}^{-1}$; $\lambda_{\mathrm{pl}} = \sqrt{A_1} = 1275\ \mathrm{sec}^{-1}$.

Treating the plate as the band-shaped beam and using formulas (6.62) and (6.66), we obtain the following eigenfrequencies for the plate attached to the stiffeners: $\lambda_1 = 755\ \mathrm{sec}^{-1}$; $\lambda_2 = 5440\ \mathrm{sec}^{-1}$.

If the stiffeners are freely supported at the ends and the plate is rigidly attached to the stiffeners and freely supported on the short edges (see Fig. 6.17), then the eigenfrequencies of the plate together with stiffeners are $\lambda_1 = 375\ \mathrm{sec}^{-1}$ and $\lambda_1 = 4670\ \mathrm{sec}^{-1}$.

The partial eigenfrequencies of the stiffeners and the plate are $\lambda_{\mathrm{st}} = 390\ \mathrm{sec}^{-1}$ and $\lambda_{\mathrm{pl}} = 1225\ \mathrm{sec}^{-1}$ in this case.

6.9.2 Interactions of the Ship Grillage Structural Components

When construction elements participate in a motion, which is more complex as compared to the one considered in Sect. 6.9.1, taking into account added masses also becomes more complex but it may be performed in a way analogous to the above reasonings. We estimate the influence of the added masses on oscillations of the ship grillage simultaneously taking into account the mutual influence of its elements. Solving the problem by the energy method, we first find the kinetic energy of the fluid involved in motion by the oscillating grillage and its construction components.

We consider a grillage of the very general type (see Fig. 6.8), which consists of the prime set joists (stringers, floors, etc.), the plating, and the reinforcing stiffeners. Oscillations of a definite tone for such a grillage can be presented as oscillations of a system with three degrees of freedom, whose motion is determined by the three generalized coordinates. We use the solution in [202, 203]. Taking the oscillation function for the grillage prime set joists to be $X(x)$ and $Y(y)$, we describe the motion of these joists by the function

$$W = w_1(t)X(x)Y(y),$$

where $w_1(t)$ is the generalized coordinate characterizing motions of the joists.

The displacement of the panel plate (the grillage part reinforced by stiffeners and bounded by joists of the prime set) in its relative motion can be described as

$$w_{ij} = \left[w_2(t)\right]_{ij}\eta(y) + \left[w_3(t)\right]_{ij}\psi(x, y), \tag{6.67}$$

where $[w_2(t)]_{ij}$ is the generalized coordinate characterizing the displacement of the stiffeners of this panel w.r.t. the grillage prime set joists, $[w_3(t)]_{ij}$ is the generalized coordinate characterizing the plate displacement w.r.t. the stiffeners, and the functions $\eta(y)$ and $\psi(x, y)$ describe the respective oscillations of the stiffeners and the ones of the panel plate.

We assume that each panel moves progressively in the direction perpendicular to the grillage plane, whereas the motion of the contour of each of the panels is determined by the value of the function W at the center of the panel:

$$W_{ij} = w_1(t)X(x_i)Y(y_j),$$

where x_i and x_j are the coordinates of the panel center.

Because the panel contours oscillate with the same frequency with amplitudes proportional to the value of $X(x_i)Y(y_j)$, we can set

$$\left[w_2(t)\right]_{ij} = w_2(t)X(x_i)Y(y_j); \qquad \left[w_3(t)\right]_{ij} = w_3(t)X(x_i)Y(y_j).$$

Expression (6.67) then becomes

$$w_{ij} = \left[w_2(t)\eta(y) + w_3(t)\psi(x, y)\right]X(x_i)Y(y_j).$$

The kinetic energy T of fluid involved in motion by an oscillating grillage can be found under the assumption of the ideal fluid experiencing a vortex-free motion. The influence of the oscillating grillage is equivalent to the action of simple sources with capacities $q = \partial Z/\partial t$ continuously distributed over the grillage surface, where

$$Z(x, y, t) = \left[w_1(t) + w_2(t)\eta(y) + w_3(t)\psi(x, y)\right]X(x_i)Y(y_j).$$

Using formula (6.3) we transform the kinetic energy to the form

$$T = \frac{\rho}{4\pi}\sum_{i,j}\iint_S \frac{\partial Z}{\partial t}\,dS'\iint \frac{\partial Z}{\partial t}\frac{dS}{r}. \tag{6.68}$$

We integrate in expression (6.68) over the surface of every panel and sum up the results over the whole grillage (for all the panels). In the case where all the panels are equal and oscillate in the same phase, expression (6.68) becomes

$$\begin{aligned} T &= \frac{\rho}{4\pi}\iint_S (\dot{w}_1 + \dot{w}_2\eta + \dot{w}_3\psi)\,dS' \\ &\quad \times \iint (\dot{w}_1 + \dot{w}_2\eta + \dot{w}_3\psi)\frac{dS}{r}\sum_{i,j}\big[X(x_i)Y(y_j)\big]^2 \\ &= \frac{\rho}{4\pi}\bigg[\dot{w}_1^2\iint_S dS'\iint \frac{dS}{r} + \dot{w}_1\dot{w}_2\bigg(\iint_S dS'\iint \eta\frac{dS}{r} + \iint_S \eta\,dS'\iint \frac{dS}{r}\bigg) \\ &\quad + \dot{w}_1\dot{w}_3\bigg(\iint_S dS'\iint \psi\frac{dS}{r} + \iint_S \psi\,dS'\iint \frac{dS}{r}\bigg) \\ &\quad + \dot{w}_2\dot{w}_3\bigg(\iint_S \eta\,dS'\iint\psi\frac{dS}{r} + \iint_S \psi\,dS'\iint\eta\frac{dS}{r}\bigg) \\ &\quad + \dot{w}_2^2\iint_S \eta\,dS'\iint \eta\frac{dS}{r} + \dot{w}_3^2\iint_S \psi\,dS'\iint \psi\frac{dS}{r}\bigg]\sum_{i,j}\big[X(x_i)Y(y_j)\big]^2, \end{aligned} \tag{6.69}$$

where $M_1 = \frac{1}{2}\frac{\rho}{\pi}\iint_S dS'\iint \frac{dS}{r}$ is the added mass of a separate panel caused by oscillations of the whole grillage, $M_2 = \frac{1}{2}\frac{\rho}{\pi}\iint_S \eta\,dS'\iint \eta\frac{dS}{r}$ is the added mass of the separate panel oscillating together with stiffeners as a field, and $M_3 = \frac{1}{2}\frac{\rho}{\pi}\iint_S \psi\,dS'\iint \psi\frac{dS}{r}$ is the added mass of the plating of the separate panel oscillating w.r.t. the stiffeners.

We transform the sums of integrals in the parentheses in expression (6.69) using the theorem about the average [205] (see Sect. 6.9.1):

$$\begin{aligned} M_{12} &= \frac{1}{2}\frac{\rho}{\pi}\bigg(\iint_S dS'\iint \eta\frac{dS}{r} + \iint_S \eta\,dS'\iint \frac{dS}{r}\bigg) \\ &= \frac{\rho}{\pi}\sqrt{\iint_S \eta\,dS'\iint \eta\frac{dS}{r}\iint_S dS'\iint \frac{dS}{r}} = 2\sqrt{M_2M_1}. \end{aligned}$$

Analogously,

$$\begin{aligned} M_{13} &= \frac{1}{2}\frac{\rho}{\pi}\bigg(\iint_S dS'\iint \psi\frac{dS}{r} + \iint_S \psi\,dS'\iint \eta\frac{dS}{r}\bigg) = 2\sqrt{M_3M_1}; \\ M_{23} &= \frac{1}{2}\frac{\rho}{\pi}\bigg(\iint_S \eta\,dS'\iint \psi\frac{dS}{r} + \iint_S \psi\,dS'\iint \eta\frac{dS}{r}\bigg) = 2\sqrt{M_2M_3}. \end{aligned}$$

The final expression for the kinetic energy of fluid is

$$T = \frac{1}{2}\left(M_1\dot{w}_1^2 + M_{12}\dot{w}_1\dot{w}_2 + M_{13}\dot{w}_1\dot{w}_3 + M_{23}\dot{w}_2\dot{w}_3 + M_2\dot{w}_2^2 + M_3\dot{w}_3^2\right) \times \sum_{i,j}\left[X(x_i)Y(y_j)\right]^2. \tag{6.70}$$

The first term in (6.70) is the added mass of the whole grillage caused by its oscillations as a system of crossing joists, which can be calculated by the formula

$$\begin{aligned} M_G &= \frac{1}{2}M_1\dot{w}_1^2\sum_{i,j}\left[X(x_i)Y(y_j)\right]^2 \\ &= \rho\mu\left(\frac{B}{L}\right)B\int_0^L\int_0^B X^2(x)Y^2(y)\,dx\,dy. \end{aligned} \tag{6.71}$$

The quantities M_1, M_2, and M_3 follow from the expressions

$$\begin{aligned} M_1 &= \rho\mu\left(\frac{B}{L}\right)B\cdot b\cdot l; \\ M_2 &= \rho\mu\left(\frac{L}{pl}\right)\frac{L}{p}\int_0^L\int_0^b \eta^2(y)\,dx\,dy; \\ M_3 &= \rho\mu\left(\frac{L}{pl}\right)\frac{l}{n}\int_0^l\int_0^b \psi^2(x,y)\,dx\,dy, \end{aligned} \tag{6.72}$$

where L and B are the respective length and width of the grillage, l and b are the corresponding dimensions of a single panel, p the number of panels along the long side L of the grillage, and n the number of spans of the plate inside a single panel.

We determined the coefficients μ entering expressions (6.71) and (6.72) by graphs in Figs. 6.2–6.6.

Calculating the added masses M_1, M_2, and M_3 is therefore easy. It is important to use these quantities when calculating oscillations of the grillage taking into account interactions between its separate elements (prime set joists, stiffeners, and plates of the grillage).

We describe the idea of the method and formulas for calculating joint eigenfrequencies of construction elements of the general type grillage, whose plating is reinforced by stiffeners (see Fig. 6.8) [202, 203]. When using the energy method we must know the total kinetic energy of the system grillage-fluid $T_\Sigma = T_G + T$ and the potential energy P of the construction. The fluid kinetic energy T is determined by expression (6.70). The kinetic energy of the grillage equals the sum of kinetic energies of prime set joists, grillage plating, and stiffeners

$$T_G = \frac{1}{2} M_{\text{ad}} \dot{w}_1^2 + \frac{1}{2} \big[\big(M_1^{\text{pl}} + M_1^{\text{st}} \big) \dot{w}_1^2 + \big(M_2^{\text{pl}} + M_2^{\text{st}} \big) \dot{w}_2^2 + M_3^{\text{pl}} \dot{w}_3^2 + 2 \big(M_{12}^{\text{pl}} + M_{12}^{\text{st}} \big) \dot{w}_1 \dot{w}_2 + 2 M_{13}^{\text{pl}} \dot{w}_1 \dot{w}_3 + 2 M_{23}^{\text{pl}} \dot{w}_2 \dot{w}_3 \big] \times \sum_{i,j} \big[X(x_i) Y(y_j) \big]^2, \tag{6.73}$$

where

$$M_{\text{ad}} = m_1 \int_0^L Y^2(y)\, dy \sum_{i=1}^{k} X^2(\tilde{x}_i) + m_2 \int_0^B X^2(x)\, dx \sum_{j=1}^{p-1} Y^2(\tilde{y}_j);$$

$$M_1^{\text{pl}} = m_{\text{pl}} b l; \qquad M_3^{\text{pl}} = m_{\text{pl}} \int_0^l \int_0^b \psi^2(x, y)\, dx\, dy;$$

$$M_2^{\text{pl}} = m_{\text{pl}} \int_0^l \int_0^b \eta^2(y)\, dx\, dy; \qquad M_{13}^{\text{pl}} = m_{\text{pl}} \int_0^l \int_0^b \psi(x, y)\, dx\, dy;$$

$$M_{12}^{\text{pl}} = m_{\text{pl}} \int_0^l \int_0^b \eta(y)\, dx\, dy; \qquad M_{23}^{\text{pl}} = m_{\text{pl}} \int_0^l \int_0^b \eta(y) \psi(x, y)\, dx\, dy;$$

$$M_1^{\text{st}} = (n-1) m_{\text{st}} b; \qquad M_2^{\text{st}} = (n-1) m_{\text{st}} \int_0^b \eta^2(y)\, dy;$$

$$M_{12}^{\text{st}} = (n-1) m_{\text{st}} \int_0^b \eta(y)\, dy,$$

where m_1, m_2, and m_{st} are masses per unit lengths of the respective cross joist, the prime set joist, and the stiffener (masses of all frame elements are given without joining belts), m_{pl} is the mass of the unit area of the grillage plating, k is the number of cross joists, $p-1$ is the number of the prime set joists, $n-1$ is the number of stiffeners inside a single panel, and $\tilde{x}_i$ and $\tilde{y}_j$ are the coordinates for the joists of the prime set.

The potential energy of the whole grillage is

$$P_G = \frac{1}{2} \widetilde{N}_{\text{ad}} w_1^2 + \frac{1}{2} \big(C_1 w_2^2 + C w_3^2 \big) \sum_{i,j} \big[X(x_i) Y(y_j) \big]^2,$$

where

$$C_{\text{js}} = E J_1 \int_0^L \big[Y''(y) \big]^2 dy \sum_{i=1}^{k} \big[X(\tilde{x}_i) \big]^2 + E J_2 \int_0^B \big[X''(x) \big]^2 dx \sum_{j=1}^{p-1} \big[Y(\tilde{y}_j) \big]^2 \tag{6.74}$$

is the generalized stiffness of joists of the prime set, C_1 and $\widetilde{N}$ are the stiffness of the respective stiffeners and the plating within a separate panel of the grillage (they are determined by formulas (6.60)), and J_1 and J_2 are the inertia moments of the cross-sections of the respective cross joist and the joist of the principal direction.

Substituting the expressions for the kinetic T_Σ and potential P_G energies in the Lagrange equation

$$\frac{d}{dt}\left(\frac{\partial T_\Sigma}{\partial \dot{w}_i}\right) + \frac{\partial P_G}{\partial w_i} = 0$$

(the potential energy of the fluid is not taken into account since it remains constant) and introducing the notation

$$\begin{aligned}
&A = \sum_{i,j}\left[X(x_i)Y(y_j)\right]^2, \qquad A_3 = M_{13}^{\text{pl}} + \sqrt{M_1 M_3};\\
&A_1 = M_{12}^{\text{pl}} + M_{12}^{\text{st}} + \sqrt{M_1 M_2}, \qquad A_4 = M_{23}^{\text{pl}} + \sqrt{M_2 M_3};\\
&A_2 = M_{12}^{\text{pl}} + M_2^{\text{st}} + M_2; \qquad A_5 = M_3^{\text{pl}} + M_3;\\
&B_1 = M_{\text{ad}} + \left(M_1^{\text{pl}} + M_1^{\text{st}} + M_1\right)A,
\end{aligned} \tag{6.75}$$

we obtain the system of differential equations for the oscillatory motion of the grillage:

$$\begin{aligned}
&B_1\ddot{w}_1 + AA_1\ddot{w}_2 + AA_3\ddot{w}_3 + C_{\text{ad}}w_1 = 0;\\
&A_1\ddot{w}_1 + A_2\ddot{w}_2 + A_4\ddot{w}_3 + C_1 w_2 = 0;\\
&A_3\ddot{w}_1 + A_4\ddot{w}_2 + A_5\ddot{w}_3 + C w_3 = 0.
\end{aligned}$$

Looking for the solution of this system in the form

$$w_i = f_i \sin(\lambda t)$$

and equating the determinant to zero, we obtain the frequency equation

$$\begin{aligned}
&\lambda^6\left(A_2A_3B_1 - A_4^2B_1 - AA_1^2A_5 + 2AA_1A_3A_4 - AA_2A_3^2\right)\\
&\quad - \lambda^4\left(A_5B_1C_1 + A_2B_1C + A_2A_5C_{\text{js}} - A_4^2C_{\text{js}} - AA_1^2C - AA_3^2C_1\right)\\
&\quad + \lambda^2(B_1CC_1 + A_5C_1C_{\text{js}} + A_2CC_{\text{js}}) - CC_1C_{\text{js}} = 0.
\end{aligned} \tag{6.76}$$

The positive roots $\lambda_{1,2,3}$ of Eq. (6.76) are frequencies of the free oscillations of the grillage calculated with accounting for the added masses of fluid involved in motion both by the grillage as a whole and by its separate elements. The first frequency then customarily characterizes the frequency of the free oscillations of the grillage taking into account the influence of oscillations of the plating and joists, whereas the second and the third frequencies characterize free oscillations of the grillage plates and stiffeners with accounting for the mechanical compliance of the grillage carcase joists.

As was demonstrated by calculations of actual ship grillages, interactions between separate elements of a grillage may result in reducing the frequencies of the first modes of free oscillations of the plating. The influence of oscillations of the plating and the stiffeners on eigenfrequencies of the grillage is essential in the case where the frequencies of free oscillations of the grillage and the ones of its fields are close to each other (the difference between them does not exceed 50%).

The mechanical compliance of the joists of the grillage increases the joint frequencies of plate and stiffeners (calculated with accounting for their interaction but without taking into account the grillage elasticity): the lowest frequency may be increased by (40–50)% and the higher frequency increases at a lesser rate.

Example. As an example, we determine the frequencies of free oscillations of the bottom grillage and its construction elements (plates and stiffeners) taking into account their interactions and the influence of the outer water. The grillage is confined by longitudinal and transverse bulkheads.

The basic parameters of the grillage and its carcase are the following. The grillage dimensions are (see Fig. 6.8): the length $L = 7.00$ m, the width $B = 7.00$ m; the profiles of the prime set joists and their inertia moments (with the attached plating belt) are:

$$\text{the vertical keel—}\frac{0.8 \times 0.8 \cdot 10^{-2}}{0.1 \times 1.0 \cdot 10^{-2}}; \quad J_1 = 14.4 \cdot 10^{-4}\ \text{m}^4;$$

$$\text{the stringers—}\frac{0.45 \times 0.6 \cdot 10^{-2}}{9 \cdot 10^{-2} \times 0.8 \cdot 10^{-2}}; \quad J_1 = 2.801 \cdot 10^{-4}\ \text{m}^4;$$

$$\text{the floors—}\frac{0.45 \times 0.6 \cdot 10^{-2}}{9 \cdot 10^{-2} \times 0.8 \cdot 10^{-2}}; \quad J_2 = 2.728 \cdot 10^{-4}\ \text{m}^4;$$

the distance between the stringers is $l = 1.75$ m; the distance between floors is $b = 1.00$ m; the distance between the longitudinal stiffeners is $a = 0.35$ m; the profile of the stiffener and its inertia moment with the attached plating belt is the flat-bulb No. 8; $i = 1.7 \cdot 10^{-6}$ m^4; the thickness of the plating $\delta = 1.0 \cdot 10^{-2}$ m; the ship hull material is steel ($E = 19.6 \cdot 10^{10}$ kg/m^2; $\nu = 0.3$); the grillage contacts water from one side.

We need the masses of the following elements of the grillage construction.

The mass per unit length of the grillage joists (without attached plating belts): for the vertical keel $m_1 = 51.84$ kg/m; for the stringer $m_1' = 26.8$ kg/m; for the floor $m_2 = 26.8$ kg/m; for the stiffener $m_{\text{st}} = 4.57$ kg/m; the mass per unit area of the plating $m_{\text{pl}} = 78.4$ kg/m^2. The cylindrical stiffness of the plating $D = E\delta^3/12(1-\nu^2) = 1.79 \cdot 10^4$ N $\cdot$ m.

We consider the first mode of the grillage oscillation and, assuming that joists of both directions are freely supported at their ends, take the amplitudes of their oscillations to be

$$X(x) = \sin\left(\frac{\pi x}{B}\right); \qquad Y(y) = \sin\left(\frac{\pi y}{L}\right).$$

We assume the plating and stiffeners to be rigidly clamped along the supporting contour (the symmetric oscillation mode), and, therefore,

$$\eta(y) = \sin^2\left(\frac{\pi y}{b}\right); \qquad \psi(x, y) = \sin^2\left(\frac{n\pi x}{l}\right)\sin^2\left(\frac{\pi y}{b}\right).$$

We now determine from (6.73) the generalized masses of the prime set joists, of the stiffeners, and of the plates of the grillage:

$$\begin{aligned} M_{\mathrm{js}} &= 51.84 \int_0^{7.00} \sin^2\left(\frac{\pi y}{7.00}\right) dy \sin^2\left(\frac{3.50\pi}{7.00}\right) \\ &\quad + 26.8 \int_0^{7.00} \sin^2\left(\frac{\pi y}{7.00}\right) dy \left(\sin^2 \frac{1.75\pi}{7.00} + \sin^2 \frac{5.25\pi}{7.00}\right) \\ &\quad + 26.8 \int_0^{7.00} \sin^2\left(\frac{\pi x}{7.00}\right) dx \\ &\quad \times 2\left(\sin^2 \frac{1.00\pi}{7.00} + \sin^2 \frac{2.00\pi}{7.00} + \sin^2 \frac{3.00\pi}{7.00}\right) = 603 \text{ kg}; \end{aligned}$$

$$M_1^{\mathrm{pl}} = 78.4 \cdot 1.0 \cdot 1.75 = 137.5 \text{ kg};$$

$$M_2^{\mathrm{pl}} = 78.4 \int_0^{1.00} \int_0^{1.75} \sin^4\left(\frac{\pi y}{1.00}\right) dx\, dy = 51.5 \text{ kg};$$

$$M_3^{\mathrm{pl}} = 78.4 \int_0^{1.00} \int_0^{1.75} \sin^4 \frac{\pi y}{1.00} \sin^4 \frac{5\pi x}{1.75}\, dx\, dy = 19.3 \text{ kg};$$

$$M_{12}^{\mathrm{pl}} = 78.4 \int_0^{1.00} \int_0^{1.75} \sin^2 \frac{\pi y}{1.00}\, dx\, dy = 68.6 \text{ kg};$$

$$M_{13}^{\mathrm{pl}} = 78.4 \int_0^{1.00} \int_0^{1.75} \sin^2 \frac{5\pi x}{1.75} \sin^2 \frac{\pi y}{1.00}\, dx\, dy = 34.3 \text{ kg};$$

$$M_{23}^{\mathrm{pl}} = 78.4 \int_0^{1.00} \int_0^{1.75} \sin^2 \frac{5\pi x}{1.75} \sin^4 \frac{\pi y}{1.00}\, dx\, dy = 25.75 \text{ kg};$$

$$M_1^{\mathrm{st}} = 4 \cdot 4.57 \cdot 1.0 = 18.3 \text{ kg};$$

$$M_2^{\mathrm{st}} = 4 \cdot 4.57 \int_0^{1.00} \sin^4 \frac{\pi y}{1.00}\, dy = 6.88 \text{ kg};$$

$$M_{12}^{\mathrm{st}} = 4 \cdot 4.57 \int_0^{1.00} \sin^2 \frac{\pi y}{1.00}\, dy = 9.15 \text{ kg}.$$

Using expressions (6.74) and (6.60) we find the generalized rigidities of the corresponding constructions:

$$C_{\text{js}} = 19.6\cdot 10^{10}\left(14.4\cdot 10^{-4}\frac{\pi^4}{7.00^4}\sin^2\left(\frac{3.50\pi}{7.00}\right)\int_0^{7.00}\sin^2\left(\frac{\pi y}{7.00}\right)dy\right.$$
$$+2.801\cdot 10^{-4}\frac{\pi^4}{7.00^4}2\cdot 0.707^2\int_0^{7.00}\sin^2\left(\frac{\pi y}{7.00}\right)dy$$
$$\left.+2.728\cdot 10^{-4}\frac{\pi^4}{7.00^4}\cdot 2\cdot 1.746\int_0^{7.00}\sin^2\left(\frac{\pi x}{7.00}\right)dx\right) = 74.2\cdot 10^6\ \text{N/m};$$

$$C_1 = 4\cdot 19.6\cdot 1.7\cdot 10^4\frac{\pi^4}{1.00^4}\int_0^{1.00}\cos^2\frac{2\pi y}{1.00}\,dy = 260\cdot 10^6\ \text{N/m};$$

$$C = 1.79\cdot 10^4\int_0^{1.00}\int_0^{1.75}\left[4\frac{\pi^4}{1.00^4}\sin^4\frac{5\pi x}{1.75}\cos^2\frac{2\pi y}{1.00}\right.$$
$$+4\left(\frac{5\pi}{1.75}\right)^4\cos^2\left(\frac{2\cdot 5\pi x}{1.75}\right)\sin^4\left(\frac{\pi y}{1.00}\right)$$
$$+8\nu\frac{25\pi^4}{1.00^2\cdot 1.75^2}\sin^2\left(\frac{5\pi x}{1.75}\right)\cos\left(\frac{2\cdot 5\pi x}{1.75}\right)\sin^2\left(\frac{\pi y}{1.00}\right)\cos\left(\frac{2\pi y}{1.00}\right)$$
$$+32(1-\nu)\left(\frac{5\pi^2}{1.00\cdot 1.75}\right)^2\sin^2\left(\frac{5\pi x}{1.75}\right)$$
$$\left.\times\cos^2\left(\frac{5\pi x}{1.75}\right)\sin^2\left(\frac{\pi y}{1.00}\right)\cos^2\left(\frac{\pi y}{1.00}\right)\right]dx\,dy = 167.5\ \text{N/m}.$$

The panel added masses M_1, M_2, and M_3 caused by different types of its oscillations (together with plating, bending oscillations together with stiffeners and bending oscillations of the grillage plates w.r.t. the stiffeners) can be calculated by formulas (6.72):

$$M_1 = 1.0\cdot 10^3\cdot 0.4\cdot 7.00\cdot 1.75\cdot 1.00 = 4.88\cdot 10^3\ \text{kg},$$

where $\mu(B/L) = 0.4$ is the added mass coefficient caused by grillage oscillations and determined by Fig. 6.2 under the assumption that $n = 1$;

$$M_2 = 1.0\cdot 10^3\cdot 0.77\cdot 1.00\int_0^{1.00}\int_0^{1.75}\sin^4\left(\frac{\pi y}{1.00}\right)dx\,dy = 506\ \text{kg},$$

where $\mu(L/pl) = 0.77$ is the added mass coefficient caused by grillage oscillations together with stiffeners and determined by Fig. 6.3 under the assumption that $n = 4, 5$;

$$M_3 = 1.0\cdot 10^3\cdot 0.98\frac{1.75}{5}\int_0^{1.00}\int_0^{1.75}\sin^4\frac{5\pi x}{1.75}\sin^4\frac{\pi y}{1.00}\,dx\,dy = 84.5\ \text{kg}.$$

Calculating the coefficients A_i and B_1 (6.75) entering frequency equation (6.76), we reduce the latter to the form

$$\lambda^6 - 35 \cdot 10^6 \lambda^4 + 166.3 \cdot 10^{12} \lambda^2 - 34.3 \cdot 10^{16} = 0.$$

The solution of this equation determines frequencies of free oscillations of the grillage, stiffeners, and plates taking into account their interaction and the influence of surrounding fluid: $\lambda_1 = 60\ \mathrm{sec}^{-1}$, $\lambda_2 = 2380\ \mathrm{sec}^{-1}$, and $\lambda_3 = 5415\ \mathrm{sec}^{-1}$. The frequency of grillage free oscillations of the first mode calculated without taking into account plating and stiffeners vibrations practically coincides with the frequency obtained from Eq. (6.76).

The frequencies of free oscillations of the plate and the stiffeners calculated with accounting for their interaction but without taking into account the mechanical compliance of the prime set joists (see the example in Sect. 6.9.1) are $\lambda_1 = 777\ \mathrm{sec}^{-1}$ (stiffeners) and $\lambda_2 = 5645\ \mathrm{sec}^{-1}$ (plates). The partial (without taking into account interactions) frequencies of the stiffeners and plates are $\lambda_{\mathrm{st}} = 970\ \mathrm{sec}^{-1}$ and $\lambda_{\mathrm{pl}} = 1275\ \mathrm{sec}^{-1}$.

The mechanical compliance of prime set joists results therefore in a substantial increase in the second and third frequencies of the construction oscillations as compared to the corresponding partial frequencies of plates and stiffeners. The explanation is analogous to the one that explains changes of oscillation frequencies of plates and stiffeners when taking into account their interaction (see Sect. 6.9.1).

6.9.3 Cylindrical Shell Reinforced by Longitudinal Stiffeners

We consider two related co-axis cylindrical shells experiencing transversal oscillatory motions. These oscillations result in relative elastic oscillations of the external shell reinforced by equidistantly distributed equal longitudinal stiffeners supported by a solid frame. The internal shell is solid and does not experience relative motions. The fluid is outside and between the shells.

Vibration parameters of the plating and the carcase of the external shell are to be determined by taking into account dynamical interaction of the construction elements under its complex motion and especially by taking into consideration the surrounding fluid and fluid inside the construction that is involved in motion.

In this setting, the problem reduces to the problem of determination of forced relative oscillations of the plating and of the carcase of the external shell caused by a kinematic excitation, which are oscillatory motions of the system of co-axis shells as a whole. We solve the problem under the following assumptions [185]:

- translational motion of frames of the both shells is assumed to be the same;
- fluid flow in circular direction between the shells is assumed to be free;
- velocity of the fluid flow along the shell axis in sections along the frame elements is zero;
- the motion of the outer water as well as the one of the water between the shells is subject to the law of the ideal incompressible fluid.

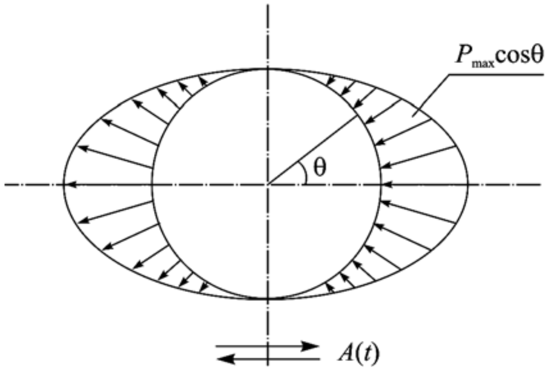

Fig. 6.20 The distribution of the fluid pressure on the shell at its oscillations in the direction perpendicular to the axis

Modes of relative oscillations of the external shell and longitudinal stiffeners (ribs are assumed to be stiff enough) are close to the modes of static bending of the shell and stiffeners under the load distributed by the law $\cos\theta$ (Fig. 6.20), which corresponds to its oscillations in fluid in the direction perpendicular to the shell axis. The form of the external shell oscillations w.r.t. the stiffeners can be therefore taken to be

$$w(\theta, x) = \frac{q_1}{4}\big(1 + \cos(n\theta)\big)\cos\theta \cdot \left(1 + \cos\frac{2\pi x}{l}\right),$$

whereas the stiffener displacement is

$$w_{\mathrm{st}} = \frac{q_2}{2}\cos\theta_i\left(1 + \cos\frac{2\pi x}{l}\right),$$

where q_1 and q_2 are the generalized coordinates representing the corresponding displacements of the shell w.r.t. the stiffeners and the ones of stiffeners w.r.t. ribs; θ and x are the cylindrical coordinates, l is the frame spacing, θ_i is the central angle determining the position of the ith stiffener (Fig. 6.21), and $2n$ is the number of longitudinal stiffeners.

Because the number of stiffeners in actual constructions is rather big, we can consider w_{st} a continuous function of the coordinate θ,

$$w_{\mathrm{st}} = \frac{q_2}{2}\cos\theta\left(1 + \frac{2\pi x}{l}\right).$$

The radial displacement of the shell w.r.t. ribs is therefore

$$w_0 = w + w_{\mathrm{st}}.$$

The absolute radial displacement (superposed with the transitional motion of the shell as a whole given by the function $A(t)$) is then

$$w_a = A(t)\cos\theta + w_0. \tag{6.77}$$

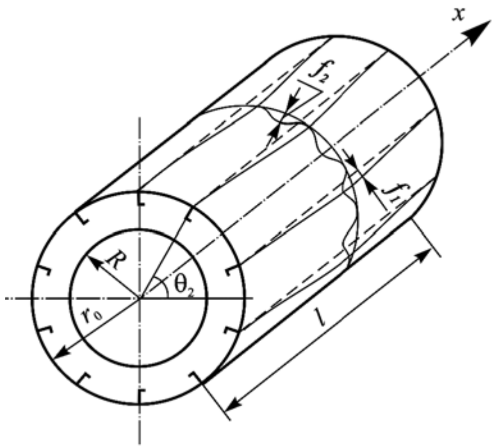

Fig. 6.21 The modes of elastic oscillations of the outer shell and longitudinal stiffeners caused by a kinematic excitation

We can find the absolute tangential shell displacement from the condition of non-stretchability of the middle surface of the shell.

To find the fluid pressure on a shell, we must find the fluid velocity potential $\varphi(x, r, \theta, t)$ on both sides of the outer shell using the Laplace equation. The latter has the form

$$\frac{\partial^2 \varphi}{\partial r^2} + \frac{1}{r}\frac{\partial \varphi}{\partial r} + \frac{1}{r^2}\frac{\partial^2 \varphi}{\partial \theta^2} + \frac{\partial^2 \varphi}{\partial x^2} = 0 \tag{6.78}$$

in the cylindrical coordinates x, r, θ.

The boundary conditions for Eq. (6.78) for fluid outside the shell are conditions of the zero normal flow on the surface of the outer shell and the condition of zero flow at infinity. For the fluid between the shells, the boundary conditions are zero normal flows on the surfaces of inner and outer shells.

Because Eq. (6.78) and the boundary conditions are linear, its solution is a superposition of solutions for each of the components of the shell motion. Expressing approximate shell oscillation functions through harmonic functions we obtain the exact solutions of the Laplace equation subsequently obtaining the fluid pressure on the shell [185].

The extra fluid pressure is determined by the linearized Lagrange–Cauchy integral

$$p = -\rho \frac{\partial \varphi}{\partial t},$$

where ρ is the fluid density.

When the law of shell motion is $q \cos(n\theta)$, the pressure of the outer fluid is

$$p_n^e = -\rho \frac{\ddot{q}}{n} r_0 \cos(n\theta), \tag{6.79}$$

where r_0 is the radius of the outer shell.

The motion of the shell by the law $q\cos(n\theta)\cos(\frac{2\pi x}{l})$ is accompanied by the outer fluid pressure

$$p_n^e = -\rho\ddot{q}\frac{1}{2\pi}\frac{\cos(n\theta)\cos(2\pi x/l)}{1+n/(2\pi r_0)}. \tag{6.80}$$

Pressure of fluid inside the construction on the inner surface of the outer shell under its oscillations by the law $A(t)\cos\theta$ is

$$p_1^i = \rho r_0\left[\ddot{A} + \left(\frac{\ddot{q}_1}{4} + \frac{\ddot{q}_2}{2}\right)\frac{1+(R/r_0)^2}{1-(R/r_0)^2}\right]\cos\theta,$$

where R is the inner shell radius.

This expression demonstrates that the pressure increases unboundedly as the distance between the shells decreases (because of presence of the solid boundary).

When the outer shell oscillates by the law $q\cos(n\theta)$ with $n > 1$, the corresponding pressure is

$$p_n^i = \rho\frac{\ddot{q}}{n}r_0\frac{1+(R/r_0)^{2n}}{1-(R/r_0)^{2n}}\cos(n\theta).$$

When the number of stiffeners is large ($n > 10$) and the ratio of the shell radiuses $R/r_0 < 0.8$, we can neglect the influence of the inner shell as a solid boundary and find the pressure by the formula that up to a sign coincides with formula (6.79) for the outer fluid pressure.

If oscillations are subject to the law $q\cos(n\theta)\cos(\frac{2\pi x}{l})$ with $n = 1, 2, \ldots$, then the influence of the solid boundary (the inner shell) on the fluid pressure on the inner side of the outer shell is negligibly small. In this case, the formula for the pressure coincides up to a sign with formula (6.80).

The added mass of the outer shell appears in the result of pressures and their superpositions caused by shell component motions. We find them by solving the problem of forced oscillations of the construction.

The equations for elastic oscillations of a shell with a frame under a kinematic excitation and with the above conditions of contact with fluid are obtained from the Lagrange equations of the second kind for which we have found preliminary expressions for the kinetic and potential energies of the construction and for the generalized forces in the generalized coordinates q_1 and q_2.

The kinetic energy of the shell is the sum of kinetic energies of the plating and the one of the stiffeners. They can be found from well-known formulas, and we omit them here.

The potential energy of the shell is also equal to the sum of potential energies of deformations of the shell and the stiffeners. We assume that the shell is initially at a stress state, determined by the forces in the middle surface for T_1 and T_2.

The generalized forces follow from the general mechanics rule

$$Q_1 = \int_{-l/2}^{l/2}\int_0^{2\pi} p_\Sigma(x,\theta,t)f_1(x,\theta)r_0\,d\theta\,dx;$$

$$Q_2 = \int_{-l/2}^{l/2} \int_0^{2\pi} p_\Sigma(x, \theta, t) f_2(x, \theta) r_0 \, d\theta \, dx,$$

where $p_\Sigma(x, \theta, t)$ is the total pressure on the shell and $f_1(x, \theta)$ and $f_2(x, \theta)$ are the respective relative displacements of the shell and the stiffeners.

As a result, we obtain the shell equations of motion as the ones for a system with two degrees of freedom:

$$M_{11}\ddot{q}_1 + \widetilde{N}_{11}q_1 + M_{21}\ddot{q}_2 + \widetilde{N}_{21}q_2 = P_1,$$
$$M_{12}\ddot{q}_1 + \widetilde{N}_{12}q_1 + M_{22}\ddot{q}_2 + \widetilde{N}_{22}q_2 = P_2.$$

In these equations, we have introduced the notation

$$M_{11} = \frac{27}{128}\pi\rho_0 h r_0 l\left[1 + \frac{8}{27}(\beta + 1)\frac{\rho r_0}{\rho_0 h}\right];$$

$$M_{12} = M_{21} = \frac{3}{8}\pi\rho_0 h r_0 l\left(1 + \frac{\beta + 1}{3}\frac{\rho r_0}{\rho_0 h}\right);$$

$$M_{22} = \frac{3}{4}\pi\rho_0 h r_0 l\left(1 + \frac{F}{bh} + \frac{\beta + 1}{3}\frac{\rho r_0}{\rho_0 h}\right);$$

$$C_{11} = \frac{3}{4}\pi^5\left(1 + \frac{l^4}{b^4} + \frac{4}{3}\frac{l^2}{b^2}\right)\frac{r_0 D}{l^3} + \frac{\pi^3}{4}\frac{r_0}{l}\left(T_1 + \frac{3}{2}\frac{l^2}{b^2}T_2\right);$$

$$C_{12} = C_{21} = \pi^5\frac{r_0 D}{l^3} + \frac{\pi^3 r_0}{4l}\left(T_1 + \frac{3}{4\pi^2}\cdot\frac{l^2}{r_0^2}T_2\right);$$

$$C_{22} = \frac{2\pi^5 E J r_0}{b l^3} + \frac{\pi^3 r_0}{2l}\left(T_1 + \frac{3}{4\pi^2}\cdot\frac{l^2}{r_0^2}T_2\right);$$

$$P_1 = -\frac{3}{4}\pi\rho_0 h r_0 l\left(1 + \frac{2}{3}\frac{\rho r_0}{\rho_0 h}\right)\ddot{A};$$

$$P_2 = -\pi\rho_0 h r_0 l\left(1 + \frac{F}{bh} + \frac{\rho r_0}{\rho_0 h}\right)\ddot{A}, \tag{6.81}$$

where D is the cylindrical rigidity of the shell, h is the shell thickness, F the area of the tangential cross-section of the longitudinal stiffener, J the inertia moment of the stiffener with the attached belt, b the distance between the neighbor stiffeners, ρ_0 the density of the construction material, and

$$\beta = \frac{(1 + R/r_0)^2}{(1 - R/r_0)^2}$$

the coefficient taking into account the influence of the inner shell as the solid boundary on the added masses.

The generalized added masses caused by oscillations of the shell with respect to the longitudinal stiffeners are given by the second term in the expression for M_{11} in (6.81). The generalized added masses caused by oscillations of the shell together with the stiffeners are given by the third term in the expression for M_{22} in (6.81). They are

$$M_{11}^* = \frac{\pi}{16}\rho r_0^2 l(\beta+1); \qquad M_{22}^* = \frac{\pi}{4}\rho r_0^2 l(\beta+1). \tag{6.82}$$

The first terms in the expressions for M_{11} and M_{22} (6.81) are the generalized masses of the construction itself corresponding to the generalized coordinates q_1 and q_2.

Note the influence of the inner shell as the solid boundary on the added mass value. The coefficient β taking into account this influence may be rather big. Say, for $R/r_0 = 0.8$, we have $\beta = 4.56$.

Example. We determine eigenfrequencies of the outer shell (the inner shell is assumed to be solid) reinforced by the longitudinal stiffeners and having contact with outer water and with water between the shells.

The initial data are $r_0 = 4.6$ m, $R = 3.7$ m, $h = 0.6$ cm, $l = 1.2$ m, $b = 0.5$ m; the longitudinal stiffeners are flat-bulb No. 8 made from steel.

We present the values of eigenfrequencies and the partial frequencies of the shell and the stiffeners in water and in air (vacuum) in Table 6.3.

The above calculations indicate that the presence of water results in a substantial decreasing (by more than 12 times) of the lowest eigenfrequency of the construction, corresponding to prevailing oscillations of stiffeners. The upper frequency corresponding to prevailing oscillations of the plating is reduced unsubstantially (by less than the factor of two) whereas the corresponding partial frequency becomes 12 times less due to the water added mass. This confirms the necessity of taking into account the collective oscillations of the shell and the reinforcing elastic stiffeners for the construction in fluid.

Table 6.3 Frequencies of the shell and the longitudinal frame in fluid

Conditions of contact with water	Eigenfrequencies, Hz		Partial frequencies, Hz	
	Shell	Stiffeners	Shell	Stiffeners
Construction in air	1670	229	1010	231
Construction in water	885	18.7	82.5	18.8

6.10 Added Masses of Plates with Cutouts

Following [10, 44, 210], the frequency of oscillation of a continuous plate in fluid is

$$\lambda_0^* = \frac{\lambda_0}{\sqrt{1 + 2\mu(a/b)\rho_0 a/(\rho_1 h)}},$$

where λ_0 is the frequency of oscillations of the continuous plate in air, $\mu(a/b)$ is the added mass coefficient for the continuous plate determined in Sect. 6.3; ρ_0 the fluid density, ρ_1 the density of the plate material, a and b are the least and biggest dimensions of the plate, and h the plate thickness.[11]

Analogously, the frequency of oscillation of the plate with cutout immersed in fluid is

$$\lambda^* = \frac{\lambda_0(1 + \xi(d/a))}{\sqrt{1 + 2\mu(a/b)\kappa(d/b)\rho_0 a/(\rho_1 h)}}.$$

Here d is the biggest dimension of the cutout (or the diameter of the circular cutout), $\xi(d/a)$ is the correction coefficient expressing the dependence of the oscillation frequency of the plate in air on the cutout size, and $\kappa(d/b)$ is the correction coefficient of the added mass taking into account the presence of the cutout.

The oscillation frequency for a continuous plate in air depends on the boundary conditions at the edges and is determined by the well-known formulas:

– For the freely supporter plates

$$\lambda_0 = \frac{\pi^2}{a^2}\left(1 + \frac{a^2}{b^2}\right)\sqrt{\frac{D}{\rho_1 h}};$$

– for the rigidly clamped plates

$$\lambda_0 = \frac{22.373}{a^2}\sqrt{\frac{D(1 + 0.605a^2/b^2 + a^4/b^4)}{\rho_1 h}}.$$

Here $D = Eh^3/(12(1-\nu^2))$ is the cylindrical rigidity, E is the elasticity modulus, and ν is the Poisson coefficient.

Introducing the correction coefficients ξ and κ we can reduce the problem of finding frequencies of oscillations of the plate with cutout in air and in fluid to the analogous problem for the continuous plate of the same dimensions, which can be easily solved.

The dependencies $\xi(d/a)$ and $\kappa(d/b)$ were found by V.N. Fedorov experimentally by comparing eigenfrequencies of oscillations in air and in fluid for a large series of plates with cutouts. It was found that the eigenfrequencies of oscillations in air and in fluid of a plate with the central cutout are always higher than those for the analogous continuous plate.

We approximate the coefficient $\xi(d/a)$ by the cubic parabola:

[11] This section was written by V.N. Fedorov.

– for the free support

$$\xi\left(\frac{d}{a}\right) = \frac{2.5}{n^2+n-1}\left(\frac{a}{b}\right)^{2+b/(4a)}\left(\frac{d}{a}\right)^3, \tag{6.83}$$

– for the rigid clamping

$$\xi\left(\frac{d}{a}\right) = \frac{5}{(n^2+n-1)^{a/b}}\left(\frac{a}{b}\right)^{2+a/(2b)}\left(\frac{d}{a}\right)^3, \tag{6.84}$$

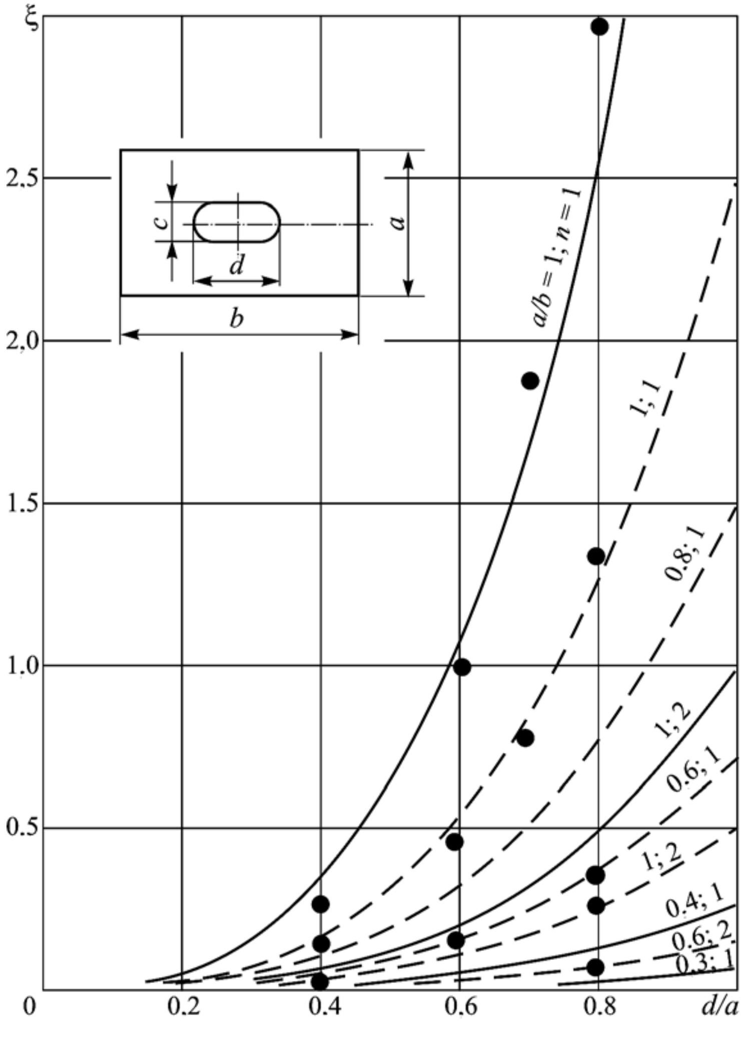

Fig. 6.22 Comparing the values of the coefficient ξ calculated by formulas (6.83) and (6.84) with experimental data; *dashed line*—free support, *solid line*—rigid clamping, ●●●—experimental data

where $n = d/c$ is the relative size of the cutout and c is the lesser dimension of the cutout.

We present the dependencies $\xi(d/a)$ for several values of a/b and n in Fig. 6.22 together with experimental data.

The frequencies determined by formulas (6.83) and (6.84) satisfy the experimental values and frequencies obtained by the energy method with error not exceeding 5% for the square plates (as the relative size b/a increases, the error diminishes).

Interpolation formulas (6.83) and (6.84) can be used in calculations of frequencies of plates having central cutouts for values b/a between 1 and 4. For plates with $b/a > 4$, the influence of the cutout on the frequency is negligible in practice.

The plate added masses decrease in the presence of the cutout. Based on experimental data, we have obtained the unified averaged dependence for the correction coefficient of added masses $\kappa(d/b)$:

$$\kappa\left(\frac{d}{b}\right) = 1 - \frac{3}{2}\frac{d}{b} + \frac{3}{2}\left(\frac{d}{b}\right)^2 - \frac{2}{3}\left(\frac{d}{b}\right)^3. \tag{6.85}$$

This dependence presented graphically in Fig. 6.23 is valid for rectangular isolated plates with arbitrary boundary conditions and arbitrary stretching having circular or oval longitudinally oriented cutouts.

Analyzing the experimental data (see Fig. 6.23) we find that the actual added mass correction coefficients for isolated rigidly clamped plates are 5–10% less and the ones for the freely supported plates are 5–10% more than those calculated by formula (6.85). Hence, the averaged dependence (6.85) ensures the least error when calculating elastically clamped plates with mixed boundary conditions, which are the most common elements of actual constructions.

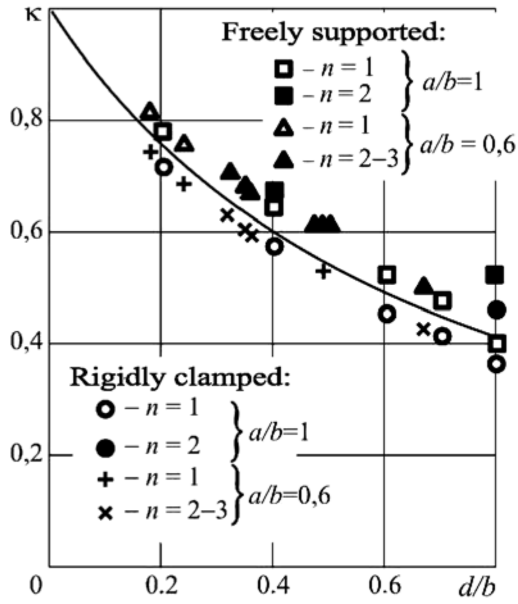

Fig. 6.23 Comparing the correction coefficient κ calculated by formula (6.85) with experimental data

Chapter 7
Elastic One-Dimensional Oscillations of an Elongated Body in Fluid: Reduction Coefficients

In this section we discuss a way to describe elastic oscillations of an elongated body (say, a hull) in a fluid along the long axis of the body.[1] Assuming that the shape of cross-sections of the body remains unchanged under oscillations (i.e., the oscillation is identical to the oscillations of an elastic rod), one can introduce the notion of a so-called *reduction coefficient*. The reduction coefficients describe three-dimensional effects: a reduction coefficient is given by the ratio of an added mass of an elongated body oscillating in one direction (vertical, horizontal of torsional) to the added mass computed by the method of planar sections.

7.1 General Discussion

In studies of low frequency *transverse* oscillations a hull or another elongated body can be modeled by an elastic rod (see for description of elastic oscillations of the rod [20, 103, 105, 107, 122, 154, 172, 178, 187, 212]).

In solution of the hydroelastic problem one can use the following simplifying assumptions:

1. Shape of free oscillations of the hull is the same under oscillations in air and in water.
2. Amplitude of the oscillations is small.
3. The oscillation frequency is high; thus one can neglect the induced free surface waves.
4. Induced fluid velocities are small.
5. The hull is considered as an elongated body whose hydrodynamics can be described by considering a two-dimensional hydrodynamic problem in each section (and then introducing a coefficient related to space effects).

Assumption 1 allows us to separate the problem into two parts: the problem of elastic oscillations of the rod (hull) and the hydromechanical problem. In [186] an error was evaluated which may be induced by the assumption 1. It was shown for example that, under this assumption, the maximal error in determining the eigenfrequency of a 12th tone or prism-shaped rod does not exceed 2%. On the other hand, the shape of the rod oscillations in water differs more essentially from the shape of rod oscillation in air. In Fig. 7.1 we show the shapes of oscillation of the 1st and 10th tone of oscillations of a lighter ship hull having the displacement 62.090 tons.

[1] Sects. 7.1–7.3 were written by E.I. Ivanjuta.

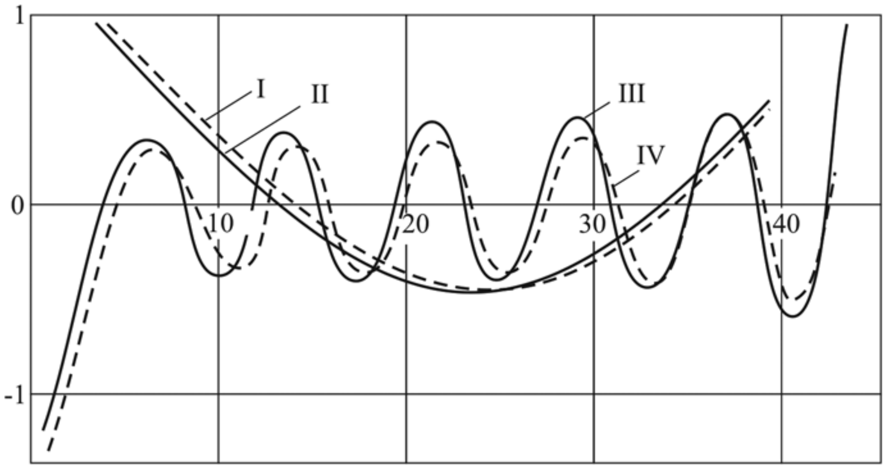

Fig. 7.1 Shape of vertical oscillations of lighter carrier: the first tone in air (*curve I*) and in water (*curve II*); the 10th tone in air (*curve III*) and in water (*curve IV*)

Assumptions 4 and 5 simplify the solution of the Laplace equation; they allow us to reduce the problem to the two-dimensional one.

According to experimental data, the rod approximation of the hull can be used up to the tone number $n = 1 + 0.7L/B$, where L is the maximal length of the hull; B is the maximal width of the hull.

The three-dimensional effects of the flow around an oscillating hull (or an elongated body in general) are captured by the so-called *reduction coefficients* J_n, where n is the number of the tone of oscillation. The coefficient J_n is defined as follows:

$$J_n = \frac{T_n}{T_n^{\text{p.s.}}}$$

where T_n is the kinetic energy of the fluid flow arising under elastic oscillations of the hull on the nth tone; $T_n^{\text{p.s.}}$ is the approximation to the kinetic energy computed by the method of planar sections. Namely, $T^{\text{p.s.}} = \int_0^L T(x)\,dx$ where x is the coordinate along the axis of oscillations, and $T(x)$ is equal to $\lambda(x)v(x)^2/2$ where $v(x)$ is the velocity of a given planar section, and $\lambda(x)$ is the added mass of this planar section in the direction of its motion.

Depending on oscillation type (horizontal, vertical or torsional) one can define three corresponding types of reduction coefficients: J_n^h, J_n^v and J_n^{tor}.

The coefficients J_n take into account both vibration and the three-dimensional nature of the flow; in all known cases they turn out to be smaller than 1.

7.2 Added Masses of Shipframes under Vibration

Let us introduce the parameters of an immersed part of the shipframe as shown in Fig. 7.2. We choose the coordinate system in a standard way: the z axis is directed downward; the x axis is directed along the central line of the hull; the y axis is parallel to the free surface. We consider the following added masses of a shipframe: the added mass λ_{22} corresponds to motion of the shipframe in a horizontal direction, λ_{33} corresponds to the motion in a vertical direction; the added mass λ_{44} corresponds to rotation with respect to the torsion center c. The position of the torsion center is described by the properties of the hull as a whole; in Table 2.3 we compute λ_{44} with respect to the point of intersection of the waterplane and the central plane of the hull. If the torsion center is shifted with respect to this point, then λ_{44} transforms accordingly.

Denote by $d(x)$ the draught and by $b(x)$ the (half of) the width of the shipframe at waterline; $S(x)$ is the area of the immersed part of the shipframe. By n we denote the tone number.

We introduce coefficients c_h, c_v and c_{tor} (denoted in Chap. 2, see Table 2.3 by k_{220}, k_{33} and k_{44} respectively). These coefficients are equal to ratios of the added masses λ_{22}, λ_{33} and λ_{44} of the immersed part of the shipframe to corresponding added masses of the ellipse the same geometric size (with half-axes b and d).

We introduce also the following notations:

$$\sigma(x) = \frac{S(x)}{2b(x)d(x)}$$

is the area coefficient of a given shipframe;

$$q = \frac{d(x)}{b(x)}$$

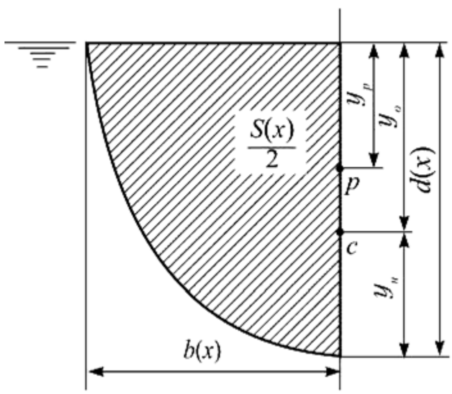

Fig. 7.2 Scheme of (half of) the immersed part of a shipframe. $S(x)$ is the area of the shipframe; p is the centroid of the immersed part of the shipframe area; c is the position of the center of torsional oscillations; the *upper horizontal line* is the waterline

is (a half of) the ratio of the draught to the width of the shipframe. We introduce the following auxiliary coefficient

$$a = \frac{1}{2}\Big[3(1+q) - \sqrt{1+10q+q^2-32\sigma q/\pi}\,\Big].$$

The following approximate formulas for coefficients c_h and c_v were proposed in [50, 128]:

$$c_v = 1 + (1+q-a)(q-a),$$

$$c_h = \frac{4}{\pi^2}\left[1 + \frac{4}{3q^2}(1+q-a)^2\right].$$

To take into account the three-dimensional effects one has to introduce also the correction (or *reduction*) coefficients J_n (which depend on the tone number); the added masses of the shipframe in a realistic situation then take the form:

$$\lambda_{22} = J_n^h c_h\left(\frac{\pi}{2}\rho d^2\right),$$

$$\lambda_{33} = J_n^v c_v\left(\frac{\pi}{2}\rho b^2\right).$$

To write down approximate empiric formulas[2] for coefficients J_n^h and J_n^v we need to introduce some additional notations:

$$\alpha_h := \frac{L}{T}, \qquad \alpha_v := \frac{L}{B},$$

$$e_h := \frac{0.16\alpha_h + 1}{0.3\alpha_h}, \qquad e_v := \frac{0.16\alpha_v + 1}{0.3\alpha_v},$$

$$p_h := 1.03 - \frac{1.7}{\alpha_h}, \qquad p_v := 1.03 - \frac{1.7}{\alpha_v},$$

$$q_h := \frac{\alpha_h - 0.125}{\alpha_h + 2.5}, \qquad q_v := \frac{\alpha_v - 0.125}{\alpha_v + 2.5},$$

$$f_h := \frac{p_h q_h (e_h + 5)}{1 - p_h q_h}, \qquad f_v := \frac{p_v q_v (e_v + 5)}{1 - p_v q_v},$$

and, finally,

$$R_n^h := \frac{f_h}{p_h(e_h + f_h + n)}, \qquad R_n^v := \frac{f_v}{p_v(e_v + f_v + n)}.$$

[2] These formulas were derived as a result of efforts of several authors (technical reports of Krylov Research Shipbuilding Institute, 1970–1980, unpublished).

Then coefficients J_n obtained using the model of elongated ellipsoid of revolution (i.e., the ratio B/T is assumed to be 2) are given by:

$$J_1^h = 1.035 - 1.674\frac{L}{\alpha_h}, \qquad J_1^v = 1.035 - 1.674\frac{L}{\alpha_v} \tag{7.1}$$

and

$$J_n^v = J_1^v R_n^v, \qquad J_n^v = J_1^v R_n^v. \tag{7.2}$$

The reduction coefficients obtained using the model of a three-axial ellipsoid (in that case the ratio B/T can be arbitrary) have the following form:

$$J_n^{h*} = J_n^h\left(1 + \frac{0.02(B/T-2)}{J_n^h}\right), \qquad J_n^{v*} = J_n^v\left(1 + \frac{0.02(B/T-2)}{J_n^v}\right). \tag{7.3}$$

For bulb-type shipframes, whose form coefficient is greater than 1, one can use the above formulas by substituting the maximal width of the shipframe $b_{\max}$ instead of b.

Values of coefficients c_v, c_n, c_{tor} and c_{incl} presented in Table 2.4 are computed for shipframes with $b/d < 2$ (however, for some ships one can have $b/d > 3$). To evaluate the dependence of c_v and c_h on b/d for various form coefficients (close to 1) one can use graphs shown in Fig. 2.49 [122].

7.3 Reduction Coefficients of Simplest Elongated Bodies Vibrating in Transverse Direction

7.3.1 Reduction Coefficients for a Circular Cylinder under Transversal Oscillations

Consider transverse oscillations of an infinitely long circular cylinder of radius a. Introduce the cylindrical coordinate system (x, r, θ) (see Fig. 7.3). Consider bending oscillations of the cylinder in the xy-plane, such that velocities of points of the

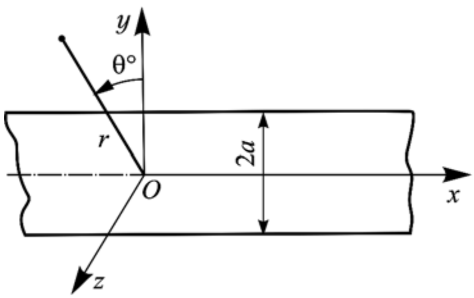

Fig. 7.3 Cylindrical coordinate system

surface of the cylinder depend on x and θ as follows:

$$v(r=a,\theta,x)=v_0\cos kx\cos\theta. \tag{7.4}$$

Solutions of the Laplace equation for velocity potential

$$\frac{\partial^2\varphi}{\partial x^2}+\frac{\partial^2\varphi}{\partial r^2}+\frac{1}{r}\frac{\partial\varphi}{\partial r}+\frac{1}{r^2}\frac{\partial^2\varphi}{\partial\theta^2}=0,$$

taking into account (7.4), can be represented in the form

$$\varphi(x,r,\theta)=R(r)\cos kx\cos\theta;$$

this leads to the following ODE for the function R:

$$R''+\frac{1}{r}R'-\left(k^2+\frac{1}{R^2}\right)R=0. \tag{7.5}$$

Solution of Eq. (7.5), vanishing for $r\to\infty$, is given by the Bessel function of second kind of first order $R(r)=CK_1(kr)$ where an arbitrary constant C is determined from the boundary condition (7.4):

$$\left.\frac{\partial\varphi}{\partial r}\right|_{r=a}=v_0\cos ks\cos\theta=CkK_1'(ka)\cos kx\cos\theta;$$

$$C=\frac{v_0}{kK_1'(ka)}.$$

Therefore, the expression for velocity potential near vibrating cylinder looks as follows:

$$\varphi(x,r,\theta)=\frac{v_0}{kK_1'(ka)}K_1(kr)\cos kx\cos\theta. \tag{7.6}$$

Computing the kinetic energy of fluid using (7.6) we find

$$T=-\frac{1}{2}\rho\int_0^{2\pi}\varphi\frac{\partial\varphi}{\partial r}a\,d\theta=-\frac{1}{2}\rho\frac{K_1(ak)}{akK_1'(ak)}a^2\pi v_0^2\cos^2 kx.$$

Dividing the kinetic energy by the square of local velocity in the y-direction $(1/2)v_0^2\cos^2 kx$, we get the added mass λ_{22} of the circular cylinder vibrating in the xOy plane:

$$\lambda_{22}=-\rho a^2\pi\frac{K_1(ak)}{akK_1'(ak)}=\rho a^2\pi\frac{1}{1+ak[K_0(ak)/K_1(ak)]},$$

where K_0 is the Bessel function of second kind of 0th order; in computations leading to this formula one has to use the identity

$$-K_1'(z)=K_0(z)+\frac{1}{z}K_1(z).$$

We see that the added mass of a vibrating cylinder differs from the added mass of a cylinder moving without changing its shape (equal to $\rho\pi a^2$) by the multiplier

$$J = \frac{1}{1 + ak[K_0/K_1(ak)]}. \tag{7.7}$$

Consider now vibrations of a cylinder of finite length L. Let us choose in (7.7) $k := J_n = \pi n/L$ $(n = 1, 2, \ldots)$. Then on the cylinder of length L one has n nodes, since the distribution of velocities is determined by formula (7.4). Then $ak = a\pi n/L$ and the coefficient (7.7) takes the form

$$J_n = \frac{1}{1 + a\pi n/L[K_0(a\pi n/L)/K_1(a\pi n/L)]} \tag{7.8}$$

which depends on the number of nodes and on the ratio a/L.

The formula (7.8) gives reduction coefficients for the circular cylinder.

In fact, under vibration of a cylinder of finite length L, boundary conditions on its ends differ from the case of an infinite cylinder. More precise formulas for J_n which take into account these boundary conditions are given in [144].

Coefficient J_n remains the same when a cylinder is floating horizontally on a free surface in half-submerged position since corresponding added masses (the added mass of a vibrating cylinder and the added mass of a cylinder of stationary shape) decrease by the factor of 2 in comparison with cylinders in an infinite fluid.

In Fig. 7.4 we show graphs of $J_n(L/B)$ $(B = 2a$ is the diameter of the cylinder) for $n = 2, 3, 4$ obtained for the circular cylinder by different authors. Curve 1 is computed by the formula (7.8); the curve 2 was obtained in [124]; curve 3 was obtained in [144]. In the same figure we show experimental points (circles) obtained in [144]. The curves shown in bold give the shape of bending oscillations for $n = 2, 3, 4$ in water; circles on these curves correspond to the shape of oscillations in air.

7.3.2 Reduction Coefficients for a Vibrating Elliptic Cylinder

To determine the added mass of an elliptic cylinder vibrating in a vertical plane in an infinite fluid or being half-submerged, one can use reduction coefficients J_n, which are given in Fig. 7.5 for $n = 2, 3, 4$ and the ratio of axes $B/2d$ equal to 2 and 4. The numbers assigned to separate points show the value of n.

7.3.3 Reduction Coefficients for a Vibrating Rectangular Pontoon

Explicit theoretical solution of the problem of vibration of a floating rectangular pontoon of infinite length is not known (to the best of the author's knowledge). Here

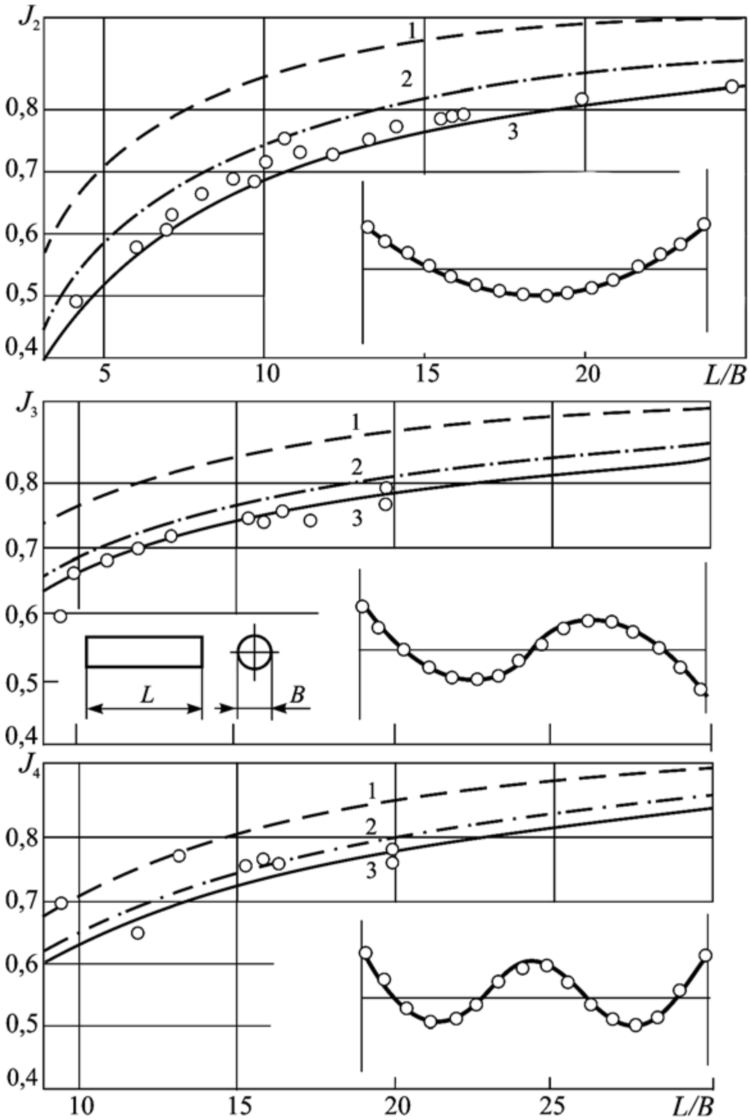

Fig. 7.4 Dependence of reduction coefficients on elongation of a circular cylinder

we present experimental data for the coefficient J_2 [144] for different combinations of values of B/D (and $B/2d$, where D is the height, B is the width and d is the draught of the pontoon), see Fig. 7.6. The added mass of a plane section of a non-vibrating rectangular pontoon necessary for computation of J_2, was computed via

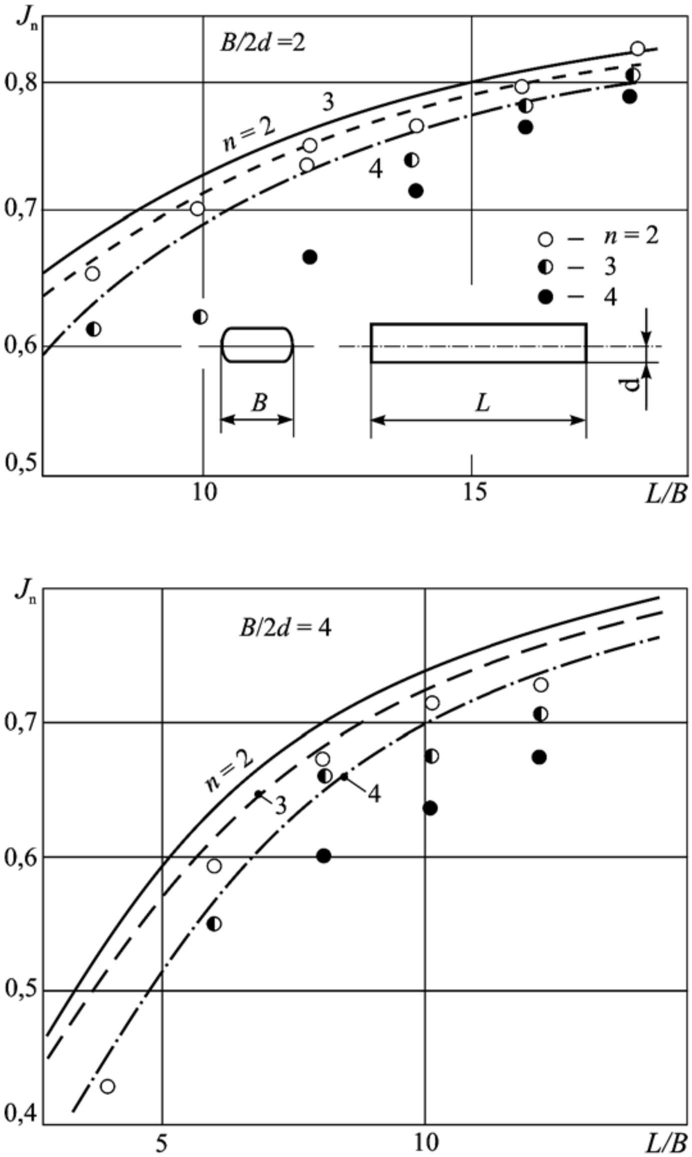

Fig. 7.5 Reduction coefficients for an elliptic cylinder

the formula $\lambda_{22} = k_{22}\rho\pi(B/2)^2$, where the coefficient k_{22} (see Fig. 7.7) is taken from the work [131]. The added mass of a plane section of a vibrating pontoon is given by $\lambda_{22}^{\mathrm{vib}} = J_2\lambda_{22}$.

For a pontoon of finite length L and square section we present in Fig. 7.8 the experimental curve showing dependence of J_2 on $B/2d$ for various L/B.

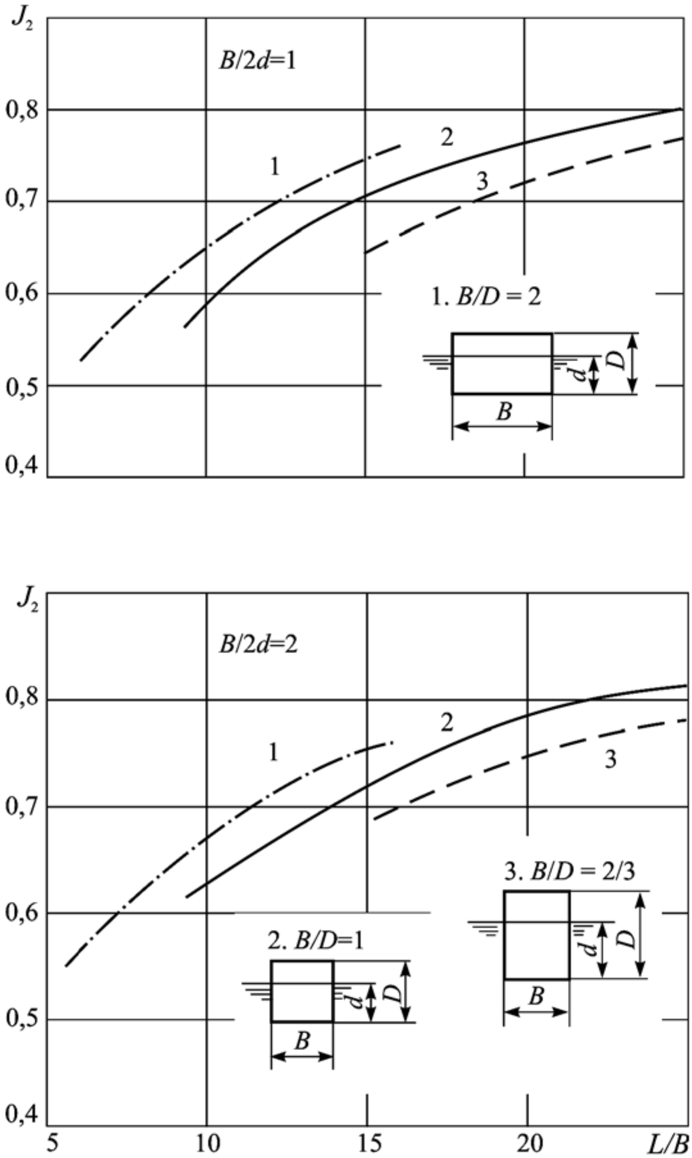

Fig. 7.6 Reduction coefficients for a rectangular pontoon: *1*—for the model 1; *2*—for the model 2; *3*—for the model 3

7.3.4 Reduction Coefficients for Vibrating Ellipsoid of Revolution

Theoretically the added masses of a vibrating ellipsoid of revolution were considered in [131, 142, 143]. Curves showing dependence of reduction coefficients J_n for $n = 2, 3, 4, 5$ on the ratio L/B (L is the length and B is the width of the ellip-

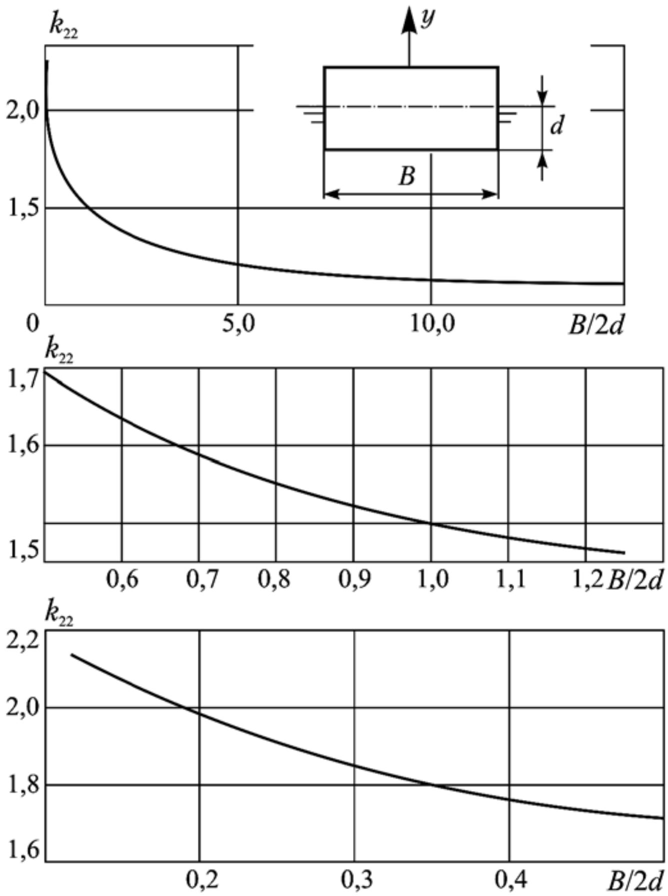

Fig. 7.7 Coefficient k_{22} of added mass of a rectangular pontoon under vertical motion

soid of revolution) are given in Fig. 7.9. The curves in the right lower corners of the graphs correspond to the shape of the central line of the ellipsoid under oscillation for $L/B = 20$.

Curves 1 correspond to the data of [131]; curves 2 were obtained in [143]; curves 3—in [142]. In the same graphs we show the experimental points [144].

Consider the influence of the shape of the axial line of the ellipsoid under vibration with the same number of nodes on reduction coefficients J_n. In [144] dependence of J_n on b/a (where a is the deviation of the end of vibration body, b is the deviation of the point situated in the middle between two nodes) were studied for the circular cylinder with $L/B = 9$ (Fig. 7.10a) and the ellipsoid of revolution with $L/B = 11$ (Fig. 7.10b) for $n = 2, 3, 4$.

If a cylinder is vibrating between two boundaries such that its ends are close to the vertical walls, the reduction coefficient changes. Dependence $J_n(L_0/L)$ where L

Fig. 7.8 Experimental data on reduction coefficients of a rectangular pontoon of finite length

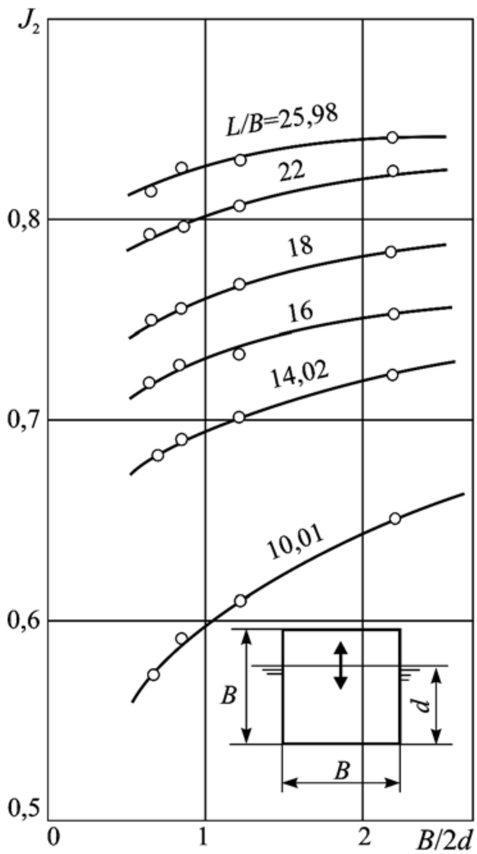

is the length of the vibrating cylinder, L_0 is the distance between two walls, $n = 2, 3$ was obtained experimentally in [144], see Fig. 7.11.

When the half-immersed floating cylinder is vibrating in a horizontal plane, its reduction coefficient differs from the coefficient corresponding to vibration in a vertical plane. Corresponding coefficients $J_2(L/B)$ and $J_3(L/B)$ are represented by curves 4 in Fig. 7.9 [143]. In the case of two-node vibration ($n = 2$) the nodes were situated at the distance $x = \pm 0.223L$ from the center; for $n = 3$ the positions of nodes were at $x = 0$ and $x = \pm 0.3L$.

There exist numerous publications devoted to computation of the reduction coefficients (see for example [50, 122, 186]). In most of these works the hull was schematically represented as one or another body of revolution: the circular or elliptic cylinder of finite length [186], ellipsoid of revolution [128] or three-axial ellipsoid. Modeling the hull by a three-axial ellipsoid allows us to take into account both ratios L/B and B/T (L is the length, B is the width, T is the draught). It turns out that compressibility of fluid does not essentially influence the reduction coefficients.

In Table 7.1 we present values of reduction coefficient J_n^v for the first six modes of vertical oscillations of a three-axial ellipsoid.

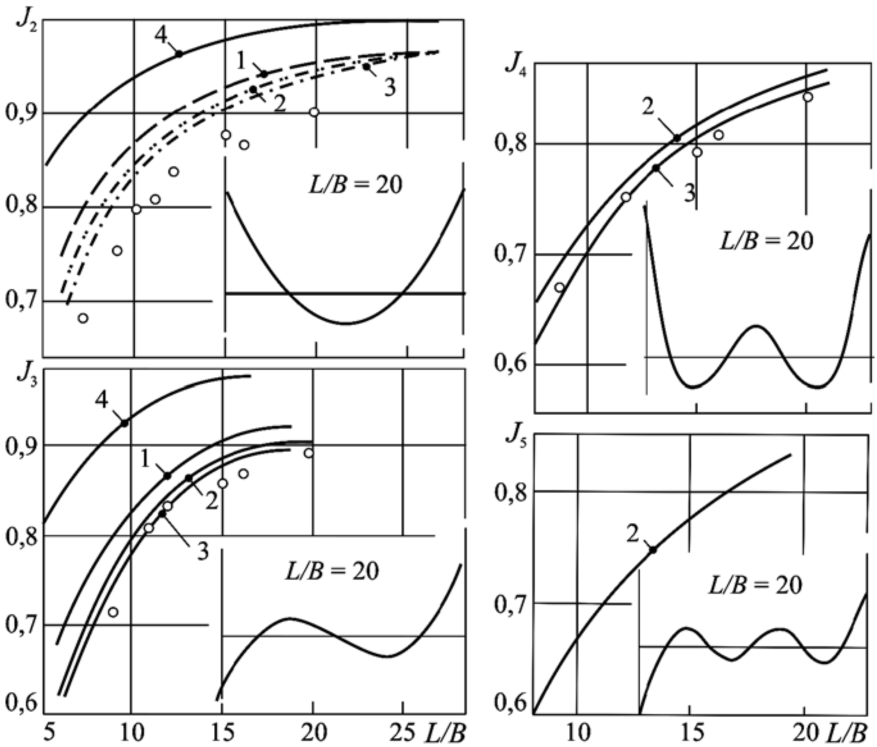

Fig. 7.9 Reduction coefficients of an ellipsoid of revolution

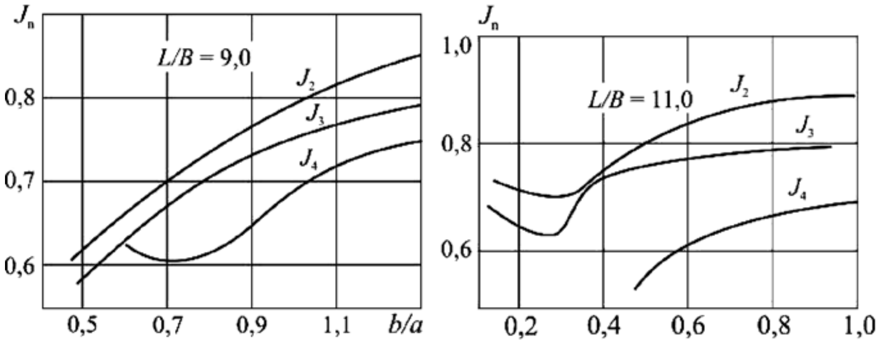

Fig. 7.10 Influence of a bending shape of vibrating body on reduction coefficients

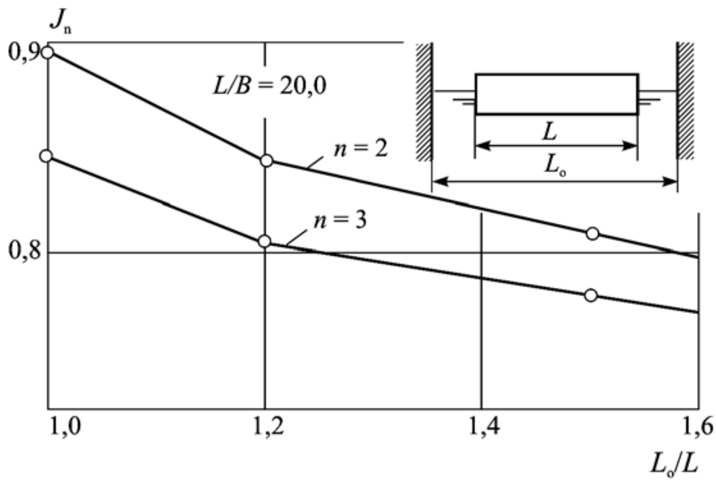

Fig. 7.11 Influence of walls on the values of reduction coefficients

7.3.5 *Added Moments of Inertia under Torsional Oscillations of the Hull*

The influence of the shape of torsional oscillations and three-dimensional effects on the value of the torsional added moment of inertia was studied in [50, 157]. In [157] the hull was modeled by an elliptic cylinder and a three-axial ellipsoid.

In Fig. 7.12 we show the dependence of coefficients corresponding to the first two tones, J_1^{tor} and J_2^{tor}, on the ratio L/B for constant ratio $B/T = 3$.

Table 7.1 Reduction coefficients for three-axial ellipsoid

Tone	L/B	B/T					
		2.2	2.5	3.0	3.5	4	5
$n = 1$	4	0.526576	0.561010	0.602126	0.630189	0.650272	0.676660
	6	0.690928	0.715381	0.743838	0.763020	0.776687	0.794696
	7	0.742383	0.763185	0.787374	0.803641	0.815237	0.830543
	8	0.781685	0.799643	0.820435	0.834426	0.844411	0.857608
	9	0.812395	0.828044	0.846150	0.858352	0.867046	0.878558
	10	0.836870	0.850640	0.866580	0.877285	0.884934	0.895136
	12	0.873018	0.883964	0.896598	0.905111	0.911179	0.919266

(*continued on next page*)

Table 7.1 (continued)

Tone	L/B	B/T					
		2.2	2.5	3.0	3.5	4	5
$n=2$	4	0.430890	0.436994	0.506621	0.537417	0.559876	0.589816
	6	0.602164	0.630541	0.664228	0.687235	0.703731	0.725525
	7	0.661495	0.686570	0.716040	0.736052	0.750390	0.769302
	8	0.708427	0.730604	0.757494	0.774099	0.786657	0.830277
	9	0.746081	0.765795	0.788773	0.834313	0.815445	0.830180
	10	0.776729	0.794355	0.814867	0.828721	0.838639	0.851775
	12	0.823100	0.837439	0.854095	0.865353	0.873399	0.884120
$n=3$	4	0.374299	0.398268	0.435538	0.465065	0.487686	0.518743
	6	0.530859	0.560111	0.596026	0.621104	0.621104	0.639279
	7	0.529963	0.620075	0.652619	0.675026	0.691180	0.712661
	8	0.644012	0.668750	0.698077	0.718141	0.732558	0.751701
	9	0.686126	0.708586	0.735061	0.753098	0.766069	0.783292
	10	0.712121	0.741550	0.765532	0.781834	0.793548	0.809091
	12	0.775369	0.792387	0.812310	0.825826	0.835545	0.848377
$n=4$	4	0.350578	0.358463	0.384063	0.409436	0.430430	0.460736
	6	0.475267	0.502765	0.538386	0.564109	0.583057	0.608529
	7	0.536092	0.563354	0.597078	0.620768	0.638013	0.661049
	8	0.588426	0.614250	0.646492	0.667146	0.682831	0.703736
	9	0.632882	0.656941	0.685694	0.705489	0.719794	0.738845
	10	0.670652	0.692934	0.719386	0.737506	0.750580	0.768062
	12	0.730562	0.749659	0.772133	0.787490	0.798543	0.813323
$n=5$	4	0.355378	0.340601	0.349047	0.367315	0.385180	0.413249
	6	0.433518	0.456935	0.490081	0.515266	0.534274	0.560230
	7	0.489777	0.515531	0.548828	0.572893	0.590660	0.614697
	8	0.541068	0.566724	0.598619	0.621146	0.637585	0.659640
	9	0.586156	0.610800	0.640812	0.661731	0.676947	0.697312
	10	0.625399	0.648680	0.676731	0.696151	0.710214	0.729017
	12	0.689149	0.709622	0.734008	0.750805	0.762924	0.779038
$n=6$	4	0.385145	0.341501	0.327651	0.336226	0.349646	0.374215
	6	0.403881	0.421084	0.449860	0.473522	0.491996	0.517793
	7	0.452839	0.475589	0.507109	0.530787	0.548595	0.572907
	8	0.501191	0.525568	0.557067	0.579813	0.596632	0.619365
	9	0.545485	0.569837	0.600226	0.621782	0.637559	0.658786
	10	0.585029	0.608648	0.637558	0.657806	0.672675	0.692415
	12	0.650944	0.672412	0.698186	0.716033	0.728981	0.746281

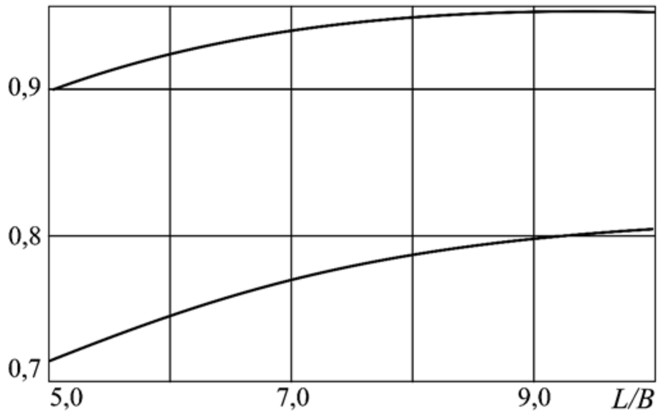

Fig. 7.12 Reduction coefficients J_1^{tor} (the upper curve) and J_2^{tor} (the lower curve) under torsional oscillations of a three-axial ellipsoid for $B/T = 3$

7.4 Influence of Shallow Water on Added Masses of a Hull under Vertical Vibrations

Here we present the results of experimental study of vertical oscillations of the hull of a cargo ship (vegetable carrier) of inland type ST-1302 on shallow and deep water, and results of studies of a model of this ship.[3] The main goal of this study was to determine the dependence of frequency and shape of hull oscillation on the depth of water; thus obtaining information about dependence of added masses of the hull on the depth.

By analyzing the influence of water depth on eigenfrequencies we get information on influence of the water depth on added masses of the ship. Parameters of this ship were as follows: length at waterline: $L = 83.6$ m; width at waterline $B = 12$ m, average draught $T = 1.2$ m. The depth water: $H = 12$ m (which corresponds to $h = 10.8$ m under the keel) in experiments on "deep" water. The depth of water in experiments on shallow water was $H = 3.2$ m (which corresponds to $h = 2$ m under the keel).

The vibrogenerator of eccentric type (see Fig. 7.13) was installed on the transom of the ship; the vibrosensors collecting the information about oscillations of the hull were installed on sides and on bulkheads.

Shapes and frequencies of the ship oscillations for these values of h are shown in Fig. 7.14.

To study a possibility of obtaining realistic results on models of a hull, there were constructed four elastic models of the hull; all models had length 3 m, width 0.43 m, had the same mass and elasticity, but different configurations of the hull.

The models were constructed as follows: 10 synthetic foam blocks were attached by bolts to a channel bar of 3 m length; a gap between two blocks was equal to 1 cm;

[3]This section was written by A.S. Samsonov.

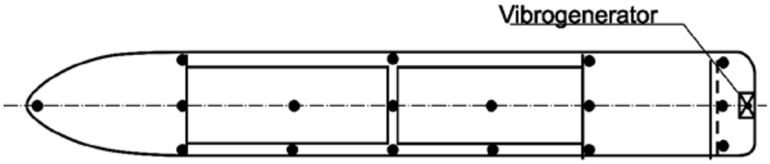

Fig. 7.13 Positions of vibrogenerator and vibrosensors on the hull of ST-1302

Fig. 7.14 Shapes of vertical oscillations of the hull. Small circles correspond to deep water ($h = 10.8$ m); crosses correspond to shallow water ($h = 2.0$ m). A denotes the amplitude of the oscillations

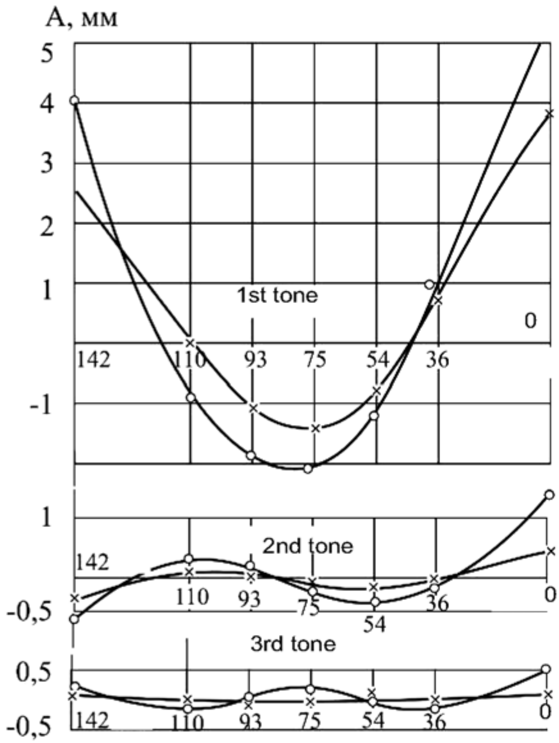

this gap was covered by a thin elastic film, which provided water-tightness of the hull, but did not influence its oscillations (Fig. 7.15 and Fig. 7.16). Elasticity of the hull of such a model was completely determined by elasticity of the central channel bar. Therefore, on each model one could easily excite the first five eigenmodes of vertical oscillations; the difference between these oscillations was determined only by the difference in added masses.

The configuration of the hull of the 1st model was exactly identical to the shape of ST-1302; however, the elasticity of the hull of ST-1302 was not modeled. The other three models were studied to understand the influence of the shape of the keel on eigenfrequencies and shapes of oscillations of inland ships of this kind. These three models had the identical shape of shipframes over the length; the difference between them was in the angle of inclination of sides at the waterline level (90°, 60° and 30°

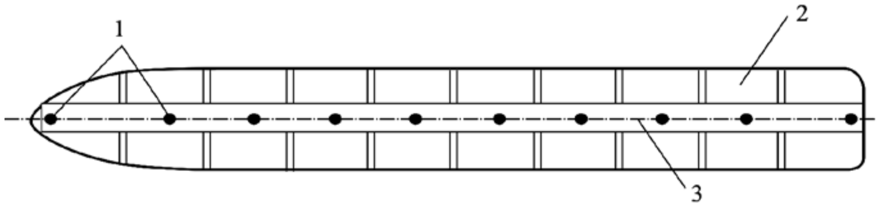

Fig. 7.15 The main model of the ship ST-1302 and positions of vibrosensors. *1*—vibrosensors, *2*—synthetic foam blocks; *3*—channel bar

Fig. 7.16 Cross-section of the model of the ship ST-1302

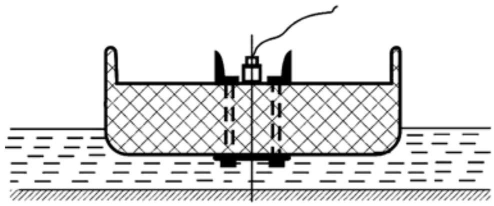

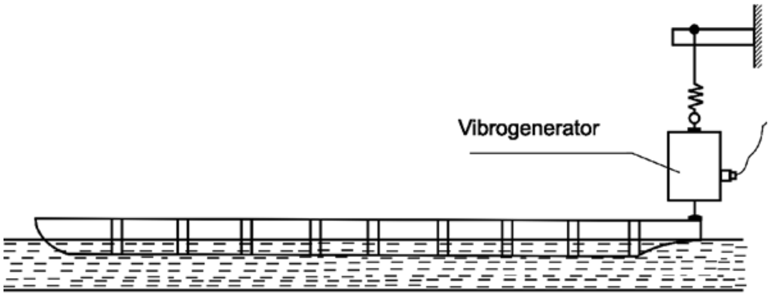

Fig. 7.17 Position of vibrogenerator on the models

respectively); therefore, while all of these models had the same displacement, the draught and width at waterline was slightly different.

Vertical oscillations of each model were generated by a vibrogenerator installed at the stern (see Fig. 7.17; the amplitude of the generated oscillations was independent of frequency); oscillations were measured by 10 vibrosensors.

The oscillations of the model were studied at nine depths which were changing from minimal value $h/B = 0.02$ (B is the width at waterline, h is the depth under the keel) to the value $h/B = 2$; further increase of the depth did not show any change in eigenfrequencies (and, therefore added masses) of the models.

It was shown that for $h/B = 0.02$ all five eigenfrequencies were about 45% smaller than the eigenfrequencies for $h/B > 2$. Moreover, the amplitude of oscillations at the ends of the models was $3 - 5$ times smaller for $h/B = 0.02$ in comparison with the same amplitude for $h/B > 2$ (Fig. 7.18). Analogous effects were observed for the ship ST-1302 itself (Fig. 7.14).

Table 7.2 Comparison of experimental frequencies (Hz) of vertical oscillations of three inland cargo ships on shallow and deep water with theoretical results obtained via the formula (7.10). "D"—deep, "S"—shallow, "exp"—experiment; "th"—theory

Tone	ST-1302			"Kujbyshev GES"			"Soviet Azarbajdjan"		
	D., exp.	S., exp.	S., th.	D., exp.	S., exp.	S., th.	D., exp.	S., exp.	S., th.
1	1.6	1.36	1.33	1.68	1.45	1.43	1.60	1.48	1.38
2	3.25	2.64	2.71	3.37	2.92	2.85	3.05	2.53	2.63
3	–	–	–	4.97	4.03	4.22	4.13	3.47	3.57
4	–	–	–	6.52	5.53	5.53	5.25	4.33	4.53
5	–	–	–	7.80	6.37	6.42	–	–	–

To evaluate the influence of shallow water on eigenfrequencies of vertical oscillations and added masses one can use the following formula:

$$\eta^i := \left(\frac{N^i_{\text{deep}}}{N^i_{\text{shallow}}}\right)^2 = \frac{D + M^i_{\text{shallow}}}{D + M^i_{\text{deep}}} \tag{7.9}$$

where N^i_{shallow} are eigenfrequency number i $(i = 1, \ldots, 5)$ of vertical oscillations of the hull on shallow water; N^i_{deep} are eigenfrequency number i $(i = 1, \ldots, 5)$ of vertical oscillations of the hull on deep water; D is the displacement of the ship; M^i_{shallow} and M^i_{deep} are added masses on shallow and deep water, respectively.[4]

If the coefficients η^i and added masses M^i_{deep} of the hull on deep water are known, one can determine the added masses M^i_{shallow} on shallow water.

Experiments on a model allowed us to determine the dependence of η^i on the ratio h/B; these coefficients turn out to be almost coinciding for all four models, and, moreover, they are almost the same for all i, i.e., are in fact independent of the mode of oscillation.

Therefore, one can propose a general averaged dependence of η^i on h/B which looks as follows:

$$\eta_{(i)} = 0.075\frac{B}{h} + 1. \tag{7.10}$$

Applicability of this formula can be evaluated using the following Table 7.2 where we show the eigenfrequencies of the first five modes of vertical oscillations for ST-1302 as well as two other ships obtained experimentally at different times, and compare them with theoretical values obtained by the formula (7.10). The maximal deviation of theoretical values from the experimental data equals 7%.

[4]Here one uses the naive notion of added mass: one assumes that the hull oscillates as an elastic rod of two different masses both in air and in water. The mass of the rod oscillating in air is its real mass; the mass of the rod oscillating in water is assumed to be a sum of its real mass and the added mass. Relationship of this notion of added mass to the general notion of added mass of vibrating body from Chap. 6 is not obvious, although these notions do coincide in the main order.

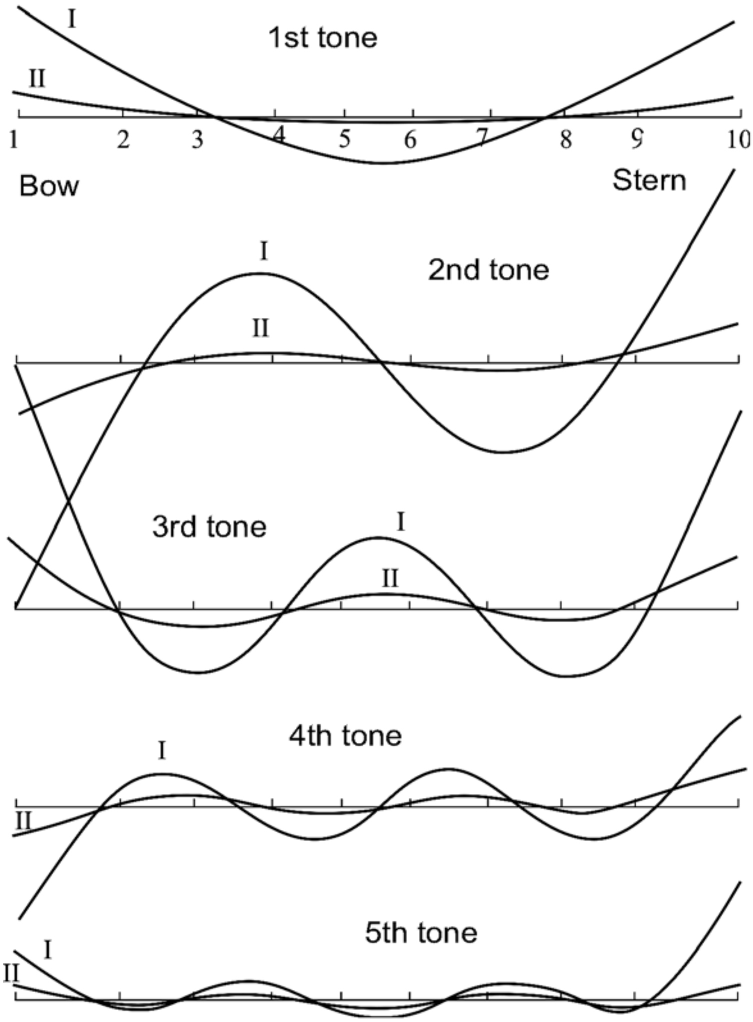

Fig. 7.18 Shapes of first 5 model of vertical oscillation of the model of ship ST-1302. The first mode is shown on *top*; the 5th in the *bottom*. *I*—deep water ($h/B = 1.89$); *II*—shallow water ($h/B = 0.02$). The *stern* is at the *right side* of the graphs; the bow is at the *left*

The experiments on the ship ST-1302 (the length at waterline 83.6 m, width 12 m, depth under keel on deep water 10.8 m, on shallow water 2 m) were carried out in 1983 by A.S. Samsonov. Experiments on cargo ship "Kujbyshev GES" (length at waterline 131 m, width 16.8 m, depth under keel in deep water 72 m, on shallow water 3.25 m) were carried out in 1964 by M.M. Bolesko and O.N. Lychev. The experiments on ferry "Soviet Azerbajdjan" (length at waterline 127.2 m, width 17.5 m, depth under keel on deep water 14 m, on shallow water 3.75 m) were carried out in 1964 by F.P. Shujgin.

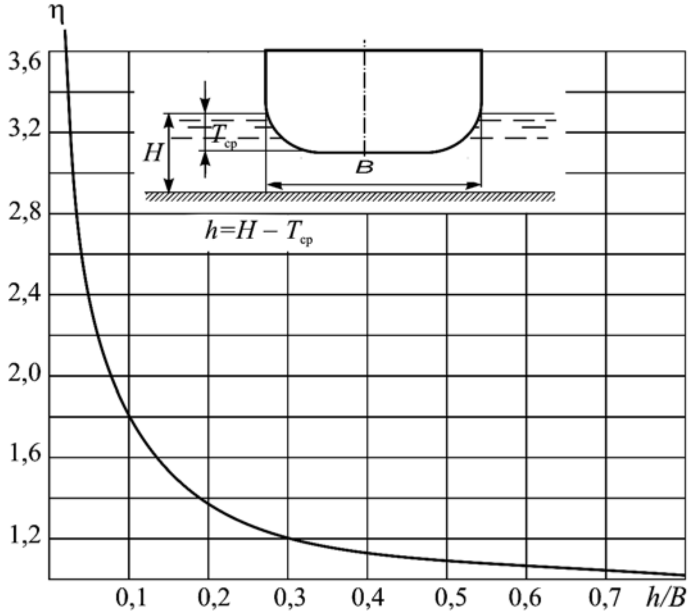

Fig. 7.19 Dependence of coefficient η on h/B for first five vertical eigenmodes of inland cargo ships; h is the depth under the keel; B is the width of the hull at waterline

Chapter 8
Added Masses of a Propeller

Here we discuss the properties and methods of determination of added masses of a propeller, as well as the influence of the hull on the added masses.

8.1 Forces and Torques of Inertial Nature Acting on a Propeller

Let us introduce the coordinate system xyz associated to the propeller (Fig. 8.1) such that the origin O is situated at the axis; the Ox axis is directed along the propeller axis; the Oz axis is directed along one of the blades. The number of the blades we denote by Z. If the coordinate system xyz is rotated around the axis Ox by the angle $\beta = 2\pi/Z$, then the axis Oz_1 of the new coordinate system is also directed along a blade of the propeller, i.e., the position of the propeller in the new coordinate system xy_1z_1 is the same as its position under the old coordinate system xyz. Therefore the added masses of the propeller in the new coordinate system xy_1z_1 are the same as the added masses in the coordinate system xyz. Consider kinetic energy of the fluid flow around the propeller (see (1.13)) in the coordinate systems xyz and xy_1z_1.

Let in coordinate system xyz the linear and angular velocities of the propeller be denoted by u_i $(i = 1, \ldots, 6)$. Then in the coordinate system xy_1z_1 these velocities have the form

$$u_1' = u_1; \qquad u_2' = u_2 \cos\beta + u_3 \sin\beta;$$

$$u_3' = -u_2 \sin\beta + u_3 \cos\beta; \qquad u_4' = u_4;$$

$$u_5' = u_5 \cos\beta + u_6 \sin\beta; \qquad u_6' = -u_5 \sin\beta + u_6 \cos\beta.$$

Kinetic energy of the fluid in the coordinate system xyz can be written as follows:

$$\begin{aligned} 2T = {} & \lambda_{11}u_1^2 + \lambda_{22}u_2^2 + \lambda_{33}u_3^2 + 2\lambda_{12}u_1u_2 + 2\lambda_{13}u_1u_3 + 2\lambda_{23}u_2u_3 \\ & + 2u_1(\lambda_{14}u_4 + \lambda_{15}u_5 + \lambda_{16}u_6) + 2u_2(\lambda_{24}u_4 + \lambda_{25}u_5 + \lambda_{26}u_6) \\ & + 2u_3(\lambda_{34}u_4 + \lambda_{35}u_5 + \lambda_{36}u_6) + \lambda_{44}u_4^2 + \lambda_{55}u_5^2 \\ & + \lambda_{66}u_6^2 + 2\lambda_{45}u_4u_5 + 2\lambda_{46}u_4u_6 + 2\lambda_{56}u_5u_6. \end{aligned} \tag{8.1}$$

A.I. Korotkin, *Added Masses of Ship Structures*,

Fig. 8.1 Coordinate system associated to a propeller. R is the maximal radius of the propeller; r_0 is the radius of the propeller's hub

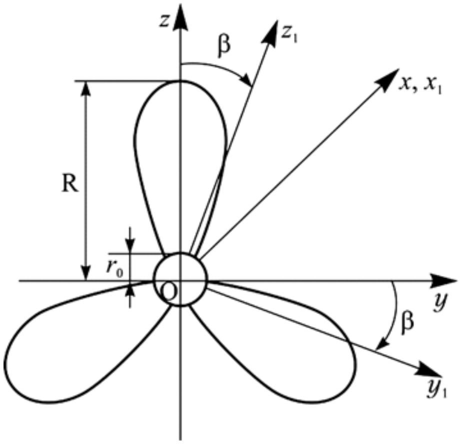

The same kinetic energy in the coordinate system xy_1z_1 can be written as follows:

$$\begin{aligned}
2T = {} & \lambda_{11}u_1^2 + \lambda_{22}(u_2\cos\beta + u_3\sin\beta)^2 + \lambda_{33}(-u_2\sin\beta + u_3\cos\beta)^2 \\
& + 2\lambda_{12}(u_2\cos\beta + u_3\sin\beta)u_1 + 2\lambda_{13}u_1(-u_2\sin\beta + u_3\cos\beta) \\
& + 2\lambda_{23}(u_2\cos\beta + u_3\sin\beta)(-u_2\sin\beta + u_3\cos\beta) \\
& + 2u_1\big[\lambda_{14}u_4 + \lambda_{15}(u_5\cos\beta + u_6\sin\beta) + \lambda_{16}(-u_5\sin\beta + u_6\cos\beta)\big] \\
& + 2(u_2\cos\beta + u_3\sin\beta)\big[\lambda_{24}u_4 + \lambda_{25}(u_5\cos\beta + u_6\sin\beta) \\
& + \lambda_{26}(-u_5\sin\beta + u_6\cos\beta)\big] \\
& + 2(-u_2\sin\beta + u_3\cos\beta)\big[\lambda_{34}u_4 + \lambda_{35}(u_5\cos\beta + u_6\sin\beta) \\
& + \lambda_{36}(-u_5\sin\beta + u_6\cos\beta)\big] \\
& + \lambda_{44}u_4^2 + \lambda_{55}(u_5\cos\beta + u_6\sin\beta)^2 \\
& + \lambda_{66}(-u_5\sin\beta + u_6\cos\beta)^2 + 2\lambda_{45}u_4(u_5\cos\beta + u_6\sin\beta) \\
& + 2\lambda_{46}u_4(-u_5\sin\beta + u_6\cos\beta) \\
& + 2\lambda_{56}(u_5\cos\beta + u_6\sin\beta)(-u_5\sin\beta + u_6\cos\beta).
\end{aligned} \tag{8.2}$$

Expressions (8.1) and (8.2) are identically equal for arbitrary values of u_i ($i = 1, 2, \ldots, 6$), since they define the same kinetic energy. Comparing various terms in these formulas we can get relationships between the added masses λ_{ik} ($i, k = 1, 2, \ldots, 6$), which follow from the discrete rotational symmetry of the propeller.

For two-blade propeller $Z = 2$, $\beta = \pi$. The formula (8.2) takes the form

$$\begin{aligned}
2T = {} & \lambda_{11}u_1^2 + \lambda_{22}u_2^2 + \lambda_{33}u_3^2 - 2\lambda_{12}u_1u_2 - 2\lambda_{13}u_1u_2 + 2\lambda_{23}u_2u_3 \\
& + 2u_1(\lambda_{14}u_4 - \lambda_{15}u_5 - \lambda_{16}u_6) \\
& - 2u_2(\lambda_{24}u_4 - \lambda_{25}u_5 - \lambda_{26}u_6) - 2u_3(\lambda_{34}u_4 - \lambda_{35}u_5 - \lambda_{36}u_6) \\
& + \lambda_{44}u_4^2 + \lambda_{55}u_5^2 + \lambda_{66}u_6^2 \\
& - 2\lambda_{45}u_4u_5 - 2\lambda_{46}u_4u_6 + 2\lambda_{56}u_5u_6.
\end{aligned} \tag{8.3}$$

Since (8.3) must identically coincide with (8.1), taking into account that the added masses λ_{ik} coincide in both formulas, we get

$$\lambda_{12} = \lambda_{13} = \lambda_{15} = \lambda_{16} = \lambda_{24} = \lambda_{34} = \lambda_{45} = \lambda_{46} = 0. \tag{8.4}$$

For four-blade propeller, when $Z = 4$ and $\beta = \pi/2$, the formula (8.2) takes the form

$$\begin{aligned} 2T = {} & \lambda_{11}u_1^2 + \lambda_{22}u_3^2 + \lambda_{33}u_2^2 + 2\lambda_{12}u_1u_3 \\ & - 2\lambda_{13}u_1u_2 - 2\lambda_{23}u_2u_3 + 2u_1(\lambda_{14}u_4 + \lambda_{15}u_6 - \lambda_{16}u_5) \\ & + 2u_3(\lambda_{24}u_4 + \lambda_{25}u_6 - \lambda_{26}u_5) - 2u_2(\lambda_{34}u_4 + \lambda_{35}u_6 - \lambda_{36}u_5) \\ & + \lambda_{44}u_4^2 + \lambda_{55}u_6^2 + \lambda_{66}u_5^2 + 2\lambda_{45}u_4u_6 - 2\lambda_{46}u_4u_5 - 2\lambda_{56}u_5u_6. \end{aligned} \tag{8.5}$$

Comparing (8.1) with (8.5), we get the following relations between the added masses of a four-blade propeller:

$$\lambda_{22} = \lambda_{33}; \qquad \lambda_{55} = \lambda_{66}; \qquad \lambda_{25} = \lambda_{36}; \qquad \lambda_{26} = -\lambda_{35};$$

$$\lambda_{12} = \lambda_{13} = \lambda_{23} = \lambda_{15} = \lambda_{16} = \lambda_{24} = \lambda_{34} = \lambda_{45} = \lambda_{46} = \lambda_{56} = 0. \tag{8.6}$$

For a three-blade propeller ($Z = 3$), as well as for propellers with higher number of blades ($Z \geq 5$) one has to compare the formulas (8.1) and (8.2). Coincidence of coefficients in front of pairwise products $u_i u_k$ for $i = 1, \ldots, 6$ implies

$$\lambda_{22} = \lambda_{33}; \qquad \lambda_{55} = \lambda_{66}; \qquad \lambda_{25} = \lambda_{36}; \qquad \lambda_{26} = -\lambda_{35};$$

$$\lambda_{12} = \lambda_{13} = \lambda_{23} = \lambda_{15} = \lambda_{16} = \lambda_{24} = \lambda_{34} = \lambda_{45} = \lambda_{46} = \lambda_{56} = 0. \tag{8.7}$$

We notice that for a two-blade propeller the condition $\lambda_{23} = 0$ is not included in (8.4); this is due to the fact that the position of the axis Oz on the blade is considered arbitrary. However, according to the transformation formulas from Chap. 1 one can always choose the Oz axis in the Oyz plane such that λ_{23} vanishes.

Taking into account the expressions (8.4), (8.6) and (8.7), let us give the formulas for kinetic energy of the flow around propellers with different numbers of blades:

For a two-blade propeller:

$$\begin{aligned} 2T = {} & \lambda_{11}u_1^2 + \lambda_{22}u_2^2 + \lambda_{33}u_3^2 + 2\lambda_{23}u_2u_3 + 2\lambda_{14}u_1u_4 \\ & + 2\lambda_{25}u_2u_5 + 2\lambda_{26}u_2u_6 + 2\lambda_{35}u_3u_5 + 2\lambda_{36}u_3u_6 + \lambda_{44}u_4^2 \\ & + \lambda_{55}u_5^2 + \lambda_{66}u_6^2 + 2\lambda_{56}u_5u_6. \end{aligned} \tag{8.8}$$

For a four-blade propeller:

$$\begin{aligned} 2T = {} & \lambda_{11}u_1^2 + \lambda_{22}\left(u_2^2 + u_3^2\right) + 2\lambda_{14}u_1u_4 \\ & + 2\lambda_{25}(u_2u_5 + u_3u_6) - 2\lambda_{26}(u_3u_5 - u_2u_6) \\ & + \lambda_{44}u_4^2 + \lambda_{55}\left(u_5^2 + u_6^2\right). \end{aligned} \tag{8.9}$$

For a three-blade propeller and a propeller with a number of blades $Z \geq 5$:

$$2T = \lambda_{11}u_1^2 + \lambda_{22}\big(u_2^2 + u_3^2\big) + 2\lambda_{14}u_1u_4 + 2\lambda_{25}(u_2u_5 + u_3u_6) + \lambda_{44}u_4^2 + \lambda_{55}\big(u_5^2 + u_6^2\big). \tag{8.10}$$

Expressions (8.8)–(8.10) can be used to find forces and torques acting on a propeller according to formulas of Sect. 1.4. The components of hydrodynamic forces and torques of inertial nature acting on a propeller arbitrarily moving in an immovable fluid are determined by (1.22)–(1.27), taking into account (8.4), (8.6) or (8.7) depending on the number of blades of the propeller.

The formulas for forces and torques of inertial nature acting on a propeller which moves in a changing velocity field, are given in [137].

If a propeller with the number of blades $Z \geq 2$ is moving in immovable fluid with velocities $u_1(t)$ and $u_4(t)$, then, according to formulas (1.22)–(1.27), it is acted upon by the following force and torque of inertial nature:

$$R_x = -\lambda_{11}\frac{du_1}{dt} - \lambda_{14}\frac{du_4}{dt}; \qquad L_x = -\lambda_{14}\frac{du_1}{dt} - \lambda_{44}\frac{du_4}{dt}.$$

8.2 Added Masses of Propeller Blades

Added masses of propeller blades are usually determined by the method of plane sections [41, 136]. Consider an element of the propeller blade (see Fig. 8.2). The origin of coordinate system xOy is assumed to belong to the chord of the profile; it is assumed to coincide with the center of mass of the section. Let us assume that for all sections of the blade these points belong to one line (coinciding with the Oz axis), i.e., the blade is not twisted. The added masses of a given section are denoted by λ_x, λ_y, λ_{xy}, $\lambda_{x\omega}$, $\lambda_{y\omega}$, λ_ω. According to the method of planar sections the added masses of the blade λ_{ik}^0 can be obtained by integration of added masses of planar sections with respect to the radius r in the limits from r_0 to R (see Fig. 8.1):

$$\lambda_{11}^0 = \int_{r_0}^{R} \lambda_x\, dr; \qquad \lambda_{12}^0 = \int_{r_0}^{R} \lambda_{xy}\, dr; \qquad \lambda_{22}^0 = \int_{r_0}^{R} \lambda_y\, dr;$$

$$\lambda_{14}^0 = -\int_{r_0}^{R} \lambda_{xy} r\, dr; \qquad \lambda_{15}^0 = \int_{r_0}^{R} \lambda_x r\, dr; \qquad \lambda_{16}^0 = \int_{r_0}^{R} \lambda_{x\omega}\, dr;$$

$$\lambda_{24}^0 = -\int_{r_0}^{R} \lambda_y r\, dr; \qquad \lambda_{26}^0 = \int_{r_0}^{r} \lambda_{y\omega}\, dr; \qquad \lambda_{25}^0 = -\lambda_{14}^0;$$

$$\lambda_{44}^0 = \int_{r_0}^{R} \lambda_y r^2\, dr; \qquad \lambda_{55}^0 = \int_{r_0}^{R} \lambda_x r^2\, dr; \qquad \lambda_{66}^0 = \int_{r_0}^{R} \lambda_\varpi\, dr;$$

Fig. 8.2 Propeller blade

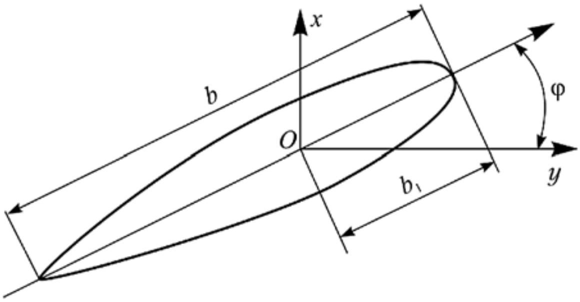

$$\lambda^0_{45} = \int_{r_0}^{R} \lambda_{xy} r^2 \, dr; \qquad \lambda^0_{46} = -\int_{r_0}^{R} \lambda_{y\varpi} r \, dr; \qquad \lambda^0_{56} = \int_{r_0}^{R} \lambda_{x\varpi} r \, dr. \quad (8.11)$$

Signs in front of the integrals were chosen according to the rules discussed in Sect. 3.5.1, as well as the transformation formulas (1.21).

Added masses of the profile can be found in the coordinate system xOy taking into account its width and curvature (see Chap. 2).

In approximate computations, taking into account a relatively small thickness of the profile and small curvature of the middle chord, one can substitute the profile by a thin plate of width b. Then the added masses of an element of the blade, taking into account (1.20) can be written as follows:

$$\lambda_x = \rho \frac{\pi}{4} b^2 \cos^2 \varphi; \qquad \lambda_y = \rho \frac{\pi}{4} b^2 \sin^2 \varphi; \qquad \lambda_{xy} = -\frac{1}{2} \rho \frac{\pi}{4} b^2 \sin 2\varphi;$$

$$\lambda_{x\omega} = \rho \frac{\pi}{4} b^3 (0.5 - \bar{b}_1) \cos \varphi; \qquad \lambda_{y\omega} = -\rho \frac{\pi}{4} b^3 (0,5 - \bar{b}_1) \sin \varphi;$$

$$\lambda_\omega = \rho \frac{\pi}{4} b^4 \left[\frac{9}{32} - \bar{b}_1 (1 - \bar{b}_1) \right], \quad (8.12)$$

where φ is the angle shown in Fig. 8.2; b is the width of profile of an element of the blade; b_1 is the distance between the front point of the blade to its center (Fig. 8.2); $\bar{b}_1 = b_1/b$.

If we assume that the blade profile is symmetric with respect to the axis Oz, i.e., $\bar{b}_1 = 0.5$, then $\lambda_{x\omega} = \lambda_{y\omega} = 0$. In this case, as it follows from (8.11),

$$\lambda^0_{16} = \lambda^0_{26} = \lambda^0_{46} = \lambda^0_{56} = 0.$$

Substituting (8.12) into (8.11), we get the following formulas for the remaining added masses of the blade:

$$\lambda_{11}^0 = m\int_{\bar r_0}^1 \bar b^2 \cos^2\varphi\, d\bar r; \qquad \lambda_{22}^0 = m\int_{\bar r_0}^1 \bar b^2 \sin^2\varphi\, d\bar r;$$

$$\lambda_{12}^0 = -\frac{m}{2}\int_{\bar r_0}^1 \bar b^2 \sin 2\varphi\, dr; \qquad \lambda_{14}^0 = \frac{mR}{2}\int_{\bar r_0}^1 \bar b^2 \bar r \sin 2\varphi\, d\bar r;$$

$$\lambda_{15}^0 = mR\int_{\bar r_0}^1 \bar b^2 \bar r \cos^2\varphi\, d\bar r; \qquad \lambda_{24}^0 = -mR\int_{\bar r_0}^1 \bar b^2 \bar r \sin^2\varphi\, d\bar r;$$

$$\lambda_{44}^0 = mR^2\int_{\bar r_0}^1 \bar b^2 \bar r^2 \sin^2\varphi\, d\bar r; \qquad \lambda_{55}^0 = mR^2\int_{\bar r_0}^1 \bar b^2 \bar r^2 \cos^2\varphi\, d\bar r;$$

$$\lambda_{66}^0 = \frac{mR^2}{8}\bar b_m^2\int_{\bar r_0}^1 \bar b^4\, d\bar r; \qquad \lambda_{45}^0 = -\frac{mR^2}{2}\int_{\bar r_0}^1 \bar b^2 \bar r^2 \sin 2\varphi\, d\bar r \tag{8.13}$$

where $m = (1/8)\pi\rho\bar b_m^2 D^3$; $\bar b_m = b_m/D$; b_m is the maximal width of the blade; D is the diameter of the propeller; $\bar b = b/b_m$; $\bar r = r/R$. The variable m in (8.13) has the meaning of mass of the fluid contained in the cylinder of height R and diameter b_m. Variables mR and mR^2 are proportional to the static moment and the moment of inertia of this mass with respect to the axis of the propeller. Integrals in (8.13) are coefficients of influence of blade geometry. They depend on the radius of the hub, as well as of radial distribution of the width of the blade, and the pitch between the blades. Variable b_m depends on blade-area ratio, number of blades and radius of the hub.

For Troost propellers of B-series family the integrals in (8.13) were computed by V. Lipis [137]; for $\bar r_0 = 0.2$ he obtained the following formulas:

$$\lambda_{11}^0 = 2.1\rho\frac{D^3\theta^2}{Z^2} f_1\left(\frac{H}{D}\right); \qquad \lambda_{22}^0 = 0.319\left(\frac{H}{D}\right)^2 \frac{f_0(H/D)}{f_1(H/D)}\lambda_{11}^0;$$

$$\lambda_{12}^0 = -0.6\left(\frac{H}{D}\right)\lambda_{11}^0; \qquad \lambda_{14}^0 = 0.159D\left(\frac{H}{D}\right)\lambda_{11}^0;$$

$$\lambda_{24}^0 = -0.0955D\left(\frac{H}{D}\right)^2\lambda_{11}^0; \qquad \lambda_{15}^0 = 0.3D\lambda_{11}^0;$$

$$\lambda_{44}^0 = 0.0253D^2\left(\frac{H}{D}\right)^2\lambda_{11}^0; \qquad \lambda_{55}^0 = \left[\frac{0.056}{f_1} - 0.102\left(\frac{H}{D}\right)^2\right]D^2\lambda_{11}^0;$$

$$\lambda_{66}^0 = 0.0854D^2(\theta^2/Z^2)\left(\frac{1}{f_1}\right)\lambda_{11}^0; \qquad \lambda_{45}^0 = -0.0479D^2\left(\frac{H}{D}\right)^2\lambda_{11}^0. \tag{8.14}$$

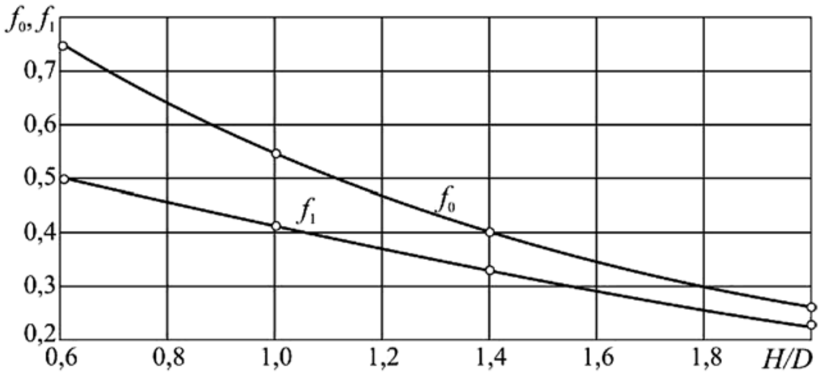

Fig. 8.3 Functions defining added masses of Troost B propellers

Here the functions $f_0(H/D)$ and $f_1(H/D)$ are determined by Fig. 8.3, θ is the blade-area ratio; H/D is the pitch ratio. The function f_1 can be approximated by the formula [136] $f_1 = 0.61 - 0.19H/D$.

The following added masses of the propeller as a whole can be approximately found in terms of coefficients λ^0_{ik} as follows:

$$\lambda_{11} = Z\lambda^0_{11}; \qquad \lambda_{14} = Z\lambda^0_{14};$$

$$\lambda_{44} = Z\lambda^0_{44}; \qquad \lambda_{25} = 0.5Z\lambda^0_{25}.$$

It is more difficult to find other added masses; these computations should in particular take into account relationships (8.4), (8.6) and (8.7). In derivation of the formulas (8.14) the formulas for added masses of isolated plates were used. Lattice effects lead to increase of corresponding values of λ_{ik} [86]. Taking these effects into account the following expressions were obtained in this work:

$$\lambda_{11} = 2.31\rho D^3\left(\frac{\theta^2}{Z}\right)A;$$

$$\lambda_{14} = 0.368\rho D^4\left(\frac{\theta^2}{Z}\right)\left(\frac{H}{D}\right)A;$$

$$\lambda_{44} = 0.0585\rho D^5\left(\frac{\theta^2}{Z}\right)\left(\frac{H}{D}\right)^2 A, \tag{8.15}$$

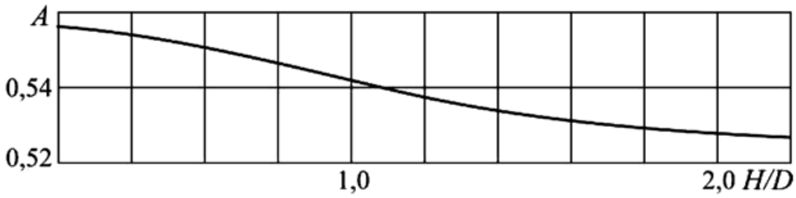

Fig. 8.4 Graph of function $A(H/D)$

where

$$A = 0.56 - 0.26\left(\frac{H}{D}\right)^2 + \left[0.362\left(\frac{H}{D}\right)^3 - 0.031\left(\frac{H}{D}\right)^5\right]$$
$$\times \arctan\frac{0.255(H/D)}{0.2 + 0.101(H/D)^2}$$
$$+ 0.0703\left(\frac{H}{D}\right)^4 - \left[0.099\left(\frac{H}{D}\right)^4 - 0.00075\left(\frac{H}{D}\right)^6\right]$$
$$\times \ln\frac{1 + 0.101(H/D)^2}{0.04 + 0.101(H/D)^2}.$$

The graph of function $A(H/D)$ is shown in Fig. 8.4. Notice that the signs of the added masses λ_{14}^0 (8.14) and λ_{14} (8.15) are chosen taking into account (8.11).

Besides theoretical results, very often one uses experimental data on a propeller's added masses. In particular, there is the following formula by L.M. Kutuzov for λ_{44} (for the case of water):

$$\lambda_{44} = \frac{111\theta^2 D^5}{Z}\frac{(H/D)^2}{3.8 + (H/D)^2}\sqrt{\frac{1 + 0.23\theta/Z}{1 + (6\theta/Z)^2}}\ \text{kg} \times \text{m}^2.$$

There exists also the following experimental formula relating λ_{44} and λ_{11}:

$$\lambda_{44} = kH^2\lambda_{11},$$

where the coefficient k lies between 0.023 and 0.025.

On the other hand, computations using (8.14) give the following formula: $\lambda_{44} = 0.0253H^2\lambda_{11}$. Formulas (8.14) show that the added masses of the blade (and, therefore, of the propeller as a whole) can be expressed via the variable λ_{11}^0 (for propeller via λ_{11}). Therefore, the λ_{11}^0 (and λ_{11}) should be determined as exactly as possible. Analysis of experimental data [137] suggested that we introduce a correction $\alpha(\theta)$ (see Fig. 8.5) which is introduced in the formula for the added mass of the propeller:

$$\lambda_{11} = 2.1\rho\frac{D^3\theta^2}{Z} f_1\left(\frac{H}{D}\right)\alpha(\theta).$$

Some results on added masses of four-blade propeller for $0.4 \le \theta \le 1.0$, $0.5 \le H/D \le 1.2$ are contained in [102]. In the work [74] the added masses of three

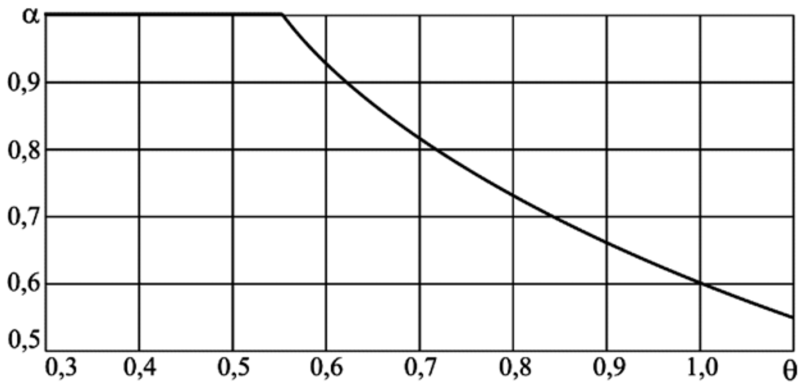

Fig. 8.5 Experimental correction $\alpha(\theta)$ for added mass of a propeller

propellers were computed: propeller 1 (with diameter $D = 5.3$ m, number of blades $Z = 4$, pitch ratio at radius $0.7R$ given by $H/D = 1.23$, blade-area ratio $\theta = 0.586$), propeller 2 (with diameter $D = 5.8$ m, number of blades $Z = 5$, pitch ratio at radius $0.7R$ given by $H/D = 1.16$, blade-area ratio $\theta = 0.650$), propeller 3 (with diameter $D = 4.25$ m, number of blades $Z = 4$, pitch ratio at radius $0.7R$ given by $H/D = 1.17$, blade-area ratio $\theta = 0.550$).

In Table 8.1 we give the complete matrix of coefficients $\lambda_{ik}/\rho D^m$ for the propeller No. 1, where $m = 3$ for $i, k \leq 3$, $m = 4$ for $i > 3$, $k \leq 3$, $m = 5$ for $i, k > 3$.

Each of the blades was covered by 308 panels (i.e., the complete surface of the propeller was covered by 1232 panels). Theoretical considerations show that $\lambda_{ik} = \lambda_{ki}$; however, in Table 8.1 we observe certain disagreements with this prediction; for example $\lambda_{14} = -0.01225$ while $\lambda_{41} = -0.01237$; $\lambda_{35} = -0.00037$ while $\lambda_{53} = -0.00042$.

In Table 8.1 we also observe that $\lambda_{23} \neq 0$ and $\lambda_{56} \neq 0$, which contradicts theoretical predictions; however, these values are relatively small (0.00001 and 0.00005 respectively). These disagreements with theoretical predictions are due to discretization error.

Table 8.1 Matrix of coefficients $\lambda_{ik}/(\rho D^m)$

i/k	1	2	3	4	5	6
1	0.06759	0	0	−0.01225	0	0
2	0	0.01399	−0.00001	0	0.00620	0.00037
3	0	0.00001	0.01399	0	−0.00037	0.00620
4	−0.01237	0	0	0.00232	0	0
5	0	0.00603	−0.00042	0	0.00386	0.00005
6	0	0.00042	0.00603	0	0.00005	0.00386

Table 8.2 Results of computation of added masses of propellers by different methods

		Prop. 1	Prop. 2	Prop. 3
$\frac{\lambda_{11}}{\rho D^3}$	a	0.0623	0.0594	0.0615
	b	0.0519	0.0607	0.0532
	c	0.0541	0.0574	0.0503
	f	0.0676	0.0535	0.0484
$\frac{\lambda_{14}}{\rho D^4}$	a	−0.0121	−0.0110	−0.0114
	b	−0.0102	−0.0112	−0.00991
	f	−0.0122	−0.0093	−0.00841
$\frac{\lambda_{44}}{\rho D^5}$	a	0.00239	0.00202	0.00213
	b	0.00199	0.00207	0.00184
	c	0.00207	0.00196	0.00174
	f	0.00232	0.00171	0.00153
$\frac{\lambda_{22}}{\rho D^3}$	a	0.0365	0.0313	0.0329
	d	0.0474	0.0386	0.0426
	f	0.0140	0.0114	0.0182
$\frac{\lambda_{25}}{\rho D^4}$	a	0.00609	0.00548	0.00572
	f	0.00620	0.00467	0.00453
$\frac{\lambda_{55}}{\rho D^5}$	e	0.00190	0.00203	0.00171
	f	0.00386	0.00287	0.00267

On the other hand, for a 4-blade propeller the symmetries related to $\pi/2$ rotational symmetry of the propeller: $\lambda_{22} = \lambda_{33}$, $\lambda_{55} = \lambda_{66}$, $\lambda_{25} = \lambda_{36}$, and $\lambda_{12} = \lambda_{13} = \lambda_{15} = \lambda_{16} = \lambda_{24} = \lambda_{34} = \lambda_{45} = \lambda_{46} = 0$ are fulfilled exactly.

Comparison of results of computation of the added masses of the three propellers mentioned above by the panel method and results obtained theoretically by various authors is given in Table 8.2. Theoretical results of different authors are enumerated as follows:

a—method of V. Lipis,
b—method of M. Grechin,
c—method of D. Kutuzov,
d—method of S. Dorofeuk and G. Solomatina,
e—method of L. Kutuzov and M. Yakovleva,
f—panel method used in [74].

As one can see from Table 8.2, the different methods give close values of λ_{11}, λ_{14}, λ_{44} and λ_{25}. However, values of λ_{22} and λ_{55} computed via the panel method significantly differ from approximate theoretical predictions.

8.3 Added Masses of a Propeller under Transversal Oscillations of Shafting

In dynamical computations one has to find the added masses of the system which consists of propeller and shafting.[1]

In [184] the added masses were computed experimentally by comparing the frequencies of oscillations of a rod with a propeller attached to its end in air and in water (in the case of oscillations in water the propeller was immersed deeply enough to exclude the influence of the water surface). The added masses of the rod itself can also be neglected if its diameter is sufficiently small compared to the diameter of the propeller.

The frequency of free oscillations of a rod with a propeller attached to its end is determined by the well-known formula:

$$N = \frac{a^2}{l^2}\sqrt{\frac{EJ}{m}} \tag{8.16}$$

where E is the modulus of elongation of the material of the rod; J is the moment of inertia of the cross-section of the rod; l is the length of the rod; m is the linear mass of the rod.

In the air the frequency equation for the coefficient a has the form

$$A(a) - naB(a) = 0 \tag{8.17}$$

where $A(a) = 1 + \cosh a \cos a$; $B(a) = \cosh a \sin a + \operatorname{sh} a \cos a$; $n = M_p/ml$; M_p is the mass of the propeller.

If the propeller is immersed in water, one has to add the added mass M (which corresponds to the standard notation λ_{22} used in the rest of the book) to the propeller mass M_p; in this way we get the frequency equation

$$A(a_1) - n_1 a_1 B(a_1) = 0 \tag{8.18}$$

where $n_1 = (M_p + M)/ml$; we have

$$\frac{M}{M_p} = \frac{n_1 - n}{n}. \tag{8.19}$$

The frequencies of oscillations of the system in the air and in the water can be found experimentally; then one can find corresponding coefficients a from (8.16), a_1 from (8.18), which give coefficients n and n_1; substituting these coefficients in (8.19) we find M.

In [51] there were tested 41 propellers of the same diameter ($D = 200$ mm) with different numbers of blades (2, 3 and 5), with different pitch ratio and blade-area ratio.

---

[1] This section was written by E.N. Schukina.

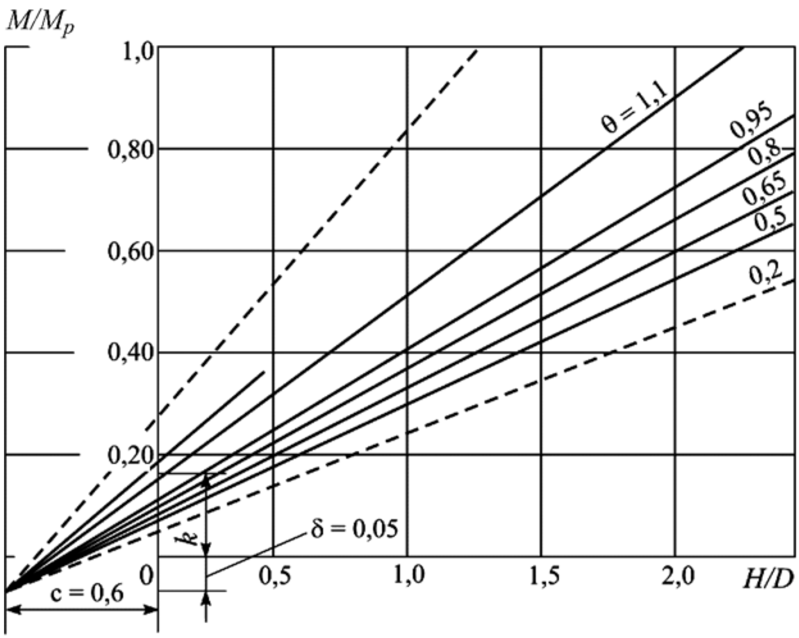

Fig. 8.6 Dependence of transversal added mass of propeller on pitch ratio

For three-blade propellers on the basis of experimental results there were found graphs of M/M_∂ as functions of pitch ratio H/D for different values of the blade-area ratio θ (Fig. 8.6). As one can see from these graphs, dependence $M/M_p = f(H/D)$ is approximately linear for each value of θ; moreover, all of these lines intersect at one point.

Each of the lines $M/M_p = f(H/D)$ can be expressed by the formula

$$\frac{M}{M_p} = \frac{k+\delta}{c}\frac{H}{D} + k = k\left(\frac{1}{c}\frac{H}{D} + 1\right) + \frac{\delta}{c}\frac{H}{D}. \tag{8.20}$$

The values of k, c and δ are shown in Fig. 8.6. Since $c = 0.6$ and $\delta = 0.05$, the values of added masses of the tested three-blade propellers can be determined as follows:

$$M = \left[k\left(1 + 1.66\frac{H}{D}\right) + 0.083\frac{H}{D}\right]M_p. \tag{8.21}$$

The coefficient k depends on the blade-area ratio θ; the graph $\theta(k)$ is shown in Fig. 8.7.

The formula (8.21) was derived for three-blade propellers. For propellers with another number of blades one can introduce a correction; to determine this correction experimental investigation was carried out for propellers with number of blades equal to 2, 3 and 5 with the same blade-area ratio $\theta = 0.55$ and pitch ratio $H/D = 1.0$. The experimental curve showing dependence of M/M_p on the number

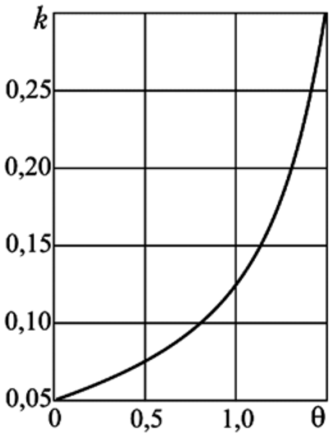

Fig. 8.7 Dependence of coefficient k on blade-area ratio θ

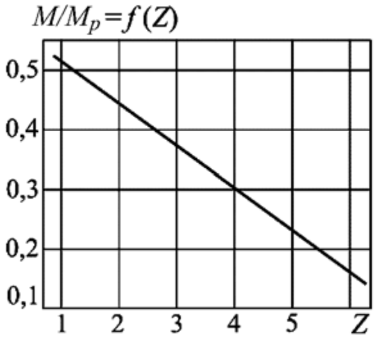

Fig. 8.8 Dependence of added mass of a propeller on the number of blades

of blades Z is shown in Fig. 8.8; this curve is a linear function in a good approximation.

If we denote the point of intersection of the graph of this function $M/M_0 = f(Z)$ with Z-axis by Z_0, we get

$$\frac{f(Z)}{f(Z_0)} = \frac{Z_0 - Z}{Z_0 - 3}.$$

Since $(Z_0 - 5)/(Z_0 - 2) = f(5)/f(2)$ then

$$Z_0 = \left[2 - 5\frac{f(2)}{f(5)}\right]\left[1 - \frac{f(2)}{f(5)}\right]^{-1} = 7.85.$$

Therefore,

$$f(Z) = \frac{7.85 - Z}{4.85} f(3) \quad \text{or} \quad \frac{M}{M_p} = \frac{7.85 - Z}{4.85}\left(\frac{M}{M_p}\right)_3 \tag{8.22}$$

where $(M/M_p)_3$ is the value of the ratio M/M_p for a three-blade propeller.

Introduce in (8.21) the correction related to the number of blades according to (8.22). Let us also introduce another correction, related to the density of propeller

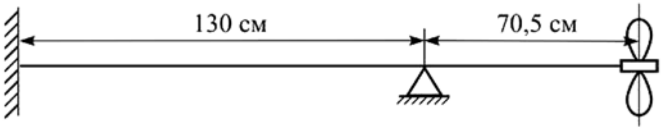

Fig. 8.9 Model of a propeller shaft

material (the tested propellers were made of white metal with density $\gamma_0 = 7.26 \times 10^4$ N/m^3), we get the final formula for the added mass of an arbitrary propeller:

$$M = \left[k\left(1 + 1.66\frac{H}{D}\right) + 0.083\frac{H}{D}\right]\frac{7.85 - Z}{4.85}\frac{\gamma_0}{\gamma_p}M_p \tag{8.23}$$

where γ_p is the density of the propeller.

The formula (8.23) is valid for all propellers, independently of their diameter, which was verified by comparing the data obtained using (8.23) with experimental data for frequencies of free oscillations of the propeller shaft in water (Fig. 8.9). Propellers of diameter 250 mm and 300 mm were attached to the end of the shaft. The frequencies of free transversal oscillations of the propeller shaft, obtained theoretically (using (8.23)) and experimentally, are given below.

	$D = 250$ mm	$D = 300$ mm
Mass P, kg	3.15	5.43
Number of blades Z	3	3
Blade-area ratio θ	1.03	1.10
Pitch ratio H/D	1.03	1.03
Theoretical frequency of free oscillations N_t, osc./min.	395	328
Experimental frequency of free oscillations N_e, osc./min.	400	316

Experiment also shows that the rotation of the propeller does not significantly influence its added masses.

The added moment of inertia of the propeller can be found using the following approximate formula[2]:

$$J = 33 \cdot 10^{-4}\rho D^5 z\left(\frac{H}{D} - 0.4\right)\left(\frac{\theta}{Z} + 0.04\right)\left(1.3 - 0.3\frac{H}{D}\right),$$

where ρ is the density of the fluid; D is the diameter of the propeller; Z is the number of blades; H/D is the pitch ratio; θ is the blade-area ratio.

[2]Obtained by L.M. Kutuzov and M.V. Yakovleva.

8.4 Added Masses of a Propeller in a Shroud

The added mass λ_{11} of a propeller working in a shroud was found in [198] by experimental analysis of the frequencies of vibration of propeller models in the air and in the water.

All propellers had diameter 0.5 m; the form of blades was assumed to be of Kaplan type. The blade-area ratio varied in the limits between $0.4 \le \theta \le 0.7$; the pitch ratio varied in the limits between $0.5 \le H/D \le 1.4$. The shroud of length 0.5 m had the shape of a ring cylinder with inner diameter 0.505 m. The relative gap between the blade ends and the inner surface of the shroud was therefore equal to $\varDelta = (505 - 500)/500 = 0.01$.

Analysis of experimental data gave the following formula for the added mass of propeller in the shroud:

$$\lambda_{11} = 0.74\rho D^3 \frac{\theta^2}{Z}\left(1 + 0.25\frac{H}{D}\right)\left[1 - (\theta - 0.4)^2\right],$$

where Z is the number of blades. Using this formula together with (8.14) we get the following formulas for λ_{14} and λ_{44}:

$$\lambda_{14} = \frac{1}{2}\pi D\lambda_{11}\frac{H}{D} = 0.118\rho\frac{\theta^2}{Z}\frac{H}{D}\left(1 + 0.25\frac{H}{D}\right)\left[1 - (\theta - 0.4)^2\right]D^4,$$

$$\begin{aligned}\lambda_{44} &= 0.0253D^2\frac{H^2}{D^2}\lambda_{11}\\ &= 0.0187\rho\frac{\theta^2}{Z}\frac{H^2}{D^2}\left(1 + 0.25\frac{H}{D}\right)\left[1 - (\theta - 0.4)^2\right]D^5.\end{aligned}$$

The comparison with experimental data on propellers without a shroud shows that the shroud increases the added mass λ_{11} by 5% to 30% depending on geometric characteristics of the propeller.

8.5 Influence of a Boundary on Added Masses of a Propeller

In computation of added masses of propeller it is common to used the software STAR3D Electric which was originally developed for computation of the stationary electrical field of multi-electrode galvanic systems [229].[3] The possibility to use this program in hydrodynamics is based on a well-known electro-hydrodynamic analogy (EHDA) between the electric field E and the velocity field in an ideal fluid. In the static case the field E is potential: $E = -\operatorname{grad}\varphi$, and the potential φ satisfies the Laplace equation $\varDelta\varphi = 0$.

[3]This section was written by A.M. Vishnevskij, A.J. Lapovok and S.A. Kirillov.

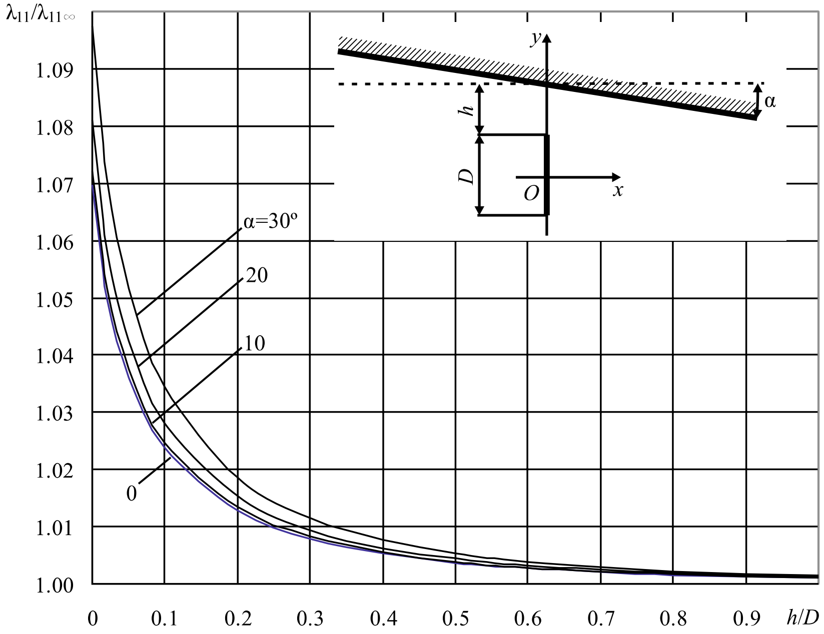

Fig. 8.10 Coefficient of added mass of a disc under its motion near a hard boundary

In particular, STAR3D Electric allows us to consider the isolating surfaces where the boundary condition

$$\frac{\partial \varphi}{\partial n} = E_{0n} \tag{8.24}$$

is satisfied. Here E_{0n} is the normal component of an external homogeneous electric field. The boundary value problem (8.24) for the Laplace equation corresponds to the Laplace equation (1.2) and the water-tightness condition (1.3) from Chap. 1.

To solve the boundary-value problem (8.24), STAR3D Electric uses the method of boundary elements (MBE), which, in contrast to the method of finite elements (MFE), does not require the use of a three-dimensional net; instead, one triangulates the isolating surface only.

In the case of boundary-value problem (8.24) for the Laplace equation, the method of boundary elements gives rise to solution of an integral equation for the density of an equivalent double layer of electrical charges situated on an isolating surface; we use a method of approximation of the density of the double layer which allows us to take into account the branching of the surface [229].

The corresponding system of linear algebraic equations has a symmetric and positively-defined matrix; thus the problem can be solved by methods of iteration. In large dimensions (10^4–10^5 boundary elements) the program STAR3D Electric uses the multi-level fast multi-pole algorithm [38].

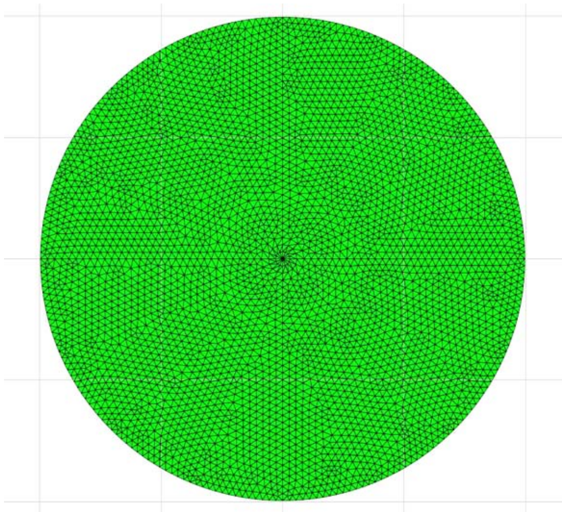

Fig. 8.11 Disc with triangulation

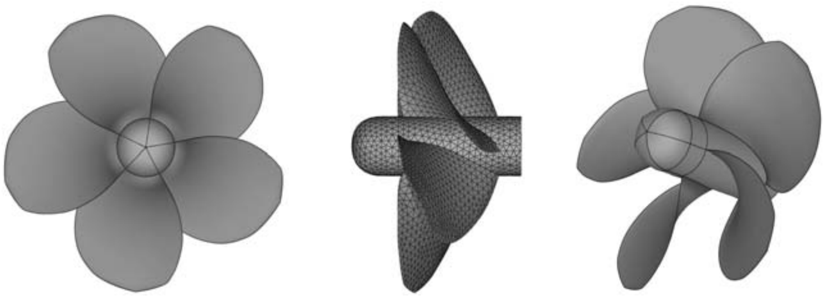

Fig. 8.12 Model of a propeller with blade-area ratio 1.08 with triangulation

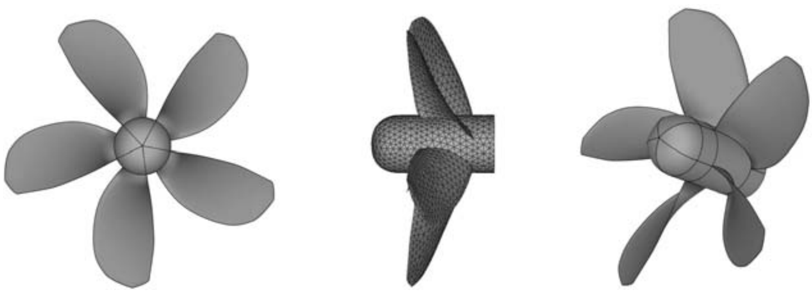

Fig. 8.13 Model of a propeller with blade-area ratio 0.61 with triangulation

In STAR3D Electric there exists a possibility to take into account the boundary conditions $\varphi = 0$ or $\partial\varphi/\partial n = 0$ automatically, via the method of mirror imaging of equivalent sources.

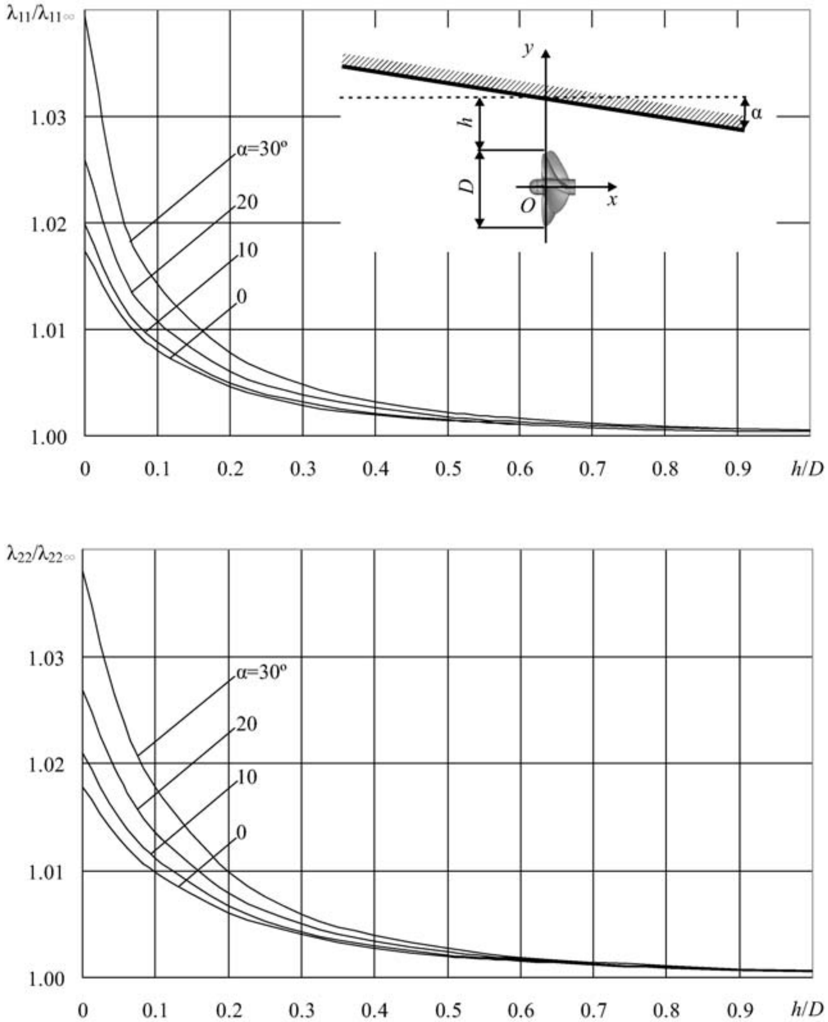

Fig. 8.14 Coefficients of added masses of a propeller with blade-area ratio 1.08 under its motion near a hard boundary

Below we collect some results of numerical computation of added masses of a disc and two models of propellers when they move close to a solid boundary. We considered two five-blade propellers with the values of blade-area ratio equal to 1.08 and 0.61. The blades of real geometry were modeled by thin plates (i.e. the effects related to finiteness and variability of the thickness of a blade were neglected).

Below we consider the added masses of a disc and two blades in the presence of a solid boundary divided by corresponding values in an infinite fluid. For the case of longitudinal motion this ratio is denoted by $\lambda_{11}/\lambda_{11\infty}$; for the case of transversal motion it is denoted by $\lambda_{22}/\lambda_{22\infty}$.

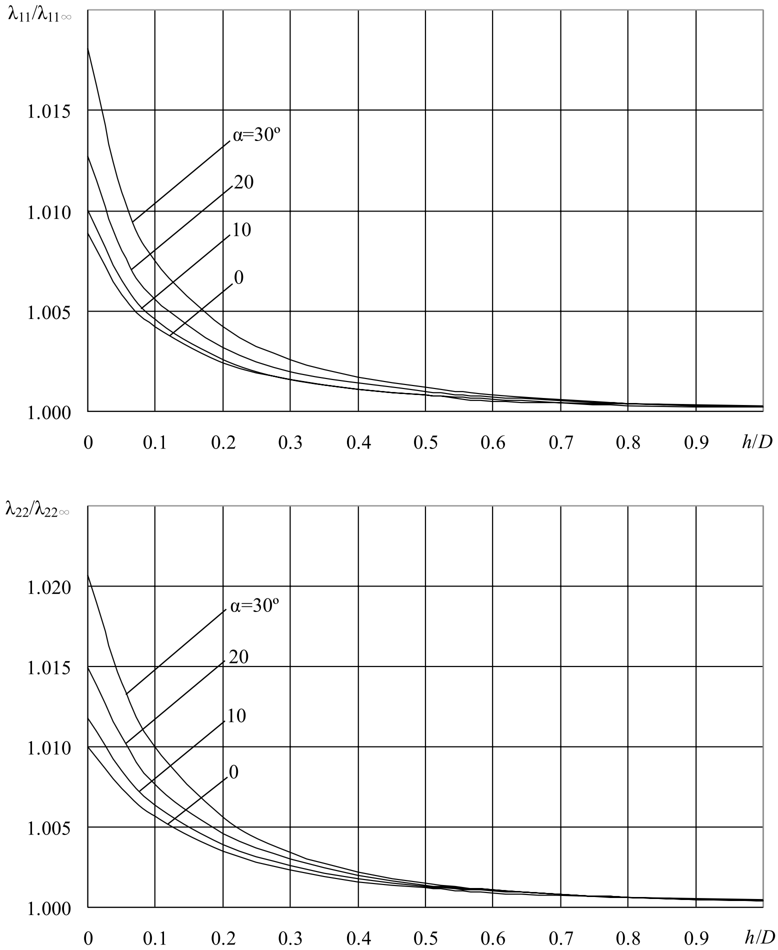

Fig. 8.15 Coefficients of added masses of a propeller with blade-area ratio 0.61 under its motion near a hard boundary

Disc Moving Near a Flat Boundary

Consider a disc or diameter D situated at a distance h from the solid plane; the angle between the plane and the axis of the disc is denoted by φ (see Fig. 8.10). The model of the disc with the triangulation is shown in Fig. 8.11. The total number of triangles in the triangulation equals 8056. Computations were performed for different values of relative distance of the disc to the boundary h/D and angle φ. The ratio $\lambda_{11}/\lambda_{11\infty}$ as a function of h/D and φ is shown in Fig. 8.10.

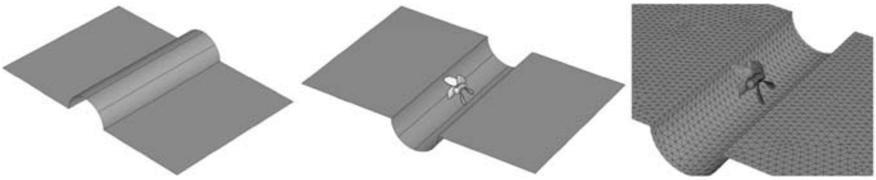

Fig. 8.16 A propeller near a flat boundary with a channel; triangulation of the boundary

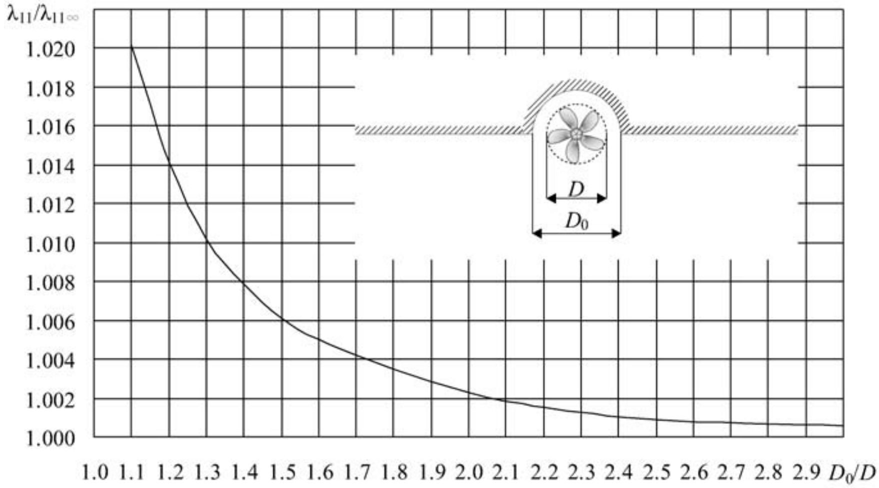

Fig. 8.17 The coefficient of added masses of a propeller under motion near a hard boundary with a channel

Propeller with Blade-Area Ratio 1.08 Moving Near Flat Boundary

The position of the propeller with respect to hard boundary is shown in Fig. 8.14. The geometric model of the propeller is shown in Fig. 8.12. The number of boundary elements of the propeller equals 4890. Graphs of coefficients $\lambda_{11}/\lambda_{11\infty}$ and $\lambda_{22}/\lambda_{22\infty}$ as functions of h/D and φ are shown in Fig. 8.14.

Propeller with Blade-Area Ratio 0.61 Moving Near Flat Boundary

The geometric model of considered propeller is shown in Fig. 8.13. The number of boundary elements was equal to 3160. Results of computation of coefficients $\lambda_{11}/\lambda_{11\infty}$ and $\lambda_{22}/\lambda_{22\infty}$ as functions of h/D and φ are shown in Fig. 8.15.

Propeller with Blade-Area Ratio 0.61 Moving Near Flat Boundary with a Channel

The geometric picture is shown in Fig. 8.17. The channel represents a half-cylinder of diameter D_0. The axis of the propeller coincides with the axis of the channel. In this problem the boundary was also triangulated (in contrast to the previous cases of flat boundary when we used the method of mirror images). The added masses were computed for different values of D_0. The number of boundary elements for different values of D_0 was between 6520 and 11724. In Fig. 8.16 we show a triangulation for $D_0/D = 1.5$. The graph of coefficient $\lambda_{11}/\lambda_{11\infty}$ as a function of D_0/D is shown in Fig. 8.17.

Chapter 9
Methods for Experimental Determination of Added Masses

There exist two main methods of experimental determination of added masses: the method of small oscillations and the method of electro-hydrodynamic analogy (EHDA). Below we consider these two methods in detail. In the last section we briefly review the existing numerical methods of computation of added masses.

9.1 Method of Small Oscillations

Consider a spring-mass system completely immersed in liquid. The equation of small oscillations of the mass along the x-axis has the form

$$(m+\lambda_{11})\ddot{x}+2\bar{n}\dot{x}+\bar{k}^2x=0 \tag{9.1}$$

where m is the mass and λ_{11} is the added mass of the body; dot denotes derivative with respect to time t; the first term corresponds to inertial force; the second term equals the damping force; the third term equals the restoring force.

The frequency of oscillations is given by the formula $k_1=\sqrt{k^2-n^2}$ where the condition of under-damping $k^2=\bar{k}^2/(m+\lambda_{11})\gg\bar{n}^2/(m+\lambda_{11})=n^2$ is provided by using springs with sufficiently small spring constants.

If we neglect damping n^2 in comparison with k^2 and experimentally determine the frequency of oscillations in water $k_0^2=\bar{k}^2/(m+\lambda_{11})$ and in air $k_\star^2=\bar{k}^2/m$, one gets the relation

$$\frac{k_\star^2}{k_0^2}=1+\frac{\lambda_{11}}{m},$$

which allows computation of the added mass

$$\lambda_{11}=m\left(\frac{k_\star^2}{k_0^2}-1\right). \tag{9.2}$$

This simple formula is derived under assumption of constancy of $\bar{k}$, assumption of small resistance and also under assumption $\rho_0\ll\rho$ (ρ_0 is the air density, ρ is the water density) which allows us to neglect the added mass of the air.

In derivation of (9.2) we used Eq. (9.1) with linear dependence of damping on velocity. However, it is well known that hydrodynamic resistance is in most cases proportional to the square of velocity. A detailed analysis of the equation with quadratic

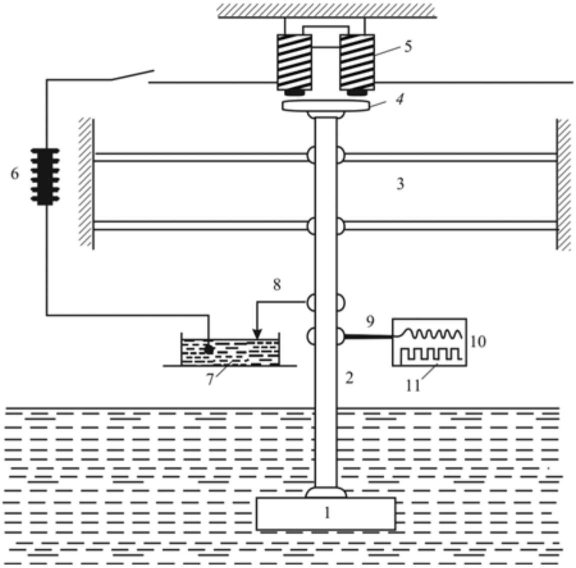

Fig. 9.1 Scheme of experimental facility to determine added masses by the method of small oscillations

damping shows [25] that for small amplitudes the frequency of oscillations is essentially independent of damping and is defined by the formulas $k_0^2 = \bar{k}^2/(m + \lambda_{11})$, $k_\star^2 = \bar{k}^2/m$, i.e., expression (9.2) in the case of quadratic damping is more accurate than in the case of linear damping. In practice the measurements are usually carried out when the oscillation regime is stable, which is provided by the impulse pumping of energy, which does not essentially change the eigenfrequency of oscillations of the system [183].

The installation scheme is shown in Fig. 9.1. The model (1) immersed in a fluid using the rod (2) is attached to springs (3); other ends of the springs are attached to the main body of the installation. A metallic plate (4) is attached to the upper end of the rod. Electrical magnet (5) connected to the battery (6) attracts the plate (4). The switch (7, 8) disconnects the battery when the rod is in highest upper position; then the rod falls down, the switch (7, 8) connects the battery and the rod returns to the upper position. Then the process repeats. The whole process is recorded using recording device (9, 10, 11).

An analogous scheme is used to determine the added moments of inertia.

9.2 Small Oscillations for Determining Added Masses of Bodies Floating on Water Surface

The scheme of installation for determining the added masses of floating bodies is shown in Fig. 9.2.[1] A crankgear transforms the rotation of the motor into a linear

[1]The method and the installation were developed by Huskind and Riman [101].

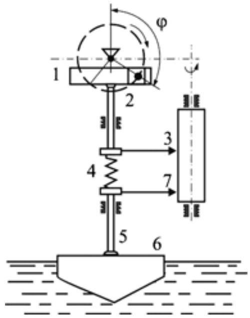

Fig. 9.2 Installation for determining added masses of ship models

harmonic motion of the rod $y = r\cos\sigma t$. This motion is recorded by a recording device (3). A spring is attached to the low end of the rod, and another rod (5) connects the other end of the spring with the model (6). The displacement of the rod (5) and the displacement of the model are recorded by the recording device (7).

Denote the mass of the model (including the lower rod) by m; the added mass by λ_{33}; the damping coefficient by n_{33}; the density of water by γ, the area of the model at waterline by S; the spring coefficient by C; the vertical displacement of the model by z. The differential equation for $z(t)$ looks as follows:

$$(m+\lambda_{33})\frac{d^2z}{dt^2} + n_{33}\frac{dz}{dt} + (\gamma S + C)z = Cr\cos\sigma t. \tag{9.3}$$

A particular solution corresponding to oscillations of the model induced by the driven force have the form

$$z_p = Ae^{i(\sigma t-\delta)} \tag{9.4}$$

where A is the amplitude of oscillations; δ is the phase shift between the driven force and oscillations of the model. Substituting (9.4) in (9.3) we get

$$\left[\gamma S + C - \sigma^2(m+\lambda_{33}) + i\sigma n_{33}\right]A = Cre^{i\delta},$$

or, separating the real and imaginary parts,

$$\lambda_{33} = \frac{1}{\sigma^2}\left[\gamma S + C - \frac{Cr}{A}\cos\delta\right] - m$$

and

$$n_{33} = \frac{Cr}{\sigma A}\sin\delta.$$

Determining A and δ experimentally from the recording devices one can easily compute λ_{33}, as well as damping n_{33}.

A similar scheme is used to determine λ_{55} when the model oscillates along the trim angle [100].

The same method can be applied when the model is tugged with constant velocity. In Fig. 9.3 we show experimental data [245] for added masses of an ellipsoid

Fig. 9.3 Coefficient of added mass of the ellipsoid of revolution for various tugging velocities

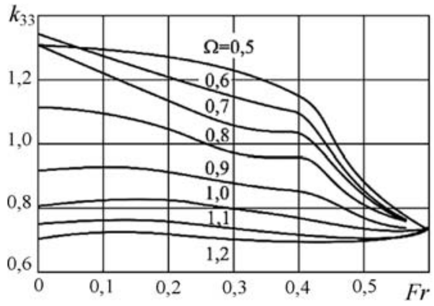

Fig. 9.4 Coefficient of added mass of catamaran

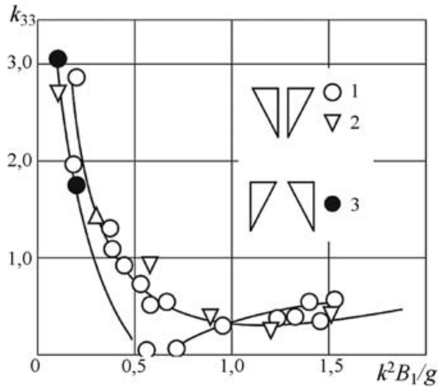

of revolution with elongation $L/B = 7$, obtained when the ellipsoid oscillates near the water surface. Here $k_{33} = \lambda_{33}/V$, where V is the volume of the ellipsoid; the immersion depth of the long axis of the ellipsoid is $h = B$; the Froude number (the normalized velocity) is $Fr = v/\sqrt{gL}$ where v is the speed of tugging, $\Omega = \sigma\sqrt{B/g}$ where σ is the frequency of oscillations of the model.

The method of small oscillation to find λ_{33} was applied by Avramenko [8] for catamaran models. The length of the models was 0.866 m, the draft and width of the models was changing. The cross-section of the hulls was chosen in the shape of rectangle, semi-circle and right-angled triangle (Fig. 9.4). These experiments were carried out for various frequencies of oscillations of the model k ($k = 2\pi/\tau$, where τ is the period of oscillations) and different distances between hulls (measured at the level of waterline). Dependence of coefficient $k_{33} = \lambda_{33}/m$ (where m is the mass of model) on dimensionless frequency k^2B_1/g, where g is the free fall acceleration, is shown for triangle hulls in Fig. 9.4.

Points shown by white circles (points "1") correspond to value $b/B_1 = 0$ (B_1 is the width of one hull of the model); points shown by white triangles (points "2") correspond to $b/B_1 = 1$; points shown by black circles (points "3") correspond to $b/B_1 = 3.7$. The mutual positions of the hulls is shown in Fig. 9.4. The author of [8] noticed that the added mass λ_{33} of catamarans is smaller than λ_{33} of a single hull whose width equals twice the width of a single hull of a catamaran.

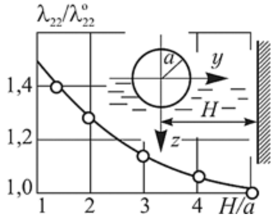

Fig. 9.5 Dependence of coefficient $\lambda_{22}/\lambda_{22}^{0}$ of a half-immersed cylinder on the distance to the wall under horizontal oscillations. Here λ_{22}^{0} is the added mass of the half-immersed cylinder of radius a in absence of the wall

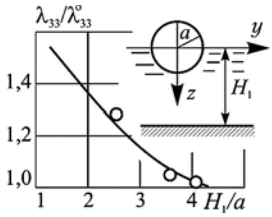

Fig. 9.6 Dependence of coefficient $\lambda_{33}/\lambda_{33}^{0}$ of a half-immersed cylinder on the distance to the bottom under vertical oscillations. Here λ_{33}^{0} is the added mass of the half-immersed cylinder of radius a at infinite depth

Using the method of small free oscillations, Dorofeuk investigated dependence of added masses of a half-immersed floating cylinder on the distance to a vertical wall (Fig. 9.5) and on the distance to the bottom (Fig. 9.6).

9.3 Experimental Method of Determining Added Mass of a Ship at Acceleration and Deceleration

Sometimes added mass can be determined using the so-called inertial method [232]. Under non-stationary linear motion of a ship the equations of motion have the form

$$(m+\lambda_{11})\frac{du_1}{dt} = P - R, \tag{9.5}$$

where m is the mass of the model, λ_{11} is the added mass of the ship; $u_1(t)$ is the linear velocity along the x-axis; P is the driving force (which is usually equal to zero in experiments with deceleration); P is resistance force.

If the driving force $P = const$, one can choose an interval of velocities $[u_1(t_1), u_2(t_2)]$ such that the resistance coefficient c_x in the formula $R = (1/2)c_x \rho u_1^2(t) S$ can be considered constant. Then Eq. (9.5) gives differential equation

$$(m+\lambda_{11})\frac{du_1}{n^2 - u_1^2} = \frac{1}{2} c_x \rho S\, dt, \tag{9.6}$$

where $n^2 = 2P/c_x \rho S$. Integrating (9.6) over the interval $[t_1, t_2]$, we get the expression

$$(m+\lambda_{11}) \ln\left[\frac{u_1(t_2) + n u_1(t_1) - n}{u_1(t_1) + n u_1(t_2) - n}\right] = n c_x \rho S (t_2 - t_1).$$

Measuring velocities $u_1(t_2)$ and $u_1(t_1)$ at the moments t_2 and t_1 and knowing P, c_x, S and m, we can easily find λ_{11} from the last equality.

If the added mass is determined in the process of deceleration under the action of the force of hydrodynamic resistance, Eq. (9.5) takes the form

$$-(m+\lambda_{11})\frac{du_1}{u_1^2} = \frac{1}{2}c_x\rho S\,dt. \tag{9.7}$$

Integrating (9.7) between t_1 and t_2 we find

$$(m+\lambda_{11})\left(\frac{1}{u_1(t_2)} - \frac{1}{u_1(t_1)}\right) = \frac{1}{2}c_x\rho S(t_2-t_1).$$

From this equality we determine λ_{11} for known t_1, t_2, $u_1(t_1)$ and $u_1(t_2)$.

In principle, an added mass should not depend on the regime of the motion of a model. However, in presence of viscosity one observes some difference in values of added masses computed under acceleration and deceleration [232].

9.4 Experimental Determination of Added Masses of Vibrating Models

The installation used to experimentally determine added masses of vibrating models is shown in Fig. 9.7 [144]. The model ("2") is posed on a free surface of liquid filling the tank ("1"). The model is supported by strings ("4") attached to the model at the points which are supposed to remain at rest under vibration ("node points"). Other ends of the strings are attached to the installation frame ("5"). On the surface of the model one installs a generator of vibrations ("3") and a device measuring acceleration in a given section of the model ("6").

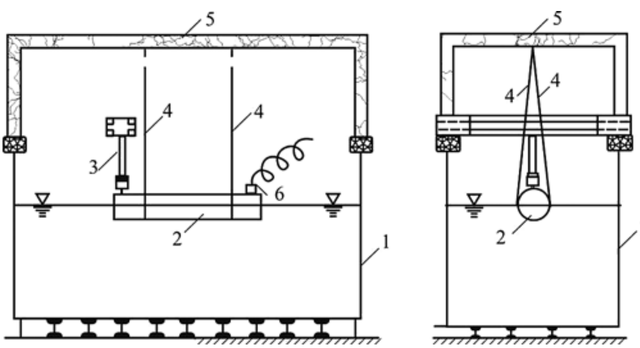

Fig. 9.7 Installation for determining added masses of vibrating models

In the simple case of investigation of homogeneous cylinder (not necessarily circular) its oscillation frequency is given by expression

$$f_n^{\text{air}} = k_n^2 \sqrt{\frac{EJ}{m}}$$

where E is the coefficient of elasticity; J is the moment of inertia of the cross-section of the cylinder with respect to the central axis; m is the linear density of the cylinder; k_n is the coefficient depending on type of oscillation (for a given length of the cylinder on a number of nodes) and boundary conditions at the ends of the cylinder.

By measuring the frequency of free oscillations of the cylinder in air f_n^{air} and in water

$$f_n^{\text{water}} = \sqrt{\frac{EI}{m + \Delta m} k_n^4}$$

under the same conditions, we get the relation

$$\left(\frac{f_n^{\text{air}}}{f_n^{\text{water}}} \right)^2 = 1 + \frac{\Delta m}{m},$$

which implies the formula for the linear added density of the cylinder:

$$\Delta m = m \left[\left(\frac{f_n^{\text{air}}}{f_n^{\text{water}}} \right)^2 - 1 \right].$$

The added mass of air is usually neglected.

Consider the added linear density of the cylinder moving as a solid body in the direction of vibration (y-axis):

$$\Delta m' = k_{22} \rho \pi a^2,$$

where a is half of the width of the cylinder in the direction orthogonal to the direction of motion; k_{22} is a coefficient depending on the shape of a cross-section of the cylinder. The ratio

$$J_n = \frac{\Delta m}{\Delta m'},$$

depending on the number of nodes n, is the reduction coefficient introduced above in Sect. 7.1.

If Δm is determined for a circular cylinder half-immersed in a liquid, then

$$k_n = \frac{2m}{\pi \rho k_{22} a^2} \left[\left(\frac{f_n^{\text{air}}}{f_n^{\text{water}}} \right)^2 - 1 \right],$$

since in that case

$$\Delta m' = \frac{1}{2} k_{22} \rho \pi a^2.$$

Let us describe some details of experiments carried out by Dorofeuk. The model was chosen to be an ellipsoid of revolution of length $L = 150$ cm, with elongation $L/B = 10$. The interior base of the model was a steel plate 3 cm wide and 0.3 cm thick (to study vibrations of 4th and 5th tones the thickness of the plate was taken to be 0.1 cm). The "shipframes" were disks made of plywood 0.5 cm thick. The radius of the disks was changing over the length of the plate by elliptic law. The intervals between plywood disks were 0.2 cm; the disks were separated by washers 0.2 cm thick. At the ends of the model small metallic cups were attached. From outside the model was covered by a rubber shell 0.1 cm thick which prevented penetration of water inside of the model. The weight of the model was chosen to make sure that it was floating when half-immersed in water. The rigidity of the ellipsoid was constant over its length and was equal to the rigidity of the central plate. The linear mass of the model was a combination of mass of the central plate, the washers, and plywood disks.

To carry out experiments in the air, two carriers were attached to the central plate; two strings were attached to the carriers. The positions of the carriers were chosen to coincide with nodes under oscillations of the model with given frequency. The rod of the vibrating mechanism was at the end of the model; it was connected to the model by a steel spring. Oscillations of various points of the model were recorded by vibrograph.

When the model was oscillating in water, the vertical supporting strings were removed, and the position of the model in water was fixed by horizontal bracings attached to the model at both ends.

At small frequencies of the driven force the model was oscillating as a solid body. This regime corresponds to conditions of motion considered above (method by Huskind and Riman). When the frequency increases, these oscillations quickly decay and elastic oscillations of the model appear, whose amplitude is increasing until it reaches its maximum when the frequency of the driven force coincides with the 1st tone of the model. Two nodes of oscillations of the first tone were clearly seen. When the frequency of the driven force increases further, the model becomes immovable again, until the frequency reaches the second tone, etc.

For the model whose interior steel plate was 0.3 cm thick, in this way one can excite the 1st, 2nd and 3rd resonance tones. Due to high rigidity of such a plate, higher tones could not be excited. Oscillations of 4th and 5th tones were excited by substitution of the 0.3 cm plate by a 0.1 cm thick plate. However, in that case the 1st, 2nd and 3rd modes could not be excited due to insufficient power of an electrical motor at small frequencies.

It is interesting to notice that in water one can easily see the nodes of oscillations; counting them one can determine the tone. In Fig. 9.8 (obtained by E.N. Schukina) we clearly see these points for the case of oscillations of a rectangular pontoon.

In Table 9.1 both experimental and theoretical results are shown for reduction coefficients k_n ($n = 1, \dots, 5$) for an ellipsoid of revolution.

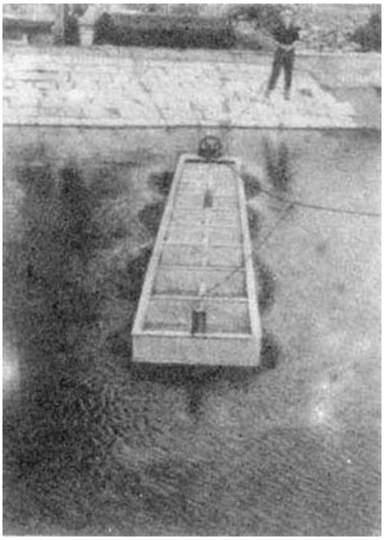

Fig. 9.8 Rectangular pontoon vibrating on a water surface

Table 9.1 Values of reduction coefficients (due to Dorofeuk) for vertical oscillations of a floating ellipsoid of revolution

Tone number	Frequency of free oscillations		$k_{n\,\mathrm{exp}}$	$k_{n\mathrm{th}}$
	in air, osc/min	in water, osc/min		
1	195	150	0.875	0.858
2	460	360	0.810	0.808
3	825	655	0.760	0.759
4	290	228	0.716	0.716
5	460	365	0.689	0.677

9.5 Determination of Added Mass Coefficients by Methods of Electromagnetic Modeling

In the general case, to determine added masses of an arbitrary geometric form moving in unbounded flow gives rise to computation of integrals (see Chap. 1):

$$\lambda_{ik} = -\rho \iint_S \varphi_k \frac{\partial \varphi_i}{\partial n}\, dS, \quad i, k = 1, \ldots, 6, \tag{9.8}$$

where ρ is the density of the fluid, φ_i are elementary potentials of velocity defined after (1.9); n is surface normal; S is the surface of the body.[2]

One approach to experimental determination of these integrals is based on mathematical analogy between the flow of an ideal fluid and electrical and magnetic fields.

[2]This section was written by S.N. Okunev.

Table 9.2 Electro-hydrodynamic analogy (EHDA)

Field of velocities in liquid caused by linear motion of a body	Field of stationary electrical charges in conducting media (EHDA)
Velocity of fluid v	Electric field of induced charges E
Velocity of body v_0	External homogeneous electric field E_0
Potential of fluid velocity φ	Potential of induced charges φ
Relation between velocity and potential $v = \operatorname{grad} \varphi$	Relation between electric field and potential $E = -\operatorname{grad} \varphi$
Boundary condition on body surface $v_n = v_0 \cos(v_0, n)$	Boundary condition on non-conducting body surface $E_n = -E_0 \cos(E_0, n)$
Boundary condition on watertight boundaries of the flow $v_n = 0$	Boundary conditions on non-conducting external boundaries $E_n = 0$
Condition of continuity in the flow: Laplace equation $\Delta\varphi = 0$	Condition of continuity in conducting medium $\Delta\varphi = 0$
Added masses $\lambda_{ik} = -\rho \iint_S \varphi_i \frac{\partial \varphi_k}{\partial n}\, dS$, $i, k = 1, \ldots, 6$; S is the area of body surface; ρ density of fluid	$\lambda_{ik} = -\rho \iint_S \varphi_i \frac{\partial \varphi_k}{\partial n}\, dS$; φ_i-elementary electric potentials

Correspondence between hydrodynamic and electrical variables is represented in Table 9.2 [189] (in [189] a correspondence between hydrodynamic and magnetic variables is also given). It follows from these tables that in geometrically identical electrical model, under appropriate boundary conditions one can mathematically rigorously reproduce the flow of ideal fluid around a solid body.

Advantages of electromagnetic analog models are the following:

- Use of standard devices which can measure electrical and magnetic fields with high precision.
- Existence of conducting materials (metallic foil, electrolytes) possessing standard properties and technically convenient for model construction.
- Existence of well-known methods of analogous modeling in continuous media, which allow reproduction of a model of the flow induced by the motion of a body or a flat contour of an arbitrary shape. The flow can be bounded by walls of an arbitrary shape; in this case complexity of the modeling increases insignificantly (for example, analysis of the flow around a hull near a wall of an arbitrary shape is only 2–3 times more laborious than the analysis of the same flow in an infinite fluid).
- High visualization of the method.
- For most measured variables such as potential, velocity, contour integrals etc., one can tune-up the model in advance and determine coefficients translating electrical and magnetic parameters into hydrodynamic ones.

The disadvantages of analogous models are related mainly to inaccuracy of obtained data having the following origins:

1. Insufficiently complete formulation of the problem and insufficiently precise translation of boundary conditions (especially in the case of body motion near the free surface).
2. Discreteness of boundary conditions; inhomogeneity of conduction medium.
3. Systematic error related to jump of potential on conducting elements while working with electrolytes.

Solution of these problems is taken into account in development of modeling methods [49, 189].

In electromagnetic models, precision is influenced by working frequency of the electromagnetic field, relation between size of the model and size of the electromagnetic sensor. Detailed analysis of these parameters is given in [189].

The main methods of electrical and magnetic modeling, taking into account boundary conditions as well as their practical implementations, are considered below.

9.5.1 Added Masses of Planar Contours

Added masses of a flat contour can be most conveniently determined via the formula (9.8) on EHDA installation for the model of reversed flow (Fig. 9.9). The installation includes a rectangular conducting sheet (a model of the domain of the flow), bus bars to get the difference of potentials E_0 and an electric battery. The investigated contour is cut out from a sheet (conducting material is removed from the inside of the contour) such that the axis Ox, parallel to E_0, coincides with the direction of the body motion. A point of the contour is chosen as an origin of the coordinate system ($x = 0$, $y = 0$). At the origin one installs a needle of a sensor; at this point one assumes $\varphi_k = 0$. The second needle is installed in other points of the contour; potential φ_{mi} of contour points with respect to the origin is measured.

Taking into account the boundary condition on the contour when it moves along the Ox axis with unit velocity, one gets from (9.8) the following expression for the added mass:

$$\lambda_{11} = -\rho \int_0^{y_M} \varphi_1 \, dy. \tag{9.9}$$

In this formula y_M is the y-coordinate of the point M of the contour l which has a maximal distance to Ox axis; $\varphi_1 := \varphi_{1m} - \varphi_{0m}$, where φ_{1m} is the potential at a given point of the contour l; φ_{0m} is the potential at the same point if the investigated contour is not cut out.

Value φ_{0m} can be determined by one measurement on a conducting sheet before the model is cut out between points 0 and M (see Fig. 9.9).

For contours of an arbitrary shape the measurements should be carried out for all points of the contour; for symmetric contours one can measure only one half of the contour, and then double the result. To determine $\varphi_{0m} = f(y)$ one can use an "etalon"—a rectangular model of conducting medium, included in the chain together with the model (see Fig. 9.9). For coinciding widths of the sheets $h = H$ the

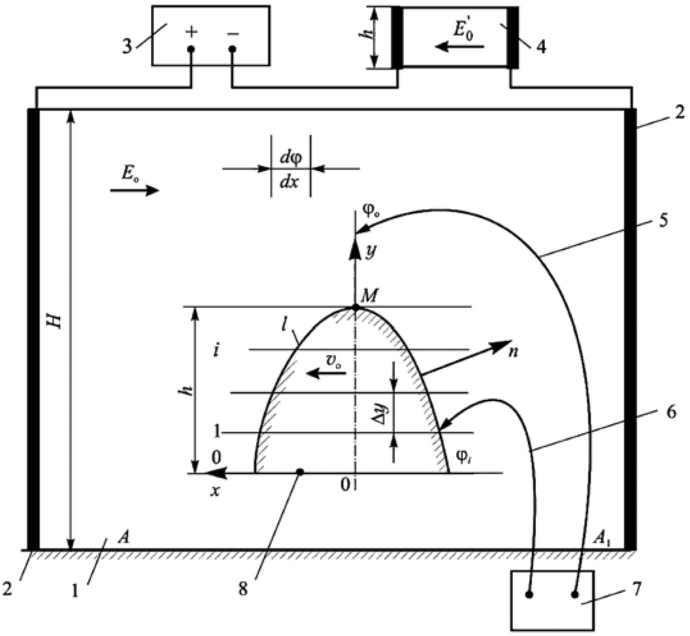

Fig. 9.9 EHDA installation to determine added masses of planar contours. Notations: *1*—conducting media; *2*—electrodes creating difference of potentials; *3*—battery; *4*—device controlling the magnitude of current in the model; *5*—static sensor measuring reference potential φ_0; *6*—moving sensor to measure potential at the contour l; *7*—measuring device; *8*—non-conducting contour l

rate of increase of the potential (per unit of length) is the same; for different widths the rate of increase of the potential is inversely proportional to the ratio of heights of the working sheet and the etalon, since $E_0 H = E_0' h$. This scheme is convenient for modeling a motion parallel to a flat boundary (screen) which is modeled by a non-conducting edge AA_1 of the sheet (see Fig. 9.9) from one or from both sides. To imitate a motion of the contour towards the screen one can cut an edge of the sheet, which changes electrical parameters of the model.

The EHDA method allows us to reproduce the model of induced flow by setting appropriate potentials on contours via discrete electrodes (Fig. 9.10). Contour S can be split by several equidistant lines parallel to the direction of motion (the x-axis); the interval between two lines equals $\Delta y = const$. Change of potential on these intervals (which is equal by magnitude) is added or subtracted depending on the angle between the y-axis and normal to the interval ΔS of the boundary. Discrete electrodes (via resistors) and "etalon" are connected to batteries with variable voltage. Such a scheme allows us to introduce sources of the same magnitude; the "etalon" controls the total flow (i.e., defines velocity of the contour). The induced potentials φ_i are measured between the electrodes. For 20–25 sources and sinks the error due to discreteness does not exceed 2–4%. This method allows us to investigate, for ex-

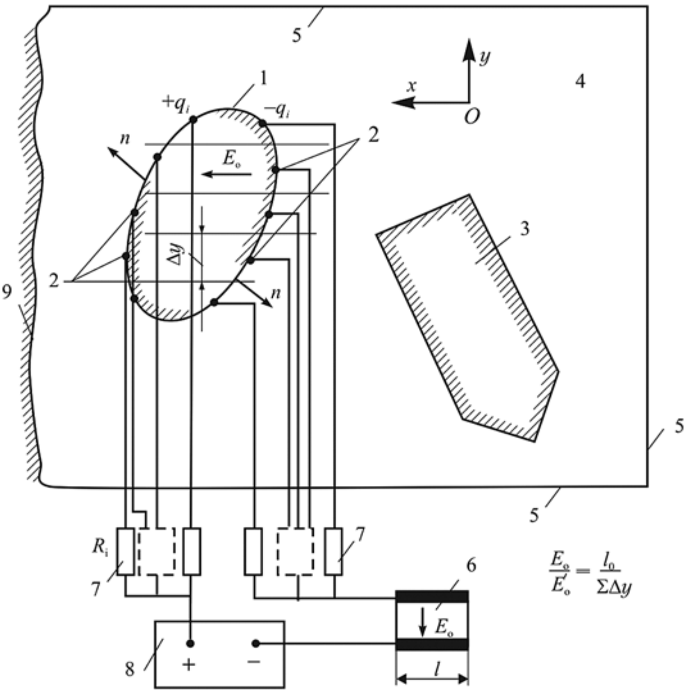

Fig. 9.10 Electrical model of non-inversed motion of contour. Notations: *1*—contour S, moving in the direction of axis Ox; *2*—discrete sources (sinks) of intensity q_i; *3*—immovable contour S_1; *4*—conducting medium; *5*—boundaries of the flow; *6*—device for determining total flow $\sum q_i$; *7*—resistors R_i; *8*—battery; the contour is moving in the direction of the screen 9

ample, motion of a contour over a screen of an arbitrary shape in presence of other (immovable) contours.

To increase the precision of measurement on the contour (if the contour is relatively small, or has a complicated shape) one applies a combined model of motion. In this model the inverted flow is defined with respect to the moving contour while on other contours and a curved screen one installs sources and sinks (through "etalons") which compensate the field of inverted flow on these contours (in this way one models their "motion" in the direction of inverted flow (Fig. 9.11)). In such models the discreteness of sources and sinks is significant at lengths which do not exceed 2–3 distances between the sources (sinks).

9.5.2 Added Masses of 3D Bodies

To determine added masses of a 3D body by the EHDA method one immerses a model made of dielectric into a tank filled with an electrolyte. The surface of the model is marked by two families of equidistant parallel planes (xOy and xOz)

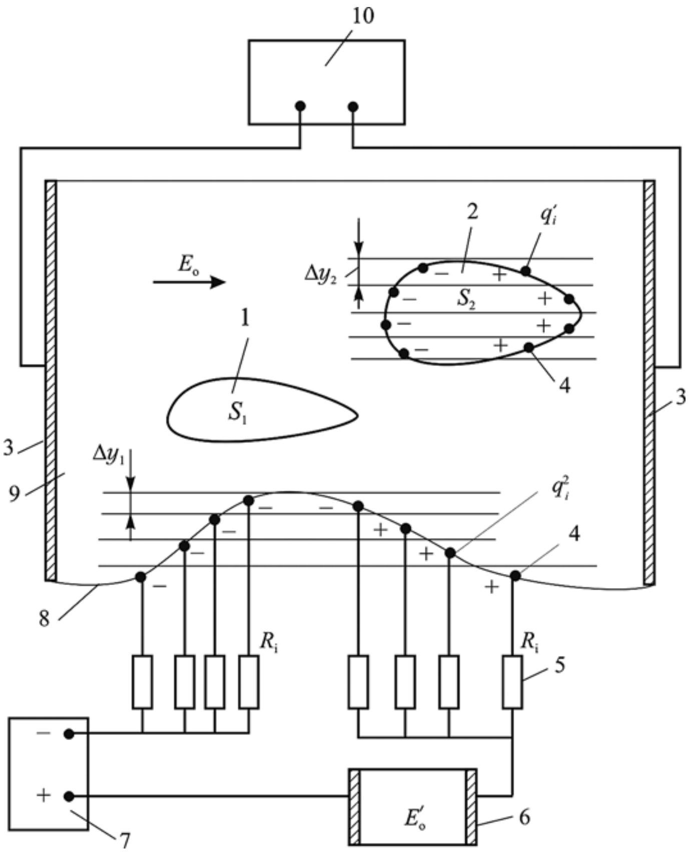

Fig. 9.11 Combined scheme of modeling of motion on EHDA installation. Notations: *1*—investigated contour; *2*—immovable contour; *3*—electrodes; *4*—discrete sources (sinks); *5*—resistors; *6*—etalon; *7*—battery; *8*—curved boundary; *9*—domain of the flow; *10*—battery

such that projections ΔS of all surface elements on the orthogonal plane are equal (Fig. 9.12). Discrete electrodes (sources and sinks of different intensity) are posed at the center of each surface element. The measurement of induced potentials is carried out over the marking curves between the electrodes.

The problems of this method are related to complexity of installation of many electrodes. An advantage of the method is the possibility to model boundaries of arbitrary shape, and the possibility to consider a superposition of several moving bodies. If one models the motion in an infinite medium, or in a medium bounded by flat screens which are parallel to the direction of the motion, it makes sense to apply the model of inverted flow.

Within a tank filled with an electrolyte (Fig. 9.13) one creates a homogeneous electric field; then one inserts in the tank a model of the body made of a dielectric. On the surface of the body one measures the potential (with respect to an arbitrary initial point) by a needle sensor. The choice of measurement points is arbitrary,

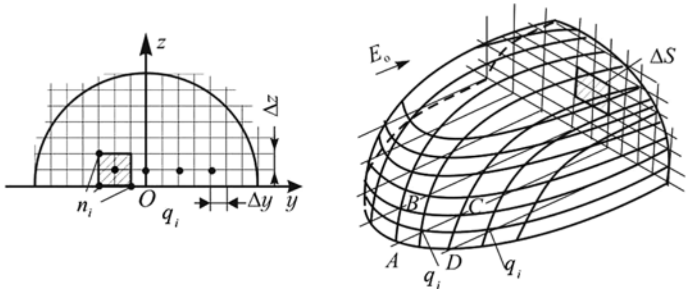

Fig. 9.12 Marking of the surface of a model: $\Delta S = 4\Delta z \Delta y$—projections of bow and after-part elements of hull surface to the plane of middle shipframe; E_0—domain of electrolyte; n_i—points of measurement of potential

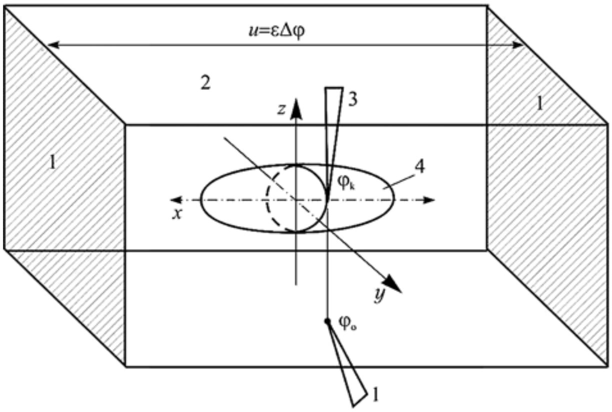

Fig. 9.13 Scheme of space EHDA installation. Notations: *1*—electrodes; *2*—electrolyte; *3*—1-needle sensors; *4*—non-conducting surface of the model; φ_k—potential at point k of surface S

which is convenient in studies of models of complicated structure with elements of different scale (for example, immersed parts of floating drilling vessels). The measurement and summation of potentials should be carried out over the complete surface.

Similar methods can be applied to determine added moments of inertia [189].

9.5.3 Determination of Added Masses on the Basis of Magneto-hydrodynamic Analogy (MHDA)

Analog models for determining added masses can be constructed on the basis of magneto-hydrodynamic analogy (MHDA). The MHDA installation is shown in Fig. 9.14. A homogeneous magnetic field is created inside a closed solenoid which,

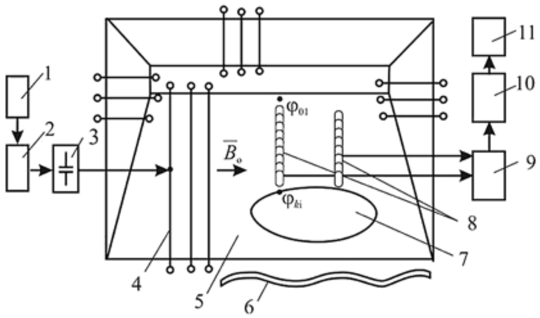

Fig. 9.14 Scheme of installation of magnetohydrodynamic analogy (MHDA). Here *1*—generator; *2*—amplifier; *3*—block of capacitors; *4*—solenoid; *5*—homogeneous magnetic field; *6*—metallic screen; *7*—metallic model; *8*—solenoid sensors; *9*—commutator; *10*—measuring amplifier; *11*—results recorder

together with a block of capacitors, creates an oscillating circuit with resonant frequency 30–50 kHz. A metallic model is put inside the solenoid; screens made of metallic sheets 0.3–0.5 mm thick are posed both inside and outside of the solenoid; the screen can have an arbitrary shape.

Magnetic potentials are measured using thin long solenoids which are moved orthogonally to the vector of unperturbed field B_0, such that one end of the solenoid is posed near the model surface, where $\varphi_i = \varphi_{0i} + \varphi_{bi}$; another end is posed far from the model, where the field is unperturbed, $\varphi_i = \varphi_{0i}$. Therefore, the potential of induced motion φ_{bi} can be found by one measurement. The potential φ_b is measured over the whole surface and integrated.

Advantages of the MHDA method (compared to the EHDA method) are absence of electrolytes, possibility to consider large models (up to 3–5 m), simplification of measurements, absence of flow boundaries (since solenoid winding does not bound the magnetic field). Restrictions of the method are related to necessity to build models from metal, and to take into account the size of sensors for measuring magnetic potentials (usually diameter of the solenoid is $d = 4$–8 mm and length is 500–1000 mm). If characteristic linear size l of the model is chosen such that $l/d > 20$, the error of measurement does not exceed 3%; for $l/d > 100$, the error does not exceed 0.3%.

9.5.4 Some Data on Added Masses of Planar Contours Determined Using EHDA Method

1. Cylinder of radius R with rectangular attachment. The sides of rectangle h and l are chosen according to Fig. 9.15, where one shows also the choice of coordinate system.

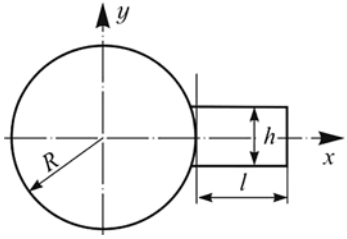

Fig. 9.15 Cylinder with rectangular attachment

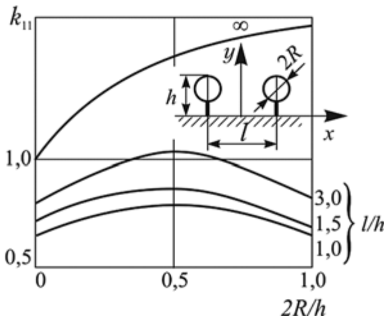

Fig. 9.16 Coefficient of added mass of parallel plates with cylindrical attachments as a function of $2R/h$

$h/2R$	0.40	0.60	0.60	0.60	0.60	–	–	–
$l/2R$	0.25	0.25	0.35	0.45	0.5	–	–	–
$\lambda_{11}/(\pi\rho R^2)$	1.08	1.30	1.42	1.45	1.48	–	–	–
$h/2R$	0.10	0.10	0.10	0.20	0.30	0.40	0.50	0.50
$l/2R$	0.10	0.20	0.30	0.30	0.30	0.40	0.40	0.50
$\lambda_{22}/(\pi\rho R^2)$	1.16	1.42	1.68	1.77	1.83	2.10	2.15	2.67

2. Two parallel plates of height h with cylindrical attachments of radius R posed at distance l from each other have a coefficient of added masses determined by the graph shown in Fig. 9.16. Variable $k_{11} = 2\lambda_{11}/\pi\rho R^2$ corresponds to added mass of one plate.

3. Coefficient of added mass of the system consisting of a vertical plate and a circular cylinder posed under the plate. The graph of $k_{11} = 2\lambda_{11}/\rho\pi R^2$ as a function of D/H is shown in Fig. 9.17; here $h = 0.4H$, where H is the total height of the system (see Fig. 9.17).

4. Added mass $\lambda_{11} = k_{11}\pi\rho R^2$ of a circular cylinder with edges of height l posed with gap $h - l$ near its surface (see Fig. 9.18) is shown in terms of coefficient $k_{11}(l/R)$ for $h/R = 0.5$.

Added masses of a cylinder with central slit is shown in Fig. 9.19 via dependence of coefficients $k_{11} = \lambda_{11}/\pi\rho R^2$ and $k_2 = \lambda_{22}/\pi\rho R^2$ on dimensionless parameter $(D - h)/D$ determining the width of slit ($D = 2R$ is diameter of the cylinder, h is the width of the slit).

Fig. 9.17 Coefficient of added mass of the system plate-cylinder as a function of D/H

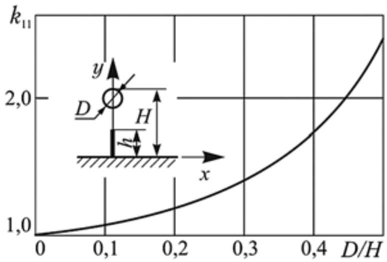

Fig. 9.18 Coefficient of added mass of cylinder with edges posed close to its surface as a function of l/R

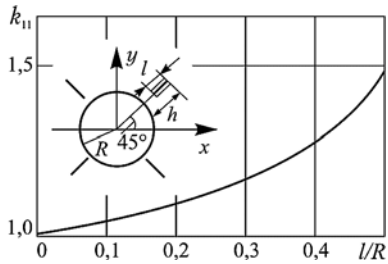

Fig. 9.19 Coefficient of added mass of cylinder with slit as a function of $(D-h)/D$

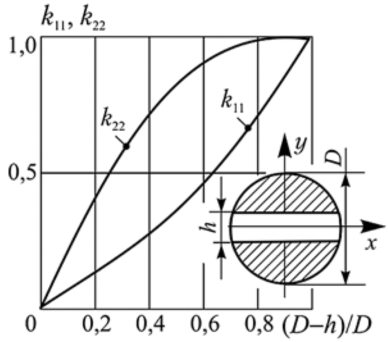

9.6 On Numerical Methods of Computation of Added Masses

There exist two main ways of mathematical description of problems of mechanics of continua: the first one is based on differential equations, and the second one is based on variational principles.[3]

The most common numerical method based on a differential equations description is the method of finite differences [45, 179]. The idea of this method is to substitute all derivatives in the differential equations and boundary conditions by their approximate difference values, which are determined by values of the function at a chosen set of lattice points inside the domain. Then the original problem reduces to a system of algebraic equations.

[3] This section was written by V.S. Boyanovsky and O.I. Babko.

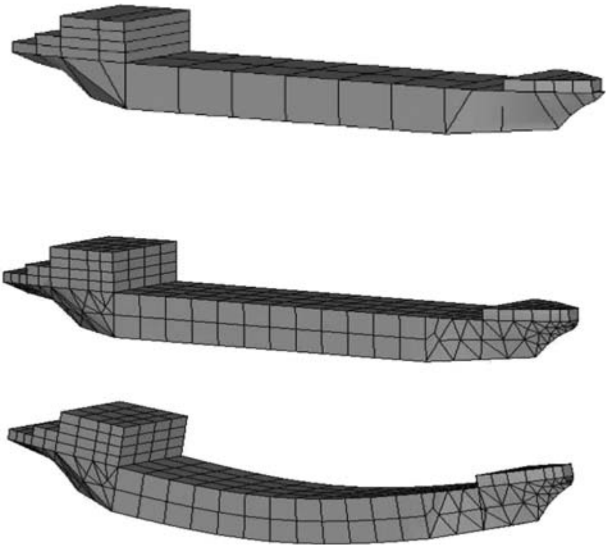

Fig. 9.20 Finite-element models (above) and results of computations of the shape of oscillations of the first mode of a hull of a medium-size tanker (below)

The most common numerical method based on variational principles is the method of finite elements [1, 46, 47, 66, 118, 119, 179, 257, 258]. The method of finite elements (MFE) is very stable with respect to change of geometry of the considered object and boundary conditions. The main idea of the method is in substitution of a system with infinite degrees of freedom as a system of a finite number of separate elements connected to each other at certain points (junction points).

There are the following steps of computations via the MFE:

1. The domain (structure) under investigation is split into finite elements interacting with each other at junction points (see Fig. 9.20). The choice of the shape and size of the finite elements depends on the shape of the object and precision of computation.
2. The values of a function at junction points are assumed to be unknown; then the total number of degrees of freedom equals the product of the number of junction points with the number of unknown functions.

   After the set of unknowns is chosen, one performs the main step: the choice of interpolating polynomial which describes the unknown function inside the finite element via the values of unknown variables at the junction points. When polynomials of first order are used the finite elements are called first order; polynomials of second order determine quadratic finite elements. Under certain general conditions on these polynomials the value of the functional χ (whose physical meaning depends on the problem) for the whole domain is defined as follows:

$$\chi = \sum_{i=1}^{N} \chi_i$$

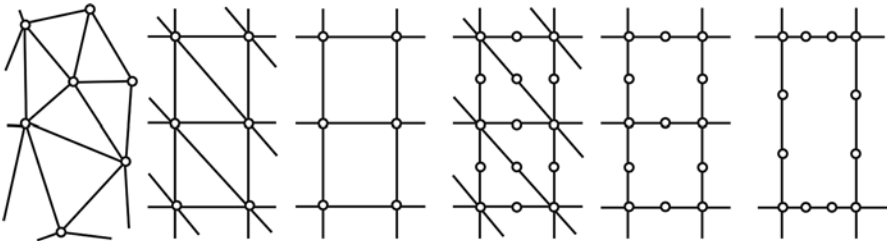

Fig. 9.21 Different ways to partition a domain to finite elements

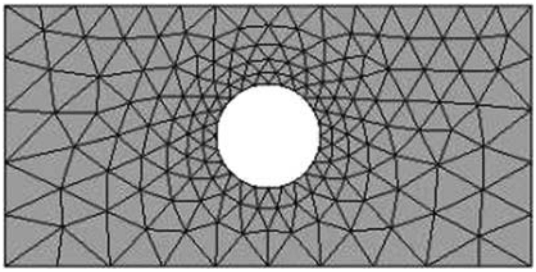

Fig. 9.22 Finite-element model of a plate with a hole

where χ_i is the value of the functional on the ith element; N is the total number of elements.

3. Finding of stationary value of the functional χ under variation of the values of the function at the junction points; stationarity of the functional gives a system of algebraic equations for these values.

When the size of finite elements decreases, the method gives more precise result; however, this leads to exponential growth of computation time.

In Fig. 9.21 we show various ways of partitioning a domain in finite elements. Generically, in a domain of high gradients of a function one should use smaller finite elements. For example, a typical way of partition of a plate with a hole in finite elements is shown in Fig. 9.22.

As an illustration of application of MFE consider a rectangular pontoon and a circular cylinder airfoil of finite length.

In the case of an oscillating rectangular pontoon for various ratios L/B (L is the length, B is the width) and constant ratios $B/H = 2$ and $H/T = 2$ (H and T are the height and the draught, respectively) the results of application of MFE show that the added masses of a given section are rather inhomogeneously distributed over the length of the pontoon (Figs. 9.23–9.25). In particular, we can conclude from these figures that as the ratio L/B grows, the relative length of the zones near the pontoon ends, where the added masses of plane sections significantly drop, decreases.

Let us now compare the theoretical results obtained in [21] with numerical results of computation of added masses by MFE for a cylindrical airfoil (see Fig. 3.12).

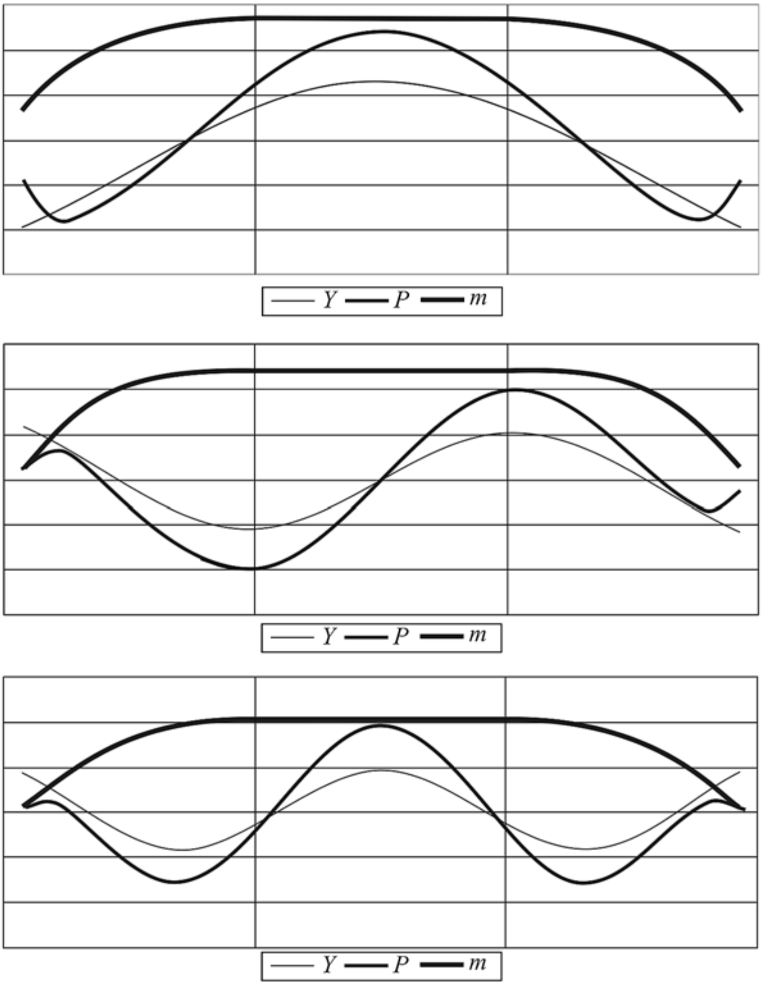

Fig. 9.23 Distribution of amplitude of oscillations Y, the pressure P and added mass m over the length of the pontoon ($L/B = 3$) under vertical vibration of the 1st 2nd and 3rd modes (from top to bottom)

Introduce the coefficients of added masses

$$k_{22} = \frac{\lambda_{22}}{\rho D b^2},$$

where λ_{22} is the total added mass of cylindrical airfoil in a direction orthogonal to the axis; ρ is the fluid density, D is the diameter of the cylinder, b is the length of the cylinder.

In Fig. 9.26 we show dependence of the coefficient λ_{22} on parameter $\lambda := D/b$. The solid curve corresponds to analytical results obtained in [21]; the points show

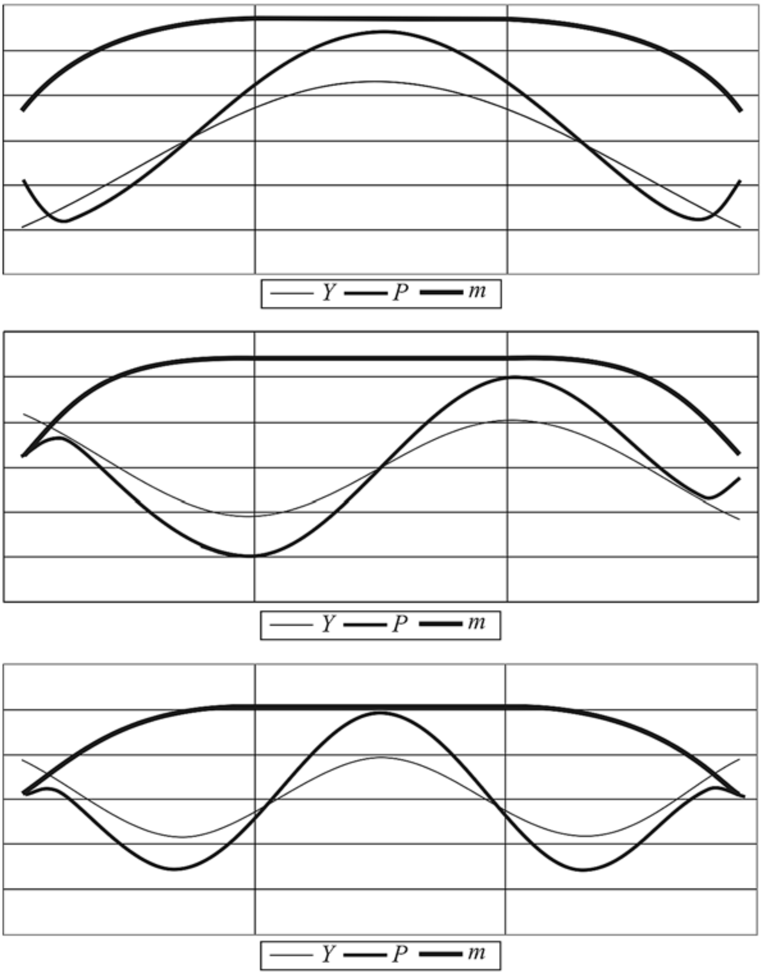

Fig. 9.24 Distribution of amplitude of oscillations Y, the pressure P and added mass m over the length of the pontoon ($L/B = 5$) under vertical vibration of the 1st, 2nd and 3rd modes (from top to bottom)

the results of numerical computation by the MFE. One observes a good correspondence between analytical and numerical results.

Using numerical methods one can study the added mass λ_{22} of cone-type circular airfoil. It turns out that under the same length and the same average diameter the following approximate formula holds:

$$\lambda_{22}^{\alpha} = \lambda_{22}\left(1 + \frac{\alpha}{100}\right),$$

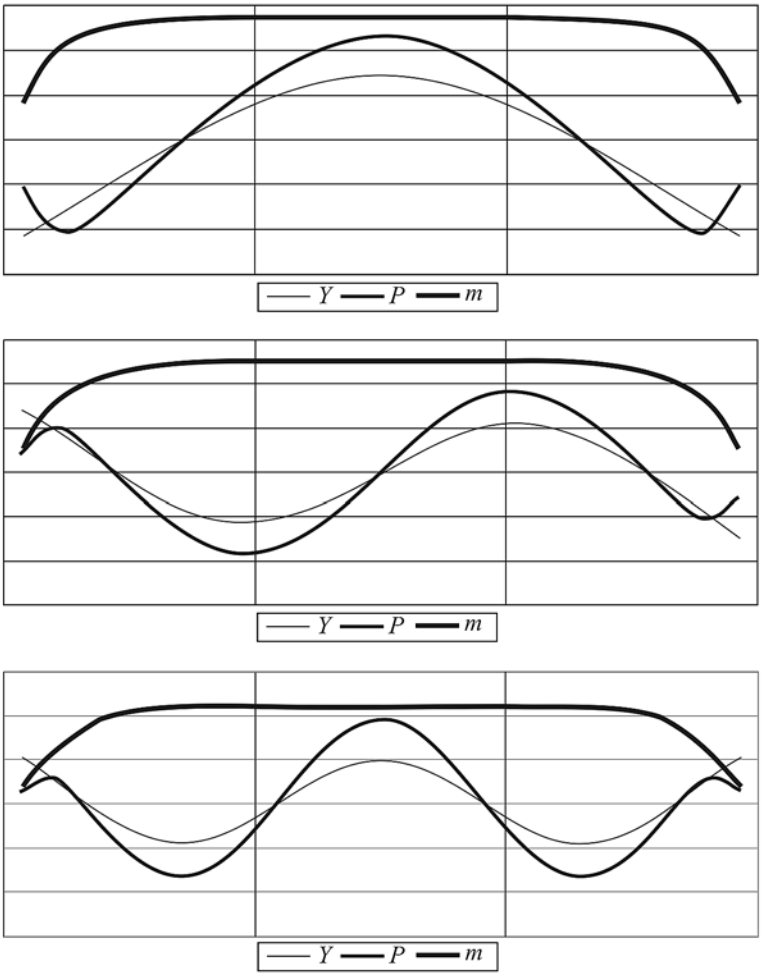

Fig. 9.25 Distribution of amplitude of oscillations Y, the pressure P and added mass m over the length of the pontoon ($L/B = 10$) under vertical vibration of the 1st, 2nd and 3rd modes (from top to bottom)

where λ_{22} is the added mass of a circular cylindrical airfoil; λ_{22}^{α} is the added mass of cone-type airfoil of the same length and average width, where α is the angle between the central line of the airfoil and generating line of its surface.

Another observation one can make on the basis of numerical results is that the added mass of elliptic airfoil in the direction of one of the main axes is in fact independent of the value of eccentricity (as long as the axis orthogonal to the direction of motion remains the same).

Using MFE one can also evaluate the influence of hard boundary and free surface on total added mass of circular cylindrical airfoil (Figs. 9.27, 9.28). Comparison of the results for the circular airfoil and for the solid cylinder shows that the presence

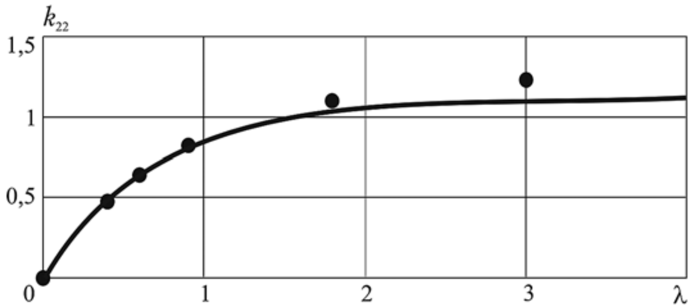

Fig. 9.26 Coefficients of added masses of a circular airfoil: the *curve* corresponds to theoretical results of [21]; *dots* correspond to computations via the method of finite elements

Fig. 9.27 Dependence of added mass of circular cylinder airfoil (*solid line*) and of a solid cylinder (*dashed line*) on the ratio of the distance from the axis to flat solid boundary to the radius

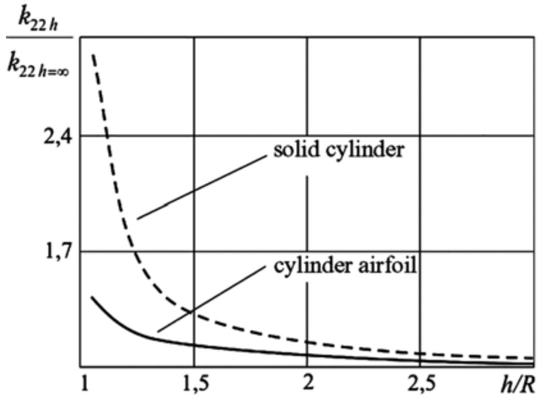

Fig. 9.28 Dependence of added mass of circular cylinder airfoil (*solid line*) and of a solid cylinder (*dashed line*) on the ratio of the distance from the axis to the free surface to the radius

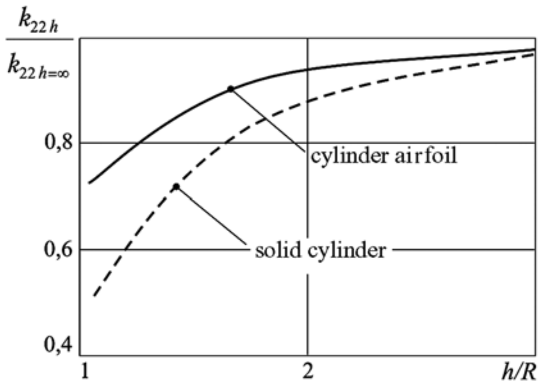

of fluid inside of the cylinder essentially decreases the influence of the distance to the solid boundary on the value of added mass.

There exist various program complexes for computation of added masses: ANSYS [19, 108], NASTRAN, COSMOS, etc.; most of these complexes are based on the method of finite elements and allow one to describe numerically highly complicated interactions of bodies moving in fluid (see for example [5]).

Bibliography

1. Aleksandrov, V.L., Matlah, A.P., Polyakov, V.I.: *Fighting Ship Vibrations*. MorWest, St. Petersburg (2005), in Russian
2. Atlas of hydrodynamic characteristics of ship rudders. Publications of Novosibirsk Institute of Water Transport **72** (1972), in Russian
3. Amabili, M.: Flexural vibration of cylindrical shells partially coupled with external and internal fluids. Trans. ASME J. Vibr. Acoust. **119**(3), 476–484 (1997)
4. Anderson, W.J., Shah, G.N.: Park Jungsun, Added mass of high-amplitude balloons. J. Aircraft **32**(2), 285–289 (1995)
5. Program complex ANSYS, version 8, Russian edition. Eng. Tech. J. **1** (2005)
6. Athanassoulis, G.A., Kaklis, P.D., Politis, C.G.: The limiting values of added masses of a partially submerged cylinder of arbitrary shape. J. Ship Res. **32**(1), 1–18 (1988)
7. Athanassoulis, G.A., Kaklis, P.D., Politis, C.G.: Low-frequency oscillations of a partially submerged cylinder of arbitrary shape. J. Ship Res. **39**(2), 123–138 (1995)
8. Avramenko, P.G.: On added masses of catamarans. Hydromechanics **15**, 19–23 (1969), Kiev, in Russian
9. Avramenko, P.G.: Added mass of elliptic cylinder near the boundary. Hydrot. Hydromech., 14–26 (1964), Kiev, in Russian
10. Babaev, N.N.: Free oscillations of rectangular plates on water. Proceedings of Krylov Shipbuilding Institute **16**, 1–42 (1947), in Russian
11. Bai, K.J.: Added mass of a rectangular cylinder in a rectangular canal. Hydronaut. **11**(1), 29–32 (1977)
12. Bai, K.J.: Sway added mass of a cylinder in a canal using dual-extremum principles. Ship Res. **21**(4), 193–199 (1977)
13. Bai, K.J.: The added mass of two-dimensional cylinders heaving in water of finite depth. Fluid Mech. **81**(1), 85–105 (1977)
14. Bai, K.J.: Zero-frequency hydrodynamic coefficients of vertical axisymmetric bodies at a free surface. Hydronaut. **11**(2), 53–57 (1977)
15. Balbuh, L.I.: Interaction of shells with gas and fluid. In: *Theory of Shells and Plates*. Nauka, Moscow (1967), in Russian
16. Basin, M.A.: *Theory of Course-Keeping Ability and Maneuverability of Vessels*. Gostehizdat, Leningrad (1949), in Russian
17. Basin, A.M., Velednitskij, I.O., Ljahovitskij, A.G.: *Hydrodynamics of Ships on Shallow Water*. Sudostroenie, Leningrad (1976), in Russian
18. Basin, A.M., Shadrin, V.P.: *Hydrodynamics of Airfoil Near the Interface of Media*. Sudostroenie, Leningrad (1980), in Russian
19. Basov, K.A.: *ANSYS in Examples and Problems*. Computer Press, Moscow (2002), in Russian
20. Belanger, F., Paldoussis, M.P., Langre, E.: Time-marching analysis of fluid-coupled systems with large added mass. AJAA J. **33**(4), 752–757 (1995)
21. Belocerkovsky, S.M.: *Thin Lifting Surface in Subsonic Flow of Gas*. Nauka, Moscow (1965), in Russian
22. Belocerkovsky, S.M., Skripach, B.K., Tabachnikov, V.G.: *Airfoil in Non-stationary Flow of Gas*. Nauka, Moscow (1971), in Russian
23. Biminskij, Yu.S.: Added masses of vertical plate in fluid of finite depth. In: *Ship Hydrodynamics*, pp. 10–16. Nikolaev (1988), in Russian
24. Birkhoff, G.: *Hydrodynamics*. Princeton Univ. Press, Princeton (1960)
25. Blagoveschenskij, S.N.: *Ship Rolling*. Sudpromgiz, Leningrad (1954), in Russian
26. Blagoveschenskij, S.N., Kholodilin, A.N.: *Reference Book on Statics and Dynamics of Ship, vol 2. Dynamics (Rolling) of a Ship*. Sudostroenie, Leningrad (1969), 976 pp., in Russian

27. Bloch, E.L.: Influence of immersion depth to coefficient of added mass of a sphere under horisontal impact. Appl. Math. Mech. **19**(3), 353–358 (1955), in Russian
28. Bloch, E.L.: Horizontal impact of ellipsoid of revolution floating in fluid close to free surface. Appl. Math. Mech. **17**(6), 579–592 (1953), in Russian
29. Bloch, E.L.: On ellipsoid of revolution floating on a free surface of heavy fluid. Appl. Math. Mech. **18**(5), 631–636 (1954), in Russian
30. Bloch, E.L., Ginevsky, A.S.: On motion of a system of bodies in ideal fluid. Proceedings of Krylov Shipbuilding Institute **47**, 131–143 (1963), in Russian
31. Borisov, R.V., Mikhailov, B.V.: Experimental investigation of added moments of inertia and damping under rolling of small vessels on shallow water. Proceedings of Leningrad Shipbuilding University **96**, 17–22 (1975), in Russian
32. Borodaj, I.K., Necvetaev, Yu.A.: *Rolling of a Ship on Waves*. Sudostroenie, Leningrad (1969), in Russian
33. Borodachev, N.M., Borodacheva, F.N.: On influence of boundaries on impact of a disc on water surface. Eng. J. (1), 177–182 (1967), in Russian
34. Botvinkov, V.M., Polunin, A.M.: Five problems on influence of hard boundary on added mass of floating cylindrical bodies under vertical impact. Izvestia AN USSR, Mechanics of Fluid and Gas (1), 124–129 (1969), in Russian
35. Boyanovsky, V.S.: Estimate of the influence of three-dimensional effects on added masses in computation of vibration of a hull. Proceedings of Krylov Shipbuilding Institute **351**, 11–14 (1981), in Russian
36. Brennan, C.E.: A review of added mass and fluid interaction forces. Naval Civil Engineering Laboratory, Port Hueneme, California, Report CP 82.010, pp. 1–50 (1982)
37. Brix, J.: Hydrodynamische Massen und Massentragheitsmomente von Schiffsrudern. Hansa **114**(12), 1151–1156 (1977)
38. Buchau, A., Nuber, C.J., Rieger, W., Rucker, W.M.: Fast BEM computations with the adaptive multilevel fast multipole method. IEEE Trans. Magn. **36**(4), 680–684 (2000)
39. Bugaenko, B.A.: Estimate of added mass of elliptic contour under its lifting from fluid surface. Proceedings of Nikolaev Shipbuilding Institute **78**, 91–99 (1973), in Russian
40. Bujvol, V.N.: *Oscillations and Stability of Deforming Systems in Fluid*. Naukova Dumka, Kiev (1975), in Russian
41. Burril, L.C., Robson, W.: Virtual mass and moment of inertia of propellers. Tr. NECJ **78**(6), 325–360 (1962)
42. Chakrabarti, S.K.: Wave interaction with multiple horizontal cylinders. Appl. Ocean Res. **1**(4), 213–216 (1979)
43. Chung, S. Jin, Added mass and damping on an oscillating surface-piercing circular column with a circular footing. In: *Proc. 4th Int. Offshore and Polar Eng. Conf., Osaka, Apr. 10–15*, **3**, pp. 182–189 (1994)
44. Chuvikovskij, V.S.: *Numerical Methods in Shipbuilding*. Sudostroenie, Leningrad (1971), in Russian
45. Chuvikovskij, V.S.: *Numerical Methods of Solution of Problems of Building Mechanics of a Ship*. Sudostroenie, Leningrad (1976), in Russian
46. Connor, J., Brebbia, K.: *Method of Finite Elements in Fluid Mechanics*. Sudostroenie, Leningrad (1979), in Russian
47. Davydov, V.V., Mattes, I.V.: *Dynamic Computations of Strength of Ship Structures*. Sudostroenie, Leningrad (1974), in Russian
48. Ditman, A.O., Kovalenko, B.P., Mastushkin, Yu.M.: Determination of added masses by the method of EHDA. In: *Methods of Mathematical Modeling of Technical Problems, Kiev*, pp. 85–91 (1975), in Russian
49. Ditman, A.O., Okunev, S.N.: Experimental precision of magneto-hydrodynamic analogy. Some Problems of Applied Mathematics **4**, 21–25 (1969), in Russian
50. Dorofeuk, S.K.: Studies of added masses under elastic oscillations of a hull. Proceedings of Krylov Shipbuilding Institute **84**, 3–74 (1954), in Russian

51. Dorofeuk, S.K., Salomatin, G.A.: Experimental studies of added masses of propeller under flexural oscillations of shafting. Proceedings of Krylov Shipbuilding Institute **152**, 92–101 (1960), in Russian
52. Dudchenko, O.N.: Numerical computation of inertial characteristics of a body moving parallel to flat boundary. In: *Ship Hydrodynamics*, pp. 17–21. Nikolaev Shipbuilding Institute, Nikolaev (1988), in Russian
53. Eatock, R. Taylor, Hu, C.S.: Multipole expansions for wave diffraction and radiation in deep water. Ocean Eng. **18**(3), 191–224 (1991)
54. Eatock, R. Taylor, Zietsman, J.: A comparison of localized finite element formulations for two-dimensional wave diffraction and radiation problems. Int. J. Numer. Methods Eng. **17**(9), 1355–1384 (1981)
55. Elis, Ya.M.: Hydrodynamic pressures, added masses and damping coefficients of inclined rolling ship on shallow water. In: Shipbuilding and Marine Constructions. Proceedings of Kharkov State University **9**, 71–76 (1968), in Russian
56. Elis, Ya.M.: Hydrodynamic coefficients of inclined shipframes. Proceedings of TIRPIH **90**, 42–93 (1980), Kaliningrad, in Russian
57. Elis, Ya.M.: Added masses and damping of inclined shipframes. Proceedings of TIRPIH **90**, 30–41 (1980), Kaliningrad, in Russian
58. Egorov, I.T.: Impact on a surface of compressible fluid. Appl. Math. Mech. **20**(1), 67–72 (1956), in Russian
59. Egorov, I.T., Sokolov, V.T.: *Hydrodynamics of High-Speed Ships*. Sudostroenie, Leningrad (1971), in Russian
60. Ermanyuk, E.V.: The use of impulse response functions for evaluation of added mass and damping coefficient of a circular cylinder oscillating in a linearly stratified fluid. Exp. Fluids **28**, 152–159 (2000)
61. Ermanjuk, E.V., Gavrilov, N.V.: On oscillations of cylinders in linearly stratified fluid. Appl. Math. Theor. Phys. **43**(4), 15–26 (2002), in Russian
62. Ermanyuk, E.V.: The rule of affine similitude for the force coefficients of a body oscillating in a uniformly stratified fluid. Exp. Fluids **32**(2), 242–251 (2002)
63. Ermanyuk, E.V., Gavrilov, N.V.: Force on a body in a continuously stratified fluid. Part 1. Circular cylinder. J. Fluid Mech. **451**, 421–443 (2002)
64. Ermanyuk, E.V., Gavrilov, N.V.: Force on a body in a continuously stratified fluid. Part 2. Sphere. J. Fluid Mech. **494**, 33–50 (2003)
65. Efimov, N.V.: *Brief Course of Analytic Geometry*. GITTL, Moscow (1954), in Russian
66. Erschov, N.F., Shahverdi, G.G.: *Finite Elements Method in Hydrodynamics and Hydroelasticity*. Sudostroenie, Leningrad (1984), in Russian
67. Falkovich, S.V., Kalinin, N.K.: On impact of floating cylinder. Notices of Saratov State University. Math. Phys. Ser. **14**(2), 206–213 (1938), in Russian
68. Farell, C.: On the flow about a spheroid near a plane wall. J. Ship Res. **15**(3), 246–252 (1971)
69. Fetisov, S.P.: Analysis of mutual influence of oscillations of structures in fluid. Izvestia VUZOV: Building and Architecture **10**, 77–80 (1989), in Russian
70. Fine, N.E., Uhlman, J.S.: Calculation of the added mass and damping forces on supercavitating bodies. In: *High Speed Hydrodynamics (HSH-2002). Proc. of the Int. Summer Scientific School. Cheboksary, Russia, June 16–23*, pp. 127–138 (2002)
71. Filippov, S.I.: *Hydrodynamics of Airfoil Near the Boundary Separating Two Fluids*. Publisher of Kazan' Mathematical Society, Kazan' (2004), in Russian
72. Fujino, M.: The effects of the restricted waters on the added mass of a rectangular cylinder. In: *The Eleventh Symposium on Naval Hydrodynamics, London*, pp. 655–670 (1965)
73. Fung, D.P.K.: Added mass and damping of circular moonpools. In: *Proc. 6th Int. Offshore and Polar Eng. Conf., Los Angeles, Calif., May 26–31*, **3**, pp. 247–254 (1996)
74. Gabbercettel', F.I., Pustoshny, A.V., Timoshin, Yu.S.: Computation of added mass of propeller by panel method. In: *Problems of Seaworthiness of Ships and Ship Hydromechanics*. Krylov Shipbuilding Research Institute, St. Petersburg (2003), in Russian

75. Galitsyn, D.A., Trotsenko, V.A.: Determination of frequencies and added masses of fluid in a parallelepiped with barriers. Izvestia RAH, Mechanics of Gas and Fluid **2**, 175–192 (2001), in Russian
76. Galkin, M.S., Zhmurin, I.P., Rudkovskij, N.I.: Mathematical model of fluid oscillation in rigid vessels. Proceedings of Central Institute of Aero- and Hydrodynamics **21**(4), 42–53 (1990), in Russian
77. Garrison, C.J., Added mass of a circular cylinder in contact with a rigid boundary. Hydronaut. **6**(1), 59–60 (1972)
78. Gofman, A.D.: *Theory and Computation of Manoevrability of Inland Vessels*. Sudostroenie, Leningrad (1971), in Russian
79. Gontkevich, V.S.: *Oscillations of Shells Immersed in Fluid*. Naukova Dumka, Kiev (1964), in Russian
80. Goodman, T.R., Sargent, T.P.: Effect of body perturbations on added mass with application to nonlinear heaving of ships. Ship Res. **4**(4), 22–28 (1961)
81. Gorban', I.N.: Hydrodynamic characteristics of elliptic cylinder moving close to non-flat boundary. Gydromechanics **59**, 64–68 (1989), Kiev, in Russian
82. Gorban', V.A., Srebnuk, S.M.: On dded masses of a system of ellipsoids. In: *Applied Problems of Hydromechanics, Kiev*, pp. 126–132 (1981), in Russian
83. Gordeev, O.I.: Inertial coefficients of composition of barges. Proceedings of Novosibirsk Institute of Water Transport **44**, 75–82 (1970), in Russian
84. Gordeev, O.I.: On added masses of inertia of composition of barges under transverse and rotational motion. Proceedings of Novosibirsk Institute of Water Transport **44**, 108–116 (1970), in Russian
85. Gordeev, O.I., Vorobjov, P.S.: On the motion of ellipsoid of revolution in bisecting plane of dihedral angle. Proceedings of Novosibirsk Institute of Water Transport **21**, 85–97 (1966), in Russian
86. Grechin, M.A.: On added masses of propeller. Proceedings of Central Research Institute for Marine Fleet **27**, 72–79 (1960), in Russian
87. Greenhow, M., Ahn, S.I.: Added mass and damping of horizontal circular cylinder sections. Ocean Eng. **15**(5), 495–504 (1988)
88. Grigoljuk, E.I., Gorshkov, A.G.: *Interaction of Elastic Structures with Fluid*. Sudostroenie, Leningrad (1976), in Russian
89. Grue, J.: Time-periodic wave loading on a submerged circular cylinder in a current. J. Ship Res. **30**(3), 153–158 (1986)
90. Guliev, Yu.M.: Added masses under vertical oscillations of flat contours on free surface of ideal fluid. Proceedings of Nikolaev Shipbuilding Institute **74**, 11–16 (1973), in Russian
91. Gurevich, M.I.: Added mass of a lattice of rectangles. Appl. Math. Mech. **4**(2), 93–100 (1940), in Russian
92. Gurevich, M.I.: Impact of a plate with separation of flow. Appl. Math. Mech. **16**(1), 116–118 (1952), in Russian
93. Gurevich, M.I.: Impact of a plate in fluid filling the vessel of half-cylindrical shape. Appl. Math. Mech. **3**(2), 241–244 (1939), in Russian
94. Gurjev, Yu.V.: Generalization of the method of added masses to the case of motion of two bodies in fluid. In: *Proceedings of 2nd Conference Morintech-97, St. Petersburg*, pp. 121–123 (1997), in Russian
95. Gurjev, Yu.V.: Practical application of generalized added masses under interaction of two bodies in fluid. In: *Proceedings of 38th Conference, Krylov Readings, St. Petersburg*, pp. 251–259. Krylov Shipbuilding Research Institute, St. Petersburg (1997), in Russian
96. Gurjev, Yu.V.: Differential equations of motion of two ships under simultaneous maneuvering. In: *Proceedings of 2nd International Shipbuilding Conference, ISC98*, pp. 187–195. Krylov Shipbuilding Research Institute, St. Petersburg (1998), in Russian
97. Havelock, T.H.: Ship vibrations: The virtual inertia of a spheroid in shallow water. TINA **95**(1), 1–9 (1953)
98. Hsu, Hu-Hsiao, Wu, Yung-Chao, The hydrodynamic coefficients for an oscillating rectangular structure on a free surface with sidewall. Ocean Eng. **24**(2), 177–199 (1997)

99. Hurley, D.G.: The generation of internal waves by vibrating elliptic cylinders. Part 1. Inviscid solution. J. Fluid Mech. **351**, 105–118 (1997)
100. Huskind, M.D.: *Hydrodynamic Theory of Ship Rolling*. Nauka, Moscow (1978), in Russian
101. Huskind, M.D., Riman, I.S.: A method of determining the characteristics of ship rolling. Izvestia AN USSR **10**, 1379–1384 (1946), Department of Technical Sciences, in Russian
102. Hylarides, S., Gent, W.: Hydrodynamic reactions to propeller vibrations. Ship Werf **46**(19), 383–393 (1979)
103. Ishii, Noriaki: Flow-induced vibration of long-span gates. Verification of added mass and fluid damping. JSME Jnt. J. Ser. 2 **33**(4), 642–648 (1990)
104. Iljin, V.P., Riad, Butris: On influence of added mass of fluid and hydrostatic pressure on oscillations and stability of cylindrical shell. In: *Studies on Mechanics of Bulding Constructions and Materials*, pp. 5–9. Sudostroenie, St. Petersburg (1989)
105. Ivanjuta, E.I., Sochinskij, S.V.: Determination of parameters of hull vibration by taking into account an interaction of elements of its construction. Shipbuilding **6**, 9–12 (1974), in Russian
106. Iwashita, H., Ohkusu, M.: The Green function method for ship motions at forward speed. J. Ship Res. **39**(2), 3–21 (1992)
107. Kanev, N.G.: The added mass of monopole and dipole in narrow pipe. Acoust. Phys. **53**(5), 553–556 (2007)
108. Kaplun, A.B., Morozov, E.M., Olfer'eva, M.A.: *ANSYS in Engineer's Hands. Practical Guidebook*. URSS, Moscow (2003), in Russian
109. Kapustjanskij, S.M., Marchenko, D.V.: Theoretical recommendations on determination of added masses under motion of ships in channels. Proceedings of Leningrad Polytechnical Institute **346**, 63–67 (1976), in Russian
110. Karafoli, E.: *Aerodynamics of Airfoil*. AN USSR Publishing House, Moscow (1956), in Russian
111. Kashiwagi, M., Varyani, K., Ohkusu, M.: Forward-speed effects on hydrodynamic forces acting on a submerged cylinder in waves. Repts Res. Inst. Appl. Mech. **34**(102), 26 (1987)
112. Kashiwagi, M., Varyani, K., Ohkusu, M.: Hydrodynamic forces acting on a submerged elliptic cylinder translating and oscillating in waves. Trans. West-Japan Soc. Naval Archit. **74**, 64–78 (1987)
113. Keldysh, M.V.: Impact of a plate on free surface of water of finite depth. Proceedings of Central Institute of Aero- and Hydrodynamics **152**, 13–20 (1935), Moscow, in Russian
114. Keulegan, G.H., Carpenter, L.H.: Forces on cylinders and plates in an oscillating fluid. J. Res. Nat. Bur. Stand. **60**(5), 423–440 (1958)
115. Kogan, V.I., Bochin, M.K.: Added masses of inland vessels on deep and shallow water. Proceedings of Leningrad Institute of Water Transport **98**, 53–59 (1968), in Russian
116. Kochin, N.E., Kibel, I.A., Rose, N.V.: *Theoretical Hydromechanics, Parts I and II*. State Publisher of Physical and Mathematical Literature, Moscow (1963), in Russian
117. Kostjukov, A.A.: *Interaction of Bodies Moving in Fluid*. Sudostroenie, Leningrad (1972), in Russian
118. Kryzhevich, G.B.: *Hydroelasticity of Ship Structures*. Publications of Krylov Shipbuilding Research Institute, St. Petersburg (2006), in Russian
119. Kurkov, S.V.: *Method of Finite Elements in Problems of Dynamics of Mechanisms and Drives*. Polytechnika, St. Petersburg (1992), in Russian
120. Kudrjavceva, N.A.: Horizontal impact of an ellipse floating in incompressible fluid. Appl. Math. Mech. **24**(2), 258–261 (1960), in Russian
121. Kudrjavceva, N.A.: Forces and moments of inertial nature, acting on a section of inclined hull. Proceedings of A.N. Krylov Society **2**, 21–27 (1957), in Russian
122. Kurdjumov, A.A.: *Vibrations of Ships*. Sudpromgiz, Leningrad (1961), in Russian
123. Kumai, T.: On the three-dimensional entrained water in vibration of Lewis section cylinder with finite length. Trans. West-Japan Soc. Naval Archit. **50**, 173–179 (1975)
124. Kumai, T.: On the virtual inertia coefficients of the vertical vibration of ships. J.S.N.A. of Japan **105**, 16–32 (1959)

125. Kwak Moon, K.: Hydroelastic vibration of rectangular plates. Trans. ASME J. Appl. Mech. **63**(1), 110–115 (1996)
126. Lai, R.Y.S., Lee, C.-M.: Added mass of a spheroid oscillating in a linearly stratified fluid. Int. J. Eng. Sci. **19**, 1411–1420 (1981)
127. Landweber, L., Chwang, A.T.: Generalization of Taylor's added-mass formula for two bodies. J. Ship Res. **33**(1), 1–9 (1989)
128. Landweber, L., Macagno, M.: Added mass of two-dimensional forms oscillating in a free surface. Ship Res. **1**(3), 114–117 (1957)
129. Landweber, L., Macagno, M.: Added mass of two-dimensional forms by conformal mapping. Ship Res. **11**(2), 101–105 (1967)
130. Landweber, L., Shahshahan, A.: Added masses and forces acting on two bodies approaching central impact in an inviscid fluid. Iova Inst. Hydraulic Res. Report (346), 1–82 (1991)
131. Lewis, F.M.: The inertia of the water surrounding in a vibrating ship. Trans. SNAME **37**, 1–20 (1929)
132. Lindholm, U.S., Kana, D.D., Chu, W.H., Abramson, H.N.: Elastic vibration characteristics of cantilever plates in water. Ship Res. **9**(1), 25–30 (1965)
133. Lamb, G.: *Hydrodynamics*. Cambridge University Press, Cambridge (1932)
134. Linton, C.M.: Radiation and diffraction of water waves by a submerged sphere in finite depth. Ocean Eng. **18**(1/2), 61–74 (1991)
135. Linton, C.M., McIver, P.: *Handbook of Mathematical Techniques for Wave/Structure Interactions*. Chapman & Hall/CRC, Boca Raton (2001), 320 pp.
136. Lipis, V.B.: *Hydrodynamics of Propeller under Rolling of the Ship*. Sudostroenie, Leningrad (1975), in Russian
137. Lipis, V.B.: Determination of inertial forces and moments acting on propeller under its motion in non-stationary flow. Proceedings of Central Research Institute for Marine Fleet **49**, 115–129 (1963), in Russian
138. Logvinovich, G.V.: Initial motion of a body in fluid with developed cavitation. In: *Collection of Works on Hydrodynamics*, pp. 3–40. Central Institute of Aero- and Hydrodynamics Publisher, Moscow (1959), in Russian
139. Lojcjanskij, L.G.: *Mechanics of Fluid and Gas*. Nauka, Moscow (1970), in Russian
140. Ljakhovitskij, A.G.: Determination of hydrodynamic forces and trimming moment acting on thin ship on shallow water. Proceedings of Leningrad Institute of Water Transport **92**, 47–60 (1968), in Russian
141. Maheri, M.R., Severn, R.T.: Experimental added-mass in modal vibration of cylindrical structures. Eng. Struct. **14**(3), 163–175 (1992)
142. Matsuura, Y.: An analysis of vertical vibration of cargo ships. J.S.N.A. of Japan **108**, 41–49 (1960)
143. Matsuura, Y., Arima, K.: A study on the added virtual mass ellipsoid of revolution in vertical vibration in water. J.K.S.N.A. **167**, 11–18 (1977)
144. Matsuura, Y., Arima, K.: A study on the virtual mass reduction factors for ship vibration. The Hitachi Zosen Technical Review **40**(2), 108–115 (1970)
145. Mastushkin, Yu.M.: *Controllability of Catcher Boats*. Light and Food Industry, Moscow (1981), in Russian
146. McIver, P.: Low-frequency asymptotics of hydrodynamic forces on fixed and floating structures. In: Rahman, M. (ed.) *Ocean Waves Engineering*, pp. 1–49. Comput. Mech. Publ., Southampton (1994)
147. McIver, P., Evans, D.V.: The occurrence of negative added mass in free-surface problems involving submerged oscillating bodies. J. Eng. Math. **18**(1), 7–22 (1984)
148. Mikelis, N.E., Parkinson, A.G., Price, W.G.: The added mass of confocal ellipsoid. Iner. Shipbuilding Progress **28**(318), 40–47 (1981)
149. Miloh, T., Waisman, G., Weihs, D.: The added-mass coefficients of a torus. J. Eng. Math. **12**(1), 1–13 (1978) 10.1007/BF00042801
150. Mnev, E.I., Pertcev, A.K.: *Hydroelasticity of Shells*. Sudostroenie, Leningrad (1970), in Russian

151. Morenshildt, V.A.: Computation of added moment of inertia under rolling of ships. Proceedings of Krylov Shipbuilding Institute **136**, 76–85 (1959), in Russian
152. Motygin, O.V., Sturova, I.V.: Wave motion in two-layer fluid induced by small oscillations of a cylinder crossing the boundary. Izvestia RAN, Mechanics of Gas and Fluid **4**, 105–119 (2002), in Russian
153. Mastushkin, Yu.M.: *Determination of Manoevrability Characteristics of Two-hull Vessels*. Sudostroenie, Leningrad (1976), in Russian
154. Nakorenjuk, A.L.: Numerical studies of influence of transverse response of a ship on the spectrum of its vibration frequencies. Proceedings of A.N. Krylov Society **351**, 51–59 (1981), in Russian
155. Nestegard, A., Sclavounos, P.D.: A numerical solution of two-dimensional deep water wave-body problems. J. Ship Res. **28**(1), 48–54 (1984)
156. Newman, J.N.: The theory of ship motions. Adv. Appl. Mech. **18**, 221–283 (1978)
157. Nikiforov, E.M.: Estimation of influence of the type of torsional vibrations of a hull on added moments of inertia. Sudostroenie **11**, 16–18 (1964), in Russian
158. Nilsen, D.: *Aerodynamics of Controllable Shells*. Oborongiz, Moscow (1962)
159. Newman, J.N.: Some theories for ship maneuvering. Mech. Eng. Sci. **14**(7), 34–42 (1972)
160. Norkin, M.V.: On influence of walls of a vessel or an arbitrary shape under non-separating impact of floating body. Appl. Mech. Tech. Phys. **42**(1), 77–81 (2001), in Russian
161. Norkin, M.V.: An body of revolution immersed in fluid of infinite depth under an impact. Appl. Mech. Tech. Phys. **37**(1), 36–41 (1996), in Russian
162. Norkin, M.V.: A solid body floating on free surface of ideal fluid of finite depth under vertical impact. Izvestia RAN, Mechanics of Gas and Fluid **1**, 74–81 (1999), in Russian
163. Norkin, M.V.: Thin torus of elliptic cross-section floating on a surface of ideal incompressible fluid. Izvestia RAN, Mechanics of Gas and Fluid **2**, 144–152 (2000), in Russian
164. Padmanabhan, B., Ertekin, R.C.: On the interaction of waves with intake/discharge flows originating from a freely-floating body. J. Offshore Mech. Arc. Eng. **125**, 41–47 (2003)
165. Palagushkin, B.V., Vjugov, V.V.: Experimental estimate of added masses of passenger and cargo ships. In: *Improvement of Hydromechanical Properties of River Boats and Consists*, pp. 87–98. Novosibirsk Institute of Engineers of Water Transport, Novosibirsk (1995), in Russian
166. Palagushkin, B.V.: Determination of added masses of river cargo boats. In: *Candidate of Sciences Thesis*. Novosibirsk Institute of Engineers of Water Transport, Novosibirsk (1988), in Russian
167. Palagushkin, B.V.: Experimental estimate of influence of viscosity and scale of modelling to added mass of a ship. In: *Improvement of Hydromechanical Properties of River Boats and Consists*, pp. 81–86. Novosibirsk Institute of Engineers of Water Transport, Novosibirsk (1991), in Russian
168. Parhomovskij, S.I.: Asymptotical formulas for coefficients of added masses of acute wedge under impact: Flow with separation. Sudostroenie **39**, 38–44 (1990), Kiev
169. Pavlenko, V.G.: *Elements of Inland Ship Navigation. Inertial Properties of Vessels and Consists*. Transport, Moscow (1971), in Russian
170. Pavlenko, V.G.: *Manoevrability of River Boats*. Transport, Moscow (1979), in Russian
171. Paschenko, Yu.N.: On computation of hydrodynamic characteristics of shipframes under rolling. Proceedings of Nikolaev Shipbuilding Institute **126**, 43–47 (1977), in Russian
172. Pekelnij, M.Ya.: On computation of added mass under high-frequency vibration of a hull. Proceedings of A.N. Krylov Society **110**, 61–68 (1968), in Russian
173. Perrault, D., Bose, N., O'Young, S., Williams, C.D.: Sensitivity of AUV added mass coefficients to variations in hull and control plane geometry. Ocean Eng. **30**, 645–671 (2003)
174. Polunin, A.M.: Influence of the channel wall on added moment of inertia of flat plate and elliptic cylinder under the action of impact moment. Proceedings of Novosibirsk Institute of Water Transport **44**, 52–61 (1970), in Russian
175. Polunin, A.M.: Influence of boundaries on the added mass of bodies of various shape under vertical impact. Proceedings of Novosibirsk Institute of Computational Methods **21**, 98–115 (1966), in Russian

176. Polunin, A.M.: Added mass of an ellipsoid of revolution floating in a vessel of ellipsoidal shape, under vertical impact. Proceedings of Novosibirsk Institute of Computational Methods **21**, 116–128 (1966), in Russian
177. Polunin, A.M.: Added masses of bending chains of vessels and catamarans. Proceedings of A.N. Krylov Society **200**, 53–68 (1973)
178. Postnov, V.A., Charchurim, I.Ya.: *Method of Finite Elements in Computions of Ship Structures*. Sudostroenie, Leningrad (1974), in Russian
179. Postnov, V.A.: *Numerical Method of Modelling of Ship Structures*. Sudostroenie, Leningrad (1977), in Russian
180. Preobrajenskij, I.N.: *Stability and Vibrations of Plates and Shells with Holes*. Mashinostroenije, Moscow (1981), in Russian
181. Rasziller, H., Durst, F.: Short-distance asymptotics of the added-mass matrix of two spheres of equal diameter. Quart. J. Mech. Appl. Math. **42**(1), 85–98 (1989)
182. Remez, Yu.V.: *Rolling of Ships*. Sudostroenie, Leningrad (1983), in Russian
183. Riman, I.S., Kreps, R.L.: Added masses of bodies of various shape. Proceedings of Central Institute of Aero- and Hydrodynamics **635**, 1–46 (1947), in Russian
184. Rodosskij, V.A.: Influence of oscillations of a system propeller-shaft-support arm on vibrations of a ship. Proceedings of A.N. Krylov Society **40**, 172–188 (1961), in Russian
185. Rodosskij, V.A., Schukina, E.N.: Determination of vibration parameters of a shell and its frame under oscillations in fluid. In: *Proceedings of 2nd International Shipbuilding Conference ISC-98, St. Petersburg*, pp. 325–330 (1998), in Russian
186. Rostovtsev, D.M.: Studies of hydroelastic oscillations of ship structures. Doctor of Sciences Thesis. Leningrad Shipbuilding Institute (1972), in Russian
187. Rostovtsev, D.M.: Added masses under vibration of bottom frames. In: *Problems of Ship Building, Leningrad*, pp. 185–195 (1973), in Russian
188. Rudin, S.N.: On the motion of three-axial ellipsoid in bounded flow. Proceedings of Novosibirsk Institute of Computational Methods **21**, 10–24 (1966), in Russian
189. Rjazanov, G.A.: *Electric Modelling with Application of Vortex Fields*. Nauka, Moscow (1969), in Russian
190. Sabaneev, V.S.: A non-separating impact acting on elliptic cylinder floating on a surface of incompressible fluid in a channel. Vestnik of Leningrad State University. Math. Mech. Astron. **4**, 99–105 (1969), in Russian
191. Sabaneev, V.S.: Influence of submersion depth on added mass of ellipsoid of a sphere. Notices of Leningrad State University, Mathematics **35**(280), 238–241 (1960), in Russian
192. Sabaneev, V.S.: Influence of submersion depth on added mass of ellipsoid of revolution. Notices of Leningrad State University, Mathematics **35**(280), 242–253 (1960), in Russian
193. Sabaneev, V.S.: Added mass of ellipsoid of revolution moving in fluid bounded by a flat boundary. Notices of Leningrad State University, Series Mathematics. Mech. Astron. **4**(19), 170–186 (1958), in Russian
194. Sabaneev, V.S.: Added masses of elliptic cylinder moving in fluid bounded by a flat boundary or free surface. Notices of Leningrad State University. Ser. Math. Mech. Astron. **7**(1), 115–123 (1963), in Russian
195. Salenjuk, V.V.: Added masses and moments of inertia under flat motion of a raft taking into account bending. Proceedings of Novosibirsk Institute of Water Transport **44**, 83–92 (1970), in Russian
196. Salkaev, A.Z.: Hydrodynamic forces acting on a contour of an arbitrary shape, and equations of rolling. Proceedings of Krylov Shipbuilding Institute **235**, 3–25 (1967), in Russian
197. Salkaev, A.Z.: Estimation of hydrodynamic forces acting on ships with large ratio of width to drought under regular rolling. Sudostroenie **4**, 19–21 (1980), in Russian
198. Sandler, L.B., Dolgushin, G.S., Vorobjov, P.S.: Added mass of propeller in shafting. Proceedings of Novosibirsk Institute of Water Transport **34**, 209–214 (1969), in Russian
199. Sayer, P.: An integral-equation method for determining the fluid motion due to a cylinder heaving on water of finite depth. Proc. R. Soc. London A **372**(1748), 93–110 (1980)
200. Shebalov, A.N.: *Added Masses*. Publisher of Leningrad Shipbuilding Institute, Leningrad (1975), in Russian

201. Shhinek, K.N.: Method of determining of added masses of flat contours by the method of electro-hydrodynamic analogy. Proceedings of Leningrad Shipbuilding Institute **22**, 24–27 (1958), in Russian
202. Schukina, E.N.: On the influence of added masses of fluid on oscillations of elements of ship structures. Proceedings of A.N. Krylov Society **66**, 18–24 (1965), in Russian
203. Schukina, E.N.: On free oscillations of ship structures touching the fluid. Proceedings of Krylov Shipbuilding Institute **217**, 16–22 (1964), in Russian
204. Schukina, E.N.: *Computations of Vibrational Strength of Hull Structures*. Sbornik Registra USSR, vol. 6, pp. 12–23. Transport, Leningrad (1976) in Russian
205. Schukina, E.N.: Computation of vibration of ship plates with ribs immersed in water. Proceedings of Krylov Shipbuilding Institute **186**, 35–39 (1962), in Russian
206. Sedov, L.I.: *Planar Problems of Hydrodynamics and Aerodynamics*. Nauka, Moscow (1966), in Russian
207. Segava, Yorihide: Analysis of the destabilizing effect of a rigid wall on the elastic one-dimensional flat plat placed in irrotational flows adjoining the rigid wall. JSME Jnt. J. B. **36**(1), 26–33 (1993)
208. Semenova, V.Yu.: Development of software for computation of nonlinear hydrodynamic forces arising under oscillations of contours of hull type of free surface. Candidate of Sciences Thesis. St. Petersburg State Marine Technical University (1999), in Russian
209. Simon, M.J.: The high-frequency radiation of water waves by oscillating bodies. Proc. R. Soc. London A **401**, 89–115 (1985)
210. Sinha, J.K., Singh, S., Rao, A.R.: Added mass and damping of submerged perforated plates. J. Sound Vibr. **260**(3), 549–564 (2003)
211. Srokosz, M.A.: The submerged sphere as an absorber of wave power. J. Fluid Mech. **95**(4), 717–741 (1979)
212. Sochinskij, S.V.: On computation of added masses under hull vibrations. Sudostroenie **6**, 12–17 (1973), in Russian
213. Srebnjuk, V.A., Gorban', V.A.: On added masses of a system of bubbles. Hydromechanics **37**, 13–19 (1978), in Russian
214. Sturova, I.V.: Radiation and diffraction problems for circular cylinder in stratified fluid. Izvestia RAN, Mechanics of Gas and Fluid **4**, 81–94 (1999), in Russian
215. Sturova, I.V.: Oscillations of circular cylinder in a layer of linearly stratified fluid. Izvestia RAN, Mechanics of Gas and Fluid **3**, 155–163 (2001), in Russian
216. Sturova, I.V.: Added masses of a cylinder crossing the separation boundary of two-layer weightless fluid of finite depth. Appl. Mech. Tech. Phys. **44**(4), 76–14 (2003), in Russian
217. Sturova, I.V.: Planar problem of rolling of a two-dimensional immersed body with zero linear velocity in two-layer fluid. Izvestia RAN, Mechanics of Gas and Fluid **3**, 144–155 (1994), in Russian
218. Sturova, I.V.: Planar problem of rolling of a two-dimensional immersed body with non-zero linear velocity in two-layer fluid. Appl. Math. Tech. Phys. **5**, 32–44 (1994), in Russian
219. Sturova, I.V.: Oscillations of a cylinder crossing a layer of linearly stratified fluid. Izvestia RAN, Mechanics of Gas and Fluid **4**, 149–159 (2006), in Russian
220. Sturova, I.V., Suj, Ch.: Hydrodynamic forces arising under oscillations of a cylinder on the boundary separating two-layer fluid of finite depth. Izvestia RAN, Mechanics of Gas and Fluid **2**, 122–131 (2005), in Russian
221. Taylor, J.L.: Some hydrodynamical inertia coefficients. Phil. Mag. Ser. 7 **9**(55), 161–183 (1930)
222. Ten, I., Kashiwagi, M.: Hydrodynamics of a body floating in a two-layer fluid of finite depth. Part 1. Radiation problem. J. Mar. Sci. Technol. **9**, 127–141 (2004)
223. Terskih, V.P.: Torsional oscillations of the shafting of power units. Sudostroenie **1** (1969), **2** (1970), **3** (1970), **4** (1971), in Russian
224. Tikhonov, A.I.: Hydrodynamic forces acting on flat plates with keels under non-established gliding. In: *Works on Hydrodynamics. Central Institute of Aero- and Hydrodynamics*, pp. 167–182 (1959), in Russian

225. Usachev, Yu.K.: Added masses of shipframes under broadside motion. Proceedings of Krylov Shipbuilding Institute **147**, 90–99 (1959), in Russian
226. Veklich, N.A.: Impact of rectangular plate on fluid half-space. Izvestia RAN, Mechanics of Gas and Fluid **5**, 120–126 (1992), in Russian
227. Veklich, N.A.: Impact of disc and planar ring in cylindrical vessel. Izvestia RAN, Mechanics of Gas and Fluid **1**, 101–103 (1995), in Russian
228. Veklich, N.A., Malyshev, B.M.: Planar problem about impact of a plate in a channel of rectangular section. Appl. Math. Mech. **52**(3), 511–516 (1988), in Russian
229. Vishnevsky, A.M., Lapovok, A.J.: Boundary integral computation of electric fields in multi-electrode galvanic systems using normally continuous elements. IEE Proc. Sci. Meas. Technol. **147**(3), 145–151 (2000)
230. Voda, Ya.M., Vorobjov, P.S., Pavlenko, V.G.: Determination of potential moment of twin rudders of river boats. Proceedings of Novosibirsk Institute of Water Transport **44** (1970), in Russian
231. Vojtkunskij, Ya.I., Pershitz, R.Ya., Titov, I.A.: *Reference Book on Theory of Ships: Propulsion and Manoevrability*. Sudostroenie, Leningrad (1973), in Russian
232. Vorobjov, P.S.: Estimates of influence of free surface on added mass of a ship under acceleration and deceleration. Proceedings of Novosibirsk Institute of Water Transport **45**, 126–136 (1970), in Russian
233. Vorobjov, P.S.: Experimental investigation of added masses of parallelepipeds on shallow water. Proceedings of Novosibirsk Institute of Water Transport **21**, 3–9 (1966), in Russian
234. Vorobjov, P.S., Dolgushin, G.S.: Coefficient of added mass of elliptic cylinder under its motion along one boundary or between two boundaries. Proceedings of Novosibirsk Institute of Water Transport **21**, 81–84 (1966), in Russian
235. Vorobjov, P.S., Pavlenko, V.G., Rudin, S.N.: Analysis of coefficients of added inertia used in studies of maneuverability of vessels on shallow water. Proceedings of Novosibirsk Institute of Water Transport **44**, 3–51 (1970), in Russian
236. Vorobjov, P.S., Rudin, S.N.: On influence of boundedness of a flow on added mass of three-axial ellipsoid. Proceedings of Novosibirsk Institute of Water Transport **21**, 25–80 (1966), in Russian
237. Vorobjov, P.S., Rudin, S.N.: Added masses of a lattice of three-axial ellipsoids. Proceedings of Novosibirsk Institute of Water Transport **24**, 3–11 (1966), in Russian
238. Vorobjov, Yu.L.: Hydrodynamic problem about longitudinal rolling of catamaran on shallow water. Izvestia AN USSR, Mechanics of Fluid and Gas (2), 147–151 (1980), in Russian
239. Vorobjov, Yu.L.: Potentials of fluid velocities under longitudinal rolling of thin ship on shallow water. Izvestia AN USSR, Mechanics of Fluid and Gas (1), 204–208 (1979), in Russian
240. Vorobjov, Yu.L.: Added mass of a shipframe under high frequency vertical oscillations on shallow water. In: *Applied Problems of Hydromechanics, Proceedings of the Institute of Hydromechanics of AN of Ukraine SSR, Kiev*, pp. 26–35 (1981), in Russian
241. Vorovich, L.S.: Vertical impact of a ball half-submerged in fluid of finite depth. Izvestia AN USSR, Mechanics of Fluid and Gas **6**, 101–113 (1966), in Russian
242. Vorovich, I.I., Yudovich, V.I.: Impact of a disc floating on free surface of a fluid of finite depth. Appl. Math. Mech. **21**(4), 525–532 (1957), in Russian
243. Vugts, J.H.: The hydrodynamic coefficients for swaying, heaving and rolling cylinders in a free surface. Report No. 194. Laboratorium voor Scheepsbovwkunde, Technische Hogeschool, Delft, The Netherlands (1968)
244. Wang, S.: Motions of a spherical submarine in waves. Ocean Eng. **13**(3), 249–271 (1986)
245. Weinblum, G., Brooks, S., Golovato, P.: Experimental investigation of the inertia and damping coefficients of a spheroid and surface ship in free heave. Int. Shipbuilding Progress **6**(54), 45–62 (1959)
246. Wendel, K.: Hydrodynamische Massen und hydrodynamische Massen-tragheitmomente. Jahrb. d. STG **44**, 207–255 (1950)
247. Wu, G.X.: Hydrodynamic forces on a submerged cylinder advancing in water waves of finite depth. J. Fluid Mech. **224**, 645–659 (1991)

248. Wu, G.X.: Radiation and diffraction of water waves by a submerged circular cylinder at forward speed. J. Hydrodyn. B **5**(4), 85–96 (1993)
249. Wu, G.X.: Radiation and diffraction by a submerged sphere advancing in water waves of finite depth. Proc. R. Soc. London A **448**(1932), 1995, 29–14
250. Wu, G.X.: The interaction of water waves with a group of submerged spheres. Appl. Ocean Res. **17**, 165–184 (1995)
251. Wu, G.X.: Wave radiation and diffraction by a submerged sphere in a channel. Quart. J. Mech. Appl. Math. **51**(4), 647–666 (1998)
252. Wu, G.X., Eatock Taylor, R.: Hydrodynamic forces on submerged oscillating cylinders at forward speed. Proc. R. Soc. London A **414**(1846), 149–170 (1987)
253. Wu, G.X., Eatock Taylor, R.: Radiation and diffraction of water waves by a submerged sphere at forward speed. Proc. R. Soc. London A **417**(1853), 433–461 (1988)
254. Wu, G.X., Eatock Taylor, R.: On the radiation and diffraction of surface waves by submerged spheroids. J. Ship Res. **33**(2), 84–92 (1989)
255. Wu, G.X., Eatock Taylor, R.: The hydrodynamic force on an oscillating ship with low forward speed. J. Fluid Mech. **211**, 333–353 (1990)
256. Yeung, R.W., Nguyen, T.W.: Radiation and diffraction of waves in a two-layer fluid. In: *Proc. 22nd Symp. on Naval Hydrodynamics*, pp. 875–891 (1999)
257. Zenkevich, O.: *Method of Finite Elements in Engineering*. Mir, Moscow (1975), in Russian
258. Zenkevich, O., Chang, I.: *Method of Finite Elements in Building Construction and in the Theory of Continuous Medium*. Nedra, Moscow (1974), in Russian
259. Zhang, Sheng-ming: Added mass of underwater plates and beam stiffened plates in vibration. J. Hydrodyn. B **3**(2), 13–20 (1991)
260. Zhuravlev, Yu.F.: Immersion of a disc in fluid under an arbitrary angle to free surface. In: *Collected works on hydrodynamics. Central Institute of Aero- and Hydrodynamics*, pp. 227–232 (1959), in Russian
261. Zhow, Z.X., Lo, E.Y.M., Tan, S.K.: Effect of shallow and narrow water on added mass of cylinders with various cross-ration shapes. Ocean Eng. **35**, 1199–1215 (2005)
262. Zhon, Q., Zhang, W., Joseph, P.F.: A new method for determining acoustic added mass and damping coefficients of fluid-structure interaction. Practical Design of Ships and Other Floating Structures. Proc. of the 8th Int. Symp. **2**, 1185–1195 (2001)
263. Zhukovsky, N.E.: *On Impact of Two Balls, One of Those is Floating in Fluid, Selected Works, vol. 1*. AN USSR Publishing House, Moscow (1948), in Russian
264. Zilman, G., Kagan, L., Miloh, T.: Hydrodynamics of a body moving over a mud layer, Part II: Added mass and damping coefficients. J. Ship Res. **40**(1), 39–45 (1996)